Playing LEGO with macromolecules : connecting polymer chains using terpyridine metal complexes

Playing LEGO with macromolecules:

connecting polymer chains using terpyridine metal complexes

PROEFSCHRIFT

ter verkrijging van de graad van doctor aan de
Technische Universiteit Eindhoven, op gezag van de
Rector Magnificus, prof.dr. R.A. van Santen, voor
een commissie aangewezen door het College voor
Promoties in het openbaar te verdedigen op
woensdag 17 november 2004 om 16.00 uur.

door

Bastiaan Gabriël Gerardus Lohmeijer

geboren te Groningen

Dit proefschrift is goedgekeurd door de promotoren:

prof.dr. U.S. Schubert
en
prof.dr. I. Manners

Het onderzoek beschreven in dit proefschrift is gefinancierd door de Technische Universiteit Eindhoven.

Omslagontwerp: Paul Verspaget

Druk: universiteitsdrukkerij, TUE

CIP-DATA LIBRARY TECHNISCHE UNIVERSITEIT EINDHOVEN

Lohmeijer, Bas G.G.

Playing LEGO with macromolecules: connecting polymer chains with terpyridine metal complexes / by Bas G. G. Lohmeijer
Eindhoven: Technische Universiteit Eindhoven, 2004.
Proefschrift. – ISBN
NUR 913
Trefwoorden: supramoleculaire chemie; zelforganisatie / polymeermorfologie / polymeersynthese / blokcopolymeren / micellen / overgangmetaalcomplexen / coördinatieverbindingen; terpyridine / nanotechnologie
Subject headings: supramolecular chemistry; self-assembly / polymer morphology / polymer synthesis / block copolymers / micelles / transition metal complexes / coordination compounds; terpyridine / nanotechnology

Table of contents

Chapter 1

Chapter 2

Chapter 3

Chapter 4

Chapter 5

Chapter 1

Design and Construction Principles of Macromolecular Architectures Based on *Bis*-Terpyridine Metal Complexes

Abstract

Current miniaturization efforts using top-down approaches such as lithography are reaching their limits in terms of technological and economical versatility. A bottom-up approach using self-assembly of macromolecules into well-defined 2D- and 3D-morphologies is a promising development. Especially block copolymers with labile groups at the block junction may provide an easy-accessible route towards functional nanomaterials. This chapter functions as a basic introduction into the field of block copolymers regarding their self-assembly into different morphologies and into the field of supramolecular chemistry where non-covalent interactions can give rise to a self-assembly process into fascinating architectures. Bis-terpyridine metal complexes are then introduced as versatile linkages for the connection of a variety of terpyridine-functionalized polymer chains. A wide range macromolecular architectures can be envisioned using the construction principles of homo- and heteroleptic bis-terpyridine metal complexes. This leads to the formulation of the aims of this thesis.

Parts of this chapter have been published: B. G. G. Lohmeijer, U. S. Schubert, *J. Polym. Sci. Part A Polym. Chem.* **2003**, *41*, 1413-1427; J.-F. Gohy, B. G. G. Lohmeijer, U. S. Schubert, *Chem. Eur. J.* **2003**, *9*, 3472-3479.

1.1 Motivation

The need for highly sophisticated materials keeps increasing with current miniaturization efforts in both academia and industry.[1-4] More data storage capacity on smaller area's and faster devices, sensors for lab-on-a-chip applications and photonics are a few of the main driving forces for active interest in new materials.[5-7] Now that top down approaches using expensive lithographic techniques are reaching their limits, bottom-up approaches using inexpensive self-assembly processes are of particular interest. Currently, state-of-the-art interferometric lithography enables periodic patterning of a photoresist-coated substrate with sub-100 nm precision using 193 nm lasers.[8-12] Envisaged for the future is the use of 157 nm lasers enabling even smaller patterning precisions, although several challenges need to be overcome.[8,13,14] Every step down in laser wavelength requires besides new optical equipment also new resist materials in terms of UV-absorption properties, solubility in organic solvent for spincasting as well as in aqueous acid/base for development, film forming properties, adhesion, etch resistance and compatibility with photoactive compounds.[8,15] On the other hand, simple diblock copolymers can give rise to highly regular patterns on a surface. By controlling the self-assembly processes involved, well-defined long range order and high topological regularity can be obtained.[16-21] The next step is to selectively remove one of the polymer blocks, e.g. by exposure to UV-light.[22] In such a way, highly regular 2D patterns can be acquired and periodicities from ~10 nm and up can be obtained. These patterned surfaces can then be used as templates in the fabrication of nano-devices by, e.g., filling the nanopores with magnetic material. In the same vein, molecular machines and nano-devices are expected to revolutionize our capabilities in the micro- and nanoworld. One can think of area's as display technology, medical treatments, nanofluidics and tissue engineering.[23-26] Again, thorough control over the morphology of the materials involved is the first step towards successful development of such materials. For example, the latest technological developments in two-photon 3D lithography show a patterning precision of 200 nm across and 800 nm in depth, but these limits are pushed further.[27,28] Nature on the other hand uses self-assembly processes to create nanometer-sized functional materials such as proteins and enzymes. The information contained in the molecular structure is responsible for the shape of the final assembly. Moreover, the programmed positioning of binding sites for interaction with other (macro)molecules enables specific functions.[29] The advances in biochemistry utilizing the Merrifield-synthesis[30] have resulted in a good control over molecular structure of biomacromolecules and also genetic engineering provides ways for exploitation of functional biomacromolecules.[31-34] Man-made well-defined self-assembled 3D nano-sized objects are far less developed but comprise important examples such as dendrimers, block copolymer micelles and vesicles, which may be used e.g. as drug delivery agents.[35-42] The important point to make is that simply by utilizing self-assembly processes control over the morphology, the shape and the function of a material can be gained relatively easy by implementing the information in the backbone of the macromolecule in contrast with lengthy and costly assembly techniques as clever and efficient as they have proven to be. The main challenges lie in understanding and fine-tuning the interactions involved that lead to a specific morphology and the subsequent design of macromolecules that contain the information necessary for a certain morphology and associated function. In this chapter self-assembly processes regarding block copolymer morphologies in the bulk, in thin films and in solution as well as the implementation of specific supramolecular binding motifs into polymer backbones which give rise to self-assembly and self-

organization are briefly discussed. This leads to the formulation of the aims and the outline of this thesis.

1.2 Block copolymers and their morphologies

Block copolymers have gained much attention due to their remarkable phase behavior. They are industrially important as thermoplastic elastomers, impact modifyers and compatibilization agents. In solution they are well-recognized for their surfactant properties with applications as foams, oil additives, solubilizers, thickeners and dispersion agents.[43-46] In a block copolymer two or more chemically distinct polymers blocks are covalently linked to each other. Examples of linear and branched block copolymers consisting of two or three monomers are depicted in Figure 1.1.[47]

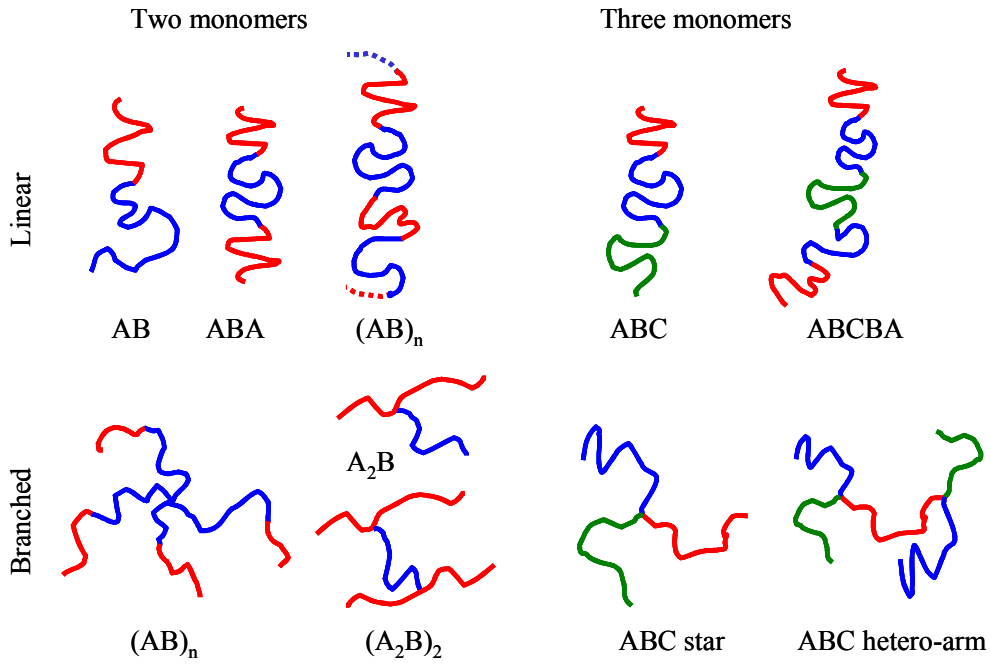

Figure 1.1. *Linear and branched block copolymers consisting of two or three monomers.*

Prerequisite for a well-defined phase behavior is a low polydispersity index in each of the blocks (PDI < 1.3) and synthetic techniques generally require living polymerization processes. In particular anionic polymerization has been successfully applied for their synthesis.[48,49] Several other routes have been realized as well, for example controlled radical polymerization,[50-53] living cationic polymerization,[54-56] group transfer[57-59] and metathesis polymerization[60-62] or combinations of such techniques. Nevertheless, block copolymer synthesis remains a challenge due to the fact that all techniques suffer from limitations. Anionic polymerization,[63] for example, suffers from monomer addition sequence issues and this becomes even more a limitation when preparing triblock and multiblock copolymers. For example, the only possible way of preparing low-polydispersity polystyrene-*block*-poly(ethylene oxide) is by first polymerizing styrene and then to use the living chain for the polymerization of ethylene oxide. The reason for this is the fact that initiation of ethylene oxide by the more nucleophilic polystyrene carbanion proceeds faster than the propagation of ethylene oxide: in this way an efficient cross-over reaction takes place and low polydispersity block copolymers are the result. This would obviously not be the case if styrene was to be polymerized as the second monomer. Moreover,

special care has to be taken regarding the required ultra-high purity of the second monomer in order to prevent unwanted termination reactions. Further limitations of anionic polymerization are the required stringent purification levels of monomer and solvent as well as the intolerance to functional groups. On the other hand, functional groups such as hydroxyl groups may be introduced by end-capping reactions[64] or by making use of (protected) functionalized initiators.[65] This will eventually allow the coupling of other functionalized polymers in a second step. Controlled radical polymerization techniques are a valuable alternative due to the practicality and versatility associated with radical polymerizations.[66,67] Moreover, the starting block may be isolated and purified first before adding the second monomer. Also, initiating groups for different polymerization mechanisms may be present, allowing in some cases the one-pot synthesis of block copolymers.[68-70] Nevertheless, also here monomer addition sequence issues apply because of macro-initiator end group functionality and re-initiation efficiency that largely determine the success of a block copolymerization.

Important reason for the interest in well-defined block copolymers is the remarkable micro- and nanophase behavior and the therefrom resulting useful properties. In diblock copolymers this simply stems from the covalent junction between two different polymer chains. Two competing effects are responsible for the phase behavior: phase separation may take place due to energetically favorable demixing of the two blocks, but entropically this is unfavorable due to a more constrained chain configuration. Since both blocks are connected to each other and cannot come loose, macrophase separation cannot occur and nano-sized phase separated domains rich in either polymer block are formed. The extent to which block copolymers phase separate is expressed by the reduced parameter χN, where χ describes the Flory-Huggins parameter and N the degree of polymerization. The Flory-Huggins parameter is a measure of the incompatibility between two polymer blocks and represents mainly the enthalpic contribution to the free energy, whereas the degree of polymerization N represents the entropic contribution.[47,71-75] In a block copolymer melt the so-called order-disorder transition (ODT) is the transition at which a homogeneous block copolymer melt transforms into a heterogeneous melt of phase separated domains. The volume fraction of the blocks determines the type of morphology that is formed, since the interfacial area between the two blocks will be as small as possible. Figure 1.2 shows both the theoretical and experimentally determined phase diagram of amorphous polystyrene-*block*-isoprene.[76]

As can be seen, spherical, cylindrical, bicontinuous and lamellar morphologies are formed depending on the volume fraction and the χN-parameter. Experimentally also a hexagonally perforated layer has been observed.[77] Upon lowering the temperature, vitrification and/or crystallization of one or both blocks may occur, depending on the chemical composition of the individual polymer blocks. The morphology is normally retained during vitrification, but especially in case of semi-crystalline blocks a different morphology may form as a result of the crystallization process.[78-81] Moreover, in block copolymer thin films, interesting morphologies may form as a result of surface effects.[82,83] Figure 1.3 shows both experimental and theoretical results on symmetric diblock copolymer morphologies confined between two surfaces.

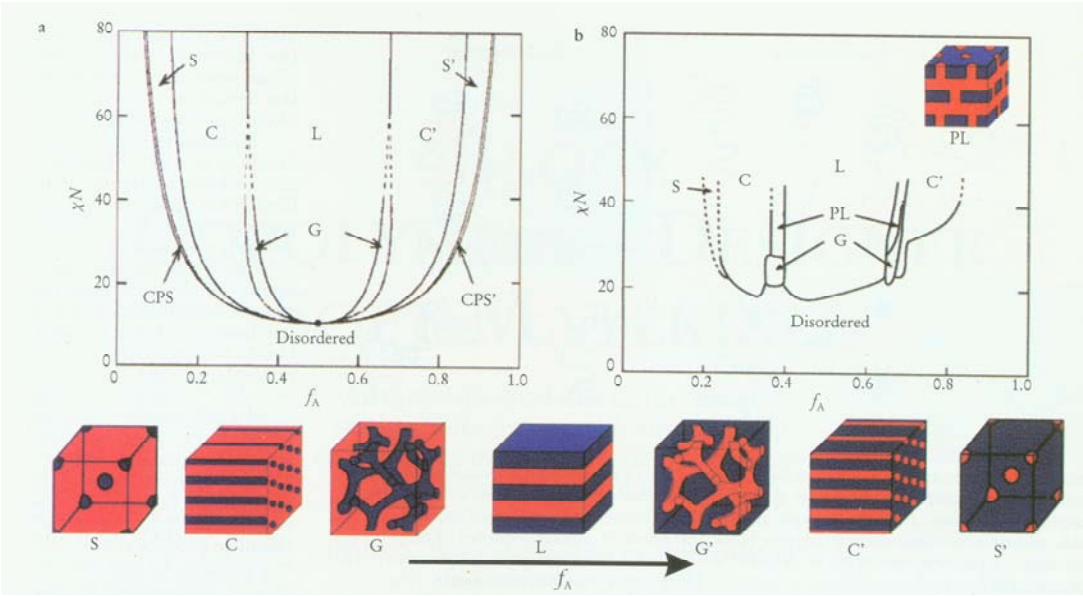

Figure 1.2. *Theoretically and experimentally determined phase diagram of polystyrene-polyisoprene diblock copolymers (from ref [97]). S, C, G and L represent the spherical, cylindrical, gyroid and lamellar phases, where PS is the minority block and S', C' and G' denote the corresponding phases, where PI is the minority block. PL represents perforated lamellae.*

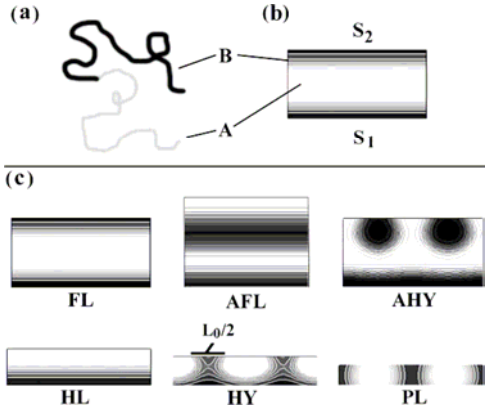

Figure 1.3. *Morphologies of a symmetric diblock copolymer thin film confined between two surfaces with surface energies S1 and S2 (after Fasolka and Mayes, ref [83]). In (c) several possible arrangments are shown, generally organized by their appearance as film thickness decreases from period L_0. FL: symmetric surface-parallel full lamellae; AFL: anti-symmetric surface parallel-lamellae; AHY: anti-symmetric hybrid structure; HL: half-lamellae; HY: symmetric hybrid structure and PL: surface perpendicular lamellae.*

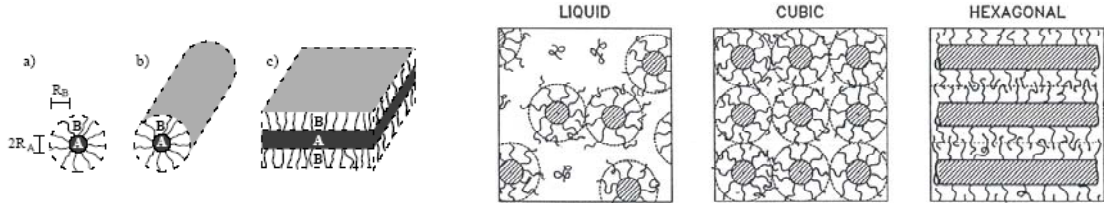

Figure 1.4. *Block copolymer micellar morphologies ranging from spherical, cylindrical to lamellae and are capable of forming of cubic and hexagonal gels (images taken from ref [47] and [95]).*

In dilute solution block copolymers may self-assemble into micelles by exposure to selective solvents.[84-91] The core of the micelle is then made up of the insoluble block, whereas the corona extends into the solvent. Spherical micelles, cylindrical micelles and vesicles may result upon increasing the concentration of the block copolymer. In

concentrated solutions, micelles can order into gels (Figure 1.4).[92-95] In summary, covalently linked diblock copolymers display a wealth of different morphologies. ABC-Triblock copolymers and their beautiful and intriguing morphologies have also been developed especially during the last decade, while a theoretical basis has been laid (Figure 1.5).[96-101]

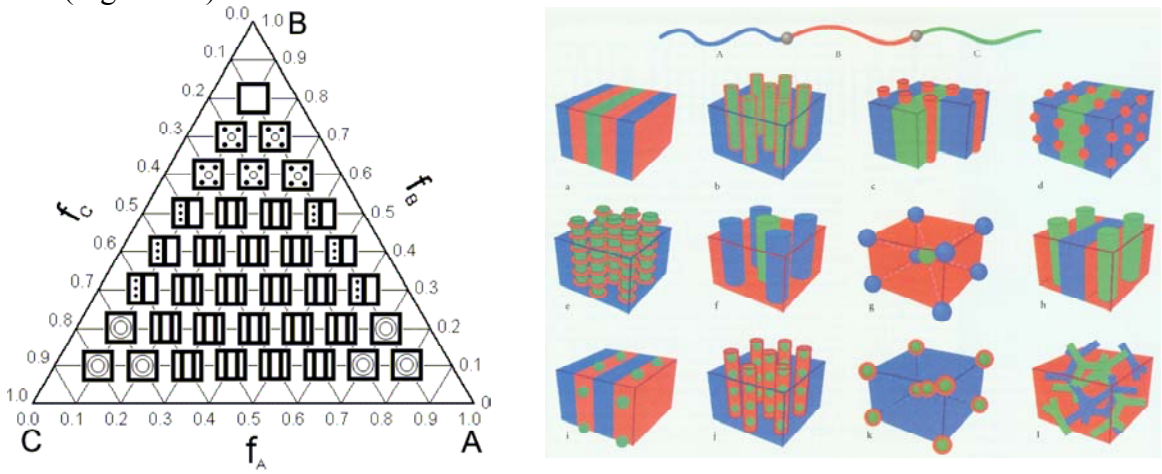

Figure 1.5. *Theoretical phase diagram of linear ABC-triblock copolymers depending on the interaction parameters between AB, AC and BC respectively. More examples can be found in ref*[97].

Very recently the first linear ABCD-tetrablock copolymers have been reported using anionic polymerization, although in a few cases one of the blocks is too short to form a distinct phase. Indeed compatibility of two phases could be troublesome in identifying real tetrablock copolymer morphologies.[102-106] Nevertheless, one true tetrablock copolymer morphology has been identified, i.e. the hexagonal triple coaxial cylinder structure.[102] Up to date only one report has appeared that deals with the synthesis of a linear pentablock copolymer, but no morphological investigations have been published yet.[106] It is expected that the phase behavior of these block copolymers is even more complex than in case of the linear triblock copolymers.

Introduction of functionality in block copolymers however will prove to be invaluable for the preparation of functional (nano)-materials. The next section will describe how supramolecular chemistry may provide some answers.

1.3 Supramolecular polymer chemistry

The directed association of synthetic molecules into defined architectures is the field of supramolecular chemistry, also known as the chemistry beyond the molecule and in a broader sense resting on principles earlier known from colloid chemistry.[107,108] Non-covalent interactions that are weaker than covalent bonds are responsible for the self-assembly processes between molecules. A dynamic binding equilibrium exists between the energetically favored associated self-assembled state(s) and the entropically favored disassembled state. This delicate equilibrium allows for reversibility and a continuous non-covalent bond formation and dissociation.[109,110] In principle, block copolymer morphologies are supramolecular structures resulting from attractive and repulsive Vanderwaals-forces between monomers of block A and block B respectively, although current supramolecular chemistry focuses on specific binding groups introducing more directionality. A large variety of non-covalent interactions can be employed as can be seen in Table 1.1, which vary in strength, lifetime and

directionality. The fact that these non-covalent interactions are weaker than covalent bonds and are governed by equilibria enables fine-tuning of the degree of association by applying external stimuli such as temperature, pressure, pH, redox state and shear forces.[111]

Table 1.1 *Supramolecular interactions after Goshe in ref [111].*

Interaction	Energy (kJ/mol)	Distance dependence	Stability	Illustration
Ion-ion	40-360	r^{-1}	High	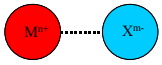
Ion-dipole	40-200	r^{-2}, r^{-4}	High	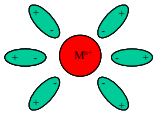
Dipole-dipole	4-150	r^{-3}, r^{-6}	Medium	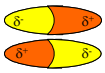
Cation-π	4-80	r^{-2}, r^{-4}	Medium	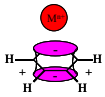
π-π stacking	4-20	r^{-3}, r^{-6}	Low	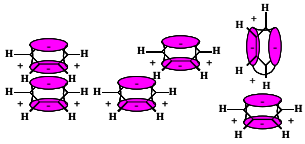
Dispersion	4-20	r^{-6}	Low	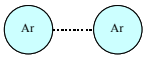
Solvent effects	4-40		High	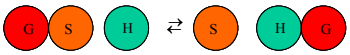

Nobel-laureate Jean-Marie Lehn described in 1993 the combination of polymer chemistry with supramolecular chemistry.[112] He proposed, that the implementation of supramolecular units into polymers should lead to a rich panorama of new materials. Lehn foresaw the birth of main chain and side chain supramolecular polymers as well as crosslinking agents through the use of mono and ditopic complementary and self-complementary supramolecular entities (Figure 1.6).

The main objective is to obtain materials that combine the desired properties from both fields: the intrinsic material properties arising from the polymer part in combination with the self-assembly and sometimes reversible binding features from the supramolecular entities that are connected to the polymer backbone. The ability to control self-organization processes of the supramolecular polymers provides access to 'intelligent' or 'smart' materials through molecular recognition of the supramolecular units: linkage(s) may be formed and broken by applying external stimuli as described above.[113-119]

In order to construct supramolecular AB diblock copolymers, the supramolecular interaction between the starting A and B end-functionalized polymers must exclusively lead to an AB "hetero-assembly" and not to AA and BB "homo-assemblies".

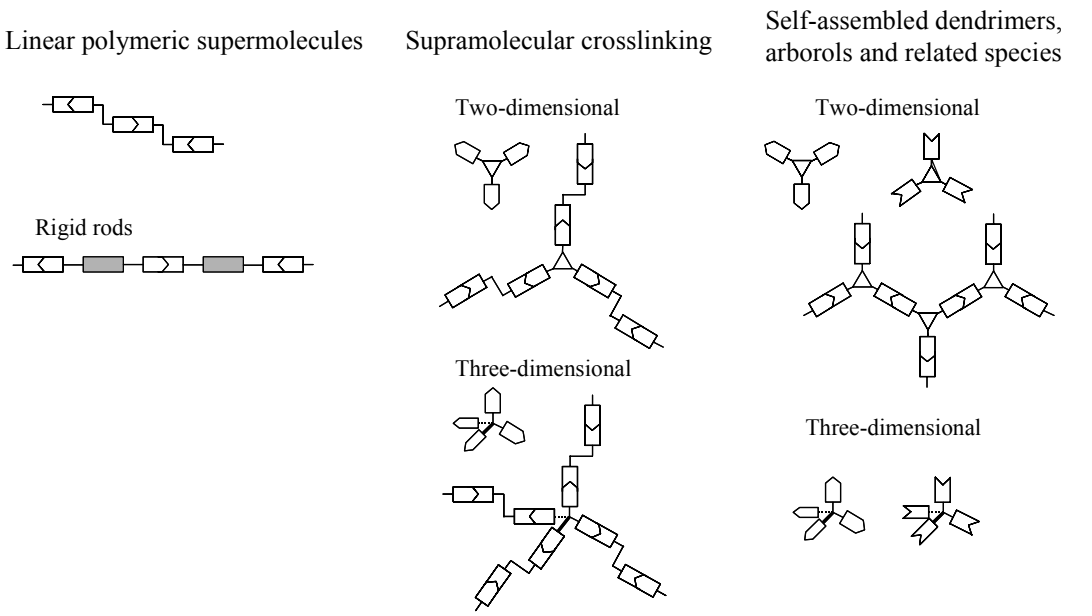

Figure 1.6. *Overview of selected macromolecular architectures from supramolecular polymer chemistry as envisioned by Lehn.*[112]

In principle, all known non-covalent interactions can be utilized for this purpose (see Table 1.1). The use of ionic interactions to form supramolecular AB block copolymers is exemplified by the work of Jérôme (Figure 1.7a).[120] The mixing of carboxylic acid end-functionalized polystyrene with tertiary amine end-functionalized polyisoprene resulted in materials that resemble covalently-bonded polystyrene-*block*-polyisoprene. The magnitude of the ionic interactions could be rather high and easily modulated through the dielectric constant.[121] However, such ionic interactions are not directional and not selective. Hydrogen-bonding in macromolecular architectures has recently received significant attention due to the thermoreversible and molecular recognition features of the resulting self-assemblies.[122-128] Complementary multiple hydrogen bonding units are good candidates to synthesize supramolecular hydrogen-bonded AB copolymers. Heterocyclic base pairing between adenine, guanine, thymine, uracil and tyrosine in DNA and RNA are well-known as tailored complementary hydrogen-bonded units in biological systems. Indeed, these typical moeities can be incorporated in synthetic polymers for the purine-thymine pair (Figure 1.7b). Recently, also complementary quadruple hydrogen bonding arrays have been developed, which certainly adds to the stability of the non-covalent linkage (Figure 1.7c).[129] However, the strength of the hydrogen-bonds is still rather weak compared to ionic or ion-dipole interactions.

The work presented in this thesis was focused on the implementation of supramolecular entities capable of ion-dipole interactions into polymer backbones. To be more precise, the chelation of one or two tridentate terpyridine-ligands around transition metal ions leading to the formation of metal complexes has been employed. Two terpyridine-ligands form octahedral complexes with a large variety of transition metal ions (Figure 1.8).[130]

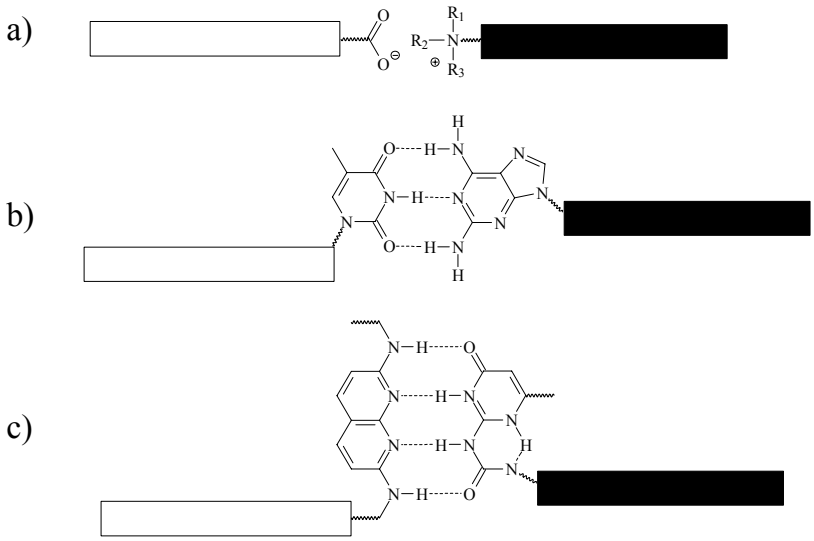

Figure 1.7. *Possible complementary non-covalent interactions for the construction of AB-block copolymer based on a) ionic interactions, b) triple hydrogen bonding scaffolds and c) quadruple hydrogen bonding scaffolds.*

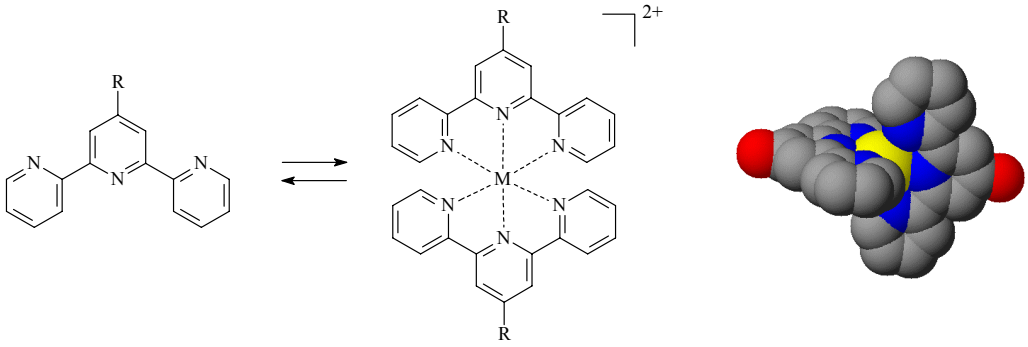

Figure 1.8. *Metal complex formation between terpyridine and transition metal ions (left), leading to an octahedral surrounding of the metal ion by two meriodinally coordinated terpyridine-ligands (right).*

Most common metal ions are Mn, Fe, Ru, Os, Co, Ir, Ni, Pt, Cu, Ag, Zn, Cd, and Hg, all in low oxidation states. There is only one possible way in which two terpyridine ligands can chelate around the metal ion to form the octahedral complex (Figure 1.8):[131] the outer rings cooperatively rotate along the central C-C bonds connecting the rings in order to create a stable binding site through the lone pairs of the three nitrogen atoms. The stability of the ion-dipole interaction stems from an efficient backdonation of the metal to the ligand.[132] In contrast, three didentate ligands such as bipyridine or phenantroline give rise to two different conformations (*fac* and *mer* stereoisomers, Figure 1.9) around an octahedral metal ion,[133] which unfortunately is not easy to selectively control.[134] Nevertheless, such ligands have been used for the preparation of star block copolymers.[135-137]

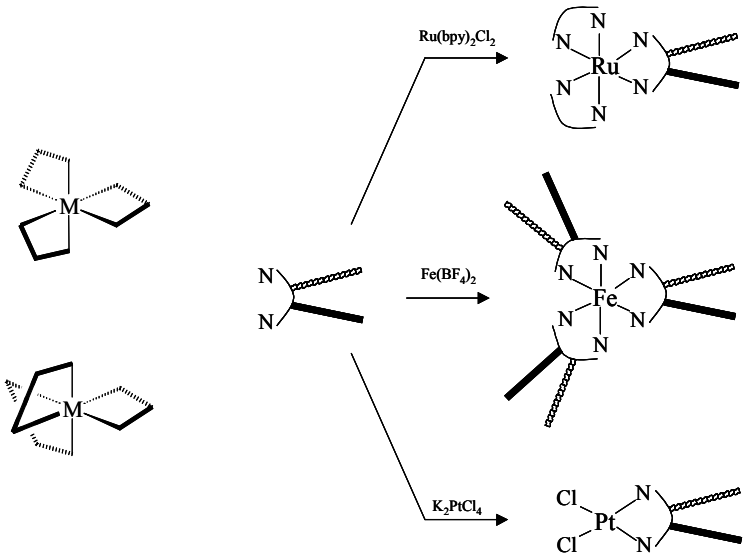

Figure 1.9. *Fac- and mer-stereo-isomers of octahedral complexes with three bidentate ligands (left) and an example of bidentate ligands in polymer architectures by Fraser.*[137]

Interestingly, a large variety of lifetimes and bond strengths can be accessed simply by changing the metal ion or even only the oxidation state while using the same ligand. [138,139] In fact, completely inert metal complexes can also be made using the terpyridine-ligand. This case is particularly interesting because of the fact that a material containing such a metal complex can be isolated, characterized and processed while the metal complex keeps its integrity, i.e. no exchange takes place due to the absence of any equilibrium.[140] Actually, such a metal complex may be regarded as a dormant switch present in the macromolecule. Of course, applying the right external stimuli may lead to labilization of the metal complex with subsequent ligand exchange, again leading to an equilibrium situation between associated and non-associated species. Inert heteroleptic *bis*-terpyridine complexes allow the connection of two different polymer chains in a two-step synthesis and hence the formation of block copolymers.[141] Examples of inert terpyridine metal complexes are of chromium(III), cobalt(III), ruthenium(II), osmium(II) and iridium(III). Selective formation of heteroleptic complexes is to the best of our knowledge at present limited to $Ru^{III}Cl_3$[142] and $Os^{III}Cl_3$.[143] Here the focus is on $Ru^{III}Cl_3$. In the first step the polymer is slowly added to an excess of this salt in an appropriate solvent, after which the *mono*-complex can be isolated by precipitation or extraction and purified. In the second step the corresponding Ru^{III} *mono*-complex is reduced to Ru^{II} in the presence of an organic reductor such as triethylamine or *N*-ethylmorpholine[144] and the chlorides are replaced by the second terpyridine ligand.[145] Since both the *mono*- and *bis*-terpyridine complexes of Ru^{III} and Ru^{II} respectively are more or less inert with respect to the terpyridine ligand, it is possible to selectively form a heteroleptic complex in two steps (Figure 1.10).

The inertness of the metal complex is actually the key to stable block copolymers. If a labile metal complex was to be used, ligand exchange would take place. Apart from AB block copolymers, AA and BB homopolymers would form, most probably in a worse than statistical mixture (1:2:1 for AA:AB:BB) due to the inherent immiscibility of polymer chains of different chemical composition. That may actually also pose problems for hydrogen-bonded supramolecular block copolymers, where

complementary triple or quadruple hydrogen bonding units may become self-complementary by using less than the maximum attainable hydrogen-bonds: a favorable enthalpy of demixing of the polymer chains may be the driving force.

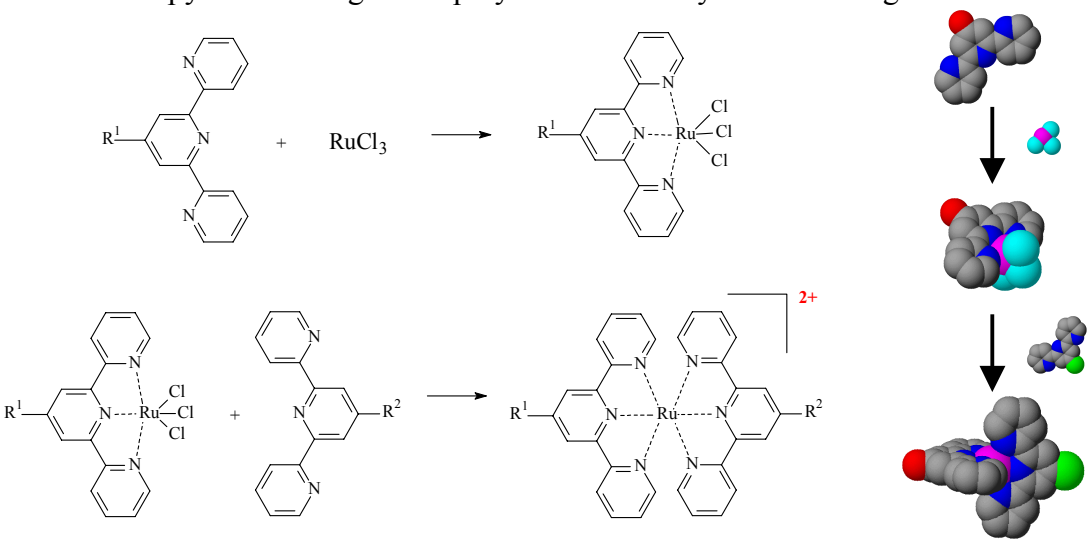

Figure 1.10. *Two-step synthesis of heteroleptic bis-terpyridine ruthenium(II) complexes via the reduction of a ruthenium(III)chloride mono complex (left) again yielding an octahedral complex (right).*

Functionalized terpyridine-ligands can be synthesized in many ways.[146-150] The most interesting route regarding the combination with polymer chemistry and also from an economical point of view is by introducing a synthetic handle at the 4'-position of the ligand. The importance and versatility of the 4'-position of the terpyridine ligand becomes evident when looking at the process of complex formation. The outer rings need to rotate in order to establish the tridentate coordination. There is no influence on the 4'-position upon rotation and therefore a (polymer) substituent can be attached to this position without introducing any conformational strain. Moreover, the symmetry of the metal complex is not distorted when placing substituents at the 4'-position. Other interesting positions that do not impose too much conformational strain are the 5- and 5"-position of the two outer rings. Functional groups in these positions are not as readily synthetically accessible as in the 4'-position. However, 5,5"-dimethyl-2,2':6',2"-terpyridine[151] has proven to be a useful starting material, e.g. for the synthesis of helicates.[152] As far as preparation of supramolecular polymers is concerned, only a single report is known utilizing these positions for modification.[153] Functional groups have been introduced at other positions on the terpyridine ligand as well, but are less attractive from steric and electronic considerations.[147] The presence of a functional group in a polymer backbone can be established by conventional polymerization routes utilizing end capping reactions, co-monomers or (protected) functionalized initiators.[154] Actually, many amino-, chloro-, carboxy- and hydroxy-functionalized polymers are commercially available. It is this functional group that needs to be converted into a terpyridine ligand for the preparation of the building blocks. Figure 1.11 shows some possibilities for the introduction of a terpyridine ligand into a polymer backbone: end group modification of ω- and/or α-functional homo- and diblock copolymers, polymerization utilizing functional initiators and copolymerization of functionalized monomers. The latter case will not be dealt with in this thesis although several reports in the literature describe this approach.[117,118,155-158] In this thesis end group modification reactions of commercial hydroxy-functionalized polymers have been carried out using

etherification and urethane-formation. A terpyridine-functionalized initiator has been synthesized and used for the polymerization of a variety of monomers. Upon introduction of metal ions a variety of macromolecular architectures may be formed (Figure 1.12).

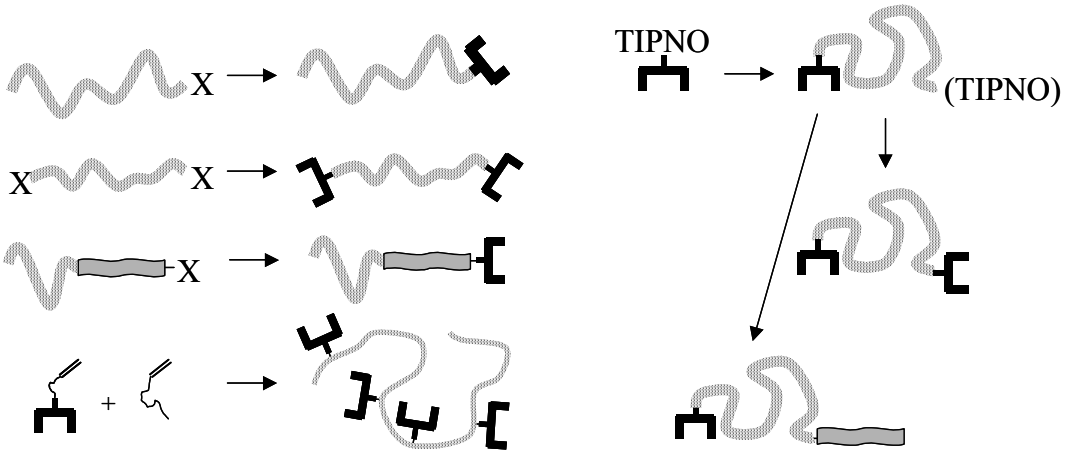

Figure 1.11. *Possible ways of introducing terpyridine-ligands into a polymer backbone using end group modification reactions (left) and functionalized initiators (right) for the preparation of mono- and telechelic terpyridine functionalized (block co) polymers. TIPNO represents a commonly used name for the nitroxide radical developed by Hawker (T=tert-butyl, I=isopropyl, P=phenyl, NO=nitroxide).*[51]

The nature of the macromolecular architecture largely depends on the applied metal ion: homo-dimers (I), chain-extended polymers (II) and AB block copolymer dimers (VI) can be prepared with any metal ion regardless of the dynamics or lability of the metal complex, because the metal complex is homoleptic and in the center of symmetry in these cases. Random multiblock copolymers (VIII) can also be connected using any metal ion. Block copolymers (III), (IV), (V), (VII) and (IX) require the inert metal ion approach in order to maintain only heteroleptic linkages between the different polymer blocks.

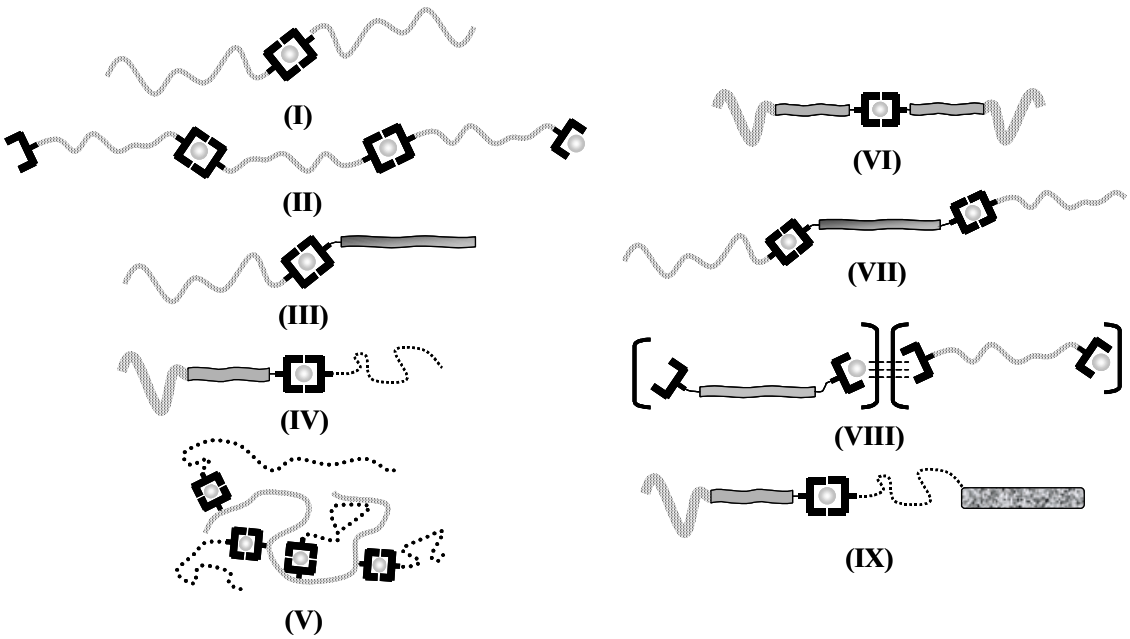

Figure 1.12. *Possible macromolecular structures upon introducing metal ions. Included are homo-dimers (I), chain-extended polymers (II), diblock copolymers (III), triblock copolymers (IV, VI, VII), tetrablock copolymers (IX), random multiblock copolymers (VIII) and graft copolymers (V).*

The versatility of this approach is obvious, since only few building blocks have to be prepared for allowing a wide range of possible macromolecular structures. The art is thus to select the appropriate metal ion for a specific function which is again closely related to the designed morphology. Hence, selection criteria must be known. Their derivation with respect to stability, reversibility and versatility of the applied metal ion is one of the subjects of this thesis. Furthermore, the approach allows the construction of (block co) polymer libraries. Again, only few building blocks are necessary to cover many different volume fractions and molecular weights by simply controlling the molecular weights of the starting building blocks. Also, combination of different terpyridine functionalized diblock copolymers directly leads to tetrablock copolymers. Block copolymers with more than four blocks are easily envisioned as well.

All of the *bis*-terpyridine metal-complex-containing macromolecules are expected to be subject to the same principles as covalent diblock copolymers, although some differences are obvious regarding the presence of charged metal complexes in the backbone. Nevertheless, using block copolymers (e.g. (III) and (IV)) it should be possible to prepare micelles by using selective solvents and to apply these block copolymers in thin films. The interest in having a labile junction in a block copolymer is demonstrated in Figure 1.13. The reversibility or switchability of the supramolecular interaction will be the key ingredient for interesting applications of these block copolymers. For example, a terpyridine functionalized micellar core can be utilized for nano-catalysis or as a scaffold for dynamic libraries.[140] Thin films of these block copolymers with a well-defined phase behavior and highly ordered morphology can be used to prepare highly regularly patterned functional surfaces by applying selective solvents and washing out one of the blocks.

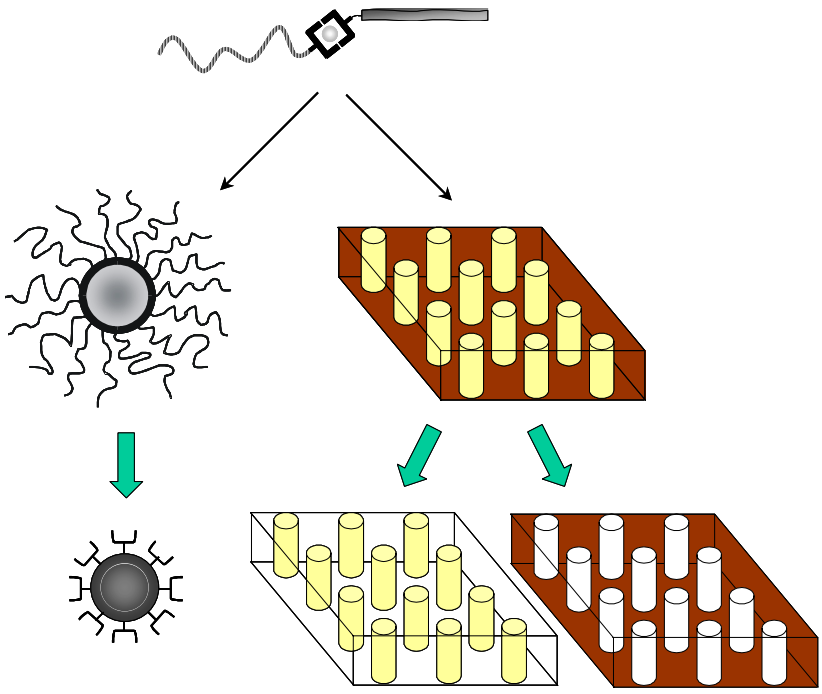

Figure 1.13. *Opening the metal complex may give rise to nano-particles with high terpyridine functionality as well as functional nano-patterned surfaces.*

1.4 Aim and outline of this thesis

This thesis focuses on how to connect polymer chains together using terpyridine metal complexes, how to disconnect them, how to characterize them and what type of morphologies the new class of block copolymers can form. By making use of homoleptic and heteroleptic *bis*-terpyridine complexes as described in the previous section, a wide range of different macromolecular architectures can be readily prepared. The generality of the approach allows a direct comparison with the well-known LEGO-system: different sizes, shapes and colors of LEGO-blocks (representing molecular weight, chemical structure and intrinsic properties of the polymers) can be connected and disconnected in a similar fashion, all using the same type of connectors – representing the metal complexes. This has led to the thesis' title "Playing LEGO with macromolecules". The thesis is subdivided in four closely related topics described in the following four chapters. Chapter 2 will deal with binding characteristics of terpyridine metal complexes. For this purpose, the synthesis, characterization and properties of model systems being *mono*- and *bis*-terpyridine metal complexes with a variety of transition metal ions have been investigated in detail. Since two ligands are sequentially chelating around the metal ion, two association constants are involved in the formation of the linkage. The absolute and relative magnitude of these constants greatly influences the final amount of *mono*- and *bis*-complexes as a function of the metal-to-ligand ratio. Moreover, special attention has been paid to the stability of the metal complexes with respect to temperature, pH and redox state. These factors in turn aids in the selection of the metal ion for making the connection between polymer chains. Chapter 3 is concerned with the synthesis and characterization of mono- and telechelic terpyridine-functionalized polymers using end-group modification routes and nitroxide mediated controlled living free radical polymerization using a terpyridine-functionalized initiator. The kinetics of the polymerization of several monomers has been studied as well as the degree of chain end functionality. Chapter 4 describes the synthesis and characterization of a variety of polymer architectures as depicted in Figure 1.10 such as homo-dimers, chain-extended polymers, di- and triblock copolymers. Due to the inherent charges present in the polymers, less-common techniques for characterization such as capillary electrophoresis and analytical ultracentrifugation have been applied as well. Chapter 5 finally introduces the morphology of several diblock copolymers in the bulk, in the melt, in thin films and in solution. The chapter is concluded with an outlook on future applications of these block copolymers.

1.5 Literature

[1] J. Tersoff, *Nature* **2001**, *412*, 135-136.
[2] P. S. Weiss, *Nature* **2001**, *413*, 585-586.
[3] V. Balzani, A. Credi, M. Venturi, *Chem. Phys. Chem.* **2003**, *3*, 49-59.
[4] C. D. Simpson, J. Wu, M. D. Watson, K. Müllen, *J. Mater. Chem.* **2004**, *14*, 494-504.
[5] C. E. Olson, M. J. R. Previte, J. T. Fourkas, *Nature Materials* **2002**, *1*, 225-228.
[6] M. Freemantle, *Chem. Eng. News* **1999**, *77*, 27-36.
[7] M. Bockstaller, R. Kolb, E. L. Thomas, *Adv. Mater.* **2001**, *13*, 1783-1786.
[8] www.almaden.ibm.com/st/chemistry/lithography/index.shtml and related links.
[9] M. Rothschild, A. J. Burns, S. G. Cann, A. R. Forte, C. L. Keast, R. R. Kunz, S. C. Palmateer, J. H. C. Sedlacek, R. Uttaro, A. Grenville, D. Corliss, *J. Vac. Sci. Technol. B*, **1996**, *14*, 4157-4161.
[10] W. Hinsberg, F. A. Houle, J. Hoffnagle, M. Sanchez, G. Wallraf, M. Morrison, S. Frank, *J. Vac. Sci. Technol. B* **1998**, *16*, 3689-3694.
[11] A. G. Timko, J. Frackoviak, L. C. Hopkins, F. P. Klemens, L. E. Trimble, O. Nalamasu, G. P. Watson, W. M. Mansfield, D. Barr, J. Li, *J. Vac. Sci. Technol. B* **2001**, *19*, 2713-2716.
[12] www.asml.nl/NASApp/asmldotcom/show.do?ctx=6720&rid=7394&%22%22
[13] T. M. Bloomstein, M. W. Horn, M. Rothschild, R. R. Kunz, S. T. Palmacci, R. B. Goodman, *J. Vac. Sci. Technol. B* **1997**, *15*, 2112-2116.
[14] E. Sarantopoulou, Z. Kollia, K. Kočevar, I. Muševič, S. Kobe, Dražić, E. Gogolides, P. Argitis, A. C. Cefalas, *Mater. Sci. Eng. C.* **2003**, *23*, 995-999.
[15] M. J. Madou, *Fundamentals of Microfabrication: the science of miniaturization*, CRC Press, London **2002**.
[16] M. Kimura, M. J. Misner, T. Xu, S. H. Kim, T. P. Russell, *Langmuir* **2003**, *19*, 9910-9913.
[17] Z. R. Chen, J. A. Kornfield, S. D. Smith, J. T. Grothaus, M. M. Satkowski, *Science* **1997**, *277*, 1248-1253.
[18] M. J. Fasolka, D. J. Harris, A. M. Mayes, M. Yoon, S. G. J. Mochrie, *Phys. Rev. Lett.* **1997**, *79*, 3018-3021.
[19] C. De Rosa, C. Park, E. L. Thomas, B. Lotz, *Nature* **2000**, *405*, 433-437.
[20] X. M. Yang, R. D. Peters, P. F. Nealey, H. H. Solak, F. Cerrina, *Macromolecules* **2000**, *33*, 9575-9582.
[21] R. A. Segalman, H. Yokoyama, E. J. Kramer, *Adv. Mat.* **2001**, *13*, 1152-1155.
[22] T. Xu, J. Stevens, J. Villa, J. T. Goldbach, K. W. Guarini, C. T. Black, C. J. Hawker, T. P. Russell, *Adv. Funct. Mater.* **2003**, *13*, 698-702.
[23] J. Knight, *Nature* **2002**, *418*, 474-475.
[24] G. M. Whitesides, *Nature Biotechnology* **2003**, *21*, 1161-1164.
[25] V. Balzani, A. Credi, F. M. Raymo, J. Fraser Stoddart, *Angew. Chem. Int. Ed.* **2000**, *39*, 3348-3391.
[26] H. Hess, G. D. Bachand, V. Vogel, *Chem. Eur. J.* **2004**, *10*, 2110-2116.
[27] http://optics.org/articles/news/10/2/23/1.
[28] M. Tormen, Businaro, M. Altissimo, F. Romanato, S. Cabrini, F. Perennes, R. Proietti, H.-B. Sun, S. Kawata, E. Di Fabrizio, *Microelectronic Eng.* **2004**, *73-74*, 535-541.
[29] L. Stryer, *Biochemistry, 4th Edition*, W. H. Freeman and Company, New York, **1995**.
[30] R. B. Merrifield, *J. Am. Chem. Soc.* **1963**, *85*, 2149-2154.
[31] www.ornl.gov/sci/techresources/Human_Genome/publicat/primer2001/PrimerColor.pdf.
[32] R. D. Schmid, *Pocket guide to biotechnology and genetic engineering*, Wiley-VCH, Weinheim, **2003**.
[33] R. W. Old, S. B. Primrose, *Principles of gene manipulation: an introduction to genetic engineering*, Blackwell Science, Oxford, **1994**.
[34] R. Langer, D. A. Tirrell, *Nature* **2004**, *428*, 487-492.
[35] M. L. Adams, A. Lavasanifar, G. S. Kwon, *J. Pharm. Sci.* **2003**, *92*, 1343-1355.
[36] F. Chécot, S. Lecommandoux, H.-A. Klok, Y. Gnanou, *Eur. Phys. J.* **2003**, *10*, 25-35.
[37] T. K. Bronich, M. Ouyang, V. A. Kabanov, A. Eisenberg, F. C. Szoka Jr., A. V. Kabanov, *J. Am. Chem. Soc.* **2002**, *124*, 11872-11873.
[38] C. Allen, D. Maysinger, A. Eisenberg, *Coll. Surf. B: Biointerfaces* **1999**, *16*, 3-27.
[39] A. Napoli, M. J. Boerakker, N. Tirelli, R. J. M. Nolte, N. A. J. M. Sommerdijk, J. A. Hubbell, *Langmuir* **2004**, *9*, 3487-3491.
[40] Y. Tang, S. Y. Liu, S. P. Armes, N. C. Billingham, *Biomacromolecules* **2003**, *4*, 1636-1645.
[41] G. Cevc, *Adv. Drug Deliv. Rev.* **2004**, *56*, 675-711.

[42] U. Boas, P. M. H. Heegaard, *Chem. Soc. Rev.* **2004**, *33*, 43-63.
[43] G. Holden, N. R. Legge, H. E. Schröder, *Thermoplastic Elastomers: a comprehensive review*, Hanser, München, **1987**.
[44] L. H. Sperling, *Polymeric Multicomponent Materials: an Introduction*, John Wiley & Sons, New York, **1997.**
[45] P. Munk, T. M. Aminabhavi, *Introduction to Macromolecular Science*, John Wiley & Sons, New York, **2002**.
[46] K. Holmberg, B. Jönsson, B. Kronberg, B. Lindman, *Surfactants and polymers in aqueous solution*, John Wiley & Sons, New York, **2003**.
[47] I. W. Hamley, *The Physics of Block Copolymers*, Oxford University Press, Oxford, **1998**.
[48] M. Szwarc, *Nature* **1956**, *178*, 1168-1169.
[49] N. Hadjichristidis, *Chem. Rev.* **2001**, *101*, 3747-3792.
[50] J. Xia, K. Matyjaszewski, *Chem. Rev.* **2001**, *101*, 2921-2990.
[51] C. J. Hawker, A. W. Bosman, E. Harth, *Chem. Rev.* **2001**, *101*, 3661-3688.
[52] J. Chiefari, Y. K. Chong, F. Ercole, J. Krstina, J. Jeffery, T. P. T. Le, R. T. A. Mayadunne, G. F. Meijs, C. L. Moad, G. Moad, E. Rizzardo, S. H. Thang, *Macromolecules* **1998**, *31*, 5559-5562.
[53] D. M. Haddleton, E. Depaquis, E. J. Kelly, D. Kuklj, S. R. Morsley, S. A. F. Bon, M. D. Eason, A. G. Steward, *J. Polm. Sci. Part A: Polym. Chem.* **2001**, *39*, 2378-2384.
[54] J. P. Kennedy, E. G. Melby, A. Vidal, *J. Macromol. Sci. Chem.* **1975**, *A9*, 833-847.
[55] M. Kamigaito, T. Ando, M. Sawamoto, *Chem. Rev.* **2001**, *101*, 3689-3745.
[56] E. J. Goethals, M. Dubreuil, Y. Wang, I. De Witte, D. Christova, S. Verbrugghe, N. Yanul, L. Tanghe, G. Mynarczuk, F. E. Du Prez, *Macromol. Symp.* **2000**, *153*, 209-216.
[57] J. P. Kennedy, R. H. Wondraczek, *Polym. Bull.* **1981**, *4*, 445-450.
[58] T. Otsu, M. Yoshida, *Makromol. Chem. Rapid Commun.* **1982**, *3*, 127-132.
[59] O. W. Webster, W. R. Hertler, D. Y. Sogah, W. B. Farnham, T. V. RajanBabu, *J. Am. Chem. Soc.* **1983**, *105*, 5706-5708.
[60] S. A. Krouse, R. R. Schrock, *Macromolecules* **1988**, *21*, 1885-1888.
[61] K. J. Ivin, J. C. Mol, *Olefin metathesis and metathesis polymerization*, Academic Press, San Diego, **1997**.
[62] P. Schwab, J. P. Ziller, R. H. Grubbs, *J. Am. Chem. Soc.* **1996**, *118*, 100-110.
[63] N. Hadjichristidis, S. Pispas, G. Floudas, *Block copolymers: synthetic strategies, physical properties and applications*, Wiley-Interscience, Hoboken, **2003**.
[64] D. N. Schulz, A. F. Halasa, A. E. Oberster, *J. Polym. Sci. Polym. Chem.* **1974**, *12*, 153-166.
[65] M. Sépulchre, G. Paulus, R. Jérôme, *Makromol. Chem.* **1983**, *184*, 1849-1859.
[66] G. Odian, *Principles of polymerization*, Wiley-Interscience, Chichester, **1991**.
[67] K. Matyjaszewski, *Controlled radical polymerization*, ACS Symposium Series, Washington, **1998**.
[68] D. Takeuchi, T. Aida, *Macromolecules* **2000**, *33*, 4607-4609.
[69] K. Matyjaszewski, D. A. Shipp, G. P. McMurty, S. G. Gaynor, T. Pakula, *J. Polym. Sci. Part A, Polym. Chem.* **2000**, *38*, 2023-2031.
[70] C. J. Hawker, J. L. Hedrick, E. E. Malmström, M. Trollss, D. Mecerreyes, G. Moineau, Ph. Dubois, R. Jérôme, *Macromolecules* **1998**, *31*, 213-219.
[71] P. J. Flory, *Principles of Polymer Chemistry*, Cornell University Press, Ithaca, **1953**.
[72] E. L. Thomas, D. M. Anderson, C. S. Henkee, D. Hoffman, *Nature* **1988**, *334*, 598-601.
[73] F. S. Bates, G. H. Fredrickson, *Annu. Rev. Phys. Chem.* **1990**, *41*, 525-557.
[74] G. H. Fredrickson, F. S. Bates, *Annu. Rev. Mater. Sci.* **1996**, *26*, 501-550.
[75] M. W. Matsen, F. S. Bates, *Macromolecules* **1996**, *29*, 7641-7648.
[76] A. K. Khandapur, S. Förster, F. S. Bates, I. W. Hamley, A. J. Ryan, W. Bras, K. Almdal, K. Mortensen, *Macromolecules* **1995**, *28*, 8796-8806.
[77] I. W. Hamley, K. A. Koppi, J. H. Rosedale, F. S. Bates, K. Almdal, K. Mortensen, *Macromolecules* **1993**, *26*, 5959-5970.
[78] I. W. Hamley, *Adv. Polym. Sci.* **1999**, *148*, 113-137.
[79] L. Zhu, Y. Chen, A. Zhang, B. H. Calhoun, M. Chun, R. P. Quirk, S. Z. D. Cheng, B. S. Hsiao, F. Yeh, T. Hashimoto, *Phys. Rev. B* **1999**, *60*, 10022-10031.
[80] R. Opitz, D. M. Lambreva, W. H. de Jeu, *Macromolecules* **2002**, *35*, 6930-6936.
[81] H. Schmalz, A. Knoll, A. J. Müller, V. Abetz, *Macromolecules* **2002**, *35*, 10004-10013.
[82] H.-C. Kim, T. P. Russell, *J. Polym. Sci. Part B: Polym. Phys.* **2001**, *39*, 663-668.
[83] M. J. Fasolko, A. M. Mayes, *Annu. Rev. Mater. Sci.* **2001**, *31*, 323-355.
[84] S. Förster, M. Antonietti, *Adv. Mater.* **1998**, *10*, 195-217.
[85] Z. Gao, S. K. Varshney, S. Wong, A. Eisenberg, *Macromolecules* **1994**, *27*, 7923-7927.

[86] J. V. M. Weaver, S. P. Armes, S. Liu, *Macromolecules* **2003**, *36*, 9994-9998.
[87] L. Cao, I. Manners, M. A. Winnik, *Macromolecules* **2002**, *35*, 8258-8260.
[88] L. Lei, J.-F. Gohy, N. Willet, J.-X. Zhang, S. K. Varshney, R Jérôme, *Macromolecules* **2004**, *37*, 1089-1094.
[89] T. P. Lodge, J. Bang, K. J. Hanley, J. Krocak, S. Dahlquist, B. Sujan, J. Ott, *Langmuir* **2003**, *19*, 2103-2109.
[90] R. Erhardt, A. Böker, H. Zettl, H. Kaya, W. Pyckout-Hintzen, G. Krausch, V. Abetz, A. H. E. Müller, *Macromolecules* **2001**, *34*, 1069-1075.
[91] F. Chécot, S. Lecommandoux, Y. Gnanou, H.-A. Klok, *Angew. Chem. Int. Ed.* **2002**, *41*, 1340-1343.
[92] H. Li, G.-E. Yu, C. Price, C. Booth, E. Hecht, H. Hoffman, *Macromolecules* **1997**, *30*, 1347-1354.
[93] K. Mortensen, J. S. Pedersen, *Macromolecules* **1993**, *26*, 805-812.
[94] O. Terreau, C. Bartels, A. Eisenberg, *Langmuir* **2004**, *20*, 637-645.
[95] K. Mortensen, *Prog. Coll. Polym. Sci.* **1993**, *93*, 72-75.
[96] C. Auschra, R. Stadler, *Macromolecules* **1993**, *26*, 2171-2174.
[97] F. S. Bates, G. H. Fredrickson, *Phys. Today* **1999**, *52(2)*, 32-38.
[98] P. Tang, F. Qui, H. Zhang, Y. Yang, *Phys. Rev. E* **2004**, *69*, 0318031-0318038.
[99] Y. Bohbot-Raviv, Z.-G. Wang, *Phys. Rev. Lett.* **2000**, *85*, 3428-3431.
[100] Y. Mogi, K. Mogi, Y. Matsushita, I. Noda, *Macromolecules* **1992**, *25*, 5412-5415.
[101] L. Bronstein, M. Seregina, P. Valetsky, U. Breiner, V. Abetz, R. Stadler, *Polymer Bull.* **1997**, *39*, 361-368.
[102] K. Takahashi, H. Hasegawa, T. Hashimoto, V. Bellas, H. Iatrou, N. Hadjichristidis, *Macromolecules* **2002**, *35*, 4859-4861.
[103] T. Tsoukatos, A. Avgeropoulos, N. Hadjichristidis, K. Hong, J. W. Mays, *Macromolecules* **2002**, *35*, 7928-7935.
[104] V. Rebizant, V. Abetz, F. Tournilhac, F. Court, L. Leibler, *Macromolecules* **2003**, *36*, 9889-9896.
[105] Z. Li, G. Liu, *Langmuir* **2003**, *19*, 10480-10486.
[106] N. Ekizoglou, N. Hadjichristidis, *J. Polym. Sci. Part A Polym. Chem.* **2002**, *40*, 2166-2170.
[107] J.-M. Lehn, *Supramolecular Chemistry*, VCH, Weinheim, **1995**.
[108] I. W. Hamley, *Introduction to Soft Matter: Polymers, Colloids, Amphiphiles and Liquid Crystals*, John Wiley & Sons, New York, **2000**.
[109] A. Ciferri, *Supramolecular Polymers*, Marcel Dekker, New York, **2000**.
[110] P. D. Beer, P. A. Gale, D. K. Smith, *Supramolecular Chemistry*, Oxford University Press, Oxford, **1999**.
[111] A. J. Goshe, I. M. Steele, C. Ceccarelli, A. L. Rheingold, B. Bosnich, *Proc. Natl. Acad. Sci.* **2002**, *99*, 4823-4829.
[112] J.-M. Lehn, *Makromol. Chem. Macromol. Symp.* **1993**, *69*, 1-17.
[113] C. Hilger, M. Draeger, R. Stadler, *Macromolecules* **1992**, *25*, 2498-2501.
[114] J. Burgert, R. Stadler, *Makromol. Chem.* **1986**, *187*, 1681-1690.
[115] Y. Chujo, K. Sada, T. Saegusa, *Macromolecules* **1993**, *26*, 6315-6319.
[116] Y. Chujo, K. Sada, T. Saegusa, *Macromolecules* **1993**, *26*, 6320-6323.
[117] K. Hanabusa, K. Nakano, T. Koyama, H. Shirai, N. Hojo, A. Kurose, *Makromol. Chem.* **1990**, *191*, 391-396.
[118] K. Hanabusa, A. Nakamura, T. Koyama, H. Shirai, *Makromol. Chem.* **1992**, *193*, 1309-1319.
[119] C. D. Eisenbach, U. S. Schubert, *Macromolecules* **1993**, *26*, 7372-7374.
[120] T. P. Russell, R. Jérôme, P. Charlier, M. Foucart, *Macromolecules* **1988**, *21*, 1709-1717.
[121] J. Horrion, R. Jérôme, P. Teyssié, *J. Polym. Sci., Part A.: Polym. Chem.* **1990**, *28*, 153-171.
[122] R. Deans, F. Ilhan, V. M. Rotello, *Macromolecules* **1999**, *32*, 4956-4960.
[123] M. Müller, A. Dardin, U. Seidel, V. Balsamo, B. Ivan, H. W. Spiess, R. Stadler, *Macromolecules* **1996**, *29*, 2577-2583.
[124] K. Yamauchi, J. R. Lizotte, D. M. Hercules, M. J. Vergne, T. E. Long, *J. Am. Chem. Soc.* **2002**, *124*, 8599-8604.
[125] K. Yamauchi, J. R. Lizotte, T. E. Long, *Macromolecules* **2002**, *35*, 8745-8750.
[126] T. Kato, J. M. J. Fréchet, *Macromolecules* **1989**, *22*, 3818-3819.
[127] S. I. Choi, X. Li, E. E. Simanek, R. Akaba, G. M. Whitesides, *Chem. Mater.* **1999**, *11*, 684-690.
[128] R. P. Sijbesma, F. H. Beijer, L. Brunsveld, B. J. B. Folmer, J. H. K. K. Hirschberg, R. F. M. Lange, J. K. L. Lowe, E. W. Meijer, *Science* **1997**, *278*, 1601-1604.

[129] X.-Z. Wang, X.-Q. Li, X.-B. Shao, X. Zhao, P. Deng, X.-K. Jiang, Z.-T. Li, Y.-Q. Chen, *Chem. Eur. J.* **2003**, *9*, 2904-2913.
[130] E. C. Constable, *Adv. Inorg. Chem. Radiochem.* **1986**, *30*, 69-121.
[131] U. S. Schubert, C. Eschbaumer, P. R. Andres, H. Hofmeier, C. H. Weidl, E. Herdtweck, E. Dulkeith, A. Morteani, N. E. Hecker, J. Feldmann, *Synth. Metals* **2001**, *121*, 1249-1252.
[132] B. Kovac, L. Klasine, *Z. Naturforsch. A* **1978**, *23A*, 247-251.
[133] M. J. Cook, A. P. Lewis, G. S. G. McAuliffe, A. J. Thomson, *Inorg. Chim. Acta* **1982**, *64*, L25-L28.
[134] R. Hage, J. G. Haasnoot, J. Reedijk, J. G. Vos, *Inorg. Chem. Acta* **1986**, *118*, 73-76.
[135] C. L. Fraser, A. P. Smith, X. Wu, *J. Am. Chem. Soc.* **2000**, *122*, 9026-9027.
[136] X. Wu, J. E. Collins, J. E. McAlvin, R. W. Cutts, C. L. Fraser, *Macromolecules* **2001**, *34*, 2812-2821.
[137] A. P. Smith, C. L. Fraser, *Macromolecules* **2002**, *35*, 594-596.
[138] R. Hogg, R. G. Wilkins, *J. Chem. Soc.* **1962**, 341-350.
[139] G. Morgan, F. H. Burstall, *J. Chem. Soc.* **1937**, 1649-1655.
[140] J.-F. Gohy, B. G. G. Lohmeijer, U. S. Schubert, *Chem. Eur. J.* **2003**, *9*, 3472-3479.
[141] B. G. G. Lohmeijer, U. S. Schubert, *Angew. Chem. Int. Ed.* **2002**, *41*, 3825-3829.
[142] B. P. Sullivan, J. M. Calvert, T. J. Meyer, *Inorg. Chem.* **1980**, *19*, 1404-1407.
[143] D. A. Buckingham, F. P. Dwyer, A. M. Sargeson, *Aust. J. Chem.* **1964**, *17*, 622-631.
[144] B. A. Moyer, M. S. Thompson, T. J. Meyer, *J. Am. Chem. Soc.* **1980**, *102*, 2310-2312.
[145] M. Maestri, N. Armaroli, V. Balzani, E. C. Constable, A. M. W. Cargill Thompson, *Inorg. Chem.* **1995**, *34*, 2759-2767.
[146] F. Kröhnke, *Synthesis* **1976**, 1-24.
[147] A. M. W. Cargill Thompson, *Coord. Chem. Rev.* **1997**, *160*, 1-52.
[148] E. C. Constable, M. D. Ward, *J. Chem. Soc. Dalton Trans.* **1990**, 1405-1406.
[149] U. S. Schubert, S. Schmatloch, A. A. Precup, *Design. Monom. Polym.* **2002**, *5*, 211-221.
[150] M. Heller, U. S. Schubert, *Eur. J. Org. Chem.* **2003**, *6*, 947-961.
[151] L. Giuse, D. L. Jameson, *Tetrahedron Lett.* **1991**, *32*, 1999-2002.
[152] B. Hasenknopf, J.-M. Lehn, *Helv. Chim. Acta*, **1996**, *79*, 1643-1650.
[153] U. S. Schubert, C. Eschbaumer, C. Weidl, *Design. Monom. Polym.* **1999**, *2*, 185-189.
[154] B. G. G. Lohmeijer, U. S. Schubert, *J. Polym. Chem. Part A: Polym. Sci.* **2003**, *41*, 1413-1427.
[155] K. T. Potts, D. A. Usifer, A. Guadalupe, H. D. Abruna, *J. Am. Chem. Soc.* **1987**, *109*, 3961-3967.
[156] K. T. Potts, D. A. Usifer, *Macromolecules* **1988**, *21*, 1985-1991.
[157] K. J. Calzia, G. N. Tew, *Macromolecules* **2002**, *35*, 6090-6093.
[158] U. S. Schubert, H. Hofmeier, *Macromol. Rapid Commun.* **2002**, *23*, 411-415.

Chapter 2

Synthesis, Characterization and Stability Studies of *Bis*-Terpyridine Metal Complexes: A Comparative Study of Model Complexes

Abstract

Terpyridine metal complexes with two different substituents at the 4'-position of the ligand have been investigated in detail. The chapter starts with modeling of the equilibrium constants, since in principle mono- and bis-complexes may be formed based on the stoechiometry and stability constants of the metal-ligand system. Titration of metal ions to terpyridine ligands in solution is performed and this process is followed by UV/vis spectroscopy to identify differences between the absorbance spectra of mono- and bis-complexes. A partition method is introduced for the derivation of stability constants for one of the ligands with zinc(II)-ions. For cobalt(II)-ions a method was developed using ^{1}H-NMR, where paramagnetic shifts of the mono- and bis-complexes allow for careful integration. Mass-spectrometry techniques have been applied as well. Subsequently, the synthesis and characterization of bis-terpyridine complexes is described using counter-ion exchange/precipitation strategies to isolate the pure bis-complexes. X-Ray structures have been determined for one full set of metal complexes. Other characterization techniques include UV/vis and FT-IR-spectroscopy, elemental analysis, NMR and mass spectrometry. The stability of the metal complexes is investigated by changes in pH, spectroelectrochemistry and thermal analysis. Finally, the synthesis and characterization of two heteroleptic complexes based on inert ruthenium(II) and cobalt(III)-ions is described. The results in this chapter allow the selection of suitable metal-ions for implementation into macromolecular structures.

Parts of this chapter have been published: M. A. R. Meier, B. G. G. Lohmeijer, U. S. Schubert, *J. Mass Spectrom.* **2003**, 38, 510-516; P. R. Andres, H. Hofmeier, B. G. G. Lohmeijer, U. S. Schubert, *Synthesis* **2003**, 18, 2865-2871.

2.1 Introduction

The coordination chemistry of terpyridine-ligands with transition metal ions has been the subject of many studies, ever since the ligand's discovery in 1932 by Morgan and Burstall.[1,2] Terpyridine is a terdentate chelating ligand and forms 1:1 or 2:1 adducts with transition metal ions.[3] The chelation requires an all-cis configuration of the pyridine-rings in contrast to the all-trans configuration of the uncoordinated ligand in solution as well as in the crystalline state.[4-6] Most commonly encountered geometries of the resulting 2:1 complexes are octahedral,[3,6] whereas 1:1 adducts can form octahedral,[3,7] trigonal bipyramidal[3,8-10] and square planar[3,11,12] geometries depending on the metal ion and on the other coordinated ligands. In principle, mono- and bidentate coordination modes of the ligand could exist, but only little experimental evidence has been found for a few pre-organized inert complexes,[13] although these modes are most likely intermediates upon chelation. Of course, this is no surprise since the chelate effect is operative: a negative enthalpy and a positive entropy term will always favor the formation of fully chelated ligands.[14,15] The only relatively stable intermediate in the formation of a *bis*-terpyridine metal complex is therefore the *mono*-terpyridine complex.

Obviously, the introduction of a terpyridine ligand into a polymer backbone requires a linkage to connect to the ligand. In all the cases described in this thesis, the ligand is connected through an oxygen-atom at the 4'-position of the ligand for synthetic reasons, which could have some consequences for the stability and coordination behavior of the corresponding metal complexes through electronic effects. This chapter is therefore devoted to the synthesis, characterization and stability of *bis*-terpyridine metal complexes using model ligands with an oxygen-substituent at the 4'-position in order to gain an insight into the coordination characteristics and geometries of these particular metal complexes. First the synthesis and characterization of the ligands is described. Then the coordination chemistry of these ligands with a variety of transition metal ions is addressed: the two association constants involved for the formation of the *mono*- and *bis*-complex (K_1 and K_2 respectively) have been determined before. The literature values have been applied in a simple model where the equilibrium concentrations of *mono*- and *bis*-complex are displayed as a function of the metal-to-ligand ratio. This demonstrates the need for accurate knowledge of K_1 and K_2, in particular their relative values. The next sections deal with the quest for the stability constants using titrations followed by UV/vis-spectroscopy, the partition method in case of Zn^{II}-complexes and ^{1}H-NMR in case of Co^{II}-complexes. Mass spectrometry has been investigated as a tool for the derivation of the relative stabilities of the metal complexes. Then the synthesis and characterization of *bis*-terpyridine metal complexes is described. Next, the stability of these metal complexes is addressed by thermogravimetric analysis, by UV/vis-spectroscopy upon changing the pH and by spectroelectrochemistry. Of special interest are those conditions where the metal complex can be (re)opened. In the final section the synthesis and characterization of heteroleptic Ru^{II}- and Co^{III}-complexes is described. A study of their stability with respect to scrambling and reversibility is conducted as well. All these results combined give a better understanding of the coordination behavior of the 4'-oxysubstitued terpyridine ligand and are of great importance for the terpyridine-functionalized polymers that are going to be connected with metal ions in the following chapters.

2.2 Synthesis and characterization of the ligands

A useful starting material for 4'-modified terpyridines is 2,6-*bis*-(2'-pyridyl)-4-pyridone, depicted as compound **1** in Figure 2.1. This compound can be prepared in large quantities from cheap starting materials in a two-step synthesis (Figure 2.1) utilizing a double Claisen condensation and a subsequent ring closure reaction.[16,17] A broad range of substitution reactions can be envisioned and realized utilizing S_N2 reactions: terpyridine ω- and/or α-functionalized polymers, initiator groups, monomeric species and ligands having other functionalities as amines, isocyanates, thiols or tosylates.[18-20]

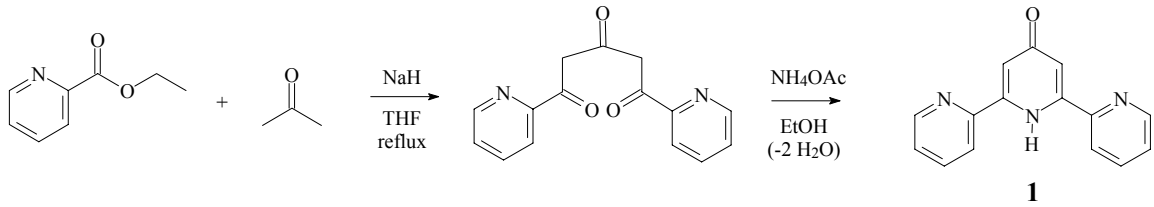

Figure 2.1. *Synthesis of 2,6-bis-(2'-pyridyl)-4-pyridone **1**.*

Compound **1** has been used for the synthesis of two ligands suitable for the above discussed model complexes and experiments regarding the complex stability (Figure 2.2). Compound **3** has improved solubility in polar solvents, whereas compound **4** contains a phenyl ring that should aid in the formation of single crystals of the corresponding metal complexes for structural analysis in the solid state, presumably through π-π stacking of the aromatic substituent.

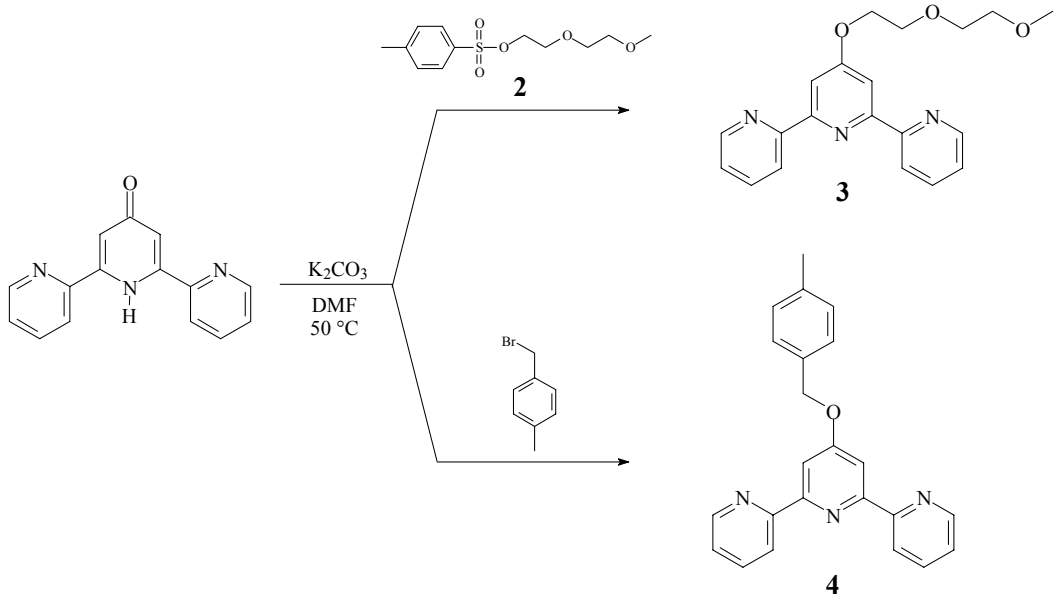

Figure 2.2. *Synthetic route to two model ligands by an S_N2-reaction.*

The mild base K_2CO_3 abstracts the acidic proton from the ligand, effectively producing a phenolate nucleophile which is highly reactive in DMF-solution. In a S_N2-reaction this ligand displaces the tosylate and bromide respectively, which are excellent leaving groups. In view of facile work-up procedures, a slight excess of **2** is used: a simple filtration column on neutral AlOx is sufficient to obtain the pure product **3**. The ligands have been fully characterized by ^{1}H-NMR, ^{13}C-NMR, UV/vis, FT-IR, GC-MS and elemental analysis. Figure 2.3 shows the assigned ^{1}H-NMR-

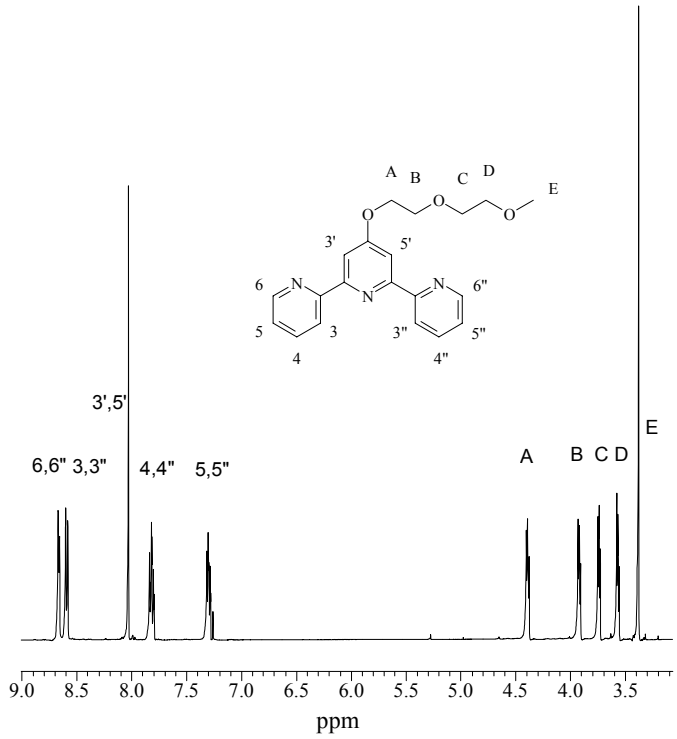

spectrum of **3** in $CDCl_3$. Of interest in the aromatic region is the singlet of the protons in the 3'- and 5'-position at 8.04 ppm, whereas the signal at 4.48 ppm can be attributed to the methylene protons directly attached to the central pyridine ring via the oxygen atom.

Figure 2.3. *Assigned ^{1}H-NMR spectrum of **3** in $CDCl_3$: of interest are the signals of protons in the 3',5'- the 6,6"- and the A-position.*

The UV/vis-spectrum shows the two characteristic bands of the two π-π* excitations and can be interpreted as the all-trans configuration of the terpyridine-ligand.[21] In FT-IR a typical pattern is observed for ring deformations of the terpyridine ligand in the region between 1620 and 1550 cm^{-1} (Figure 2.4). It is evident that these signals will change upon complexation of the ligand with transition metal ions.

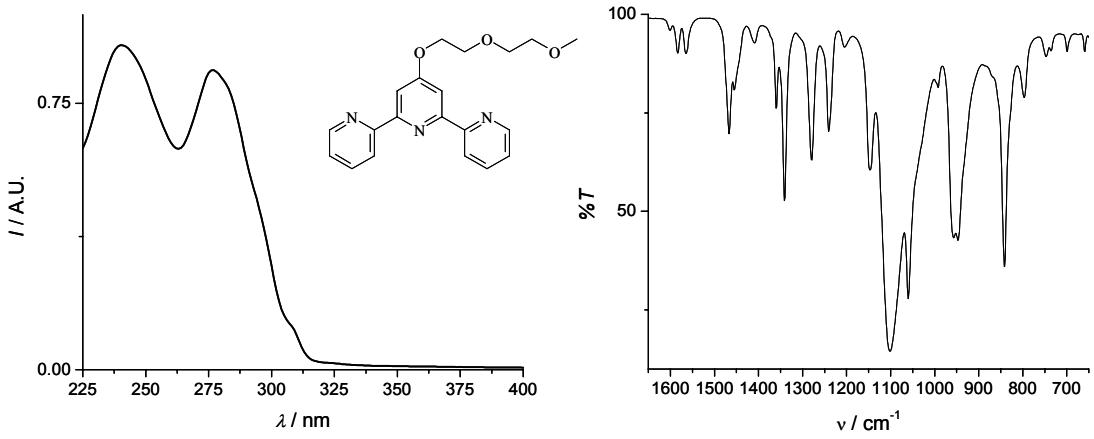

Figure 2.4. *UV/vis- and FT-IR-spectra of **3** in CH_3CN-solution and ATR-mode, respectively.*

Compound **4** was characterized using the same techniques. These two ligands have been used for the synthesis of model metal complexes with respect to their characterization, properties and stability.

2.3 Complex formation

Several studies have been conducted in order to derive stability constants for terpyridine *mono*- and *bis*-complexation with a variety of transition metal ions.[15,22-27] This is not an easy task due to the fact that in general their values are very high: determination of the stability constants requires accurate knowledge about the

equilibrium concentrations[1)] of all species involved, i.e. uncoordinated ligand, 'free' metal ion, *mono*-complex and *bis*-complex. However, due to the high stability constants the equilibrium concentration of one or more species is extremely low compared to the other(s), complicating detection and concomitant quantification. The values that have appeared for terpyridine in the literature are based on kinetic measurements from both metal and ligand exchange experiments by radioactive decay[22] or from stopped-flow measurements.[23-27] It requires measurement of the complex formation rate constant of both complexation steps individually as well as measurement of the complex dissociation rate constants. When pseudo-first-order kinetics are applicable, the equilibrium constant follows from the ratio of the rate constants of formation and dissociation. Later, calorimetric methods have been used.[15] The values for the known stability constants are summarized in Table 2.1.

Table 2.1. *Metal complex stabilities measured at 25°C in water (from ref [23])*

Metal-ion	**Log K_1**	**Log K_2**	**Log β_2**
Mn^{II}	4.4		
Fe^{II}	7.1	13.8	20.9
Co^{II}	8.4	9.9	18.3
Ni^{II}	10.7	11.1	21.8
Zn^{II}	6.0 6.7[33]	5.2[33]	
Cd^{II}	5.1		

The drawback of using these values is the fact that the data stems from kinetic measurements and especially the existence of the reported *mono*-complexes can be questioned as soon as they are dissolved (vide infra). To circumvent kinetic measurements, the equilibrium concentrations of a system in thermodynamic equilibrium should be assessed. As already mentioned, due to the high stability constants this is complicated, if not impossible. Varying the ratio of metal to ligand is the solution, if the equilibrium concentrations of one or more of the active species can be determined accurately at all these ratio's. Subsequent fitting of the data may provide the stability constants.[28] However, many spectroscopic techniques suffer from overlapping signals and spectrum deconvolution is usually not straightforward. Therefore, in the following section, modeling has been used to show the profound influence of the two equilibrium constants of *mono*- and *bis*-complex formation, to gain insight into the distributions of *mono*- and *bis*-complexes if different metal to ligand ratio's are employed. Also, the pKa-values of the ligand have been determined and titrations with different transition metal ions have been carried out. Finally, attempts have been made to derive stability constants of selected terpyridine metal complexes. For Zn^{II}-ions a partition method has been developed to determine the free ligand concentration and for Co^{II}-ions ^{1}H-NMR has been used to determine the concentration of *mono*- and *bis*-complex. Finally, the relative binding strength of all metal complexes has been evaluated by mass spectrometry techniques. All these experiments have involved **3** for solubility reasons: solutions up to 10^{-3} M can be prepared in water, whereas **4** is insoluble in water.

[1)] Activities have been replaced by concentrations due to the low concentrations used.

2.3.1 Modeling

In the previous section it was established that only two metal complexes play a significant role in the complex formation, namely the *mono*- and the *bis*-complex. Scheme 2.1 shows schematically the reactions, the representative equilibrium constants and the mass balances for the metal and the ligand.

$$M + L \rightleftharpoons ML \qquad \text{with} \qquad K_1 = \frac{[ML]}{[M][L]}$$

$$ML + L \rightleftharpoons ML_2 \qquad \text{with} \qquad K_2 = \frac{[ML_2]}{[ML][L]}$$

$$c_M = [M] + [ML] + [ML_2]$$

$$c_L = [L] + [ML] + 2 \bullet [ML_2]$$

Scheme 2.1. *Simplified reaction scheme with the associated equilbrium constants and mass balances.*

Here, [M], [L], [ML] and [ML_2] denote the equilibrium concentrations of metal, ligand, *mono*-complex and *bis*-complex respectively. Rewriting these equations leads to the expression 2.1 that can be solved analytically for the equilibrium concentration of ligand ([L]) using computer software (Maple 8.0), if the equilibrium constant K_1 and K_2 and the initial concentration of metal (c_M) and ligand (c_L) are known.

$$\frac{c_M}{1 + K_1[L] + K_2K_1[L]^2} = \frac{-c_L + [L]}{K_1[L] * (1 + 2K_2[L])} \qquad (2.1)$$

The equilibrium constants from the literature (see Table 2.1) have been used, the initial concentration of ligand was held constant at 0.1 mM and the initial concentration of metal was varied from 0.1 μM to 0.1 M. The equilibrium concentrations were calculated and subsequently plotted as a function of metal-to-ligand ratio (Figure 2.5). This provides a clear view on what happens during a titration of metal ion, of course assuming that the system is under thermodynamic control. In this way it should not matter whether the metal is titrated to the ligand or the ligand to the metal. In reality, hysteresis may play an important role, especially if the association constants are high.

In all four cases, the predominant species in the beginning of the titrations is apart from the ligand the *bis*-complex. The second complexation constant favors this as long as the ligand is in excess.

a. In case of Fe^{II}-ions, the second equilibrium constant is very much higher than the first by a factor of ~5×10^6. This implies that *bis*-complex formation will always predominate, even when there are (much) more metal-ions than ligand present. Also, the only species present at the 1:2 metal to ligand ratio is the *bis*-terpyridine iron(II) complex, since all metal and ligand present in the system is complexed. The concentration of *bis*-complex therefore reaches half the original ligand concentration. At the 1:1 ratio of metal to ligand, as can be seen from Figure 2.5 (top left), no appreciable amount of *mono*-complex forms. In fact, the concentration of 'free' metal increases almost linearly upon increasing c_M:c_L. Even at extreme c_M:c_L (1000:1), *mono*-complexes will still not form. Of course, experimentally such high concentrations of Fe^{II}-ions will not be attainable.

b. In the case of Co^{II}-ions, the second equilibrium constant is also higher than the first, but only by a factor of ~30. Also here the *bis*-terpyridine cobalt(II) complex dominates and is the only species present at the 1:2 ratio of metal to ligand. However, some formation of *mono*-complex can be seen, if $c_M:c_L > 0.5$. Actually, at a 10:1 ratio of metal to ligand (not shown), virtually identical concentrations of *mono*- and *bis*-complex are present.

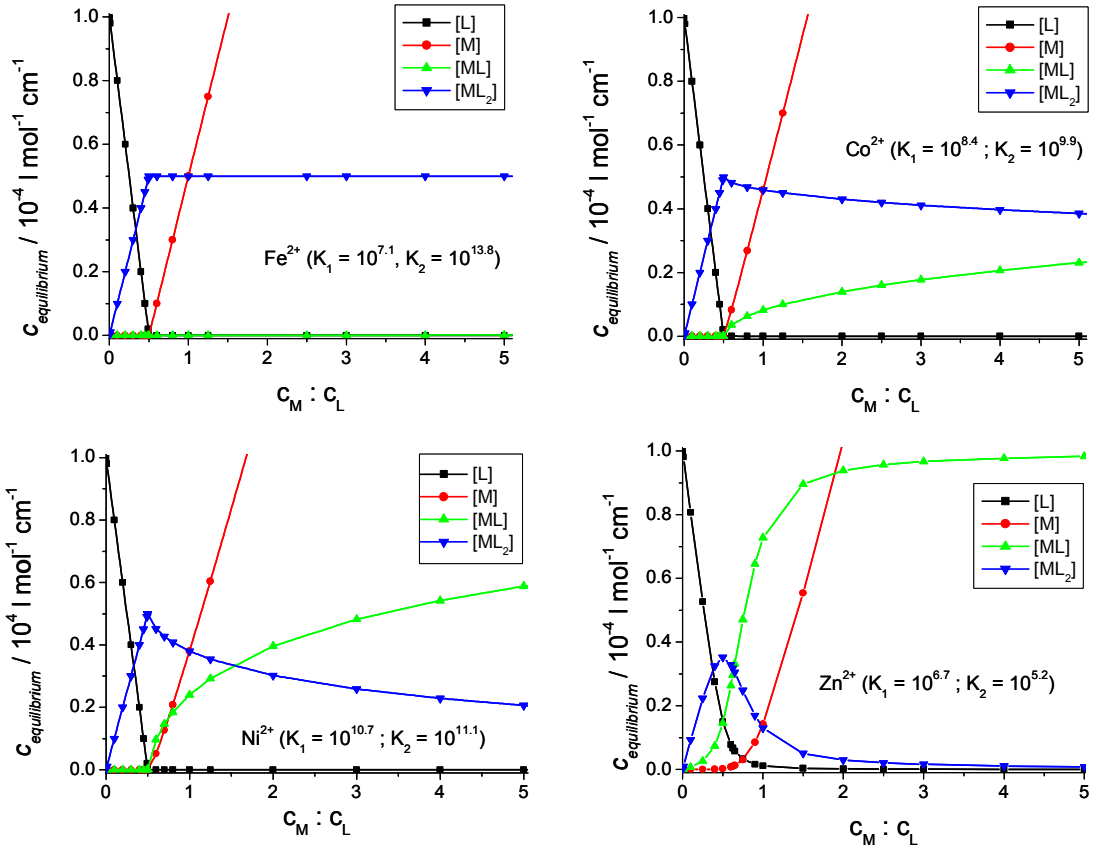

Figure 2.5. *Modeling of the equilibrium concentrations of ligand [L], metal [M], mono-complex [ML] and bis-complex [ML_2] as a function of the initial ratio of metal to ligand $c_M:c_L$ using the equilibrium constants K_1 and K_2 from Table 2.1: Fe^{2+} (top left), Co^{2+} (top right), Ni^{2+} (bottom left) and Zn^{2+} (bottom right).*

c. In the case of Ni^{II}-ions, both equilibrium constants are very high, but the second equilibrium constant is only slightly larger than the first by a factor of ~2. Again, if $c_M:c_L < 0.5$, *bis*-complex formation will dominate and due to the high value of the second stability constant – as was also the case for Fe^{II} and Co^{II}-ions – only *bis*-complex is present at the 1:2 ratio of metal to ligand. However, increasing the nickel(II)-to-ligand ratio gives rise to appreciable formation of *mono*-complex due to the similar value of the first equilibrium constant. At a 3:2 ratio there is almost as much *mono*- as *bis*-complex present. At a 5:1 ratio of metal-to-ligand there is only little *bis*-complex present.

d. In the case of Zn^{II}, the equilibrium constants are relatively small. Here the second equilibrium constant is smaller than the first, actually by a factor of ~30. Although a maximum in the *bis*-complex concentration is reached at the 1:2 ratio of metal to ligand, there is still free ligand as well as already an appreciable amount of *mono*-complex present at that ratio. Increasing the metal-ligand ratio leads to

increased formation of the *mono*-complex and already at a 2:1 ratio of metal to ligand no *bis*-complex is any longer present.
In summary, this simple model has some predictive power about the equilibrium concentrations of the species involved in complex formation. In fact, it gives useful information for the synthesis of metal complexes and further analysis in solution. The limitation of the model is that it is very much simplified and would need the implementation of acid-base equilibria of both metal and ligand, and solubility parameters in order to better predict the equilibrium concentrations. Also, 'free' metal-ions do not exist and thus the partitioning of the 'free' metal in equilibrium with solvent molecules and anions must be taken into account.

2.3.2 Determination of the pKa

Terpyridine-ligands are weak bases and depending on the pH of the solution, competition between metal complex formation and ligand protonation may occur. It is therefore imperative to have good knowledge about the pKa-values of the ligand. As a first experiment, the pKa-values of compound **3** have been determined. An acidic solution of the ligand was titrated with base (NaOH) and a UV-spectrum was recorded after each titration: steps of ~0.1 in pH were made and the pH was verified by measuring with a pH-electrode. A plot of the absorbance as a function of pH at different wavelengths was used to determine the pKa values, since the UV-spectra of the unprotonated, *mono*- and *bis*-protonated ligand are distinctly different (Figure 2.6). In an excellent article from Nakamoto, the UV-spectra have been explained in terms of the all-trans configuration of the ligand in basic environment, the all-cis configuration in acidic environment and the cis-trans configuration at intermediate pH.[21] In his case, the pKa-values were derived from the inflection points of the absorbance curves measured at two wavelengths (280 nm and 320 nm). For our purposes, a Matlab-program was written that analyzes the entire spectral range and performs a fit on the data at each wavelength *vs* pH to a sigmoidal curve. The inflection point of the curve then represents the pKa-values of the respective protonation and were found to be 3.1 and 4.2, which is in good agreement with literature values of 2.6 and 4.2 or 3.3 and 4.7 respectively, reported for 2,2':6',2"-terpyridine.[21,29]

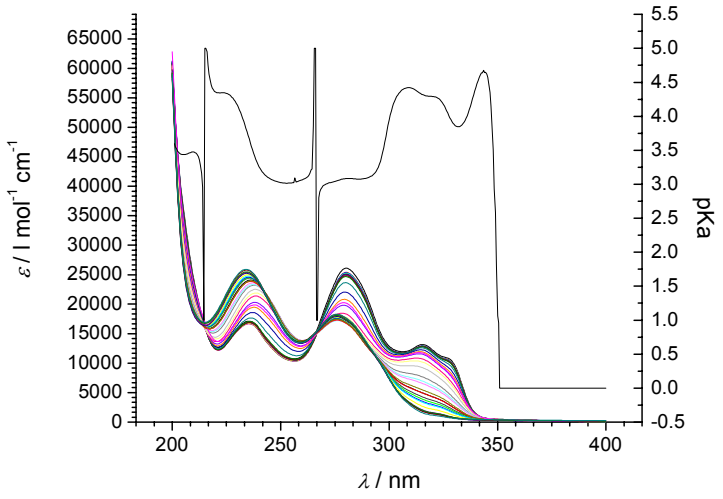

Figure 2.6. *Determination of the pKa-values of **3** by UV/vis-spectroscopy and monitoring of the pH.*

2.3.3 Metal-titration

The ligand has been titrated with metal ions in a buffer-solution of pH=9 in order to minimize the influence of ligand protonation and prevent precipitation of the metal ion as its hydroxide salt. This facilitates the analysis of UV/vis-spectra that were recorded after each titration step. The ligand will be in the all-trans configuration upon the start of the titrations. Figure 2.7 shows the titration curves of **3** with the acetate-salts of Fe^{II}, Co^{II}, Ni^{II}, Cu^{II}, Zn^{II}, Cd^{II} and Hg^{II}. Upon addition of metal-ions, a new electronic absorption band can be observed in all cases between ~290-330 nm and originates from the all-cis configuration of the ligand: all three nitrogen of the ligand coordinate to the metal ion. Maximum absorption in all cases is reached at or slightly beyond the 1:2 metal to ligand ratio proving the formation of *bis*-complexes. Upon overtitration with Co^{II}-, Ni^{II}- and Cd^{II}-ions, the UV-spectra of the ligand do not seem to change. On the other hand, the spectra of the ligand with Fe^{II}-, Cu^{II}-, Zn^{II}- and Hg^{II}-ions undergo some changes. This can be explained as follows:

In case of Zn^{II}-ions, a very slight blue-shift of the peaks at 310 and 322 nm can be observed. In light of the stability constants discussed in the previous section, the *mono*- and the *bis*-complex can thus be identified. However, due to the overlap of the peaks it will be impossible to derive reliable data for the stability constants.

a. In case of Cu^{II}-ions, a large difference can be observed: clearly, the *mono*-complex is being formed. The fact that there is such a large difference between absorption of the *mono*- and *bis*-complex comes from a Jahn-Teller distortion commonly observed in octahedral Cu^{II}-complexes[14] and is supported by X-Ray crystallography (vide infra). Apparently the *mono*-complex has a different symmetry and resembles the UV-spectrum of the zinc *mono*-complex. In spite of the more pronounced differences in the UV-spectra of the *mono*- and the *bis*-complex, peak overlap prevents again the calculation of the equilibrium constants. The same story is true for Hg^{II}-ions.

b. In case of Co^{II}-, Ni^{II}- and Cd^{II}-ions, there are three possible explanations for the fact that the UV-spectra do not change upon overtitration. First, the UV-spectra of both *mono*- and *bis*-complex are the same. This may be true, because in the spectra the absorptions of interest are ligand-centered. If no changes in geometry of the coordinating ligand take place in the *mono*- and the *bis*-complex and the corresponding electronic repulsion effects are negligible, the UV-spectra will appear to be the same. This also explains the similarity of the UV-spectra of *mono*- and *bis*-complexes in case of Zn^{II}- and Hg^{II}-ions. In analogy with the titrations with Zn^{II}- and Hg^{II}-ions (also d^{10}-complexes for which $K_2<K_1$) Cd^{II}-complexes probably behave the same. The second explanation for this behavior is that due to the higher second equilibrium constant ($K_2>K_1$), *bis*-complex formation is favored even at overtitration and *mono*-complexes are not being formed in detectable quantities. Following the discussion in the section 2.3.1, this second argument may very well be true for the titrations with Co^{II}-ions. The third explanation is hysteresis: due to the high overall stability constant, especially in case of Fe^{II}, Co^{II} and Ni^{II}, the dynamics of the system may be very low. Therefore, on the timescale of the titrations, no exchange is taking place and a kinetically determined state (being the bis-complex) is observed by UV/vis-spectroscopy.

c. In case of titrating the ligand with Fe^{II}-ions, a band at 360 nm appears to grow upon overtitration with Fe^{II}-ions. This band can be attributed to d-d bands of the metal salt. It seems therefore likely that upon overtitration only *bis*-complex is present, as can also be expected from the stability constants in Table 2.1.

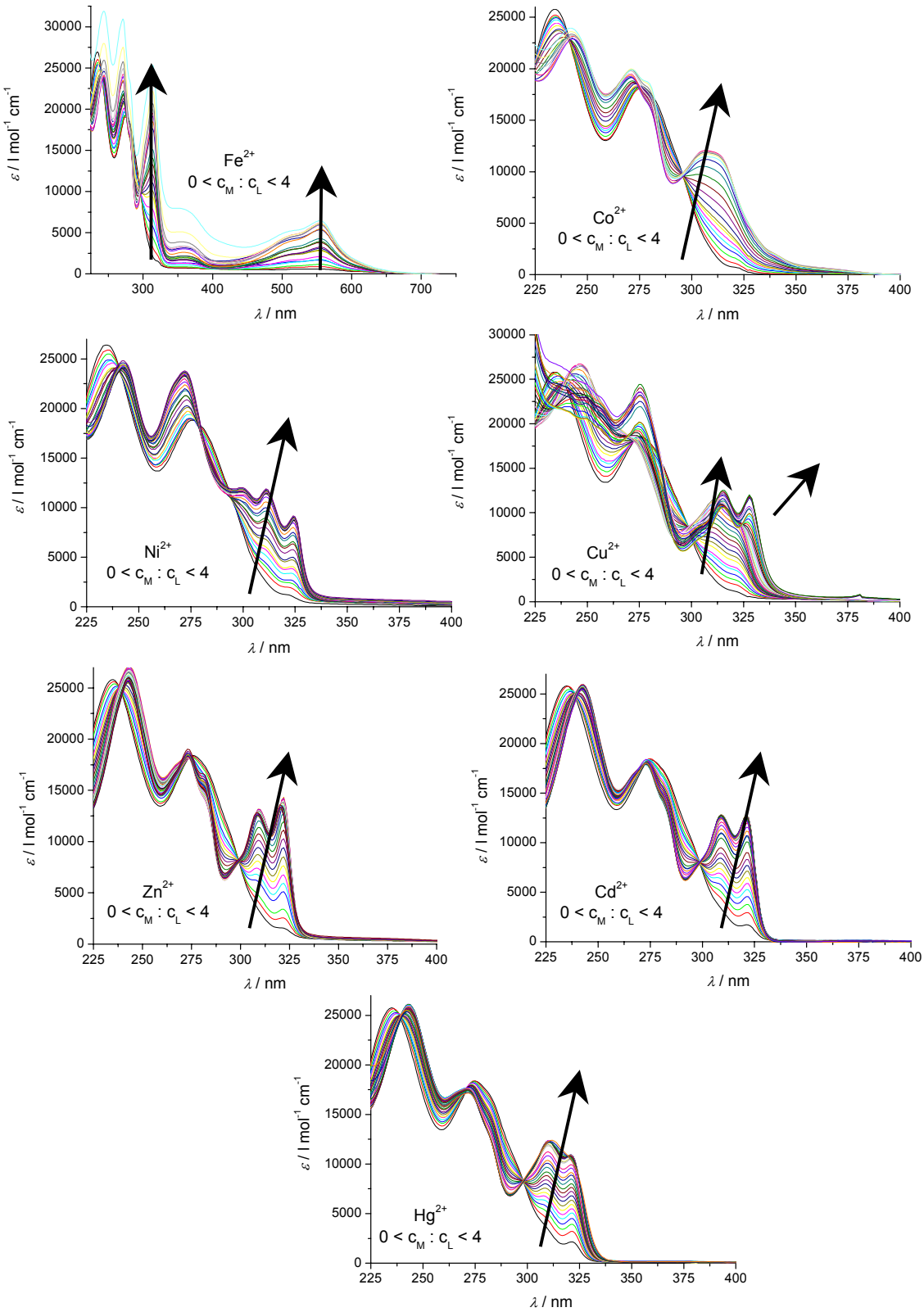

Figure 2.7. *Titration of metal-acetate to* ***3*** *in water followed by UV/vis-spectroscopy: Fe^{II} (top left), Co^{II} (top right), Ni^{II} (middle left), Cu^{II} (middle right), Zn^{II} (bottom left), Cd^{II} (bottom right) and Hg^{II} (bottom).*

These titrations have given insight into the complexation behavior of several metal ions and the formation of *mono*-complexes can be accounted for. Nevertheless, actual

values of equilibrium constants could not be derived using the titration data due to severe spectral overlap. The determination of stability constants will be subject of the following chapters.

2.3.4 Partition method

The difficulty of determining the equilibrium concentrations of uncoordinated ligand, 'free' metal-ion, *mono*-complex and *bis*-complex using spectrum deconvolution as described before or by kinetic measurements as performed in the literature can be circumvented by using the partition method. This method was successfully applied by Irving and Williams on a series of bipyridine complexes.[30-32] Overall stability constants of 10^{24} (!) could be determined. In their paper an outlook is mentioned to use the same method for terpyridine metal complexes, but unfortunately that follow-up paper has not appeared.[32] The partition method derives its name from the partitioning of the uncoordinated metal-ion-free ligand between an organic and an aqueous phase. The partition coefficient is defined as:

$$p_L = \frac{[L]_o}{[L]_{aq}}$$

$[L]_o$ is the ligand in the organic phase and [L] in the aqueous phase. A high partition coefficient is desired in order to accommodate high stability constants and this solely depends on solvent choice. Moreover, only the free ligand should participate in partitioning between the two phases: protonated and metal complexed species should stay in the aqueous phase. This can easily be verified by analysis of the organic layer. In order to derive the stability constants, different solutions need to be prepared in which the initial ligand concentration remains constant, but the initial metal concentration is varied. All these solutions are allowed to equilibrate for a sufficient amount of time with the organic phase in order to reach the thermodynamic equilibrium. The amount of free ligand in the organic phase is then determined using spectroscopic techniques for all cases. From this the equilibrium concentrations of the free ligand in the aqueous phase can be determined. Subsequent curve fitting of the degree of complex formation versus the aqueous ligand concentration yields the stability constants. The degree of complex formation is defined as the ratio of the total ligand bound to the metal ion over the total metal ion concentration. In this term, the *mono*- and *bis*-complex formation are accounted for as well as the competitive effect of the acid/base equilibrium. The necessary equations are listed below.

For the stability constants:

$$\beta_n = \frac{[ML_n]}{[M][L]^n}$$

For the acid constants:

$$K_{a_n} = \frac{[H_nL]}{[H_{n-1}L][H^+]}$$

For the mass balances at all time:

$$n_L = ([L] + [HL] + [H_2L] + [ML] + 2[ML_2]) * V + [L]_o * V_o$$
$$n_M = ([M] + [ML] + [ML_2]) * V$$

If the volumes of the aqueous phase and the organic phase are equal, this reduces to:

$$c_L = [L] + [HL] + [H_2L] + [ML] + 2[ML_2] + [L]_o$$
$$c_M = [M] + [ML] + [ML_2]$$

Rewriting the partition coefficient in terms of pH and of the free ligand in the organic phase leads to:

$$p_L = \frac{[L]_o * (1 + K_{a1} * [H^+] + K_{a1} * K_{a2} * [H^+]^2)}{c_L - [L]_o}$$

The degree of formation of metal complexes, $\bar{n}$, in the aqueous phase is given by:

$$\bar{n} = \frac{[ML] + 2[ML_2]}{c_M} = \frac{c_L - [L]_o(\frac{1}{p_L} + \frac{K_{a1} * [H^+]}{p_L} + \frac{K_{a1} * K_{a2} * [H^+]^2}{p_L} + 1)}{c_M}$$

and is related to the stability constants by:

$$\bar{n} = \frac{\beta_1 * [L] + 2\beta_2 * [L]^2}{1 + \beta_1 * [L] + \beta_2 * [L]^2}$$

Thus, by determining $[L]_o$ for various initial concentrations of ligand and metal, the degree of formation can be calculated as a function of [L]. Plotting the degree of metal complex formation as a function of [L] and perform curve-fitting will then lead to the values for the stability constants. In this case, the degree of metal complex formation lies between 0 and 2.

The partition method has been applied to terpyridine ligand **3** and zinc metal ions using hydrated zinc(II)perchlorate. The counter-ion plays an important role: it must not facilitate extraction of the metal-ion into the organic phase. This is especially true if non-ionic *mono*-complexes can be formed. As solvent HPLC-grade dichloromethane (ethanol stabilized) was chosen and the pH of the aqueous phase was adjusted to 9.5. Subsequently the partition coefficient of the ligand was determined at room temperature using UV/vis spectroscopy and was found to be 205±6. By taking into account the solubility of **3** in water (10^{-3} M) and the detection limit of UV/vis-spectroscopy (2×10^{-6} M) after partitioning, such a value is in principle sufficient to measure an overall stability constant of $\beta_2=10^{13}$. Twenty different metal-to-ligand ratio's have been applied. The experiment was repeated twice and reasonably good statistics were found. Figure 2.8 shows the result of plotting the degree of metal complex formation as a function of [L]. Fitting the data leads to equilibrium constants of $K_1=3.0\pm0.3\times10^6$ and $K_2=1.3\pm0.1*10^6$ with an overall stability constant of $\beta_2=4.0\pm0.1\times10^{12}$. Interestingly, these values are in the same order-range as determined by isothermal calorimetry (ITC), although a different solvent and differently substituted terpyridine was used.[33] From stopped-flow measurements a value for $K_1=1.0\times10^6$ for 2,2':6'2"-terpyridine in water was found.[23] In principle, stability constants could be determined for other metal ions as well. However, a different solvent should be used that has a higher partition coefficient. Preliminary experiments reveal that chloroform indeed shows a much higher partition coefficient, in the range of 10^3-10^4. This leads to much higher upper limits for the determination

of the stability constants. Nonetheless, the zinc-case already displays the power of the partition method.

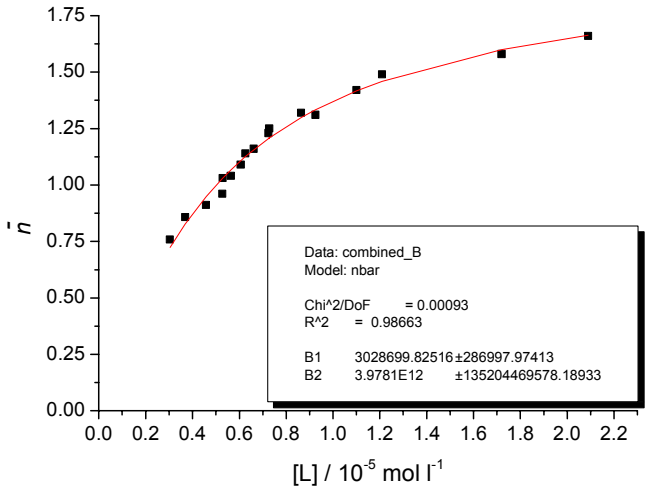

Figure 2.8. *Degree of complex formation as a function of equilibrium concentration of the ligand in water. Subsequent curve-fitting yields to the successive stability constants.*

It is interesting to note that the values for K_1 and K_2 are almost the same. It implies that there are no steric effects and only minor electronic effects upon coordination of the second ligand. This is probably also the reason why the UV/vis-spectra of the *mono*- and *bis*-terpyridine zinc complex are comparable.

Other methods have been applied as well to obtain an idea of the stability constants for other metal ions. The next section deals with ^{1}H-NMR spectroscopy as a tool.

2.3.5 ^{1}H-NMR for cobalt(II)-complexes

Determination of the stability constants requires accurate knowledge of one or more equilibrium concentrations. UV/vis-spectroscopy was found to be unsuitable due to severe band overlap. Other techniques such as fluoresence spectroscopy which is frequently employed when high association constants are to be determined will fail, because the metal complexes are efficient quenchers of the fluorescence. However, there are some spectroscopic techniques that can identify the equilibrium concentration of all species involved. For example, Li has shown that it is possible to deconvolute IR-spectra into the pure components, even if the signals of some of the species involved are very weak. Further calculations subsequently gave the equilibrium constants.[34] ^{1}H-NMR techniques are also frequently employed.[35] From modeling in section 2.3.1 we have seen that the distribution between *mono*- and *bis*-complexes is influenced by the relative values of K_1 and K_2 upon increasing the metal-ligand ratio beyond 1:2. Thus, making a series of known metal-ligand ratio's and subsequent quantification of the amount of *mono*- and *bis*-complex should enable calculation of the stability constants. For cobalt(II)-complexes the technique of choice is ^{1}H-NMR spectroscopy. ^{1}H-NMR-spectra of diamagnetic metal complexes such as those of Fe^{II} and Zn^{II}, Cd^{II} and Hg^{II} show chemical shifts that arise only from the applied magnetic field. Paramagnetic complexes on the other hand have unpaired electrons and this can give rise to two effects in ^{1}H-NMR: first of all, the local magnetic field at the protons will be significantly different from the applied field due to the presence of unpaired electrons at the metal center. Second, the signals will be

broadened as a result of interaction of the nuclear spins with the electron spins providing efficient relaxation mechanisms.[36] In case of Ni^{II}- and Cu^{II}-complexes with terpyridine-ligands this relaxation is apparently really efficient because the signals are broadened in such a way that actually no signals are observed. In case of Co^{II}-ions however, ^{1}H-NMR-signals are shifted over a chemical shift range of up to 150 ppm, but are still significantly sharp. J-coupling information is partially lost, so assignment of the peaks becomes rather difficult. Nevertheless, *mono*- and *bis*-complexes of terpyridine with cobalt(II) can be identified (Figure 2.9).

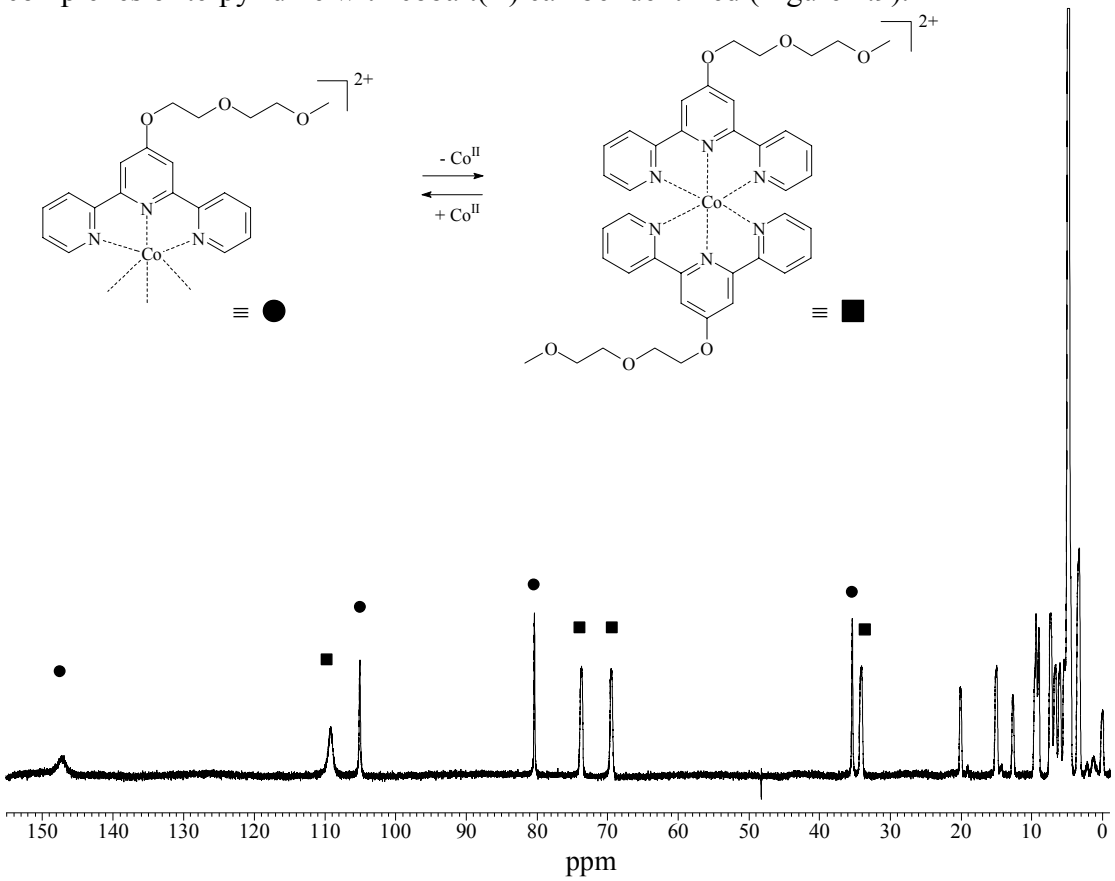

Figure 2.9. *^{1}H-NMR-spectrum of cobalt(II) mono- and bis-complexes. In this particular case $c_M : c_L$ = 1.5. The boxes represent signals coming from the bis-complex, whereas the dots represent signals from the mono-complex. For the integrations and subsequent calculations of $[ML_2]/[ML]$ the signals at 105 and 82 ppm for the mono-complex and the signals at 74 and 68 ppm for the bis-complex have been used.*

The fact that signals are shifted over such a broad ppm-range means that no peak overlaps are present and all signals can be perfectly integrated in contrast to e.g. zinc(II)-complexes. By varying the amount of metal to ligand beyond the 1:2 ratio, the equilibrium concentrations of *mono*- and *bis*-complexes can be calculated through an iterative process. Again, twenty different solutions have been prepared in which the initial concentration of ligand **3** was kept constant and the amount of metal (cobalt(II)acetate tetrahydrate) was varied in CD_3OD. After proper sealing of the NMR-tubes, the solutions were allowed to equilibrate for 24 hours before measurement. Measurements were conducted at 25 °C with a relaxation time of 10 seconds and 128 scans per sample. The relative amounts of *mono*- and *bis*-complex have been determined by integration of the spectra using the signals at 105, 82, 74 and 68 ppm. Figure 2.10 shows the results: $[ML_2]$:[ML] is plotted as a function of c_M:c_L. For comparison, the curves for Fe^{II}, Co^{II}, Ni^{II} and Zn^{II} based on the calculations in

section 2.3.1 are displayed as well. It is directly evident that the titration does not follow the model. The flaw of the model is that it uses the concentrations instead of the activities: for the NMR-measurements the concentrations are as high as 0.075-0.3 mol L^{-1} and this requires the use of activities instead of concentrations. Upon increasing the ionic strength the activity coefficients decrease. When this would be implemented into the model by using the (extended) Debye-Hückel law, a value for K_2:K_1 may be derived. Still, the absolute values of K_1 and K_2 are then not known, since this requires exact knowledge of one of the equilibrium concentrations. Unfortunately, this can not be retrieved from the NMR-measurements. From Figure 2.10 it can be concluded though, that $K_2 > K_1$ and that their relative values are between those of Co^{II} and Ni^{II}, i.e. $5 > K_2:K_1 > 30$.

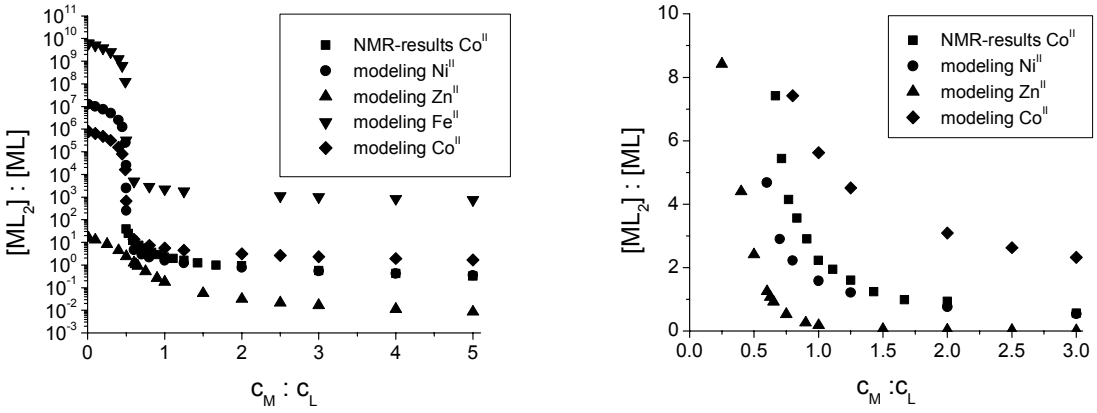

Figure 2.10. *Results of the ratio of the equilibrium concentrations of [ML_2]:[ML] vs the ratio of c_M : c_L. from integration of the ^{1}H-NMR of paramagnetically shifted cobalt(II) mono- and bis-complexes with ligand **3** in CD_3OD at 25 °C and compared to the modeling-results. The right Figure is a close-up of the region of interest: the NMR-results are represented by the black boxes.*

In summary, two types of experiments have been performed in order to derive stability constants. Surely these methods can and should be applied for the other metal ions to obtain a clear view and a better understanding of the complex formation of transition metal ions and terpyridine. However, it is possible to get an idea about the relative stability of all metal complexes using MS-techniques.

2.3.6 ESI-QTOF-MS/MS

Mass spectrometry is a versatile tool for the characterization of metal complexes, especially when soft ionization techniques like electrospray ionization or matrix-assisted laser desorption ionization are applied.[37] In contrast to hard ionization techniques that allow identification of a compound through analysis of its fragments, soft ionization techniques are less- or even non-destructive meaning that non-covalent assemblies remain intact during the ionization process. Thus, the exact molecular mass of a metal complex with its coordinated ligands and associated counter-ions may be determined while the isotopic pattern of a transition metal ion may further help to identify the metal complex. MS/MS- or tandem MS-techniques are used to identify the fragmentation pathway(s) of the selected ion. This works as follows: only an ion of a certain molecular mass is selected in a quadrupole of the first mass spectrometer. This ion (the precursor ion) is subsequently accelerated and then fragmented in a collision cell with an inert gas. These collisions result in the transfer of kinetic energy to internal energy, which subsequently leads to fragmentation of the precursor ion. These fragments can then be analyzed in a second MS spectrometer and the

fragmentation pathway per ion in the mass spectrum of the original sample can be studied. In fact, depending on the kinetic energy of the precursor ion, the distribution of the fragments may be differently populated: a higher kinetic energy results in more transfer into internal energy and hence higher fragmentation. Thus, by varying the kinetic energy of the precursor ion, the intensity of a certain fragment after collision can be probed. The kinetic energy then becomes a measure of the stability of the precursor ion. Now, a point needs to be defined through which the intensity of precursor ion and its fragment(s) are related in order to compare isostructural precursor ions with one another. For simplicity, this is the point where equal amounts of the precursor ion and its fragment are present. Comparing the kinetic energies of isostructural compounds such as metal complexes with the same ligands but with different metal ions provides information about the relative binding constants assuming that the same amount of kinetic energy is transferred into internal energy for each metal complex. For *bis*-terpyridine metal complexes the molecular ion with only one or no counter-ions can be selected in the first mass spectrometer. This *bis*-complex is then accelerated and fragmented into the *mono*-complex and the free ligand (which is of course not detected due to the fact that it is uncharged). This yields information about the dissociation energy of the complex. However, exact quantification of this energy will be difficult: first the exact amount of kinetic energy that is transferred into internal energy must be known and second the amount of internal energy leading to fragmentation must also be known. Nevertheless, for a relative comparison of metal complex stabilities, tandem MS is a powerful tool.[38-40]

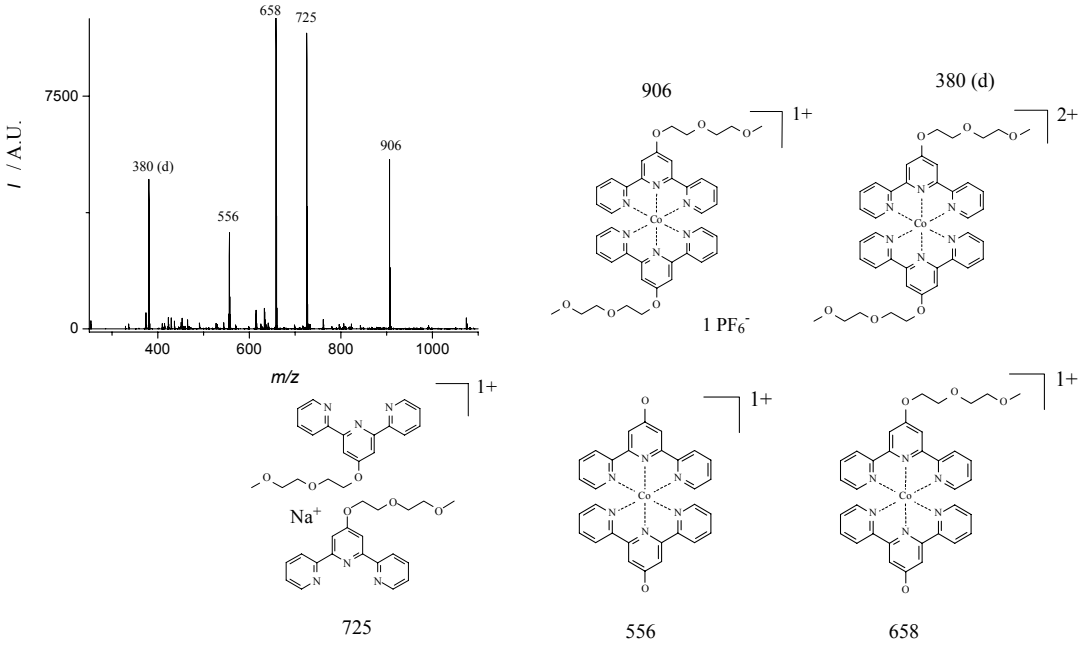

Figure 2.11. *ESI-MS spectrum of bis-terpyridine cobalt(II) complex of **3** (left) and identification of the fragments (right). Note the net charge of the fragments, where d represents the doubly-charged species.*

The synthesis, characterization and properties of the different metal complexes under investigation is described in the following sections. However, here we will use already the *bis*-complex of ligand **3** with Co^{II}-ions. Figure 2.11 shows the ESI-MS spectrum and the identification of the fragments. Interestingly, the molecular ion is not observed, but the compound with m/z = 906 (one associated PF_6^--counter-ion) and the doubly-charged species with m/z = 380 are clear evidence for the presence of the *bis*-**3**-cobalt(II) complex. The peak at m/z = 725 was identified as the sodium-adduct

of two ligands by analogy with other metal complexes where this peak was also present and by addition of 15-crown-5 which led to a reduction of the intensity of this peak. MS/MS after selecting this ion revealed a fragmentation into the protonated ligand and the sodium adduct of the ligand. Even more peculiar are the peaks at m/z = 658 and 556, where one or both oligo-ethylene oxide tail are fragmented off of the metal complex. Apparently, under ESI-MS-conditions the oxygen-linkage between the ligand and the substituent is weaker than the coordination bond between terpyridine and cobalt. For our purposes, the fragmentation of m/z = 380 is of interest for the stability of the *bis*-complex. The MS-spectrum of the precursor ion with m/z = 380 after collision is shown in Figure 2.12 together with its fragments.

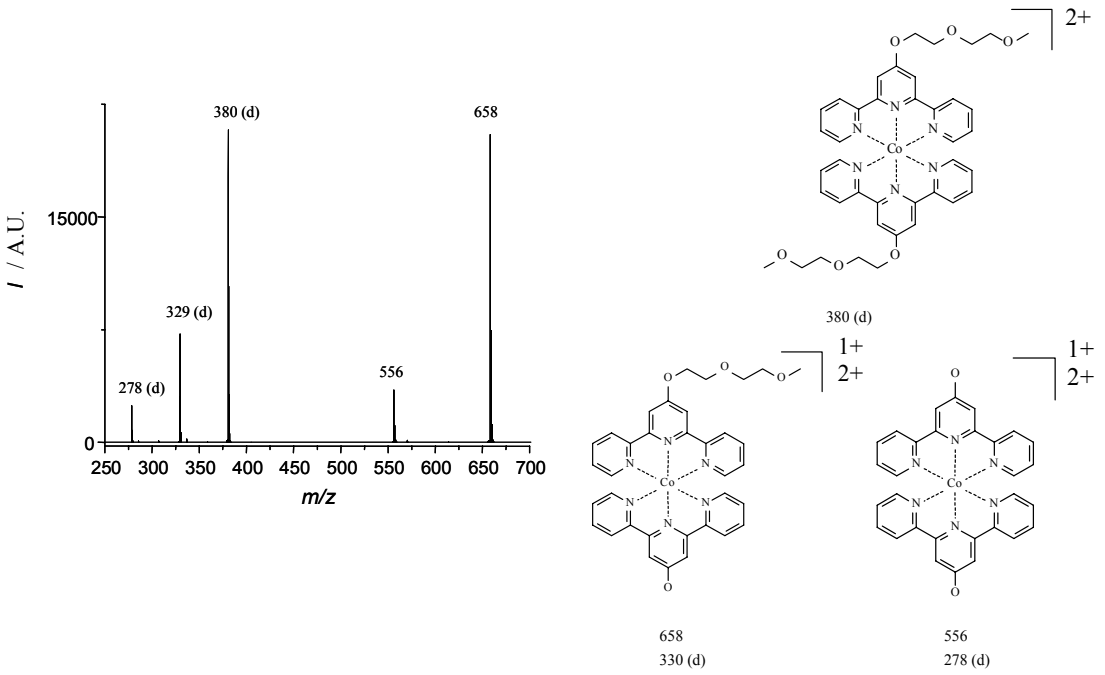

Figure 2.12. *ESI mass spectrum of precursor ion with m/z = 380 after collision (left) and assignment of the observed fragments (right); d represents doubly charged species.*

This spectrum shows to our disappointment that indeed first the substituents are fragmented off before the coordination is affected. It would be possible, though, to select this ion for comparison. However, not all metal complexes showed this ion upon fragmentation and comparing relative stabilities will be impossible. To circumvent this complicated fragmentation behavior, a *bis*-terpyridine cobalt(II) complex of 2,2':6',2"-terpyridine (no substituents) was synthesized according to literature procedures[4] in order to provide at least a proof of principle. The ESI-MS-spectrum is depicted in Figure 2.13 with the identification of the fragments. Clearly, the spectrum is much less complicated with only four peaks. It is interesting to note that two of the peaks arise from the fragmentation of the hexafluorophosphate counter-ion. A neutral pentafluorophosphate molecule is released and can lead to the formation of *mono*-complexes. This could also be observed in case of some of the complexes of **3**. More important for our purposes is the peak at m/z = 262, which is the molecular ion without counter-ions. Selecting this as precursor ion for tandem MS-experiments gives rise to a fragmentation pattern as shown in Figure 2.14.

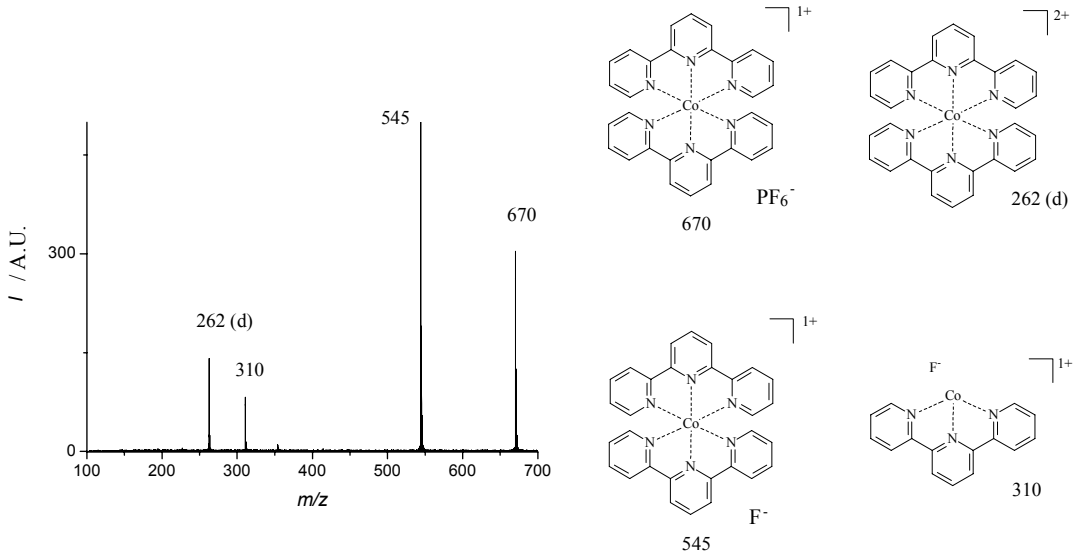

Figure 2.13. *ESI-QTOF mass spectrum of bis-terpyridine cobalt(II) complex (left) and assignment of the observed peaks (right); d represents doubly charged species.*

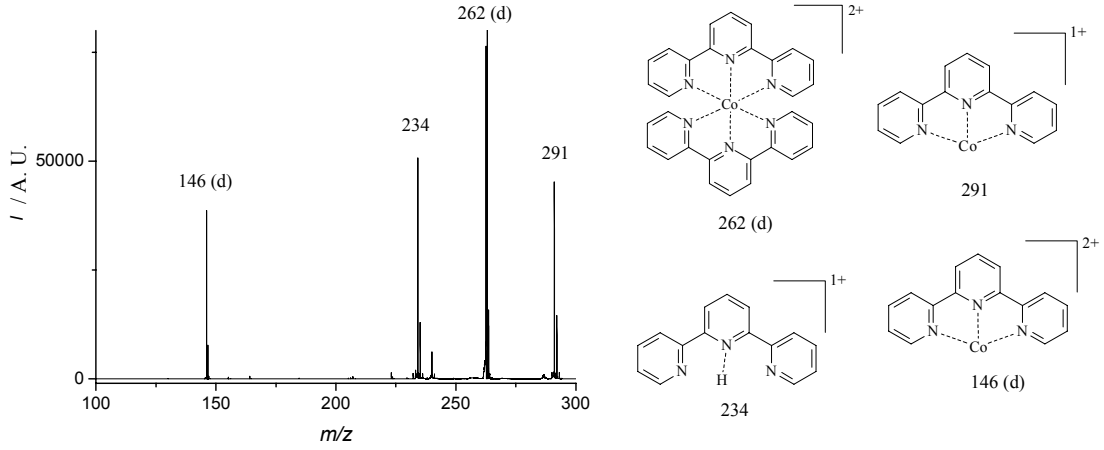

Figure 2.14. *Fragmentation pattern of precursor ion with m/z = 262 at an acceleration voltage of 20 V (left) and the assignment of the observed fragments (rights).*

Three fragmentation products are obtained, which seem puzzling at first. Eventually, by carefully looking at the masses of these fragments, there must be two possible fragmentation pathways for this precursor ion (Figure 2.15). The first one gives a doubly charged and a non-charged species (unobserved), which is the fragmentation of interest. The second fragmentation pathway results in two singly charged products. In fact, a proton is transferred from one ligand to the other. The acceleration voltage which is proportional to the kinetic energy of the precursor ion for the first process requires 26.6 V, whereas the second pathway requires only 24.0 V to reach the 1:1 ratio between products and precursor ion.

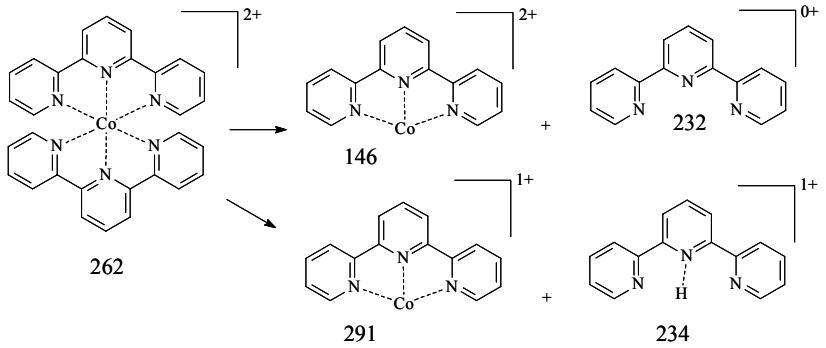

Figure 2.15. *The two fragmentation pathways of precursor ion with m/z = 262.*

Unfortunately, for a comparison not only the fragmentation patterns must be the same, but also the fragmentation mechanisms. Obviously, it will be hard to compare any data if different fragmentation mechanisms are taking place for the same precursor ion. Measurements are complicated further due to the fact that a steel needle is used for making the spray. Labile and weaker metal complexes such as mercury show exchange of the metal ion for iron that can only be originating from the needle. A solution would be to use a glass needle, but this is not straightforward from an instrumental point of view. Therefore we have turned to the use of MALDI-TOF MS to obtain more reliable data on the stability of the metal complexes in the gas phase.

2.3.7 MALDI-TOF MS

For the ionization in matrix-assisted laser desorption ionization time of flight mass spectrometry (MALDI-TOF MS) a matrix is used in which the analyte is dispersed. A laser ablates bulk portions of the sample through short but intense pulses. These pulses excite the matrix molecules and the large amount of energy that locally accumulates in the sample leads to desorption from the target. The gas phase contains apart from matrix molecules the analyte. It is thought that ions are being formed from gas-phase proton transfer reactions from photo-ionized matrix molecules, but the exact mechanism is still unclear.[37,41] The formed ions are separated in a time-of-flight (TOF) analyzer according to their mass-to-charge ratio and analyzed by a detector. Nevertheless, the intensity of the laser, i.e. duration and number of laser pulses, can be varied. Higher intensities generally result in more fragmentation of an ion of interest. The relative intensity of the ion of interest versus its fragment can be compared as a function of the laser intensity. The laser intensity is then used as a measure for the stability of isostructural compounds such as the metal complexes. Important assumptions are that the matrix absorbs all the energy from the laser and that the analyte remains intact during desorption. In other words, fragmentation occurs after sublimation and is not due to absorption of the analyte by the laser. Since the instrument uses a 337 nm nitrogen-laser, absorption within this region is little for the metal complexes involved, but does show some small differences. However, the number of matrix molecules by far exceeds that of the analyte. Therefore, these assumptions may be valid, but must be accounted for. The MALDI-TOF mass spectra of all metal complexes are shown in Figure 2.16, except for zinc and mercury. The latter two species did not give reproducible results.

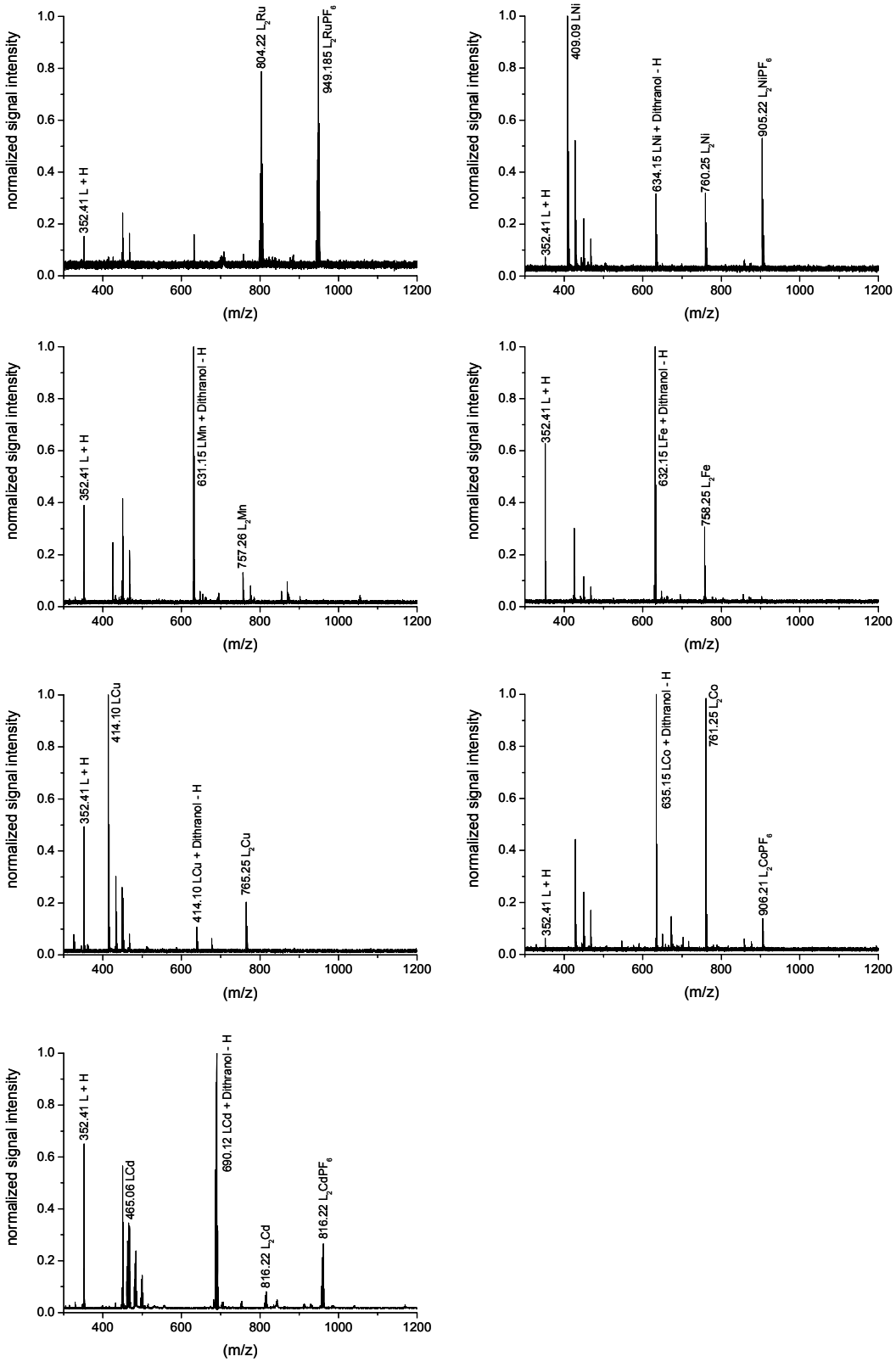

Figure 2.16. *MALDI-TOF MS spectra of all investigated bis-complexes of **3**: Ru^{II} (top left), Ni^{II} (top right), Mn^{II} (middle left), Fe^{II} (middle right), Cu^{II} (bottom left), Co^{II} (bottom right), Cd^{II} (last bottom figure).*

The spectrum reveals a fragmentation pattern as given below:

$$ML_2 \bullet 2PF_6 + d \xrightarrow{h\nu} L^+ + MLd^+ + ML_2PF_6^+ + ML_2^+ + ML^+ + d^+ + d_2^+$$

where d represents the matrix dithranol, M the metal ion, L the ligand and PF_6 the counter-ion. All compounds are singly-charged, which has been explained by Karas.[42] The metal complexes and their fragments are easily identified by making use of their isotopic pattern. It is interesting to see what happens with the distribution of the intensity of the fragments upon varying the laser intensity. Of interest is the ratio of L^+/ML_2^+, because this describes the overall stability of the complex. This ratio may be affected by further fragmentation of other fragmentation products upon increasing the laser intensity, especially MLd^+, $ML_2PF_6^+$ and ML^+. Fragmentation reactions that may be occuring involve:

$$MLd^+ \rightarrow ML^+ + L^+$$
$$ML_2PF_6^+ \rightarrow ML_2^+ + ML^+ + L^+$$
$$ML_2^+ \rightarrow ML^+ + L^+$$
$$ML^+ \rightarrow L^+$$

In total, eight different fragmentation pathways of these four precursor ions are possible and in principle, fragmentation of each ion contributes to the formation of L^+. Thus, the ratio of L^+/ML_2^+ as a function of the applied laser intensity may be regarded as a measure of the stability, since this reflects the cascade of binding energies from the *bis*-complex to the free ligand. Since the fragmentation pathways differ from complex to complex, it can be argued that the comparison between the complexes is not allowed. On the other hand, the order is highly reproducible and valid for other complexes as well. The actual experiment is shown in Figure 2.17 for the iron-complex.

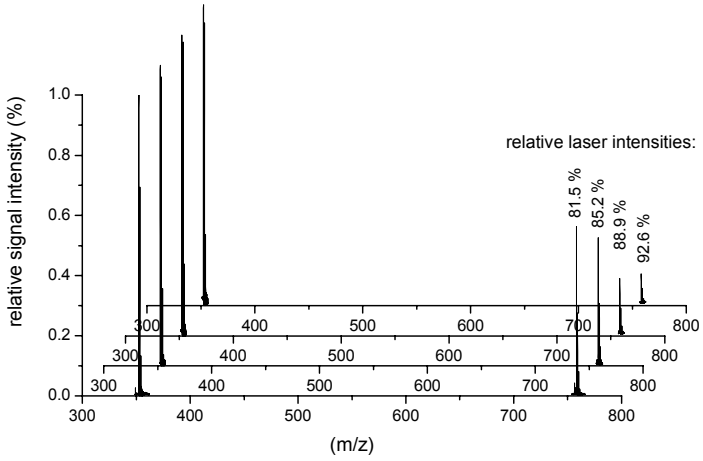

Figure 2.17. *MALDI-TOF mass spectra of the bis-terpyridine iron(II) complex of **3** at different laser intensities. Peaks were omitted in order to demonstrate the laser intensity-signal intensity more explicitly.*

Three mass spectra with 50 laser pulses per spectrum were recorded for each laser intensity. The relative signal intensities for the ligand L and the *bis*-complex ML_2 were taken from the calibrated mass spectra to calculate the ratio of L^+/ML_2^+. These ratio's were subsequently averaged over the three spectra corresponding to a single

laser intensity. The acceleration potential was left constant at 25 kV throughout all measurements. All data is combined into one plot as shown in Figure 2.18.

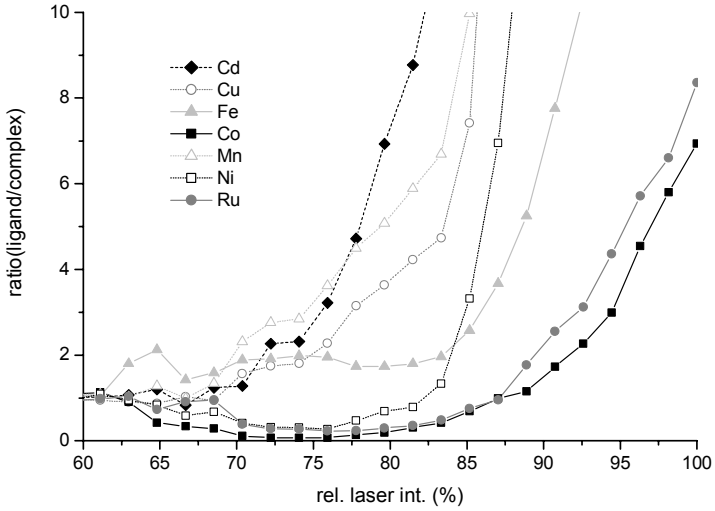

Figure 2.18. *Metal complex dissociation as a function of increasing laser intensity for the different metal complexes.*

If the point of complete complex dissociation is considered to be the point where the ratio of L^+/ML_2^+ is ~10, a relative binding strength can be derived from the plot: Co > Ru > Fe > Ni > Cu > Mn > Cd. Taking a ratio of ~5 still leads to the same order of the series. These results are actually in quite good agreement with data from Satterfield and Brodbelt who investigated the relative binding strength of 2,2':6',2"-terpyridine with cobalt, nickel and copper by using energy-variable collisionally activated dissociation in a quadrupole ion trap mass spectrometer.[43] They found an order for the relative binding strength of Co > Ni > Cu, which is the same in our case. However, as compared with the data in Table 2.1, the order shows some differences. This can be explained by the fact that those data have been acquired in solution in contrast to the gas-phase using MALDI-TOF MS and e.g. solvation energies are thus not taken into account. The applied laser intensity will be valuable for the evalution of MALDI-spectra of supramolecular polymers (see chapter 4).

This section has dealt more specifically with the binding characteristics of the metal complexes. Titration of metal ions to the ligand have shown that *mono*-complexes could be identified by UV/vis spectroscopy with certainty in case of Cu^{II}, Zn^{II} and Hg^{II} and that in these cases $K_1>K_2$. For Zn^{II} complexes a partition method yielded values of $K_1=3.0\pm0.3\times10^6$ and $K_2=1.3\pm0.1*10^6$. In case of Co^{II}, the *mono*-complex could be identified by means of ^{1}H-NMR, but not by UV/vis. Here it was found that $K_2>K_1$, but the exact quantification remains to be done. Furthermore, ESI MS/MS experiments have shown that 4'-oxy substituents are fragmented off of the Co^{II} complex before the metal coordination is affected. A similar phenomenon is observed in case of Ru^{II}-complexes and demonstrates the high stability of these metal complexes. A series of relative binding strengths has been derived from MALDI-TOF MS experiments and obeys the following sequence Co > Ru > Fe > Ni > Cu > Mn > Cd.

2.4 Synthesis and characterization of model metal complexes

Ligands **3** and **4** have been reacted with the acetate-salts of transition metal ions of manganese(II), iron(II), cobalt(II), nickel(II), copper(II), zinc(II), cadmium(II) and mercury(II) in methanol or in methanol-chloroform mixtures at a ratio of 2:1 ligand-to-metal ratio in order to ensure the *bis*-complex to be the predominant species (Figure 2.19). From the modeling it can be seen that *mono*-complexes may be present at the thermodynamic equilibrium at the 2:1 ligand to metal ratio. In order to isolate the *bis*-terpyridine metal complex, it was precipitated by addition of an excess of NH_4PF_6, leading to the exclusive precipitation of the *bis*-complex.[6] Simple filtration, washing and drying leads to the pure *bis*-complexes in reasonable to excellent yields (60%-90%).

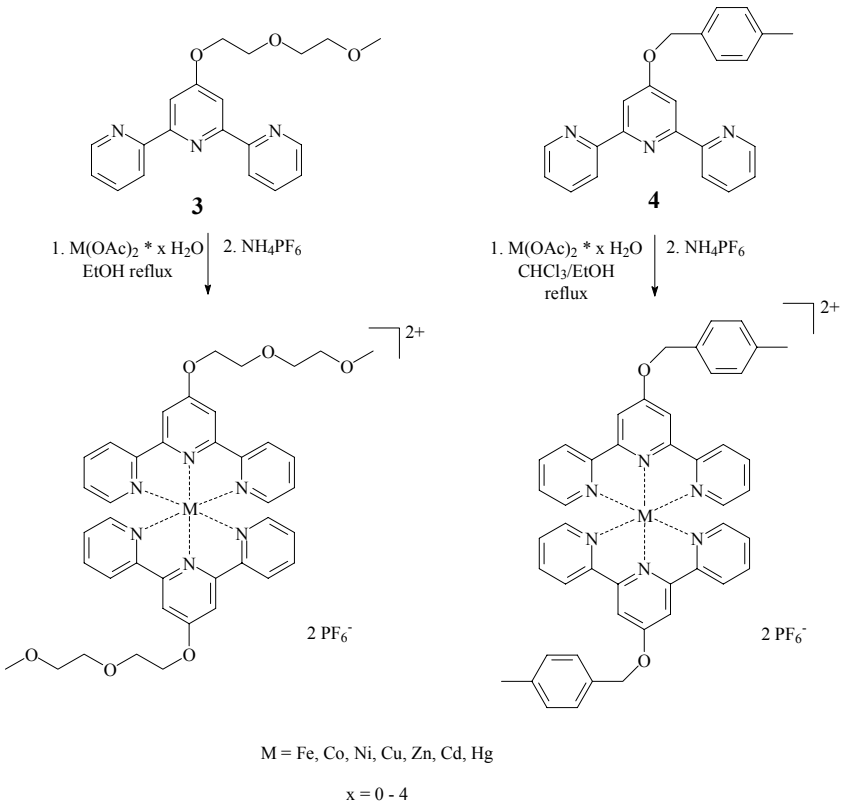

Figure 2.19. *Synthetic routes for the bis-terpyridine metal complex formation of **3** and **4** with Fe^{II}, Co^{II}, Ni^{II}, Cu^{II}, Zn^{II}, Cd^{II} and Hg^{II} ions.*

All compounds have been characterized by a variety of techniques such as ^{1}H-NMR, ^{13}C-NMR, UV/vis, FT-IR, MS, cyclic voltammetry, thermal gravimetric analysis and elemental analysis. From the metal complexes of **4**, single crystals were grown and analyzed by X-Ray diffraction in order to establish the different bond lengths and angles.

Figure 2.20 shows an ^{1}H-NMR-spectrum of an assigned Fe^{II}-complex with ligand **3**. In ^{1}H-NMR the coordination of the two ligands in a meriodinal fashion locates the π-system of one ligand in close proximity of the other ligand at an angle of around 90°. Especially the protons in the 6,6”- and in the 3’,5’-position are influenced by the coordination of the second ligand and their resonances shown a significant shift. This gives rise to typical chemical shifts of these protons in acetonitril solution.[44] Moreover, due to the introduction of the metal ion, the protons of the substituent are

more effectively shielded and shift to higher frequencies. The signals were assigned through their J-couplings and using 2D-NMR techniques.

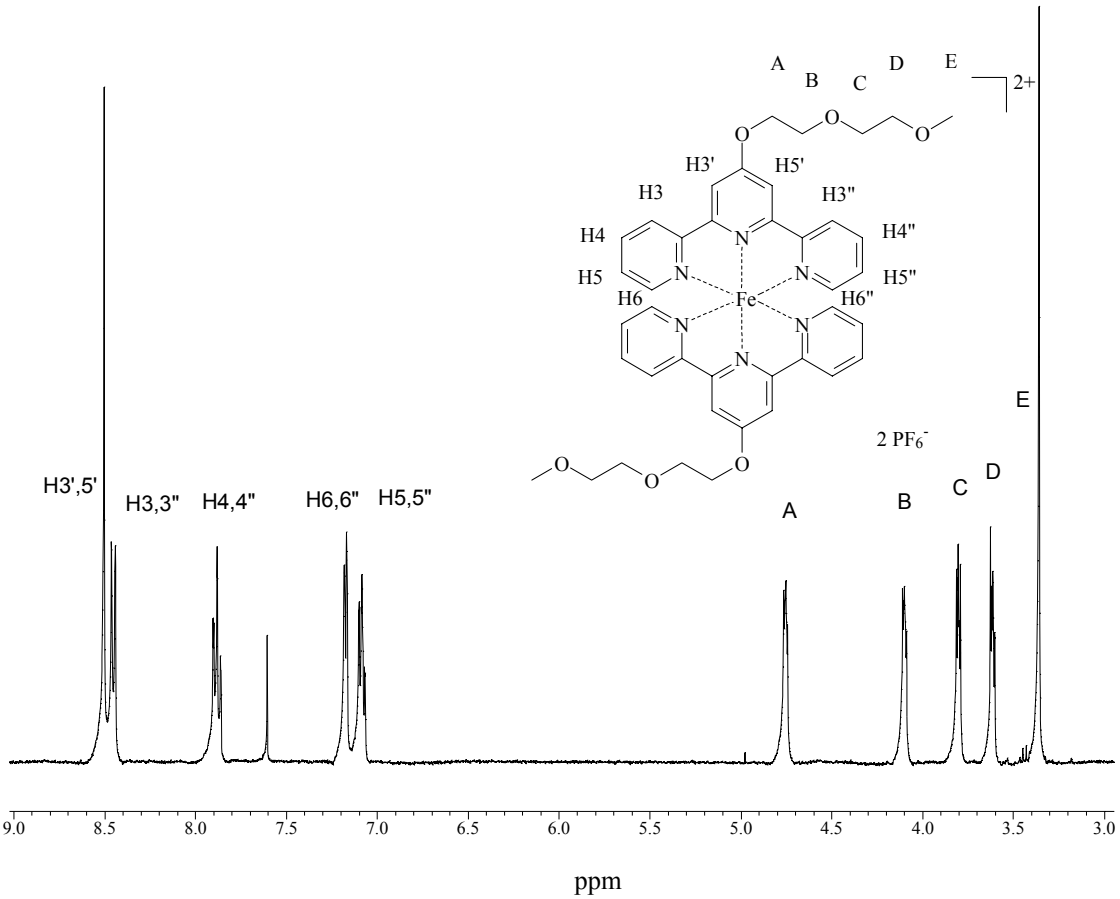

Figure 2.20. *^{1}H-NMR spectrum of the bis-terpyridine iron(II) complex of **3** in CD_3CN. Compare with Figure 2.3 to see the actual shifts.*

Only in case of Co^{II}-complexes paramagnetic or Knight shifts of the protons could be observed as explained in section 2.3.3. Nevertheless, assignment of these peaks is not easy due to the fact that J-coupling information is lost for some peaks. Comparison of different Co^{II}-complexes have led to a tentative assignment. The 6,6"-protons can be identified because they are located closest to the cobalt metal center and thus experience the largest paramagnetic shift.[45] The intensity of the 4'-proton in *bis*-complexes of 2,2':6',2" terpyridine with cobalt(II) ions can be assigned through integration. Luckily, using 2D-COSY-NMR techniques a coupling of this proton was found with the 3',5'-protons. Also, couplings between the 4,4"- and 5,5"-protons were found. This then leaves only the 3,3"-protons left over to be assigned in this complex. Using these findings then allows for the assignment of the 4'-substituted Co^{II}-complexes (see experimental section for more details). See Figure 2.9 for a spectrum of Co^{II} *mono*- and *bis*-complexes.

The all-cis-configuration gives in UV/vis-spectroscopy rise to a new intraligand transition between 290 and 340 nm. Figure 2.21 shows the UV-spectra of all compounds of **3**, where the substituent has no absorption. The similarity between the spectra of the d^5- and d^{10}-complexes of Mn^{II}, Zn^{II}, Cd^{II} and Hg^{II} is striking as well as that between the d^6-complexes of iron and ruthenium. This is not suprising due to the

same electronic configuration of the metal complex and thus similar ligand-centered excitations of the ligand can be expected. Moreover, for the same reason, the coordination of the ligand will be comparable for these complexes. The ruthenium and iron complexes show also a metal-to-ligand charge transfer band at 486 and 558 nm for Ru^{II} and Fe^{II} respectively.

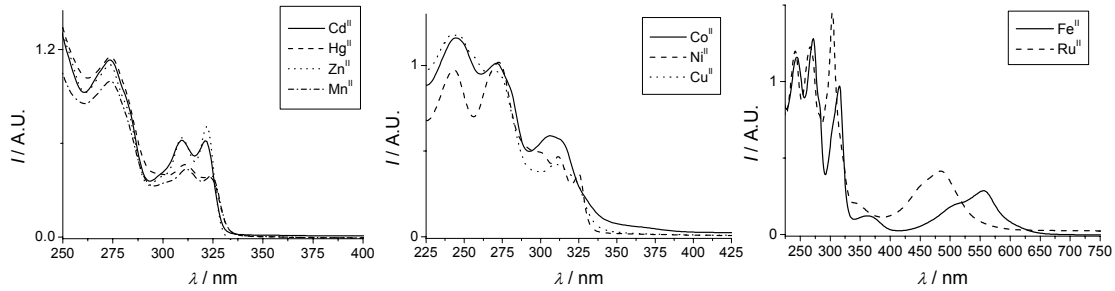

Figure 2.21. *UV/vis spectra of bis-terpyridine complexes of **3**: Mn^{II}, Zn^{II}, Cd^{II} and Hg^{II} (left), Co^{II}, Ni^{II} and Cu^{II} (middle) and Fe^{II} and Ru^{II} (right).*

A complete assignment of the IR- and Raman-spectra of 2,2':6',2"-terpyridine has been carried out by normal coordinate analysis.[46] This method predicts the frequencies and atomic displacements of normal modes by constructing a force field of the important bonded and non-bonded interactions. The parameters for such a force field are the atomic masses, the equilibrium bond lengths (usually from X-Ray crystallography) and the force constants. In FT-IR the region between 1700 and 1500 cm^{-1} is of particular interest, since here the ring deformations of terpyridine are located and there are no absorptions from the substituent that may overlap. The normal modes of vibration, also those between 1700 and 1500 cm^{-1}, for the ligand have been described in detail in the literature.[46]

Bis-terpyridine Ru^{II}-complexes have also been analyzed by normal coordinate analysis in order to assign the vibrational spectra based on symmetry arguments, although not all metal-complexes have exact octahedral, D_{2d}- or C_{2v}-symmetry.[47] In the case of the model metal complexes, symmetry will be even worse due to the orientation of the substituents. Nevertheless, comparison of the IR-spectra of the different metal complexes in the region between 1700 and 1500 cm^{-1} shows a similar pattern for all metal complexes (Figure 2.22), i.e. two sets of two peaks, although in case of Fe^{II} and Ru^{II} the splitting is blurred. This indeed indicates that the ligands have a similar conformation around the different metal ions. The differences no doubt arise from the subtle differences in coordination behavior regarding bond lenghts and angles.

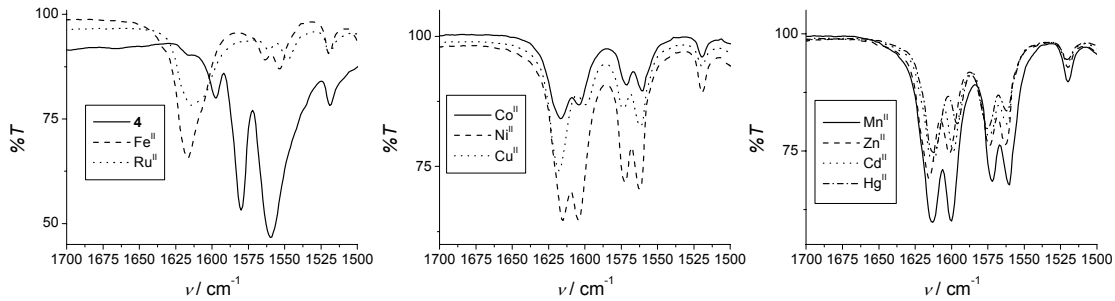

Figure 2.22. *IR-spectra of bis-terpyridine complexes of **4** in the region between 1700 and 1500 cm^{-1}: **4**, Fe^{II} and Ru^{II} (left), Co^{II}, Ni^{II} and Cu^{II} (middle) and Mn^{II}, Zn^{II}, Cd^{II} and Hg^{II} (right).*

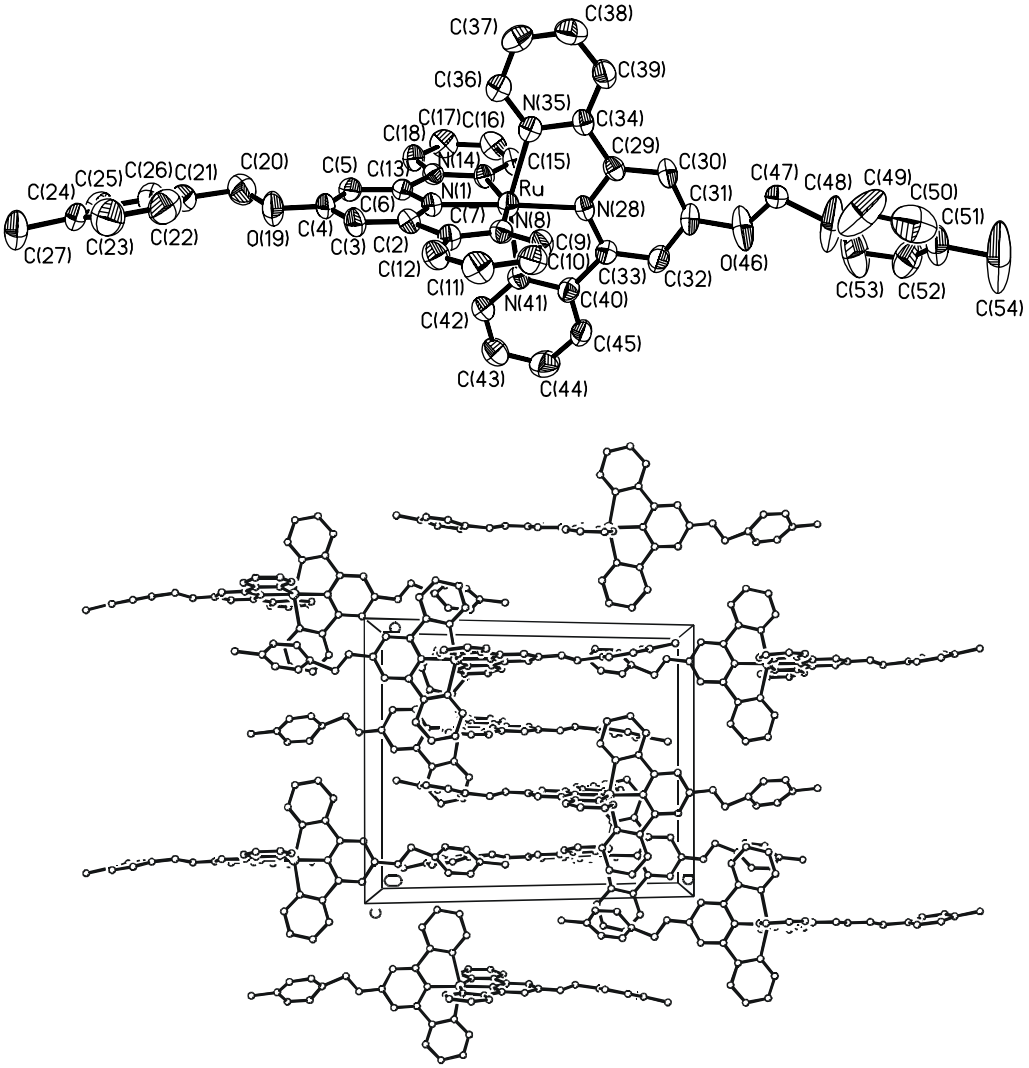

Figure 2.23. *X-Ray structure of the ruthenium(II) bis-complex of **4** with thermal ellipsoids (top) and the crystalline lattice (bottom).*

X-Ray crystallography on the metal complexes of **4** show in all cases octahedral surrounding of the metal complex. Figure 2.23 shows the crystal structure of the *bis*-complex of **4** with Ru^{II}. The PF_6^--counter-ions have been omitted for clarity, but show to fit perfectly between two adjacent metal complexes. Also, π-π stacking is occuring between the aromatic substituents of neighboring metal complexes. Undoubtedly, these two built-in prerequisites lead to the formation of suitably large single crystals in contrast to the *bis*-complexes of ligand **3** with metal ions. The nitrogens of the central rings are at almost identical distances from the ruthenium metal center, whereas the other four nitrogens have almost similar but slightly longer bond lengths. This may be a reason for the superb stability of the metal complex. Table 2.2 shows the differences in bond lengths between the different nitrogens and the metal center. The same numeration as in Figure 2.23 is adopted.

Table 2.2. *Selected bond lengths in different metal complexes of **4**.*

	M-N(8)	M-N(1)	M-N(14)	M-N(35)	M-N(28)	M-N(41)
Mn(II)	2.251(2)	2.197(0)	2.262(2)	2.245(2)	2.180(9)	2.253(2)
Fe(II)	1.986(3)	1.897(3)	1.992(3)	1.986(3)	1.898(3)	1.974(3)
Ru(II)	2.088(4)	1.981(4)	2.079(4)	2.100(4)	1.985(4)	2.101(4)
Co(II)	2.140(5)	1.988(5)	2.132(5)	2.108(5)	1.973(4)	2.079(5)
Ni(II)	2.126(3)	1.994(3)	2.120(3)	2.123(3)	1.989(3)	2.097(3)
Cu(II)	2.122(4)	1.949(4)	2.119(4)	2.244(4)	1.993(4)	2.080(6)
Zn(II)	2.203(6)	2.064(6)	2.227(6)	2.187(7)	2.080(6)	2.201(6)

Table 2.2 reveals that the bond length of the metal ion to the central nitrogens is in all cases shorter than to the respective terminal nitrogens. This stems from geometrical constraints of the ligand. Interestingly, in comparison with literature,[6,48-50] the bond lengths are comparable although it seems that the bond length to the central nitrogen atom is slightly shorter in all cases (ranging between 0.01 and 0.04 Å). Although this may be experimental error, it could also be explained by electronic effects from the substituent. Anyhow, the influence is in the latter case still not large. Another point is the coordination position of the first ligand with respect to the second. Especially in the case of copper, the second ligand shows a longer bond length of the central nitrogen to the metal ion, but more importantly the distances of the terminal nitrogens of the second ligand to the metal ion are much larger as compared with those of the first ligand. This has previously been explained as a Jahn-Teller-distortion,[14] for which this is the definite proof: the complex is indeed slightly elongated along one of its central axes. The other metal complexes show basically the same bond lengths of the nitrogens from the first and second ligand to the metal ion, albeit that in case of cobalt(II) the differences are slightly larger. The zinc-complex as well as the manganese-complex have longer overall bond lengths in comparison with the others and this may explain the lower stability of these *bis*-complexes. In case of iron the shortest bond lengths can be observed.

2.5 Stability

Supramolecular interactions are in general weaker than covalent interactions. In principle, they can be influenced by temperature, pH, redox state and shear forces. The following section deals with the results from thermal gravimetric analysis (TGA), UV-spectroscopy of the metal complexes in different pH-buffers and spectro-electrochemistry, where the metal complex is being oxidized and reduced while recording the corresponding UV-spectra.

2.5.1 Thermal stability

The thermal stability of the complexes has been studied by thermogravimetric analysis (TGA) under nitrogen-atmosphere. Uncoordinated ligand **3** shows an onset of 5% weight loss at 235 °C, whereas ligand **4** shows this at 284 °C. The metal complexes also reveal different onsets as summarized in Table 2.3. The bis-complexes of ligand **4** are in general more thermally stable than those of ligand **3**. Several complexes show an earlier onset than the uncoordinated ligand. This can be explained by involvement of the metal-ion upon dissociation of one of the ligands from the complex. It has to be noted that for the metal complexes the weight loss occurs more gradual than in case of the uncoordinated ligand. The relative thermal stabilities for ligand **3** are Co > Ru > Ni > Cu > Fe > Hg > Cd > Zn and for ligand **4**

between the relative thermal stabilities of the two series, the high stability of *bis*-terpyridine complexes of Ru^{II}, Ni^{II} and Co^{II} is demonstrated.

Table 2.3. *TGA-results indicating the thermal stability of bis-terpyridine metal complexes with **3** and **4**. The table lists the temperature at which 5 % weight loss was observed.*

Metal ion	T / ºC (ligand **3**)	T / ºC (ligand **4**)
none	235	284
Mn^{II}	203	310
Fe^{II}	256	227
Ru^{II}	293	340
Co^{II}	306	331
Ni^{II}	286	339
Cu^{II}	261	279
Zn^{II}	211	218
Cd^{II}	240	313
Hg^{II}	246	271

Using a polarized light-microscope with a heating plate in order to follow any transitions in colored complexes (Fe^{II}, Ru^{II} and Co^{II}) proved unsuccessful: the compounds degraded before a clear color change – indicative of decomplexation – could be observed.

2.5.2 pH-stability of the complexes

By adjusting the pH of a solution of the metal complex, competition may take place between ligand protonation and metal hydroxide formation on the one hand and metal complex formation on the other hand.[52] The metal complexes of ligand **3** have been solubilized in a series of buffer solutions of different pH and UV-spectra were recorded.

Table 2.4. *Stability of the bis-terpyridine metal complexes of **3** at various pH. a + represents an intact complex, whereas a – indicates that the UV/vis-spectrum resembled that of the protonated or uncoordinated ligand.*

Metal ion	**pH=1.0**	**pH=3.0**	**pH=5.0**	**pH=7.0**	**pH=10.0**	**pH=13.0**
Mn^{II}	-	-	+	+	+	-
Fe^{II}	-	+	+	+	+	-
Ru^{II}	+	+	+	+	+	+
Co^{II}	-	+	+	+	+	-
Ni^{II}	+	+	+	+	+	+
Cu^{II}	-	+	+	+	+	-
Zn^{II}	-	+	+	+	+	-
Cd^{II}	-	+	+	+	+	-
Hg^{II}	-	+	+	+	+	-

The results are summarized in Table 2.4. Clearly, all metal complexes remain intact by varying the pH from 3.0 to 10.0, although it seems decomplexation is already occuring for the Mn^{II} complex at pH = 3.0. This could be related to lower stability constants. At pH = 1.0 the UV-spectra of the original complexes of Fe^{II}, Co^{II}, Cu^{II}, Zn^{II}, Cd^{II} and Hg^{II} resemble that of the protonated free ligand. Thus, the connection between the two ligands via the metal ion is broken. In case of the Ru^{II} and Ni^{II} complexes, no changes have appeared in the spectrum, indicating that the metal complexes are stable at low pH. At pH = 13.0 the UV-spectra of the original complexes of Fe^{II}, Co^{II}, Cu^{II}, Zn^{II}, Cd^{II} and Hg^{II} resemble that of the free ligand at pH = 13.0, although for copper it takes prolonged periods of time. Also in case of Co^{II}, a small absorption remains at 320 nm. The UV-spectra of the Ru^{II} and Ni^{II} complexes are unchanged. This indicates that these two complexes are stable over the whole pH-range. From Ru^{II} it is known that its complexes are generally inert and thus no changes would be expected. However, Ni^{II} also seems to behave as an inert metal ion. This could explain the results from the titrations in section 2.3.1, where upon overtitration no changes were occuring in the UV-spectrum. The degree of inertness of Ni^{II}-complexes can be established by performing an exchange-experiment with a stronger coordinating ligand or metal ion. The results in Table 2.4 indicate that metal complexes of Fe^{II}, Co^{II}, Cu^{II}, Zn^{II}, Cd^{II} and Hg^{II} are sufficiently labile and lead to decomplexation. The reversibility of this decomplexation process was further investigated by preparing a solution of the Fe^{II}-complex in water of neutral pH. Subsequently, the solution was titrated with 0.1 M HCl until the color had fully disappeared. Then, an equal amount of 0.1 M NaOH was added and indeed, the purple color was reinstalled, albeit that the intensity was slightly lowered (Figure 2.24). On the other hand, when the solution was first titrated with 0.1 M NaOH until the color had disappeared, the purple color never re-appeared upon addition of 0.1 M HCl. This probably stems from the fact that Fe^{II}-ions are not stable in alkaline solution and in the presence of oxygen they may rapidly be oxidized to Fe^{III}-ions and subsequently precipitate as the hydroxide-salt. Leaving the solution stand for some time gave indeed a brown precipitate.

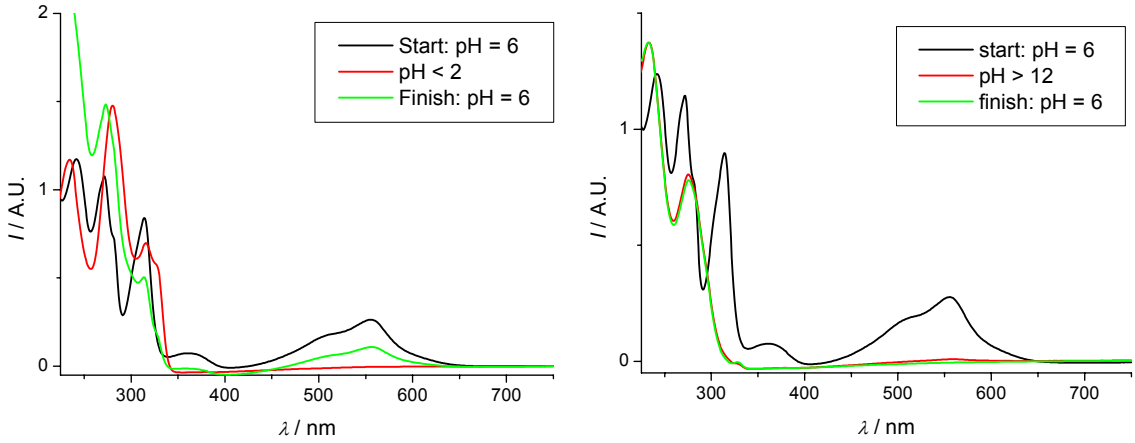

Figure 2.24. *Cycling of the pH followed by UV/vis-spectroscopy on the bis-terpyridine iron complex of* ***3*** *in water: first acid, then base (left) and first base, then acid (right).*

2.5.3 Spectroelectrochemistry

The electrochemical responses of the ligands and the complexes were characterized by cyclic voltammetry in 0.1 M NBu_4PF_6 in acetonitrile against a SSCE reference

electrode at scan rates of 25, 50, 100 and 200 mV/s. This revealed one-electron processes for all the steps involved.[53] Table 2.5 summarizes the results.

Table 2.5. *Results of cyclic voltammetry of the bis-terpyridine metal complexes of **3** in acetonitrile using SSCE as the reference electrode and 0.1 M [NBu$_4$][PF$_6$] as electrolyte.*

Complex	M(III)/M(II)	M(II)/M(I)	tpy/tpy^{-}
[Co**3**$_2$][PF$_6$]$_2$	0.28	-0.89	-1.67
[Fe**3**$_2$][PF$_6$]$_2$	1.04		-1.28, -1.45
[Ni**3**$_2$][PF$_6$]$_2$ *			-1.25, -1.43
[Cu**3**$_2$][PF$_6$]$_2$ *		-0.29	
[Zn**3**$_2$][PF$_6$]$_2$			-1.37, -1.52
[Ru**3**$_2$][PF$_6$]$_2$	1.19		-1.27, -1.46

*Ni and Cu are irreversible. Both compounds show a stripping peak in the reverse scan. The electrochemically irreversible nature of the reduction couples can be attributed to a rearrangement followed by absorption on the electrode.

The Co^{II}, Fe^{II} and Ru^{II} complexes all showed reversible oxidation and reduction waves, both in the cathodic and anodic scan, whereas Ni^{II} (**3**) and Cu^{II} (**4**) were irreversible. It is noteworthy to mention that the free ligand does not show any activity in both the anodic and cathodic scans. The irreversible nature of the reduction of *bis*-terpyridine nickel and copper complexes has previously been attributed to rearrangement of the complexes into other geometries. The reduced species absorb onto the electrode and then give rise to a stripping peak in the reverse scan.[54-56] In all cases except for [Co**3**$_2$][PF$_6$]$_2$ two close lying reduction waves are observed and they have been attributed to stepwise reduction of one of the coordinated ligands followed by reduction of the second coordinated ligand according to the formula given below.

$$[ML_2]^{2+} \xrightarrow{e^-} [L - M^{2+} - L^{\bullet -}]^{+} \xrightarrow{e^-} [M^{2+} L_2^{\bullet -}]$$

For the Co^{II} complex the metal ion is reduced to Co^{I} and this occurs at a different potential. In cooperation with the group of professor Salbeck (University of Kassel), spectroelectrochemistry (SPEL) investigations have been performed. By using this technique, it is possible to record *in-situ* UV-spectra when performing electrochemistry. It is therefore an excellent tool to study what could be happening during oxidition and/or reduction. New transitions may appear as a result of a newly occupied orbital via reduction or as a result of a newly partially unoccupied orbital upon oxidation. Shifts in transitions not involving the redox orbital can also occur, although these shifts will be not so dramatic. The complexes of interest are the previously described complexes of Zn^{II}, Co^{II}, Ru^{II} and Fe^{II}. The interpretation of the results is unfortunately not straightforward. Figure 2.25 show the results of spectroelectrochemistry – reduction only – on the Ru^{II}, Fe^{II} and Zn^{II} and Co^{II} complexes. It is interesting to note that in literature the first and second peak in the reduction are attributed to ligand centered reductions for the zinc complex: no metal-centered reductions are expected, since the d-shell of the zinc-complex is completely filled.[55] In the UV/vis spectrum of the Zn^{II} complex the absorption at 319 nm is attributed to a ligand-centered transition. From CV the first reduction should give rise to a radical anion on the ligand. Usually, radical anions display a rich absorption spectrum in the visible light stemming from new π^*-π^*-transitions. For 2,2':6',2"-terpyridine the radical anion has been prepared by reaction with alkali metal ions and has been studied mainly by ESR.[57] A short communication by Nakamura however shows the UV/vis spectra in the visible range, where indeed broad absorptions with a maximum between 550 and 620 nm are observed depending on the solvent and the

alkali metal ion.[58] Thus, the radical anion of terpyridine is expected to have broad absorptions in the visible range. It is interesting to see that in SPEL the UV/vis-spectrum accompanying the first reduction wave is very similar to the UV/vis-spectrum of the free ligand. If it really is the free ligand, then this implies that zinc is released from the complex. The exact mechanism on how this may occur remains puzzling. On the other hand, if the electron that is being transferred to the complex occupies one of the π^*-orbitals on one of the ligands, it is also expected that this particular ligand-centered transition is less likely to take place and could shift to higher energies. Then however, a radical anion should form on the ligand and in the UV/vis-spectrum we would then also expect absorptions that indicate the presence of a radical anion. These absorptions are not observed. They are indeed visible during the second reduction, where broad bands appear in the visible region of the spectrum. Thus, after a two-electron reduction of the complex, the radical anion of the ligand appears. The fact that the absorption maxima are different than those reported in literature for the reduction of the ligand by alkali metal ions must be the result of the presence and/or stabilization of the ligand by zinc-ions and/or the substituent on the central ring.[58] In summary, during the first reduction wave the UV/vis-spectrum of the free ligand is observed. It might be that the zinc metal ion is involved and leads to complex dissociation. During the second reduction, the radical anion of the ligand is formed.

In case of cobalt, the band at 305 nm decreases until it has almost half the intensity and there are new bands arising at 416 and 595 nm during the first reduction wave, which involves the formation of a Co^{I} complex according to CV-measurements.[59,60,61] However, the formation of a radical anion can not be excluded due to the broad band observed at 595 nm, which was also observed in case of the zinc after the second reduction. Alternatively, this band could be attributed to MLCT- and/or d-d bands, but the analogy with the zinc-complex is more obvious. It is interesting to note that the UV/vis-spectrum in the region between 235 and 300 nm reveals bands that are similar to the free ligand after the second reduction. Thus, the ligand centered transitions characteristic of complex formation (between 280 and 320 nm) disappear or shift to higher energies and radical anions on both ligands are being formed.

The results of SPEL upon reduction of the Ru^{II}- and Fe^{II}-complexes also remain difficult to explain, even qualitatively. In literature, the *bis*-terpyridine complexes of these two metal-ions have been studied the most with respect to their electrochemical behavior in light of photophysical properties, although there are only few accompanying UV/vis spectra regarding spectroelectrochemistry.[62-66] The results on the reduction of *bis*-2,2':6',2"-terpyridine iron(II) ditetrafluoroborate are comparable.[67] Upon the first reduction, the MLCT-band decreases in intensity and shifts only slightly. The band at 311 nm decreases to half its intensity and a strong absorption band at 355 nm appears. Upon reducing the complex further the MLCT-band shift to higher energies (486 nm). The same story is more or less true for reduction of the ruthenium-complex: the MLCT-band decreases in intensity and shifts slightly, the band at 307 nm decreases and a new band appears at 350 nm. Upon reducing the complex further a strong band at 445 nm appears, which may be attributed to a shift of the MLCT.

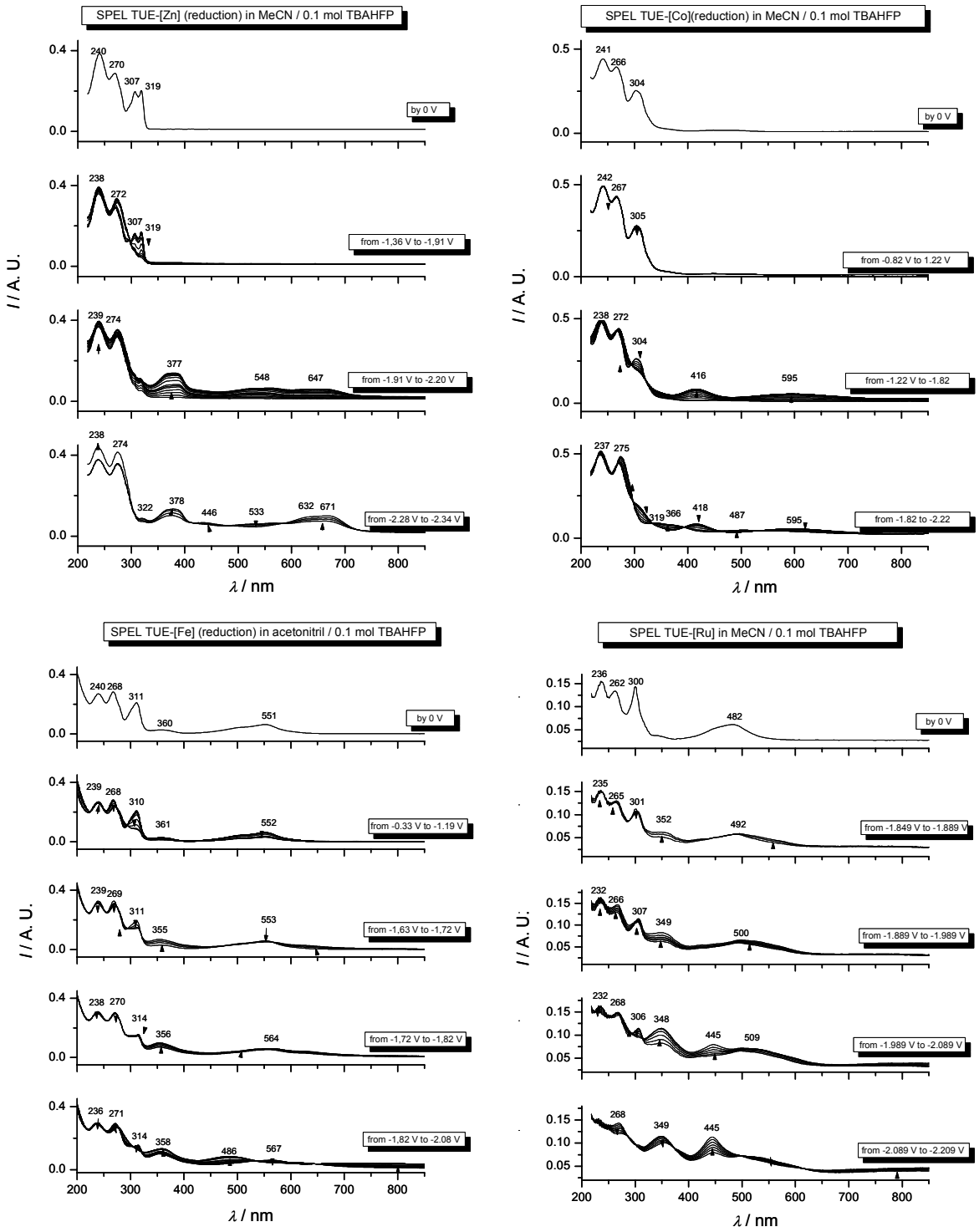

Figure 2.25. *Spectroelectrochemistry of the bis-terpyridine complexes of **3** with Zn^{II} (top left), Co^{II} (top right), Fe^{II} (bottom left) and Ru^{II} (bottom right). UV/vis-spectra have been recorded at and between those potentials as denoted in the legend and represent the reduction waves observed in CV. Note that the reference has changed from the SSCE-electrode to the ferrocene/ferrocenium-ion couple.*

The results strongly suggest that when the complex is singly reduced, the added electron is localized on one of the coordinated ligands, because absorptions of both the coordinated radical anion as well as the neutral coordinated ligand are visible. The

fact that the absorption of the neutral coordinated ligand further decreases upon the second reduction suggests that the second electron is localized on the other ligand.

In summary, spectroelectrochemistry during reduction of Fe^{II}, Ru^{II}, Co^{II} and Zn^{II}-complexes has given some insight into the metal complex stabilities with respect to reduction. In case of iron, ruthenium and cobalt, the singly and doubly reduced species can be identified as *bis*-terpyridine complexes with radical anions on both ligands, whereas in case of zinc it appears that the first reduction leads to decomplexation followed by the formation of the radical anion on the uncoordinated ligand.

The ruthenium-complex was oxidized by means of an acidic solution of $Ce(IV)(SO_4)_2$ in 0.1 M H_2SO_4 (pH = 1). At higher pH $Ce(IV)(SO_4)_2$ is unstable. The other complexes are unstable towards the acidic experimental conditions. Because the oxidation potential of this system is slightly higher than the Ru^{II}/Ru^{III} couple, the following reaction occurs:

$$[RuL_2]^{2+} + Ce^{4+} \rightarrow [RuL_2]^{3+} + Ce^{3+}$$

First of all, some reference experiments were carried out to make sure that both Ce^{IV} and Ce^{III} do not form complexes with terpyridine in this pH-range. Luckily, this does not occur, although several Ce^{III}-complexes with terpyridine-ligands have been reported.[68,69] Apparently, they are rather labile. Also, Ce^{III} and Ce^{IV} have an absorption in the spectral region of interest. Fortunately, Ce^{III} has very little absorption and absorption from Ce^{IV} is easily identified and corrected for. Thus, a solution of $Ce(IV)(SO_4)_2$ in 0.1 M H_2SO_4 was titrated to solution of the *bis*-complex of **3**. Figure 2.26 shows the results.

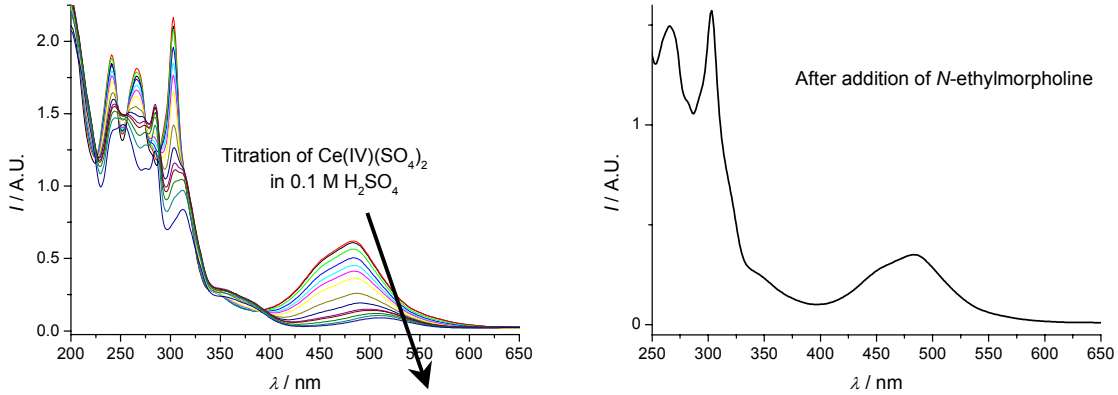

Figure 2.26. *Titration of $Ce(IV)(SO_4)_2$ in 0.1 M H_2SO_4 resulting in the oxidation of the Ru^{II} to the Ru^{III}-complex (left) and after addition of N-ethylmorpholine resulting in the reformation of the Ru^{II} complex (right).*

As can be seen, the MLCT-band at 486 nm shifts to 511 nm and becomes less intense. This is accompanied by a color change from intense red to less-intense pink. Also, changes in the ligand centered absorptions can be observed, but those arise in parts from the broad peak coming up from 400 nm (Ce^{IV}-ions). Again, the π-π^*-transition at 307 nm decreases. Upon addition of an organic reductor (*N*-ethylmorpholine), the original MLCT-band at 486 nm is being restored (Figure 2.26). However, this does not prove that the metal complex is actually opened up or that exchange has taken place. In order to do so an exchange experiment was attempted at a 10 mg scale. After

oxidation of the metal complex a solution of uncoordinated 2,2':6',2"-terpyridine in 0.1 M H_2SO_4 was added at a 1:2 molar ratio of original metal complex versus to-be-added ligand. Subsequently the solution was heated, stirred for another hour and cooled to room temperature. Then the organic reductor was added and the products were isolated by extraction and precipitation. Analysis by ^{1}H-NMR revealed that no exchange had taken place, since only the starting compounds were retrieved. Neither mixed species (AB) nor homodimers of the unsubstituted ligand (BB) had formed. Of course, at a pH of 1 the free ligand will be protonated and may prevent complex formation. However, Ru^{III} complexes can be formed in acidic medium due to their relative inertness.[70] We may therefore conclude that these *bis*-terpyridine Ru^{III} complexes are not prone to ligand exchange and are also highly inert. From a stability point of view, this is of course highly desired, but from a reversibility point of view, this is unfortunate.

2.6 Heteroleptic complexes

In chapter 1 the formation of heteroleptic complexes in two steps using ruthenium(III)chloride and osmium(III)chloride was briefly mentioned. In the first step a *mono*-complex can be isolated by a precipitation approach: the *mono*-complex is less soluble than the parent-ion and also than the *bis*-complex and will precipitate from solution. Subsequent washing or extraction will lead to the isolation of pure *mono*-complex. In the second step the corresponding Ru^{III} *mono*-complex is reduced to Ru^{II} in the presence of an organic reductor, *N*-ethylmorpholine, and the chlorides are replaced by the second terpyridine ligand.[71,72] The approach is more general, since *mono*-complexes of terpyridine have been reported with a variety of other transition metal ions such as Fe^{III}, Co^{II}, Ni^{II}, Cu^{II} and Zn^{II}.[7-12,73] Nevertheless, a selective formation of a heteroleptic complex with these metal ions is impossible, because due to the dynamic nature of the metal-ligand interaction ligand-exchange will occur upon addition of a differently substituted ligand. This will then lead to a mixture of A-A, A-B and B-B complexes. Also, it would not make sense to separate the A-B complex from the other two, because as soon as the purified A-B complex is exposed to a solvent, exchange can take place again. In case of nickel(II)-complexes however, regarding the results in section 2.3.2 and 2.5.2, it may be expected that inert heteroleptic complexes could be prepared indeed. This has not been exploited so far, since attention was focused on a different metal ion. Cobalt(II)-ions form labile metal complexes, whereas cobalt(III)-ions form inert metal complexes. Chujo has reported temperature and redox reversible hydrogels based on bipyridine functionalized poly(oxazolines) and cobalt-ions.[73] The results in section 2.5.2 reveal that cobalt(II)-ions are also labile in *bis*-terpyridine complexes. With cobalt(III)-ions the *bis*-terpyridine complex is inert. Thus, a selective approach towards heteroleptic *bis*-terpyridine cobalt(III) complexes should be possible via a *mono*-terpyridine cobalt(III) complex. The next two sections deal with the formation of heteroleptic complexes: the first deals with ruthenium(II) as metal ion, the second with cobalt(III).

2.6.1 Heteroleptic *bis*-terpyridine ruthenium(II) complexes

Mono-complexes of ruthenium have been prepared in two different ways. The first one, using literature procedures,[71] involves hydrated ruthenium(III)chloride. An excess of hydrated ruthenium(III)chloride (1:1.5 ratio of ligand to metal) is solubilized in a minimum amount of ethanol. The ligand is added portion-wise and the *mono*-complex precipitates out of solution due to its non-ionic nature. Filtration, washing and drying leads to the *mono*-complex. The second route involves anhydrous

$RuCl_3$ in anhydrous argon-purged DMF. This route presumably involves coordination of DMF as a ligand and abstraction of the carbonyl that subsequently acts as a ligand by formation of dimethylamine.[74] The latter one is the preferred route in case of polymers as will be explained in chapter 4. The two synthetic pathways are shown in Figure 2.27 and were used for the *mono*-complex formation of **3** and **4**. Other methods have been reported in the literature such as 'ruthenium-blue solutions' for the preparation of terpyridine *mono*-complexes, but the composition of the metal source is in this case unknown, presumably the metal ion or a cluster of metal ions with a mixture of solvent ligands.[70]

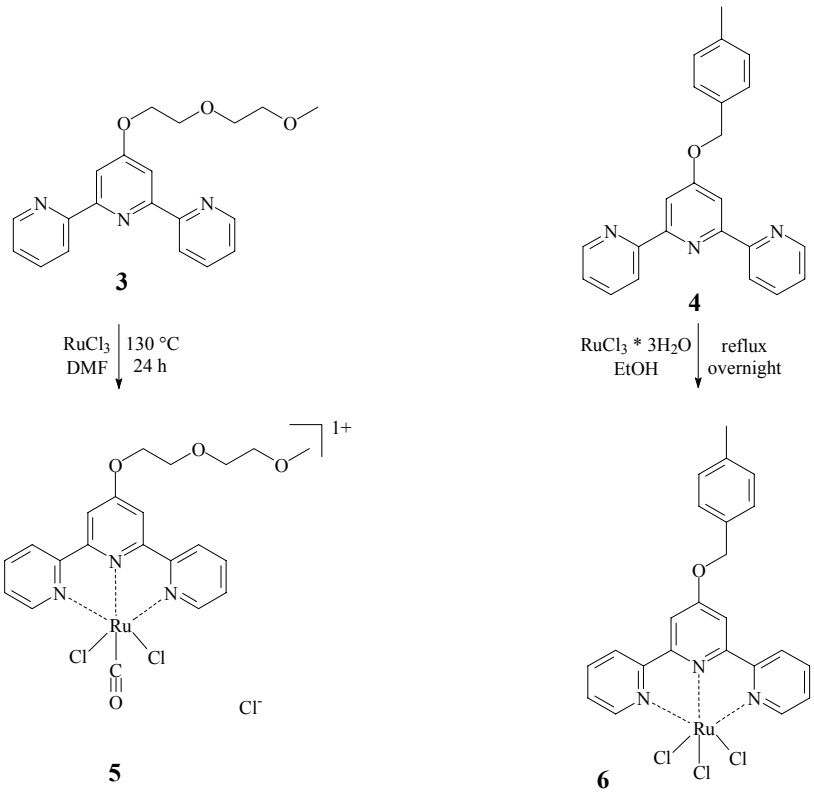

Figure 2.27. *Synthesis of mono-terpyridine ruthenium(III) complexes **5** and **6** of ligand **3** and **4**.*

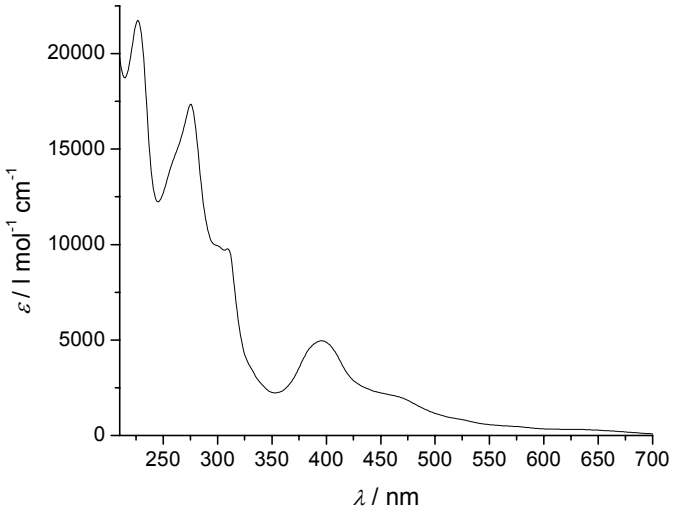

Figure 2.28. *UV/vis spectrum of **6** in acetonitrile.*

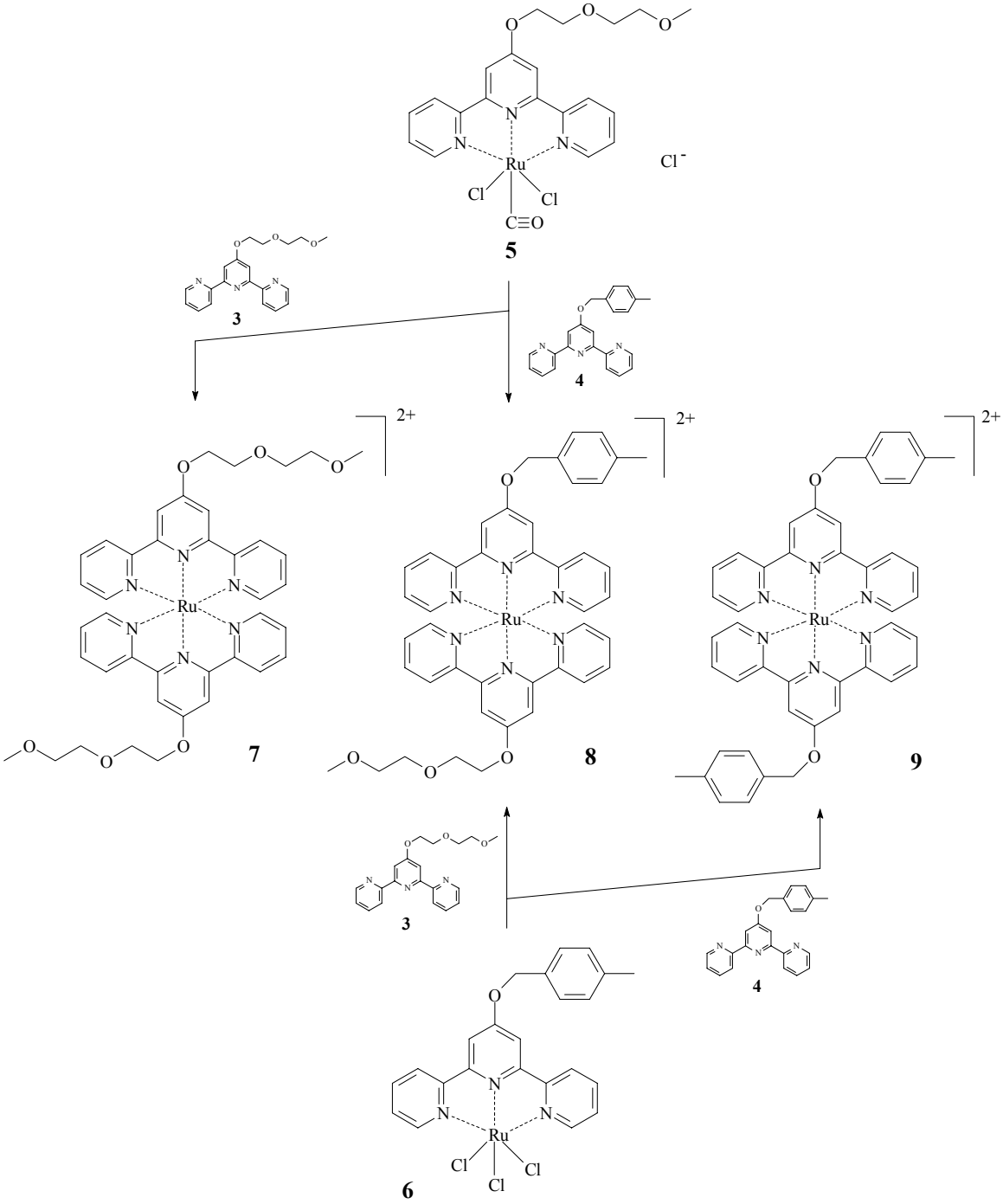

Figure 2.29. *Synthetic routes to the two homoleptic as well as the heteroleptic ruthenium(II) complexes. In all steps a catalytic amount of N-ethylmorpholine is used for the reduction.*

The *mono*-complexes have been characterized by several techniques (see experimental section). In the ^{1}H-NMR-spectrum no signals in the terpyridine-region could be observed due to the paramagnetic nature of ruthenium(III)-ions, whereas in the UV/vis-spectrum a clear metal-to-ligand-charge transfer band could be observed at 400 nm (Figure 2.28). In the FT-IR spectrum the carbonyl stretching vibration can be observed at 1941 cm^{-1}, indeed proving the abstraction of this ligand from DMF. A corresponding mass spectrum and a fitting elemental analysis prove the purity of the *mono*-complexes.

In a second step the heteroleptic complex can be formed. To a solution of the mono-complex and the uncoordinated second ligand, a few drops of an organic reductor, *N*-ethylmorpholine, is added: Ru^{III} is reduced to Ru^{II} and the second ligand displaces the remaining chlorides. For comparison, also the homoleptic complexes have been prepared (Figure 2.29). All complexes have been purified by column chromatography and were isolated in reasonable yields after reprecipitation with NH_4PF_6 (55-85%). After work-up the compound showed a single spot on a TLC-plate. Figure 2.31 shows the assigned ^{1}H-NMR spectrum as well as the UV-spectrum of the heteroleptic complex **8**. In the ^{1}H-NMR the most interesting signal shifts stem from the protons in the 3':5'- and 6:6"-position of the ligands and the OCH_2-signals from the substituents. The presence of both substituents can be observed and integration reveals the 1:1 ratio of both ligands, as expected in a heteroleptic complex. Some signals in the aromatic region clearly overlap causing loss of the fine-splitting as observed in the free ligands. Nevertheless, all peaks could be assigned by comparison with the homoleptic ruthenium(II) complexes of ligand **3** and **4**.

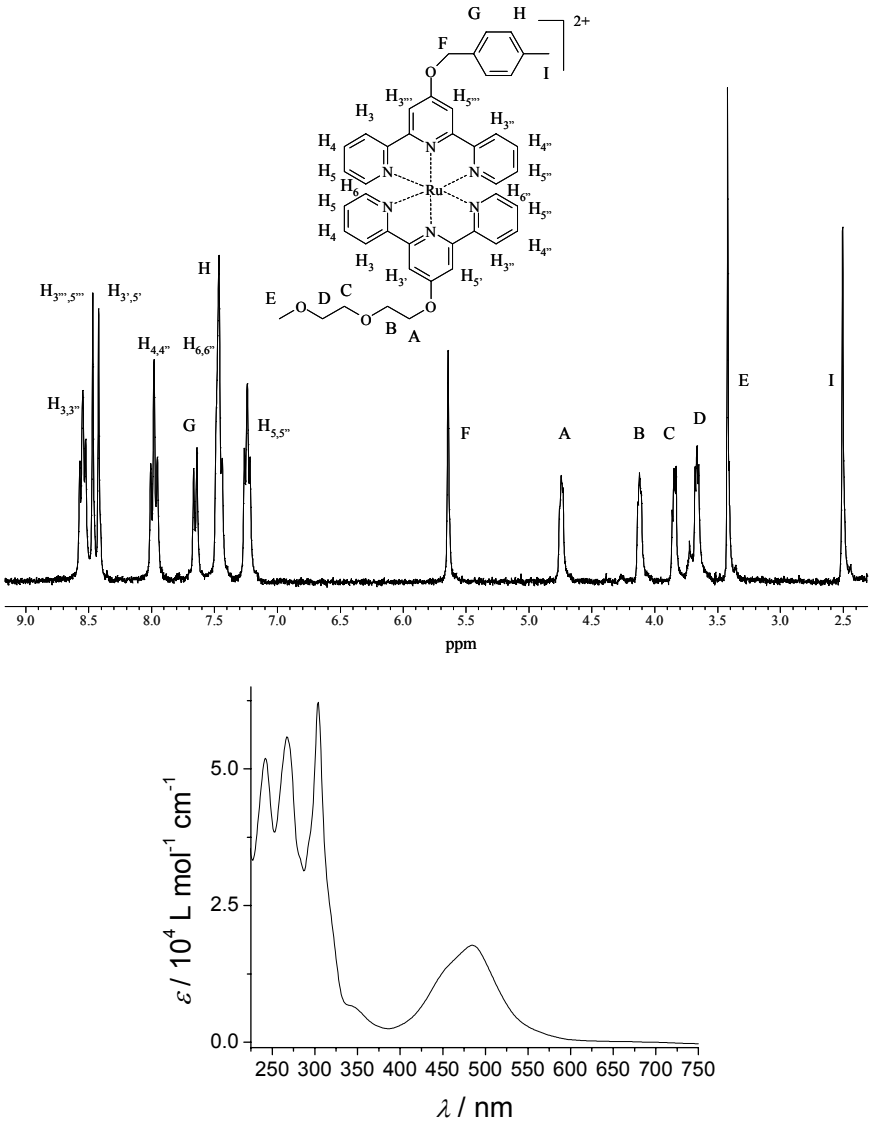

Figure 2.30. *Characterization of **8** by ^{1}H-NMR in CD_3CN (top) and UV/vis (bottom) in CH_3CN.*

The UV/vis spectrum reveals an MLCT-band at 486 nm and a new π-band at 307 nm, which are typical for *bis*-terpyridine ruthenium(II) complexes (Figure 2.30).[75] The band at 400 nm indicative of the *mono*-complex has disappeared, although the broadness of the new MLCT-band overlaps to some extent. Mass spectrometry is not very well suitable to draw conclusions on the purity of the complex, since the mass of ligand **3** and **4** differ by only 4 mass units. Nevertheless, elemental analysis in combination with the other characterization techniques proves the purity of the heteroleptic complex.Also this complex has been studied regarding its stability in acidic and basic media, its redox stability and its thermal stability. The same conclusions as for the homoleptic ruthenium(II) complexes can be drawn: the heteroleptic complex is extremely stable.

2.6.2 Heteroleptic *bis*-terpyridine cobalt(III) complexes

In the literature there are a few examples in which heteroleptic cobalt(III) complexes have been prepared by oxidation of cobalt(II)-ions in the presence of two different terpyridine ligands.[76,77] A selective approach for the formation of heteroleptic *bis*-terpyridine cobalt(III) complexes has up to now not been developed, to the best of our knowledge. This would require the formation of a *mono*-terpyridine cobalt(III) complex as an intermediate. Again, the literature describes only a few examples of *mono* terpyridine cobalt(III)-complexes, all of which were isolated in low yields and bad reproducibility.[78] The major problem in preparing a cobalt(III) *mono*-complex is the lack of an appropriate source for cobalt(III)-ions. Only cobalt(II)-salts are commercially available and the few cobalt(III)-complexes that can be bought are unsuitable for *mono*-complex formation for steric reasons. An exploration of the Gmelin database revealed a great number of cobalt(III)-salts, most of them described by the founding fathers of coordination chemistry Werner and Jörgensen.[79] Especially bidentate ligands and the associated stereo-isomerism of the complexes have been subject of many studies. An interesting lead was found in a short article from Crayton.[80] Here the coordination of a single tridentate ligand (diethylenetriamine) to cobalt(III) was described.

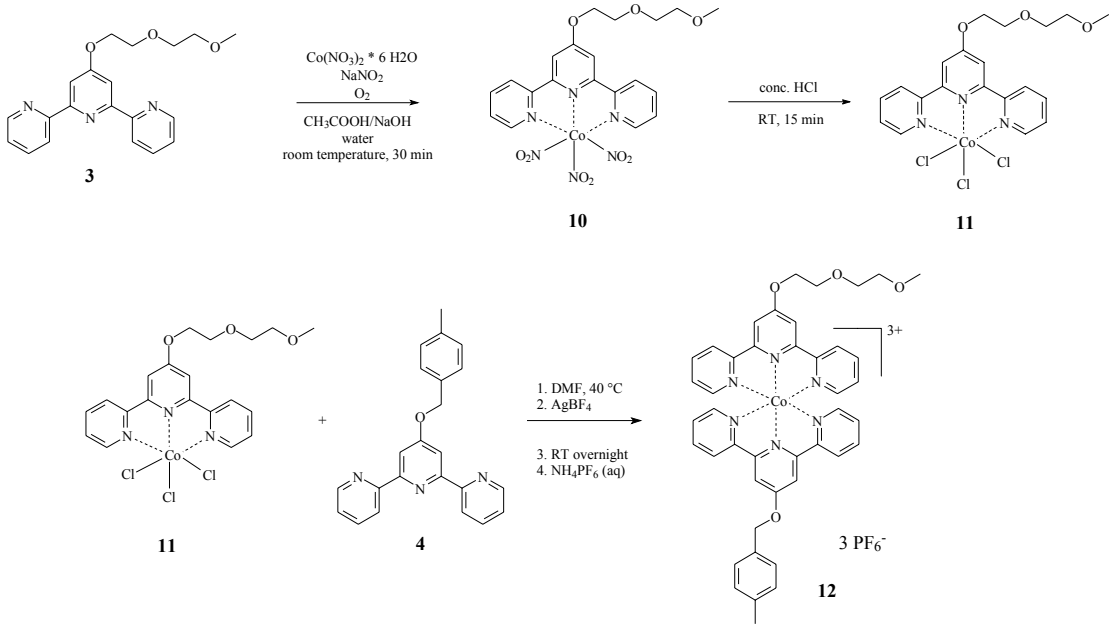

Figure 2.31. *Synthetic scheme for the preparation of heteroleptic bis-terpyridine cobalt(III) complexes.*

In this case, a solution containing Co(II)-ions was oxidized by bubbling air in the presence of sodium-nitrite in an aqueous buffer (pH = 6). The nitro-counterions played a major role in the isolation of the compound, because its precipitates from solution: it is no longer soluble due to the fact that it is uncharged. Simple filtration and drying yields the pure product. In that same article two synthetic routes were described for the replacement of the nitro-counter-ions by chlorides or nitrates. Chloride counter-ions are easily removed by precipitation with an appropriate silver-salt.[81] Based on these results, the following route was followed for the preparation of heteroleptic cobalt(III) complexes (Figure 2.31).

In a first step the *mono*-terpyridine-trinitrocobalt(III) complex is formed. In ^{1}H-NMR all signals shift slightly due to the coordination of the ligand. However, since a *mono*-complex is being formed, the ^{1}H-NMR looks distinctly different from that of a *bis*-complex. In case of a *bis*-complex especially the protons in the 3',5' and the 6,6"-positions on opposite ligands come in close vicinity of each other and therefore they influence their respective chemical shifts strongly. In case of a *mono*-complex, the π-system of the second ligand is lacking and a pattern as observed in the free ligand appears, although there are subtle differences in the respective chemical shifts. The signals could be assigned by analogy with the free ligand through their J-couplings. In FT-IR the coordination of the nitro-ligands by the N-O stretch vibrations can be derived (Figure 2.32). The absorptions at 1401 and 1306 cm^{-1} are indicative of coordination through the nitrogen-atom.[82] In the mass spectrum the molecular ion could be observed, but the spectrum was of bad quality. The elemental analysis fitted though and capillary electrophoresis revealed a single peak that overlapped with the electro-osmotic flow marker, indicating a non-charged species. Since the nitro-ligands are highly inert and resist the precipitation-strategy with silver, they must be replaced. Crayton described a procedure in which concentrated aqueous hydrochloric acid solution can be used for this purpose.[80] The resulting trichloro-compound again precipitated from the solution and a greyish-green product could be isolated. The compound is soluble in DMF and DMSO, where the green color is retained. However, addition of some drops of water showed a color change to red. Apparently, at least one of the chlorides is easily replaced (presumably the one in the trans-position) and is responsible for the color change.

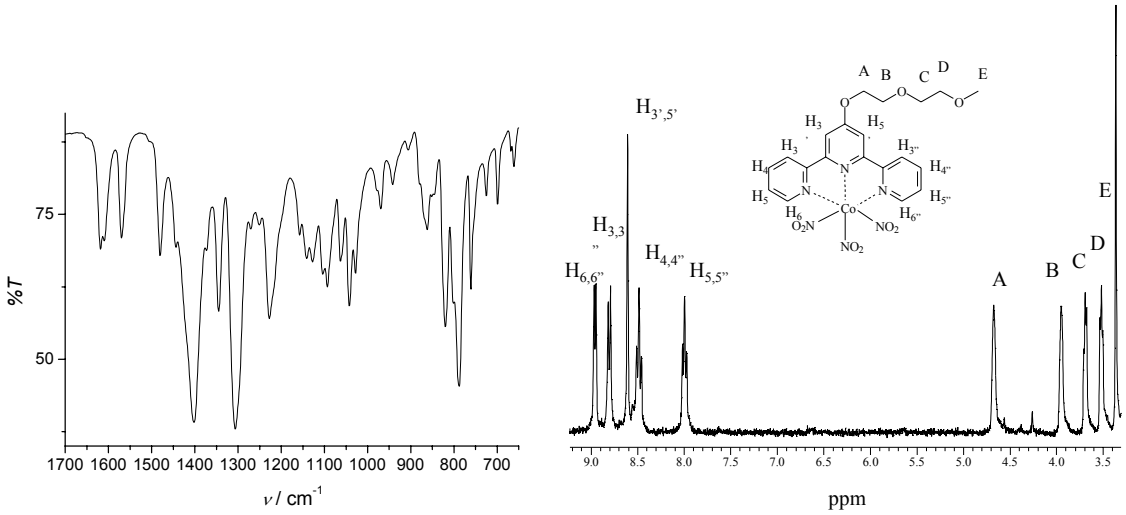

Figure 2.32. *Characterization of **10** by FT-IR (left) and ^{1}H-NMR in DMSO-d6 (right).*

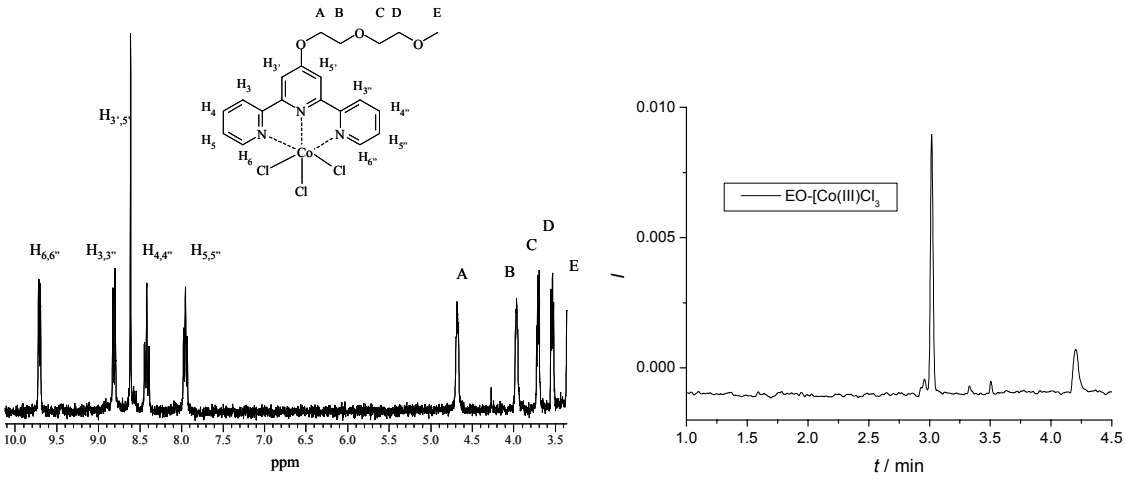

Figure 2.33. *^{1}H-NMR-spectrum of **11** (left). Note the shift of the protons in the 6,6''-position (left). The electroferogram (right) reveals two main peaks indicative of the non-charged species at 4.25 min and of the singly charged species at 3.05 min.*

Capillary electrophoresis in *N*-methylformamide showed two peaks, which stem from the non-charged compound (with three chlorides) and a charged compound in which one of the chlorides is replaced. The other three small peaks remain unassigned. No efforts were thus undertaken to further purify this compound apart from a thorough washing. The successful replacement of the nitro's by the chlorides could be proven by the absence of the NO-stretching vibrations in FT-IR. Also, the elemental analysis was in good agreement with the expected theoretical values and in ^{1}H-NMR again some shifts could be observed in the aromatic region (Figure 2.33). Interestingly, the substituent survived the hydrochloric acid treatment judging from the integrals, probably because the reaction was at room temperature and for a short time only. The final step was removal of the chlorides by precipitating them as AgCl. In the presence of a second ligand this should then in theory give rise to a heteroleptic cobalt(III) complex. However, TLC-analysis of the crude product revealed three spots. After column chromatography, the three species could be identified as the two homoleptic complexes and the heteroleptic complex, that could be isolated in a 50% yield. This implies that there is no selectivity in the formation of the heteroleptic complex, since exchange is taking place during the synthesis. However, upon resolubilization of the isolated heteroleptic cobalt(III) complex, no exchange was found even over prolonged periods of time. A small amount of cobalt(II) may be responsible for this behavior: it is known that cobalt(II)- and cobalt(III)-complexes undergo electron self-exchange reactions.[83,84] Co^{II}-ions might have been present in the starting material or may have formed because of the experimental conditions. After column chromatography, the cobalt(II)-ions are apparently removed and no more exchange takes place. In ^{1}H-NMR the protons in the 3',5'-position and 6,6''-position again experience the presence of the other ligand and chemical shifts as for a *bis*-terpyridine complex are observed. Integration of the substituent signals fits nicely for a 1:1 ratio of both ligands in the complex. It is thus possible to prepare heteroleptic *bis*-terpyridine cobalt(III) complexes (Figure 2.34).

This complex was also subjected to stability tests. Upon varying the pH from 1.0 to 13.0 no changes in the UV/vis spectrum could be observed, even over prolonged periods of time. This is thus a good proof of the inertness of the cobalt(III) complex. However, reducing the cobalt(III) complex by *N*-ethylmorpholine gave rise to the

UV-spectrum of a *bis*- terpyridine cobalt(II) complex. By adding acid it is then possible to fully remove the metal ion by ligand protonation (Figure 2.35). An excess of an alkaline solution was added and extracted with chloroform. Not surprisingly, in ^{1}H-NMR the signals of the two starting ligands could be observed.

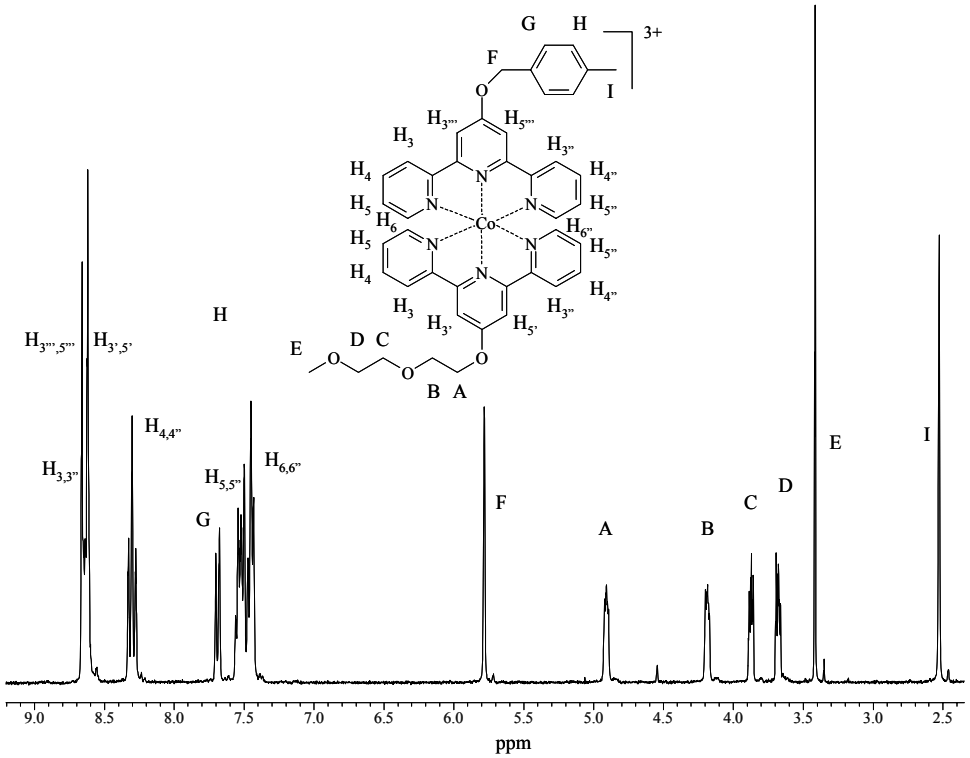

Figure 2.34: *^{1}H-NMR-spectrum of the heteroleptic cobalt(III) complex in CD_3CN.*

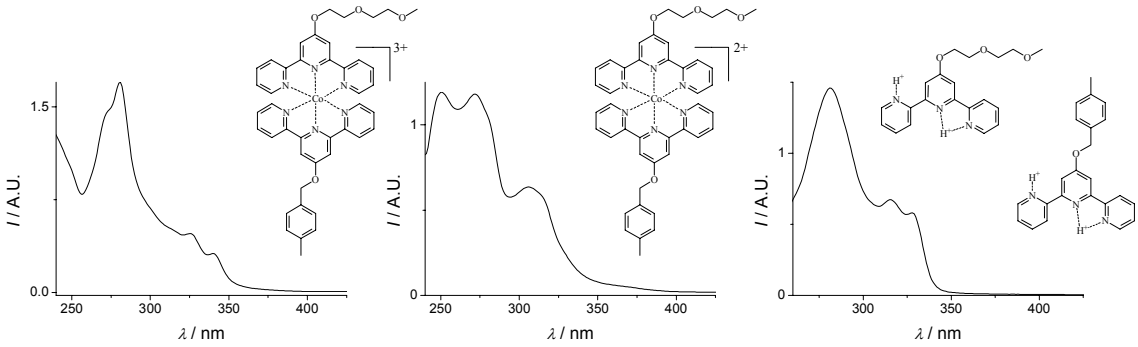

Figure 2.35. *Changes in the UV/vis-spectrum of the starting heteroleptic complex (left) upon reduction by N-ethylmorpholine (middle) and subsequent formation of the doubly protonated form of the ligand (right).*

To summarize this section, it is possible to prepare heteroleptic complexes of two differently substituted terpyridine ligands using ruthenium(II)- and cobalt(III)-ions. In the former case the stability of the linkage is so great that reversing is virtually impossible without breaking covalent bonds. In the latter case, the selectivity of the synthesis is not optimized yet. Ways to overcome this would be to use a suitable source of Co^{III}, preferably a compound such as *mer*-trinitrotriamminecobalt(III),[85] but it would even be better to have more easily replaceable counter-ions already incorporated.

2.7 Conclusions

This chapter was devoted to the synthesis, characterization and stability studies of *bis*-terpyridine metal complexes with two different substituents. The partition method has been successfully applied for *bis*-terpyridine-zinc(II) complexes, whereas ^{1}H-NMR has is a promising technique for Co^{II}-complexes, although quantification remains to be done. Mass spectrometry techniques showed the relative order in metal-complex stability. Acidic and alkaline solutions as well as spectroelectrochemistry were used to evaluate the stability of the different metal complexes in solution. Heteroleptic complexes have been prepared by using Ru^{III}/Ru^{II}-chemistry and a new route to heteroleptic *bis*-terpyridine cobalt(III) complexes has been developed, although selectivity and versatility need to be improved. For the construction of macromolecular architectures, these metal complex characteristics are of great value: it allows the selection of a suitable metal ion with respect to its binding characteristics. In general, Zn^{II}, Cd^{II} and Hg^{II} give rise to the weakest complexes and show the highest lability. By analogy with the Zn^{II}-complex, also Cd^{II} and Hg^{II} are expected to have $K_1>K_2$. This implies that there will always be a substantial dissociation of the *bis*-complex into the *mono*-complex and the uncoordinated ligand, even at the 1:2 metal-to-ligand ratio, unless concentrations are kept relatively high or the lability is decreased e.g. by using other counter-ions or a different solvent. In case of Cu^{II}-complexes, K_1 is also larger than K_2, evidenced by UV/vis-spectroscopy and X-ray crystallography due to a Jahn-Teller distortion of the *bis*-complex. For Fe^{II}-complexes, K_2 is much larger than K_1 and only *bis*-complexes are being formed, even if much more metal than ligand is present. Reversible binding was observed by cycling the pH. For Co^{II} *mono*-complexes could be detected by ^{1}H-NMR, but also here $K_2>K_1$. For Ni^{II} no suitable technique has been developed yet to identify *mono*-complexes. Due the high stability constants, the complex seems to behave as an inert complex with little exchange taking place: this explains the insensitivity of the complex to changes in pH and the high thermal stability. Ru^{II}- and Co^{III}-complexes are highly inert, although in the synthesis of the latter scrambling took place. These complexes are insensitive to changes in pH and display high thermal stabilities. Moreover, by MS-techniques it was shown that Co and Ru complexes are among the most stable complexes: the substituents are fragmented off before the metal complex opens. Nevertheless, Co^{III} complexes can easily be reduced to Co^{II}-complexes that are easily dissociated.

These heteroleptic complexes are of course the key for connecting chemically different polymer chains together, whereas homoleptic complexes can give rise to chain extended polymers, but also AB-BA triblock copolymers. The next chapter will deal with the synthesis and characterization of a variety of polymers with a terpyridine ligand at one or both chain ends, since they present the building blocks that can be connected with metal-ions.

2.8 Experimental part

Chemicals were received from Aldrich, Fluka, Strem and Acros and were used without further purification. Solvents were bought from Biosolve. Column chromatography was carried out on silica, flash silica or neutral AlOx (Fluka). DMF was dried over molsieves. ^{1}H-NMR and ^{13}C-NMR were recorded on a Varian Inova spectrometer with frequencies of 400 and 100 MHz respectively and on a Varian Mercury spectrometer with frequencies of 300 and 75 MHz at 25 °C. Chemical shifts are given in ppm downfield from TMS. UV/Vis spectra were recorded on a Perkin Elmer Lambda 45P spectrophotometer. Matrix assisted laser desorption/ionization mass spectra were obtained using dithranol as the matrix and NaI as additive on a PerSeptive BioSystems Voyager DE PRO

spectrometer. ESI-QTOF-MS/MS experiments were conducted on Q-Tof Ultima GLOBAL mass spectrometer (Micromass, Manchester UK) equipped with a Z-spray source. Samples were injected in Flow Injection Analysis mode. Ionization was achieved in positive ion mode by application of 5 kV on the needle. Argon collision gas was introduced into the central hexapole collision cell of the mass spectrometer for the MS/MS experiments. IR-spectra were measured on a Perkin Elmer 1600 FT-IR in attenuated total reflection (ATR) mode. Elemental analysis was carried out on a Perkin Elmer 2400 Series CHN Analyzer and on a Eurovector Euro EA Elemental Analyzer equipped with a EuroCAP 40-2 autosampler. TGA was conducted using a Netzsch TG209 F1 under N_2-atmosphere at a heating rate of 10 °C min^{-1}. GC-MS were recorded with a Shimadzu GC17A connected to an MS. Capillary electrophoresis was carried out on a Beckman P/ACE System 2200 using NMF as solvent and LiCl as supporting electrolyte with a standard 30 cm long fused silica capillary and an operating voltage of 20 kV using an injection pressure of 5 mbar and a P/ACE UV-Absorbance detector operating at 280 nm. Cyclic voltammetry were recorded in 0.1 M $[NBu_4][PF_6]$ in acetontrile. The following electrodes were used: a platinum disc working electrode, a platinum plate counter-electrode and a standard calomel electrode calibrated against Fc/Fc^+. SPEL was carried out using an in-house set-up. Buffer solutions (500 mL) were prepared from FIXANAL® buffer concentrate for pH 1.00, 3.00, 5.00, 7.00, 10.00 and 13.00 at 20 °C. 2,6-*Bis*-(2'-pyridyl)-4-pyridon **(1)** was synthesized according to literature procedures.[16,17] All reactions were carried out under argon-atmosphere unless stated otherwise.

2-(2-Methoxyethoxy)ethane-1-*p*-tosylate (2)

A solution of *p*-toluenesulfonyl chloride (41.26 g, 216 mmol) in THF (50 mL) was added dropwise to a stirred two-phase system of NaOH (8.64 g, 216 mmol) in water (50 mL) and 2-(2-methoxyethoxy)ethanol (20.00 g, 166 mmol) in THF (50 mL) at T < 5 °C. Subsequently the temperature was kept below 5 °C and stirring was continued for another three hours after which the reaction mixture was poured into ice-water (200 mL). The mixture was extracted with $CHCl_3$ (3 × 250 mL) and the combined organic layers were washed with 0.1 M HCl (2 × 100 mL), dried over Na_2SO_4 and evaporated *in vacuo*. Purification by column chromatography (silica starting with hexane:EtOAc (6:1) and increasing the polarity to EtOAc) yielded 40.65 g (89%) of a viscous colorless oil after drying. ^{1}H-NMR ($CDCl_3$): δ = 7.78 (d, 2 H, ^3J = 7.2 Hz; *o-H* tosyl), 7.34 (d, 2 H, ^3J = 7.2 Hz; *m-H* tosyl), 4.16 (t, 2 H, ^3J = 4.0 Hz; SO_3CH_2), 3.67 (t, 2 H, ^3J = 4.0 Hz; $SO_3CH_2CH_2$), 3.56 (t, 2 H, ^3J = 4.0 Hz; CH_2OCH_2), 3.47 (t, 2 H, ^3J = 4.0 Hz; CH_2OCH_3), 3.34 (s, 3 H; OCH_3), 2.42 (s, 3 H; CH_3); ^{13}C-NMR ($CDCl_3$): δ = 144.6, (*p-C* tosyl), 132.7 (*C*-1 tosyl), 129.6 (*m-C* tosyl), 127.7 (*o-C* tosyl), 71.5 (SO_3CH_2), 70.3 ($SO_3CH_2CH_2$), 69.1 (CH_2OCH_2), 68.4 (CH_2OCH_3), 58.7 (OCH_3), 21.3 (CH_3); Anal. Calcd for $C_{12}H_{18}SO_5$ (274.34): C, 52.54; H, 6.61; S, 11.69. Found: C, 52.11; H, 6.41; S, 11.75.

4'-(2-[1-Methoxyethoxy]ethoxy)-2,2';6',2''-terpyridine (3)

To a solution of **1** (3.55 g, 14.2 mmol) and K_2CO_3 (5.96 g, 42.5 mmol) in dry DMF (100 mL) at 80 °C was added dropwise a solution of **2** (3.55 g, 12.8 mmol) in dry DMF (50 mL). Stirring was continued overnight, after which the reaction mixture was poured in water (250 mL) and extracted with CH_2Cl_2 (3 × 150 mL). The combined organic layers were dried over Na_2SO_4, filtered and evaporated *in vacuo*. The crude product was purified by column chromatography (AlOx, CH_2Cl_2) and isolated as a white solid. Yield: 3.48 g (77%). ^{1}H NMR ($CDCl_3$): δ = 8.67 (dd, 2 H, ^3J = 4.8, ^4J = 1.8; $H_{6,6''}$), 8.60 (dd, 2 H, ^3J = 8.0, ^4J = 1.0 Hz; $H_{3,3''}$), 8.04 (s, 2 H; $H_{3',5'}$), 7.84 (td, 2 H, ^3J = 8.0, ^4J = 1.6 Hz; $H_{4,4''}$), 7.31 (ddd, 4 H, ^3J = 8.0, ^3J = 4.8 Hz, ^4J = 1.0 Hz; $H_{5,5''}$), 4.41 (t, 2 H, ^3J = 4.8 Hz; H_A), 3.94 (t, 2 H, ^3J = 4.0 Hz; H_B), 3.75 (t, 2 H, ^3J = 4.0 Hz; H_C), 3.58 (t, 2 H, ^3J = 4.4 Hz; H_D), 3.40 (s, 3 H; H_E); ^{13}C NMR ($CDCl_3$): δ = 166.9 ($C_{4'}$), 157.4 ($C_{2',6'}$), 156.0 ($C_{2,2''}$), 149.0 ($C_{6,6''}$), 136.7 ($C_{3',5'}$), 123.7 ($C_{3,3''}$), 121.2 ($C_{4,4''}$), 107.4 ($C_{5,5''}$),71.9 (C_A), 70.8 (C_B), 69.4 (C_C), 67.7 (C_D), 59.0 (C_E). GC-MS (EI): *m/z* (%) = 351 (M^+, 100); FT-IR (ATR): ν (cm^{-1}): 3100, 2910, 2804 (CH, CH_3,CH_2); 1599, 1582, 1564 (terpyridine); UV/vis (CH_3CN): λ / nm (ε / L mol^{-1} cm^{-1}): 277 (24900), 240 (26900); Anal. Calcd for $C_{20}H_{21}N_3O_3$ (351.41): C, 68.36; H, 6.02; N, 11.96. Found: C, 67.97; H, 6.17; N, 11.75.

4'-(4-Methylbenzyloxy)-2,2';6',2''-terpyridine (4)

To a solution of **1** (7.00 g, 28 mmol) and K_2CO_3 (12.94 g, 90 mmol) in dry DMF (50 mL) at 50 °C was added dropwise a solution of α-bromo-*p*-xylene (4.92 g, 27 mmol) in dry DMF (20 mL). Stirring was continued overnight, after which the reaction mixture was poured in 0.01 M HCl in water (100 mL) and extracted with CH_2Cl_2 (3 × 100 mL). The combined organic layers were dried over Na_2SO_4, filtered and evaporated *in vacuo*. The crude product was purified by column chromatography (AlOx, CH_2Cl_2) and recrystallized from ethanol to yield light-yellow needles. Yield: 6.42 g (68%). ^{1}H-NMR ($CDCl_3$): δ = 8.68 (dd, 2 H, ^3J = 4.8, ^4J = 1.8; $H_{6,6''}$), 8.61 (dd, 2 H, ^3J = 8.0, ^4J = 1.0; $H_{3,3''}$), 8.11 (s, 2 H; $H_{3',5'}$),

7.83 (td, 2 H, ^3J = 7.8, ^4J = 1.8 Hz; $H_{4,4"}$), 7.36, (d, 2 H, ^3J = 7.2 Hz; *o*-CH phenyl), 7.31 (ddd, 4 H, ^3J = 8.0, ^3J = 4.8 Hz, ^4J= 1.0 Hz; $H_{5,5"}$), 7.20 (d, 2 H, ^3J = 7.2 Hz; *m*-CH phenyl), 5.27 (s, 2 H; tpyOCH_2), 2.36 (s, 3 H; CH_3). ^{13}C NMR ($CDCl_3$): δ = 167.0 ($C_{4'}$), 157.1 ($C_{2',6'}$), 156.1 ($C_{2,2"}$), 149.0 ($C_{6,6"}$), 137.9 (*p*-C phenyl), 136.7 ($C_{3',5'}$), 133.0 (C-1 phenyl), 129.3 (*m*-C phenyl), 127.6 (*o*-C phenyl), 123.8 ($C_{3,3"}$), 121.3 ($C_{4,4"}$), 107.6 ($C_{5,5"}$), 69.9 (tpyOCH_2), 21.2 (CH_3). GC-MS (EI): *m/z* (%) = 353 (M^+, 100); FT-IR (ATR): ν (cm^{-1}): 3055, 3018, 2933, 2876 (CH, CH_3, CH_2); 1598, 1580, 1560 (terpyridine); UV/vis (CH_3CN): λ / nm (ε / L mol^{-1} cm^{-1}): 277 (23800), 239 (29000); Anal. Calcd for $C_{23}H_{19}N_3O$ (353.42): C, 78.13; H, 5.42; N, 11.89. Found: C, 78.14; H, 5.43; N, 11.60.

General procedure for the synthesis of bis-terpyridine metal complexes of 3

A solution of **3** (100 mg, 285 μmol) and exactly half an equimolar amount of the appropriate metal-acetate salt (143 μmol, i.e. 35, 25, 35, 36, 29, 31, 35 and 45 mg for Mn, Fe, Co, Ni, Cu, Zn, Cd and Hg respectively) in methanol (10 mL) was stirred for three hours at reflux. Then a ten-fold excess of NH_4PF_6 (0.5 g, 3 mmol) in methanol (5 mL) was added and the solution was allowed to cool to room temperature. Usually a precipitate formed, which was isolated by filtration. The residue was washed with ice-cold methanol (2 ×) followed by water (3 ×) and diethyl ether (2 ×). If no precipitate had formed after cooling to room temperature, the solution was allowed to stand overnight in the fridge (4 °C). The precipitate that formed then was subjected to the same work-up procedure as described above.

Mn^{II}: yellow solid, yield: 116 mg (78%); MALDI-TOF MS: 757 (M^+ - $2PF_6$); UV/vis: λ / nm (ε / L mol^{-1} cm^{-1}): 325 (22500), 312 (22300), 274 (38800), 248 (42700); FT-IR (ATR): ν / cm^{-1}: 2878 (CH_2,CH_3) 1615, 1602, 1574, 1562 (tpy), 827 (PF_6); Anal. Calcd. for $C_{40}H_{42}N_6O_6P_2F_{12}Mn$ (1047.68): C, 45.86; H, 4.04; N, 8.02; Found: C, 45.47; H, 4.02; N, 8.22.

Fe^{II}: purple solid, yield: 82 mg (55%); ^{1}H-NMR (CD_3CN): δ = 8.50 (s, 4 H, $H_{3',5'}$), 8.45 (d, 4 H, ^3J = 8.0 Hz; $H_{3,3"}$), 7.88 (td, 4 H, ^3J = 8.0, ^4J = 1.6 Hz; $H_{4,4"}$), 7.17 (d, 4 H, ^3J = 5.2 Hz; $H_{6,6"}$), 7.08 (dd, 4 H, ^3J = 8.2, ^3J = 5.2 Hz; $H_{5,5"}$), 4.75 (t, 4 H, ^3J = 4.4 Hz; tpyOCH_2), 4.10 (t, 4 H, ^3J = 4.2 Hz; tpyOCH_2CH_2), 3.80 (m, 4 H; CH_2OCH_2), 3.61 (m, 4 H; CH_2OCH_3), 3.36 (s, 6 H; OCH_3); ^{13}C-NMR (CD_3CN): δ = 168.6, 161.6, 158.8, 154.1, 139.2, 128.0, 124.4, 112.3, 72.7, 71.4, 71.0, 69.9, 59.0 (OCH_3); MALDI-TOF MS: 903 (M^+ - PF_6), 758 (M^+ - $2PF_6$); UV/vis: λ / nm (ε / L mol^{-1} cm^{-1}): 555 (11750), shoulder at 505 (7880), 361 (4790), 315 (39280), 271 (54150), 245 (47590); FT-IR (ATR): ν / cm^{-1}: 2879 (CH_2,CH_3) 1615, 1601, 1563, 1552 (tpy), 827 (PF_6); Anal. Calcd. for $C_{40}H_{42}N_6O_6P_2F_{12}Fe$ (1048.59): C, 45.82; H, 4.04; N, 8.01; Found: C, 46.11; H, 4.08; N, 7.63.

Co^{II}: light-brown solid, yield: 94 mg (63%); ^{1}H-NMR (CD_3CN): δ = 111.39 (bs, 2 H; $H_{6,6"}$), 74.20 (bs, 4 H; $H_{3',5'}$), 70.16 (bs, 4 H; $H_{5,5"}$), 34.59 (bs, 4 H; $H_{3,3"}$), 14.88 (t, 4 H, ^3J = 4.0 Hz; tpyOCH_2), 9.41 (t, 2 H, ^3J = 4.8 Hz; tpyOCH_2CH_2), 7.12 (t, 4 H, ^3J = 3.8 Hz; CH_2OCH_2), 6.54 (bs, 4 H, $H_{4,4"}$), 5.96 (t, 4 H, ^3J = 4.0 Hz; CH_2OCH_3), 4.66 (s, 6 H, OCH_3); MALDI-TOF MS: 906 (M^+ - PF_6), 761 (M^+ - $2PF_6$); UV/vis: λ / nm (ε / L mol^{-1} cm^{-1}): 505 (700), 450 (1000), 306 (26500), 271 (45600), 245 (52300); FT-IR (ATR): ν / cm^{-1}: 2879 (CH_2, CH_3), 1615, 1603, 1573, 1561 (tpy), 828 (PF_6); Anal. Calcd. for $C_{40}H_{42}N_6O_6P_2F_{12}Co$ (1051.67): C, 45.68; H, 4.03; N, 7.99; Found: C, 45.34; H, 4.07, N, 7.71.

Ni^{II}: grey solid, yield: 127 mg (85%); MALDI-TOF MS: 905 (M^+ - PF_6), 760 (M^+ - $2PF_6$); UV/vis: λ / nm (ε / L mol^{-1} cm^{-1}): 325 (18800), 312 (23700), 300 (25100), 273 (51900), 243 (49600); FT-IR (ATR): ν / cm^{-1}: 2928 (CH_2,CH_3), 1614, 1603, 1571, 1563 (tpy), 830 (PF_6); Anal. Calcd. for $C_{40}H_{42}N_6O_6P_2F_{12}Ni$ (1051.43): C, 45.69; H, 4.03; N, 7.99; Found: C, 45.63; H, 4.07; N, 7.64.

Cu^{II}: blue solid, yield: 108 mg (72%); MALDI-TOF MS: 765 (M^+-$2PF_6$): UV/vis: λ /nm (ε / L mol^{-1} cm^{-1}): 310 (20700), 271 (47200), 246 (57700); FT-IR (ATR): ν / cm^{-1}: 2882 (CH_2,CH_3) 1616, 1601, 1575, 1561 (tpy), 827 (PF_6); Anal. Calcd. for $C_{40}H_{42}N_6O_6P_2F_{12}Cu$ (1056.29): C, 45.48; H, 4.01; N, 7.96; Found: C, 45.60; H, 3.99; N, 7.67.

Zn^{II}: white solid, yield: 86 mg (57%); ^{1}H-NMR (CD_3CN): δ = 8.54 (d, 4 H, ^3J = 8.0 Hz; $H_{3,3"}$), 8.23 (s, 4 H, $H_{3',5'}$), 8.13 (td, 4 H, ^3J = 8.0, ^4J = 1.6 Hz; $H_{4,4"}$), 7.77 (d, 4 H, ^3J = 5.4 Hz; $H_{6,6"}$), 7.38 (ddd, 4 H, ^3J = 8.0, ^3J = 5.4, ^4J= 1.4 Hz; $H_{5,5"}$), 4.67 (t, 4 H, ^3J = 4.4 Hz; tpyOCH_2), 4.02 (t, 4 H, ^3J = 4.0 Hz; tpyOCH_2CH_2), 3.75 (m, 4 H, CH_2OCH_2), 3.57 (m, 4 H, CH_2OCH_3), 3.33 (s, 6 H, OCH_3); ^{13}C-NMR (CD_3CN): δ = 172.0, 151.8, 148.7, 148.6, 141.9, 128.2, 123.7, 111.0, 72.6, 71.4, 71.1, 69.8, 59.0; MALDI-TOF MS: 768 (M^+ - $2PF_6$); UV/Vis: λ / nm (ε / L mol^{-1} cm^{-1}): 320 (26770), 307 (25120), 271

(42790), 241 (56920); FT-IR (ATR): ν / cm^{-1}: 2929 (CH_2,CH_3), 1615, 1603, 1574, 1563 (tpy), 832 (PF_6).

Cd^{II}: white solid, yield: 109 mg (66%); ^{1}H-NMR (CD_3CN): δ = 8.59 (d, 4 H, ^3J = 8.0 Hz; $H_{3,3''}$), 8.20 (s, 4 H, $H_{3',5'}$), 8.17 (td, 4 H, ^3J = 8.0, ^4J = 1.8 Hz; $H_{4,4''}$), 8.03 (d, 4 H, ^3J = 5.0 Hz; $H_{6,6''}$), 7.48 (dd, 4 H, ^3J = 8.2, ^3J = 5.4; $H_{5,5''}$), 4.65 (t, 4 H, ^3J = 4.4 Hz; tpyOCH_2), 4.01 (t, 4 H, ^3J = 4.0 Hz; tpyOCH_2CH_2), 3.74 (m, 4 H, CH_2OCH_2), 3.57 (m, 4 H, CH_2OCH_3), 3.33 (s, 6 H, OCH_3) ^{13}C-NMR (CD_3CN): δ = 171.4, 152.2, 150.2, 149.6, 141.2, 128.0, 124.3, 111.4, 72.6, 71.4, 70.8, 69.8, 59.0 (OCH_3); MALDI-TOF MS: 961 (M^+ - PF_6), 816 (M^+ - 2PF_6); UV/Vis: λ / nm (ε / L mol^{-1} cm^{-1}): shoulder at 322 (16810), 311 (21250), 273 (42570), 244 (54680); FT-IR (ATR): ν / cm^{-1}: 2934 (CH_2,CH_3), shoulder at 1608, 1599, 1575, 1563 (tpy), 829 (PF_6); Anal. Calcd. for $C_{40}H_{42}N_6O_6P_2F_{12}Cd$ (1105.15): C, 43.47; H, 3.83; N, 7.60; Found: C, 43.01; H, 3.73; N, 7.77.

Hg^{II}: white solid, yield: 101 mg (59%); ^{1}H-NMR (CD_3CN): δ = 8.62 (d, 4 H, ^3J = 8.0 Hz; $H_{3,3''}$), 8.26 (s, 4 H, $H_{3',5'}$), 8.19 (t, 4 H, ^3J = 8.0 Hz; $H_{4,4''}$), 8.03 (bs, 4 H, $H_{6,6''}$), 7.55 (m, 4 H; $H_{5,5''}$), 4.68 (t, 4 H, ^3J = 4.4 Hz; tpyOCH_2), 4.00 (t, 4 H, ^3J = 4.0 Hz; tpyOCH_2CH_2), 3.75 (m, 4 H, CH_2OCH_2), 3.57 (m, 4 H, CH_2OCH_3), 3.34 (s, 6 H, OCH_3); ^{13}C-NMR (CD_3CN): δ = 171.0, 150.8, 150.0, 147.6, 141.7, 128.1, 124.6, 112.0, 72.6, 71.3, 70.8, 69.8, 58.9 (OCH_3); MALDI-TOF MS: 961 (M^+ - PF_6), 816 (M^+ - 2PF_6); UV/Vis: λ / nm (ε / L mol^{-1} cm^{-1}): 322 (20240), 310 (20570), 274 (33250), 243 (42660); FT-IR (ATR): ν / cm^{-1}: 2894 (CH_2,CH_3), shoulder at 1610, 1597, 1576, 1562 (tpy), 828 (PF_6).

General procedure for the synthesis of bis-terpyridine metal complexes of 4

A solution of **4** (100 mg, 282 μmol) and exactly half an equimolar amount of the appropriate metal-acetate salt (141 μmol, i.e. 35, 25, 35, 36, 29, 31, 35 and 45 mg for Mn, Fe, Co, Ni, Cu, Zn, Cd and Hg respectively) in a 1:1 solvent mixture of methanol and chloroform (10 mL) was stirred for three hours at reflux. Then a ten-fold excess of NH_4PF_6 (0.5 g, 3 mmol) in methanol (5 mL) was added and the solution was allowed to cool to room temperature. In many cases immediately after counter-ion exchange a precipitate formed, which was isolated by filtration. The residue was washed with ice-cold 1:1 methanol:chloroform (2 ×) followed by water (3 ×) and diethyl ether (2 ×). Single crystals suitable for X-Ray analysis were grown by the vapor diffusion of diisopropyl ether into a solution of the complex in acetonitril unless stated otherwise. A hyperlink gives access to all relevant crystallographic data.

Mn^{II}: yellow solid, yield: 121 mg (82%); MALDI-TOF MS: UV/Vis (CH_3CN): λ / nm (ε / L mol^{-1} cm^{-1}): 325 (25900), 312 (26100), 274 (50800), 249 (54100); FT-IR (ATR): ν / cm^{-1}: 1613, 1600, 1572, 1560 (terpyridine); 827 (PF_6). Anal. Calcd. for $C_{46}H_{38}N_6O_2P_2F_{12}Mn$ (1051.72): C, 52.53; H, 3.69; N, 7.99; Found: C, 52.20; H, 3.60; N, 7.64; Crystallographic data: monoclinic, P2(1)/c; a = 9.003(7), b = 14.208(8), c = 36.022(5) Å; α = 90 °, β = 93.599(3) °, γ = 90 °; ρ = 1.519 Mg m^{-3}.

Fe^{II}: purple solid, yield: 63 mg (42%); ^{1}H-NMR (CD_3CN): δ = 8.84 (s, 4 H, $H_{3',5'}$), 8.67 (d, 4 H, ^3J = 8.0 Hz; $H_{3,3''}$), 7.91 (t, 4 H, ^3J = 8.0 Hz; $H_{4,4''}$), 7.52 (d, 4 H, ^3J = 7.2 Hz; *o-H* phenyl), 7.40 (d, 4 H, ^3J = 6.0 Hz; $H_{6,6''}$), 7.28 (m, 4 H; $H_{5,5''}$), 7.14 (d, 4 H, ^3J = 7.2 Hz; *m-H* phenyl), 5.62 (s, 4 H, tpyOCH_2), 2.32 (s, 6 H, CH_3); MALDI-TOF MS: UV/Vis (CH_3CN): λ / nm (ε / L mol^{-1} cm^{-1}): 556 (11600), shoulder at 505 (7800), 359 (5700), 316 (37800), 273 (58800), 244 (49626); FT-IR (ATR): ν / cm^{-1}: 1617, 1564, 1554 (terpyridine), 825 (PF_6); Crystallographic data: monoclinic, P2(1)/c; a = 19.458(4), b = 15.539(4), c = 15.999(7) Å; α = 90 °, β = 110.248(2) °, γ = 90 °; ρ = 1.540 Mg m^{-3}.

Co^{II}: brown solid, yield: 119 mg (80%); ^{1}H-NMR (CD_3CN): δ = 113.81 (bs, 2 H; $H_{6,6''}$), 76.79 (bs, 4 H; $H_{3',5'}$), 71.82 (bs, 4 H; $H_{5,5''}$), 35.13 (bs, 4 H; $H_{3,3''}$), 16.27 (bs, 4 H; *o*-H phenyl), 12.88 (bs, 4 H; tpyOCH_2), 9.89 (bs, 4 H; *m*-H phenyl), 6.40 (bs, 4 H; $H_{4,4''}$), 3.92 (bs, 6 H; OCH_3); MALDI-TOF MS: 910 (M^+-PF_6), 766 (M^+-2PF_6); UV/Vis (CH_3CN): λ / nm (ε / L mol^{-1} cm^{-1}): 498 (700), 450 (1000), 306 (27000), 271 (51200), 246 (56300); FT-IR (ATR): ν / cm^{-1}: 1617, 1604, 1571, 1560 (terpyridine); 827 (PF_6). Anal. Calcd. for $C_{46}H_{38}N_6O_2P_2F_{12}Co$ (1055.71): C, 52.34; H, 3.63; N, 7.96; Found: C, 52.06; H, 3.63; N, 7.90; Crystallographic data: monoclinic, P2(1)/c; a = 19.617(5), b = 15.492(4), c = 16.003(4) Å; α = 90 °, β = 110.315(5) °, γ = 90 °; ρ = 1.537 Mg m^{-3}.

Ni^{II}: grey-brown solid, yield: 106 mg (71%); MALDI-TOF MS: UV/Vis (CH_3CN): λ / nm (ε / L mol^{-1} cm^{-1}): 325 (19400), 312 (25100), shoulder at 299 (26900), 273 (62000), 244 (55500); FT-IR (ATR): ν /

cm^{-1}: 1615, 1604, 1572, 1562 (terpyridine); 826 (PF_6); Crystallographic data: monoclinic, P2(1)/c; a = 19.6847(8), b = 15.5312(6), c = 16.0512(7) Å; α = 90 °, β = 110.570(1) °, γ = 90 °; ρ = 1.526 Mg m^{-3}.

Cu^{II}: blue solid, yield: 97 mg (65%); MALDI-TOF MS: 769 (M^+-2PF_6); UV/Vis (CH_3CN): λ / nm (ε / L mol^{-1} cm^{-1}): 312 (22000), 250 (60100); FT-IR (ATR): ν / cm^{-1}: 1618, 1599, 1574, 1561 (tpy); 829 (PF_6). Anal. Calcd. for $C_{46}H_{38}N_6O_2P_2F_{12}Cu$ (1060.33): C, 52.11; H, 3.61; N, 7.93; Found: C, 52.27; H, 3.69; N, 7.47; Crystallographic data: monoclinic, P2(1); a = 19.6635(7), b = 15.5270(6), c = 16.0390(6) Å; α = 90 °, β = 109.934(0) °, γ = 90 °; ρ = 1.530 Mg m^{-3}.

Zn^{II}: white solid, yield: 98 mg (65%); ^{1}H-NMR (CD_3CN): δ = 8.53 (d, 4 H, ^3J = 8.0 Hz; $H_{3,3''}$), 8.28 (s, 4 H, $H_{3',5'}$), 8.16 (t, 4 H; ^3J = 7.8 Hz; $H_{4,4''}$), 7.78 (d, 4 H; ^3J = 5.6 Hz; $H_{6,6''}$), 7.55 (m, 8 H; $H_{5,5''}$, *o-H* phenyl), 7.38 (d, 4 H; ^3J = 7.0 Hz; *m-H* phenyl), 5.57 (s, 4 H; tpyOCH_2), 2.42 (s, 6 H; CH_3); ^{13}C-NMR (CD_3CN): δ = 171.5, 151.3, 148.1, 141.4, 139.3, 132.3, 129.8, 128.7, 127.7, 123.1, 110.5, 72.2 (CH_2), 20.6 (CH_3); MALDI-TOF MS: 909 (M^+-PF_6), 764 (M^+-2PF_6); UV/Vis (CH_3CN): λ / nm (ε / L mol^{-1} cm^{-1}): 322 (29000), 310 (26800), 274 (47600), 244 (60300); FT-IR (ATR): ν / cm^{-1}: 1615, 1601, 1574, 1563 (tpy); 829 (PF_6). Anal. Calcd. for $C_{46}H_{38}N_6O_2P_2F_{12}Zn$ (1062.17): C, 52.02; H, 3.61; N, 7.91; Found: C, 52.12; H, 3.69; N, 7.81; Crystallographic data: monoclinic, C2/c; a = 45.024(9), b = 9.141(0), c = 26.577(5) Å; α = 90 °, β = 122.40(3) °, γ = 90 °; ρ = 1.459 Mg m^{-3}.

Cd^{II}: white solid, yield: 120 mg (77%); ^{1}H-NMR (CD_3CN): δ = 8.57 (d, 4 H; ^3J = 8.4 Hz; $H_{3,3''}$), 8.25 (s, 4 H, $H_{3',5'}$), 8.19 (t, 4 H; ^3J = 8.2 Hz; $H_{4,4''}$), 8.03 (d, 4 H; ^3J = 6.2 Hz; $H_{6,6''}$), 7.54 (d, 4 H; ^3J = 7.6 Hz; *o-H* phenyl), 7.49 (m, 4 H; $H_{5,5''}$), 7.36 (d, 4 H, ^3J = 7.4 Hz; *m-H* phenyl), 5.57 (s, 4 H; tpyOCH_2), 2.42 (s, 6 H; CH_3); ^{13}C-NMR (CD_3CN): δ = 170.6, 151.6, 149.6, 148.9, 141.4, 139.0, 132.4, 129.6, 128.6, 127.4, 123.5, 110.8, 71.8 (CH_2), 20.5 (CH_3); MALDI-TOF MS: 965 (M^+-PF_6); UV/Vis (CH_3CN): λ / nm (ε / L mol^{-1} cm^{-1}): 322 (26200), 310 (27300), 274 (49000), 244 (61100); FT-IR (ATR): ν / cm^{-1}: 1613, 1599, 1575, 1562 (tpy); 829 (PF_6). Anal. Calcd. for $C_{46}H_{38}N_6O_2P_2F_{12}Cd$ (1109.19): C, 49.81; H, 3.45; N, 7.58; Found: C, 49.44; H, 3.37; N, 7.27.

Hg^{II}: white solid, yield: 83 mg (49%); ^{1}H-NMR (CD_3CN): δ = 8.59 (d, 4 H, ^3J = 8.0 Hz; $H_{3,3''}$), 8.30 (s, 4 H; $H_{3',5'}$), 8.18 (t, 4 H, ^3J = 7.8 Hz; $H_{4,4''}$), 8.02 (d, 4 H, ^3J = 4.8 Hz; $H_{6,6''}$), 7.54 (m, 8 H; *o-H* phenyl, $H_{5,5''}$), 7.36 (d, 4 H, ^3J = 7.6 Hz; *m-H* phenyl), 5.56 (s, 4 H; tpyOCH_2), 2.42 (s, 6 H; CH_3); MALDI-TOF MS: 1053 (M^+-PF_6); UV/Vis (CH_3CN): λ / nm (ε / L mol^{-1} cm^{-1}): shoulder 322 (18900), 311 (23100), 273 (46000), 245 (58300); FT-IR (ATR): ν / cm^{-1}: 1612, 1596, 1575, 1562 (tpy); 829 (PF_6).

Mono-4'-(2-[1-methoxyethoxy]ethoxy)-2,2';6',2''-terpyridine-dichlorocarbonyl-ruthenium(III) chloride (5)

To a suspension of $RuCl_3$ (142 mg, 0.68 mmol) in dry argon-purged DMF (5 mL) at 130 °C was added dropwise a solution of **3** (200 mg, 0.57 mmol) in dry DMF (10 mL). The suspension was stirred overnight, after which the solution was filtered. The filtrate was partitioned between 0.1 M HCl and CH_2Cl_2. The organic layer was separated, dried over Na_2SO_4 and evaporated *in vacuo*. The brown residue that formed was solubilized in acetonitril and precipitated into diethyl ether, filtered and washed with ice-cold ethanol until the washing fluid was colorless. Subsequently the residue was washed with water (2 ×) and diethyl ether (2 ×). After drying a fine brown powder was obtained (241 mg, 72%); UV/vis (CH_3CN): λ / nm (ε / L mol^{-1} cm^{-1}): shoulder at 460 (2100), 396 (5000), 308 (9800), 275 (17400), 227 (21700); FT-IR (ATR): ν / cm^{-1}: 3064, 2880 (CH, CH_3); 1941 (C=O), 1600, 1552 (tpy). Anal. Calcd. for $C_{21}H_{21}N_3O_4RuCl_3$ (586.87): C, 42.98; H, 3.61; N, 7.16; Found: C, 42.64; H, 3.86; N, 7.30.

Mono-4'-(4-methylbenzyloxy)-2,2';6',2''-terpyridine-trichlororuthenium(III) (6)

To a solution of $RuCl_3 \times 3\ H_2O$ (300 mg, 1.13 mmol) in refluxing ethanol (5 mL) was added dropwise a solution of **4** (200 mg, 0.57 mmol) in ethanol (10 mL). The solution was refluxed for four hours, after which a brown precipitate had formed. The solution was allowed to cool to room temperature and was then filtered, washed with ethanol until the washing fluid was colorless. Subsequently the residue was washed with water (2 ×) and diethyl ether (2 ×). After drying a dark brown powder was obtained (223 mg, 70%). UV/vis (CH_3CN): λ / nm (ε / L mol^{-1} cm^{-1}): 400 (6900), 275 (19800); FT-IR (ATR): ν / cm^{-1}: 3074, 2885 (CH, CH_3); 1612, 1602, 1564, 1554 (tpy); Anal. Calcd. for $C_{23}H_{19}N_3ORuCl_3$ (560.87): C, 49.25; H, 3.41; N, 7.49; Found: C, 48.99; H, 3.62; N, 7.19. Single crystals were grown by vapour diffusion of diisopropyl ether into a DMF-solution containing the compound (in 10 days).

***Bis*-4'-(2-[1-methoxyethoxy]ethoxy)-2,2';6',2''-terpyridine ruthenium(II) dihexafluorophosphate (7)**

A solution of **3** (30.0 mg, 30 μmol) and **5** (50.0 mg, 85 μmol) was heated to reflux in methanol (5 mL). After 15 minutes a few drops of *N*-ethylmorpholine were added and the reaction mixture turned from brown to purple. Stirring was continued overnight or until an intense red color appeared. Then 1 mL of a 0.01 M solution of NH_4PF_6 in methanol was added and the reaction mixture was allowed to cool to room temperature. The red precipitate was filtered, washed with methanol (2 ×), water (2 ×) and diethyl ether (2 ×). The crude product was purified by column chromatography (silica, acetonitril:water:KNO_3(aq) in a 14:2:1 ratio). The purified product was extracted from a 0.01 M NH_4PF_6 solution in water into chloroform. The organic layer was washed three times with water and evaporated *in vacuo*. The product was isolated by precipitation from acetonitril into diethyl ether. Yield: (68 mg, 73%). ^{1}H-NMR (CD_3CN): δ = 8.50 (d, 4 H, ^3J = 8.0 Hz; $H_{3,3''}$), 8.35 (s, 4 H, $H_{3',5'}$), 7.91 (t, 4 H, ^3J = 8.0 Hz; $H_{4,4''}$), 7.41 (d, 4 H, ^3J = 4.8 Hz; $H_{6,6''}$), 7.17 (m, 4 H; $H_{5,5''}$), 4.72 (m, 4 H, tpyOCH_2), 4.08 (m, 4 H, tpyOCH$_2$CH_2), 3.80 (m, 4 H, CH$_2$OCH_2), 3.61 (m, 4 H, CH_2OCH$_3$), 3.37 (s, 6 H, OCH$_3$); ^{13}C-NMR (CD_3CN): δ = 166.8, 159.2, 157.4, 153.4, 138.7, 128.3, 125.2, 112.0, 72.6, 71.4, 70.8, 69.9, 58.9 (OCH$_3$); MALDI-TOF MS: 950 (M^+ - PF_6), 804 (M^+ - 2PF_6); UV/Vis: λ / nm (ε / L mol^{-1} cm^{-1}): 485 (15100), shoulder at 456 (11700), 344 (5670), 303 (56500), 266 (48700), 241 (46900); FT-IR (ATR): ν / cm^{-1}: 2925 (CH_2, CH_3); 1614, 1603, 1572, 1559 (tpy); 829 (PF_6). Anal. Calcd. for $C_{40}H_{42}N_6O_6P_2F_{12}Ru$ (1093.81): C, 43.92; H, 3.87; N, 7.68; Found: C, 43.41; H, 3.48 N, 7.96.

***Bis*-4'-(4-methylbenzyloxy)-2,2';6',2''-terpyridine ruthenium(II) dihexafluorophosphate (9)**

A solution of **4** (31.5 mg, 89 μmol) and **6** (50.0 mg, 89 μmol) was heated to reflux in methanol. After 15 minutes a few drops of *N*-ethylmorpholine were added and the reaction mixture turned from brown to purple. Stirring was continued overnight or until an intense red color appeared. Then a solution of NH_4PF_6 in methanol was added and the reaction mixture was allowed to cool to room temperature. The red precipitate was filtered, washed with with methanol (2 ×), water (2 ×) and diethyl ether (2 ×). The crude product was purified by column chromatography (silica, acetonitril:water:KNO_3(aq) in a 14:2:1 ratio). The purified product was extracted from a 0.01 M NH_4PF_6 solution in water into chloroform. The organic layer was washed three times with water and evaporated *in vacuo*. Yield: 54 mg, (56%). ^{1}H-NMR (CD_3CN): δ = 8.45 (d, 4 H, ^3J = 8.0 Hz; $H_{3,3''}$), 8.39 (s, 4 H, $H_{3',5'}$), 7.89 (td, 4 H, ^3J = 8.0, ^4J = 1.4 Hz; $H_{4,4''}$), 7.56 (d, 4 H, ^3J = 7.2 Hz; *o*-H phenyl), 7.38 (m, 8 H, *m*-H phenyl; $H_{6,6''}$), 7.15 (dd, 4 H, ^3J = 8.0, ^3J = 5.7 Hz; $H_{5,5''}$), 5.56 (s, 4 H; tpyOCH$_2$), 2.42 (s, 6 H; CH$_3$). MALDI-TOF MS: 953 (M^+-PF_6); UV/Vis (CH_3CN): λ / nm (ε / L mol^{-1} cm^{-1}): 485 (17800), shoulder at 447 (11900), shoulder at 343 (6300), 304 (62600), 268 (61700), 242 (55400). FT-IR (ATR): ν / cm^{-1}: 3120, 2926 (CH, CH_2, CH_3), 1614, 1560, 1548 (tpy), 824 (PF_6). Anal. Calcd. for $C_{46}H_{38}N_6O_2P_2F_{12}Ru$ (1097.84): C, 50.33; H, 3.49; N, 7.66; Found: C, 50.18; H, 3.54; N, 7.41.

4'-(4-Methylbenzyloxy)-2,2';6',2''-terpyridine-4'-(2-[1-methoxyethoxy]ethoxy)-2,2';6',2''-terpyridine ruthenium(II) dihexafluorophosphate (8)

A solution of **3** (62.5 mg, 0.18 mmol) and **6** (100 mg, 0.18 mmol) was heated to reflux in methanol (10 mL). After 15 minutes a few drops of *N*-ethylmorpholine were added and the reaction mixture turned from brown to purple. Stirring was continued overnight or until an intense red color appeared. Then a 0.01 M solution of NH_4PF_6 in methanol was added (1 mL) and the reaction mixture was allowed to cool to room temperature. The red precipitate was filtered, washed with methanol (2 ×), water (2 ×) and diethyl ether (2 ×). The crude product was purified by column chromatography (silica, acetonitril:water:KNO_3(aq) in a 14:2:1 ratio). The purified product was extracted from a 0.01 M NH_4PF_6 solution in water into chloroform. The organic layer was washed three times with water and evaporated *in vacuo*. Yield: 158 mg, (81%). ^{1}H-NMR (CD_3CN): δ = 8.57 (d, 4 H, ^3J = 8.2 Hz; $H_{3,3''}$ phenyl), 8.53 (d, 4 H, ^3J = 8.2 Hz; $H_{3,3''}$), 8.47 (s, 2 H, $H_{3',5'}$ phenyl), 8.42 (s, 2 H, $H_{3',5'}$), 7.97 (t, 4 H, ^3J = 8.2 Hz; $H_{4,4''}$), 7.65 (d, 2 H, ^3J = 7.8 Hz; *o*-C*H* phenyl), 7.45 (m, 6 H, *m*-C*H* phenyl; $H_{6,6''}$), 7.24 (m, 4 H; $H_{5,5''}$), 5.64 (s, 2 H; tpyOCH_2 phenyl), 4.74 (m, 2 H; tpyOCH_2), 4.12 (m, 2 H; CH_2OCH$_2$), 3.84 (m, 2 H; CH$_2$OCH_2), 3.67 (m, 2 H; CH_2OCH$_3$), 3.42 (s, 3 H; OCH$_3$), 2.51 (s, 3 H; CH$_3$ phenyl). ^{13}C-NMR (CD_3CN): 166.0, 165.9, 158.4, 156.6, 156.5, 152.7, 139.0, 137.9, 137.8, 132.6, 129.7, 128.5, 127.5, 124.4, 124.3, 117.5, 111.3, 111. 2, 71.9, 71.8, 70.5 (*C*H$_2$OCH$_2$), 69.9 (CH$_2$O*C*H$_2$), 69.1 (*C*H$_2$OCH$_3$), 58.1 (OCH$_3$), 20.4 (CH$_3$). MALDI-TOF MS: m/z = 951 (M^+-PF_6); UV/Vis (CH_3CN): λ / nm (ε / L mol^{-1} cm^{-1}): 485 (17500), shoulder at 451 (12800), shoulder at 342 (6500), 304 (62000), 267 (55700), 242 (51800), ; FT-IR (ATR): ν / cm^{-1}: 3100, 2927 (CH, CH_2, CH_3); 1618, 1564 (tpy); 833 (PF_6). Anal. Calcd. for $C_{43}H_{40}N_6O_4P_2F_{12}Ru$ (1095.83): C, 47.13; H, 3.68; N, 7.67; Found: C, 47.01; H, 3.85, N, 7.49.

4'-(2-[1-Methoxyethoxy]ethoxy)-2,2';6',2''-terpyridine-trinitro-cobalt(III) (10)
A stream of air was bubbled through a solution of $Co(NO_3)_2 \times 6\ H_2O$ (1.05 g, 3.6 mmol), $NaNO_2$ (1.09 g, 16.3 mmol), NaOH (0.29 g, 7.2 mmol) and acetic acid (0.87 g, 14.5 mmol) in water (1.5 mL) at room temperature. After 15 minutes the color had changed from brown to orange. At this moment a solution of **3** (1.00 g, 2.8 mmol) in ethanol (3 mL) was added instantaneously. An orange precipitate immediately starts to form. After 15 minutes the orange precipitate was isolated by filtration. The residue was washed with ethanol (3 ×), water (3 ×) and diethyl ether (2 ×). After drying under vacuum the yield was 1.07 g (70%). ^{1}H-NMR (DMSO-d_6): δ = 8.96 (d, 2 H, ^3J = 5.4 Hz; $H_{6,6''}$), 8.80 (d, 2 H, ^3J = 7.8 Hz; $H_{3,3''}$), 8.61 (s, 2 H; $H_{3',5'}$), 8.48 (t, 2 H, ^3J = 7.8 Hz; $H_{4,4''}$), 8.00 (t, 2 H, ^3J = 6.6 Hz; $H_{5,5''}$), 4.67 (t, 2 H, ^3J = 4.4 Hz; tpyOCH_2), 3.95 (t, 2 H, , ^3J = 4.4 Hz; CH_2OCH$_2$), 3.69 (t, 2 H, ^3J = 4.4 Hz; CH$_2$OCH_2), 3.52 (t, 2 H, ^3J = 4.4 Hz; CH_2OCH$_3$), 3.36 (s, 3 H, OCH$_3$). ^{13}C-NMR (CD_3CN): δ = 170.0, 156.2, 155.8, 152.8, 141.5, 128.2, 124.0, 111.2, 71.3, 69.8, 68.4, 58.1 (OCH$_3$). MALDI-TOF MS: m/z = 546 (M^+-H^+); UV/Vis (CH_3CN): λ / nm (ε / L mol^{-1} cm^{-1}): 359 (6700), 306 (12200), 281 (21900), 273 (21100), 254 (22800); FT-IR (ATR): ν / cm^{-1}: 3100, 2927 (CH, CH$_2$, CH$_3$); 1618, 1610, 1569 (tpy); 1401, 1306 (NO_2). Anal. Calcd. for $C_{20}H_{21}N_6O_9Co$ (548.36): C, 43.81; H, 3.86; N, 15.33; Found: C, 43.33; H, 3.81; N, 15.07.

4'-(2-[1-Methoxyethoxy]ethoxy)-2,2';6',2''-terpyridine-trichloro-cobalt(III) (11)
Concentrated hydrochloric acid (15 mL) was added to **10** (500 mg, 0.91 mmol) and heated to 40 °C. From the red solution a brown-green substance precipitates. After 5 minutes of continued stirring the precipitate was isolated by filtration and washed with concentrated HCl (2 ×), 1 M HCl (2 ×), water (4 ×), acetone (3 ×) and diethyl ether (2 ×). After drying under vacuum the yield was 352 mg (75%). ^{1}H-NMR (DMSO-d_6): δ = 9.71 (d, 2 H, ^3J = 5.0 Hz; $H_{6,6''}$), 8.81 (d, 2 H, ^3J = 8.0 Hz; $H_{3,3''}$), 8.61 (s, 2 H, $H_{3',5'}$), 8.43 (t, 2 H, ^3J = 7.8 Hz; $H_{4,4''}$), 7.95 (t, 2 H, ^3J = 6.6 Hz; $H_{5,5''}$), 4.68 (t, 2 H, ^3J = 4.6 Hz; tpyOCH_2), 3.96 (t, 2 H, ^3J = 4.6 Hz; CH_2OCH$_2$), 3.70 (m, 2 H, CH$_2$OCH_2), 3.53 (m, 2 H, CH_2OCH$_3$), 3.35 (s, 3 H, OCH$_3$). MALDI-TOF MS: m/z = 445 (M^+-2Cl); UV/Vis (DMF): λ / nm (ε / L mol^{-1} cm^{-1}): 530 (600), 321 (16200), 308 (17000), 268 (35500); FT-IR (ATR): ν / cm^{-1}: 3100, 2927 (CH, CH$_2$, CH$_3$); 1616, 1569 (tpy). Anal. Calcd. for $C_{20}H_{21}N_3O_3Cl_3Co$ (516.72): C, 46.49; H, 4.10; N, 8.13; Found: C, 45.78; H, 3.95; N, 8.10.

4'-(4-Methylbenzyloxy)-2,2';6',2''-terpyridine-4'-(2-[1-methoxyethoxy]ethoxy)-2,2';6',2''-terpyridine-cobalt(III) trihexafluorophosphate (12)
To a solution of **4** (32.5 mg, 92 μmol) and **11** (50.0 mg, 97 μmol) in DMF (5 mL) at room temperature was added $AgBF_4$ (62.2 mg, 319 μmol). Immediately a precipitate formed, which was allowed to settle. The solution was decanted and partitioned between a 0.01 M NH_4PF_6-solution in water and dichloromethane. The organic layer was separated, washed with water (2 ×), dried over Na_2SO_4 and removed *in vacuo*. TLC-analysis of the crude product revealed three spots and thus the compound was purified by column chromatography (silica, acetonitril:water:KNO_3(aq) in a 14:2:1 ratio), yielding three fractions: the desired heteroleptic complex but also the two homoleptic complexes. All three complexes were extracted from a 0.01 M NH_4PF_6 solution in water into $CHCl_3$. The organic layer was washed three times with water and evaporated *in vacuo*.
12: ^{1}H-NMR (CD_3CN): δ = 8.66 (s, 2 H; $H_{3',5'}$ phenyl), 8.64 (m, 4 H; $H_{3,3''}$), 8.62 (s, 2 H; $H_{3',5'}$), 8.30 (m, 4 H; $H_{4,4''}$), 7.68 (d, 2 H, ^3J = 7.2 Hz; *o*-C*H* phenyl), 7.54-7.43 (m, 10 H; *m*-C*H* phenyl, $H_{6,6''}$, $H_{5,5''}$), 5.78 (s, 2 H; tpyOCH_2 phenyl), 4.91 (m, 2 H; tpyOCH_2), 4.20 (m, 2 H; CH_2OCH$_2$), 3.86 (m, 2 H; CH$_2$OCH_2), 3.68 (m, 2 H; CH_2OCH$_3$), 3.41 (s, 3 H; OCH$_3$), 2.53 (s, 3 H; CH$_3$ phenyl). ^{13}C-NMR (CD_3CN): δ = 172.8, 172.6, 157.0, 156.9, 156.3, 156.2, 152.4, 143.2, 143.1, 139.6, 131.5, 130.9, 129.8, 128.9, 126.9, 115.0, 114.9, 73.6, 71.8, 71.6, 70.5, 68.8, 58.1, 20.5 (CH3). MALDI-TOF MS: (dithranol): m/z = 909 ; UV/Vis (CH_3CN): λ / nm (ε / L mol^{-1} cm^{-1}): 452 (700), 340 (13000), 325 (19100), 280 (68700), 219 (117500); FT-IR (ATR): ν / cm^{-1}: 3102, 2884 (CH, CH$_2$, CH$_3$); 1619, 1564 (tpy); 824 (PF_6). Anal. Calcd. for $C_{43}H_{40}N_6O_4P_3F_{18}Co$ (1198.66): C, 43.09; H, 3.36; N, 7.01; Found: C, 43.44; H, 3.27; N, 6.69.
13: xtpy-Co-xtpy ^{1}H-NMR (CD_3CN): δ = 8.64 (s, 4 H, $H_{3',5'}$ phenyl), 8.63 (d, 4 H, ^3J = 8.0 Hz; $H_{3,3''}$), 8.28 (td, 4 H, ^3J = 7.8, ^4J = 1.5 Hz; $H_{4,4''}$), 7.68 (d, 2 H, ^3J = 7.4 Hz, *o*-C*H* phenyl), 7.54-7.43 (m, 10 H, *m*-C*H* phenyl, $H_{5,5''}$, $H_{6,6''}$), 5.78 (s, 4 H; CH_2), 2.53 (s, 6 H; CH$_3$). MALDI-TOF MS: m/z = 911 (M^+-2PF_6); UV/Vis (CH_3CN): λ / nm (ε / L mol^{-1} cm^{-1}): 452 (800), 340 (12500), 325 (19000), 281 (67400), 219 (104000); FT-IR (ATR): ν / cm^{-1}: 3097, 2960 (CH, CH$_2$, CH$_3$); 1618, 1565 (tpy); 827 (PF_6).
14: ^{1}H-NMR (CD_3CN): δ = 8.64 (m, 8 H; $H_{3,3''}$, $H_{3',5'}$), 8.30 (m, 4 H; $H_{4,4''}$), 7.54-7.43 (m, 8 H; $H_{5,5''}$, $H_{6,6''}$), 4.91 (m, 2 H; tpyOCH_2), 4.20 (m, 2 H; CH_2OCH$_2$), 3.86 (m, 2 H; CH$_2$OCH_2), 3.68 (m, 2 H; CH_2OCH$_3$), 3.41 (s, 3 H; OCH$_3$). MALDI-TOF MS: m/z = 907 (M^+-PF_6); UV/Vis (CH_3CN): λ / nm (ε /

L mol^{-1} cm^{-1}): 452 (1000), 340 (12100), 325 (17300), 280 (57600), 220 (106700); FT-IR (ATR): ν / cm^{-1}: 3100, 2927 (CH, CH_2, CH_3); 1618, 1564 (tpy); 833 (PF_6). Anal. Calcd. for $C_{40}H_{42}N_6O_6P_3F_{18}Co$ (1196.64): C, 40.15; H, 3.54; N, 7.02; Found: C, 40.26; H, 3.86; N, 7.44.

2.9 Literature

[1] G. T. Morgan, F. S. Burstall, *J. Chem. Soc.* **1932**, 20-30.
[2] E. C. Constable, *Adv. Inorg. Chem. Radiochem.* **1986**, 69-121.
[3] R. B. King, *Encyclopedia of Inorganic chemistry*, John Wiley & Sons, New York, **1994**, pages 1490-1495 and 2114-2118.
[4] C. A. Bessel, R. F. See, D. L. Jameson, M. R. Churchill, K. J. Takeuchi, *J. Chem. Soc. Dalton Trans.* **1992**, 3223-3228.
[5] P. R. Andres, R. Lunkwitz, G. R. Pabst, K. Böhn, D. Wouters, S. Schmatloch, U. S. Schubert, *Eur. J. Org. Chem.* **2003**, 3769-3776.
[6] U. S. Schubert, C. Eschbaumer, P. R. Andres, H. Hofmeier, C. H. Weidl, E. Herdtweck, E. Dulkeith, A. Morteani, N. E. Hecker, J. Feldmann, *Synth. Metals* **2001**, *121*, 1249-1252.
[7] R. A. Leising, S. A. Kubow, M. R. Churchill, L. A. Buttrey, J. W. Ziller, K. J. Takeuchi, *Inorg. Chem.* **1990**, *29*, 1306-1312.
[8] C. M. Harris, T. N. Lockyer, N. C. Stephenson, *Aust. J. Chem.* **1966**, *19*, 1741-1743.
[9] D. E. C. Corbridge, E. G. Cox, *J. Chem. Soc.* **1956**, 594-603.
[10] J. Pickardt, B. Staub, K. O. Schäfer, *Z. Anorg. Allg. Chem.* **1999**, *625*, 1217-1224.
[11] J. A. Bailey, M. G. Hill, R. E. Marsh, V. M. Miskowski, W. P. Schaefer, H. B. Gray, *Inorg. Chem.* **1995**, *34*, 4591-4599.
[12] R. D. Sommer, A. L. Rheingold, A. J. Goshe, B. Bosnich, *J. Am. Chem. Soc.* **2001**, *123*, 3940-3952.
[13] G. B. Deacon, J. M. Patrick, B. W. Skelton, N. C. Thomas, A. H. White, *Aust. J. Chem.* **1984**, *37*, 929-945.
[14] S. F. A. Kettle, *Physical Inorganic Chemistry*, Oxford University Press, Oxford, **1998**.
[15] K.-Y. Kim, G. H. Nancollas, *J. Phys. Chem.* **1977**, *81*, 948-952.
[16] M. D. Ward, E. C. Constable, *J. Chem. Soc. Dalton Trans.* **1990**, 1405-1406.
[17] U. S. Schubert, S. Schmatloch, A. A. Precup, *Design. Monom. Polym.* **2002**, *5*, 211-221.
[18] R. A. Fallahpour, *Synthesis* **2003**, 155-184.
[19] M. Heller, U. S. Schubert, *Eur. J. Org. Chem.* **2003**, *6*, 947-961.
[20] P. R. Andres, H. Hofmeier, B. G. G. Lohmeijer, U. S. Schubert, *Synthesis* **2003**, 2865-2871.
[21] K. Nakamoto, *J. Chem. Soc.* **1960**, *64*, 1420-1425.
[22] R. Hogg, R. G. Wilkins, *J. Chem. Soc.* **1962**, *66*, 341-350.
[23] R. H. Holyer, C. D. Hubbard, S. F. A. Kettle, R. G. Wilkins, *Inorg. Chem.* **1966**, *5*, 622-625.
[24] P. A. Cock, C. E. Cottrell, R. K. Boyd, *Can. J. Chem.* **1972**, *50*, 402-411.
[25] Y. Abe, G. Wada, *Bull. Chem. Soc. Jp.* **1981**, *54*, 3334-3339.
[26] H. P. Bennetto, E. F. Caldin, *J. Chem. Soc. A* **1971**, 2191-2198.
[27] G. U. Priimov, P. Moore, L. Helm, A. E. Merbach, *Inorg. React. Mech.* **2001**, *3*, 1-23.
[28] This can nowadays been carried out by any mathematical program with curve-fitting options such as Origin or Excel. Before, amongst others, Olerup's method has been used (H. Irving, *J. Chem. Soc.* **1962**, 4056-4062).
[29] P. O'D. Offenhartz, P. George, G. P. Haight Jr., *J. Chem. Soc.* **1963**, *67*, 116-118.
[30] H. Irving, R. J. P. Williams, *J. Chem. Soc.* **1949**, 1841-1847.
[31] H. Irving, D. H. Mellor, *J. Chem. Soc.* **1962**, 5222-5251.
[32] G. Anderegg, *Helv. Chim. Acta* **1963**, *46*, 2397-2410.
[33] P. R. Andres, *PhD-thesis*, Eindhoven University of Technology, **2004**.
[34] C. Li, E. Widjaja, W. Chew, M. Garland, *Angew. Chem. Int. Ed.* **2002**, *41*, 3785-3789.
[35] S. H. M. Söntjens, R. P. Sijbesma, M. H. P. van Genderen, E. W. Meijer, *J. Am. Chem. Soc.* **2000**, *122*, 7487-7493.
[36] P. J. Hore, *Nuclear magnetic resonance (Oxford chemistry primers, 32)*, Oxford University Press, Oxford, **1996**.
[37] E. de Hoffmann, V. Stroobant, *Mass Spectrometry – principles and applications 2nd Ed.*, John Wiley & Sons, Chichester, **2001**.
[38] E. Stulz, C. C. Mak, J. K. M. Sanders, *J. Chem. Soc, Dalton Trans.* **2001**, *5*, 604-613.
[39] M. A. C. Broeren, J. L. J. van Dongen, M. Pittelkow, J. B. Christensen, M. H. P. van Genderen, E. W. Meijer, *Angew. Chem. Int. Ed.* **2004**, *43*, 3557-3562.
[40] B. Salih, C. Masselon, R. Zenobi, *J. Mass Spectrom.* **1998**, *33*, 994-1002.
[41] R. Zenobi, R. Knochenmuss, *Mass Spectrom. Rev.* **1998**, *17*, 337-366.

[42] M. Karas, M. Glückmann, J. Schäfer, *J. Mass Spectrom.* **2000**, *35*, 1-12.
[43] M. Satterfield, J. S. Brodbelt, *Inorg. Chem.* **2001**, *40*, 5393-5400.
[44] H. Elsbernd, J. K. Beattie, *J. Inorg. Nucl. Chem.* **1972**, *34*, 771-774.
[45] E. C. Constable, C. E. Housecroft, T. Kulke, C. Lazzarini, E. R. Schofield, Y. Zimmermann, *Dalton* **2001**, 2864-2871.
[46] S. Schneider, G. Brehm, C.-J. Prenzel, W. Jäger, M. I. Silva, H. D. Burrows, S. T. Formosinho, *J. Raman Spectroscopy* **1996**, *27*, 163-175.
[47] P. W. Hansen, P. W. Jensen, *Spectrochim. Acta* **1994**, *50A*, 169-183.
[48] A. T. Baker, H. A. Goodwin, *Aust. J. Chem.* **1985**, *38*, 207-214.
[49] B. N. Figgis, E. S. Kucharski, A. H. White, *Aust. J. Chem.* **1983**, *36*, 1537-1561.
[50] S. Pyo, E. Pérez-Cordero, S. G. Bott, L. Echegoyen, *Inorg. Chem.* **1999**, *38*, 3337-3343.
[51] www.wellesley.edu/chemistry/chem341/jt.html.
[52] A. E. Martell, R. D. Hancock, *Metal complexes in aqueous solutions*, Plenum Press, New York, **1996**.
[53] T. Riley, C. Tomlinson, A. M. James, *Principles of electroanalytical methods*, John Wiley & sons, Chichester, **1987**.
[54] G. D. Storrier, S. B. Colbran, D. C. Craig, *J. Chem. Soc. Dalton Trans.* **1997**, 3011-3028.
[55] G. D. Storrier, S. B. Colbran, D. C. Craig, *J. Chem. Soc. Dalton Trans.* **1998**, 1351-1363.
[56] K. Hutchinson, J. C. Morris, T. A. Nile, J. L. Walsh, D. W. Thompson, J. D. Petersen, J. R. Schoonover, *Inorg. Chem.* **1999**, *38*, 2516-2523.
[57] I. M. Brown, S. I. Weissman, L. C. Snyder, *J. Chem. Phys.* **1965**, *42*, 1105-1111.
[58] K. Nakamura, *Bull. Chem. Soc. Jp.* **1972**, *45*, 1943.
[59] M. Aihara, H. Kishta, S. Misumi, *Bull. Chem. Soc. Jp.* **1975**, *48*, 680-683.
[60] J. M. Rao, M. C. Hughes, D. J. Macero, *Inorg. Chim. Acta* **1976**, *16*, 231-236.
[61] S. Musumeci, E. Rizzarelli, S. Sammartano, R. P. Bonomo, *J. Electroanal. Chem.* **1973**, *46*, 109-117.
[62] D. E. Morris, K. W. Hanck, M. K. DeArmond, *J. Electroanal. Chem.* **1983**, *149*, 115-130.
[63] R. Prasad, D. B. Scaife, *J. Electroanal. Chem.* **1977**, *84*, 373-386.
[64] L. C. Kamra, G. H. Ayres, *Anal. Chim. Acta* **1976**, *81*, 117-129.
[65] R. M. Berger, D. R. McMillin, *Inorg. Chem.* **1988**, *27*, 4245-4249.
[66] S. W. Jones, L. M. Vrana, K. J. Brewer, *J. Organomet. Chem.* **1998**, *554*, 29-40.
[67] P. S. Braterman, J.-I. Song, R. D. Peacock, *Inorg. Chem.* **1992**, *31*, 555-559.
[68] L. I. Semenova, A. N. Sobolev, B. W. Skelton, A. H. White, *Aust. J. Chem.* **1999**, *52*, 519-529.
[69] J.-C. Berthet, Y. Miquel, P. B. Iveson, M. Nierlich, P. Thuéry, C. Madic, M. Ephritikhine, *J. Chem. Soc. Dalton Trans.* **2002**, 3265-3272.
[70] T. Togano, N. Nagao, M. Tsuchida, H. Kumakura, K. Hisamatsu, F. S. Howell, M. Mukaida, *Inorg. Chim. Acta* **1992**, *195*, 221-225.
[71] B. P. Sullivan, J. M. Calvert, T. J. Meyer, *Inorg. Chem.* **1980**, *19*, 1404-1407.
[72] W. M. Reiff, W. A. Baker Jr., N. E. Erickson, *J. Am. Chem. Soc.* **1968**, *90*, 4794-4797.
[73] Y. Chujo, K. Sada, T. Saegusa, *Macromolecules* **1993**, *26*, 6320-6323.
[74] D. Choudhury, R. F. Jones, G. Smith, D. J. Cole-Hamilton, *J. Chem. Soc. Dalton Trans.* **1982**, 1143-1146.
[75] M. Maestri, N. Armaroli, V. Balzani, E. C. Constable, A. M. W. Cargill Thompson, *Inorg. Chem.* **1995**, *34*, 2759-2767.
[76] T. Yutaka, I. Mori, M. Kurihara, N. Tamai, H. Nishihara, *Inorg. Chem.* **2003**, *42*, 6306-6313.
[77] A. Yoshimura, H. Torieda, T. Ohno, *J. Phys. Chem. A* **2004**, *108*, 2149-2154.
[78] K. Jitsukawa, T. Hata, T. Yamamoto, K. Kano, H. Masuda, H. Einaga, *Chem. Lett.* **1994**, 1169-1172.
[79] Gmelin, 58 Co [B], 122, 123, 246-249, 304-307, 578-597.
[80] P. H. Crayton, J. A. Mattern, *J. Inorg. Nucl. Chem.* **1960**, *13*, 248-253.
[81] W. L. Jolly, *Synthetic inorganic chemistry*, Prentice-Hall, Englewood Cliffs, **1960**.
[82] F. A. Cotton, *Advanced inorganic chemistry, 6th Ed.*, Wiley-Interscience, New York, **1999**.
[83] R. G. Endres, M. X. LaBute, D. L. Cox, *J. Chem. Phys.* **2003**, *118*, 8706-8714.
[84] J. K. Beattie, H. Elsbernd, *Inorg. Chim. Acta* **1995**, *240*, 641-644.
[85] G. G. Schlessinger, *Inorganic laboratory preparations*, Chemical publication company, New York, **1962**, page 262.

Chapter 3

Incorporation of terpyridine ligands into polymers

Abstract

Terpyridine ligands are introduced at the chain end(s) of polymers by two different routes. The first route involves end group modification reactions of mono- and telechelic hydroxy functionalized polymers by using 4'-chloroterpyridine and an isocyanate functionalized terpyridine derivative. In this way terpyridine functionalized poly(ethylene oxide), polystyrene, poly(ethylene-co-butylene), poly(2-vinylpyridine)-block-polystyrene), polyisoprene, polybutadiene and polyferrocenyldimethylsilane were synthesized and characterized. The second route involved the use nitroxide mediated controlled living radical polymerization of styrene, n-butylacrylate, N,N-dimethylacrylamide, 4-vinylpyridine, 2-vinylpyridine and isoprene. For the former four monomers kinetic investigations were performed at differently targeted molecular weights. Auto-initiation as well as addition of excess nitroxide were found to influence the control over the polymerization. Special focus was on end group functionality and high terpyridine incorporation degrees were obtained (> 90%). Terpyridine telechelic polymers were synthesized by applying nitroxide substitution reactions using a maleimide functionalized terpyridine. Subsequently, polystyrene and poly-4-vinylpyridine prepared by nitroxide mediated polymerization have been used as macro-initiators for the controlled polymerization of isoprene and N,N-dimethylacrylamide respectively. In this fashion terpyridine-functionalized block copolymers could also be obtained. The synthetic work leads to a toolbox that allows the construction of an enormous variety of metal complexed polymers.

Parts of this chapter have been published: B. G. G. Lohmeijer, U. S. Schubert, *Angew. Chem.* **2002**, *41*, 3825-3829; B. G. G. Lohmeijer, U. S. Schubert, *J. Polym. Sci. Part A Polym. Chem.* **2004**, *42*, 4016-4027; B. G. G. Lohmeijer, U. S. Schubert, *Macromol. Chem. Phys.* **2003**, *204*, 1072-1078.

3.1 Introduction

In the previous chapter the synthesis, characterization and stability of various *bis*-terpyridine substituted metal complexes has been addressed. In order to connect polymer chains together using the results described in the previous chapter, terpyridine-ligands need to be incorporated into different polymer backbones. The most interesting architectures are expected to arise from connecting polymers through their chain end(s). Hence, terpyridine-ligands need to be introduced at the chain end(s) of a polymer. There are a variety of ways to do so. Figure 3.1 shows some of the possibilities.

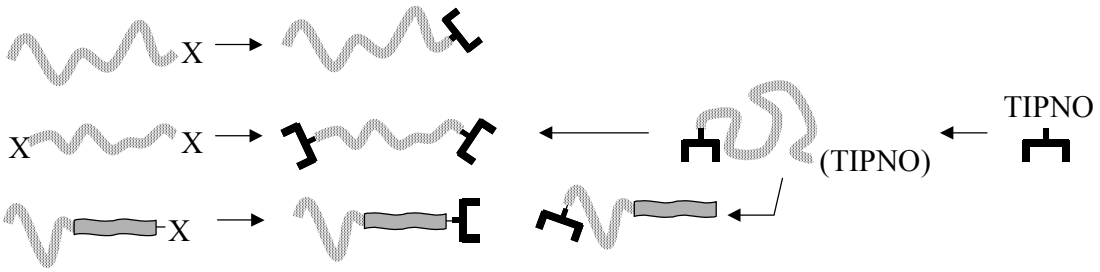

Figure 3.1. *Possible routes towards mono- and telechelic terpyridine functionalized polymers using end group modification and functionalized initiators. TIPNO represents a specific nitroxide radical (see also section 3.3).*

Rougly, there are two routes: the first route uses organic modification reactions of existing functional polymer end groups. These end-groups have been introduced by established polymerization processes. Especially mono- and telechelic hydroxy-functionalized polymers prepared by anionic polymerization are versatile starting polymers, since end-group modification can easily be established by etherification reactions using 4'-chloroterpyridine and by urethane-formation using isocyanate-functionalized terpyridine.[1] A variety of polymers can be functionalized with terpyridine units and this is described in section 3.2. The second route uses functional initiators and end-cappers that introduce the terpyridine ligand by initiation and by end-capping respectively. For this purpose a unimolecular terpyridine-functionalized initiator was synthesized enabling control over the nitroxide-mediated radical polymerization of a large variety of different vinylic monomers such as styrenes, acrylates, acrylamides, dienes and vinylpyridines. The monochelic terpyridine-functionalized polymers are described in section 3.3. The synthesis of telechelic terpyridine-functionalized polymers is described in section 3.4 using again end-group modification reactions and nitroxide-substitution reactions. The reason for controlled polymerization methods is obvious: polymers with tunable chain length and low polydispersity indices are obtained by these methods and especially in case of block copolymers this is a prerequisite for well-defined phase behavior. All terpyridine-functionalized polymers described in this chapter can be regarded as the true building blocks for the macromolecular LEGO-system. The modularity and versatility of the polymer synthesis establishes the toolbox from which to select suitable candidates for the contruction of metal-complex connected macro-molecular architectures.

3.2 End group modification

Two useful starting compounds for the end-group modification are 4'-chloroterpyridine[2] and 4'-(1-isocyanatopentoxy)-2,2':6',2"-terpyridine (Figure 3.2).[3,4] The former compound is easily prepared from 2,6-*bis*-(2-pyridyl)-4-pyridone using $POCl_3$. Other good leaving groups such as bromides and triflates are also easily prepared from the pyridon.[5-7] This 4'-chloroterpyridine can be used for the etherification of hydroxy-end groups of polymers and this is described in section 3.2.1. Alternatively, this compound can be used for the introduction of other functional groups. By reaction with 1-amino-5-hydroxypentane an amino-group may be introduced,[8] that can subsequently be turned into an isocyanate functionality using di-*tert*-butyltricarbonate.[9,10] Although isocyanates are normally easily hydrolyzed in the presence of pyridines, apparently steric hindrance of the terpyridine-system prevents this.[11] The presence of the isocyanate-functionality on the terpyridine ligand allows the urethane-formation of this compound with hydroxy-functionalized polymers that are unstable towards the etherification reactions with 4'-chloroterpyridine and this is described in section 3.2.2.

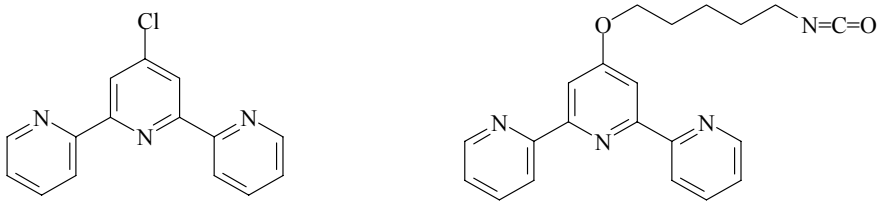

Figure 3.2. *Starting compounds for end group functionalization reactions using 4'-chloro-2,2':6',2"-terpyridine and 4'-(1-isocyanatopentoxy)-2,2':6',2"-terpyridine.*

3.2.1 End group modification via 4'-chloroterpyridine

Previously, poly(ethylene oxide) and poly(tetramethylene oxide) have been functionalized with terpyridine-units using a suspension of KOH in DMSO at 70 °C.[12,13] The base abstracts the proton of the polymer end group, effectively producing the nucleophilic anion. This nucleophile attacks at the 4'-position of the ligand and a negative charge is introduced into the central pyridine ring. Subsequently the aromaticity of the central ring is reinstalled by elimination of a chloride anion. Actually, the intermediate can be identified from the reddish color of the DMSO-suspension. This synthetic strategy has also been adopted in case of monochelic poly(ethylene oxide)s of various molecular weights (M_n = 3000, 5200, 10000, 16500 g mol^{-1}). The ^{1}H-NMR spectra of the purified products revealed in each case signals of the terpyridine-ligand in the aromatic region. Of particular interest is the singlet attributed to the 3',5'-protons on the middle ring, which has moved from 8.47 ppm to 8.04 ppm due to the substitution from a chloro to an oxygen atom at the 4'-position. Also the methylene protons of the backbone next to the ligand have shifted from 3.83 for the hydroxy substituted PEO to 4.40 and 3.93 for the terpyridine substituted end group. MALDI-TOF-MS has proven to be an excellent tool for end-group analysis of these polymers.[13,14] In Figure 3.3 a clear shift of 232 Dalton can be observed for each single peak, which corresponds to the mass of the terpyridine-ligand proving the successful and complete end group functionalization.

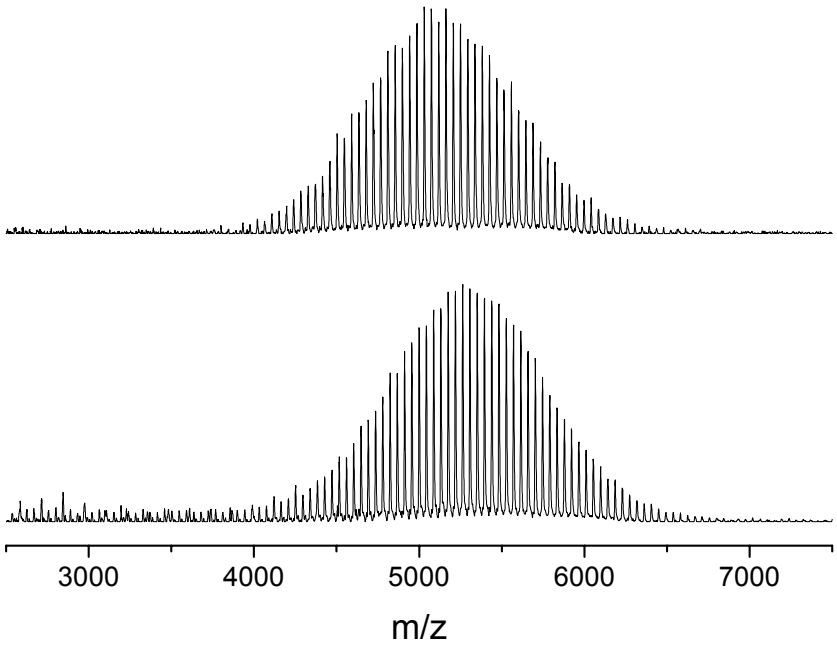

Figure 3.3. *MALDI-TOF mass spectra of poly(ethylene oxide) (DP = 125) with hydroxy end group (top) and after modification with terpyridine (bottom).*

The GPC-traces (Figure 3.4) were recorded with an eluent consisting of 94% chloroform, 4% Et_3N and 2% 2-propanol. This mixture reduced most of the column interactions of the terpyridine end functionalized polymers. Tailing of the GPC-traces, which can be observed when using pure chloroform or THF, leads to unreliable data regarding M_n and PDI. Nevertheless, also in case of the special solvent mixture, the M_n of the lower molecular weight species are still somewhat low compared to the MALDI-TOF-MS and ^{1}H-NMR data and in comparison with the starting materials, which can still be interpreted as an effect of column interactions. For the higher molecular weight species, having a lower absolute terpyridine content, the molecular weights by these three independent techniques are comparable (Table 3.1), so for the higher M_n polymers column interactions are negligible.

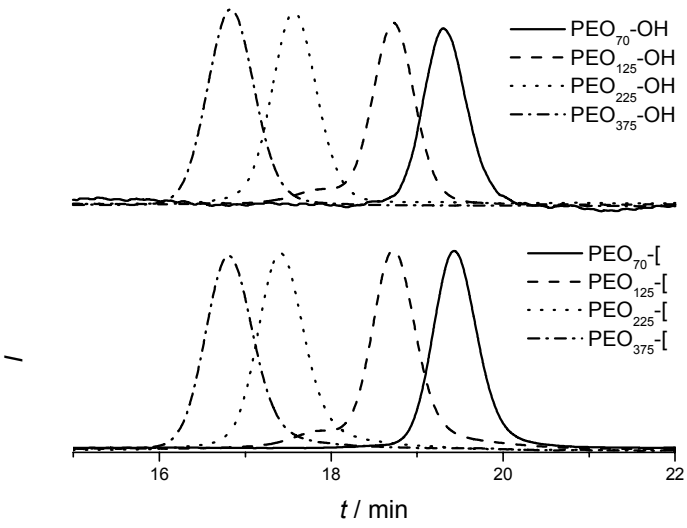

Figure 3.4. *GPC traces of poly(ethylene oxide) of various molecular weights with hydroxy end group (top) and after modification with terpyridine (bottom).*

	M_n (PDI) GPC	M_n ^{1}H-NMR	M_n MALDI-TOF MS
PEO_{70}-OH	2800 (1.04)	3000	2923
PEO_{70}-[	2500 (1.04)	3100	3123
PEO_{125}-OH	4300 (1.06)	5200	5036
PEO_{125}-[	4200 (1.09)	5400	5202
PEO_{225}-OH	9400 (1.04)	10000	10876
PEO_{225}-[	10000 (1.06)	10300	10901
PEO_{375}-OH	15400 (1.04)	16500	16863
PEO_{375}-[	15500 (1.04)	16600	17434

Table 3.1. *Determination of the molecular weights of different poly(ethylene oxide) starting materials and the corresponding terpyridine functionalized poly(ethylene oxide)s by three independent techniques, polydispersity indices (M_w/M_n) are given in parentheses.*

Hydroxy end-functionalized polystyrene is obtained by addition of the living polymer reaction mixture to a solution of ethylene oxide in THF or by addition of CO_2 and subsequent hydrogenation of the acid to the alcohol.[15] Other methods involve the use of haloalkanes with hydroxy-protected silyl ethers.[16] This hydroxy-end group can subsequently be converted into a terpyridine-end group using 4'-chloroterpyridine. However, the approach described for PEO will fail, since polystyrene is insoluble in DSMO. Therefore two different routes were developed. The first used a phase transfer catalyst, 18-crown-6, for KOH in toluene-solution. Although successful, reaction times were quite long, typically 48 hours. Hence, a different method was followed using *t*-BuOK in dry THF for the deprotonation of the polymer and the addition of an excess of the 4'-chloroterpyridine. The reaction was completed within 4 hours, costs less starting materials and is therefore an improvement to the first route. We have used commercially available hydroxy-functionalized polystyrene of two different molecular weights (2000 and 10000 g mol^{-1}) and observed comparable results. The excess 4'-chloroterpyridine was removed by a double precipitation in methanol (distilled) and subsequent washing with hexanes. Alternatively, preparative size exclusion chromatography could be carried out, but was in these cases not necessary. The terpyridine functionalized polystyrene was analyzed by ^{1}H-NMR, size exclusion chromatography (GPC), FT-IR and MALDI-TOF MS. In IR characteristic vibrations at 1600, 1582 and 1563 cm^{-1} of the terpyridine ligand can be observed. In ^{1}H-NMR the corresponding signals for the terpyridine arise and can be integrated to the backbone. This was in excellent agreement with results from GPC using polystyrene standards and MALDI-TOF MS measurements. Hydroxy-functionalized poly(ethylene-*co*-butylene) can be obtained from anionic polymerization of 1,3-butadiene after end-capping with ethylene oxide and subsequent hydrogenation of the double bonds.[17] Poly(ethylene-*co*-butylene) has been functionalized with terpyridine by the two methods described above. However, in both cases full functionalization was not obtained probably due to insufficient reaction time or not dry enough working conditions. Thus, in the reaction mixture the same polymer with two different end groups was present. Fortunately, these polymers could be separated from each other by column chromatography due to different affinity of the end-group to the stationary phase. For these reasons the yield was only 49%. Again, ^{1}H-NMR could be used to successfully integrate the signals of the terpyridine ligand to the signals of the backbone, GPC to determine the polydispersity index and the molecular weight, while MALDI-TOF MS was only successful for the product due to the presence of protonatable nitrogen atoms. The starting compound unfortunately could not be detected using MALDI-TOF MS.

Hydroxy-functionalized polystyrene-*block*-poly(2-vinylpyridine) is obtained by anionic polymerization of styrene.[18] The living anion is then introduced into a solution of 2-vinylpyridine and functions as macro-initiator. After polymerization of 2-vinylpyridine the polymer is end-capped by ethylene oxide to yield the hydroxy end group. This commercially available block copolymer has been functionalized with a terpyridine-ligand using *t*-BuOK in dry THF. Figure 3.5 shows the ^{1}H-NMR-spectrum of the polymer before and after functionalization. The signals of both blocks can be observed as well as a few terpyridine-signals, although some overlap is occuring with the 2-vinylpyridine-block. The signals at 3.3 and 3.4 ppm, indicating the terminal two methylene-groups, have quantitatively shifted to 3.8 and 3.9 ppm.

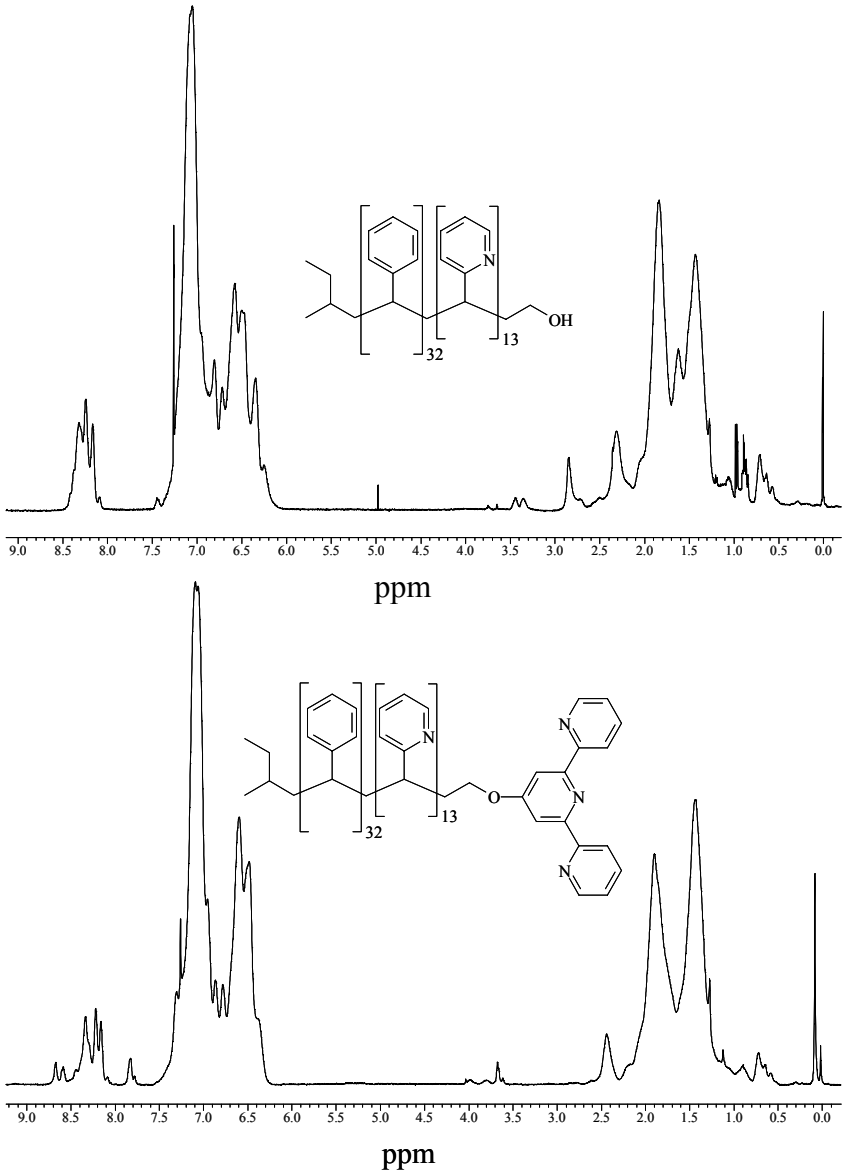

Figure 3.5. *^{1}H-NMR-spectra of hydroxy-functionalized polystyrene-block-poly-2-vinylpyridine (top) and after reaction with 4'-chloroterpyridine (bottom) in $CDCl_3$.*

GPC showed a narrow monomodal distribution. MALDI-TOF-MS revealed two distributions that could be attributed to the block copolymer and its sodium-adduct. Interestingly, a well-resolved distribution could be observed, which naturally stems from the similar masses of the monomers and the low overall molecular weight.

Normally, MALDI-TOF MS-spectra of block copolymers show broad peaks without any fine-structure, even when the polydispersity index is very low. Hydrogenated hydroxy end functional polybutadiene-*block*-poly(ethylene oxide)[19] has also been reacted with 4'-chloroterpyridine and yielded a second terpyridine-functionalized diblock copolymer.

3.2.2 End-group modification by isocyanates

The end-group modification reactions by 4'-chloroterpyridine as described in the previous section work very well for non-reactive polymer backbones. However, commercially important polymers such as polybutadiene and polyisoprene but also metal-containing polymers such as polyferrocenyldimethylsilane[20] could not be functionalized with terpyridine moeities using these methods. The conditions apparently give rise to some crosslinking of the polydienes judging from the respective GPC-traces and ^{1}H-NMR-spectra, which is highly undesired. Lowering the temperature usually did not result in any reaction. In case of the polyferrocenyldimethylsilane no reaction took place, presumably because oxidation of the backbone occurred.

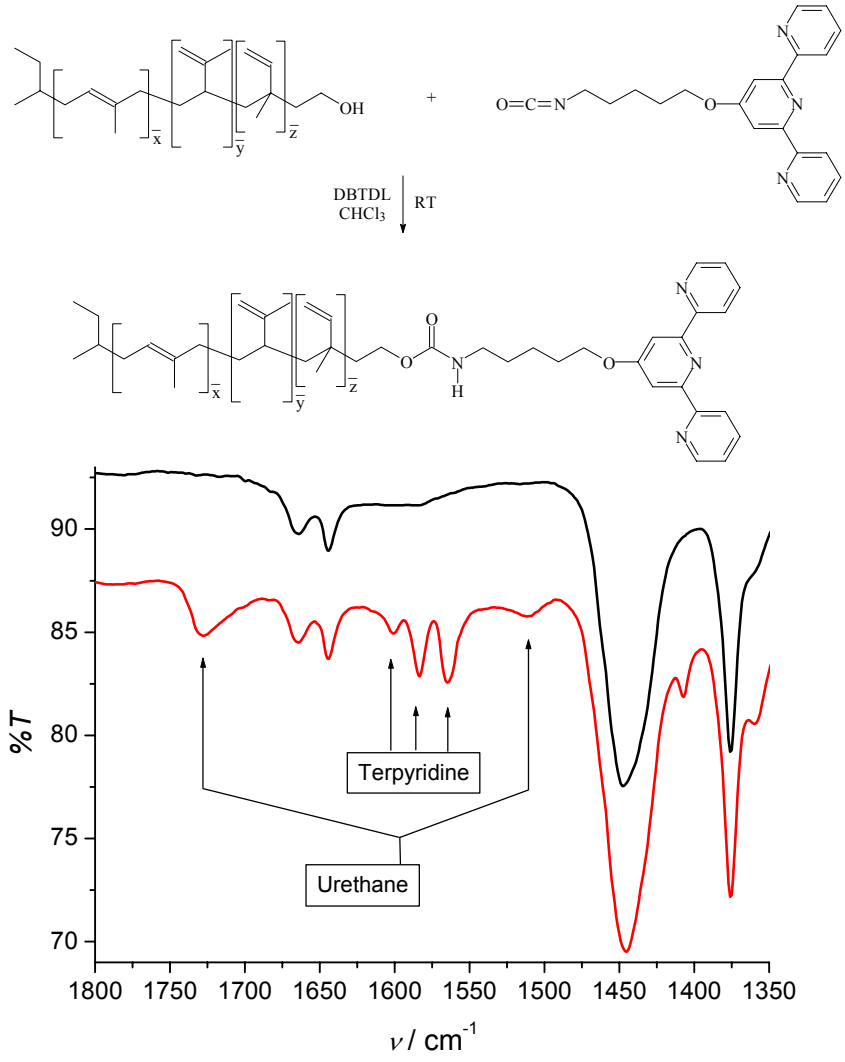

Figure 3.6. *Synthetic scheme and IR-spectra of the hydroxyfunctionalized polyisoprene and of terpyridine-functionalized polyisoprene using an isocyanate functionalized terpyridine.*

Therefore a different route was developed using isocyanates to form urethanes with the corresponding hydroxy-functionalized polymers. For polyisoprene and polybutadiene a hydroxy end group was obtained by end capping of the anionic polymerization with ethylene oxide, whereas for polyferrocenyldimethylsilane a hydroxy-protected initiator was used for the anionic ring-opening polymerization of strained monomeric silicon-bridged [1]ferrocenophanes. Isocyanate reactions are very versatile in terms of reactivity by using an appropriate catalyst.[21] Fortunately, the formation of a urethane-bond can be followed perfectly using IR-spectroscopy. The isocyanate band is clearly visible at 2250 cm^{-1} and upon formation of the urethane two bands appear at 1721 and 1515 cm^{-1}. Hydrolysis of the isocyanate into the amine and subsequent reaction could in principle give rise to the formation of urea groups with bands at 1650 and 1615 cm^{-1}.[22] In all three IR-spectra of the terpyridine-functionalized polymer only urethane-formation was observed. Moreover, precipitation in methanol was sufficient to purify the polymers from the starting isocyanate and catalyst. Also, the terpyridine-signals in the region between 1600 and 1550 cm^{-1} are present and indicate the successful incorporation (Figure 3.6). The polymers were further characterized by MALDI-TOF MS, ^{1}H-NMR and GPC as described in the previous section, although again for polybutadiene and polyisoprene the starting compounds could not be detected with MALDI-TOF MS.

Figure 3.7 summarizes the syntheses of all polymers obtained by end-group modification reactions using 4'-chloro-2,2':6',2"-terpyridine and 4'-(1-isocyanatopentoxy)-2,2':6',2"-terpyridine.

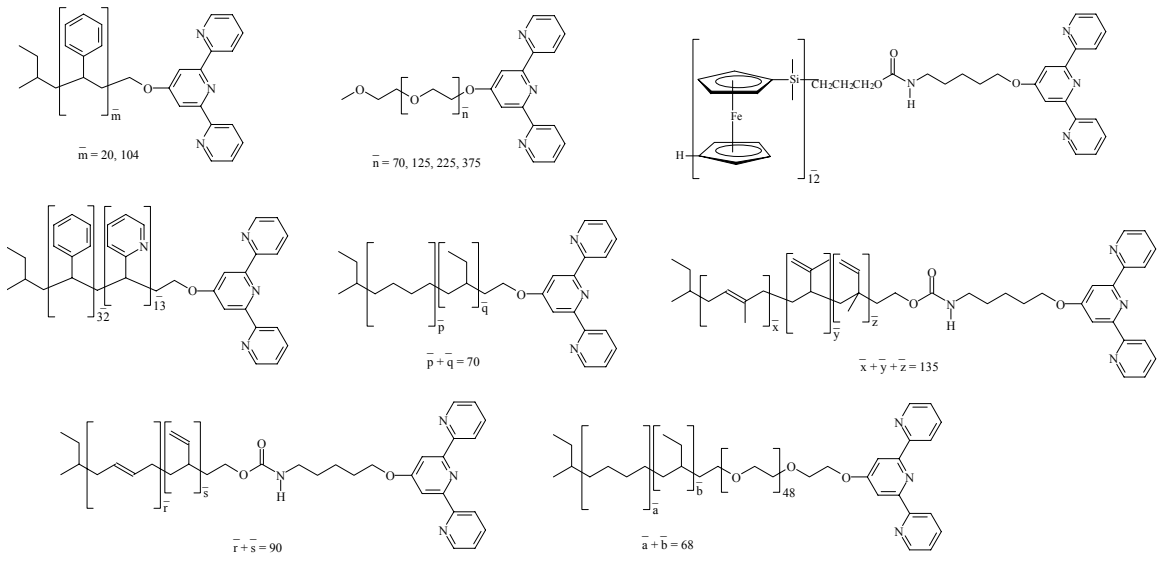

Figure 3.7. *Schematic representation of all polymers obtained by end group modification reactions, i.e. polystyrene, poly(ethylene oxide), polyferrocenyldimethylsilane, polystyrene-block-poly(2-vinylpyridine), poly(ethylene-co-butylene), polyisoprene, polybutadiene and poly(ethylene-co-butylene)-block-poly(ethylene oxide).*

3.3 Nitroxide mediated controlled living radical polymerization

The previous section has dealt with end group functionalization of polymers prepared by anionic polymerization and proved to be a valuable tool for the introduction of a terpyridine end group into polymers such as polystyrene, poly(ethylene oxide), poly(ethylene-*co*-butylene) and polystyrene-*b*-poly(2-vinylpyridine). Nevertheless, the limited range of monomers, intolerance to various monomers with important functional groups and stringent purification procedures call for other polymerization techniques than anionic. As stated before (section 3.1), perfect control over the molecular architecture is a must in the synthesis of the macromolecular LEGO building blocks, especially when connecting chains together through the metal complexes in order to form block copolymers with a well-defined morphology. Thorough control over the molecular weight and its distribution can be gained by utilizing controlled living polymerization techniques. In the last decade important advances have been made in the field of controlled living free radical polymerization (CRP). Radical polymerization is widely employed in industry and academia due to its compatibility with functional groups and its tolerance to water. Moreover, since the development of techniques such as Atom Transfer Radical Polymerization (ATRP),[23] Reversible Addition Fragmentation Chain Transfer Polymerization (RAFT)[24] as well as Nitroxide Mediated Polymerization (NMP),[25] it is possible to obtain polymers with narrow molecular weight distributions and high end-group functionality. Complete monomer-families can be polymerized by CRP-techniques such as styrene, (meth)acrylates, acrylamides, acrylonitriles, dienes and vinylpyridines. For our purposes, ATRP is unfortunately not suitable: the terpyridine ligand will compete for the transition metal ion of the ATRP catalyst and control will be lost. Of course, the terpyridine ligand could be protected by forming an inert complex and after polymerization decomplexation would give terpyridine functionalized polymers, but such a pathway is rather tedious and unnecessary. RAFT is the most versatile controlled radical polymerization technique but thorough end group control is still a major challenge.[26] In NMP however, control over the end groups can be gained relatively easy by using a functional unimolecular initiator.[27] Some termination in the beginning of a polymerization process initiated by such an initiator leads to an excess of persistent nitroxide radicals. This excess mediates in an equilibrium reaction between propagating (growing) and dormant chains: the dormant chains are reversibly turned into growing chains by continuous addition and fragmentation of the nitroxide radical, allowing an equal growth rate of each polymer chain up till high conversions (Scheme 3.1).[28]

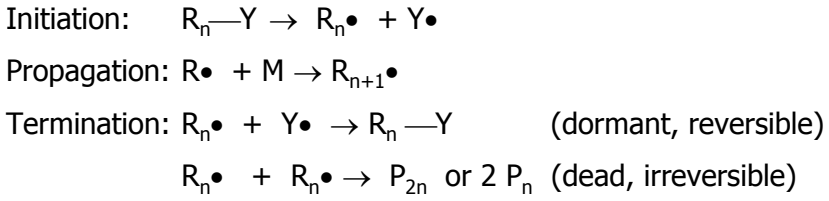

Scheme 3.1. *Simplified reaction scheme for nitroxide mediated radical polymerization.*

Hawker has developed a universal alkoxyamine with a chloro-functionality capable of polymerizing styrenes, acrylates, dienes, acrylamides and vinylpyridines.[27,29,30] After some synthetic perseverance this compound could be reproduced. In a subsequent step 2,6-*bis*-(2'-pyridyl)-4-pyridon[2] was reacted with this alkoxyamine yielding a unimolecular initiator bearing the terpyridine moiety (Figure 3.8).

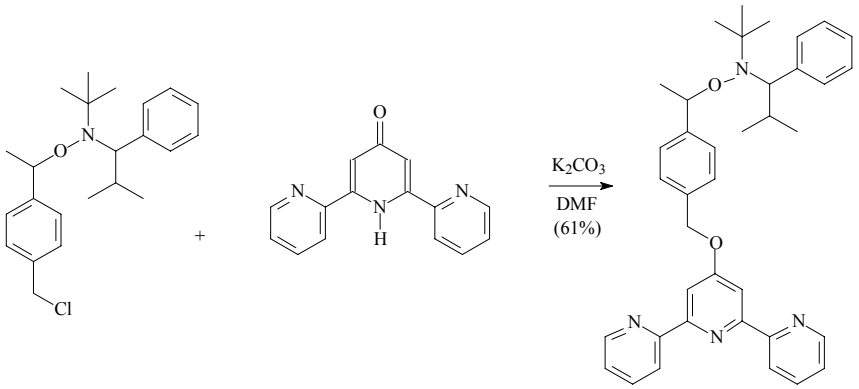

Figure 3.8. *Preparation of a terpyridine functionalized initiator suitable for nitroxide mediated controlled living free radical polymerization.*

In this way an initiator that already contains the terpyridine ligand was acquired. The chloromethyl derivate and the pyridon were synthesized as published before.[27,31,32] As discussed in chapter 2, the mild base K_2CO_3 deprotonates the pyridon and then undergoes an S_N2 reaction with the chloro-group on the alkoxyamine. In view of the facile work-up procedures, i.e. a filtration column, the pyridon was used in excess. The first fraction obtained from the column contained a small amount of some impurity that was present in the alkoxyamine and was discarded. The second and largest fraction contained the desired compound, the unimolecular initiator containing the terpyridine ligand. Figure 3.9 shows the ^{1}H-NMR, where the typical terpyridine signals are visible between 8.8 and 7.2 ppm. Also, the signal of the CH_2 connecting the terpyridine to the styrene-fragment has shifted from 4.66 to 5.35 ppm with respect to the chloromethyl derivative. Since the initiator contains two stereo-centers, four isomers can be expected. The diastereoisomers show different signals in ^{1}H-NMR and are present in a 45:55 ratio. Further assignment was carried out by 2D-NMR techniques. Although conformational changes are obvious, no large influence has been reported in initiating efficiency of the stereoisomers, making the separation of them unnecessary.[33] The polymerizations initiated by this unimolecular initiator will therefore automatically lead to polymers containing one terpyridine ligand at the chain end, at least in theory. The next sections deal with the polymerization of styrene, *n*-butylacrylate, *N,N*-dimethylacrylamide, 4-vinylpyridine, 2-vinylpyridine and isoprene. For a detailed understanding of the processes involved different molecular weights were targeted and the kinetics of several polymerization runs was investigated. Special focus will be on end group functionality of the resulting polymers with respect to the initiating fragment containing the terpyridine-ligand, but also with respect to the mediating nitroxide. The presence of the nitroxide group at the other end of the polymers allows for block copolymer synthesis using the terpyridine-functionalized polymer as macroinitiator for a different monomer or for preparing telechelics by proper nitroxide-substitution reactions (section 3.4).

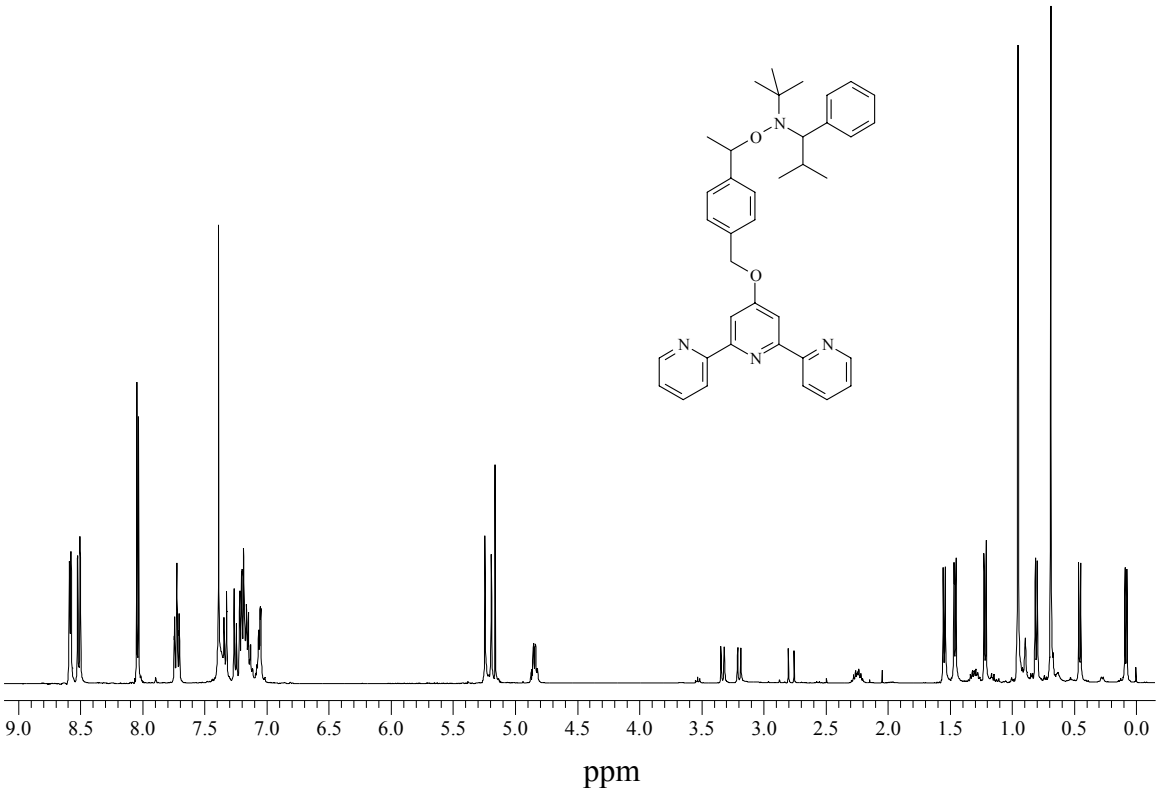

Figure 3.9. *^{1}H-NMR of the terpyridine functionalized initiator in $CDCl_3$. The typical terpyridine signals are visible between 8.8 and 7.2 ppm. From the ^{1}H-NMR the molar ratio of the diastereoisomers was calculated as 45:55.*

3.3.1 Polymerization of styrene

A stock solution of the initiator in purified styrene was prepared. This stock solution was transferred for kinetic investigations to eight reaction vessels. Three freeze-pump-thaw-cycles were applied for the removal of oxygen before the reaction vessels were immersed in an oilbath of 125 °C. The polymerization was carried out for a certain amount of time and then stopped. In total eight different polymerization times were used for the polymerization of the same stock solution. All analysis of the kinetics (conversion, molecular weight) was carried out before the samples were precipitated (twice). Again the respective molecular weights were determined (GPC, ^{1}H-NMR) and several precipitated samples were subjected to column chromatography. Table 3.2 displays some of the results obtained so far. The integration of the terpyridine signals to the polymer backbone was used to determine M_n. A few general remarks can be made when looking at Table 3.2: 1) high conversions could be reached; 2) the theoretical molecular weights are in good agreement with the observed ones, and 3) polydispersity indices are well below 1.3. The molecular weights as measured by ^{1}H-NMR for polystyrene are systematically higher than those measured by GPC. The latter technique used polystyrene standards for calibration and should therefore be more accurate, if column interactions are ruled out. Of course, the higher the M_n the less accurate ^{1}H-NMR will be. Nevertheless, all spectra were recorded with a long relaxation time (10 s) and sufficient scans were applied (128) until no differences were found upon integration.

An explanation for the non-fitting data from GPC and ^{1}H-NMR may be found in the auto-initiation of styrene. In the early literature on nitroxide mediated polymerization (using TEMPO) some reports have been published on this topic.[34-37] However, in the

last years this issue seems to be neglected due to the fact that polymerization times have been shortened drastically, thus seemingly reducing the effect of auto-initiation. But this does not mean that there will be no auto-initiation and subsequent auto-polymerization at all! Auto-initiation and auto-polymerization will lead to two types of polymers using the terpyridine functionalized initiator: one type with a terpyridine end group and the other with no terpyridine functionality. Both polymers should show a controlled growth: there is no preference for the nitroxide radical with respect to the propagating radical and the corresponding initiator fragment.

Table 3.2. *Selection of the results obtained by the polymerization of styrene by the terpyridine functionalized initiator. $M_{n,th}$ represents the targeted molecular weight (100% conversion). The M_n-data in the table is before any purification procedures.*

$M_{n,th}$ (g/mol)	Polymerization time (min)	Conversion (%)	M_n (GPC)	PDI (GPC)	M_n (^{1}H-NMR)
7000	75	54	4700	1.12	5600
10000	200	77	7300	1.08	7700
12500	240	77	8900	1.11	10300
25000	600	86	19700	1.12	22400
50000	360	66	34500	1.13	41200
80000	360	69	55600	1.33	87400

To account for these two types of polymers, polystyrene of M_n = 7300 g mol^{-1} and PDI = 1.08 (entry 2 in Table 3.2) was subjected to column chromatography (for conditions, see experimental part). The first fraction, which was the minor component (<5% by weight) contained the non-functionalized polystyrene, whereas the second fraction contained the terpyridine functionalized polymer. The starting material and the two obtained fractions were subjected to GPC-analysis using a photo diode array-detector. Figure 3.10 shows the GPC-chromatograms and the accompanying UV-spectra from the photo diode array-detector. The UV-spectra clearly demonstrate the presence of two different end-groups, since the terpyridine ligand has a characteristic absorption from 260 to 300 nm. Moreover, the M_n's and the PDI of the two polymer fractions were calculated: the terpyridine containing polymer revealed a M_n of 7700 g mol^{-1} as expected and a PDI of 1.08, indicating the living and controlled growth of the terpyridine initiated chains. The non-functional polystyrene on the other hand had an M_n of 3200 g mol^{-1} and a PDI of 1.42.

To study the effects of auto-initiation upon targeted molecular weight, a more detailed look at the kinetics of the polymerization of styrene was undertaken. Four different degrees of polymerization (DP's) were targeted (125, 250, 500 and 800, respectively) and for each a stock solution of the purified monomer containing the respective calculated amount of initiator was prepared. This stock solution was transferred to different reactors and polymerized at 125 °C for different times. The results are shown in Figure 3.11. A linear increase of molecular weight with conversion is observed as well as a linear increase of the conversion with time. This indicates that all polymers are growing at the same rate, and proves the controlled nature of the polymerization

of styrene up till at least 80000 g/mol. It also shows that auto-initiation does not influence the pseudo-livingness of the polymerization.

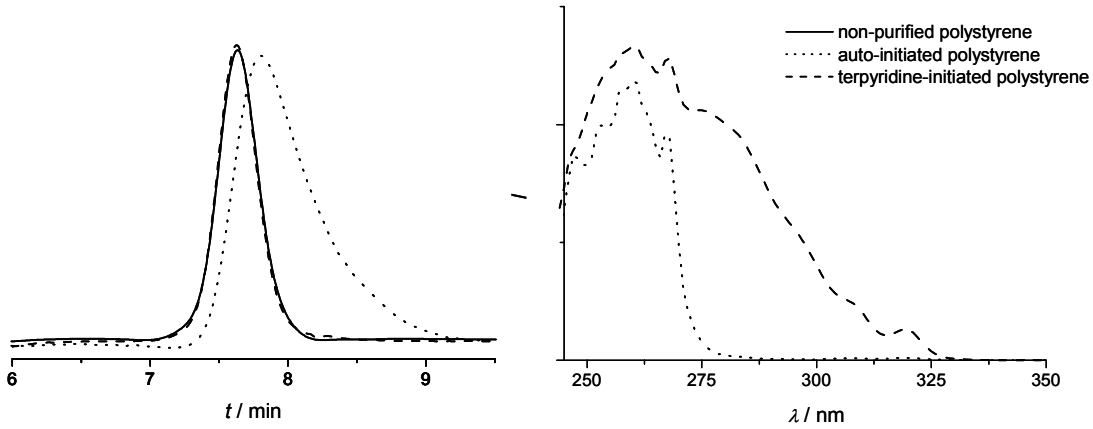

Figure 3.10. *GPC-traces of polystyrene before and after separation by column chromatography in two fractions (3 traces, left) and the corresponding UV-spectra as measured by the photo diode array-detector of the two fractions (right). The GPC-trace of the non-separated polystyrene is added to show that auto-initiated chains are not detected by UV/vis due to the low amount present and much lower optical density as compared to terpyridine-initiated polystyrene.*

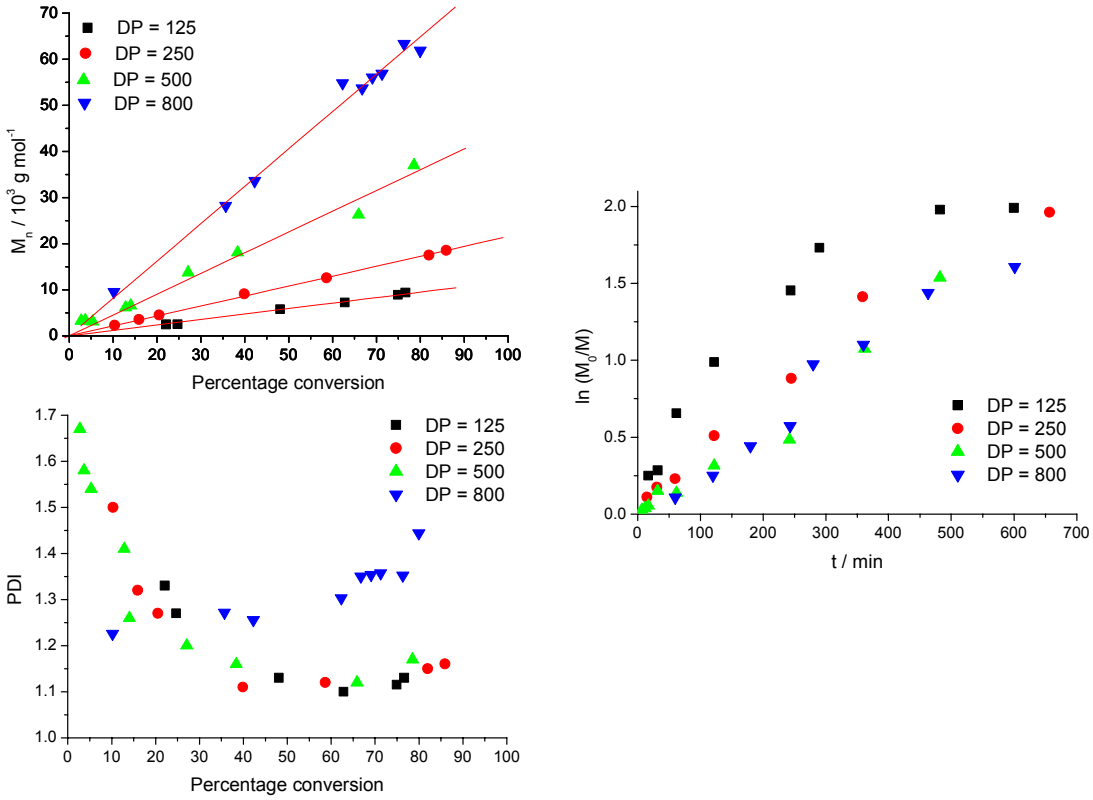

Figure 3.11. *Plot of molecular weight (top left) and polydispersity index (bottom left) as a function of conversion for four differently targeted degree's of polymerization, namely DP = 125, 250, 500 and 800 and the corrsponding plot of ln([M$_0$/M]) as a function of time for the four differently targeted degrees of polymerization (right).*

Interestingly, the polymerization rates show some striking differences: for DP = 250, 500 and 800 the rates are comparable, but for DP = 125 the polymerization rate is quite different. How can this be explained? For the former three DP's the rate is in good agreement with the thermal self-polymerization of styrene.[37] The rate of polymerization is independent of the initiator concentration due to the fact that the concentration of persistent and propagating radicals remains more or less constant. Important to note is that the effects of auto-initiation become more important at higher DP's. The number of growing chains is less upon increasing the [M]/[I]-ratio as well as the number of persistent radicals. Termination reactions thus become more important at lower radical concentrations. Since auto-initiation of styrene is a relatively slow process,[38,39] the polymerization remains controlled: the increase in the number of growing radicals is automatically counter-acted upon by termination reactions.

In this fashion, the less regulating nitroxide is present, the higher the influence of auto-initiation and concomitant termination reactions. The experimental results reflect this by looking at the chains initiated by the terpyridine fragment: the molecular weights as measured by GPC and NMR are quite different. This obviously stems from the fact that in NMR the molecular weight is calculated from the integration of the terpyridine initiator signal to the backbone, whereas by GPC this is not end group related and thus represents better the actual molecular weight. Upon increasing the targeted molecular weight, the discrepancy between the measured molecular weights becomes larger, indicating that more auto-initiated chains are participating in the polymerization. Moreover, this discrepancy becomes larger with increasing conversion. Also, the GPC-chromatograms of the kinetic investigation for DP = 800 clearly showed tailing due to the more pronounced termination reactions. The polydispersity indices for this particular kinetic investigation remain as a result rather high as compared to the other kinetic runs. As stated before, the polymerization rate for DP = 125 is quite different with respect to the other polymerization rates. This indicates a non steady-state polymerization, where the persistent radical effect is still operative. For such a case, Fischer described a $t^{2/3}$ dependence of $\ln([M_0]/[M])$: a continuous decrease of the propagating radicals through termination gives rise to this dependency.[40,41] Indeed, fitting the data with the $t^{2/3}$ time dependence reveals a perfect linear relationship. Interestingly, at one point one would expect that auto-initiation starts to play a role again, when the propagating radicals reach a concentration similar to that of under thermal self-polymerization conditions. However, before this point is reached, apparently monomer conversion has proceeded too far for DP = 125.

Upon increasing the targeted molecular weight a cross-over from controlled to uncontrolled growth of the polymer chains is apparent, where the price to pay is the control over polydispersity index and initiating group functionality. A simple way of decreasing the influence of auto-initiation would be to lower the temperature. Unfortunately, polymerization times increase tremendously due to the fact that the propagation rate is reduced as well as the rate for the homolytic C-O bond cleavage. The question remains whether auto-initiation is then really no longer an issue, since auto-initiation takes place roughly from 60 °C and up. For our purposes, the molecular weight range and corresponding polydispersity indices are already acceptable enough to serve as building blocks for the macromolecular LEGO-system.

3.3.2 Polymerization of *n*-butylacrylate

The previous section has dealt with the polymerization of styrene, where auto-initiation and auto-polymerization limit the degree of end-group functionality and obtainable polydispersity index for higher molecular weights: for the styrene polymerizations a steady-state between termination reactions (consuming existing transient radicals) and auto-initiation reactions (producing new transient radicals) led to a controlled growth of the polystyrene chains. *n*-Butylacrylate is not subject to auto-initiation, but the propagation rate of *n*-butylacrylate polymerization is much higher than of styrene (about 6 times at 120°C).[27] This means that there is no source for additional new radicals to form and that at a certain point in conversion (or time) the polymerization of *n*-butylacrylate could stop, if termination reactions occur frequently. A build-up of nitroxide in the system slows down the polymerization. For TEMPO-mediated *n*-butylacrylate polymerizations this is indeed the case. When followed by ESR spectroscopy, the nitroxide radical concentration is low in the beginning, but increases fast with time. At 8% conversion the reaction indeed stops.[42] Hence, the excess concentration of persistent radical should be kept constant and in an excellent paper from Georges control could be gained over *n*-butylacrylate polymerizations using TEMPO by removing it from the system by ascorbic acid.[43] High conversions were in this case possible, but polydispersity indices were still not great (1.32 is the lowest reported), presumably due to too little control over the decay rate of the nitroxide. Other nitroxides have been developed and they were shown to afford better control over the polymerization of *n*-butylacrylate than TEMPO-derivatives.[27,44,45] The terpyridine-initiator has the TIPNO-nitroxide connected to a functionalized styrene-fragment. For this particular nitroxide bond dissociation rate constants have been calculated and it was found that the rate constant for dissociation from the styrene-fragment has a 10 times higher value than from a *t*-butylacrylate radical ($k_d = 3.3*10^{-3}$ and $2.5*10^{-4}$ s^{-1} for TIPNO at 120 °C respectively).[33] This is beneficial for controlling the polymerization of *n*-butylacrylate, because initiation should be fast with respect to the propagation reaction. The faster the initiation, the faster the equilibrium concentrations for transient and persistent radicals are reached and hence better control over the polymerization is the result. For TEMPO this factor is more or less the same, but the absolute value is much lower. Moreover, the recombination rate constant is much higher for TEMPO. This implies that the equilbrium between dormant and transient radicals is shifted much more to the dormant species. The same amount of termination in case of *n*-butylacrylate polymerization using TEMPO or TIPNO in the beginning then leads indeed to a stop in conversion for TEMPO, but is ongoing in case of TIPNO. However, rather high polydispersity indices were reported for *n*-butylacrylate polymerization using TIPNO.[27] This problem was overcome, simply by the addition of free nitroxide radical: this shifts the equilibrium more in favor of the dormant chains, because propagating radicals are effectively scavenged by the excess of persistent radical.[27,38] The amount of termination also decreases because the probability that two chains will find another becomes smaller due to the presence of more persistent species. Although reaction times increase, the control over the polymerization is much better and polymers with low polydispersity index can be obtained.

The kinetics of the polymerization of *n*-butylacrylate were studied in a similar fashion as for styrene. Three degrees of polymerization were targeted and different amounts of free nitroxide were added to the system (DP = 100, DP = 200 and DP = 400 with 5, 2.5 and 5 mol% added nitroxide respectively). Figure 3.12 displays the results. The

conversion shows an almost perfectly linear relationship with the measured molecular weights for all three cases. This indicates that the polymerization is indeed controlled. Nevertheless, polymerization times are quite different. Figure 3.12 reveals that for a DP = 100 with 5% added free nitroxide and for a DP = 200 with 2.5% added free nitroxide, the polymerization times are virtually the same. This can be readily understood: a steady state is again achieved between persistent radicals and transient radicals and in the absence of termination the transient radical concentration is proportional to the initial radical concentration and inversely proportional to the persistent radical concentration. Therefore, halving this concentration and also halving initiator concentration leads to the same polymerization rate. However, increasing the free nitroxide concentration would slow the polymerization down further. In fact, for a DP = 400 and 5% free nitroxide, the polymerization needs a long time before significant conversions are obtained. Simply extending the previous argument would imply a four times slower polymerization rate and this is in reasonable agreement with the results displayed in Figure 3.12.

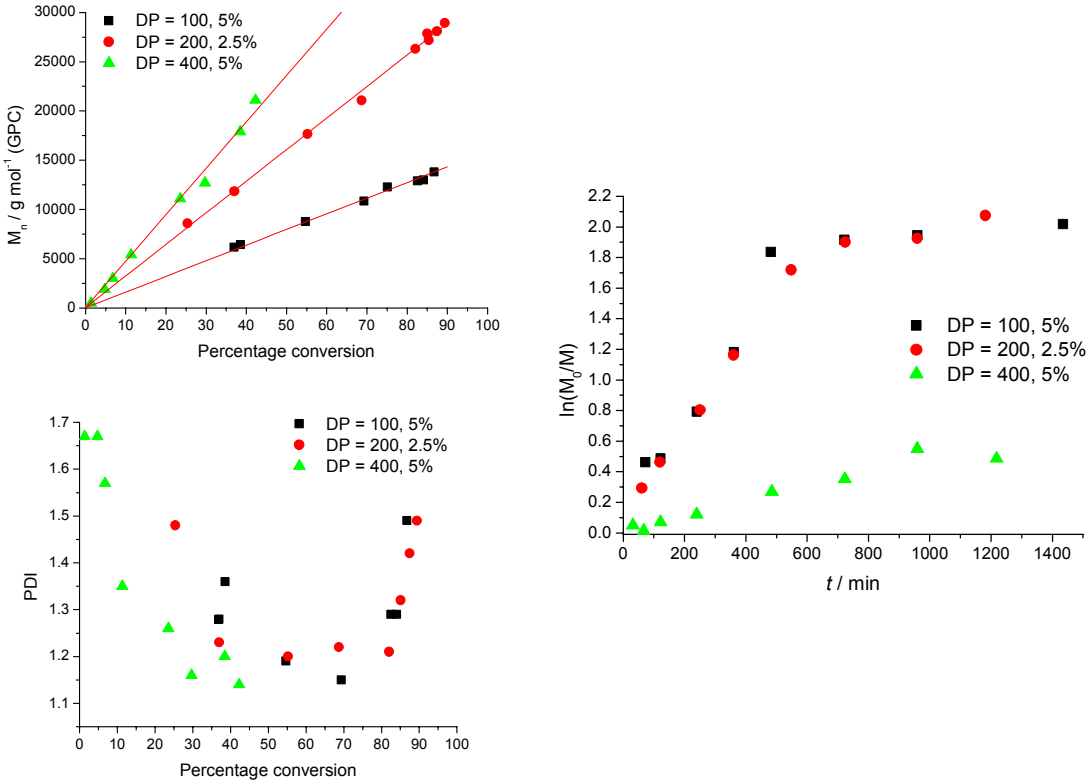

Figure 3.12. *Plot of molecular weight (top left) and polydispersity index (bottom left) as a function of conversion for three differently targeted degree's of polymerization of n-butylacrylate, namely DP = 100, 200 and 400 with 5%, 2.5% and 5% added free nitroxide respectively and the corresponding plot of ln([M_0/M]) as a function of time for the three differently targeted degrees of polymerization and added free nitroxide (right).*

The evolution of the polydispersity indices upon increasing the conversion for the three targeted molecular weights is noteworthy. In the beginning the polydispersity decreases dramatically and very acceptable polydispersity indices are reached. On the other hand, at high conversions termination reactions play a more significant role since the monomer becomes depleted. The evolution of end-group-functionality with conversion was studied in all cases by ^{1}H-NMR. Excellent agreement was found

between the GPC-values and upon integration of the terpyridine-signals with respect to the polymer backbone, proving that every chain was initiated by the terpyridine-functionalized initiator. Some reports in literature have appeared dealing with intramolecular chain transfer reactions regarding the polymerization of butylacrylates, using integration of ^{13}C-NMR spectra (branchpoint vs backbone), but no evidence for chain transfer was found in these studies.[46]

3.3.3 Polymerization of *N,N*-dimethylacrylamide

Dimethylacrylamide also has a much higher propagation rate constant as compared to styrene and *n*-butylacrylate.[47,48] Thus, a similar approach as for the polymerization of *n*-butylacrylate was undertaken. One kinetic investigation was performed for a DP = 100 and 5 mol% free nitroxide with respect to the initiator was added to the reaction vessels. The results are shown in Figure 3.13. The polymerization is controlled as evidenced from the linear relationship between molecular weight vs conversion and between ln[M_0/M] *vs* time. The molecular weights as determined by integration of the ^{1}H-NMR-spectra were found to be in good agreement with the theoretically expected molecular weights, whereas the values for the GPC were in all cases slightly higher (between 5 to 15%): this may be attributed to the calibration of the GPC-column. The polydispersity indices decrease with increasing conversion, but at high conversion increase again due to termination reactions. Indeed, in the ^{1}H-NMR-spectra of samples at conversions over 90% some signals could be observed in the region between 5.0 and 6.0 ppm, indicating termination by disproportionation. The color of the polymerization reaction mixture in those cases had turned to orange, indicating the presence of free nitroxide. A gel effect was not observed.

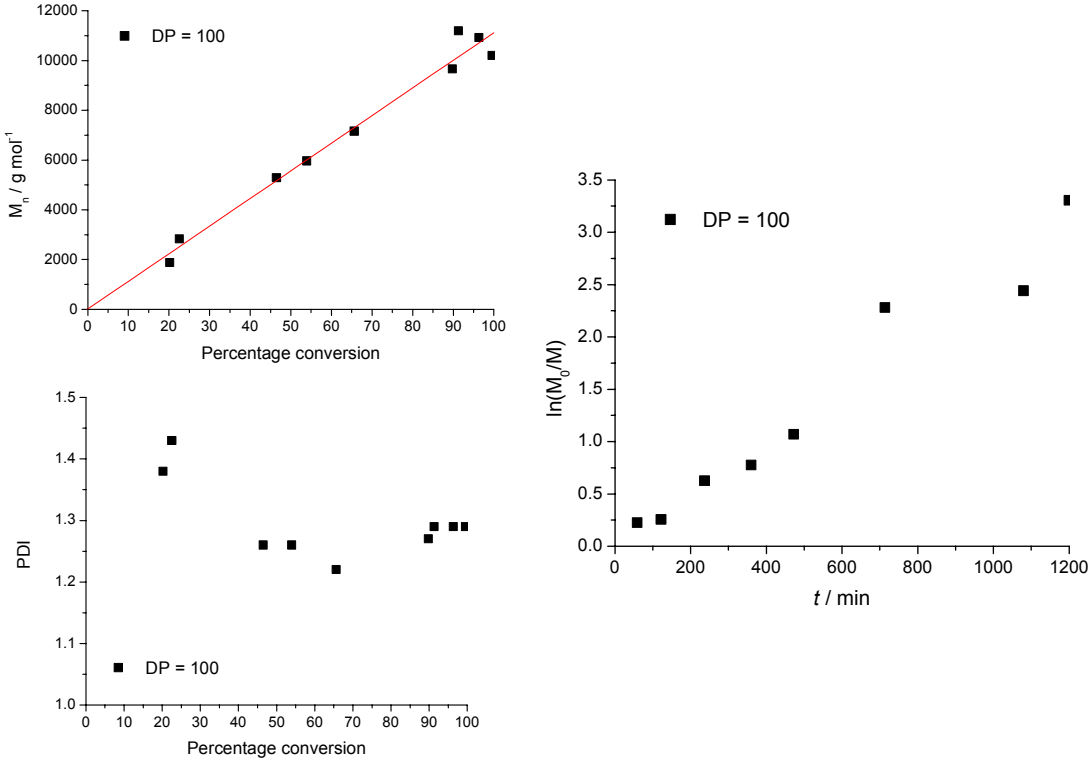

Figure 3.13. *Plot of molecular weight (top left) and polydispersity index (bottom left) as a function of conversion for a targeted degree of polymerization of N,N-dimethylacrylamide, namely DP = 100 with 5% added free nitroxide and the corresponding plot of ln([M_0/M]) as a function of time for this polymerization (right).*

3.3.4 Polymerization of 4-vinylpyridine

The controlled polymerization of 4-vinylpyridine (4VP) has up till now been carried out successfully by anionic polymerization.[49] In case of metal-ion-assisted ATRP the controlled polymerization of vinylpyridines poses severe challenges due to coordination of the monomer to the catalyst. Nitroxide-mediated controlled radical polymerization does not require transition metal ions. The free radical polymerization of 4-vinylpyridine has been well-studied,[50] but only a few reports have appeared that deal with the controlled radical polymerization of this monomer using TEMPO, HTEMPO and SG-1.[51-55] Alternatively, 2-vinylpyridine has been polymerized using TEMPO and TIPNO as mediating radicals.[30,56] For 4VP it was found that in case of TEMPO polymerization rates were dramatically lowered in comparison with styrene and that the temperature had to be increased. The explanation was that the C-O bond enthalpy for 4VP connected to a nitroxide is higher than for styrene through stabilization by the pyridine moiety.[51] A higher bond enthalpy leads again to lower dissociation rates. Thermal initiation was also addressed, but only to explain the increased polydispersity index at higher conversions. For SG-1-mediated polymerization the temperature could be lowered to 110 °C and high conversions could be reached.[55] SG-1 has a higher dissociation rate as compared to TEMPO and this explains the lower temperature. Also here thermal polymerization was mentioned, but no conclusions could be drawn due to lowered initiator efficiency having antagonistic effects on the observed molecular weights. For our purpose, the terpyridine initiator was used for the homopolymerization of 4-vinylpyridine. One molecular weight was targeted (DP = 150) and the kinetics of this polymerization were investigated as described before at 125 °C. Figure 3.14 shows the results.

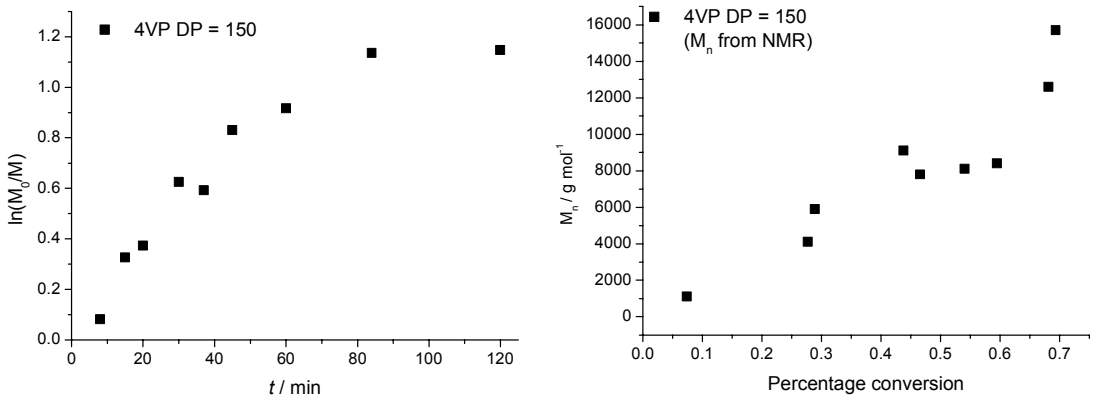

Figure 3.14. *Plot of molecular weight as a function of conversion for a targeted degree of polymerization of 4-vinylpyridine, namely DP = 150 (left) and the corresponding plot of ln([M$_0$/M]) as a function of time for this polymerization (right).*

The polymerization of 4-vinylpyridine is very fast: in one hour the polymerization is virtually completed. The plot of ln[M_0/M] as a function of time does not reveal a straight line, but instead is curved. This was previously observed in the case of styrene polymerization with a targeted molecular weight of 12500 g mol^{-1}. Hence, it can be concluded that the polymerization takes place under non-steady state conditions and during the polymerization termination happens continuously, resulting in a decrease of the transient radical concentration and an increase in the free nitroxide concentration. Monomer is depleted before a steady-state can be reached, since too little termination reactions take place. Auto-initiation would lead to polymers with no terpyridine end-group. Comparison of the molecular weights as obtained by GPC and

by ^{1}H-NMR reveals that they are in reasonable agreement with each other. Again the molecular weight by GPC is overestimated by ~25-35% as compared to ^{1}H-NMR and is due to the calibration of the column (using PMMA-standards) and also the presence of cationic species in the eluent (5 mM NH_4PF_6 in DMF) that may cause an expansion of the hydrodynamic volume of the polymer through ion-dipole interactions. It can therefore be concluded that all chains are effectively initiated by the terpyridine initiator and auto-initiation does not play a significant role. Nevertheless, the polymerization of 4-vinylpyridine could be optimized for TIPNO e.g. by addition of free nitroxide, by lowering the temperature or to increase the monomer to initiator ratio, but this remains to be done. However, polydispersity indices were already excellent (<1.15).

3.3.5 Polymerization of other monomers

In literature the controlled radical polymerization of a variety of other monomers has been reported. For example, homopolymers of acrylonitrile, isoprene, butadiene and *t*-butylmethacrylate have been reported as well as copolymers containing methyl methacrylate using various nitroxides.[25,27,29,57-60] Functionalized monomers have been reported as well. The playground for tailoring a polymer backbone with respect to composition and molecular weight is formidable and it is up the chemist to design basically any specialty polymer. Using the terpyridine-functionalized initiator the polymerization of 2-vinylpyridine and isoprene were attempted following literature procedures, although no kinetic investigations were performed. The polymerization of 2-vinylpyridine was carried out aiming at two different molecular weights (DP = 50 and DP = 140) and they were completed after 4 and 5 hours respectively. High conversions were reached and the targeted molecular weights were indeed obtained, although polydispersity indices were not great (1.27 and 1.36, respectively). Comparison of the molecular weights obtained by GPC and ^{1}H-NMR revealed a good agreement, although again GPC overestimates the molecular weight slightly. For isoprene, a kinetic investigation was attempted aiming at a molecular weight of 50000 g mol^{-1}. Only very little conversion was found in the first 24 hours of the reaction (<5%). Thereafter conversion increased rapidly and after 48 hours 60% was reached. Nevertheless, control was not good and high polydispersity indices (1.8) were the result. Two separate runs were performed with aiming at two different molecular weights (DP = 100 and DP = 250). Conversion was much better reaching 80% after 48 hours. But the control was again not good judging from polydispersity indices of 1.23 and 1.69. In parts, the reactor set-up could be responsible for this, since isoprene is a very volatile monomer and pressures in the polymerization tubes become very high. Possibly the use of an autoclave – as reported in literature as to regulate the pressure – could help. Also, decay of the nitroxide after prolonged periods of time at high temperature could be responsible for the sudden increase in conversion and the resulting poor control.[27] Nevertheless, a few of the polymerizations yielded acceptable terpyridine-functionalized polyisoprenes in terms of polydispersity index and end group functionality, although the approach described in section 3.2.2 is by far more reliable for preparing these polymers.

3.3.6 Block copolymers

One of the most interesting features of living polymerization is the possibility of preparing well-defined block copolymers. In living anionic and cationic polymerizations the first monomer is fully depleted leaving a living polymer chain end. This living chain end is immediately reacted with a second monomer, because

isolation of the first polymer block usually leads to irreversible deactivation of the living group. In controlled 'living' radical polymerizations, it is the absence of termination reactions that leads to well-defined polymers. However, at high conversions the monomer becomes depleted and termination reactions become of increasing importance. It is therefore a general rule that a controlled radical polymerization is stopped at a conversion below 85%. Ideally, all polymer chains have the same composition with respect to initiating fragment, but also to the end group. After purification from the monomer and other reaction products (usually by multiple precipitation steps), this end group can reinitiate the polymerization of a different monomer. Already in chapter 1 it was stressed that for a successful block copolymerization an efficient cross-over reaction from the macroinitiator to the monomer must take place. It implies that the reinitiation must be fast with respect to propagation, the exact same criterion that allows for a controlled growth of the first block. This criterion can not always be met due to inherent reactivities of monomers and therefore controlled living block copolymerization techniques all suffer from monomer sequence issues. Hence, in case of nitroxide-mediated polymerization techniques a polystyrene macro-initiator will not as efficiently reinitiate the polymerization of *n*-butylacrylate as does a poly(*n*-butylacrylate) macroinitiator reinitiate the polymerization of styrene.[25] Of course, control could in principle be gained by addition of free nitroxide in order to shift the equilibrium in favor of the dormant species and so try to supress high propagation rate constants. In this fashion the sequence of the blocks can be successfully altered.[45] This section deals with the synthesis of block copolymers using a few of the polymers described in the previous sections as macroinitiator in order to obtain terpyridine-functionalized block copolymers. Terpyridine-functionalized polystyrene and poly(4-vinylpyridine) macro-initiators have been used for the polymerization of isoprene and *N,N*-dimethylacrylamide, respectively. Figure 3.15 shows the ^{1}H-NMR-spectrum of polystyrene-*block*-polyisoprene and the corresponding GPC-chromatograms of the macroinitiator and the block copolymer.

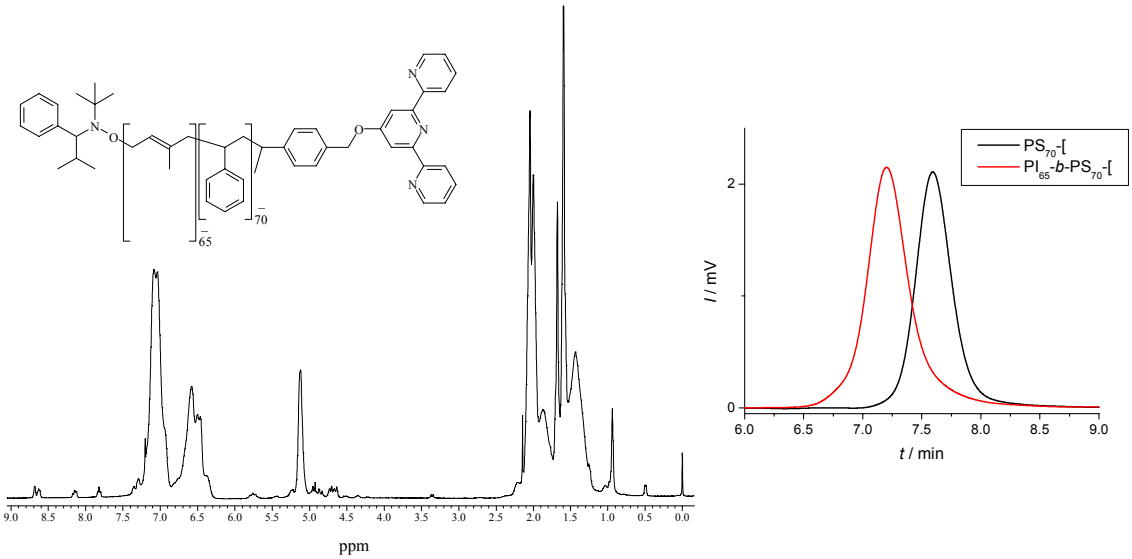

Figure 3.15. *^{1}H-NMR spectrum of terpyridine end functionalized PI_{65}-b-PS_{70} in $CDCl_3$ (left) and the GPC-chromatograms of the macroinitiator and the block copolymer showing a successful chain extension (right).*

Although there is some overlap between the GPC-chromatograms of the macro-initiator and the resulting block copolymers, the chromatogram of the block

copolymer does not show shoulders at both the high and low molecular weight side. This would be indicative of chain coupling and incomplete initiation respectively. Hence, the majority of the macroinitiator chains has successfully initiated the polymerization of the second monomer with a terpyridine-functionalized diblock copolymer as the result. The ^{1}H-NMR-spectrum has been used to calculate the respective block ratio's and molecular weight by integration with respect to the terpyridine signals. The block copolymers thus obtained are PS_{70}-*b*-PI_{65} and $P4VP_{42}$-*b*-$PDMAA_{37}$. It is interesting to note that in both cases in the ^{1}H-NMR-spectrum there are still signals visible of the nitroxide fragment and in principle a third monomer might be initiated to yield a terpyridine functionalized triblock copolymer or nitroxide substitution reactions can be performed leading to α,ω-terpyridine end-functionalized diblock copolymers (see section 3.4).

In summary, a variety of monomers can be polymerized in a controlled fashion using a terpyridine-functionalized initiator that is suitable for the nitroxide-mediated controlled radical polymerization. This means that different molecular weights of chemically different polymers are readily accessible. This is of main importance in designing the volume fractions in block copolymers. Moreover, high and low Tg polymers (PS and P*n*BA) can be prepared as well as crosslinkable (PI), watersoluble (PDMAA) and stimuli-responsive systems (P4VP). It was also demonstrated that block copolymers can be prepared by using the obtained polymers as macroinitiators (Figure 3.16).

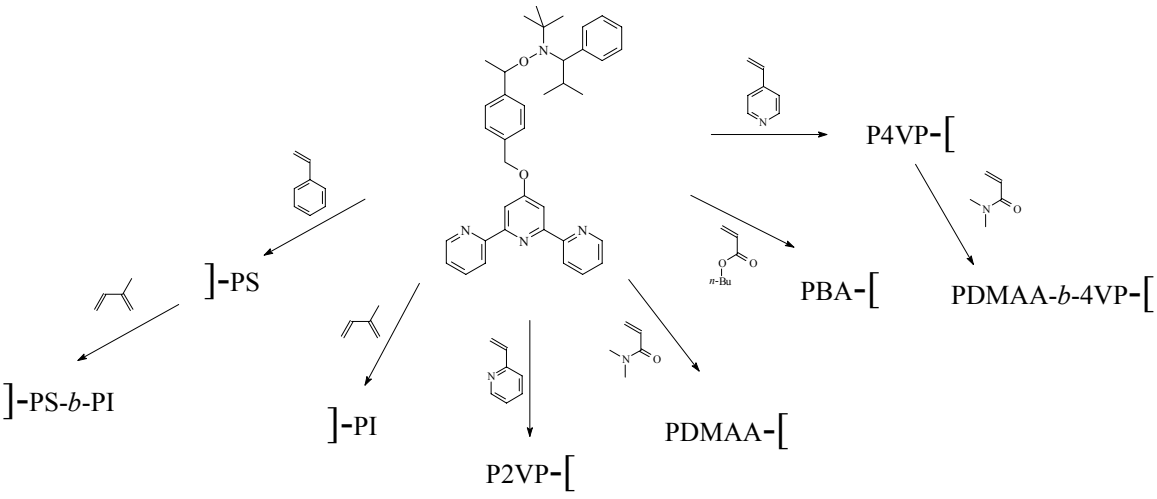

Figure 3.16. *All polymers prepared by nitroxide mediated controlled radical polymerization.* –[*represents the terpyridine-ligand.*

3.4 Terpyridine-functionalized telechelics

Telechelic terpyridine functionalized polymers can also be prepared in two ways. The first route again involves the modification of hydroxy end groups as described in section 3.2, whereas the second route uses radical substitution reactions of polymers using the unimolecular terpyridine-functionalized initiator as described in section 3.3. The first route is exemplified by the modification of α,ω-hydroxy-functionalized poly(ethylene-*co*-butylene). This polymer is prepared by anionic polymerization of butadiene using a protected hydroxy-group in the initiator molecule. Subsequent end-capping of the polybutadiene by ethylene oxide results in the first hydroxy group.

Afterwards, hydrogenation leads to an aliphatic backbone as well as a deprotection resulting in two hydroxy-end groups. Unfortunately, end group functionality is only 1.9 after this treatment, instead of the maximum theoretical value of 2.0. Nevertheless, by using *t*-BuOK and 4'-chloroterpyridine in dry THF, α,ω-terpyridine functionalized poly(ethylene-*co*-butylene) was prepared from commercially available α,ω-hydroxy-functionalized poly(ethylene-*co*-butylene). After a double precipitation, this polymer was analyzed by a combination of techniques. ^{1}H-NMR gives the clearest indication for full conversion of the hydroxy group into the terpyridine ligands. Moreover, the end-group functionality can be calculated from integration of the methylene protons at the two different chain ends and was found to be 1.92±0.03 (Figure 3.17).

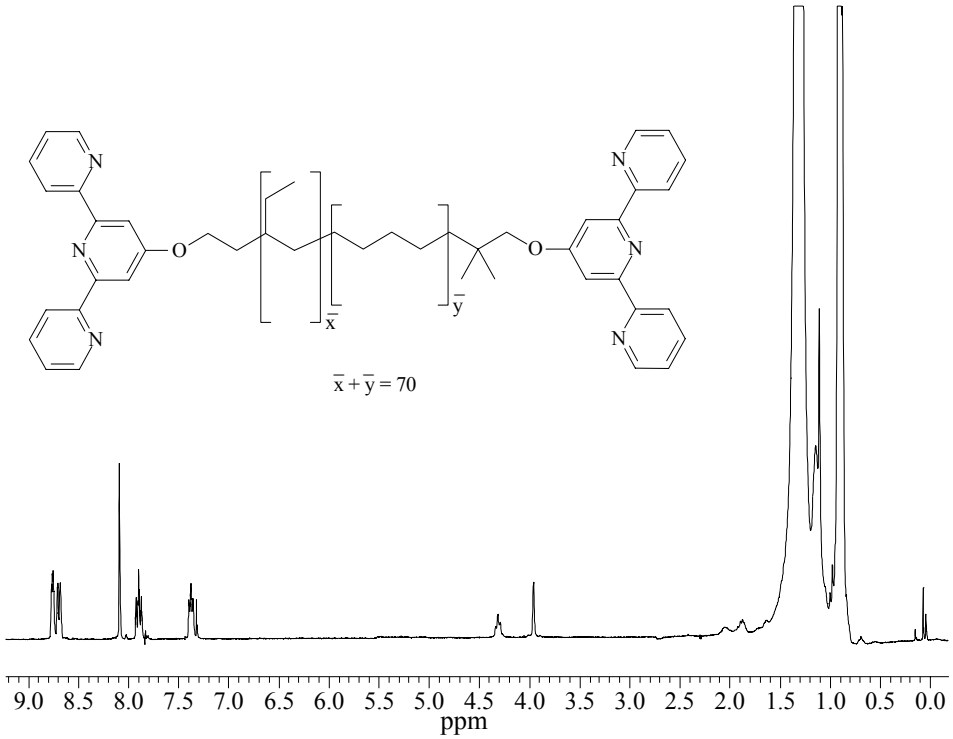

Figure 3.17. *^{1}H-NMR-spectrum of α,ω-terpyridine functionalized poly(ethylene-co-butylene) in $CDCl_3$. Note the singlet at 3.89 ppm of the methylene group at one chain end and the triplet 4.32 ppm at of the methylene group at the other chain end.*

The second route involved the polymers prepared by the unimolecular terpyridine-functionalized initiator suitable for nitroxide mediated controlled living radical polymerization. The presence of the nitroxide end group in these polymers opens not only possibilities for block copolymerizations (section 3.3.6), but also to further end-functionalized polymers prepared in this way. If the dormant chain is again thermally initiated, the terminal radical can be reacted with a maleimide.[31,32] Maleimides resist homo-polymerization, therefore allowing facile functionalization of nitroxide end capped polymers since only one maleimide will add to the chain. Enough excess of the maleimide with respect to the nitroxide is a must for preventing chain coupling. Moreover, the intermediate where the maleimide group is capped by the nitroxide must give rise to a clean and high-yielding disproportionation reaction. In literature this reaction has been exploited to introduce fluorescent labels at the chain end and/or to improve the thermal stability. [31,32] Other radical addition reactions have been reported by Matyjaszewski.[61] To prepare telechelic polystyrene bearing a terpyridine

ligand at each chain end, a terpyridine functionalized maleimide is required as building block. This compound was prepared by refluxing the corresponding amine functionalized terpyridine with maleic anhydride in *p*-xylene (Figure 3.18).[62]

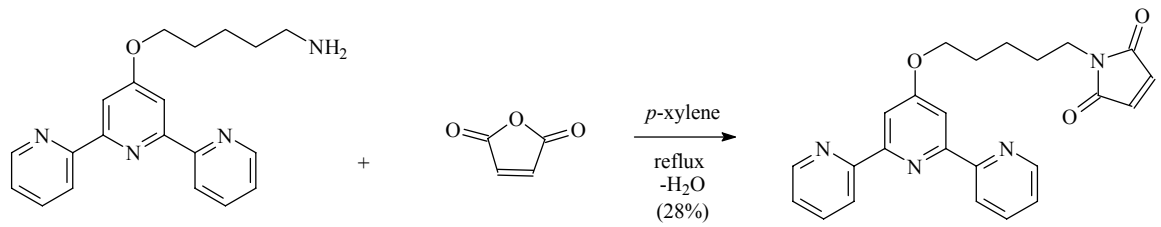

4 **5**

Figure 3.18. *Synthesis of terpyridine modified maleimide.*

Although the yields are not that good, the purification procedure is straightforward using an AlOx filtration column. Mitsunobe-coupling[63] utilizing hydroxy functional terpyridine and maleimide was tried as well, but the yields were not better after purification.

The purified polystyrene (M_n = 7700 g mol^{-1}) was used for further modification by the terpyridine functionalized maleimide in order to obtain telechelic polystyrene (Figure 3.19). In literature this maleimide modification reaction is described in two steps: first the polymer and the maleimide in DMF are heated at 100 °C for two hours in order to prepare the intermediate and then increase the temperature to 125 °C to establish the disproportionation.

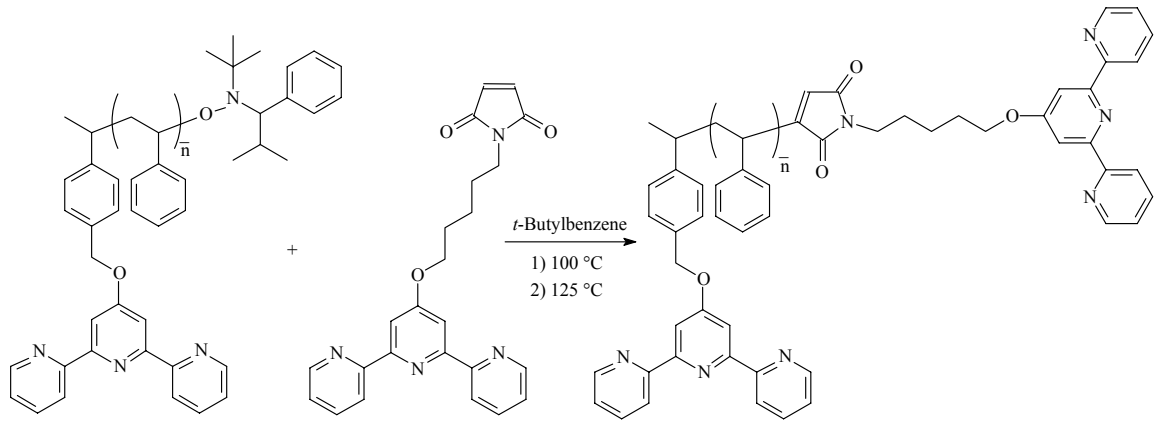

5

Figure 3.19. *Synthesis of α,ω-terpyridine functionalized polystyrene.*

However, in our hands the product contained only 60% *bis*-functionalized compounds as judged from ^{1}H-NMR, which may be due to chain transfer to the solvent. We therefore changed the solvent to *t*-butylbenzene, which is known for its low transfer constant, while all other conditions remained unchanged. Much better incorporation of the terpyridine functionalized maleimide was established, >95% as judged from the ^{1}H-NMR. The GPC chromatogram showed no higher molecular weight shoulders, which would be indicative of chain coupling. Accordingly, the molecular weight and polydispersity index did not change significantly (7800 g mol^{-1}, PDI = 1.09). Using MALDI-TOF MS we were able to identify the end groups of the *bis*-functionalized polystyrene as well as a shift of 414 mass units with respect to the starting nitroxide polymer (Figure 3.20), although the starting nitroxide functional polystyrene showed

depolymerization during the MALDI-process as a function of the laser intensity. Trying to suppress depolymerization effects using various matrices has been subject of investigation in the past, but was not further investigated for these samples.[64,65]

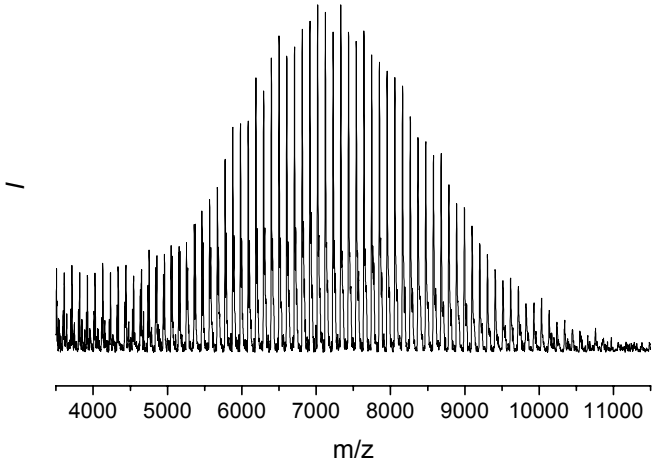

Figure 3.20. *MALDI-TOF mass spectrum of α,ω-terpyridine functionalized polystyrene.*

3.5 Conclusions

This chapter has been devoted to the introduction of terpyridine ligands at one or both chain ends of a polymer. Successful routes were developed by end group modifcation reactions using 4'-chloro-2,2':6',2"-terpyridine and 4'-(1-isocyanatopentoxy)-2,2':6',2"-terpyridine and by a functional initiator capable of controlling the radical polymerization of a variety of monomers. Kinetics of the polymerizations have been investigated for styrene, *n*-butylacrylate, *N,N*-dimethylacrylamide and 4-vinylpyridine. In all cases controlled polymerization were found, although auto-initiation and non-steady state kinetics can play important roles with respect to end-group functionality and polydispersity index. Some of the obtained polymers have been successfully applied as macroinitiators for the polymerization of a second monomer in order to obtain block copolymers. Terpyridine functionalized telechelics have also been prepared by end group modification reactions and nitroxide substitution reactions. Hence, the toolbox for preparing polymers with terpyridine end groups has been established and in principle each polymer can be used in the construction of more complex macromolecular architectures by connecting them with one another using metal ions. This will be the topic of the next chapter.

3.6 Experimental part

Chemicals were received from Aldrich, Fluka, Strem, Polymersource as well as Shearwater and used without further purification. Solvents were bought from Biosolve. DMSO was dried over BaO, THF and toluene were distilled over Na/K/benzophenone and Na, respectively, before use. All monomers were freshly purified on an AlOx-filtration column prior to use in order to remove the inhibitor. For preparative size exclusion chromatography, Bio-Rad SX-1 Beads swollen in CH_2Cl_2 or THF were used. ^{1}H-NMR-spectra were recorded on a Varian Inova spectrometer with frequencies of 500 MHz at 25 °C in addition to the NMR-spectrometers described in Chapter 2. Chemical shifts are given in ppm downfield from TMS. Three different GPC-set-ups have been used: 1) Size exclusion chromatography was performed on a 30 cm long Waters Styragel HT4-column and analyzed with an RI-detector (Waters 1414) with chloroform as the eluent with 4 vol% Et_3N and 2 vol% 2-propanol as additives to reduce column interactions at a flow of 0.5 mL/min utilizing a Waters 1515-pump. 2) Alternatively the solvent used was 5 mM NH_4PF_6 in DMF. Poly(ethylene oxide) and PMMA-standards were used for calibration; 3) (München) Size exclusion chromatography was performed on a 90 cm long mixed C-column (Waters Ultrastyragel, pore size 10000 and 100000 Å) and analyzed with a UV- and RI-detector (Waters 486 at 254 nm and Waters 410) with chloroform as the eluent at a flow of 1.0 mL min$^-$

[1] utilizing a Waters 510-pump. Polystyrene standards were used for calibration. For further information on experimental set-ups, see section 2.8.

4'-(1-Aminopentyloxy)-2,2';6',2''-terpyridine
To a suspension of KOH (37.25 g, 651 mmol) and 1-amino-pentan-5-ol (10.60 g, 103 mmol) in DMSO (500 mL) at 60 °C was added in small portions 4'-chloro-2,2':6',2"-terpyridine (25.00 g, 93 mmol). Stirring was continued overnight, after which the reaction mixture was poured into water (1000 mL). The yellow precipitate was filtered, washed with water (3 × 250 mL) and diethyl ether (2 × 100 mL). The crude product was recrystallized from hot ethanol and isolated as a yellow solid. Yield: 21.32 g (68%). ^{1}H NMR (400 MHz, $CDCl_3$): δ = 8.68 (dd, 2 H, ^3J = 5.0, ^4J = 1.8; $H_{6,6''}$), 8.61 (dd, 2 H, ^3J = 8.0, ^4J = 1.0; $H_{3,3''}$), 8.00 (s, 2 H, $H_{3',5'}$), 7.84 (dt, 2 H, ^3J = 8.0, ^4J = 1.6 Hz; $H_{4,4''}$), 7.32 (ddd, 2 H, ^3J = 8.0, ^3J = 4.8, ^4J = 1.2 Hz; $H_{5,5''}$), 4.23 (t, 2 H, ^3J = 6.2 Hz; H_ε), 2.73 (m, 2 H; H_α), 1.87 (m, 4 H; $H_{\delta,NH2}$), 1.54 (m, 4 H; $H_{\beta,\gamma}$). ^{13}C NMR (100 MHz, $CDCl_3$): δ = 166.8 ($C_{4'}$), 157.1 ($C_{2',6'}$), 155.9 ($C_{2,2''}$), 148.9 ($C_{6,6''}$), 136.7 ($C_{3',5'}$), 123.7 ($C_{3,3''}$), 121.2 ($C_{4,4''}$), 107.5 ($C_{5,5''}$), 68.0 (C_ε), 42.0 (C_α), 33.2 (C_δ), 28.8 (C_β), 23.3 (C_γ). MALDI-TOFMS (matrix: dithranol): *m/z* = 335 (MH^+). IR (ATR): ν (cm^{-1}): 3352, 3294 (NH_2); 3050, 3014, 2936, 2859 (CH_2); 1599, 1581, 1563 (tpy). UV/vis (CH_3CN): λ / nm (ε / L mol^{-1} cm^{-1}): 277 (21000), 241 (24800). Anal. Calcd. For $C_{20}H_{22}N_4O$ (334.18): C, 71.82; H, 6.63; N, 16.76; Found: C, 71.74; H, 6.46; N, 16.66.

General procedure for the synthesis of terpyridine end-functionalized poly(ethylene oxide)
Powdered KOH and *α*-methoxy-*ω*-hydroxy-poly(ethylene oxide) (with M_n = 3000, 5200, 10000, 16500 g/mol) were stirred under argon in dry DMSO at 70 °C. After 30 minutes a two times excess of 4'-chloro-2,2':6',2"-terpyridine[9] was added. The mixture was stirred for 24 h, then poured into cold water and extracted with CH_2Cl_2. The combined organic layers were dried over Na_2SO_4 and removed *in vacuo*. The compounds were purified by preparative size exclusion chromatography (BioBeads SX-1, CH_2Cl_2), followed by a double precipitation from THF into diethyl ether. Analytical data are for PEO_{70}, PEO_{125}, PEO_{225} and PEO_{375}, respectively. ^{1}H-NMR ($CDCl_3$): δ = 8.68 (d, 2 H, ^3J = 5.0 Hz; $H_{6,6''}$), 8.61 (d, 2 H, ^3J = 8.0 Hz; $H_{3,3''}$), 8.04 (s, 2 H; $H_{3',5'}$), 7.85 (td, 2 H, ^3J = 8.0 Hz, ^4J = 1.8 Hz; $H_{4,4''}$), 7.34 (dd, 2 H, ^3J = 8.0, ^3J = 5.0 Hz; $H_{5,5''}$), 4.40 (m, 2 H; tpyOCH_2), 3.93 (m, 2 H; tpyOCH_2CH_2), 3.83-3.45 (m, PEO backbone), 3.38 (s, 3 H, OCH_3). ^{13}C-NMR ($CDCl_3$): δ = 166.6 ($C_{4'}$), 156.7 ($C_{2',6'}$), 155.6 (C_2, $C_{2''}$), 148.7 ($C_{6,6''}$), 136.4 ($C_{4,4''}$), 123.5 ($C_{5,5''}$), 120.9 ($C_{3,3''}$), 107.0 ($C_{3',5'}$), 72.2-67.4 (*C* $_{\text{PEO backbone}}$), 58.6 (O*C*H_3). UV/Vis (H_2O): λ_{max} (ε) = 278 (13200), 234 (17000). IR (ATR): 2884, 2741 (CH_2); 1601, 1583, 1565 (tpy). MALDI-TOF-MS (PEO_{70}): M_n = 3123; (PEO_{125}) M_n = 5202; (PEO_{225}) M_n = 10901; (PEO_{375}) M_n = 17434 g/mol. GPC (RI) (PEO_{70}): M_n = 2500, PDI = 1.04; (PEO_{125}) M_n = 4200, PDI = 1.09 ; (PEO_{225}) M_n = 10000, PDI = 1.06; (PEO_{375}) M_n = 15500, PDI = 1.04.

Synthesis of terpyridine end-functionalized poly(ethylene-*co*-butylene)
A solution of powdered KOH (0.70 g, 12.3 mmol), 18-crown-6 (0.54 g, 2.05 mmol) and hydroxy-terminated poly(ethylene-*co*-butylene) (M_n = 3900 g/mol) (7.800 g, 2.05 mmol) was stirred at 90 °C in dry toluene (150 mL). After 1 h 4'-chloro-2,2':6',2"-terpyridine (0.80 g, 3.0 mmol) in dry toluene (30 mL) was added dropwise. The reaction mixture was stirred for 48 h, then concentrated and poured into water. The water-layer was extracted with $CHCl_3$ (3 × 25 mL). The combined organic layers were dried over Na_2SO_4 and removed *in vacuo*. The compound was purified by column chromatography (silica, CH_2Cl_2 followed with CH_2Cl_2:Et_3N = 9:1) yielding 3.9 g of product (46%). ^{1}H-NMR ($CDCl_3$): δ = 8.69 (m, 2 H; $H_{6,6''}$), 8.62 (m, 2 H; $H_{3,3''}$), 8.01 (s, 2 H; $H_{3',5'}$), 7.85 (m, 2 H; $H_{4,4''}$), 7.32 (m, 2 H; $H_{5,5''}$), 4.25 (m, 2 H; tpyOCH_2), 1.58-0.68 (m, 569 H; $H_{\text{PEB backbone}}$). ^{13}C-NMR ($CDCl_3$): δ = 166.5 ($C_{4'}$), 158.8 ($C_{2',6'}$), 156.1 ($C_{2,2''}$), 148.8 ($C_{6,6''}$), 136.5 ($C_{4,4''}$), 123.6 ($C_{5,5''}$), 121.2 ($C_{3,3''}$), 107.4 ($C_{3',5'}$), 59.0 (tpyOCH_2), 39.0-24.5 ($C_{\text{PEB backbone}}$), 11.1-9.8 ($C_{\text{PEB backbone}}$). UV/Vis (CH_2Cl_2): λ / nm (ε / L mol^{-1} cm^{-1}) = 278 (19600), 243 (21100). MALDI-TOF MS: M_n = 4151 g mol^{-1}. GPC (UV): M_n = 4450, PDI = 1.19.

Synthesis of terpyridine end-functionalized polystyrene (KOH-route)
A solution of powdered KOH (0.372 g, 6.52 mmol), 18-crown-6 (0.345 g, 1.31 mmol) and hydroxy-terminated polystyrene (M_n = 1900 g/mol) (2.500 g, 1.31 mmol) was stirred at 90 °C in dry toluene (25 ml). After 1 h 4'-chloro-2,2':6',2"-terpyridine (0.700 g, 2.61 mmol) in dry toluene (5 mL) was added dropwise. The reaction mixture was stirred for 48 h, then concentrated and precipitated into methanol. The precipitate was collected by filtration and centrifugation. The compound was purified by preparative size exclusion chromatography (BioBeads SX-1, CH_2Cl_2) followed by a second precipitation from toluene into methanol (2.10 g, 75%). ^{1}H-NMR ($CDCl_3$): δ

= 8.67 (m, 2 H; $H_{6,6"}$), 8.60 (m, 2 H; $H_{3,3"}$), 7.91 (s, 2 H; $H_{3',5'}$), 7.83 (m, 2 H; $H_{4,4"}$), 7.31-6.39 (m, 102 H; $H_{\text{aromatic PS backbone}}$; $H_{5,5"}$), 4.11-3.96 (m, 2 H; tpyOCH_2), 2.66 (m, 2 H; CH_2CH$_2$Otpy), 2.18-1.10 (m, 63 H; CH_2, CH $_{\text{PS backbone}}$), 0.78 (m, 6 H; CH_3). UV/Vis (CH_2Cl_2): λ / nm (ε / L mol^{-1} cm^{-1}) = 278 (19300), 243 (21500). MALDI-TOF MS: M_n = 2104 g mol^{-1}. GPC (UV): M_n (PDI): 1850 g mol^{-1} (1.10).

Synthesis of terpyridine end-functionalized polystyrene (*t*-BuOK route)
Hydroxy end functionalized polystyrene and *t*-BuOK (3 eq.) were refluxed for 15 min in dry THF under argon. Via an addition funnel a 2-fold excess of 4'-chloroterpyridine was added to the solution and was refluxed for an additional 4 hours. Hereafter the solution was directly precipitated in methanol (1:10 v/v). The white precipitate was reprecipitated from THF into methanol and washed with hexane. Yields varied from 76-85%. Analytical data are given for PS with DP = 104: ^{1}H-NMR: ($CDCl_3$): δ = 8.67 (m, 2 H; $H_{6,6"}$), 8.60 (m, 2 H; $H_{3,3"}$), 7.91 (s, 2 H; $H_{3',5'}$), 7.83 (m, 2 H; $H_{4,4"}$), 7.31-6.39 (m, 522 H; $H_{\text{aromatic PS backbone}}$, $H_{5,5"}$), 4.11-3.96 (m, 2 H; tpyOCH_2), 2.66 (m, 2 H; CH_2CH$_2$Otpy), 2.18-1.10 (m, 315 H; $H_{\text{PS backbone}}$), 0.78 (m, 6 H; CH_3). UV/Vis (CH_2Cl_2): λ / nm (ε / L mol^{-1} cm^{-1}) = 278, 243. MALDI-TOF MS: M_n = 9487 g/mol. GPC (RI): M_n = 9800, PDI = 1.13.

Synthesis of terpyridine end-functionalized PS_{32}-*b*-$P2VP_{13}$
Hydroxy end functionalized PS_{32}-*b*-$P2VP_{13}$ (0.250 g, 0.0556 mmol) (M_n = 4500 g/mol) and *t*-BuOK (0.019 g, 0.167 mmol) was stirred at reflux in dry THF (5 mL). After 15 minutes 4'-chloro-2,2':6',2''-terpyridine (0.030 g, 0.111 mmol) in dry THF (5 mL) was added dropwise. The reaction mixture was stirred overnight, after which the solvent was removed *in vacuo*. The resulting solid was partitioned between water and chloroform. The chloroform-layer was washed with water (3 × 25 mL). The organic layer, containing the product, was dried over Na_2SO_4 and removed *in vacuo*. The compound was purified by a double size exclusion chromatography (BioBeads SX-1, first column in THF, second column in CH_2Cl_2) yielding 0.187 g of product (72%). ^{1}H-NMR ($CDCl_3$): δ = 8.65 (m, 2 H; $H_{6,6"}$), 8.57 (m, 2 H; $H_{3,3"}$), 8.43-8.07 (m, 15 H; $H_{\text{P2VP backbone aromatic}}$, $H_{3',5'}$), 7.79 (m, 2 H; $H_{4,4"}$), 7.29-6.47 (m, 201 H; $H_{\text{P2VP \& PS backbone aromatic}}$, $H_{5,5"}$), 3.96 (m, 2 H; tpyOCH_2), 3.79 (m, 2 H; tpyOCH$_2$CH_2), 2.42-0.56 (m, 118 H; $H_{\text{P2VP \& PS backbone}}$). UV/Vis ($CH_2Cl_2$): λ / nm (ε / L mol^{-1} cm^{-1}) = 263 (69800). MALDI-TOF MS(dithranol): distribution with Δ(m/z) = 105 g mol^{-1}, peak of highest intensity m/z = 4526 g mol^{-1}; M_n = 4752 g mol^{-1}, PDI = 1.04. GPC (UV): M_n (PDI): 3500 g mol^{-1} (1.28).

Synthesis of terpyridine end-functionalized PEB_{68}-*b*-PEO_{48}
Hydroxy end functionalized PEB_{68}-*b*-PEO_{48} (0.500 g, 0.085 mmol) and *t*-BuOK (0.032 g, 0.280 mmol) was stirred at reflux in dry THF (5 mL). After 15 minutes 4'-chloro-2,2':6',2''-terpyridine **4** (0.057 g, 0.210 mmol) in dry THF (10 mL) was added dropwise. The reaction mixture was stirred overnight, after which the solvent was removed *in vacuo*. The resulting solid was partitioned between water and chloroform. The chloroform-layer was washed with water (3 × 25 mL). The organic layer, containing the product, was dried over Na_2SO_4 and removed *in vacuo*. The compound was purified by size exclusion chromatography (BioBeads SX-1, CH_2Cl_2). ^{1}H-NMR ($CDCl_3$): δ = 8.72 (m, 2 H; $H_{6,6"}$), 8.67 (m, 2 H; $H_{3,3"}$), 8.04 (bs, 2 H; $H_{3',5'}$), 7.85 (m, 2 H; $H_{4,4"}$), 7.37 (m, 2 H; $_{H5,5"}$), 4.41 (m, 2 H; tpyOCH_2), 3.96 (m, 2 H; tpyOCH$_2$CH_2), 3.83-3.45 (m, 188 H; $CH_2O_{\text{PEO backbone}}$), 1.62-0.78 (m, 539 H; $H_{\text{PEB backbone}}$, CH_2, CH_3). GPC (RI): M_n (PDI): 5400 g mol^{-1} (1.15).

Synthesis of 4'-(1-isocyanatopentyloxy)-2,2';6',2''-terpyridine
Di-*tert*butyltricarbonate (0.823 g, 3.14 mmol) was stirred in dry chloroform (50 mL). After 15 minutes a solution of 4'-(1-aminopentyloxy)-2,2':6',2''-terpyridine (1.000 g, 2.99 mmol) in dry chloroform (50 mL) was added by syringe in the stirring solution. Stirring was continued for another 20 minutes, after which the solvent was evaporated *in vacuo*. No further purification of the remaining brown oil that contained some of the excess tricarbonate was attempted and used as such. The oil was stored in the freezer (-25°C) until further use. Yield: 1.15 g (>99%). IR (ATR): ν (cm^{-1}): 3055, 2945, 2875 (CH terpyridine, alkyl CH_2); 2261 (NCO); 1600, 1582, 1563 (terpyridine). ^{1}H-NMR ($CDCl_3$): δ = 8.67 (dd, 2 H, ^3J = 4.8, ^4J = 1.8; $H_{6,6"}$), 8.60 (dd, 2 H, ^3J = 8.0, ^4J = 1.0; $H_{3,3"}$), 8.00 (s, 2 H; $H_{3',5'}$), 7.84 (td, 2 H, ^3J = 8.0, ^4J = 1.6 Hz; $H_{4,4"}$), 7.31 (ddd, 2 H, ^3J = 7.8, ^3J = 4.8, ^4J = 1.0 Hz; $H_{5,5"}$), 4.21 (t, 2 H, ^3J = 6.2 Hz; H_ε), 3.33 (t, 2 H, ^3J = 6.2 Hz; H_α), 1.86 (m, 2 H; H_δ), 1.66 (m, 2 H; H_β),1.52 (m, 2 H, H_γ). ^{13}C-NMR ($CDCl_3$): δ = 167.0 ($C_{4'}$), 157.0 ($C_{2',6'}$), 156.0 ($C_{2,2"}$), 148.9 ($C_{6,6"}$), 136.7 ($C_{3',5'}$), 123.7 ($C_{3,3"}$), 121.2 (N*C*O, $C_{4,4"}$), 107.2 ($C_{5,5"}$), 67.6 (C_ε), 42.7 (C_α), 30.8 (C_δ), 28.3 (C_β), 23.0 (C_γ).

Synthesis of α-hydrido-ω-terpyridinyl-polyferrocenyldimethylsilane
α-Hydrido-ω-hydroxy-polyferrocenyldimethylsilane (200 mg, 0.071 mmol), 4'-(1-isocyanatopentyloxy)-2,2':6',2"-terpyridine (50 mg, 0.142 mmol) and a catalytic amount dibutyltindilaurate (DBTDL) were stirred in dry chloroform (10 mL) under reflux. Stirring was continued overnight, after which the solvent was removed *in vacuo*. The crude product was purified by column chromatography (SiO_2, $CHCl_3$) and preparative size exclusion chromatography (BioBeads SX-1, CH_2Cl_2) and precipitated from THF in hexanes. Yield: 105 mg (46%). ^{1}H-NMR ($CDCl_3$): δ = 8.73 (d, ^3J = 5.2 Hz, 2 H; $H_{6,6"}$), 8.67 (d, ^3J = 8.0 Hz, 2 H; $H_{3,3"}$), 8.06 (bs, 2 H; $H_{3',5'}$), 7.87 (td, ^3J = 8.0, ^4J = 1.8 Hz, 2 H; $H_{4,4"}$), 7.35 (dd, ^3J = 8.0, ^4J= 5.2 Hz, 2 H; $H_{5,5"}$), 4.71 (bs, 1 H; N*H*CO), 4.37 (m, 2 H; tpyOCH_2), 4.32-3.89 (m, 99 H; fc PFS, C(=O)OCH_2), 3.22 (m, 2 H; CH_2NH), 1.88 (m, 2 H; tpyOCH$_2$CH_2), 1.59 (m, 6 H; CH_2), 0.70-0.27 (m, 74 H; SiCH_2, SiCH_3 PFS). UV/vis (CH_2Cl_2): λ / nm (ε / L mol^{-1} cm^{-1}): 453 (1800), continuously increasing absorption from 369 to 245 (400-93000). IR (ATR): ν (cm^{-1}): 3082, 2954 (alkyl CH_2, CH terpyridine); 1721, 1515 (NHCOO); 1600, 1583, 1564 (C=C, C=N, tpy); 1249, 1163, 1034, 797, 767 (PFS). GPC (RI): M_n = 2700 g mol^{-1}, PDI = 1.13. MALDI-TOF MS (dithranol): distribution with Δ(m/z) = 242 Da, peak of highest intensity m/z = 3080 g mol^{-1}; M_n = 3150 g mol^{-1}, PDI = 1.03.

Synthesis of terpyridine end-functionalized polybutadiene
ω-Hydroxy-polybutadiene (0.530 g, 0.110 mmol), 4'-(1-isocyanatopentyloxy)-2,2':6',2"-terpyridine (80 mg, 0.220 mmol) and a catalytic amount dibutyltindilaurate (DBTDL) were stirred in dry chloroform (15 mL) under reflux. Stirring was continued overnight, after which the solvent was removed *in vacuo*. The crude product was purified by precipitation from $CHCl_3$ in methanol. Yield: 0.443 (78%). ^{1}H-NMR ($CDCl_3$): δ = 8.68 (d, ^3J = 5.2 Hz, 2 H; $H_{6,6"}$), 8.63 (d, ^3J = 8.0 Hz, 2 H; $H_{3,3"}$), 8.01 (bs, 2 H; $H_{3',5'}$), 7.83 (td, ^3J = 8.0, ^4J = 1.8 Hz, 2 H; $H_{4,4"}$), 7.36 (dd, ^3J = 8.0, ^4J= 5.2 Hz, 2 H; $H_{5,5"}$), 5.80-4.92 (m, 168 H; $H_{PBD\ backbone}$), 4.84 (bs, 1 H; N*H*CO), 4.25 (m, 2 H; tpyOCH_2), 4.12 (m, 2 H; C(=O)OCH$_2$), 3.22 (m, 2 H; CH_2NH), 2.38-1.25 (m, 354 H; $H_{PBD\ backbone}$, CH_2). IR (ATR): ν (cm^{-1}): 3082, 3006, 2916, 2844 (CH_3, CH_2, CH backbone, CH terpyridine); 1728, 1515 (NHCOO); 1650, 1640 (PBD backbone); 1601, 1583, 1565 (C=C, C=N, tpy); 1444, 964 (PBD backbone). GPC (RI): M_n = 8000 g mol^{-1}, PDI = 1.08.

Synthesis of terpyridine end-functionalized polyisoprene
ω-Hydroxy-isoprene (7.00 g, 0.70 mmol), 4'-(1-isocyanatopentyloxy)-2,2':6',2"-terpyridine (500 mg, 1.39 mmol) and a catalytic amount dibutyltindilaurate (DBTDL) were stirred in dry chloroform (50 mL) under reflux. Stirring was continued overnight, after which the solvent was removed *in vacuo*. The crude product was purified by precipitation from $CHCl_3$ in methanol. Yield: 5.31 g (69%). ^{1}H-NMR ($CDCl_3$): δ = 8.71 (d, ^3J = 5.2 Hz, 2 H; $H_{6,6"}$), 8.64 (d, ^3J = 8.0 Hz, 2 H; $H_{3,3"}$), 8.03 (bs, 2 H; $H_{3',5'}$), 7.83 (td, ^3J = 8.0, ^4J = 1.8 Hz, 2 H; $H_{4,4"}$), 7.37 (dd, ^3J = 8.0, ^4J= 5.2 Hz, 2 H; $H_{5,5"}$), 5.04 (m, 100 H; PI backbone, 1,4-addition), 4.81-4.65 (m, 20 H, PI backbone, 1,2 addition), 4.93 (bs, 1 H; N*H*CO), 4.27 (m, 2 H; tpyOCH_2), 4.02 (m, 2 H; C(=O)OCH$_2$), 3.21 (m, 2 H; CH_2NH), 2.38-1.25 (m, 758 H; $H_{PI\ backbone}$, CH_2). IR (ATR): ν (cm^{-1}): 3036, 2961, 2922, 2854 (CH_3, CH_2, CH backbone, CH terpyridine); 1728, 1511 (NHCOO); 1664, 1644 (PI backbone); 1601, 1583, 1565 (C=C, C=N, tpy); 1445, 1376 (PI). GPC (RI): M_n = 14900 g mol^{-1}, PDI = 1.04.

Synthesis of α,ω-terpyridine end-functionalized poly(ethylene-*co*-butylene)
Hydroxy end functionalized poly(ethylene-*co*-butylene) (43.35 g, 10.8 mmol) and *t*-BuOK (7.35 g, 65 mmol) were refluxed for 60 min in dry THF (250 mL) under argon. Via an addition funnel an excess of 4'-chloroterpyridine (11.61 g, 43 mmol) in dry THF (100 mL) was added to the solution and refluxing continued overnight. Hereafter the solution was directly precipitated in methanol. The brown oil was reprecipitated from $CHCl_3$ into methanol. Yield: 26.83 g (52%). ^{1}H-NMR: ($CDCl_3$): δ = 8.69 (m, 2 H; $H_{6,6"}$), 8.62 (m, 2 H; $H_{3,3"}$), 8.01 (s, 2 H; $H_{3',5'}$), 7.85 (m, 2 H; $H_{4,4"}$), 7.32 (m, 2 H; $H_{5,5"}$), 4.25 (m, 2 H; tpyOCH_2), 1.58-0.68 (m, 569 H; $H_{PEB\ backbone}$). ^{13}C-NMR ($CDCl_3$): δ = 166.5 ($C_{4'}$), 158.8 ($C_{2',6'}$), 156.1 ($C_{2,2"}$), 148.8 ($C_{6,6"}$), 136.5 ($C_{4,4"}$), 123.6 ($C_{5,5"}$), 121.2 ($C_{3,3"}$), 107.4 ($C_{3',5'}$), 59.0 (tpyOCH$_2$), 39.0-24.5 ($C_{PEB\ backbone}$), 11.1-9.8 ($C_{PEB\ backbone}$). UV/Vis (CH_2Cl_2): λ / nm (ε / L mol^{-1} cm^{-1}) = 278 (19600), 243 (21100). MALDI-TOF MS: M_n = 4151 g mol^{-1}. GPC (UV): M_n = 4500, PDI = 1.19.

Synthesis of terpyridine functionalized initiator (2,2,5-trimethyl-3-(1-(4'-(4"-terpyridinyloxy)-methyl)phenylethoxy)-4-phenyl-3-azahexane)
To a suspension of 2,6-*bis*-(2'-pyridyl)-4-pyridon **2** (7.50 g, 0.030 mol) and K_2CO_3 (14.70 g, 0.110 mol) in dry DMF (75 mL) at 50 °C, a solution of 2,2,5-trimethyl-3-(1-(4'-chloromethyl)phenylethoxy)-

4-phenyl-3-azahexane[27] (10.65 g, 0.029 mol) in dry DMF (25 mL) was added dropwise. Stirring was continued overnight, after which the reaction mixture was cooled, poured into cold water (500 mL) and extracted with CH_2Cl_2 (3 × 300 mL). The combined organic layers were dried over Na_2SO_4, filtered and removed *in vacuo*. The light brown residue was subjected to a filtration column (AlOx, hexane:CH_2Cl_2, 1:1) and recrystallized twice from ethanol, yielding 10.15 g (61%) of a polycrystalline white powder. The presence of diastereomers makes the normally well-defined *J*-couplings in the terpyridine-region loose the fine-splitting into ddd, td or dd and only multiplets or doublets remain. ^{1}H-NMR ($CDCl_3$, both diastereomers): δ = 8.69 (m, 4 H; $H_{6,6''}$), 8.62 (d, 4 H, *J* = 7.5 Hz; $H_{3,3''}$), 8.17 (s, 2 H; $H_{3',5'}$, major), 8.16 (s, 2 H; $H_{3',5'}$, minor), 7.82 (t, 4 H, *J* = 7.4 Hz; $H_{4,4''}$), 7.57-7.18 (m, 22 H; aromatic & $H_{5,5''}$) 5.35 (s, 2 H; tpyOCH_2, minor), 5.30 (s, 2 H; tpyOCH_2, major), 4.97 (q + q, 2 H, *J* = 6.0 Hz; *H*C-ON, both diastereomers), 3.47 (d, 1 H, *J* = 10.5 Hz; ON-C*H*, major), 3.36 (d, 1 H, *J* = 10.5 Hz; ON-C*H*, minor), 2.38 (m, 1 H; CH_3CHCH_3, major) 1.67 (d, 3 H; *J* = 6.0 Hz, CH_3CH-ON, major), 1.58 (d, 3 H, *J* = 6.0 Hz; CH_3CH-O-N, minor), 1.43 (m, 1 H; CH_3CHCH_3, minor), 1.34 (d, 3 H, *J* = 6.0 Hz; CH_3CHCH$_3$, major), 1.08 (s, 9 H; C(CH_3)$_3$, minor), 0.93 (d, 3 H, *J* = 6.0 Hz; CH$_3$CHCH_3, major), 0.81 (s, 9 H; C(CH_3)$_3$, major), 0.56 (d, 3 H, *J* = 6.0 Hz; CH_3CHCH$_3$, minor), 0.21 (d, 3 H, *J* = 6.0 Hz; CH$_3$CHCH_3, minor). ^{13}C-NMR (125 MHz, $CDCl_3$, 25 °C): 166.9 ($C_{4'}$), 157.0 ($C_{2',6'}$), 155.9 ($C_{2,2''}$), 148.9 ($C_{6,6''}$), 145.7, 144.9, 142.3, 142.1 (q, C aromatic), 136.7 ($C_{3',5'}$), 135.0, 134.3 (q, C aromatic), 130.9, 130.8, 127.3-126.1 (*C*-H aromatic), 123.7 ($C_{3,3''}$), 121.3 ($C_{4,4''}$), 107.7, 107.6 ($C_{5,5''}$), 83.1 (*C*-O-N, major), 82.3 (*C*-O-N, minor), 72.1 (O-N-*C*, major), 72.0 (O-N-*C*, minor), 69.9 (tpyO*C*H$_2$, major), 69.8 (tpyO*C*H$_2$, minor), 60.4 (*C*(CH$_3$)$_3$, major), 60.3 (*C*(CH$_3$)$_3$, minor), 31.9, 31.6, 28.3 (C(*C*H$_3$)$_3$, minor), 28.2 (C(*C*H$_3$)$_3$, major), 24.5, 23.0, 22.0, 21.9, 21.1, 20.9. UV/vis (CH_2Cl_2): λ / nm (ε / l mol^{-1} cm^{-1}): 278 (20100), 240 (25300). IR (ATR): ν (cm^{-1}): 3060 (CH_2, CH_3); 2973, 2868 (CH); 1600, 1582, 1563 (C-C, C-N terpyridine), 1516, 1468, 1385, 1354, 1195, 1063, 1015, 821, 793, 743, 733, 701. MALDI-TOF MS (dithranol): m/z: 587 ($M+H^+$, 80%), 336 (M^+-nitroxide, 20%). Anal. Calcd. for $C_{38}H_{42}N_4O_2$ (586.40): 77.83% C, 7.22% H, 9.55% N; found: 77.94% C, 7.18% H, 9.34% N.

General procedure for the polymerization of styrene

A stock solution of the initiator in 25 mL of purified styrene (0.210 mol) was prepared. For a degree of polymerization (DP) of 125, 250 and 500 the corresponding amounts of initiator were 0.968 g (166 mmol), 0.499 g (85 mmol), 0.247 g (42 mmol). For a DP of 800, 0.128 g (21 mmol) were dissolved in 20 mL of purified styrene. The stock solution was transferred for the various kinetic investigations to 7-9 reaction vessels. Three freeze-pump-thaw-cycles were applied for removal of oxygen before the reaction vessels were immersed in an oilbath of 125 °C. The polymerization was carried out for a certain amount of time and then stopped. In total 7-9 different polymerization times were used for the polymerization of the same stock solution. The conversion was measured gravimetrically. Molecular weights and polydispersity indices were measured by size exclusion chromatography, whereas ^{1}H-NMR was used for the determination of end group functionality and molecular weight by careful integration of the polymer backbone to the terpyridine signals. Purification by column chromatography of terpyridine-functionalized from non-functionalized polystyrene was carried out on silica, eluting first with hexane:CH_2Cl_2 (1:3), then CH_2Cl_2 and finally increasing the gradient with THF. For M_n above 10,000 g mol^{-1} of the terpyridine functional polystyrene, adding THF was not necessary. After analysis the polystyrene was precipitated twice from chloroform into methanol. Analytical data are for PS_{70}. ^{1}H-NMR ($CDCl_3$): δ = 8.68 (m, 2 H; $H_{6:6''}$), 8.62 (m, 2 H; $H_{3:3''}$), 8.21 (m, 2 H; $H_{3':5'}$), 7.93 (m, 2 H; $H_{4:4''}$), 7.47-6.32 (m, 353 H; $H_{PS\ backbone\ aromatic}$; $H_{aromatic}$, $H_{5,5''}$), 5.34 (m, 2 H; tpyOCH_2), 4.27-4.07 (broad, 1 H; *H*C-ON), 3.50-3.15 (m, 1 H; ON-C*H*), 2.45-0.53 (m, 225 H, $H_{PS\ backbone\ aliphatic}$; C(C$H_3$)$_3$; C$H_3$CHCH$_3$; C$H_{3\ initiating\ fragment}$). GPC (UV): M_n (PDI): 7700 g mol^{-1} (1.08).

General procedure for the polymerization of *n*-butylacrylate

A stock solution of the initiator in 25 mL of purified *n*-butylacrylate (0.175 mol) was prepared. To each stock solution an appropriate amount of free nitroxide was added. For a DP of 100, 200 and 400 the corresponding amounts of initiator were 1.025 g (1.75 mmol), 0.514 g (0.875 mmol) and 0.265 g (0.451 mmol) and the corresponding amounts of nitroxide were 19.1 mg (86 μmol), 5.0 mg (23 μmol) and 4.9 mg (22 μmol) respectively. The stock solution was then divided over 7-9 different reaction vessels. Three freeze-pump-thaw cycles were applied for removal of oxygen before the reaction vessels were immersed in an oilbath of 125 °C. The polymerization was carried out for a certain amount of time and then stopped. In total 7-9 different polymerization times were used for the polymerization of the same stock solution. The conversion was measured gravimetrically. Molecular weights and polydispersity indices were measured by size exclusion chromatography, whereas ^{1}H-NMR was used for the determination of end group functionality and molecular weight by careful integration of the polymer backbone to the terpyridine signals. After analysis of the relevant data for the kinetic

investigations, the polymers were precipitated from CH_2Cl_2 into methanol. Analytical data are for P(*n*-BA) of M_n = 4500 g mol^{-1}. ^{1}H-NMR ($CDCl_3$): δ = 8.69 (m, 4 H; $H_{6,6"}$), 8.63 (m, 4 H; $H_{3,3"}$), 8.17 (bs, 4 H; $H_{3',5'}$), 7.83 (m, 4 H; $H_{4,4"}$), 7.44-7.18 (m, 22 H; $H_{aromatic}$, $H_{5,5"}$) 5.31 (m, 4 H; tpyOCH_2, both diastereomers), 4.38 (m, 2 H; *H*C-ON, both diastereomers), 4.08 (m, 140 H; $OCH_{2\ PBA\ backbone}$), 3.41 (m, 1 H; ON-C*H* minor), 3.31 (m, 1 H; ON-C*H* major), 2.72 (bs, 1 H; CH_3CHCH_3 major), 2.37 (m, 35 H; $OCH_2CH_{2\ PBA\ backbone}$), 1.96-1.17 (m, 292 H; $CH_{2\ PBA\ backbone}$, CH_3CHCH_3 major, CH_3CHCH_3 minor, $CH_{3\ initiating\ fragment}$), 0.96 (m, 228 H; $CH_{3\ PBA\ backbone}$, $C(CH_3)_3$ both diastereomers), 0.57 (m, 3H; CH_3CHCH_3 minor), 0.42 (m, 3H; CH_3CHCH_3 major). GPC (RI): M_n (PDI): 4500 (1.28).

General procedure for the polymerization of *N,N*-dimethylacrylamide

A stock solution of the initiator (1.412 g, 2.41 mmol) in 25 mL of purified *N,N*-dimethylacrylamide (0.241 mol) containing 5 mol% free nitroxide (26.5 mg, 120 μmol) was prepared. The stock solution was then divided over 7-9 different reaction vessels. Three freeze-pump-thaw cycles were applied for removal of oxygen before the reaction vessels were immersed in an oilbath of 125 °C. The polymerization was carried out for a certain amount of time and then stopped. In total 7-9 different polymerization times were used for the polymerization of the same stock solution. The conversion was measured gravimetrically. Molecular weights and polydispersity indices were measured by size exclusion chromatography, whereas ^{1}H-NMR was used for the determination of end group functionality and molecular weight by careful integration of the polymer backbone to the terpyridine signals. After analysis of the relevant data for the kinetic investigations, the polymers were precipitated from $CHCl_3$ into diethyl ether. Analytical data are for PDMAA of M_n = 4200 g mol^{-1}. ^{1}H-NMR ($CDCl_3$): δ = 8.68 (m, 4 H; $H_{6,6"}$), 8.61 (m, 4 H; $H_{3,3"}$), 8.13 (bs, 2 H; $H_{3',5'}$ major), 8.09 (bs, 2 H; $H_{3',5'}$ minor), 7.84 (m, 4 H; $H_{4,4"}$), 7.44-7.08 (m, 22 H; $H_{aromatic}$, $H_{5,5"}$), 5.30 (m, 4 H, tpyOCH_2), 4.88 (m, 1 H; *H*C-ON, major), 4.04 (m, 1 H; *H*C-ON, minor), 3.52-2.13 (m, 534 H; $N(CH_3)_{2\ PDMAA\ backbone}$, $CH_{PDMAA\ backbone}$, ON-C*H*, $CH_{3\ initiating\ fragment}$, CH_3CHCH_3, CH_3CHCH_3 major, CH_3CHCH_3 minor), 2.05-0.80 (m, 166 H; $CH_{2\ PDMAA\ backbone}$, $C(CH_3)_3$), 0.57 (m, 3H; CH_3CHCH_3 minor), 0.42 (m, 3H; CH_3CHCH_3 major). GPC (RI): M_n (PDI): 5200 g mol^{-1} (1.27).

General procedure for the polymerization of 4-vinylpyridine

A stock solution of the initiator (0.921 g, 1.57 mmol) in 25 mL of purified 4-vinylpyridine (0.235 mol). The stock solution was then divided over 7-9 different reaction vessels. Three freeze-pump-thaw cycles were applied for removal of oxygen before the reaction vessels were immersed in an oilbath of 125 °C. The polymerization was carried out for a certain amount of time and then stopped. In total 7-9 different polymerization times were used for the polymerization of the same stock solution. The conversion was measured gravimetrically. Molecular weights and polydispersity indices were measured by size exclusion chromatography, whereas ^{1}H-NMR was used for the determination of end group functionality and molecular weight by careful integration of the polymer backbone to the terpyridine signals. After analysis of the relevant data for the kinetic investigations, the polymers were precipitated from $CHCl_3$ into diethyl ether. Analytical data is for poly(4-vinylpyridine) of M_n = 4000 g mol^{-1}. ^{1}H-NMR ($CDCl_3$): δ = 8.66 (m, 4 H; $H_{6,6"}$), 8.63 (m, 4 H; $H_{3,3"}$), 8.60-8.01 (m, 138 H; *o*-$H_{P4VP\ backbone}$, $H_{3',5'}$), 7.84 (m, 4 H; $H_{4,4"}$), 7.42-7.08 (m, 22 H; $H_{aromatic}$, $H_{5,5"}$), 6.80-6.10 (m, 136 H; *m*-$H_{P4VP\ backbone}$), 5.24 (m, 4 H; tpyOCH_2), 4.45 (m, 1 H; *H*C-ON minor), 4.07 (m, 1 H; *H*C-ON major), 2.53-0-44 (m, 244 H; $CH_{2\ P4VP\ backbone}$, $CH_{P4VP\ backbone}$, nitroxide (34 H), initiating fragment (6 H)). GPC (RI): M_n (PDI): 4000 g mol^{-1} (1.14).

Synthesis of terpyridine end-functionalized polyisoprene

Isoprene (7.50 g, 0.037 mol) and the initiator (0.240 g, 0.37 mmol) were transferred into a reactor vessel. After three freeze-pump-thaw-cycles the vessel was immersed in an oilbath of 125 °C. The polymerization was stopped after 48 hours by cooling the reaction mixture to room temperature. The resulting viscous oil was diluted with chloroform and precipitated into methanol. Yield: 3.48 g (45%). ^{1}H-NMR ($CDCl_3$): δ = 8.68 (m, 4 H; $H_{6,6"}$), 8.62 (m, 4 H; $H_{3,3"}$), 8.13 (bs, 4 H; $H_{3',5'}$), 7.84 (m, 4 H; $H_{4,4"}$), 7.42-7.15 (m, 22 H; $H_{nitroxide}$, $H_{initiating\ fragment}$, $H_{5,5"}$), 5.77 (m, 4 H; tpyOCH_2), 5.42-4.63 (m, 45 H; PI backbone), 4.53 (m, 2 H; H_2C-ON minor), 4.37 (m, 2 H; H_2C-ON major), 4.22 (m, 1 H; ON-C*H* minor), 3.38 (m, 1 H; ON-C*H* major), 2.88 (m, 1 H; CH_3CHCH_3 major), 2.76 (m, 1 H; CH_3CHCH_3 minor), 2.38-1.25 (m, 630 H; $H_{PI\ backbone,\ nitroxide}$), 1.20 (m, 3 H; CH_3CHCH_3 minor), 0.93 (m, 18 H; $C(CH_3)_3$, both), 0.51 (m, 3 H; CH_3CHCH_3 major). GPC (RI): M_n (PDI) = 4700 g mol^{-1} (1.23).

Synthesis of terpyridine end-functionalized poly(2-vinylpyridine)

2-Vinylpyridine (5.230 g, 0.051 mol) and the initiator (0.573 g, 1.0 mmol) were transferred into a reactor vessel. After three freeze-pump-thaw-cycles the vessel was immersed in an oilbath of 125 °C.

The polymerization was stopped after 3.5 hours by cooling the reaction mixture to room temperature. At this point the solution had become so viscous that stirring had stopped. The glassy solid was solubilized in dichloromethane and precipitated in hexane. Yield: 4.89 g (90%). Analytical data are for P2VP with M_n = 5100 g mol^{-1}. ^{1}H-NMR ($CDCl_3$): 8.70 (m, 2 H; $H_{6,6''}$), 8.62 (m, 2 H; $H_{3,3''}$), 8.53-7.99 (m, 46 H; $H_{P2VP\ backbone}$, $H_{3',5'}$), 7.82 (m, 2 H; $H_{4,4''}$), 7.43-6.19 (m, 143 H; $H_{6,\ P2VP\ backbone}$, $H_{nitroxide}$, $H_{initiating\ fragment}$, $H_{5,5''}$), 5.22 (m, 2 H; tpyOCH_2), 4.32-4.18 (m, 1 H; *H*C-ON), 3.40-3.07 (m, 1 H; ON-CH), 2.18-0.51 (m, 148 H; $H_{P2VP\ backbone}$, $H_{nitroxide}$, $H_{initiating\ fragment}$). GPC (RI): M_n (PDI) = 5100 g mol^{-1} (1.27). MALDI-TOF MS: two distributions (parent, parent - nitroxide) with $\Delta m/z$ = 105; M_n (PDI) = 3854 g mol^{-1} (1.14).

Synthesis of terpyridine-functionalized polyisoprene-*block*-polystyrene

A terpyridine-functionalized polystyrene macro-initiator (1.00 g, DP = 70, 143 μmol) and isoprene (2.43 g, 35.7 mmol) were transferred into a reactor vessel. After three freeze-pump-thaw-cycles the vessel was immersed in an oilbath of 125 °C. The polymerization was stopped after 24 hours. The reaction mixture was diluted with chloroform and precipitated twice into methanol. Yield: 1.53 g (44%). ^{1}H-NMR ($CDCl_3$): δ = 8.68 (m, 4 H; $H_{6,6''}$), 8.62 (m, 4 H; $H_{3,3''}$), 8.14 (m, 4 H; $H_{3',5'}$), 7.82 (m, 4 H; $H_{4,4''}$), 7.41-6.28 (m, 363 H; $H_{PS\ backbone\ aromatic}$; $H_{aromatic}$, $H_{5,5''}$), 5.74 (m, 4 H; tpyOCH_2) 5.45-4.59 (m, 130 H; $H_{vinylic\ PI\ backbone}$), 4.51 (m, 2 H; H_2C-ON minor), 4.36 (m, 2 H; H_2C-ON major), 4.22 (m, 1 H; ON-C*H* minor), 3.37 (m, 1 H; ON-C*H* major), 2.70 (m, 1 H; CH_3CHCH_3 major), 2.46-0.83 (m, 1147 H; $H_{aliphatic\ PI\ backbone,\ nitroxide}$) 0.48 (m, 3 H; CH_3CHCH_3 major). GPC (RI): M_n (PDI): 13900 g mol^{-1} (1.23).

Synthesis of terpyridine-functionalized poly(*N,N*-dimethylacrylamide)-*block*-poly(4-vinyl-pyridine)

A terpyridine-functionalized poly(4-vinylpyridine) macro-initiator (278 mg, DP = 39, 62 μmol), *N,N*-dimethylacrylamide (1.554 g, 15.5 mmol) and the nitroxide (0.49 mg, 2.2 μmol) were transferred to a reactor vessel. After three freeze-pump-thaw-cycles the vessel was immersed in an oilbath of 115 °C. The polymerization was stopped after 4 hours. The reaction mixture was diluted with chloroform and precipitated twice into diethyl ether. Yield: 733 mg (38%). ^{1}H-NMR ($CDCl_3$): δ = 8.68 (m, 4 H; $H_{6,6''}$), 8.62 (m, 4 H; $H_{3,3''}$), 8.60-8.11 (m, 172 H; *o*-H $_{P4VP\ backbone}$, $H_{3',5'}$) 7.84 (m, 4 H; $H_{4,4''}$), 7.42-7.17 (m, 22 H; $H_{aromatic}$, $H_{5,5''}$) , 6.84-6.19 (m, 168 H; *m*-H $_{P4VP\ backbone}$), 5.25 (m, 2 H; tpyOCH_2), 4.78 (m, 1 H; *H*C-ON, major), 4.04 (m, 1 H; *H*C-ON, minor), 3.22-2.21 (m, 530 H; N($C\!H_3$)$_{2\ PDMAA\ backbone}$, $C\!H_{\ PDMAA\ backbone}$, ON-C*H*, $C\!H_{3\ initiating\ fragment}$, $CH_3C\!HCH_3$, $C\!H_3CHCH_3$ major, $CH_3CHC\!H_3$ minor), 2.20-0.88 (m, 218 H; $CH_{2\ PDMAA\ backbone}$, $H_{aliphatic\ P4VP\ backbone}$, $C(CH_3)_3$), 0.49 (m, 3H; $C\!H_3CHCH_3$ minor), 0.33 (m, 3H; $CH_3CHC\!H_3$ major). GPC (RI): M_n (PDI): no signal!

Synthesis of *N*-(4'-terpyridinyl)pent-5-oxy)maleimide (5)

(a). A solution of 1-amino-5-(4'-terpyridinyl)oxypentane[8] (5.16 g, 15 mmol) and maleic anhydride (1.47 g, 15 mmol) in dry *p*-xylene (50 mL) was refluxed overnight, while the produced water was removed by a Dean-Stark-trap. After reaction, the solvent was removed *in vacuo*. The brown residue was subjected to column chromatography (AlOx, CH_2Cl_2) and the product was isolated as a white solid (1.73 g, 28%).

(b). Mitsunobe coupling: A solution of Ph_3P (0.393 g, 1.50 mmol) in dry THF (20 mL) was cooled to -78°C. DIAD (0.313 g, 1.55 mmol) was added over 2-3 min. To the yellow reaction mixture 1-hydroxy-5-(4'-terpyridinyl)oxypentane (0.544 g, 1.62 mmol) was added, followed by neopentylalcohol (0.073 g) and subsequently maleimide (0.146 g, 1.50 mmol). The resulting suspension was stirred for 5 min, after which the reaction mixture was allowed to heat up to room temperature and stirred overnight. THF was removed *in vacuo* and the residue was purified by column chromatography (AlOx, hexane:EtOAc 1:2, gradually increasing to EtOAc), yielding an off-white solid (116 mg, 19%). TLC-analysis showed one spot, however judging from the ^{1}H-NMR and elemental analysis the compound was not pure. No further purification efforts were undertaken, since route (a) was less time-consuming and more straightforward.

^{1}H-NMR ($CDCl_3$): δ = 8.68 (dd, 2 H, J = 4.8, 1.5 Hz; $H_{6,6''}$), 8.60 (dd, 2 H, J = 7.2, 1.0 Hz; $H_{3,3''}$), 7.99 (s, 2 H; $H_{3',5'}$), 7.83 (td, 2 H, ^3J = 7.2, ^4J = 1.6 Hz; $H_{4,4''}$), 7.31 (ddd, 2 H, J = 7.2, 4.8, 1.6 Hz; $H_{5,5''}$), 6.68 (d, 2 H, J = 0.4 Hz; H vinylic), 4.21 (t, 2 H, J = 8.0 Hz; O$C\!H_2$) 3.56 (t, 2 H, J = 9.2 Hz; N$C\!H_2$), 1.89 (m, 2 H; $OCH_2C\!H_2$), 1.68 (m, 2 H; $NCH_2C\!H_2$), 1.52 (m, 2 H; $CH_2C\!H_2CH_2$). ^{13}C-NMR ($CDCl_3$): δ = 170.7 (*C*O), 167.1 ($C_{4'}$), 156.9 ($C_{2',6'}$), 156.0 ($C_{2,2''}$), 148.9 ($C_{6,6''}$), 136.6 ($C_{3',5'}$), 133.9 (*C* vinylic), 123.7 ($C_{3,3''}$), 121.2 ($C_{4,4''}$), 107.2 ($C_{5,5''}$), 67.7 (O$C\!H_2$), 37.5 (N$C\!H_2$), 28.4 ($OCH_2C\!H_2$), 28.1 ($NCH_2C\!H_2$), 23.2 ($CH_2C\!H_2CH_2$). UV/vis (CH_2Cl_2): λ / nm (ε / l mol^{-1} cm^{-1}): 279 (24400), 243 (24900). IR (ATR): ν

(cm^{-1}): 3083, 3069, 3014 (CH_3, CH_2), 2938, 2908, 2865 (CH), 1698 (C=O), 1601, 1581, 1562 (tpy). MALDI-TOF MS (dithranol): m/z = 415 ($M+H^+$, 100%). Elem. Anal.: calculated for $C_{24}H_{22}N_4O_3$: 69.55% C, 5.35% H, 13.52% N. Found: 69.14% C, 5.43% H, 13.48% N.

Synthesis of α,ω-maleimido terpyridine-functionalized polystyrene

Terpyridine functionalized polystyrene (after purification by column chromatography, 300 mg, 4 μmol) and **5** (66 mg, 16 μmol) were heated under argon at 100 °C in degassed *t*-butylbenzene for 2 hours. The temperature was then increased to 125 °C and heating was continued for another 4 hours. The solution was allowed to cool to room temperature and precipitated into methanol. The white precipitate was isolated and reprecipitated from THF into methanol. Yield: 240 mg (78%). ^{1}H-NMR ($CDCl_3$): δ = 8.67 (m, 4 H; $H_{6:6"}$), 8.61 (m, 4 H; $H_{3:3"}$), 8.18 (s, 2 H; $H_{3':5',\ initiating\ fragment}$), 7.98 (s, 2 H; $H_{3':5',\ maleimide}$), 7.79 (m, 4 H; $H_{4,4"}$), 7.37-6.21 (m, 349H, $H_{PS\ backbone\ aromatic}$; $CH_{maleimide}$, $H_{5,5"}$), 5.28 (m, 2 H; tpyO$CH_{2,\ initiating\ fragment}$), 4.19 (m, 2 H; tpyO$CH_{2,\ maleimide}$), 3.70 (m, 2 H; NC$H_{2,\ maleimide}$), 2.28-0.60 (m, 215 H; $H_{PS\ bacbone\ aliphatic}$; $CH_{2,\ maleimide}$; $CH_{3,\ initiating\ fragment}$). GPC (UV): M_n (PDI): 7800 g mol^{-1} (1.09). MALDI-TOF MS (dithranol): M_n (PDI): 7200 g mol^{-1} (1.04).

Synthesis of α,ω-maleimido terpyridine-functionalized poly(*n*-butylacrylate)

Terpyridine functionalized poly(*n*-butylacrylate) (200 mg, 2.9 μmol) and maleimide (30 mg, 7 μmol) were heated under argon at 100 °C in degassed *t*-butylbenzene for 2 hours. The temperature was then increased to 125 °C and heating was continued for another 4 hours. The solution was allowed to cool to room temperature and precipitated into methanol. The oil was isolated by decantation and reprecipitated from THF into methanol. Yield: 134 mg (66%). ^{1}H-NMR ($CDCl_3$): δ = 8.69 (m, 4 H; $H_{6:6"}$), 8.63 (m, 4 H; $H_{3:3"}$), 8.12 (s, 2 H; $H_{3':5',\ initiating\ fragment}$), 7.99 (s, 2 H; $H_{3':5',\ maleimide}$), 7.84 (m, 4 H; $H_{4,4"}$), 7.41-7.18 (m, 8 H; $H_{aromatic\ initiating\ fragment}$, $H_{5,5"}$), 6.70 (s, 1 H; $H_{aromatic\ maleimide}$), 5.28 (m, 2 H; tpyO$CH_{2,\ initiating\ fragment}$), 4.21 (m, 2 H; tpyO$CH_{2,\ maleimide}$), 4.07-3.77 (m, 110 H; $OCH_{2,PBA}$), 3.70 (m, 2 H; NC$H_{2,\ maleimide}$), 2.22-0.88 (m, 559 H; $H_{PBA\ backbone}$ $CH_{2,\ maleimide}$; $CH_{3,\ initiating\ fragment}$). GPC (UV): M_n (PDI): 8200 g mol^{-1} (1.17). MALDI-TOF MS (dithranol): M_n (PDI): 6200 g mol^{-1} (1.14).

3.7 Literature

[1] B. G. G. Lohmeijer, U. S. Schubert, *J. Polym. Sci. Part A Polym. Chem.* **2003**, *41*, 1413-1427.
[2] E. C. Constable, M. D. Ward, *J. Chem. Soc. Dalton Trans.* **1990**, 1405-1409.
[3] J. Pahnke, *Diplomarbeit*, Eindhoven University of Technology, **2001**.
[4] P. R. Andres, *PhD-Thesis*, Eindhoven University of Technology, **2004**.
[5] A. M. W. Cargill Thompson, *Coord. Chem. Rev.* **1997**, *160*, 1-52.
[6] P. Pechy, F. P. Rotzinger, M. K. Nazeeruddin, O. Kohle, S. M. Zakeeruddin, *J. Chem. Soc. Chem. Comm.* **1995**, 65-66.
[7] K. T. Potts, D. Konwar, *J. Org. Chem.* **1991**, *56*, 4815-4816.
[8] G. R. Newkome, E. He, *J. Mater. Chem.* **1997**, *7*, 1237-1244.
[9] C. S. Dean, D. S. Tarbell, A. W. Friederang, *J. Org. Chem.* **1970**, *35*, 3393-3397.
[10] H. W. I. Peerlings, E. W. Meijer, *Tetrahedron Lett.* **1999**, *40*, 1021-1024.
[11] K. Schwetlick, R. Noack, F. Stebner, *J. Chem. Soc. Perkin Trans. 2* **1994**, 599-608.
[12] U. S. Schubert, O. Hien, C. Eschbaumer, *Macromol. Rapid Commun.* **2000**, *21*, 1156-1161.
[13] U. S. Schubert, C. Eschbaumer, *Macromol. Symp.* **2001**, *163*, 177-187.
[14] H. Pasch, W. Schrepp, *MALDI-TOF Mass spectrometry of synthetic polymers,* Springer, Berlin, **2003**.
[15] H. Brody, D. H. Richards, M. Szwarc, *Chem. & Industry* **1958**, *45*, 1473-1474.
[16] M. Tohyama, A. Hirao, S. Nakahama, K. Takenaka, *Macromol. Chem. Phys.* **1996**, *197*, 3135-3148.
[17] H. M. Keizer, R. van Kessel, R. P. Sijbesma, E. W. Meijer, *Polymer* **2003**, *44*, 5505-5511.
[18] J. P. Spatz, S. Mössmer, C. Hartmann, M. Möller, T. Herzog, M. Krieger, H.-G. Boyen, P. Ziemann, B. Kabius, *Langmuir* **2000**, *16*, 407-415.
[19] P. Hoerner, G. Riess, F. Rittig, G. Fleischer, *Macromol. Chem. Phys.* **1998**, *199*, 343-352.
[20] X.-S. Wang, M. A. Winnik, I. Manners, *Macromol. Rapid Commun.* **2002**, *23*, 210-213.
[21] A. J. Bloodworth, A. G. Davies, *J. Chem. Soc.* **1965**, 5238-5244.
[22] M. Hesse, H. Meier, B. Zeeh, *Spektroskopische Methoden in der Organischen Chemie*, Georg Thieme Verlag, Stuttgart, **1991**.
[23] J. Xia, K. Matyjaszewski, *Chem. Rev.* **2001**, *101*, 2921-2990.

[24] J. Chiefari, Y. K. Chong, F. Ercole, J. Krstina, J. Jeffery, T. P. T. Le, R. T. A. Mayadunne, G. F. Meijs, C. L. Moad, G. Moad, E. Rizzardo, S. H. Thang, *Macromolecules* **1998**, *31*, 5559-5562.
[25] C. J. Hawker, A. W. Bosman, E. Harth, *Chem. Rev.* **2001**, *101*, 3661-3688.
[26] F. D'Agosto, R. Hughes, M.-T. Charreyre, C. Pichot, R. G. Gilbert, *Macromolecules* **2003**, *36*, 621-629.
[27] D. Benoit, V. Chaplinski, R. Braslau, C. J. Hawker, *J. Am. Chem. Soc.* **1999**, *121*, 3904-3920.
[28] H. Fischer, *Chem. Rev.* **2001**, *101*, 3581-3610.
[29] D. Benoit, E. Harth, P. Fox, R. M. Waymouth, C. J. Hawker, *Macromolecules* **2000**, *33*, 363-370.
[30] A. W. Bosman, R. Vestberg, A. Heumann, J. M. J. Fréchet, C. J. Hawker, *J. Am. Chem. Soc.* **2003**, *125*, 715-728.
[31] M. Rodlert, E. Harth, I. Rees, C. J. Hawker, *J. Polym. Sci. Part A Polym. Chem.* **2000**, *38*, 4749-4763.
[32] E. Harth, C. J. Hawker, W. Fan, R. M. Waymouth, *Macromolecules* **2001**, *34*, 3856-3862.
[33] S. Marque, C. Le Mercier, P. Tordo, H. Fischer, *Macromolecules* **2000**, *33*, 4403-4410.
[34] K. Matyjasewski, S. Gaynor, D. Greszta, D. Mardare, T. Shigemoto, *Macromol. Symp.* **1995**, *98*, 73-89.
[35] M. K. Georges, R. A. Kee, R. P. N. Veregin, G. K. Hamer, P. M. Kazmaier, *J. Phys. Org. Chem.* **1995**, *8*, 301-305.
[36] T. Fukuda, T. Terauchi, A. Goto, K. Ohno, Y. Tsuji, T. Miyamoto, S. Kobatake, B. Yamada, *Macromolecules* **1996**, *29*, 6393-6398.
[37] E. Malmstrom, R. D. Miller, C. J. Hawker, *Tetrahedron* **1997**, *53*, 15225-15236.
[38] M. Souaille, H. Fischer, *Macromolecules* **2002**, *35*, 248-261.
[39] D. Greszta, K. Matyjaszewski, *Macromolecules* **1996**, *29*, 7661-7670.
[40] H. Fischer, *J. Polym. Sci. Part A Polym. Chem.* **1999**, *37*, 1885-1901.
[41] H. Zhang, B. Klumperman, W. Ming, H. Fischer, R. van der Linde, *Macromolecules* **2001**, *34*, 6169-6173.
[42] M. K. Georges, P. G. Odell, N. A. Listigovers, M. H. Quinlan, *ACS Symp. Ser.* **1998**, *713*, 80-95.
[43] M. K. Georges, J. L. Lukkarila, A. R. Szkurhan, *Macromolecules* **2004**, *37*, 1297-1303.
[44] S. Grimaldi, J.-P. Finet, F. Le Moigne, A. Zeghdaoui, P. Tordo, D. Benoit, M. Fontanille, Y. Gnanou, *Macromolecules* **2000**, *33*, 1141-1147.
[45] P. Lacroix-Desmazes, J.-P. Lutz, F. Chauvin, R. Severac, B. Boutevin, *Macromolecules* **2001**, *34*, 8866-8871.
[46] C. Farcet, J. Belleney, B. Charleux, R. Pirri, *Macromolecules* **2002**, *35*, 4912-4918.
[47] A. M. North, A. M. Scallan, *Polymer* **1964**, *5*, 447-455.
[48] G. Brandrup, Polymer Handbook, II80-II82.
[49] S. Creutz, P. Teyssier, R. Jérôme, *Macromolecules* **1997**, *30*, 1-5.
[50] P. Molyneux, *Watersoluble synthetic polymers vol. 2*, CRC Press, **1984**, p. 50.
[51] J. Bohrisch, U. Wendler, W. Jaeger, *Macromol. Rapid Commun*. **1997**, *18*, 975-982.
[52] A. Fischer, A. Brembilla, P. Lochon, *Macromolecules* **1999**, *32*, 6069-6072.
[53] M. Baumann, G. Schmidt-Naake, *Macromol. Chem. Phys.* **2000**, *201*, 2751-2755.
[54] Z. Chen, J. Cia, X. Jiang, C. Yang, *J. Appl. Polym. Sci.* **2002**, *86*, 2687-2692.
[55] T. Diaz, A. Fischer, A. Jonquières, A. Brembilla, P. Lochon, *Macromolecules* **2003**, *36*, 2235-2241.
[56] I. Chalari, S. Pispas, N. Hadjichristidis, *J. Polym. Sci. Part A Polym. Chem.* **2001**, *39*, 2889-2895.
[57] T. Wannemacher, D. Braun, R. Pfaendner, *Macromol. Symp.* **2003**, *202*, 11-23.
[58] Y. Sun, D. Wan, J. Huang, *J. Polym. Sci Part A Polym. Chem.* **2001**, *39*, 604-612.
[59] C. Tang, T. Kowalewski, K. Matyjaszewski, *Macromolecules* **2003**, *35*, 7214-7223.
[60] J.-F. Lutz, D. Neugebauer, K. Matyjaszewski, *J. Am. Chem. Soc.* **2001**, *125*, 6986-6993.
[61] V. Coessens, J. Pyun, P. J. Miller, S. G. Gaynor, K. Matyjaszewki, *Macromol. Rapid Commun.* **2000**, *21*, 103-109.
[62] L. E. Coleman Jr., J. F. Bork, H. Dunn Jr., *J. Org. Chem.* **1959**, *24*, 135-136.
[63] M. A. Walker, *J. Org. Chem.* **1995**, *60*, 5352-5355.
[64] M.-A. Dourges, B. Charleux, J.-P. Vairon, J.-C. Blais, G. Bolbach, J.-C. Tabet, *Macromolecules* **1999**, *32*, 2495-2502.
[65] C. Burguiere, M.-A. Dourges, B. Charleux, J.-P. Vairon, *Macromolecules* **1999**, *32*, 3883-3890.

Chapter 4

Playing LEGO: Synthesis and Characterization of Various Terpyridine Metal Complex Connected Macromolecules

Abstract

The polymers prepared in Chapter 3 and the construction principles described in Chapter 2 are combined for the construction of new polymeric materials, in which the building blocks are held together via bis terpyridine metal complexes. The introduction explains the nomenclature for these polymers and subsequently different examples are presented. These include polymer mono-complexes, A-[•]-A homo dimers, (A-[•]-)$_n$ chain extended polymers, A-[•]-B diblock copolymers and ABA and ABC triblock copolymers. Characterization techniques include capillary zone electrophoresis, analytical ultracentrifugation, ^{1}H-NMR, GPC with unusual eluentia, mass spectrometry and other spectroscopic tools. Decomplexation issues are dealt with in case of the A-[•]-A homo dimers. The strength of the approach is demonstrated by the construction of a library of polystyrene-block-poly(ethylene oxide) diblock copolymers in order to enable the study of structure-property relationships.

Parts of this chapter have been published: B. G. G. Lohmeijer, U. S. Schubert, *Angew. Chem. Int. Ed.* **2002**, *41*, 3825-3829; J.-F. Gohy, B. G. G. Lohmeijer, S. K. Varshney, B. Décamps, E. Leroy, S. Boileau, U. S. Schubert, *Macromolecules* **2002**, *35*, 9748-9755; B. G. G. Lohmeijer, U. S. Schubert, *J. Polym. Sci. Part A Polym. Chem.* **2003**, *41*, 1413-1427; B. G. G. Lohmeijer, U. S. Schubert, *Macromol. Chem. Phys.* **2003**, *204*, 1072-1078; B. G. G. Lohmeijer, H. Schlaad, U. S. Schubert, *Macromol. Symp.* **2003**, *196*, 125-135; M. A. R. Meier, B. G. G. Lohmeijer, U. S. Schubert, *Macromol. Rapid Commun.* **2003**, *24*, 852-857; J.-F. Gohy, B. G. G. Lohmeijer, X.-S. Wang, A. Alexeev, M. A. W. Winnik, I. Manners, U. S. Schubert, *Chem. Eur. J.* **2004**, *10*, 4315-4323; C. Tziatzios, A. A. Precup, B. G. G. Lohmeijer, L. Börger, U. S. Schubert, D. Schubert, *Coll. Polym. Sci.* **2004**, in press.

4.1 Introduction

The previous two chapters have dealt with *bis*-terpyridine metal complex formation and their stability, and the introduction of terpyridine ligands at the chain ends of polymers. This enables the synthesis of a large variety of possible macromolecular structures, the nature of which largely depending on the metal ion. Homoleptic complexes can lead to homo-dimers, chain-extended polymers, AB block copolymer dimers as well as random chain extended multiblock copolymers. Inert metal ions that allow a stepwise contruction of the metal complex using differently substituted ligands (section 2.3.6) lead to block copolymers, where the metal complex is located at the interface between the two blocks. Of course, this requires the synthesis of a polymer *mono*-complex, which is described in section 4.2. The design of the macromolecular architecture is facilitated by the numerous mono and disubstituted terpyridine functionalized polymers described in chapter 3. Having metal complexes as the linkage between polymer backbones has prompted us in using a modified nomenclature regarding these metal containing polymers. We propose to use acronyms such as A_x-[•]-B_y, where A represents block A with degree of polymerization x. The same is true for block B with degree of polymerization y. The symbol –[represents the terpyridine ligand and • is the metal-ion in its 2+ state unless stated otherwise. For example, a triblock copolymer consisting of a terpyridine functionalized diblock of poly(2-vinyl pyridine) of DP = 32 and polystyrene of DP = 13, a *bis*-terpyridine ruthenium complex and a terpyridine functionalized poly(ethylene oxide) of DP = 70 can then be referred to as $P2VP_{32}$-*b*-PS_{13}-[Ru]-PEO_{70} (Figure 4.1). In the following parts this nomenclature is used for the description of the obtained polymers.

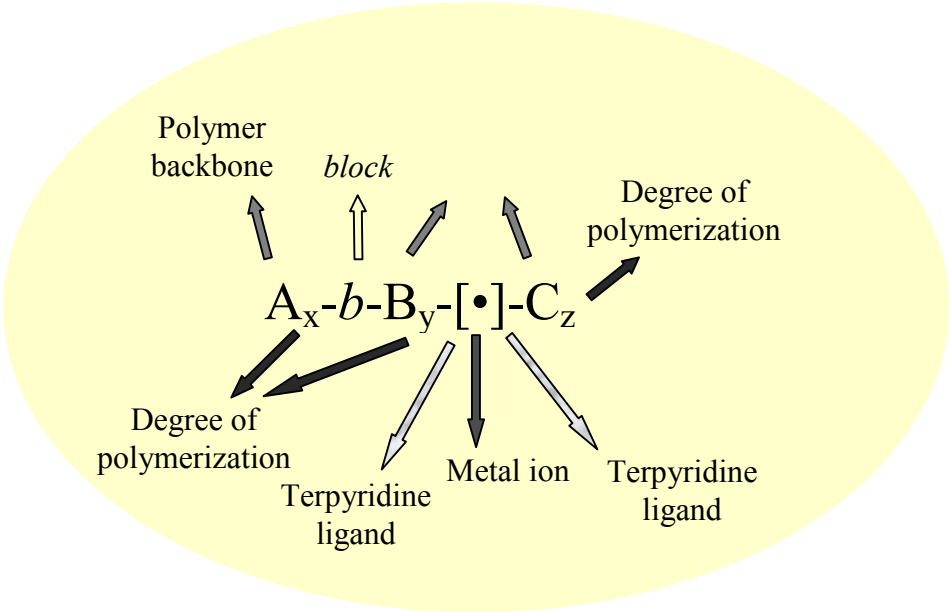

Figure 4.1. *Schematic explanation of the nomenclature for polymers that are linked together by bis-terpyridine metal complexes. Represented is a triblock copolymer. In actual systems, • may be replaced with the symbol for the metal ion such as Fe, Ru, Co etc.*

Combination of different blocks can lead to amphiphilic block copolymers, thermoplastic elastomers and stimuli-responsive systems. This chapter describes the synthesis of different macromolecular architectures simply by adding appropriate metal ions. After polymer *mono*-complex formation in section 4.2, the synthesis and

characterization of A-[•]-A homo-dimers based on poly(ethylene oxide) is described. Chain-extended (A-[•]-)$_n$ are dealt with in the next section. A-[•]-B diblock and AB-[•]-AB, AB-[•]-C and A-[•]-B-[•]-A triblock copolymers are discussed in sections 4.5 and 4.6. A first example of an AB-[•]-CD tetrablock copolymer is described in section 4.7. Characterization techniques that have been used include ^{1}H-NMR, UV/vis, FT-IR, MALDI-TOF mass spectrometry, GPC using unusual eluentia, analytical ultracentrifugation and capillary electrophoresis. The combination of these techniques is needed for assessment of the purity, of the molar mass distribution and of the block lengths.

4.2 Polymer *mono*-complexes

Section 2.6.1 has dealt with the synthesis of the *mono*-complexes of terpyridines with small organic substituents at the 4'-position using $Ru^{III}Cl_3$ and Co^{II}-salts. These syntheses were based on a precipitation strategy: addition of the ligand to a solution of the metal salt resulted in the precipitation of the *mono*-complex. Simple filtration and thorough washing of the residue gave analytically pure *mono*-complexes. When using polymers, however, the solubility of the metal complex is governed mostly by the solubility of the polymer and not the complex. A precipitation strategy will therefore fail. This is one of the reasons that up to now the successful formation of pure cobalt(III) polymer *mono*-complexes has failed, although the use of a preformed cobalt(III) salt is likely to solve these problems.[1,2] Nevertheless, for $Ru^{III}Cl_3$ a route was developed that led to successful *mono*-complex formation, also described in chapter 2.6.1.[3] Here, the anhydrous salt is partially dissolved, partially suspended in dry degassed DMF. Heating at 130 °C for 30 minutes shows a color change of the solution from black to blue to green to dark brown. Although the exact intermediates have been subject of much debate in the literature, the blue and green color are thought to originate from ruthenium clusters with metal-metal interactions, whereas the brown color presumably originates from molecularly dissolved ruthenium(III) having three chloride and one to three solvent ligands.[4-7] Despite proper knowledge of the starting salt, polymer *mono*-complexes can be prepared when adding the dried polymer in dry degassed DMF dropwise to the brown-colored solution of $Ru^{III}Cl_3$ in DMF (Figure 4.2). The formation of the *mono*-complex can be followed by UV/vis spectroscopy and ^{1}H-NMR. In UV/vis a band appears at ca. 400 nm (dependent on the solvent) and can be attributed to a metal-to-ligand charge transfer band, whereas in ^{1}H-NMR the signals of the terpyridine ligand disappear due to the paramagnetic nature of the metal ion.[8-10] The polymers that could be prepared using this method were poly(ethylene oxide)s of 3000, 5200, 10000 and 16500 g mol^{-1}, polystyrene of 2000, 7700 and 30000 g mol^{-1} and polystyrene-*block*-polyisoprene as prepared in chapter 3. These polymers will be refered to as e.g. PEO_{70}-[$RuCl_3$, PS_{68}-[$RuCl_3$ and PI_{65}-*b*-PS_{70}-[$RuCl_3$. Figure 4.3 shows the UV/vis- and the ^{1}H-NMR-spectrum of PI_{65}-*b*-PS_{70}-[$RuCl_3$.

The best proof for the purity and molar mass distribution comes from GPC. After screening of many different eluentia with varying concentrations of several metal salts, a suitable set-up was found with 5 mM NH_4PF_6 in DMF.[11] Using a photo-diode-array detector allows for inspection of the UV/vis-spectrum of the eluent (containing the analyte) at any retention time. Figure 4.4 shows the GPC-traces of PEO_{70}-[$RuCl_3$, PEO_{225}-[$RuCl_3$ and PEO_{375}-[$RuCl_3$ as well as the accompanying UV/vis spectrum of PEO_{375}-[$RuCl_3$ as measured by the photo-diode array detector.

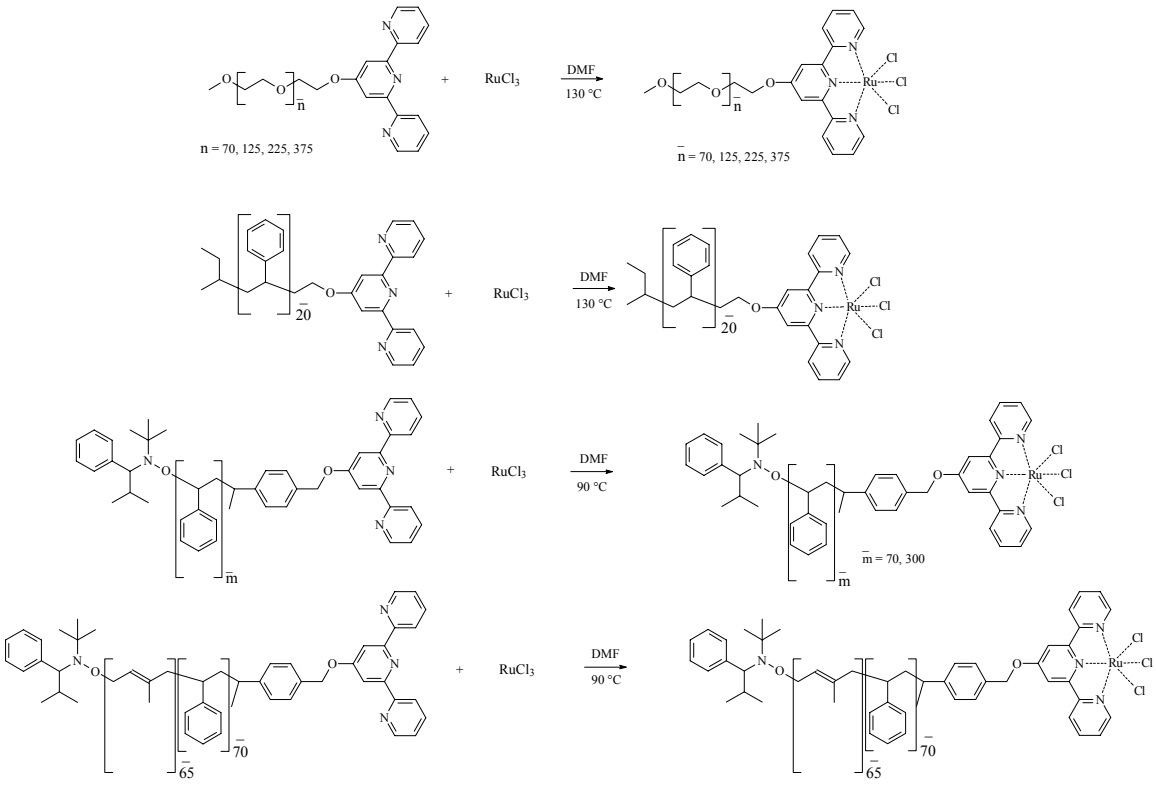

Figure 4.2. *Overview of the synthesis of the different polymer mono-complexes*.

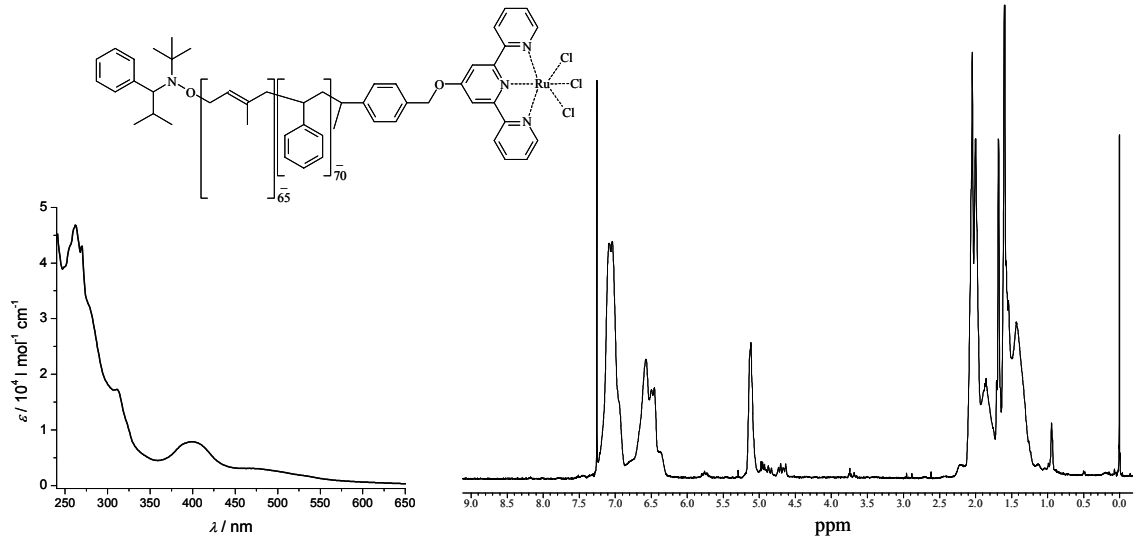

Figure 4.3. *UV/Vis spectrum in chloroform of PI_{65}-b-PS_{70}-[$RuCl_3$ (left) and its corresponding ^{1}H-NMR-spectrum in $CDCl_3$ (right). Note the band at 400 nm in the UV-spectrum and the absence of the terpyridine-signals between 7.5 and 8.8 ppm in the ^{1}H-NMR spectrum.*

Interestingly, PI_{65}-*b*-PS_{70}-[$RuCl_3$ could be measured by GPC using chloroform with 4% Et_3N and 2% isopropanol as the eluent, revealing a monomodal distribution. The PS and PEO *mono*-complexes have also been investigated by MALDI-TOF mass spectrometry. However, the presence of two or three distributions owing to the loss of counter-ions (chlorides) and the low signal-to-noise ratio's apparent for *mono*-complexes make this technique less attractive.

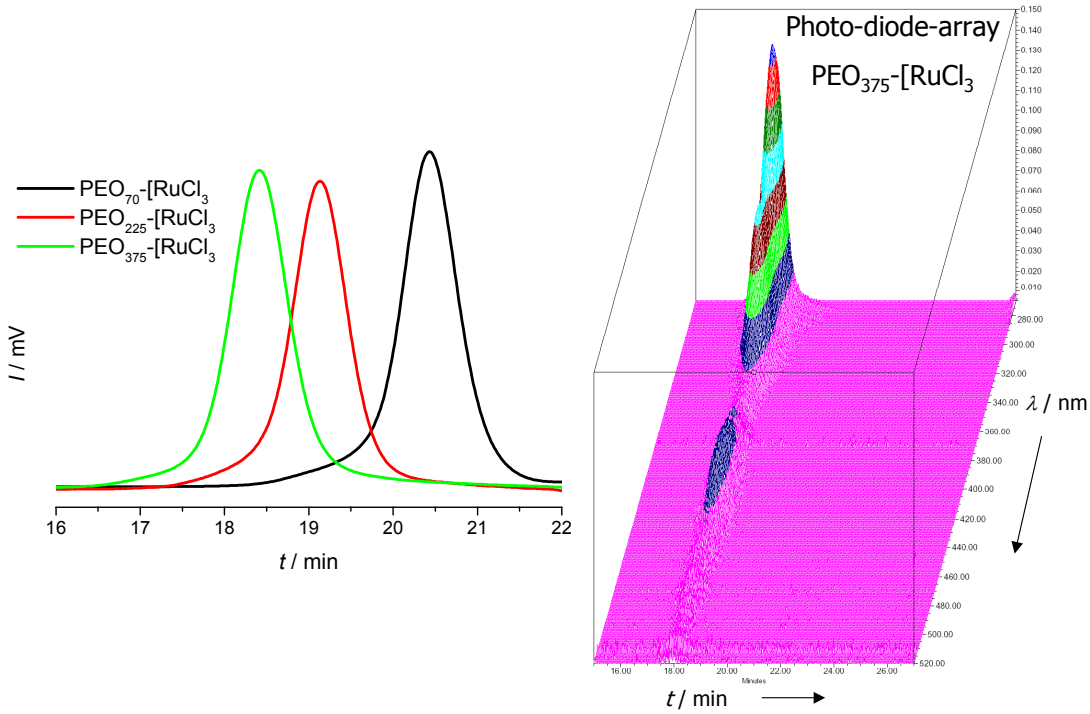

Figure 4.4. *GPC chromatograms of PEO_{70}-[$RuCl_3$, PEO_{225}-[$RuCl_3$ and PEO_{375}-[$RuCl_3$ and the corresponding UV-spectra for PEO_{375}-[$RuCl_3$ as measured by the photo-diode array detector.*

In summary, polymer *mono*-complexes can be prepared, but a different synthetic strategy as to the precipitation strategy for model complexes needed to be developed. For ruthenium(III) polymer *mono*-complexes this was successfully done by changing the solvent and working under dry and oxygen-free conditions. Successful *mono*-complex synthesis is the key towards the formation of block copolymers where the blocks are linked together via the metal complex.

4.3 Synthesis and characterization A-[•]-A homo dimers

Terpyridine functionalized PEO_{70} has been employed for the synthesis of A-[•]-A homo dimers. These homo-dimers are ideal candidates to study the stability of the metal complex as well as to serve as model systems for characterization techniques such as capillary electrophoresis and analytical ultracentrifugation. PEO_{70}-[was complexed with the acetate salts of Fe^{II}, Co^{II}, Ni^{II}, Cu^{II}, Zn^{II} and Cd^{II} and in a two-step synthesis PEO_{70}-[Ru]-PEO_{70} was prepared from the *mono*-complex using *N*-ethylmorpholine for the reduction (Figure 4.5). A very slight excess of the metal-ion was added to establish full complexation to the *bis*-complex. An excess of NH_4PF_6 was added for counter-ion exchange. Purification of these homo dimers was carried out by extraction, preparative size exclusion chromatography and precipitation. These systems were characterized, where possible, by GPC, MALDI-TOF-MS, UV/Vis, FT-IR and ^{1}H-NMR for diamagnetic complexes (i.e. Fe^{II}, Ru^{II}, Zn^{II} and Cd^{II}). In these cases shifts for the singlet of 3',5'-protons, for the 6,6"-protons and for the methylene protons were observed as also described in chapter 2.3.4. Due to the octahedral surrounding of the complex, the ligand protons in the 6,6''-position are located above the middle ring of the other terpyridine-ligand. The Co^{II}-complex revealed again strong paramagnetic shifts in ^{1}H-NMR due to specific coupling of the electronic and

nuclear spin, giving rise to proton shifts of up to 110 ppm from TMS. The UV/Vis spectra of the polymers are similar to the model complexes described in chapter 2.

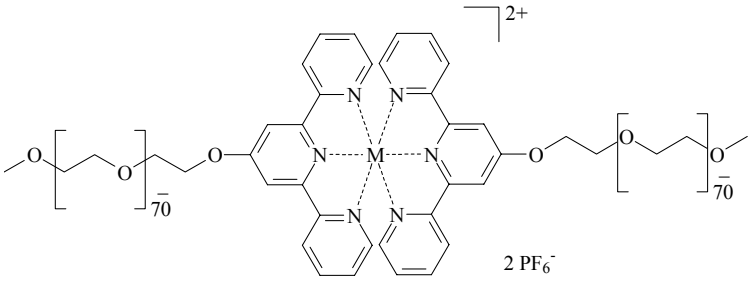

M = Fe, Ru, Co, Ni, Cu, Zn, Cd

Figure 4.5. *Schematic representation of the A-[•]-A homo dimers of PEO_{70}-[•]-PEO_{70}.*

IR-spectroscopy revealed again clear shifts in the region between 1650 and 1550 cm^{-1}. From these investigations complete complex formation can be concluded. Using the GPC setup with 5 mM NH_4PF_6 in DMF, a breakage of all complexes except the Ru^{II}-complex could be observed. This may be explained through shear forces, interaction with the column material and the labile nature of the metal ions employed and has been observed by other groups as well.[12-14] The GPC-chromatogram of PEO_{70}-[Ru]-PEO_{70} reveals a single monomodal distribution that is shifted with respect to both the uncoordinated and *mono*-complex of PEO_{70}. Using a PEO-calibration for the column it could be deduced that the molar mass is indeed doubled as expected.

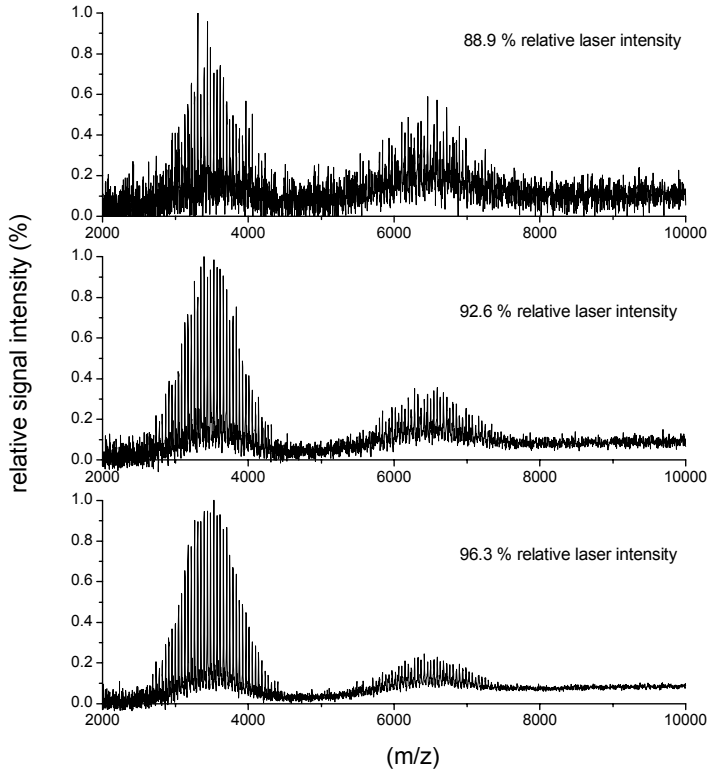

Figure 4.6. *MALDI-TOF mass spectra of PEO_{70}-[Ru]-PEO_{70} at different laser intensities.*

In MALDI-TOF-MS breakage occured due to the relatively high energy required to ionize and desorb the polymers. When all other machine settings are kept the same, the relative laser intensity to desorb the uncoordinated ligand attached to the polymer is already 90%. This can be related to the binding strengths and stabilities of the model metal complexes as described in section 2.3.6. It implies that only the polymers containing Co^{II} and Ru^{II}-ions might be detected intact at such high laser intensities, which is indeed the case (Figure 4.6). The other homo-dimers could not be detected: a single distribution that consisted of the corresponding polymer *mono*-complex was visible.

To establish the purity and molecular weight of the homo-dimers two less-used techniques in polymer chemistry were applied in cooperation with the University of Amsterdam and with the University of Frankfurt for capillary electrophoresis and analytical ultracentrifugation respectively. In short, in capillary electrophoresis charged species are separated by an electric field according to differences in their mobility. A high voltage is applied over a capillary that is filled with a background electrolyte. The analyte is introduced at one side of the capillary and is separated according to its charge and size. The velocity of the ion is a function of its electrophoretic mobility and the applied voltage. The ion is attracted to the electrode of opposite charge, but also experiences friction from the medium. Each ion has a specific constant mobility in a particular medium.[15,16] For our purpose, first different solvents and background electrolytes have been tested for capillary electrophoresis on the PEO homo-dimers: non-aqueous capillary electrophoresis is required due to insolubility of polystyrene in water.[17,18] DMF, acetonitrile and NMF have been tested as solvents. NMF was selected as the solvent and $Ba(ClO_4)_2$ has been used as background electrolyte after testing several different salts. In case of Cu^{II}, Zn^{II} and Cd^{II} electrodispersion effects caused zone fronting. For these metal-ions this set-up is thus unsuitable, but might be overcome by increasing the ionic strength of the background electrolyte.[16] Nevertheless, this system provided reproducible separations for the homo-dimers of Fe^{II}, Ru^{II} and Ni^{II}. The fact that these compounds proved to be stable during the measurement led to the synthesis of PEO_{125}-[•]-PEO_{125} and PEO_{225}-[•]-PEO_{225}, where • represents Fe^{II} and Ru^{II}. Also PS_{20}-[•]-PS_{20} homo-dimers have been prepared for all three metal ions. The electropherograms obtained experimentally showed similar peak top mobilities for the investigated compounds. This demonstrates that the type of transition metal ion has no significant influence on the charge-to-size ratio of the polymers. Unfortunately, this makes the separation of a mixture of polymers with different metal ions impossible. On the other hand, it allows for a simple molecular mass distribution characterization of the polymer samples using just one set of reference materials. Previously, it has been demonstrated that capillary electrophoresis can be a useful tool to determine the molecular mass distribution of linear synthetic polymers with a fixed charge.[19] Since all metal ions in the A-[•]-A homo polymers have the same oxidation state (2+), for this kind of polymers it can also be expected that their electrophoretic mobility reflects the effective size of the polymer. Analyses were performed with symmetrical ruthenium *bis*-terpyridine complexes with PEO chain lengths between 2 and 225 monomeric units. It was found that the inverse of the electrophoretic mobility increased linearly with the degree of polymerization of the symmetrical diblock PEO polymers. This observed relationship was used for the determination of the polydispersity of the polymer samples. Table 4.1 summarizes the results.

Table 4.1. *Experimental values of the average molar masses and polydispersity indices of the polymers as determined by capillary electrophoresis (data is calculated using calibration curve obtained using PEO-[Ru]-PEO standards).*

Polymer	nominal MM	M_p (Da)	M_w (Da)	polydispersity
PEO_{70}-[Ru]-PEO_{70}	6700	7100	7200	1.02
PEO_{125}-[Ru]-PEO_{125}	11600	11200	12700	1.03
PEO_{225}-[Ru]-PEO_{225}	20400	21600	27000	1.06
PS_{20}-[Ru]-PS_{20}	4800	3900	4400	1.03
PEO_{70}-[Fe]-PEO_{70}	6700	7400	8000	1.02
PS_{20}-[Fe]-PS_{20}	4800	4200	4600	1.03
PEO_{70}-[Ni]-PEO_{70}	6700	7100	7500	1.02
PS_{20}-[Ni]-PS_{20}	4800	4000	4900	1.06

In all cases, although less clear in case of Ru^{II}, two peaks are visible. There are a few explanations possible: 1) *mono*- and *bis*-complexes are present having the same charge or 2) *bis*-complexes with single and double charges are present having the same mass. The second explanation is easily ruled out by comparing the mobilities. The first explanation can have two reasons: due to wrong stoechiometry in the synthesis *mono*- and *bis*-complexes are present in the sample or due to the solvent NMF a new equilibrium between the ratio of *mono*- and *bis*-complexes is established. The fact that in ^{1}H-NMR only signals for the *bis*-complex of Fe^{II} and Ru^{II} are observed suggest the latter, although stoechiometric inaccuracies cannot be ruled out. On the other hand the relative amounts of *mono*- and *bis*-complex are almost equal in the electroferogram. It is difficult to compare ^{1}H-NMR data and capillary electrophoresis data because the difference in concentration is very large (concentration in CE is ~10^{-6} M, while in ^{1}H-NMR the concentration is ~10^{-2} M). This may very well imply that indeed *mono*- and *bis*-complexes are present in the Fe^{II} and Ni^{II}-dimers at the low concentrations used in CE. It may be expected that the equilibrium constants are lower in NMF as compared to the literature values measured in water due to stronger interactions between the solvent and the metal ions. The dynamic equilibrium that exists in *bis*-terpyridine Fe^{II} complexes and presumably also in Ni^{II} complexes could then be responsible for the appearance of two peaks in the electroferograms and can be attributed to *mono*- and *bis*-complexes. However, in case of Ru^{II} complexes the complexes are inert and no dynamic equilibrium exists. The only explanation then is that in the synthesis something must have gone wrong. Nevertheless, the small peak represents only 2.9% of the total area of the two peaks. In analogy with the Fe^{II} and Ni^{II} homo-dimers, this peak can be attributed to a Ru^{II} *mono*-complex. Indeed, in the synthesis the (uncharged) *mono*-complex is reduced from Ru^{III} to Ru^{II} and coupled with the second terpyridine-functionalized PEO. It may be that this coupling reaction has not gone to completion and thus some reduced Ru^{III} *mono*-complex remains. Ruthenium(II) *mono*-complexes have been reported in literature.[20] However, in GPC and also in analytical ultracentrifugation (vide infra), the *mono*-complex is not detected for PEO_{70}-[Ru]-PEO_{70}. Still, since electrophoresis has a much higher efficiency as compared to size exclusion chromatography in terms of plate number, the presence of *mono*-complex can not be ruled out completely.

In analytical ultracentrifugation separation is based on mass, density and shape. A cell containing the analyte and a reference cell is spinned at high angular velocities. The centrifugal forces are sufficient to force particles as small as several nanometers in diameter to sediment in relatively short periods of time. During the sedimentation process, the concentration profiles in the sample cell are registered using optical systems, providing time- and locally-resolved information on the mass, density and shape. Several experiments can be carried out with the AUC, of which sedimentation velocity and sedimentation equilibrium are the most important ones. In sedimentation velocity, the sedimentation coefficient distribution is obtained and this provides the number of compounds, the polydispersity and sedimentation speeds. Using established models particle size distributions, particle density distributions, molar mass distributions and diffusion coefficients may be derived. This requires proper knowledge of the particle density that can be established using density variation techniques, where the sedimentation coefficient distribution is determined in two solvents of different density or by using density gradients by mixing two solvents in different ratio's.[20-22] Alternatively, the buoyant density method can be used by sedimentation equilibrium experiments.[23] The effective molar mass is the quantity that can be determined by these experiments according to the following equation:[24,25]

$$\ln \frac{A_r}{A_{r_0}} = M_{eff} \frac{\omega^2}{2RT}(r^2 - r_0^{\,2})$$

where A_{r0} is the absorbance at a certain reference radial distance, M_{eff} the effective molar mass, ω the angular velocity and r_0 the reference radial distance. A_r and r are the absorbance at any radial position and r is that radial position. Curve-fitting of the data of a sedimentation equilibrium experiment yields M_{eff}, which is related to the actual molecular mass through:

$$M_{eff} = M(1 - \bar{v}\rho_0)$$

where v-bar is the partial specific volume of the compound and ρ_0 the density of the solution. The buoyant density experiment is focussed on finding the value of v-bar by varying the density of the solution by varying the ratio's between two solvents in such a way that the compound either floats or sediments in the analytical ultracentrifuge. By selecting several densities a linear relationship between M_{eff} and ρ_0 is established. At the point where the compound is buoyant its partial specific volume, v-bar, can be established, since this is equivalent to the reciprocal of the solvent density.

Analytical ultracentrifugation has already previously been used for the characterization of metallo-supramolecular grids.[25] The A-[•]-A homo dimers of PEO_{70} with Fe^{II} and Ru^{II} have been investigated by sedimentation equilibrium analysis. Solvent mixtures of THF and propylene carbonate with 10 mM of $[NBu_4][PF_6]$ have been used for the determination of v-bar for the different compounds. The salt is needed to suppress the primary electrostatic effect, which would otherwise lead to incorrect particle masses. Figure 4.7 shows the results for PEO_{70}, PEO_{70}-[Fe]-PEO_{70} and PEO_{70}-[Ru]-PEO_{70}.

It is interesting to note that at lower concentrations the fraction of the homo-dimer becomes less in favor of the formation of a species of half its molecular weight, presumably the *mono*-complex or the uncoordinated species. This was also assumed to take place in capillary electrophoresis. However, this fraction of *mono*-complex increased in time, whereas addition of 2-mercaptoethanol (a reducing agent) in the

AUC prevented this accumulation. Taking into account that Fe^{II} complex formation is a dynamic process and that Fe^{III} does not form *bis*-terpyridine complexes, the interpretation is as follows. Due to the lowered concentration, the amount of complexed Fe^{II} is reduced in both *mono*- and *bis*-complexes and the amount of uncoordinated Fe^{II} is increased. Oxidation then removes Fe^{II} from the system until only uncoordinated ligand and Fe^{III} *mono*-complexes are present. The question remains whether it is the *mono*-complex or the uncoordinated Fe^{II} that is apparently not stable. Addition of a reducing agent prevents the oxidation and allows for the equilibrium to remain intact. In capillary electrophoresis no evidence was found for Fe^{III}-complexes based on the expected mobilities.

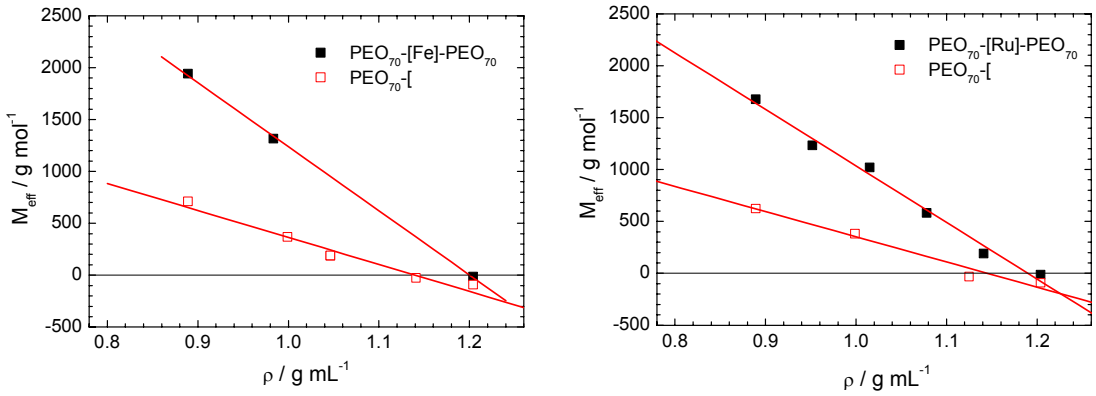

Figure 4.7. *Effective molar mass, M_{eff}, of the uncomplexed PEO-terpyridine unit (□) and of the Fe and Ru homo dimer (■) as a function of solvent density using mixtures of THF/propylene carbonate containing 10 mM tetrabutylammonium hexafluorophosphate.*

The stability of the PEO_{70}-[•]-PEO_{70} homo-dimers towards pH has been investigated by a similar experiment as described in section 2.5.2 using pH-buffers and UV/vis-spectroscopy, enabled by the solubility of the homo dimers in water. Not surprising, the same results were found as in case of the model complexes: all complexations can be reversed at pH ≤ 1 and at pH ≥ 13 except for Ni^{II} and Ru^{II}. Nevertheless, decomplexation requires more time. This clearly demonstrates that the characteristics of the metal complex formation or destruction are retained upon introduction into polymers.

In summary, the fact that a precipitation strategy can no longer be used for the isolation of the A-[•]-A homo dimers clearly complicates the synthesis. The A-[•]-A homo dimers have functioned as model systems for characterization techniques such as capillary electrophoresis and analytical ultracentrifugation. The stability of the A-[•]-A homo-dimers was found not be influenced by the presence of the polymer substituents.

4.4 Chain extended (A-[•]-)$_n$ polymers

Chain extended polymers based on reversible interactions are of great interest, since the reversible association implies that the molecular weight of these polymers is not fixed, but a function of external factors such as concentration and temperature.[26,27] This is turn is of interest for applications where low viscosities are desired for processing, but high viscosities are crucial for the performance of these materials in their final application. Telechelic polymers with self-assembling groups at the chain ends such as hydrogen bonding and metal-ligand coordination are well-suited for

these purposes. Numerous examples can be found in the literature.[26-37] In chapter 3 a few examples of *bis*-functionalized terpyridine telechelic polymers such as poly(ethylene-*co*-butylene), polystyrene and poly(*n*-butylacrylate) were described, which are the precursors for chain extended polymers. Addition of metal-ions leads to *bis*-complexes, effectively connecting polymer chains together through the metal ion. Of major importance is the stoechiometry of the metal ions versus the polymer. Chain-extended polymers based on terpyridine functionalized telechelic poly(ethylene oxide) have also been studied in our group, where different metal ions were applied. The concentration range, however, was rather low and as a consequence the obtained viscosities were relatively low.[36] Here, attention will be focused on the chain extension of poly(ethylene-*co*-butylene), PEB, by Co^{II}-ions. The tool for studying chain extension was capillary flow viscosimetry and a 9:1 ratio of chloroform to methanol was used to ensure complete solubilization of the chain extended polymers. Four different concentration ranges were investigated (i.e. 5, 10, 17.5 and 25 mM of PEB) and the ratio of metal to ligand was varied accordingly. Figure 4.8 shows the results. All solutions with varying metal to ligand ratio's and varying concentration were prepared separately and allowed to equilibrate overnight before measuring. The results can be explained qualitatively in the following way. For all concentrations it can be seen that the specific viscosity is increased upon adding metal ions. The maximum is in all cases at the 1:2 metal-to-ligand ratio, which is due to the presence of some mono-functional compound (see chapter 3) NOT exactly equal to the 1:1 molar ratio of the metal ion *vs* the polymer, but slightly lower. At this point, however, the amount of *bis*-complexes is the highest and since only the *bis*-complex can be responsible for chain extension and a concomitant increase in molecular weight, the highest viscosities are indeed expected here. Upon overtitration the viscosity again drops. This can be readily understood, since overtitration leads to the formation of *mono*-complexes that function as chain stopper. This in turn leads to shorter polymer chains and hence the viscosity decreases.

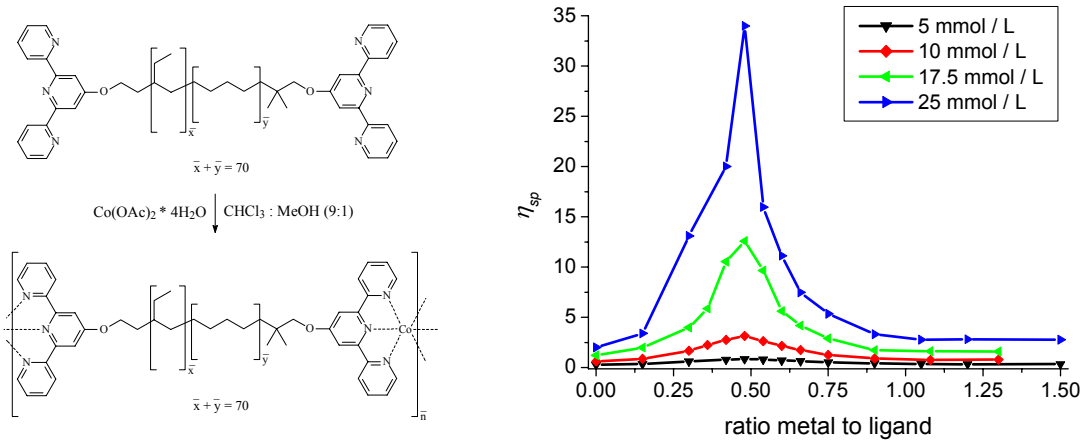

Figure 4.8. *Chain extenstion of telechelic terpyridine functionalized PEB with Co^{2+}-ions (left) and the specific viscosity as a function of the metal-to-ligand ratio at four different concentrations of PEB (right).*

The exact number of *mono*-complexes beyond the 1:1 metal-to-ligand ratio depends on the equilibrium constants K_1 and K_2. From the ^{1}H-NMR-experiments on different ratio's of Co^{II}-ions and a 4'-oxysubstituted terpyridine ligand it was found that K_2 is

larger than K_1. Figure 4.8 shows that at the 1:1 ratio of metal to ligand, the viscosity has dropped to its minimum value. Nevertheless, at the 1:1 ratio of metal-to-ligand, the NMR-experiments showed that the concentration of *bis*- *vs mono*-complexes was still slightly below 2. A higher viscosity is therefore expected, because if $K_2>K_1$ a less steep decline in viscosity as a function of the metal to ligand ratio is expected. Probably the presence of chain stopper in the starting polymer[39] plays an important role. Upon increasing the concentration of PEB the viscosity increases and this is attributed to the contribution from the equilibrium between rings and chains: at low concentrations rings are present that do not contribute significantly to the viscosity, whereas at higher concentrations the fraction of *bis*-complexes that lead to chain extension – and thus an increase in viscosity – increases.[38]

The results merit a more thorough investigation of the effect of chain stopper and the role of the relative values of K_1 and K_2 on the viscosity by modeling. Recently a model has been introduced by Van der Gucht,[37] which would form an ideal starting point to explain the results in a more quantitative way.

4.5 Synthesis and characterization of A-[Ru]-B diblock copolymers

One of the most interesting polymer architectures are the block copolymers, where chemically different polymers are linked together via covalent bonds.[41,42] The inherent immiscibility of the polymer blocks leads to a microphase-separation, because of the fact that they are covalently connected to each other. This microphase separation gives rise to interesting properties, as mentioned in chapter 1. The simplest of the family of block copolymers is the AB diblock copolymer, where only two chemically different blocks are linked together. Block copolymers, in which the polymer blocks are held together through a metal complex, can be synthesized in the two-step approach relying on the Ru^{III}/Ru^{II}-chemistry described in chapter 2. The synthesis of polymer *mono*-complexes has been dealt with in section 4.2 and in principle they can be coupled with any of the polymers synthesized in chapter 3.

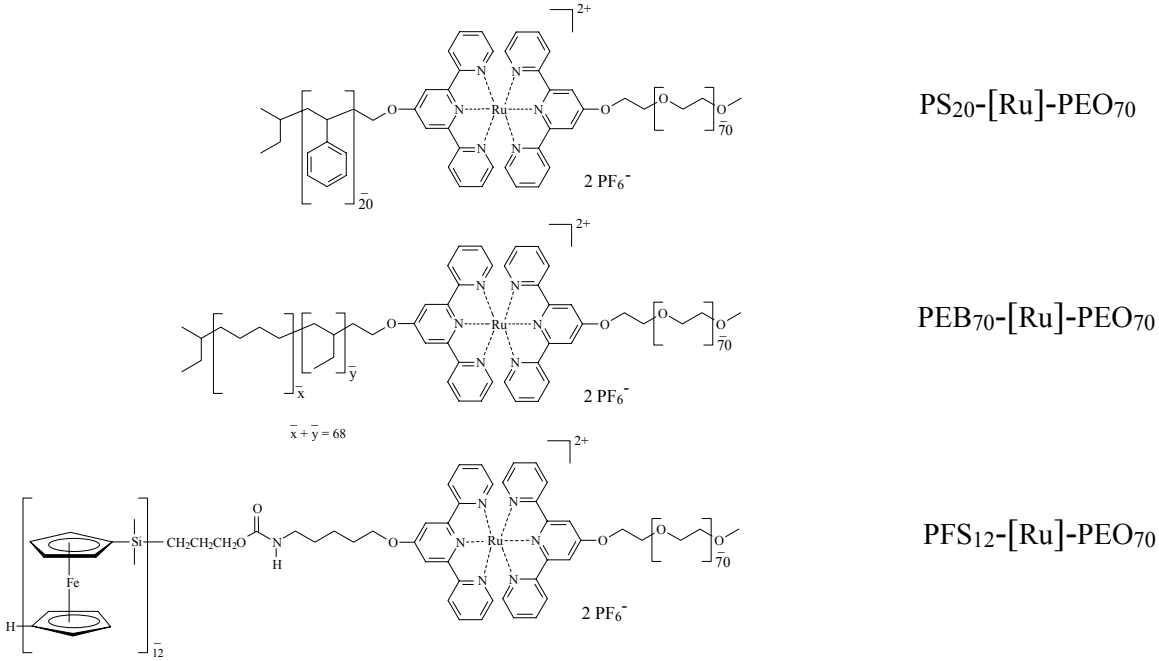

Figure 4.9. *Schematic representation of three types of A-[Ru]-B diblock copolymers.*

In first instance PEO_{70}-[$RuCl_3$ has been used for the formation of amphiphilic diblocks with several polymers as shown in Figure 4.9. The uncoordinated terpyridine-functionalized polymer and the polymer *mono*-complex are solubilized in a common solvent mixture containing *N*-ethylmorpholine that is required for the reduction of Ru^{III} to Ru^{II}. A slight excess of the uncoordinated polymer is used, since this facilitates purification procedures by preparative size exclusion chromatography on BioBeads and/or column chromatography on silica. The former method works well for block copolymers up to molecular weights of 10000 g mol^{-1}, whereas the latter method can be applied in general, although it is a bit more elaborate because of finding the right solvent and solvent-salt combinations for elution of the column. Nevertheless, a successful separation can be easily followed due to the colors of the components.

4.5.1 PS_{20}-[Ru]-PEO_{70}

Figure 4.10 shows the synthetic scheme as well as a photograph of a BioBeads-column where PS_{20}-[Ru]-PEO_{70} is separated from the starting materials in a reaction that had not gone to full completion. First the counter-ions were exchanged in order to enhance solubility in organic solvent by addition of an excess of NH_4PF_6. Subsequent extraction gave the crude product that was subjected to preparative size exclusion chromatography. The product has a red color, the largest hydrodynamic volume and is the first fraction to be isolated. The second fraction has a very intense purple color, but the absolute amount is very little (<5%), and was found to contain PEO originating from the *mono*-complex. The yellow fraction contained the terpyridine-functionalized polystyrene that had been added in excess.

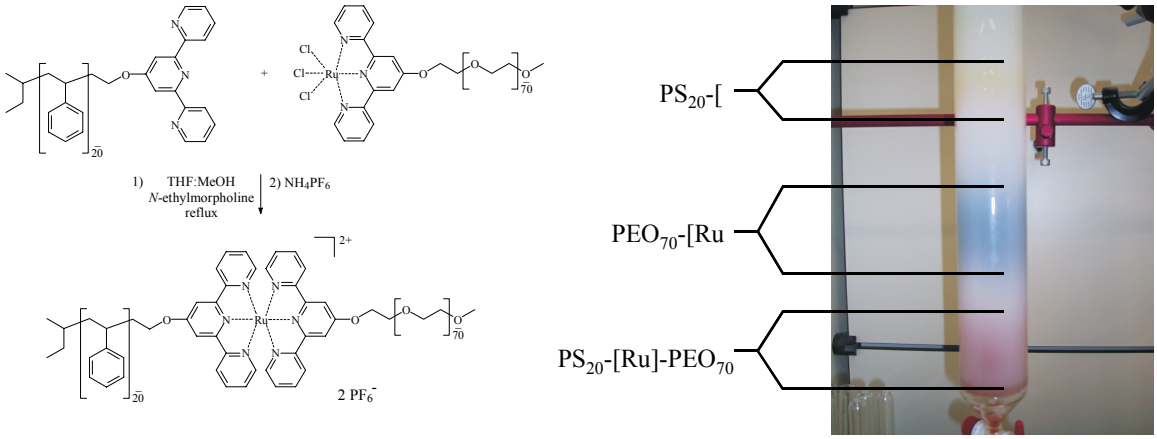

Figure 4.10. *Synthesis of PS_{20}-[Ru]-PEO_{70} (left) and subsequent purification by preparative size exclusion chromatography (right).*

Isolation of the product was carried out by washing three times with water in order to remove any excess NH_4PF_6 and precipitation. The block copolymer was characterized by GPC using 5 mM NH_4PF_6 in DMF as the eluent,[11] ^{1}H-NMR, capillary electrophoresis and analytical ultracentrifugation. Figure 4.11 shows the photo-diode-array spectrum and the ^{1}H-NMR-spectrum. The former reveals that over the full range of the peak, the UV-spectrum corresponds to that of a *bis*-terpyridine ruthenium(II) complex. From the latter the block ratio's can be determined with respect to the terpyridine-signals. These signals have shifted and are also indicative of successful complex formation.

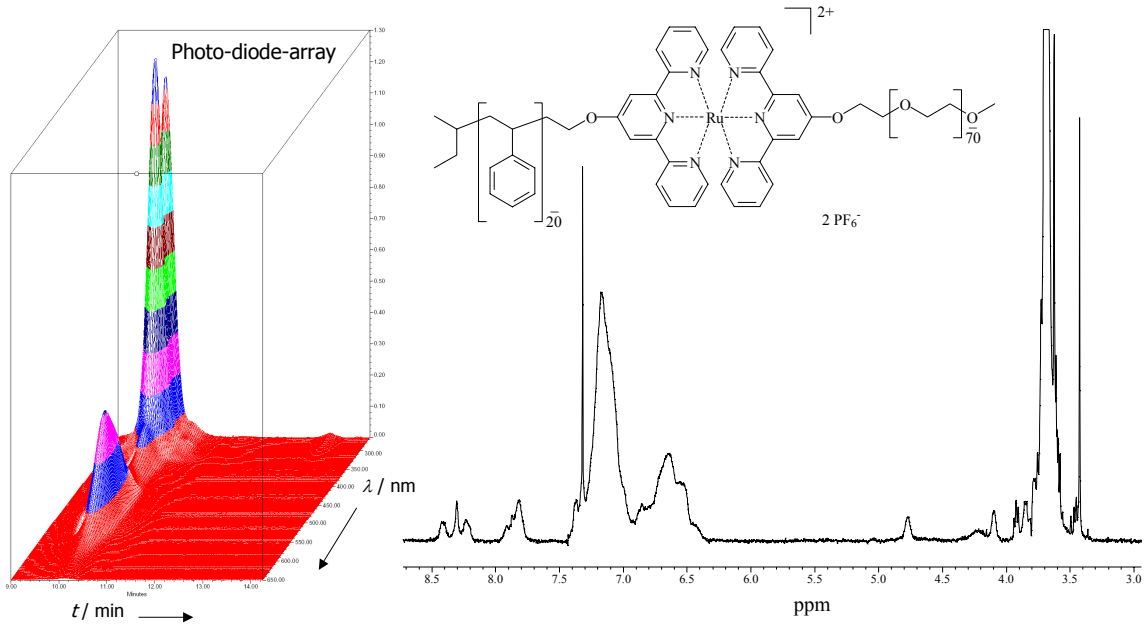

Figure 4.11. *GPC-chromatogram and corresponding UV-spectra of PS_{20}-[Ru]-PEO_{70} at each elution time (left) and its ^{1}H-NMR-spectrum in $CDCl_3$. Note the shifts in the aromatic region as well as the shifts of methylene protons connected to each polymer, which is broadened for PS at 4.23 ppm.*

The absence of homo-dimers of PS_{20}-[Ru]-PS_{20} and PEO_{70}-[Ru]-PEO_{70} was proven by capillary electrophoresis and analytical ultracentrifugation (Figure 4.13). The inertness of the complex and hence the robustness of the synthesis is demonstrated, since no scrambling takes place. Interestingly, in both capillary electrophoresis and analytical ultracentrifugation the presence of higher molecular weight compounds could be observed, which might be explained by aggregation of the block copolymer, presumably through ionic interactions. (see also chapter 5).

The influence of the counter-ion on the morphology of the resulting block copolymer has been studied by using a larger counter-ion, tetraphenylborate instead of hexafluoro-phosphate. The synthesis was started from a new batch of polystyrene and poly(ethylene oxide), so very slight differences in molecular weight and polydispersity index could result. Moreover, in addition to preparative size-exclusion chromatography, a dialysis step was necessary for the removal of excess $NaBPh_4$ from the block copolymer. Nevertheless, the GPC-chromatograms are almost identical and in ^{1}H-NMR and FT-IR the presence of the tetraphenylborate counter-ions could be proven (Figure 4.13).

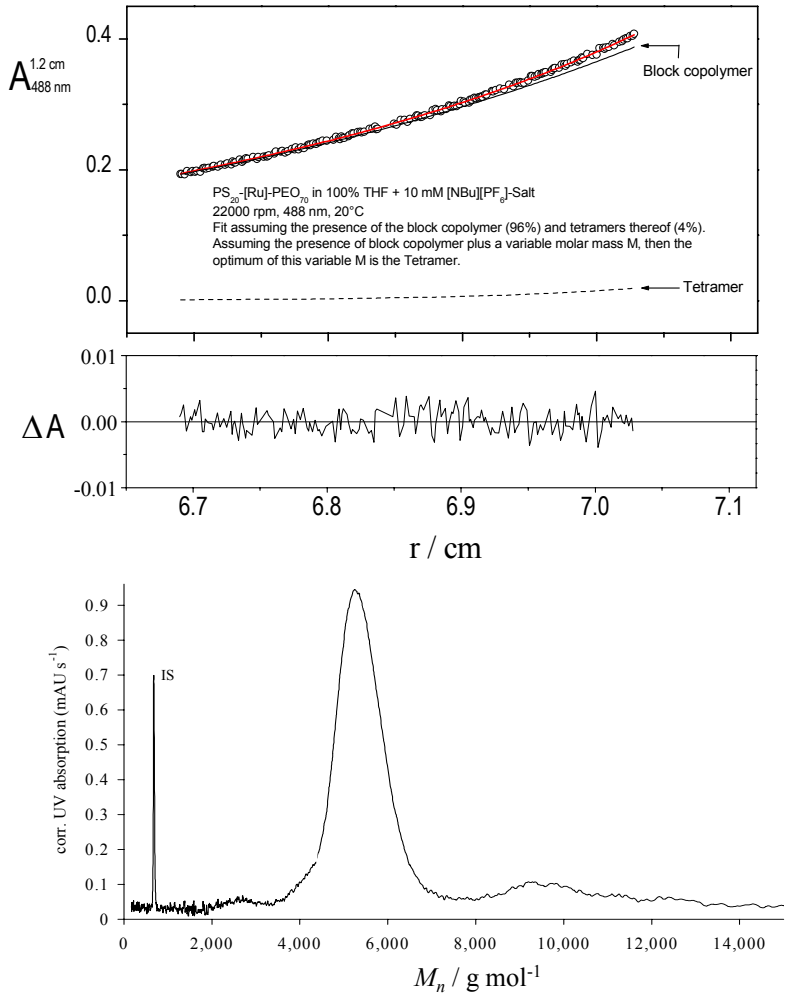

Figure 4.12. *Sedimentation equilibrium analysis on PS_{20}-[Ru]-PEO_{70}: experimental absorbance values A(r) at 488 nm (O), curve fitted to them assuming the presence of the block copolymer itself and tetramers (top) and residuals of the fit (middle) and the corresponding capillary electroferogram (bottom). From both techniques a molecular weight of 5800 g mol^{-1} is found for the block copolymer.*

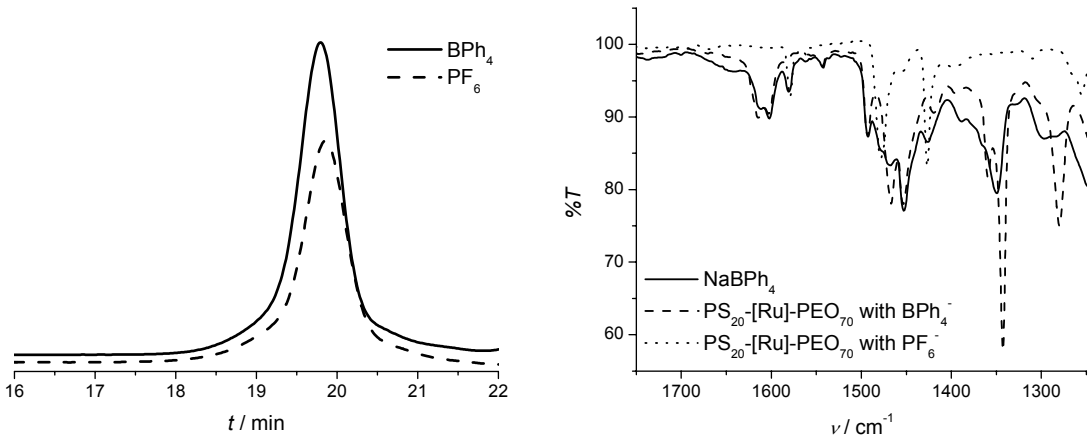

Figure 4.13. *GPC chromatograms of PS_{20}-[Ru]-PEO_{70} with PF_6 and BPh_4 counter-ions (left) and the corresponding IR-spectra including the IR-spectrum of $NaBPh_4$ (right).*

4.5.2 PEB_{70}-[Ru]-PEO_{70}

The PS_{20}-[Ru]-PEO_{70} described in the previous section contains the hydrophobic PS-block that has a high T_g. For micellization experiments in water (see chapter 5), the synthesis of an amphiphilic block copolymer with a low T_g was carried out. For this purpose, terpyridine-functionalized poly(ethylene-*co*-butylene), PEB_{70}-[, was coupled with the polymer *mono*-complex PEO_{70}-[$RuCl_3$. Purification was carried out by two preparative size exclusion columns. In ^{1}H-NMR all signals in the aromatic region could be attributed to the two differently substituted ligands coordinated to the ruthenium-metal center, by analogy with model complexes.[43] The GPC-setup in DMF showed broad peaks and also in capillary electrophoresis proved unsuitable because of the limited solubility of the PEB-block in the applied solvents. A GPC-chromatogram could be measured on a column from the Technical University in München in chloroform. The PEO_{70}-[Ru]-PEO_{70} homo-dimer and the PS_{20}-[Ru]-PEO_{70} block copolymer have been measured as well on this column. Even less stable metal complexed polymers based on terpyridine-iron(II) complexes have been reported to reach the detector intact.[44] Interestingly, all the three GPC-traces showed a monomodal distribution. Figure 4.14 shows the GPC-chromatogram and the ^{1}H-NMR-spectrum of PEB_{70}-[Ru]-PEO_{70}. These complentary techniques prove the purity of this block copolymer.

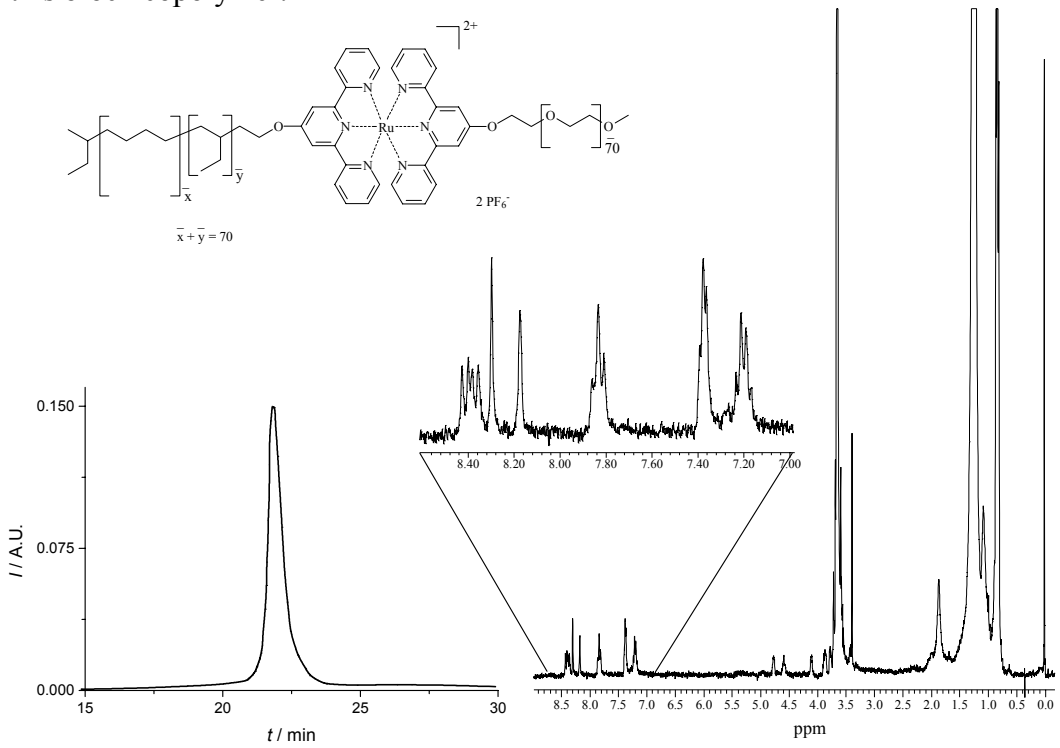

Figure 4.14. *GPC chromatogram of PEB_{70}-[Ru]-PEO_{70} in $CHCl_3$, measured on an old column, and the ^{1}H-NMR-spectrum in $CDCl_3$. The expansion shows the respective shift in the aromatic region for the differently substituted ligands.*

4.5.3 PFS_{12}-[Ru]-PEO_{70}

Block copolymers containing poly(ferrocenylsilane) (PFS) blocks are of special interest in nanotechnology because they possess interacting metal ions in the polymer chains that can lead to charge-transport materials or they can act as precursors to ferromagnetic ceramics including superparamagnetic nanoclusters by pyrolysis.[45,46] Low molecular weight PFS is a semi-crystalline polymer, which is of interest again in the formation of micelles. Indeed, crystallization of the PFS-block has resulted in the

formation of cylindrical micelles in aprotic solvents. Here, the terpyridine-functionalized PFS as described in section 3.2.1, obtained by reaction of a terpyridine having an isocyanate-functionality, was coupled with PEO_{70}-[$RuCl_3$. Purification by preparative size exclusion chromatography and subsequent precipitation in hexane yielded the pure block copolymer. Figure 4.15 shows the GPC chromatogram with the accompanying photo-diode array spectrum and the ^{1}H-NMR spectrum Moreover, the IR-spectrum shows the presence of complexed terpyridines, the urethane bands as well as both polymer backbones. The MALDI-TOF mass spectrum is shown in Figure 4.16. In MALDI-TOF breakage of the metal complex occurs and results in three distributions: one for PEO, one for PFS and the third for the block copolymer. The first two nicely show the two distributions with a mass difference corresponding to the monomeric units ($\Delta m/z$ = 242 for PFS and $\Delta m/z$ =44 for PEO). The block copolymer on the other hand reveals a broad peak, since many combinations of PFS and PEO-chains with different degrees of polymerization are possible.

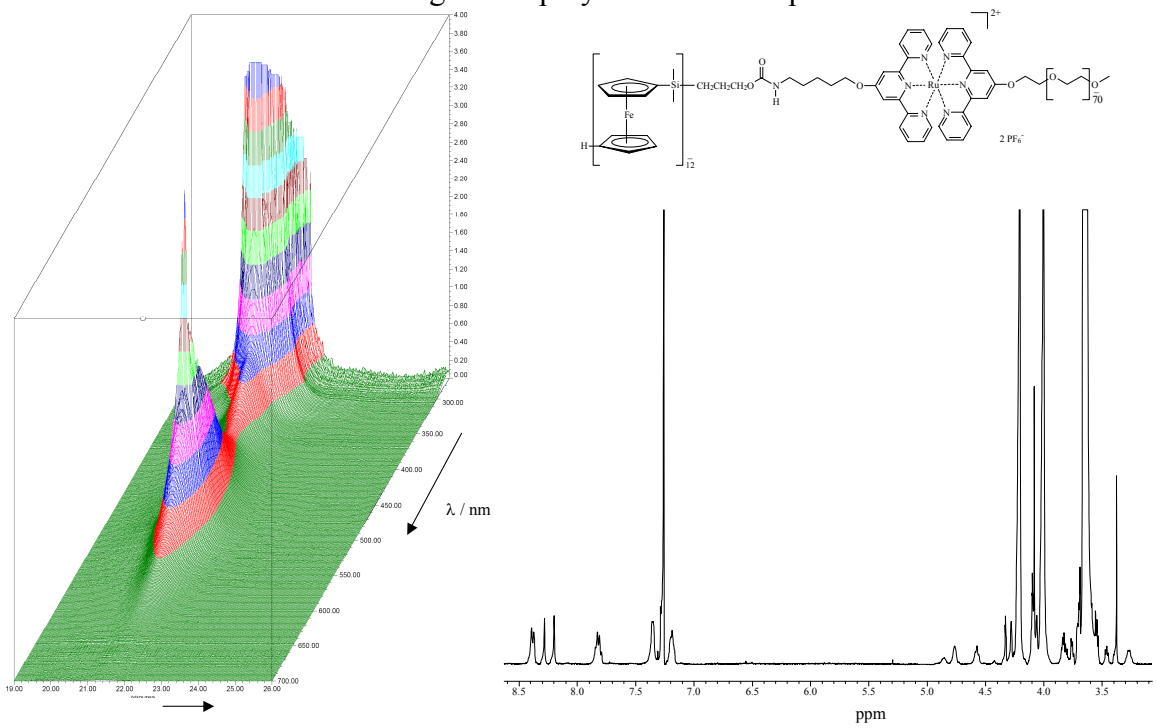

Figure 4.15. *GPC-chromatogram and corresponding UV-spectra of PFS_{12}-[Ru]-PEO_{70} at each elution time (left) and its ^{1}H-NMR-spectrum in $CDCl_3$.*

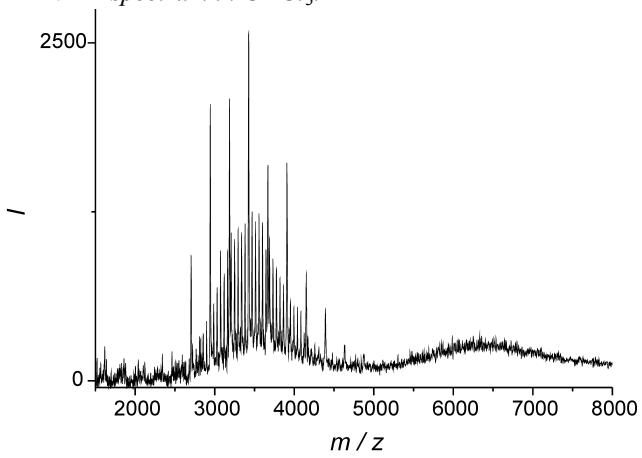

Figure 4.16. *MALDI-TOF MS of PFS_{12}-[Ru]-PEO_{70} revealing three distributions with $\Delta m/z$ = 242, $\Delta m/z$ = 44 and a peak maximum of the diblock at 6600 g mol^{-1}.*

4.5.4 Block copolymer libraries of PS_x-[Ru]-PEO_y

For block copolymers the obtained morphology is a function of the interaction parameter, the volume fraction and the overall molecular weight. Since the method for preparing metallo-supramolecular block copolymers relies on the coupling of two polymer chains via a two-step synthesis, it is straightforward to prepare a library of block copolymers connected through a metal complex with different volume fractions and molecular weights.[12] Block copolymers based on polystyrene and poly(ethylene oxide) were selected as suitable candidates, since the *mono*-complexes could all be successfully prepared for PEO and by nitroxide mediated polymerization the molecular weight of polystyrene can be tuned. The versatility of this approach is further demonstrated by the fact that the same starting blocks are used for all combinations, meaning that there is no bias regarding polydispersity and molecular weight: a 4×4 library of 16 compounds requires only 8 starting compounds, while e.g. a 10×10 library of 100 compounds would only require 20 starting compounds (Figure 4.17). Alternatively, living polymerization methods using macroinitiators can be employed for the preparation of block copolymer libraries, but such an approach requires more steps and suffers from monomer sequence issues.

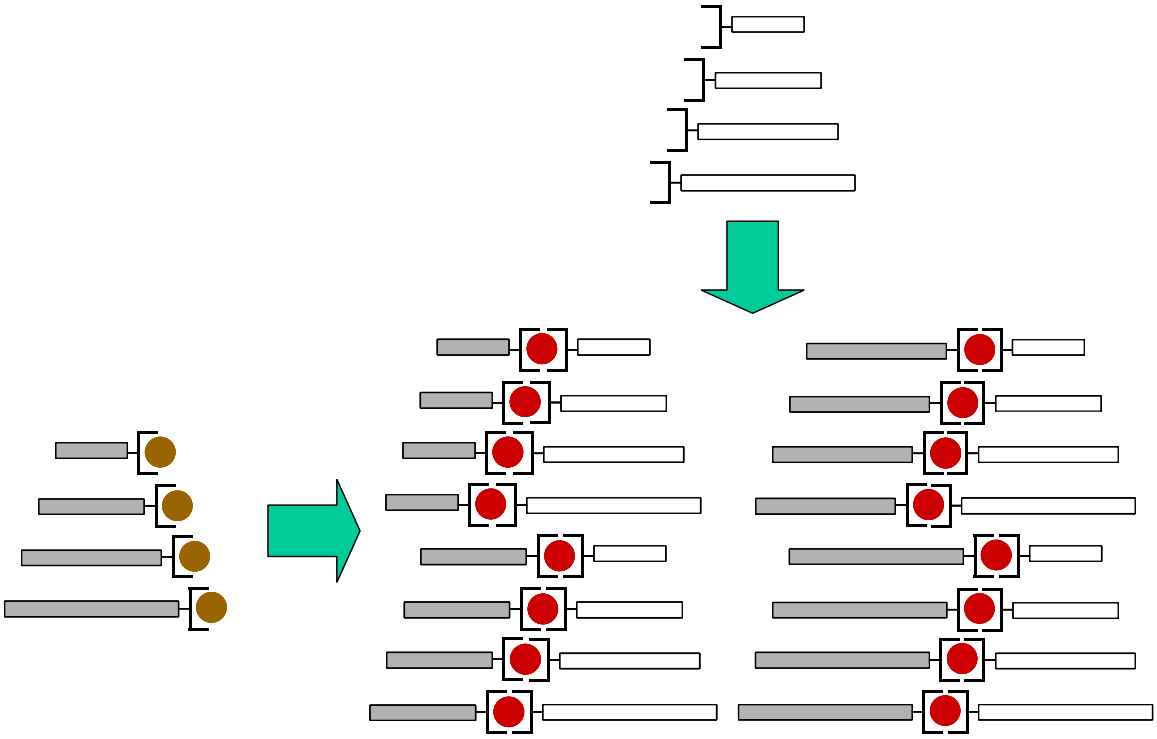

Figure 4.17. *Schematic representation of a 4 × 4-library of diblock copolymers using only 8 starting compounds.*

The starting blocks were the PEO-[$RuCl_3$ *mono*-complexes, as described in section 4.2, having degrees of polymerization of 70, 125, 225 and 375 respectively. Two types of terpyridine-functionalized polystyrenes were used: PS with a DP of 20 (using end group modification) and polystyrenes prepared by nitroxide mediated polymerization with DP's of 70, 200 and 240. All the block copolymers have been purified by preparative size exclusion chromatography and column chromatography with isolated yields between 10 and 80%: the low yields are due to non-optimized purification procedures. Figure 4.18 shows the GPC-chromatograms for a selected number of library constituents. An increase of the molecular weights can be observed

upon reacting the PEO *mono*-complex with the four polystyrenes. Moreover, the accompanying photo-diode-array spectra clearly indicate a shift of the metal-to-ligand charge transfer band (MLCT) from 390 nm for the *mono*-complex to 490 nm for the *bis*-complex. This red-shift additionally proves the successful formation of an asymmetrical *bis*-terpyridine ruthenium(II) complex.

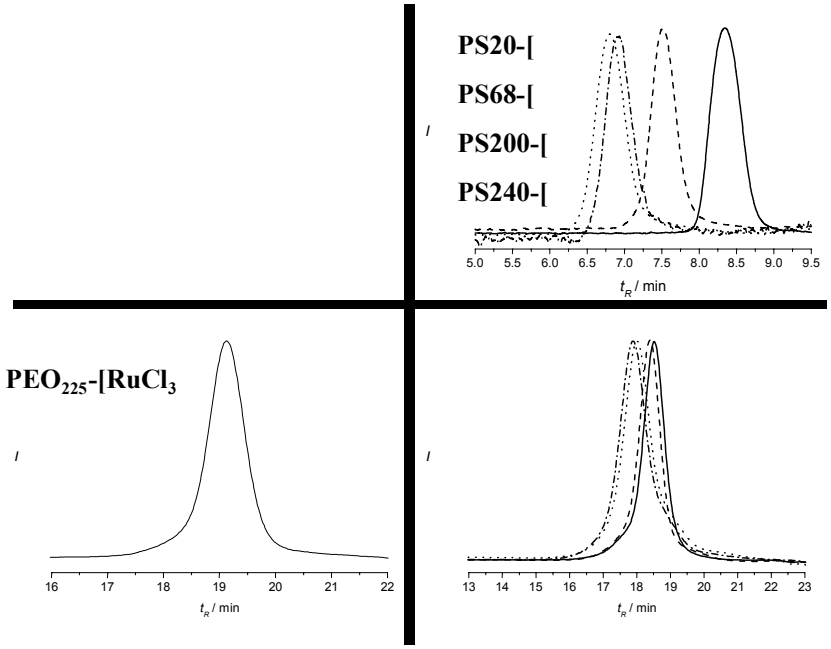

Figure 4.18. *GPC-chromatograms of PS_x-[Ru]-PEO_{225} where x represent the degrees of polymerization for the polystyrene block (DP = 20, 70, 200 and 240 respectively).*

To check whether the degree of polymerization in each block was not changed due to the severe purification efforts, ^{1}H-NMR-spectra were recorded of each compound: integration of the signals gave the expected ratio's for all components in the library within 10% error in each block. Table 4.2 displays the resulting compounds.

Table 4.2. *The block copolymers in the library are displayed in the table by name, by the molecular weights, by the volume fractions of PS, -[Ru]- and PEO (annotated between brackets) and a number designated to each block copolymer.*

	PS_{20}-[	**PS_{70}-[**	**PS_{200}-[**	**PS_{240}-[**
PEO_{70}-[$RuCl_3$	PS_{20}-[Ru]-PEO_{70} M_n = 6100 g/mol (35/16/49) **1**	PS_{70}-[Ru]-PEO_{70} M_n = 11400 g/mol (65/8/27) **2**	PS_{200}-[Ru]-PEO_{70} M_n = 25100 g/mol (84/4/12) **3**	PS_{240}-[Ru]-PEO_{70} M_n = 29300 g/mol (87/3/10) **4**
PEO_{125}-[$RuCl_3$	PS_{20}-[Ru]-PEO_{125} M_n = 8400 g/mol (25/11/64) **5**	PS_{70}-[Ru]-PEO_{125} M_n = 13700 g/mol (54/7/39) **6**	PS_{200}-[Ru]-PEO_{125} M_n = 27400 g/mol (77/4/19) **7**	PS_{240}-[Ru]-PEO_{125} M_n = 31600 g/mol (80/3/17) **8**
PEO_{225}-[$RuCl_3$	PS_{20}-[Ru]-PEO_{225} M_n = 12800 g/mol (16/8/76) **9**	PS_{70}-[Ru]-PEO_{225} M_n = 18100 g/mol (41/5/54) **10**	PS_{200}-[Ru]-PEO_{225} M_n = 31800 g/mol (67/3/30) **11**	PS_{240}-[Ru]-PEO_{225} M_n = 36000 g/mol (71/3/26) **12**
PEO_{375}-[$RuCl_3$	PS_{20}-[Ru]-PEO_{375} M_n = 19400 g/mol (11/5/84) **13**	PS_{70}-[Ru]-PEO_{375} M_n = 24700 g/mol (31/4/65) **14**	PS_{200}-[Ru]-PEO_{375} M_n = 38400 g/mol (56/3/41) **15**	PS_{240}-[Ru]-PEO_{375} M_n = 42600 g/mol (60/2/38) **16**

In short overview, a number A-[Ru]-B diblock copolymers have been prepared and fully characterized. A special GPC-setup utilizing 5 mM of NH_4PF_6 in DMF was required to measure reliable GPC-chromatograms for these compounds. Also, ^{1}H-NMR was indispensable for establishing the block ratio's. Once again capillary electrophoresis and analytical ultracentrifugation were found to be very valuable methods for the characterization and determination of the molecular weight.

4.6 Triblock copolymers

Already in chapter 1, different possibilities were shown for triblock copolymer architectures. In principle there are two types of triblock copolymers, being ABA and ABC triblock copolymer. The positioning of the connecting metal complex offers further possibilities to control the triblock copolymer morphology (Figure 4.19).

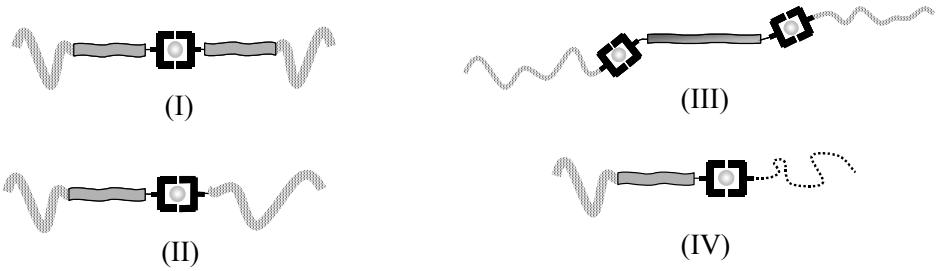

Figure 4.19. *Four different types of triblock copolymer architectures, AB-[•]-BA (I), AB-[•]-A (II), A-[•]-B-[•]-A (III) and AB-[•]-C (IV).*

Of these four, there are different requirements regarding the nature of the metal complex. Only triblock copolymer I can be prepared using homoleptic complexes, so basically any metal ion can be used for this purpose. Copolymers II, III and IV can only be prepared by using heteroleptic metal complexes, thus the choice of metal ion is up to now restricted to ruthenium.

4.6.1 PI_{65}-*b*-PS_{70}-[Fe]-PS_{70}-*b*-PI_{65}

This triblock copolymer is as type I shown in Figure 4.19. One of the block copolymers prepared by nitroxide mediated polymerization of styrene followed by isoprene was reacted with $Fe^{II}(OAc)_2$. The reaction itself required a long time, presumably due to concentration and steric effects and was monitored by UV/vis and ^{1}H-NMR. The Fe^{II} metal ion was chosen because of its high second stability constant and thus the presence of *mono*-complexes can be ruled out, even if the stoechiometry is slightly off. This is directly evident from the ^{1}H-NMR: in the course of the reaction, the signals of the starting compound disappear and a new set of signals appears in the aromatic region. By analogy with the model complexes, they can be attributed to the *bis*-terpyridine signals upon complexation with Fe^{II}. In UV/vis the typical metal-to-ligand charge transfer band (MLCT-band) of *bis*-terpyridine Fe^{II} complexes at 557 nm is observed. Unfortunately, a reliable GPC-set-up is currently lacking: the metal complex breaks on the system using chloroform with 4% Et_3N and 2% isopropanol and polyisoprene is insoluble in DMF. Information on the molecular weight is therefore available only from integration of the ^{1}H-NMR-spectrum.

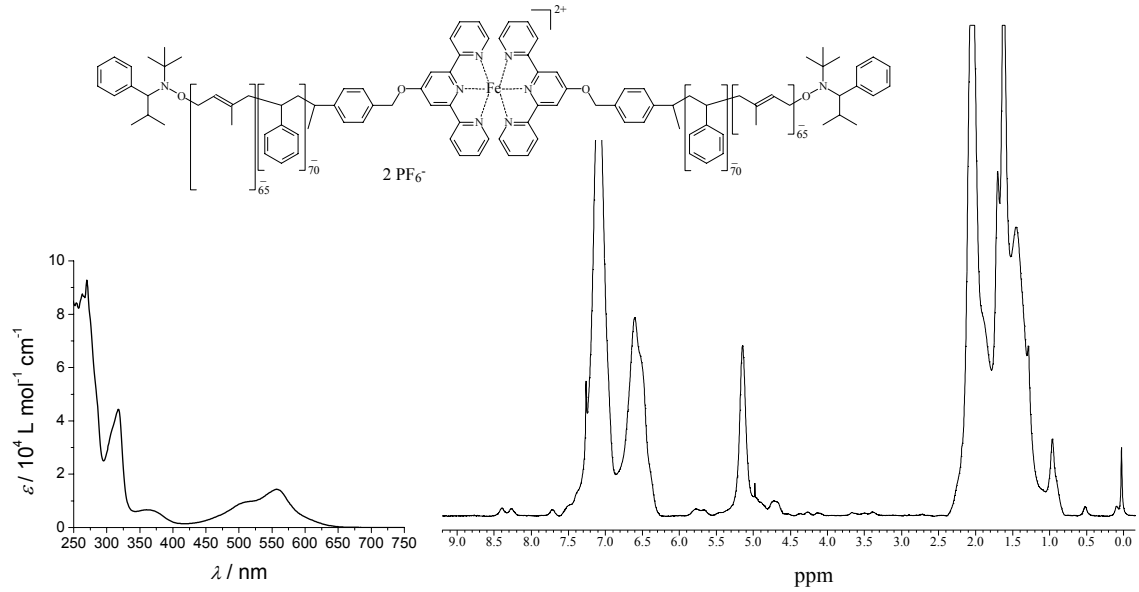

Figure 4.20. *UV/vis-spectrum of PI_{65}-b-PS_{70}-[Fe]-PS_{70}-b-PI_{65} in $CHCl_3$ (left) and its ^{1}H-NMR-spectrum in $CDCl_3$ (right). Compare with Figure 3.15 for the chemical shifts with respect to the starting terpyridine-functionalized diblock PI_{65}-b-PS_{70}.*

The material properties of the AB-[Fe]-BA triblock copolymer and the corresponding starting diblock copolymer have been studied by nano-indentation. By nano-indentation the hardness and elastic modulus can be determined by indenting an object with a certain shape into a material. The indentation process has been described in models in terms of force, displacement, E-modulus and hardness and follows contact mechanics theories. For an overview, see the reference section.[47-52] In addition, dynamic mechanical analysis was carried out. An oscillating load is applied with a certain frequency and the system shows a dynamic response, where the amplitude and phase of the displacement signal can be measured. Altogether, this provides information on the E-modulus as a function of indentation depth, and on the storage and the loss modulus as a function of frequency. Figure 4.21 shows the results. The standard deviation is because of the limited amount of measurements rather high, but can be improved. The trends are however clearly visible: the PI_{65}-*b*-PS_{70} diblock copolymer has a smaller E-modulus than the triblock copolymer for lower indentation depths and less deformation. At low frequencies the storage modulus of the triblock copolymer is three times higher than that of the diblock copolymer. The loss modulus is more or less the same for both copolymer. At high frequencies the storage modulus of the diblock copolymer approaches that of the triblock copolymer. However, the loss modulus of the diblock does not increase as much as that for the triblock copolymer. These results demonstrate that the triblock copolymer is better capable of energy dissipation than the diblock copolymer and it also has a higher elasticity. This needs to be coupled back to the morphology: the phase separation of both the di- and triblock copolymer are expected to be more or less the same. Also, because of the fact that the indentation object has a size in the order of micrometers and phase separation is usually in the order of several tens of nanometers, physical crosslinks between the outer polymer blocks might explain the differences in material properties, even though the outer blocks consist of low T_g polyisoprene.

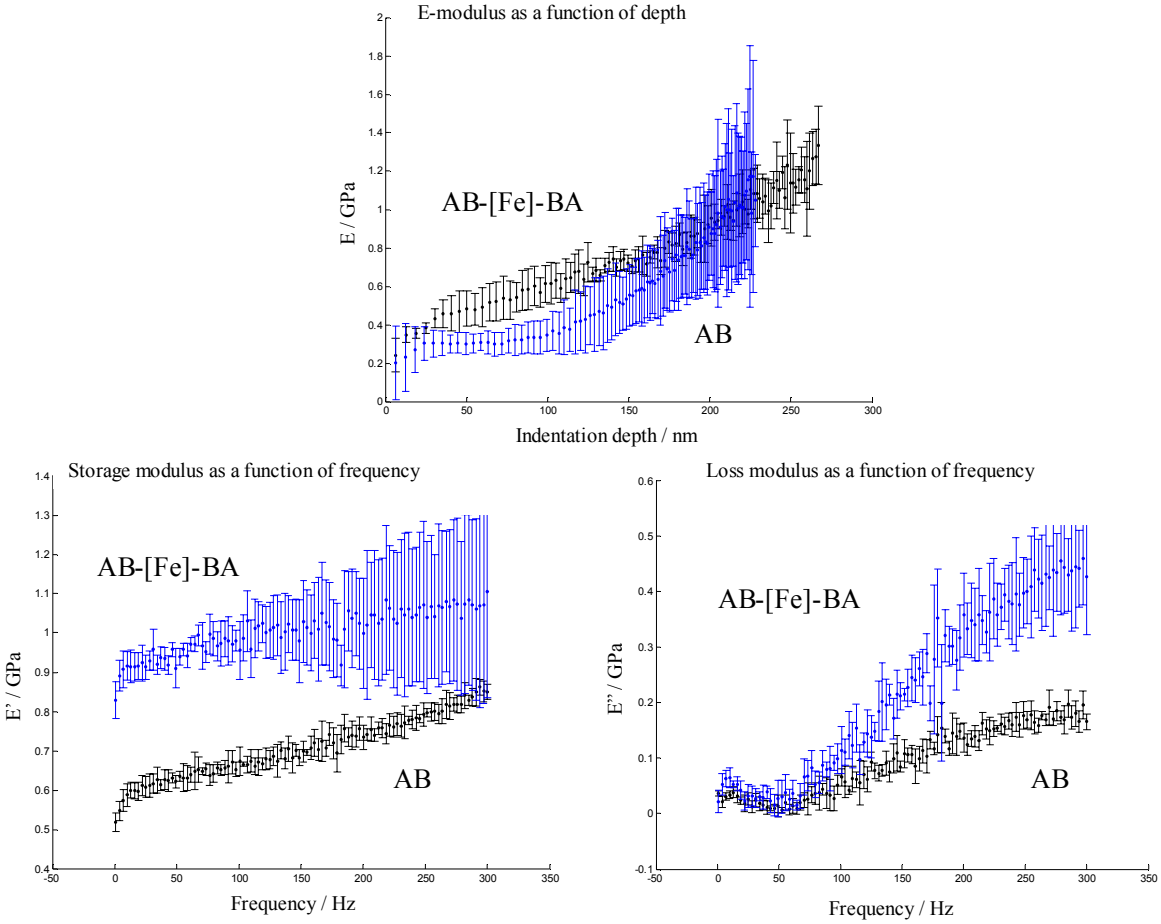

Figure 4.21. *Results from nano-indentation experiments on PI_{65}-b-PS_{70} (AB) and PI_{65}-b-PS_{70}-[Fe]-PS_{70}-b-PI_{65} (AB-[Fe]-BA): E-modulus as a function of indentation depth (top), storage modulus (bottom left) and loss modulus (bottom right) as a function of frequency.*

4.6.2 PS_{70}-[Ru]-PEB_{70}-[Ru]-PS_{70}

This triblock copolymer is as type III as shown in Figure 4.19. The polystyrene *mono*-complex is reacted with telechelic]-PEB-[: a slight excess of the *mono*-complex was used in order to establish full complexation of the free terpyridine ligand. The compound was extensively purified by column chromatography: first the polystyrene *mono*-complex was separated by elution with THF. Addition of methanol and NH_4PF_6 to the eluent rendered the block copolymer. Because of the fact that the PEB is not fully bifunctional also some AB block copolymer must be present. However, analysis by GPC could not be performed because of limited solubility of the central PEB-block in DMF. The reddish polymer was then subjected to fractionation by preparative size exclusion chromatography on BioBeads in THF. ^{1}H-NMR revealed after the extensive purification the expected block ratio's. In the aromatic region of the spectrum no signals for uncomplexed terpyridine could be detected. The UV/vis-spectrum was characteristic of *bis*-terpyridine ruthenium(II) complexes and another indication of the presence of two complexes per copolymer chain can be derived from the calculated extinction coefficients. This strongly suggests that indeed the ABA triblock copolymer is the major product (Figure 4.22). Proof for the presence of a triblock copolymer is carried out experimentally by the formation of a gel. Unfortunately, the volume fraction of the PS-blocks prevents solubilization in a selective solvent for PEB, such as hexane, so a gel could not be obtained. Also in this case, a reliable way

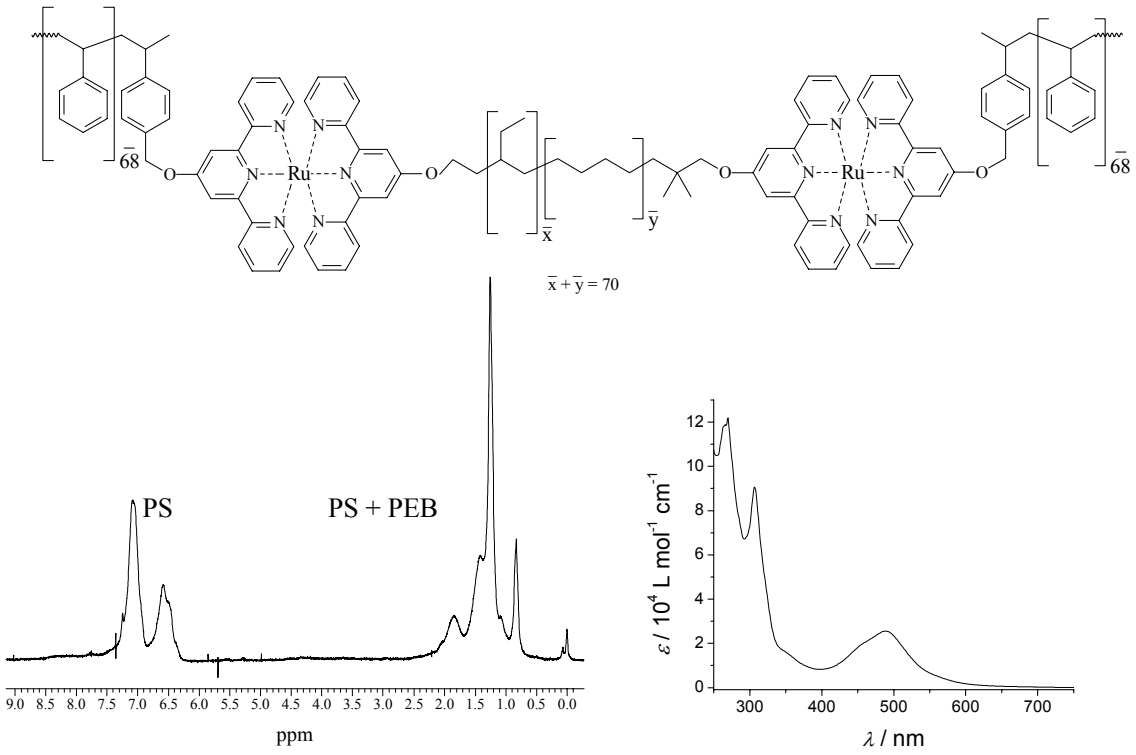

Figure 4.22. *^{1}H-NMR spectrum of PS_{70}-[Ru]-PEB_{70}-[Ru]-PS_{70} in $CDCl_3$ (left) and its corresponding UV-spectrum in $CHCl_3$ (right).*

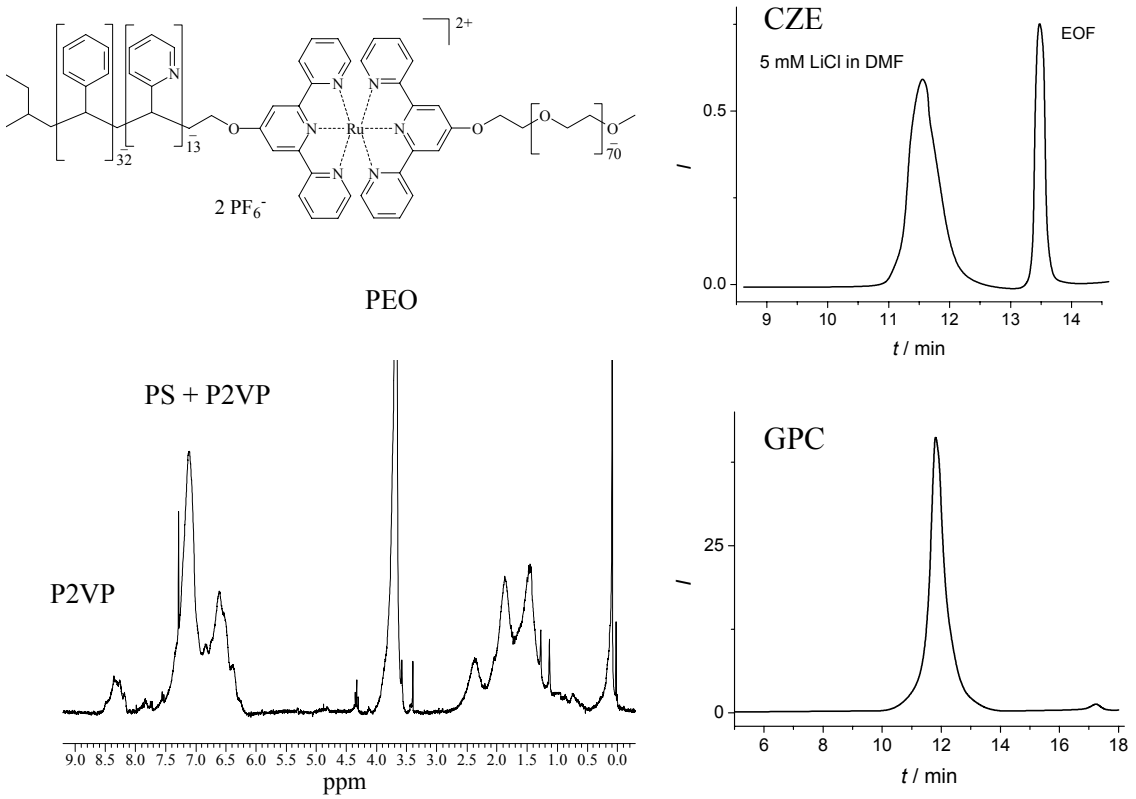

Figure 4.23. *^{1}H-NMR-spectrum of PS_{32}-b-$P2VP_{13}$-[Ru]-PEO_{70} in $CDCl_3$ (left), the corresponding CE-electroferogram (top right) and the GPC-chromatogram (bottom right).*

for establishing the purity, molecular weight and polydispersity index by GPC or CE is currently unavailable due to the low solubility of the block copolymer in the eluentia needed for these techniques. Currently analytical ultracentrifugation is tried for an indication of the molecular weight and the purity.

4.6.3 PS_{32}-*b*-$P2VP_{13}$-[Ru]-PEO_{70}

This triblock copolymer is as type IV as shown in Figure 4.19. Again PEO_{70}-[$RuCl_3$ has been employed for the synthesis of an amphiphilic ABC triblock copolymer. The interest in these block copolymers stems from the stimuli-responsive nature of the 2-vinylpyridine block: this is easily protonated/deprotonated and this causes expansion or contraction of the polymer chain through ionic interactions.[47] The yield of the reaction was not very good, presumably due to competition of the P2VP-block for the ruthenium metal ion. Nevertheless, after two preparative size exclusion columns, the pure ABC triblock copolymer could be obtained. Characterization was carried out by ^{1}H-NMR, GPC, capillary electrophoresis, FT-IR and UV/vis spectroscopy. Figure 4.23 shows the ^{1}H-NMR spectrum as well as the GPC-chromatogram and the CE-electroferogram.

In summary, three different types of triblock copolymers were prepared and characterized by the techniques described earlier in this chapter.

4.7 Conclusions

In this chapter the LEGO-principle has been applied: many different building blocks can be glued together with a universal type of connector. This leads to a variety of macromolecular architectures. Techniques such as ^{1}H-NMR, GPC using 5 mM NH_4PF_6 in DMF, capillary electrophoresis using 5 mM LiCl in NMF and analytical ultracentrifugation using 10 mM [NBu_4][PF_6] in THF/propylene carbonate were successfully applied in the determination of the molecular weight and chemical composition of several of the obtained polymers. Simple homo-dimers could be obtained by reaction with any transition metal ion. Chain extended polymers were studied by viscosimetry: a very clear increase in molecular weight was observed. Di-, and triblock copolymers were prepared and characterized by a variety of techniques. The ABBA triblock copolymer showed distinctly different material properties from the corresponding diblock copolymer as measured by nano-indentation. Also, the Ru^{III}/Ru^{II}-approach is highly suitable for the preparation of block copolymer libraries to study sturcture-property relationships. Still, a quantitative analysis of the chain extended needs to be developed, especially in the presence of chain stoppers. Furthermore, analytical tools need to be optimized for several polymers, since insolubility of one of the blocks prevents detailed analysis of the molecular weight and polydispersity. Nevertheless, the impact of having numerous building blocks at ones disposal allowing for smart combination of various terpyridine-functionalized macromolecules has been demonstrated in this chapter.

The investigation of the morphology of the new class of block copolymers in the bulk, in thin films and in solution will be the topic of the next chapter.

4.8 Experimental part

In addition to the experimental set-ups described in Chapter 2 and 3, the following specifications are applicable for the measurements described in this chapter. CE experiments were carried out on an Agilent CE instrument equipped with a diode-array detector (Waldbronn, Germany). The Chemstation CE software (Agilent) was used for instrument control and data acquisition. UV detection was performed at a wavelength of 316 nm with a bandwidth of 16 nm. Absorption spectra in the range of 220 – 350 nm were acquired. A solution of $Ba(ClO_4)_2$ in NMF (ionic strength of 5 mM) were applied as the background electrolyte. Most experiments were performed with fused-silica capillaries deactivated with OV-1701-OH, which were obtained from BGB Analytik (Adliswil, Switzerland). The capillary dimensions were 75 µm I.D. × 375 µm O.D. with a total length of 38.8 cm and a UV detection window at 30 cm. The polyimide coating was removed from both the capillary ends to avoid undesired effects on the repeatability of the injection. New capillaries were pretreated by flushing the background solution at 1 bar for 5 min followed by a voltage of 20 kV for 15 min. Prior to the separation the capillary was flushed with the background solutions at 1 bar for 1 min. Injections were performed hydrodynamically, typically by a pressure of 20 mbar for 3 s. The analyses were carried out with a voltage of 20 kV at a temperature of 25 ˚C. Sedimentation equilibrium experiments were performed using a Beckman Optima XL-A ultracentrifuge, an An-50Ti rotor, titanium double-sector centrepieces of pathlength 12 mm (BASF) and polyethylene gaskets. Rotor speed was 35,000-40,000 rpm and rotor temperature 20 °C. Sample volume was 200 µL. The absorbance-versus-radius profiles A(r) were recorded at 555 nm (PEO_{70}-[Fe]-PEO_{70}) or 486 nm (ruthenium(II) complexes), those on the uncomplexed precursor of compound I at 280 nm. The evaluations were performed as described earlier,[23] using the computer program DISCREEQ by P. Schuck. [53,54] Determination of the partial specific volume, $\bar{\nu}$, of the compounds applied the "buoyant density method" [23,25] and the solvent pair THF/propylene carbonate.[23] Nano-indentation experiments were carried out on a Hysitron triboindenter equipped with a nanoDMA unit for dynamic mechanical analysis and continuous stiffness measurement. It was however only operated in quasi-static mode. The analysis by Oliver and Pharr is incorporated in the software of the triboindenter.[48] The correction factor β is not taken into account by the software. The tip used by the triboindenter was a conical tip with 5 µm radius. Indentation with the triboindenter was load controlled. However the control was not very accurate. There was on average an 8% error, but for very small loads this could even be 20%. On every sample 5 measurements were done. One measurement consisted of 10 indents starting from 2 till 20 µN with steps of 2 µN and 20 indents starting at 25 µN up till 1000 µN with steps of 51 µN. The indents were made in a grid with 25 µm spacing between the indents. The loading and unloading rates were set at P/4 µN/s assuming that at these rates no time dependent effects would take place.

General procedure for the preparation of $RuCl_3$ poly(ethylene oxide) *mono*-complexes

A three-fold excess of anhydrous $RuCl_3$ with respect to the terpyridine end functionalized polymer was heated in dry degassed DMF to 130 °C. After the color of the suspension changed from blue to green to brown, a solution of the corresponding poly(ethylene oxide) in dry degassed DMF was added dropwise. For DP = 70, 125, 225 and 375 of the poly(ethylene oxide) this required 0.800 g, 0.200 g, 0.250 g and 0.500 g of polymer and 0.096 g, 0.050 g, 0.011 g and 0.011 g of $RuCl_3$ respectively. Stirring was continued overnight at 130 °C and then the solution was allowed to cool to room temperature. The resulting mixture was partitioned between water and CH_2Cl_2. The organic layer was separated, dried over Na_2SO_4, filtered and evaporated *in vacuo*. The brown residue was taken up in a minimum amount of THF and precipitated twice in ice-cold diethyl ether. Yields were between 79-88%. UV/vis: λ / nm (ε / L mol^{-1} cm^{-1}): PEO_{70}-[$RuCl_3$: 401 (8700), 311 (16500), 276 (31000); PEO_{125}-[$RuCl_3$: 400 (8700), 311 (16300), 277 (30600); PEO_{225}-[$RuCl_3$: 397 (8800), 311 (16900), 277 (30900); PEO_{375}-[$RuCl_3$: 395 (8200), 311 (15900), 277 (29800); GPC (RI): M_n (PDI): PEO_{70}-[$RuCl_3$: 7300 g mol^{-1} (1.08); PEO_{125}-[$RuCl_3$: 11000 g mol^{-1} (1.12); PEO_{225}-[$RuCl_3$: 17000 g mol^{-1} (1.08); PEO_{375}-[$RuCl_3$: 28000 g mol^{-1} (1.08). In ^{1}H-NMR only the polymer backbone was visible due to the paramagnetic nature of the ruthenium(III)-complex. MALDI-TOF MS could be recorded for PEO_{70}-[$RuCl_3$: M_n (PDI) = 3500 g mol^{-1} (1.02) and PEO_{125}-[$RuCl_3$: M_n (PDI) =5600 g mol^{-1} (1.01). In both cases a single distribution was observed, corresponding to the molecular ion without all three counter-ions. Decreasing the laser intensity gave rise to multiple distributions owing to the stepwise loss of chloride counter-ions.

General procedure for the preparation of $RuCl_3$ polystyrene *mono*-complexes

A suspension of anhydrous $RuCl_3$ in dry degassed DMF was heated under argon at 130°C. Not until the color of the suspension had turned dark brown, a 1/3-fold equivalent of the polystyrene in dry degassed

DMF was added slowly. Terpyridine functionalized PS_{20} (200 mg, 0.1 mmol) required 30 mg (0.3 mmol) of $RuCl_3$, whereas for PS_{70} (1.30 g, 0.17 mmol) 100 mg (0.5 mmol) of $RuCl_3$ was used. The reaction mixture was stirred overnight at 130 °C, after which it was allowed to cool to room temperature and partitioned between water and CH_2Cl_2. The organic layer was separated and dried over Na_2SO_4 and removed *in vacuo*. The resulting solid was precipitated from CH_2Cl_2 in methanol. After a short filtration column of the crude *mono*-complex using THF as the eluent, the yields were 187 mg (89%) of PS_{20}-[$RuCl_3$ and 1.13 g (84%) of PS_{70}-[$RuCl_3$. Analytical data: PS_{20}-[$RuCl_3$: UV/vis (CH_2Cl_2): λ / nm (ε / L mol^{-1} cm^{-1}): 400 (8400), 312 (16200), 270 (44500), 259 (47200); GPC (RI): M_n (PDI): 1600 g mol^{-1} (1.15). PS_{70}-[$RuCl_3$: UV/vis (CH_2Cl_2): λ / nm (ε / L mol^{-1} cm^{-1}): 395 (8500), 311 (15800), 269 (47000), 262 (53000); GPC (RI): M_n (PDI): 5800 g mol^{-1} (1.12). In ^{1}H-NMR only the polymer backbone was visible due to the paramagnetic nature of the ruthenium(III)-complex. MALDI-TOF MS could be recorded for PS_{20}-[$RuCl_3$: M_n (PDI) = 3500 g mol^{-1} (1.12). Multiple distributions were observed, corresponding to the molecular ion and the stepwise loss of chloride counter-ions.

Synthesis of $RuCl_3$ polyisoprene-*block*-polystyrene *mono*-complex
A suspension of anhydrous $RuCl_3$ (28 mg, 0.14 mmol) in dry degassed DMF (10 mL) was heated under argon at 130 °C. Not until the color of the suspension had turned dark brown, a 1/3-fold equivalent of terpyridine functionalized PI_{65}-*b*-PS_{70} (500 mg, 45 μmol) in dry degassed DMF (20 mL) was added slowly. The reaction mixture was stirred overnight at 130 °C, after which it was allowed to cool to room temperature and partitioned between water and CH_2Cl_2. The organic layer was separated and dried over Na_2SO_4 and removed *in vacuo*. The resulting solid was precipitated from CH_2Cl_2 in methanol. After a short filtration column of the crude *mono*-complex using THF as the eluent, the yield was 416 mg (82%). UV/vis (CH_2Cl_2): λ / nm (ε / L mol^{-1} cm^{-1}): 399 (7900), 311 (17300), 270 (43000), 262 (46800). In ^{1}H-NMR only the polymer backbone was visible due to the paramagnetic nature of the ruthenium(III)-complex (see Figure 4.3). However, the PS and PI-backbone can be integrated with respect to each other. From this a 65:70 ratio of PI:PS was found. GPC (RI): M_n (PDI) = 16300 g mol^{-1} (1.28).

General procedure for the synthesis of PEO_{70}-[•]-PEO_{70}: 0.250 g of the terpyridine functionalized poly(ethylene oxide) (DP = 70) and the metal salt $M(OAc)_2 \bullet n\ H_2O$ (M = Fe, Co, Ni, Cu, Zn, Cd; 0 < n < 4) in a molar ratio of 2:1 were stirred under reflux in 10 mL of MeOH for at least 4 hours. The reaction was followed by UV/Vis: when no more changes were observed in the UV-spectrum, 0.120 g of solid NH_4PF_6 (0.73 mmol, 10-fold excess) was added to the solution. Stirring was continued for another 15 minutes, after which the reaction mixture was cooled to room temperature and partitioned between dichloromethane (50 mL) and water (25 mL). The organic layer was washed 3 times to remove excess salts, then dried over Na_2SO_4 and removed *in vacuo*. From the resulting solid a ^{1}H-NMR spectrum was recorded. If uncomplexed starting polymer was present (deduced from the singlet at 8.0 ppm in ^{1}H-NMR), preparative size exclusion chromatography was carried out (BioBeads SX-1, CH_2Cl_2). Finally, the polymer was precipitated from THF into diethyl ether, filtered and dried for 2 days in a vacuum stove at 40 °C. Yields varied from 64 to 87 %. ^{1}H-NMR-spectra of PEO_{70}-[Ni]-PEO_{70} and PEO_{70}-[Cu]-PEO_{70} did not show any peaks in the aromatic region, due to the paramagnetic nature of the metal complexes. Uncooordinated terpyridine-functionalized PEO_{70} could not be observed.

PEO_{70}-[Fe]-PEO_{70}: ^{1}H-NMR (CD_3CN): δ = 8.57 (s, 4 H; $H_{3',5'}$), 8.51 (d, 4 H, ^3J = 7.4 Hz; $H_{3,3''}$), 7.93 (td, 4 H, ^3J = 7.4, ^4J = 1.6 Hz; $H_{4,4''}$), 7.20 (d, 4 H, ^3J = 5.2 Hz; $H_{6,6''}$), 7.12 (dd, 4 H, ^3J = 8.2, ^3J = 5.2 Hz; $H_{5,5''}$), 4.80 (t, ^3J = 4.8 Hz, 4 H, tpyOCH_2), 4.14 (t, ^3J = 4.8 Hz, 4 H; tpyOCH_2CH_2), 3.83-3.39 (m, 560 H, PEO backbone), 3.34 (s, 6 H; OCH_3); UV/Vis (H_2O): λ / nm (ε / L mol^{-1} cm$_{-1}$): 556 (8400), shoulder at 506 (5700), 361 (5300), 315 (31000), 271 (39200), 245 (39200); FT-IR (ATR): ν / cm^{-1}: 2883 (CH_3, CH_2) 1616, 1563, 1551 (terpyridine) 793 (PF_6); CE: M_n (PDI): 6700 g mol^{-1} (1.02); AUC: M_n = 7100 g mol^{-1}.

PEO_{70}-[Co]-PEO_{70}: ^{1}H-NMR (CD_3CN): δ = 111.12 (bs, 2 H; $H_{6,6''}$), 74.22 (bs, 4 H; $H_{3',5'}$), 70.17 (bs, 4 H; $H_{5,5''}$), 34.52 (bs, 4 H; $H_{3,3''}$), 14.93 (m, 4 H; tpyOCH_2), 9.35 (m, 4 H; tpyOCH_2CH_2), 7.13 (m, 4 H; CH_2OCH_2), 6.07 (bs, 4 H; $H_{4,4''}$), 5.22 (m, 4 H; tpyOCH_2CH_2OCH_2), 4.73 (m, 4 H; tpyOCH_2CH_2OCH_2CH_2), 4.35-3.36 (m, 552 H, PEO-backbone), 3.35 (s, 6 H, OCH_3). UV/Vis (H_2O): λ / nm (ε / L mol^{-1} cm^{-1}): 453 (730), 306 (22600), 272 (40800), 241 (43300). FT-IR (ATR): ν / cm^{-1}: 2883, 2741 (CH_3, CH_2); 1615, 1572, 1560 (terpyridine); 797 (PF_6). MALDI-TOF MS: two distributions with Δ m/z = 44 due to fractionation, one with M_n = 6600 g mol^{-1} and one with M_n = 3400 g mol^{-1}.

PEO_{70}-[Ni]-PEO_{70}: UV/Vis (H_2O): λ / nm (ε / L mol^{-1} cm^{-1}): 324 (16700), 311 (20400), 299 (19700), 273 (41000), 243 (43000). FT-IR (ATR): ν / cm^{-1}: 2883, 2742 (CH_3, CH_2); 1614, 1604, 1573, 1563 (terpyridine); 797 (PF_6). CE: M_n (PDI): 6700 g mol^{-1} (1.02).

PEO_{70}-[Cu]-PEO_{70}: UV/Vis (H_2O): λ / nm (ε / L mol^{-1} cm^{-1}): 329 (20400), 316 (21400), 275 (44700), 251 (45300). FT-IR (ATR): ν / cm^{-1}: 2883, 2742 (CH_3, CH_2); 1616, 1574, 1562 (terpy) 797 (PF_6).

PEO_{70}-[Zn]-PEO_{70}: ^{1}H-NMR (CD_3CN): δ = 8.62 (d, 4 H, ^3J = 7.6 Hz; $H_{3,3''}$), 8.31 (s, 4 H; $H_{3',5'}$), 8.20 (td, 4 H, ^3J = 7.6, ^4J = 1.6 Hz; $H_{4,4''}$), 7.81 (d, 4 H, ^3J = 5.4 Hz; $H_{6,6''}$), 7.44 (ddd, 4 H, ^3J = 8.0, ^3J = 5.4, ^4J= 1.4 Hz; $H_{5,5''}$), 4.74 (t, 4 H, ^3J = 4.8 Hz; tpyOCH_2), 4.08 (t, 4 H, ^3J = 4.8 Hz; tpyOCH_2CH_2), 3.80-3.43 (m, PEO backbone), 3.35 (s, 6 H; OCH_3). UV/Vis (H_2O): λ / nm (ε / L mol^{-1} cm^{-1}): 322 (28800), 309 (26500), 273 (38100), 243 (53900). FT-IR (ATR): ν / cm^{-1}: 2883, 2742 (CH_3, CH_2); 1614, 1603, 1575, 1563 (terpyridine); 798 (PF_6).

PEO_{70}-[Cd]-PEO_{70}: ^{1}H-NMR (CD_3CN): δ = 8.63 (d, 4 H, ^3J = 8.0 Hz; $H_{3,3''}$), 8.23 (s, 4 H; $H_{3',5'}$), 8.22 td, 4 H, ^3J = 8.0, ^4J = 1.8 Hz; $H_{4,4''}$), 8.06 (d, 4 H, ^3J = 5.0 Hz; $H_{6,6''}$), 7.52 (dd, 4 H, ^3J = 8.2, ^3J = 5.4; $H_{5,5''}$), 4.69 (t, 4 H, ^3J = 4.4 Hz; tpyOCH_2), 4.06 (t, 4 H, ^3J = 4.4 Hz; tpyOCH_2CH_2), 3.82-3.49 (m, PEO backbone), 3.39 (s, 6 H; OCH_3). UV/Vis (H_2O): λ / nm (ε / L mol^{-1} cm^{-1}): 320 (21200), 309 (22900), 274 (37100), 242 (52500). FT-IR (ATR): ν / cm^{-1}: 2883, 2742 (CH_3, CH_2); 1611, 1600, 1575, 1562 (terpy); 797 (PF_6).

PEO_{70}-[Ru]-PEO_{70}: A solution of PEO_{70}-[$RuCl_3$ (0.100 g, 0.027 mmol) and PEO_{70}-[(0.094 g, 0.027 mmol) in MeOH (5 mL) was stirred for 30 minutes under reflux. A few drops of *N*-ethylmorpholine were added and the solution turned from orange to red. Stirring under reflux was continued overnight, after which an excess of solid NH_4PF_6 (45 mg, 0.27 mmol) was added. The solution was cooled to –20 °C. The red precipitate was collected by filtration and further purified by preparative size exclusion chromatography. Excess NH_4PF_6 was washed out with water, yielding 97 mg of product (50%). ^{1}H-NMR (CD_3CN): δ = 8.49 (d, 4 H, ^3J = 7.8 Hz; $H_{3,3''}$), 8.35 (s, 4 H; $H_{3',5'}$), 7.91 (td, 4 H, ^3J = 8.0, ^4J = 1.4 Hz; $H_{4,4''}$), 7.37 (d, 4 H, ^3J = 4.8 Hz; $H_{6,6''}$), 7.16 (dd, 4 H, ^3J = 7.5, ^3J = 5.0 Hz; $H_{5,5''}$), 4.67 (t, 4 H, ^3J = 4.6 Hz; tpyOCH_2), 4.05 (t, 4H, ^3J = 4.6 Hz; tpyOCH_2CH_2), 3.80-3.38 (m, 560 H; PEO backbone), 3.31 (s, 6 H; OCH_3). ^{13}C-NMR (CD_3CN): δ = 165.0, 157.2, 155.4, 151.4, 136.9, 126.7, 123.5, 110.1, 71.4-68.1, 57.2. UV/Vis (CH_3CN): λ / nm (ε / L mol^{-1} cm^{-1}): 486 (22800), 304 (85600), 267 (74300); GPC-München (UV): M_n (PDI): 16780 g mol^{-1} (1.13); GPC DMF (RI): Mn (PDI): 17600 g mol^{-1} (1.06); MALDI-TOF MS: two distributions with Δ m/z = 44 due to fractionation, one with M_n = 6600 g mol^{-1} and one with M_n = 3400 g mol^{-1}; CE: M_n (PDI): 6700 g mol^{-1} (1.03); AUC: M_n = 7100 g mol^{-1}.

PEO_{125}-[Ru]-PEO_{125}, PEO_{225}-[Ru]-PEO_{225} and PEO_{375}-[Ru]-PEO_{375} were prepared in a similar fashion to PEO_{70}-[Ru]-PEO_{70} as described above. Unfortunately, from GPC, CE and AUC it was deduced that the compounds were not pure. The major side-product in all cases had the M_n of the *mono*-complex. Purification efforts on silica, BioBeads and Sephadex LH-20 as well as prolonged reaction periods and/or increasing the reaction temperature to 150 °C in ethylene glycol proved unsatisfactory. Nevertheless, the unpurified compounds could be used for the construction of a calibration curve in CE, where an excellent relationship between mobility and molecular weight was found.[55]

Synthesis of PS_{20}-[Fe]-PS_{20}

A 5 mL solution of terpyridine-functionalized PS_{20} (36.6 mg, 18 μmol) and $Fe(OAc)_2$ (1.6 mg, 9.2 μmol) in a mixture of THF:MeOH (7:3) was refluxed overnight. An excess of solid NH_4PF_6 (15 mg, 90 μmol) was added. The reaction mixture was poured into water (25 mL) and extracted with CH_2Cl_2 (2 × 25 mL). The organic layer was washed with water (2 × 25 mL), dried over Na_2SO_4 and removed in vacuo. Purification of the crude product was carried out by preparative size exclusion chromatography (BioBeads SX-1, swollen in CH_2Cl_2). The purple compound was isolated and precipitated from THF into methanol, yielding 24 mg of product (63%). ^{1}H-NMR ($CDCl_3$): δ = 8.16 (bm, 4 H; $H_{3,3''}$), 8.08-7.92 (bm, 4 H; $H_{3',5'}$) 7.73 (bm, 4 H; $H_{4,4''}$), 7.43-6.32 (m, 108 H; $H_{aromatic\ PS\ backbone}$, $H_{6,6''}$, $H_{5,5''}$), 4.31 (bm, 4 H; tpyOCH_2), 2.64-0.55 (bm, 71 H; tpyOCH_2CH_2, $H_{aliphatic\ PS\ backbone,\ initiator}$); UV/vis ($CHCl_3$): λ / nm (ε / L mol^{-1} cm^{-1}): 558 (14200), shoulder at 507 (9400), 364 (6000), 317 (44200), 273 (68500), CE: M_n (PDI): 4800 g mol^{-1} (1.03).

Synthesis of PS_{20}-[Ru]-PS_{20}
A 5 mL solution of terpyridine-functionalized PS_{20} (150 mg, 75 μmol) and $RuCl_3$ (8.3 mg, 37 μmol) in a mixture of THF:MeOH (7:3) was refluxed for three days. An excess of solid NH_4PF_6 (123 mg, 750 μmol) was added. The reaction mixture was poured into water (25 mL) and extracted with CH_2Cl_2 (2 × 25 mL). The organic layer was washed with water (2 × 25 mL), dried over Na_2SO_4 and removed *in vacuo*. Purification of the crude product was carried out by preparative size exclusion chromatography (BioBeads SX-1, swollen in CH_2Cl_2) and column chromatography (silica, 5% MeOH in $CHCl_3$). The red compound was isolated and precipitated from THF into methanol, yielding 24 mg of product (63%). ^{1}H-NMR ($CDCl_3$): δ = 8.18 (bm, 4 H; $H_{3,3"}$), 7.99-7.80 (bm, 4 H; $H_{3',5'}$), 7.73 (bm, 4 H; $H_{4,4"}$), 7.40-6.34 (m, 108 H; $H_{aromatic\ PS\ backbone}$, $H_{6,6"}$, $H_{5,5"}$), 4.22 (bm, 4 H; tpyOCH_2), 2.61-0.55 (bm, 71 H; tpyOCH$_2$CH_2, $H_{aliphatic\ PS\ backbone,\ initiator}$); UV/vis: ($CHCl_3$): λ / nm (ε / L mol^{-1} cm^{-1}): 489 (12900), 446 (7800), 343 (6200), 306 (46800), 270 (55800); GPC (RI): M_n (PDI) = 8000 g mol^{-1} (1.06); MALDI-TOF MS (dithranol): two distributions with Δ m/z = 104 due to fractionation, one with M_n = 2300 g mol^{-1} and one with M_n = 4500 g mol^{-1}; CE: M_n (PDI): 4800 g mol^{-1} (1.02).

Synthesis of PS_{20}-[Ni]-PS_{20}
A 5 mL solution of terpyridine-functionalized PS_{20} (50 mg, 25 μmol) and $Fe(OAc)_2$ (3.1 mg, 12.5 μmol) in a mixture of THF:MeOH (7:3) was refluxed for four hours. An excess of NH_4PF_6 (20 mg, 120 μmol) was added. The reaction mixture was poured into water (25 mL) and extracted with CH_2Cl_2 (2 × 25 mL). The organic layer was washed with water (2 × 25 mL), dried over Na_2SO_4 and removed *in vacuo*. Purification of the crude product was carried out by preparative size exclusion chromatography (BioBeads SX-1, swollen in CH_2Cl_2). The compound was isolated and precipitated from CH_2Cl_2 into methanol, yielding 20 mg of product (36%). UV/vis ($CHCl_3$): λ / nm (ε / L mol^{-1} cm^{-1}): 325 (15400), 311 (23700), 301 (27600), 270 (51400); CE: M_n (PDI): 4800 g mol^{-1} (1.06).

Synthesis of PS_{20}-[Ru]-PEO_{70} with PF_6 counter-ions
A solution of terpyridine-functionalized PS_{20} (0.630 g, 0.314 mmol) and PEO_{70}-[$RuCl_3$ (1.00 g, 0.286 mmol) in a mixture of $CHCl_3$:MeOH (8:1) (50 mL) was refluxed for 60 minutes. A few drops of *N*-ethylmorpholine were added and stirring under reflux was continued overnight. Then an excess of solid NH_4PF_6 (700 mg, 6 mmol) was added and the solution was allowed to cool to room temperature and poured into water (100 mL). The water-layer was extracted with $CHCl_3$ (3 × 50 mL) and the combined organic layers were washed with water (3 × 50 mL). The organic layers were dried over Na_2SO_4 and removed *in vacuo*. The compound was further purified by preparative size exclusion chromatography (BioBeads SX-1, THF followed by BioBeads SX-1, CH_2Cl_2) and a precipitation from THF into hexane, yielding 1.427 g of pure compound (84%). ^{1}H-NMR ($CDCl_3$): δ = 8.36 (m, 2 H; $H_{3,3"}$ PEO), 8.26 (bs, 2 H; $H_{3',5'}$ PEO), 8.17 (m, 2 H; $H_{3,3"}$ PS), 7.88-7.73 (m, 6 H; $H_{4,4"}$, $H_{3',5'}$ PS), 7.33-6.32 (m, 108 H; $H_{aromatic\ PS\ backbone}$, $H_{5,5"}$, $H_{6,6"}$) 4.74 (m, 2 H; tpyOCH_2 PEO), 4.28-4.04 (m, 4 H; tpyOCH$_2$CH_2 PEO, tpyOCH_2 PS), 3.92-3.42 (m, 560 H; PEO backbone), 3.38 (s, 3 H; OCH_3), 1.72-0.60 (m, 71 H; $H_{aliphatic\ PS\ backbone,\ initiator}$, tpyOCH$_2CH_2$ PS); UV/Vis (CH_3CN): λ / nm (ε / L mol^{-1} cm^{-1}): 487 (16600), shoulder at 347 (6600), 305 (59700), 269 (55900), 244 (48400); GPC-München (UV): M_n (PDI): 7810 g mol^{-1} (1.08); GPC-DMF (RI): M_n (PDI): 12400 g mol^{-1} (1.09); CE: M_n (PDI): 5800 g mol^{-1} (1.02); MALDI-TOF MS: (dithranol): three distributions: Δ(*m/z*) = 104 g mol^{-1} (PS) (M_n = 2300 g mol^{-1}), Δ(*m/z*) = 44 g mol^{-1} (PEO) (M_n = 3400 g mol^{-1}), diblock M_n = 5400 g mol^{-1}; AUC: M_n = 5800 g mol^{-1}.

Synthesis of PS_{20}-[Ru]-PEO_{70} with BPh_4 counter-ions
A solution of terpyridine-functionalized PS_{20} (0.250 g, 0.125 mmol) and PEO_{70}-[$RuCl_3$ (0.381 g, 0.120 mmol) in a mixture of $CHCl_3$:MeOH (8:1) (25 mL) was refluxed for 60 minutes. A few drops of *N*-ethylmorpholine were added and stirring under reflux was continued overnight. Then an excess of solid $NaBPh_4$ (428 mg, 1.25 mmol) was added. The solution was allowed to cool to room temperature and poured into water (100 mL). The water-layer was extracted with $CHCl_3$ (3 × 50 mL) and the combined organic layers were washed with water (3 × 50 mL). The organic layers were dried over Na_2SO_4 and removed *in vacuo*. The compound was further purified by preparative size exclusion chromatography (BioBeads SX-1, THF), dialysis against THF (Spectrapor dialysis bags with a cut-off range of M_w = 6000-8000) and a precipitation from THF into hexane, yielding 419 mg of pure compound (62%). ^{1}H-NMR ($CDCl_3$): δ = 8.36 (m, 2 H; $H_{3,3"}$ PEO), 8.26 (bs, 2 H; $H_{3',5'}$ PEO), 8.17 (m, 2 H; $H_{3,3"}$ PS), 7.88-7.73 (m, 6 H; $H_{4,4"}$, $H_{3',5'}$ PS), 7.33-6.32 (m, 148 H; $H_{aromatic\ PS\ backbone}$, $H_{5,5"}$, $H_{6,6"}$, $H_{aromatic\ BPh4}$) 4.74 (m, 2 H; tpyOCH_2 PEO), 4.28-4.04 (m, 4 H; tpyOCH$_2$CH_2 PEO, tpyOCH_2 PS), 3.92-3.42 (m, 560 H; PEO backbone), 3.38 (s, 3 H; OCH_3), 1.72-0.60 (m, 71 H; $H_{aliphatic\ PS\ backbone,\ initiator}$, tpyOCH$_2CH_2$ PS); UV/Vis (CH_3CN): λ / nm (ε / L mol^{-1} cm^{-1}): 487 (17400), shoulder at 347 (6800), 305 (60900), 269 (56400),

244 (52200); GPC-DMF (RI): M_n (PDI): 12100 g mol^{-1} (1.09); CE: M_n (PDI): 5800 g mol^{-1} (1.02); MALDI-TOF MS: (dithranol): three distributions: $\Delta(m/z)$ = 104 g mol^{-1} (PS) (M_n = 2300 g mol^{-1}), $\Delta(m/z)$ = 44 g mol^{-1} (PEO) (M_n = 3400 g mol^{-1}), diblock M_n = 5400 g mol^{-1}. FT-IR revealed the presence of BPh_4 counter-ions.

General procedure for the synthesis of PS_x-[Ru]-PEO_y

Terpyridine functionalized polystyrene (DP = 20, 70, 200 and 240) and the $RuCl_3$ *mono*-complex of terpyridine functional poly(ethylene oxide) (DP = 70, 125, 225 and 375) were reacted in a 1.05:1 molar ratio in a 4:1 solvent mixture of chloroform and methanol (15 mL) at reflux under argon. Thus, 129.8 mg, 60.2 mg, 31.5 mg and 23.5 mg of PS_{20} were reacted with 200 mg PEO_{70}-[$RuCl_3$, 151.8 mg PEO_{125}-[$RuCl_3$, 153 mg PEO_{225}-[$RuCl_3$ and 105.5 mg PEO_{375}-[$RuCl_3$, respectively; 200 mg, 200.5 mg, 100 mg and 102 mg of PS_{70} were reacted with 60.8 mg PEO_{70}-[$RuCl_3$, 100.4 mg PEO_{125}-[$RuCl_3$, 99.8 mg PEO_{225}-[$RuCl_3$ and 200 mg PEO_{375}-[$RuCl_3$, respectively; 200 mg, 206 mg, 80 mg and 112 mg of PS_{200} were reacted with 27 mg PEO_{70}-[$RuCl_3$, 46 mg PEO_{125}-[$RuCl_3$, 209 mg PEO_{225}-[$RuCl_3$ and 81 mg PEO_{375}-[$RuCl_3$, respectively; 229 mg, 217 mg, 197 mg and 150 mg of PS_{240} were reacted with 25 mg PEO_{70}-[$RuCl_3$, 40 mg PEO_{125}-[$RuCl_3$, 69.6 mg PEO_{225}-[$RuCl_3$ and 100 mg PEO_{375}-[$RuCl_3$, respectively. After 30 minutes a few drops of *N*-ethylmorpholine were added and a color change from brown to purple to red was observed. Stirring was continued overnight, after which a ten-fold excess of solid NH_4PF_6 was added. The solution was then allowed to cool to room temperature and poured into water. The water-layer was extracted twice with chloroform and the combined organic layers were dried over Na_2SO_4, filtered and evaporated *in vacuo*. The crude product was rigorously purified by a combination of preparative size exclusion chromatography on BioBeads SX-1 swollen in THF and/or CH_2Cl_2 and column chromatography (SiO_2, THF to wash down uncomplexed material, followed by 10% MeOH in THF to separate the *mono*-, if any, from the *bis*-complex, which was isolated by addition of NH_4PF_6 to the eluent). Selected analytical details for PS_{70}-[Ru]-PEO_{225} (**10**): ^{1}H-NMR ($CDCl_3$): δ = 8.41 (bm, 2 H; $H_{3;3"}$ PEO), 8.34-8.22 (bm, 6 H; $H_{3:3"}$ PS, $H_{3';5'}$ PS & PEO), 7.83 (bm, 4 H; $H_{4:4"}$ PS & PEO), 7.47 (bm, 2 H; *H*-PhCH$_2$Otpy), 7.36 (m, 6 H; $H_{5:5"}$ PS & PEO, *H*-PhCH$_2$Otpy), 7.21-6.28 (m, 349 H; PS backbone; $H_{6:6"}$ PS & PEO, *H*-Ph-nitroxide), 5.58 (m, 2 H; tpyOCH_2, PS), 4.77 (m, 2 H; tpyOCH_2, PEO), 4.11 (m, 2 H; tpyOCH$_2$CH_2), 3.88-3.46 (m, 901 H; PEO-backbone, Ph-C*H*-O-N), 3.38 (s, 3 H; OCH_3, PEO), 2.20-1.20 (m, 205 H; PS backbone, O-N-C*H*), 0.88 (m, 9 H; C(CH_3)$_3$ nitroxide), 0.66-0.28 (m, 7 H; isopropyl nitroxide); UV/vis (THF): λ / nm (ε / L mol^{-1} cm^{-1}): 487 (14800), 306 (52100), 270 (69100), 263 (69000); GPC (RI): M_n (PDI): 27000 g mol^{-1} (1.10).

Synthesis of PEO_{70}-[Ru]-PEB_{70}

A solution of PEB_{70}-[(0.107 g, 0.028 mmol) and PEO_{70}-[$RuCl_3$ (0.100 g, 0.028 mmol) in a mixture of THF:EtOH (7:3) (5 mL) was stirred under reflux for 30 minutes. A few drops of *N*-ethylmorpholine were added and stirring under reflux was continued overnight. Then an excess of solid NH_4PF_6 (50 mg, 31 mmol) was added and the solution was allowed to cool to room temperature and poured into water (25 mL). The water-layer was extracted with $CHCl_3$ (3 × 15 mL) and the combined organic layers were washed with water (3 × 50 mL). Afterwards the organic layers were dried over Na_2SO_4 and removed *in vacuo*. The compound was further purified by preparative size exclusion chromatography (BioBeads SX-1, CH_2Cl_2), yielding 76 mg of product (36%). ^{1}H-NMR ($CDCl_3$): δ = 8.40 (m, 2 H; $H_{3,3"}$ PEO), 8.36 (m, 2 H; $H_{3,3"}$ PEB), 8.29 (s, 2 H; $H_{3',5'}$ PEO), 8.17 (s, 2 H; $H_{3',5'}$ PEB), 7.81 (m, 4 H; $H_{4,4"}$), 7.37 (m, 4 H; $H_{6,6"}$), 7.18 (m, 4 H; $H_{5,5"}$), 4.76 (t, 2 H, ^3J = 4.8 Hz; tpyOCH_2 PEO), 4.58 (t, 2 H, ^3J = 4.8 Hz; tpyOCH_2 PEB), 4.09 (t, 2 H, ^3J = 4.8 Hz; tpyOCH$_2$CH_2 PEO), 3.87-3.41 (m, 560 H; PEO backbone), 3.38 (s, 3 H; OCH_3), 1.68-0.80 (m, 571 H; $H_{PEB\ backbone,\ initiator}$, tpyOCH$_2CH_2$ PEB); UV/Vis (CH_3CN): λ / nm (ε / l mol^{-1} cm^{-1}): 486 (14900), 304 (51100), 267 (48300). GPC-München (UV): M_n (PDI): 12400 g mol^{-1} (1.10). MALDI-TOF MS: (dithranol): three distributions: $\Delta(m/z)$ = 56 g mol^{-1} (PEB) (M_n = 3900 g mol^{-1}), $\Delta(m/z)$ = 44 g mol^{-1} (PEO) (M_n = 3400 g mol^{-1}), diblock M_n = 7500 g mol^{-1}.

Synthesis of PFS_{12}-[Ru]-PEO_{70}

A solution of PFS_{12}-[(50 mg, 0.016 mmol) and PEO_{70}-[$RuCl_3$ (52 mg, 0.015 mmol) was refluxed in a solvent mixture of chloroform and ethanol (4:1, 5 mL). After 30 minutes a few drops of *N*-ethylmorpholine were added. Stirring was continued overnight, after which an excess of solid NH_4PF_6 (50 mg, 0.3 mmol) was added and the solvent was evaporated *in vacuo*. The crude product was purified by preparative size exclusion chromatography (BioBeads SX-1, THF, followed by BioBeads SX-1, CH_2Cl_2) and precipitated from CH_2Cl_2 in hexanes. Yield: 78 mg (76%). ^{1}H-NMR ($CDCl_3$): δ = 8.41 (m, 4 H; $H_{3,3"}$), 8.31 (s, 2 H; $H_{3',5'\ PEO}$), 8.24 (s, 2 H; $H_{3',5'\ PFS}$), 7.81 (m, 4 H; $H_{4,4"}$), 7.39 (m, 4 H; $H_{6,6"}$), 7.20 (m, 4 H; $H_{5,5"}$), 4.93 (s, 1 H; N*H*COO), 4.80 (b, 2 H; tpyOCH_2 PEO), 4.61 (b, 2 H; tpyOCH_2 PFS),

4.40-3.51 (m, 383 H; PFS+PEO, $CH_2O(C=O)$), 3.43 (s, 3 H; OCH_3), 3.30 (m, 2 H; CH_2NHCOO), 2.08 (b, 2 H; tpyOCH_2CH_2 PFS), 2.00 (b, 2 H; tpy$OCH_2CH_2CH_2$), 1.72 (b, 2 H; CH_2CH_2NHCOO), 1.59 (m, 6 H; CH_2), 0.70-0.27 (m, 74H; $SiCH_2$, $SiCH_3$ PFS); UV/vis (CH_3CN): λ / nm (ε / L mol^{-1} cm^{-1}): 484 (17000), 304 (63000), 263 (90400). IR (ATR): ν (cm^{-1}): 3083, 2883 (CH terpyridine, CH_2 PEO backbone); 1716, 1543 (NHCOO); 1615 (terpyridine); 1342, 1104, 840 (C-O, PEO backbone); GPC (RI): M_n (PDI) = 14600 g mol^{-1} (1.07); MALDI-TOF MS (dithranol): three distributions: $\Delta(m/z)$ = 242 g mol^{-1} (PFS) (Mn = 3400 g mol^{-1}), $\Delta(m/z)$ = 44 g mol^{-1} (PEO) (M_n = 3400 g mol^{-1}), diblock m/z = 6330 g mol^{-1}.

Synthesis of PI_{65}-*b*-PS_{70}-[Fe]-PS_{70}-*b*-PI_{65}

A solution of $Fe(OAc)_2$ (1.6 mg, 9.0 μmol) and terpyridine-functionalized PI_{65}-*b*-PS_{70} (188 mg, 16.9 μmol) in a mixture of $CHCl_3$:MeOH (8:1, 5 mL) were stirred at reflux for three days. Conversion was followed by ^{1}H-NMR and UV/vis. After a complete shift of the signals in ^{1}H-NMR was observed, 20 mg of solid NH_4PF_6 (0.12 mmol) were added and stirring was continued for another hour. Then the solution was allowed to cool, poured into water and extracted with $CHCl_3$ (2 ×). The combined organic layers were washed with water (3 ×), dried over Na_2SO_4 and removed *in vacuo*. The compound was precipitated from THF into MeOH, yielding 98 mg (47%) of product. ^{1}H-NMR ($CDCl_3$): δ = 8.39 (bs, 4 H; $H_{3,3"}$), 8.27 (bs, 4 H; $H_{3',5'}$), 7.72 (bs, 4 H; $H_{4,4"}$), 7.58-6.24 (m, 726 H; $H_{\text{aromatic PS backbone, initiator, nitroxide}}$, $H_{6,6"}$, $H_{5,5"}$) 5.88-4.60 (bm, 134 H; $H_{\text{vinylic PI}}$, tpyOCH_2), 4.38, 4.27, 4.12, 3.67, 3.50, 3.38 (6 H, H_2C-ON, ON-C*H*), 2.38-0.80 (H aliphatic PS+PI, signals nitroxide), 0.52 (s, 18 H; $C(CH_3)_3$); UV/vis ($CHCl_3$): λ / nm (ε / L mol^{-1} cm^{-1}): 557 (14300), shoulder at 505 (9000), 360 (6600), 317 (44400), 270 (92800), 263 (87600), 254 (84300).

Synthesis of PS_{70}-[Ru]-PEB_{70}-[Ru]-PS_{70}

PS_{70}-[$RuCl_3$ (240 mg, 31 μmol) and telechelic terpyridine-functionalized PEB_{70} (68 mg, 18 μmol) were stirred at reflux in a mixture of THF and MeOH (4:1, 5 mL). After 30 minutes a few drops of *N*-ethylmorpholine were added. Refluxing was continued overnight, after which the color of the solution turned reddish-brown. An excess of solid NH_4PF_6 was added and the crude reaction mixture was poured into water. The organic layer was separated, dried over Na_2SO_4 and evaporated *in vacuo*. The red-brown product was subjected to a preparative size exclusion chromatography (BioBeads SX-1 swollen in THF, followed by a BioBeads SX-1 swollen in CH_2Cl_2. The red product was further purified by column chromatography (silica, 5% MeOH in THF). The red compound that was isolated after these purification efforts was partitioned between a 0.01 M NH_4PF_6 solution in water and $CHCl_3$. The organic layer was separated, washed three times with water and removed *in vacuo*. Finally, the product was solubilized in a minimum amount of THF and precipitated into methanol to yield the PS_{70}-[Ru]-PEB_{70}-[Ru]-PS_{70} triblock copolymer. ^{1}H-NMR ($CDCl_3$): δ = 8.48-7.92 ($H_{3,3"}$, $H_{3',5'}$), 7.78 ($H_{4,4"}$), 7.52-6.28 (H_{aromatic} PS backbone, $H_{5,5"}$, $H_{6,6"}$), 2.51-0.46 ($H_{\text{aliphatic}}$ PS+PEB-backbone). Spectrum difficult to integrate correctly for the terpyridine-signals: for PS_{aromatic} vs $PS_{\text{aliphatic}}$+PEB a ratio of 7:10 was found. This corresponds to the ratio expected for the triblock. UV/vis ($CHCl_3$): λ / nm (ε / L mol^{-1} cm^{-1}) = 489 (25500), shoulder at 445 (12700), shoulder at 351 (15800), 307 (90500), 270 (121700).

Synthesis of PS_{32}-*b*-$P2VP_{13}$-[Ru]-PEO_{70}

A solution of PEO_{70}-[$RuCl_3$ (0.070 g, 0.020 mmol) and terpyridine-functionalized PS_{32}-*b*-$P2VP_{13}$ (0.100 g, 0.021 mmol) in a mixture of THF:EtOH (7:3, 5 mL) was stirred for 30 minutes under reflux. A few drops of *N*-ethylmorpholine were added and the solution turned from orange to red. Stirring under reflux was continued overnight, after which an excess of solid NH_4PF_6 (45 mg, 0.27 mmol) was added. Stirring was continued for 1 h and subsequently the solvent was removed *in vacuo*. The reaction mixture was partitioned between 25 mL water and 25 mL CH_2Cl_2. The organic layer was washed with water (3 × 25 mL), dried over Na_2SO_4 and finally removed *in vacuo*, affording a reddish brown crude product. This was further purified by preparative size exclusion chromatography (BioBeads SX-1, first column in THF, second column in CH_2Cl_2), yielding 40 mg of the triblock copolymer (22%). ^{1}H-NMR (CD_3CN): δ = 8.58-8.11, 7.82 (b, 7.54-6.51, 4.82, 4.13, 3.82-3.55, 3.38, 2.29-1.26, 0.88-0.57. UV/Vis (CH_3CN): λ / nm (ε / L mol^{-1} cm^{-1}) = 486 (5800), 305 (22860), 263 (62100). GPC (RI): M_n (PDI) = 11900 g mol^{-1} (1.27).

4.9 Literature

[1] Gmelin, 58 Co [B], 122, 123, 246-249, 304-307, 578-597.
[2] P. H. Crayton, J. A. Mattern, *J. Inorg. Nucl. Chem.* **1960**, *13*, 248-253.
[3] D. Choudhury, R. F. Jones, G. Smith, D. J. Cole-Hamilton, *J. Chem. Soc. Dalton Trans.* **1982**, 1143-1146.
[4] T. Togano, N. Nagao, M. Tsuchida, H. Kumakura, K. Hisamatsu, F. S. Howell, M. Mukaida, *Inorg. Chim. Acta* **1992**, *195*, 221-225.
[5] B. P. Sullivan, J. M. Calvert, T. J. Meyer, *Inorg. Chem.* **1980**, *19*, 1404-1407.
[6] F. P. Dwyer, H. A. Goodwin, E. C. Gyarfas, *Aust. J. Chem.* **1963**, *16*, 42-46.
[7] A. Dovletoglou, S. A. Adeyemi, T. J. Meyer, *Inorg. Chem.* **1996**, *35*, 4120-4127.
[8] J. C. Dobson, B. P. Sullivan, P. Doppelt, T. J. Meyer, *Inorg. Chem.* **1988**, *27*, 3863-3866.
[9] C. Anderson, A. L. Beauchamp, *Can. J. Chem.* **1995**, *73*, 471-482.
[10] P. J. Hore, *Nuclear magnetic resonance (Oxford chemistry primers, 32)*, Oxford University Press, Oxford, **1996**.
[11] M. A. R. Meier, B. G. G. Lohmeijer, U. S. Schubert, *Macromol. Rapid Commun*. **2003**, *24*, 852-857.
[12] J. S. L. Lamba, C. L. Fraser, *J. Am. Chem. Soc.* **1997**, *119*, 1801-1802.
[13] J. R. Carlise, M. Weck, *J. Polym. Sci. Part A Polym. Chem.* **2004**, *42*, 2973-2984.
[14] G. Coppola, P. Fabbri, B. Pallesi, U. Bianchi, *J. Appl. Polym. Sci.* **1972**, *16*, 2829-2834.
[15] J. L. Beckers, J. C. Reijenga, *Werkboek voor het college/practicum Analytische Chemie; 2e proefversie*, Technische Universiteit Eindhoven, Eindhoven, **1996**, p.47-69.
[16] www.chemsoc.org/exemplarchem/entries/2003/leeds_chromatography/chromatography.
[17] Y. Walbroehl, J.W. Jorgenson *J. Chromatogr.* **1984**, *315*, 135-143.
[18] S. P. Porras, M-L. Riekkola, E. Kenndler *Electrophoresis* **2003**, *24*, 1485-1498.
[19] K. A. Oudhoff, P. J. Schoenmakers, W. Th. Kok, *J. Chromatogr. A* **2003**, *985*, 479-491.
[20] M. Franco, K. Araki, R. C. Rocha, H. E. Toma, *J. Solution Chem.* **2000**, *29*, 667-684.
[21] www.mpikg-golm.mpg.de/gf/ultracentrifugation.pdf.
[22] www.nanolytics.de/e/auz/auz_1.htm.
[23] C. Tziatzios, A. A. Precup, C. H. Weidl, U. S. Schubert, P. Schuck, H. Durchschlag, W. Mächtle, J. A. van den Broek, D. Schubert, *Progr. Colloid Polym. Sci.* **2002**, *119*, 24-30.
[24] www.beckman.com/resourcecenter/labresources/sia/ds837.asp.
[25] D. Schubert, C. Tziatzios, P. Schuck, U. S. Schubert, *Chem. Eur. J.* **1999**, *5*, 1377-1383.
[26] L. Brunsveld, B. J. B. Folmer, R. P. Sijbesma, E. W. Meijer, *Chem. Rev.* **2001**, *101*, 4071-4097.
[27] A. T. ten Cate, R. P. Sijbesma, *Macromol. Rapid Commun.* **2002**, *23*, 1094-1112.
[28] R. P. Sijbesma, F. H. Beijer, L. Brunsveld, B. J. B. Folmer, J. H. K. K. Hirschberg, R. F. M. Lange, J. K. L. Lowe, E. W. Meijer, *Science* **1997**, *278*, 1601-1604.
[29] S. Kelch, M. Rehahn, *Macromolecules* **1999**, *32*, 5818-5828.
[30] R. Dobrawa, F. Würthner, *Chem. Comm.* **2002**, 1878-1879.
[31] V. Berl, M. Schmutz, M. J. Krische, R. G. Khoury, J.-M. Lehn, *Chem. Eur. J.* **2002**, *8*, 1227-1244.
[32] D. G. Kurth, M. Schütte, J. Wen, *Colloids Surf. A* **2002**, *198-200*, 633-643.
[33] J. H. K. K. Hirschberg, F. H. Beijer, H. A. van Aert, P. C. M. M. Magusin, R. P. Sijbesma, E. W. Meijer, *Macromolecules* **1999**, *32*, 2696-2705.
[34] J. B. Beck, S. J. Rowan, *J. Am. Chem. Soc.* **2003**, *125*, 13922-13923.
[35] K. Yamauchi, A. Kanomata, T. Inoue, T. E. Long, *Macromolecules* **2004**, *37*, 3519-3522.
[36] S. Schmatloch, A. M. J. van den Berg, A. S. Alexeev, H. Hofmeier, U. S. Schubert, *Macromolecules* **2003**, *36*, 9943-9949.
[37] T. Vermonden, J. van der Gucht, P. de Waard, A. T. M. Marcelis, N. A. M. Besseling, E. J. R. Sudhölter, G. J. Fleer, M. A. Cohen Stuart, *Macromolecules* **2003**, *36*, 7035-7044.
[38] H. Jacobsen, W. H. Stockmayer, *J. Chem. Phys.* **1950**, *18*, 1600-1606.
[39] See experimental part chapter 3.
[40] J. Brandup, E. H. Immergut, E. A. Grulke, *Polymer Handbook 4th Ed.*, John Wiley & Sons, New York, **1999**.
[41] I. W. Hamley, *The Physics of Block Copolymers*, Oxford University Press, Oxford, **1998**.
[42] F. S. Bates, G. H. Fredrickson, *Phys. Today* **1999**, *52(2)*, 32-38.
[43] P. R. Andres, H. Hofmeier, B. G. G. Lohmeijer, U. S. Schubert, *Synthesis* **2003**, *18*, 2865-2872.
[44] M. Heller, U. S. Schubert, *Macromol. Rapid Commun.* **2001**, *22*, 1358-1363.
[45] I. Manners, *J. Polym. Sci., Part A*: *Polym. Chem.* **2002**, *40*, 179-191.
[46] K. Kulkuba, I. Manners, *Macromol. Rapid Commun.* **2001**, *22*, 711-724.
[47] K. L. Johnson, *Contact Mechanics*, Cambridge University Press, London, **1987**.

[48] W. C. Oliver, G. M. Pharr, *J. Mater. Res.* **1992**, *7*, 1564-1583.
[49] J. C. Hay, A. Bolshakov, G. M. Pharr, *J. Mater. Res.* **1999**, *14*, 2296-2305.
[50] W. C. Oliver, G. M. Pharr, *J. Mater. Res.* **2004**, *19*, 3-20.
[51] www.hysitron.com/applications/publications.htm
[52] L. I. J. C. Bergers, *Researchverslag*, Technische Universiteit Eindhoven, **2004**.
[53] P. Schuck, *Prog. Colloid Polym. Sci.* **1994**, *94*, 1-13.
[54] P. Schuck, B. Legrum, H. Passow, D. Schubert, *Eur. J. Biochem.* **1995**, *230*, 806-812.
[55] K. A. Oudhoff, P. J. Schoenmakers, W. Th. Kok, *Chromatographia* **2004**, in press.

Chapter 5

Morphologies of Metal Complex Connected Block Copolymers in the Bulk, in Thin Films and in Solution

Abstract

The melt morphology of PS_{20}-[Ru]-PEO_{70} has been studied by small angle X-Ray scattering. Depending on the counter-ion, aggregation of the metal complexes in multiplets or a lamellar phase separation is observed and can be explained in terms of ionic interactions between the metal complexes and enthalpic contributions from demixing of the polymer chains. The isothermal crystallization of this copolymer is briefly mentioned. The morphology of the 4 × 4 library of PS_x-[Ru]-PEO_y block copolymers as well as the triblock copolymers PS_{70}-[Ru]-PEB_{70}-[Ru]-PS_{70} and PI_{65}-b-PS_{70}-[Fe]-PS_{70}-b-PI_{65} is studied in thin films by AFM and a qualitative interpretation is given, since the morphologies are kinetically determined. Aqueous micelles were prepared from PS_{20}-[Ru]-PEO_{70}, PS_{20}-[Ru]-PEO_{375}, PEB_{70}-[Ru]-PEO_{70}, PFS_{12}-[Ru]-PEO_{70} and PS_{32}-b-$P2VP_{13}$-[Ru]-PEO_{70}. Dynamic light scattering, (cryo)-TEM and analytical ultracentrifugation revealed individual micelles, small aggregates of micelles and large aggregates of micelles in all cases. Reversible behavior with respect to temperature and concentration were found only in case of PEB_{70}-[Ru]-PEO_{70}. All other micelles are in a kinetically frozen state, highly dependent on the micelle preparation. Optimization of the distributions in the kinetically frozen micelles can be obtained by controlling the addition rate and volume of water to the common solvent. In case of PS_{20}-[Ru]-PEO_{70}, PS_{20}-[Ru]-PEO_{375} and PEB_{70}-[Ru]-PEO_{70} spherical micelles were obtained, whereas PFS_{12}-[Ru]-PEO_{70} gave rise to cylindrical micelles. PS_{32}-b-$P2VP_{13}$-[Ru]-PEO_{70} yielded pH-sensitive spherical micelles through protonation of the P2VP block at pH < 5. The addition of salt was found to have a deep influence on the size distributions of the micelles for all block copolymers and can be explained by ionic interactions due to the inherent charges present in the block copolymer. In general, ionic interactions are important for determining the final morphology of these block copolymers. The chapter is concluded with a brief outlook on preliminary results of opening the metal complex.

Parts of this chapter have been published: J.-F. Gohy, B. G. G. Lohmeijer, U.S. Schubert, *Macromolecules* **2002**, *35*, 4560-4563; J.-F. Gohy, B. G. G. Lohmeijer, S. K. Varshney, U. S. Schubert, *Macromolecules* **2002**, *35*, 7427-7435; J.-F. Gohy, B. G. G. Lohmeijer, S. K. Varshney, B. Décamps, E. Leroy, S. Boileau, U. S. Schubert, *Macromolecules* **2002**, *35*, 9748-9755; J.-F. Gohy, B. G. G. Lohmeijer, U. S. Schubert, *Macromol. Rapid Commun.* **2002**, *23*, 555-560; J.-F. Gohy, B. G. G. Lohmeijer, U. S. Schubert, *Chem. Eur. J.* **2003**, *9*, 3472-3479; M. Al-Hussein, B. G. G. Lohmeijer, U. S. Schubert, W. H. de Jeu, *Macromolecules* **2003**, *36*, 9281-9284; V. Vogel, J.-F. Gohy, B. G. G. Lohmeijer, J. A. van den Broek, W. Haase, U. S. Schubert, D. Schubert, *J. Polym. Sci. Part A Polym. Chem.* **2003**, *41*, 3159-3168; J.-F. Gohy, B. G. G. Lohmeijer, B. Décamps, E. Leroy, S. Boileau, J. A. van den Broek, D. Schubert, W. Haase, U. S. Schubert, *Polym. Int.* **2003**, *52*, 1611-1618; O. Regev, J.-F. Gohy, B. G. G. Lohmeijer, S. K. Varshney, D. H. W. Hubert, P. M. Frederik, U. S. Schubert, *Colloid Polym. Sci.* **2004**, *282*, 407-411; J.-F. Gohy, B. G. G. Lohmeijer, X.-S. Wang, A. Alexeev, M. A. W. Winnik, I. Manners, U. S. Schubert, *Chem. Eur. J.* **2004**, *10*, 4315-4323; V. Vogel, G. Mayer, B. G. G. Lohmeijer, J.-F. Gohy, J. A. van den Broek, W. Haase, U. S. Schubert, D. Schubert, *J. Polym. Sci. Part A Polym. Chem.* **2004**, *42*, 4458-4465; B. G. G. Lohmeijer, D. Wouters, Z. Yin, U. S. Schubert, *Chem. Commun.* **2004**, in press; M. Al-Hussein, B. G. G. Lohmeijer, U. S. Schubert, W. H. de Jeu, submitted; J.-F. Gohy, B. G. G. Lohmeijer, A. Alexeev, X.-S. Wang, I. Manners, M. A. Winnik, U. S. Schubert, *ACS Symp. Series*, accepted.

5.1 Introduction

The bulk morphology of block copolymers is determined by the immiscibility of the polymer blocks and their overall volume fractions.[1-3] For covalently connected di- and triblock copolymer phase diagrams of bulk morphologies were presented in chapter 1. The block copolymers described in chapter 4 are linked via a metal complex. This introduces a permanent 2+-charge on the polymer backbone that is neutralized by the presence of two single charged counter-anions. It can be expected that ionic interactions play an important role in the final morphology of these block copolymers. Important examples of ionic interactions in polymers can be found in ionomers[4] and polyelectrolytes.[5] Controlling the ion-content, even at low concentrations, offers ways to control important physical properties such modulus, glass transition, viscosity, melt strength and fatigue. Also, conductivity may be enhanced and lead to applications such as solid state electrolytes. Properties of ionomers arise mainly from the fact that ions tend to aggregate in media of low dielectric constant into so-called multiplets.[4,6] This ion aggregation has a deep impact on the morphology: understanding these phenomena leads to control of the structure-property-relationships and hence the design of new superior materials. In our case, understanding is enhanced because of the fact that there is no polydispersity in terms of charge per polymer chain, but more complex due to the presence of two different polymer chains and loosely bound counter-ions.

The morphology of these metal-complex linked block copolymers is the subject of this chapter. The diblock copolymer PS_{20}-[Ru]-PEO_{70} has been considered as a model system: it has been studied in the melt, upon crystallization and/or vitrification, in thin films and in selective solvents by the formation of (aqueous) micelles to gain insight into the morphological behavior of this new class of compounds. Moreover, the morphology has been compared with a covalent block copolymer of comparable composition (PS_{22}-*b*-PEO_{70}) where possible. Techniques used for the characterization of the morphology include atomic force microscopy (AFM), transmission electron microscopy (TEM) and wide and small angle X-ray scattering (WAXS and SAXS). In small angle X-ray scattering a low divergence X-ray beam is focused onto the sample. A coherent scattering pattern is observed due to local imhomogeneities in electron density within the sample. Since the dimensions of interest are much larger than the wavelength of the X-rays, the scattering pattern at small angles is analyzed. Using the inverse relationships between particle size and scattering angle, characteristic shapes and size features can be distinguished.[7] The first studies of the library as presented in chapter 4.6.4 have been carried out by AFM after spincasting in thin films. Although the morphology in thin films is more complex than in the melt because of surface interactions, a qualitative interpretation can be presented. The diblock copolymers of PEB_{70}-[Ru]-PEO_{70}, PS_{20}-[Ru]-PEO_{375}, PFS_{12}-[Ru]-PEO_{70} and the triblock copolymer PS_{32}-*b*-$P2VP_{13}$-[Ru]-PEO_{70} also formed micelles in aqueous solution. These micelles were investigated by techniques such as AFM, (cryo)-TEM, static and dynamic light scattering (SLS and DLS) and analytical ultracentrifugation (AUC). The effect of temperature, salt and pH have been investigated as well.

5.2 Bulk morphology

For investigation of the bulk morphology PS_{20}-[Ru]-PEO_{70} has been studied by differential scanning calorimetry (DSC), WAXS, SAXS, polarized optical microscopy, AFM and TEM. This copolymer was prepared as described in chapter 4.6.1: two different types were prepared and they differ in the type of associated counter-ions, being hexafluorophosphate (PF_6) and tetraphenylborate (BPh_4) respectively. Figure 5.1 shows the schematic structure of the copolymers.

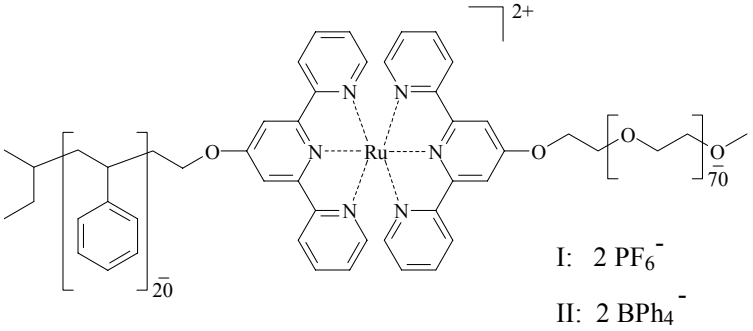

Figure 5.1. *The investigated block copolymers of PS_{20}-[Ru]-PEO_{70} with hexafluorophosphate (I) and tetraphenylborate counter-ions (II).*

5.2.1 Melt morphology of PS_{20}-[Ru]-PEO_{70}

The DSC thermogram for PS_{20}-[Ru]-PEO_{70} reveals a melting peak at 49 °C that can be attributed to melting of the semi-crystalline PEO-block (Figure 5.2). Upon cooling no crystallization of the PEO-block could be observed, but a glass transition is found at –40 °C. A subsequent heating scan reveals an exotherm recrystallization process at 5 °C. Crystallization of the PEO is hampered by the presence of PS and the metal complex at these scan rates (40 °C min^{-1}). A glass transition of the polystyrene-block is not observed, however the starting compound revealed a T_g at 74 °C. The fact that the PEO is molten at these temperatures and the low molecular weight of the PS-block are apparently responsible for sufficient mobility in the PS-block. It is noteworthy that the covalent PS_{22}-*b*-PEO_{70} revealed a melting peak at 49 °C and also no glass transition: an exotherm recrystallization peak on heating the sample from –100 °C further demonstrates the similarity. PS_{20}-[Ru]-PEO_{70} with BPh_4 counter-ions shows a similar DSC thermogram.

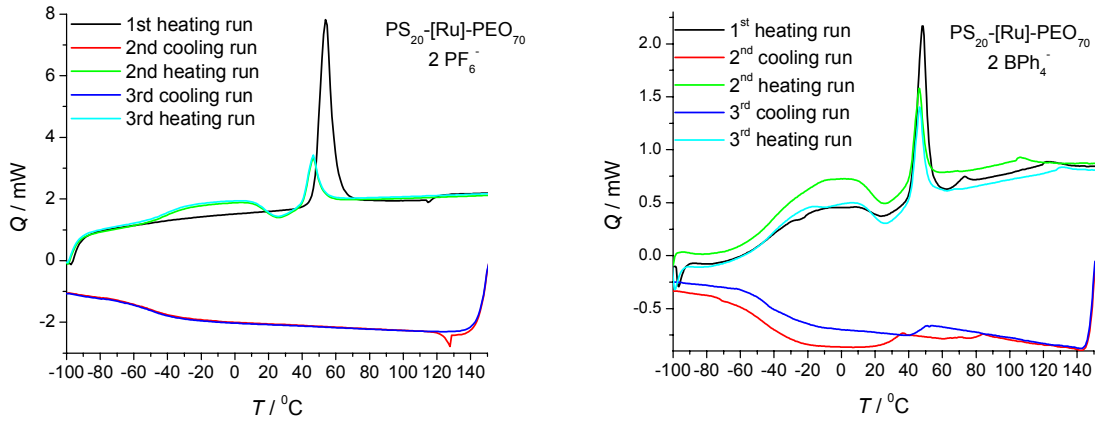

Figure 5.2. *DSC-curves of PS_{20}-[Ru]-PEO_{70} with PF_6 (left) and BPh_4 counter-ions (right) at 40 °C min^{-1}.*

For investigation of the morphology SAXS-curves have been recorded for the block copolymer melt of PS_{20}-[Ru]-PEO_{70} with PF_6 counter-ions between 55 °C and 150 °C (Figure 5.3).

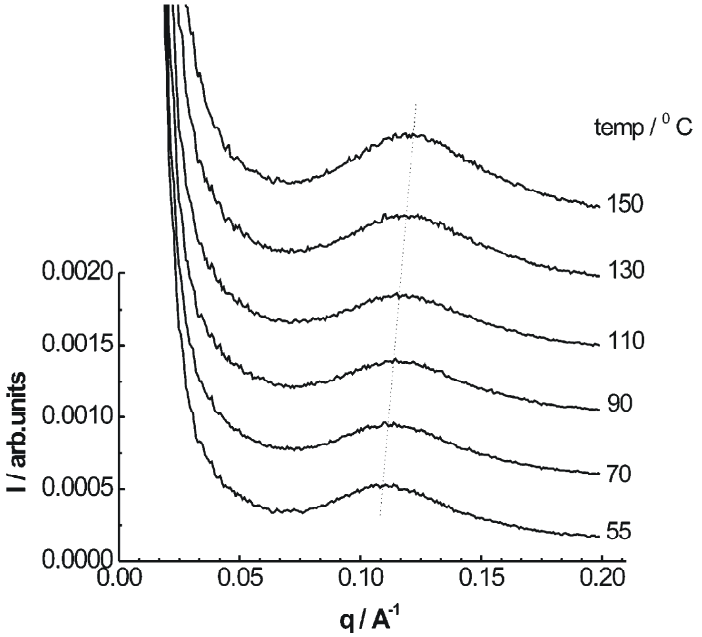

Figure 5.3. *SAXS-curve of the block copolymer melt of PS_{20}-[Ru]-PEO_{70} with PF_6^- counter-ions at various temperatures.*

A broad peak can be observed at q-values between 0.68 and 2.0 nm^{-1}. Interestingly, the covalent block copolymer does not reveal any features in the SAXS-curve, indicating a homogeneous block copolymer melt. This can be attributed to the low molecular weight of the block copolymer: the entropy arising from chain stretching compensates for the enthalpy of demixing and hence a homogeneous block copolymer melt can be obtained. However, increasing the molecular weight does give rise to a microphase separation. Based on the volume fraction for PS (42%) a lamellar morphology for the covalent analogue is expected and for higher molecular weights this has indeed been observed.[8,9] Nevertheless, PS_{20}-[Ru]-PEO_{70} does not reveal a SAXS-curve indicative of a lamellar phase separation, but instead a broad peak is observed. Obviously, the difference between the covalently and the metal-complexed linked block copolymer is the presence of the metal complex at the interface between the two polymer blocks. The difference in polarity between the metal complex and the two polymer blocks adds an additional driving force to the enthalpic and entropic forces already present. From this point of view, PS_{20}-[Ru]-PEO_{70} may be considered as a triblock copolymer with a short middle block. The difference in polarity introduced by the metal complex will trigger off a microphase separation, while the interplay between the various driving forces determines the final melt morphology. Such behavior has also been observed in the field of ionomers: due to the large difference in polarity a phase separation takes place of the ionic groups into domains in the hydrophobic polymer matrix.[4,10,11] The SAXS-curves of ionomers reveal a broad peak at q-values between 1-4 nm^{-1} and this is in perfect agreement with the SAXS-curve as displayed in Figure 5.3. Thus, the interaction between the metal complexes and the counter-ions on neighboring chains is responsible for a phase separation between domains of metal complexes in a polymer matrix. This aggregation obviously leads to unfavorable mixing of the PS and PEO chains and concomittant chain stretching. Apparently, the gain in energy for aggregation

outweighs both the enthalpic penalty for mixing as well as the restoring entropic forces for chain stretching. Simply put, random ionic aggregation of the metal complexes determines the final morphology and no influence of either block plays a role. Of course, the randomness of the aggregation is restricted by the size of the block copolymer. The origin of the SAXS-curve has been dealt with by Eisenberg: intermultiplet scattering is responsible for the appearance of the peak and is related to the distance between the scattering centers (the multiplets).[4,10,12-14] The Yarusso-Cooper model is well-suited for the interpretation of the SAXS-curves of ionomers.[15-18] The ionic aggregates are considered to be spherical particles consisiting of an ionic core of radius R_1 and a shell of outer radius R_{ca}, also known as the region of restricted mobility. These spheres are dispersed in the polymer matrix with a liquid-like order constrained by the distance of closest approach (=2 R_{ca}). When applied to PS_{20}-[Ru]-PEO_{70} the shell layer includes the metal complex with counter-ions as well as parts of the polymer chains as shown in Figure 5.4.

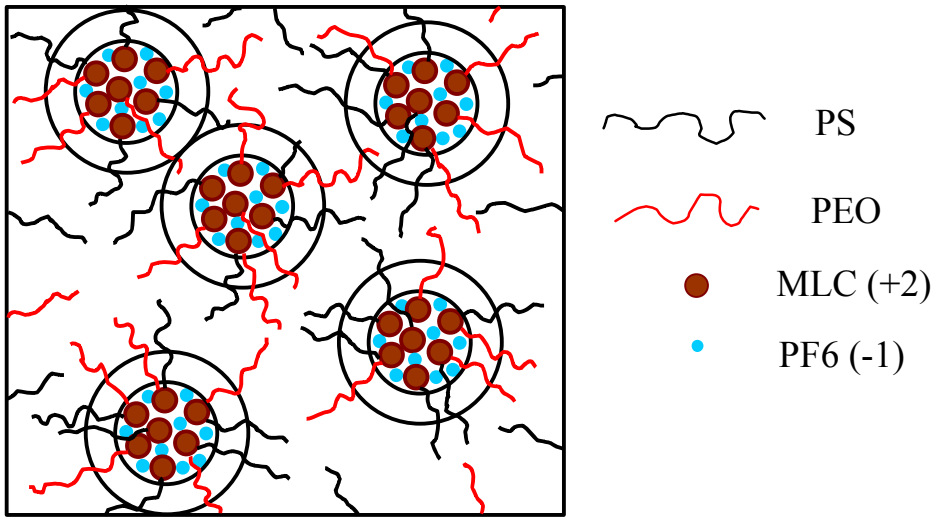

Figure 5.4. *Schematic representation of the melt morphology of PS_{20}-[Ru]-PEO_{70} with PF_6 counter-ions.*

The Yarusso-Cooper model can fit the data very well, but fails to predict the upturn at very low q-values. This can be included into the model, but would only reveal the non-randomness of the long-range distribution of the ionic aggregates.[16] For simplicity, only the broad peak has therefore been fitted with the Yarusso-Cooper model. Interestingly, upon increasing the temperature a slight shift of the peak maximum to higher q-values can be observed. In agreement with observations for ionomers, the ionic interactions persist even far above the T_g of the material.[19] The fact that the peak shifts to higher q-values implies that the aggregation becomes less, since the correlation length decreases. Nevertheless, this still does not give rise to a phase separation between PEO and PS. The values for R_1, R_{ca} and V_p (total volume of the aggregate including the metal complexes and both copolymer chains) as calculated using the Y-C model are displayed in Table 5.1.

For further quantification, the partial molar volume of the metal complex must be known. The density and volume of a metal complex can be derived from X-Ray analysis. For *bis*-terpyridine ruthenium with two hexafluorophosphate-counter-ions, the density and the volume are reported in the literature. Unfortunately, data on the same complex with tetraphenylborate-counter-ions is unavailable. On the other hand, the volume of the complex without counter-ions is also known. Thus, the volume of

the counter-ions in the complex can be calculated assuming a close packing. This is subsequently multiplied by the ratio of the partial specific volumes of BPh_4 *vs* PF_6 counter-ions.[19] Hence, the volume of the complex with tetraphenylborate counter-ions is obtained. For polystyrene and poly(ethylene oxide) the partial volumes can be calculated based on their degrees of polymerization and densities. Hence, the volume fractions of polystyrene, poly(ethylene oxide) and the metal complex can be determined. For amorphous PS and PEO the densities are 1.04 and 1.10 g cm^{-3} at 55 °C respectively.[9] Table 5.2 shows the results of the calculations.

Table 5.1. *Best-fit parameters for the Y-C model at different temperatures*

T / °C	R_1 / nm	R_{ca} / nm	V_p / nm^3
55	1.51 ± 0.28	2.42 ± 0.09	119.9 ± 3.6
70	1.50 ± 0.27	2.40 ± 0.09	119.1 ± 3.6
90	1.41 ± 0.22	2.31 ± 0.08	118.5 ± 3.4
110	1.39 ± 0.23	2.25 ± 0.08	116.6 ± 3.6
130	1.35 ± 0.23	2.20 ± 0.07	109.6 ± 3.4
150	1.32 ± 0.18	2.16 ± 0.05	104.1 ± 2.6

Table 5.2. *Results of the calculations of the volume fractions of PS, PEO and the metal complex (MC) in PS_{20}-[Ru]-PEO_{70} with PF_6 or BPh_4 counter-ions at 55 °C and 150 °C.*

T / °C	Ion	V_{PS} / nm^3	V_{PEO} / nm^3	V_{MC} / nm^3	f_{PS}	f_{PEO}	f_{MC}
55	PF_6	2.00	2.80	0.904	35.1	49.1	15.8
150	PF_6	2.10	3.02	0.904	34.9	50.1	15.0
55	BPh_4	2.00	2.80	1.092	33.9	47.5	18.5
150	BPh_4	2.10	3.02	1.092	33.8	48.6	17.6

These data can now be compared with the values obtained by the Y-C model. If we assume that the core of the ionic aggregate contains the metal complexes and counter-ions only, the number of metal complexes can be calculated from the ratio V_1/V_{MC}, where V_{MC} stands for the volume of the metal complex and V_1 can be calculated by assuming that $V_1 = 4/3\times\pi\times(R_1)^3$. This amounts to 16 metal complexes at 55 °C and 11 at 150 °C. These can be considered as upper limits, since part of the chain must also be incorporated into the core. Interestingly, calculating the volume fraction of the core in the total volume of the aggregate (V_1/V_p), one finds a volume fraction of 12.0% at 55 °C and 9.3% at 150 °C. If all metal complexes were located in the core of the aggregate, the volume fraction of the core would correspond to the volume fraction of the metal complex in the block copolymer. After comparing the data it is clear that apparently not all metal complexes are aggregated into multiplets, presumably due to steric hindrance. At higher temperatures the region of restricted mobility becomes less due to reduced expression of electrostatic interactions. As a result, the size of the core as well as of the total aggregate decreases (Table 5.1). Moreover, less metal complexes are located in the core, since V_1/V_p changes more dramatic than the volume fraction of metal complex in the block copolymer at higher temperatures.

Changing the counter-ions from PF_6 to BPh_4 leads to a different morphology as shown in Figure 5.5. At 55 °C the initial melting state reveals again a broad peak. After 10 hours at least four new peaks start to develop. The intensity of the new peaks grow with time until it reaches a final value after 40 hours.

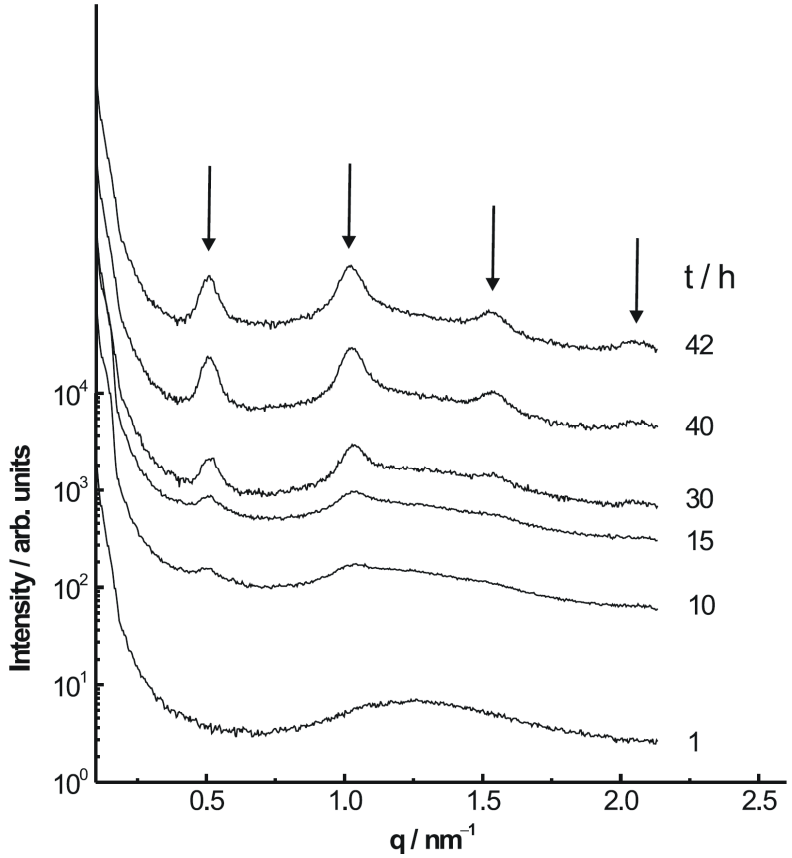

Figure 5.5. *SAXS-curves of the melt morphology of PS_{20}-[Ru]-PEO_{70} with BPh_4 counter-ions at 55 °C, where in time the broad peak transform into four distinct peaks indicating a lamellar morphology.*

The relative positions of the new peaks (1:2:3:4) indicate a highly ordered lamellar structure of the annealed melt. The first-order peak occurs at q = 0.53 nm^{-1} corresponding to a lamellar period of 11.9 nm. This value corresponds well with the size of the block copolymer. The second-order peak is more intense than the first one. This usually occurs when the second order peak introduces a new fundamental spacing, which has also been observed in liquid crystalline and side-chain liquid crystalline diblock copolymers.[20,21] In principle two types of lamellar morphologies can be envisaged due to the self-assembling of the metal complexes and counter-ions (Figure 5.6).

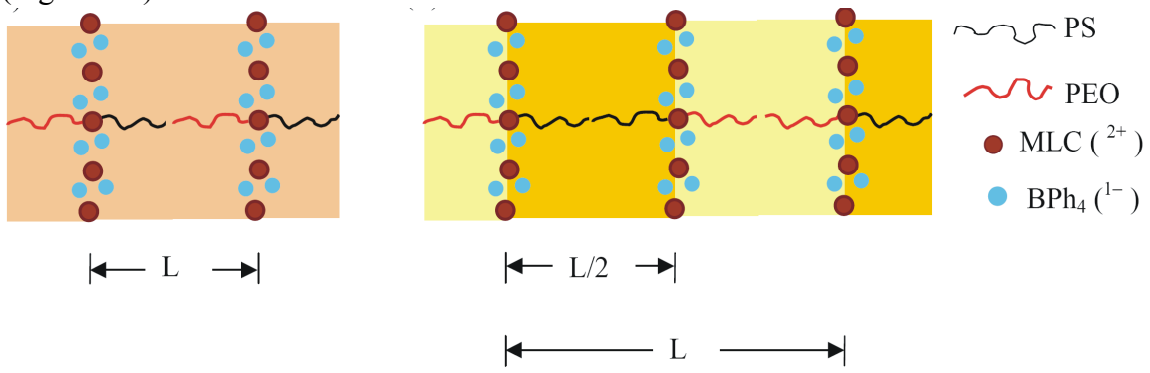

Figure 5.6. *Two possible morphologies of PS_{20}-[Ru]-PEO_{70} with BPh_4 counter-ions.*

The first one reveals intermixed PS and PEO chains and the lamellar period stems only from the metal complexes. The second option reveals a microphase separation between PS and PEO with the metal complexes confined to the interface between them. This gives rise to a lamellar period L, representing AA-[Ru]-BB. The presence of the metal complexes at the interface, however, gives rise to a lamellar period that is approximately L/2. Thus, the second-order peak can be attributed to a new fundamental spacing being that of the metal complexes. Assuming a Gaussian chain, the radius of gyration is given by $a\sqrt{N/6}$, where a is the statistical segment length and N the degree of polymerization. Given that a_{PS} = 0.68 nm and a_{PEO} = 0.28 nm, the corresponding radii of gyration for the PS and PEO chains are 1.24 and 0.96 nm.[22] From molecular mechanics modeling, the diameter of the metal complex with two BPh_4 counter-ions is approximately 2.3 nm. On the other hand, the diameter can also be recalculated from the data in Table 5.2. Then a diameter of 1.28 nm is found. Thus, a lamellar spacing L (A-[Ru]-BB-[Ru]-A) would become 11.3 nm, which corresponds quite good with the observed spacing and indicates that the chains are only slightly stretched.

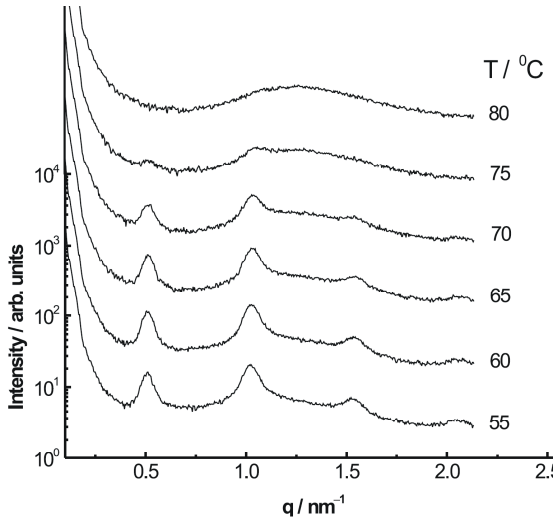

Figure 5.7. *SAXS-curves of the lamellar melt morphology of PS_{20}-[Ru]-PEO_{70} with BPh_4 counter-ions upon increasing the temperature from 55 to 80 °C.*

Figure 5.7 shows the SAXS-curves of the copolymer upon heating the lamellar melt morphology up to 80 °C. Again, the broad peak appears that was also observed before in the initial melt. It is noteworthy that the curves are identical. Fitting of this curve by the Y-C model reveals values for the diameter of the inner core of 2.0 nm and of the region of restricted mobility of 4.4 nm. It may thus be concluded that the initial melting state and that after heating the lamellar structure up to 80 °C are disordered states where the copolymer chains are dispersed uniformly. The results clearly demonstrate the difference between the melt morphology of this copolymer and that with PF6 counter-ions. Since the only difference between the two copolymers is the counter-ion, the change in morphology must be attributed to counter-ion effects. By enlarging the size of the counter-ion, the steric hindrance for metal complexes to associate becomes larger. Moreover, due to the fact that the counter-ion is much larger, its effective charge is reduced in comparison with the PF_6 counter-ion. This inherently leads to a reduced expression of ionic interactions. Furthermore, the interaction energies between the metal complex and the PS-block on one hand and the

PEO-block on the other hand will be different for different counter-ions. Currently it is not clear what the main driving forces are for the phase separation in the melt, but is likely that this must be found in the phase separation of the polymer blocks from the metal complex. Indeed, it has been shown experimentally that changing the type or size of nanoparticles in mixtures of nanoparticles and block copolymers, the morphology and the phase behavior of the system can be altered.[23-25] A theoretical approach to predict the morphology and phase diagram for such systems as a function of size, interaction energy and volume fraction of the nanoparticles has been developed by Balasz.[26,27]

Nevertheless, by simply changing the counter-ion, the morphology of the metal complexed block copolymer can be influenced dramatically. The ordering of the metal complexes in a lamellar structure or plane could be of interest for applications in electronics and photonics. Of course then the lamellar period needs to be precisely controlled. Anyhow, the counter-ion effect in combination with changing the block lengths is an issue that definitely needs to be addressed further. Moreover, it will be interesting to see what effect di-, tri- or multivalent counter-ions could have on the morphology.

5.2.2 Isothermal crystallization

Diblock copolymers containing a PEO-block belong to the class of semi-crystalline block copolymers.[28] Crystallization in block copolymers can have a profound influence on their morphology and material properties. In principle, three temperature parameters are of importance for the resulting morphology: T_{ODT}, T_g and T_{cr}, which represent the order-disorder transition, the glass transition temperature of the amorphous block and the isothermal crystallization temperature after quenching the copolymer from the melt. There are several scenario's: for cases where $T_{ODT} > T_{cr} > T_g$ results in unconfined crystallization of the crystalline block and the initial melt morphology is transformed to a lamellar structure containing alternating lamellae of the crystalline block and of the amorphous block. In cases where $T_{cr} > T_{ODT} > T_g$ a similar morphology is the result. On the other hand, when $T_{ODT} > T_g > T_{cr}$ confined crystallization is the result: the melt morphology is retained, since first vitrification of the amorphous block takes place. Crystallization can then only occur in the regions dictated by the glassy polymer block. Competition between crystallization and segregation occurs for cases where $T_{cr} \approx T_{ODT} > T_g$. Several excellent papers have dealt with the crystallization of symmetric and asymmetric PS-*b*-PEO by varying T_{cr} and recording SAXS and WAXS curves.[8,9,29,30]

Here PS_{20}-[Ru]-PEO_{70} with PF_6 counter-ions is studied. From section 5.2.1 it can be concluded that the melt morphology is dominated by ionic interactions and involved the formation of multiplets by the metal complexes and counter-ions. In comparison with covalently linked PS-*b*-PEO an additional driving force must be taken into account, i.e. the ionic aggregation. Isothermal crystallization of the melt was carried out at three different temperatures, 10 °C, 23 °C and 30 °C. The results are shown in Figure 5.8. The three SAXS-curves look rather different, although similar features can be observed. At 30 °C, at low q-values a peak comes up at 0.031 $Å^{-1}$ and an additional one arises at 0.078 $Å^{-1}$, after long periods of time. The peak present at 0.104 $Å^{-1}$ was also observed in the melt and indicated a liquid-like type of ordering of the multiplets as discussed before. At 10 °C the peak at 0.031 $Å^{-1}$ is visible, but that at 0.078 $Å^{-1}$ can not be observed. The situation at 23 °C displays a SAXS-curve that is in between

the other two. Although the peaks are all rather broad, crystallization of the PEO-block is taking place and the formation of PEO-lamellae can be deduced from the new peak at 0.31 $Å^{-1}$ visible in all three curves. Interestingly, this corresponds to a period of ~20 nm and indicates that the PEO-chains are not fully stretched. A fully stretched PEO-chain with a DP of 70 has a length of 20 nm.

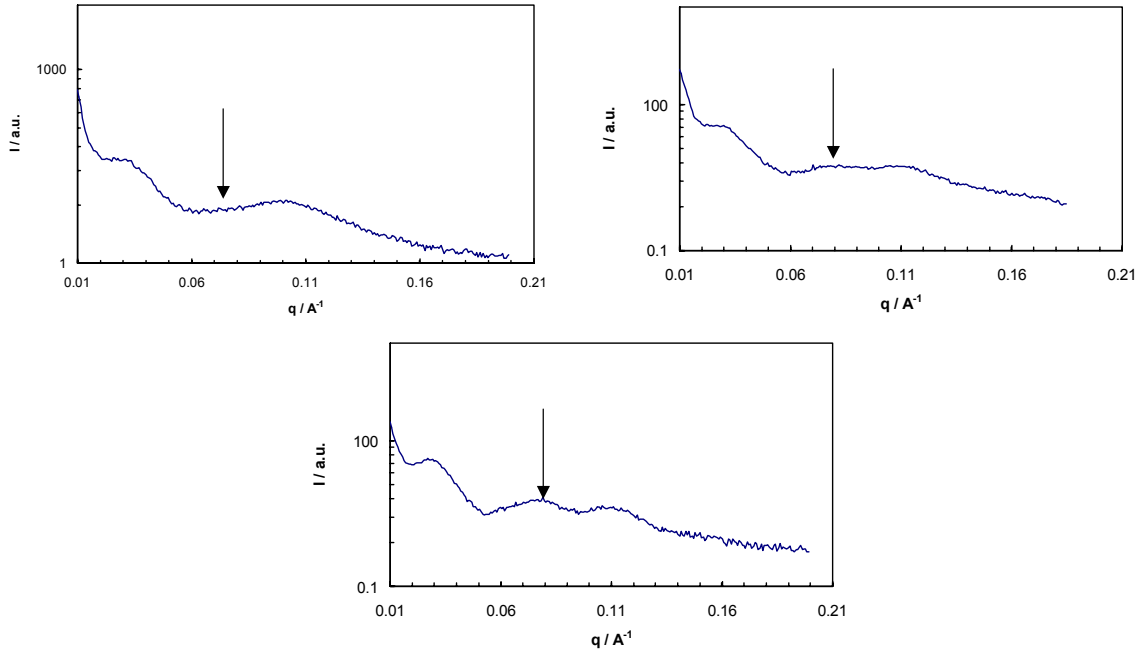

Figure 5.8. *SAXS-curves of PS_{20}-[Ru]-PEO_{70} with PF_6 counter-ions after isothermal crystallization at three different temperatures, i.e. 10 °C (top left), 23 °C (top right) and 30 °C (bottom).*

The origin of the other two peaks is difficult to explain. At 10 °C it seems that the liquid-like type of ordering is retained. This could be facilitated by crystallizing below the T_g of the polystyrene-block. Then a confined crystallization is the result and could explain the low intensity of the peak in comparison with its intensity at the two higher temperatures. One would expect that if there is sufficient mobility at higher temperatures, unconfined crystallization could take place. Due to the fact that the peak position of the PEO is only very slightly shifted to lower q-values (from 0.031 to 0.028 $Å^{-1}$ upon going from 10 to 30 °C), this is apparently not the case. The multiplets could therefore also confine the crystallization of the PEO. The question however is what the new peak at 0.078 $Å^{-1}$ represents. From WAXS, AFM and POM the formation of PEO-crystals could clearly be proven (Figure 5.9).

In summary, the morphology ot the block copolymer is changed upon isothermal crystallization from the melt. A more detailed understanding of the morphology after isothermal crystallization would require isothermal crystallization on the covalent sample for comparison.

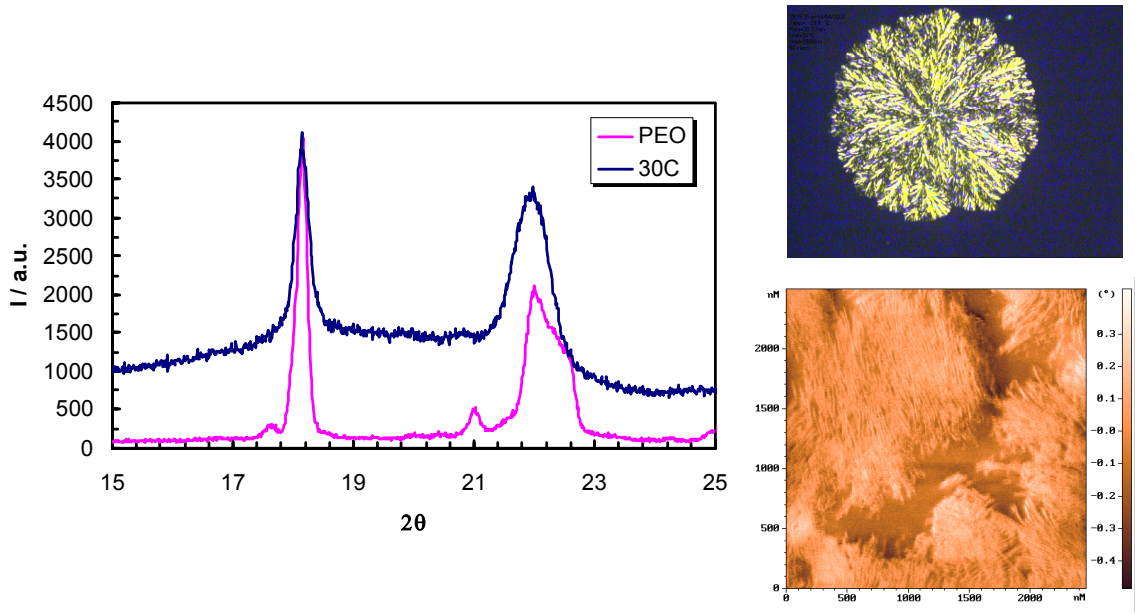

Figure 5.9. *Presence of crystalline PEO after isothermal crystallization of PS_{20}-[Ru]-PEO_{70} with PF_6 counter-ions at 30 °C, as confirmed by WAXS (left), polarized optical microscopy (top right) and AFM phase image (bottom right).*

5.3 Block copolymer thin films

The morphology of block copolymers in thin films is dictated by interfacial and surface interactions.[31] Although in theoretical work hard impenetrable surfaces have been used to model phase behavior of lamellar block copolymers using both symmetric and asymmetric boundaries, in practice only one of the surfaces is hard and impenetrable.[32-35] The existence of a free surface has important consequences for the morphology. Usually spin-cast films have thicknesses that are not an integer of the block copolymer period. Upon annealing, the morphology of such systems changes in such a way that this thickness mismatch with the copolymer periodicity is resolved. As a result, hole and island formation in the thin film surface takes place.[36,37] If the film thickness was not uniform terrace formation can also be result. Owing to their relative simplicity in terms of possible thin film morphologies, symmetric block copolymers have been studied most. Nevertheless, from a technological point of view, i.e. in the preparation of lithographic masks or templates for the fabrication of nanodots and nanocylinders, the spherical and cylindrical morphologies are of special interest.[38,39] Theoretical treatments are more scarse,[37,40] however recently cylinders standing upright and perpendicular to the surface were obtained experimentally by Russell on PS-*b*-PEO block copolymers.[41-43] The cylinders fully penetrate the thin film from top to bottom. These thin films have not been thermally annealed, but are in fact kinetically metastable structures. The existence of this morphology was explained as follows: the presence of the solvent allows for sufficient mobility of the copolymer and also reduces the differences in surface energies of both blocks. Due to the fact that evaporation in a thin film is non-uniform, a concentration gradient is established. Upon removal of solvent from the surface, the concentration increases and an order-disorder transition can take place. A phase separated state of the block copolymer in solution is thus established. The solvent gradient propagates throughout the film and functions as an ordering front. Further evaporation of the solvent leads to vitrification of the PS-block and locks in the morphology. This functions subsequently as a template until the cylinders are fully penetrating the film.[44]

5.3.1 Library of PS_x-[Ru]-PEO_y

The synthesis of a library of PS_x-[Ru]-PEO_y was described in section 4.6.4. The 16 copolymers have been spin-coated onto silicon wafers from toluene-solution and were subsequently analyzed by AFM (Figure 5.10). At first glance, the different components of the library all show different phase behavior. Although trivial, this is an important observation: interpreting the phase behavior of these block copolymers by AFM is not straightforward. Complications involve phase attribution and the relationship between topology and morphology using this AFM-technique.[45] In principle there are four individual contributors to the phase contrast: amorphous PEO, crystalline PEO, the metal complex and amorphous polystyrene. The final morphology will be determined by competitions between phase separation, crystallization of the PEO-block and vitrification of the PS-block.[8,9] Moreover, the final morphology will be further complicated by competition between phase separation of the polymer blocks and association of polymer chains through ionic interactions as described in section 5.2.1. These opposite driving forces give rise to a very rich phase behavior: annealing these thin films is therefore not straightforward, since the morphology continuously changes upon changing the temperature.

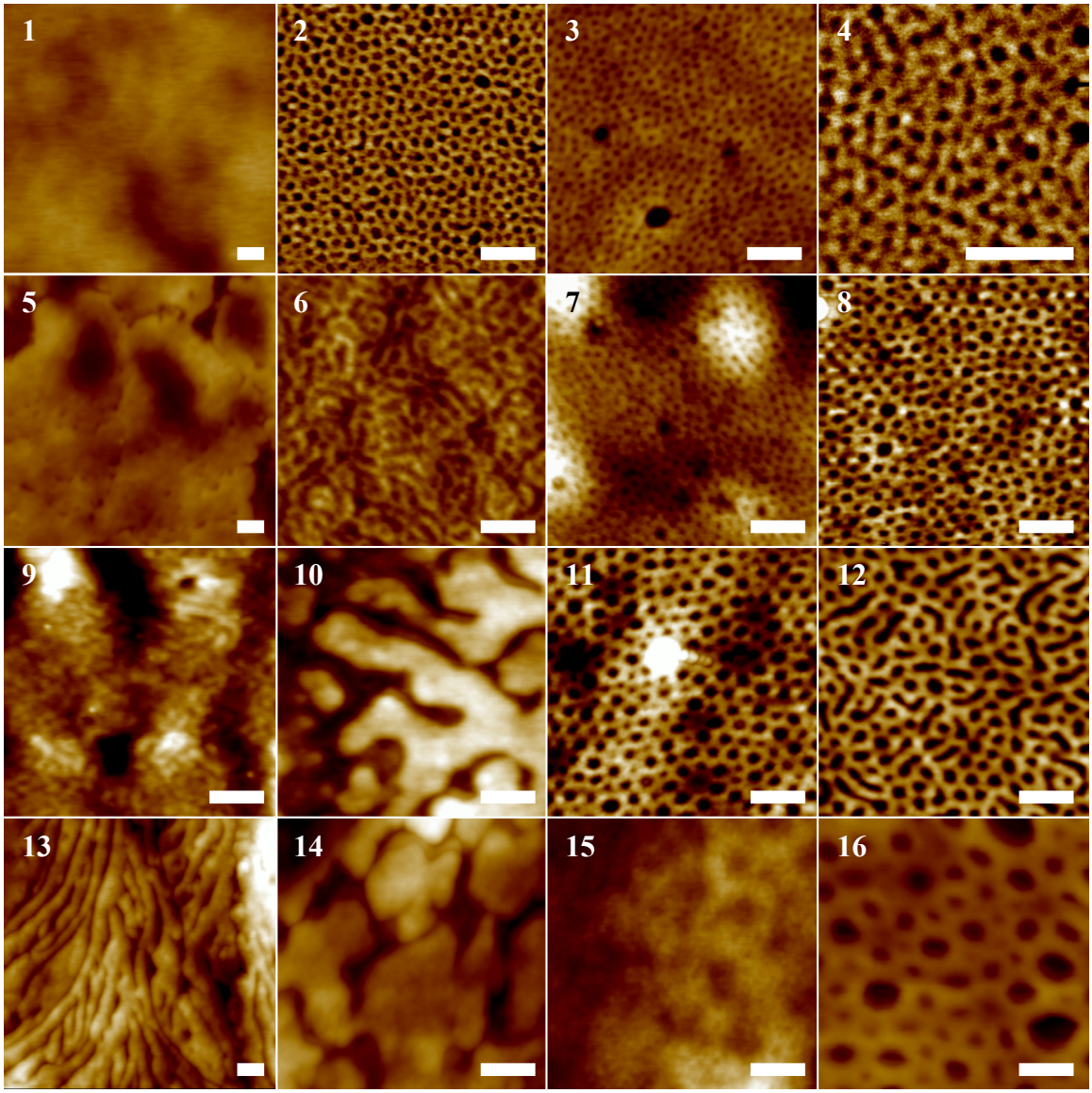

Figure 5.10. *AFM phase images of all block copolymers in the library after spin-casting from a 2 w/v% solution in toluene. No annealing has been performed. The scale bar represents 100 nm.*

As a first approach it was therefore decided to investigate the morphology after spin-casting without further annealing of the films, since this gave reproducible results. The metal complexes are assumed to be located at the interfaces between the different phases and due to their minor content and small size (~1 nm), they will be impossible to visualize. Taking in account the volume fractions displayed in Table 4.2, block copolymers **3**, **4**, **8** and **13** are expected to give rise to spherical morphologies. Indeed, spherical features can be observed for block copolymer **3**, **4** and **8**, but **13** shows only crystalline PEO-domains. Block copolymers **2**, **7**, **9**, **11** and **12** are expected to give rise to a cylindrical morphology: **2**, **7**, **11** and **12** actually show features that could be explained by cylinders that are standing upright, oriented perpendicular to the silicon substrate and fully penetrating the block copolymer film. This phenomenon of spontaneous cylinder alignment was explained before.[41] The remaining block copolymer morphologies are more difficult to understand without more measurements. In case of block copolymers **6**, **10** and **14** lamellar features appear. Lamellae are expected to form on the basis of the volume fractions. Block copolymer **6** reveals a microphase separated structure, whereas block copolymers **10** and **14** display large domains of either block. No preferential orientation of the lamellae is observed. Block copolymers **1** and **5** both contain the low molecular weight PS_{20} and a relatively high amount of metal complex, which may lead to some mixing of the chains due to favorable electrostatic interactions between the chains: no phase separation between PS and PEO was observed for the bulk morphology of **1**. Block copolymers **15** and **16** are peculiar examples, both showing reproducibly this type of morphology with holes in the film. This might be explained as the onset of dewetting or resulting from crystallization of the PEO-blocks.

PS_{20}-[Ru]-PEO_{70} with PF_6 counter-ions has also been studied after dropcasting a chloroform solution on a Formvar-coated TEM-grid. Figure 5.11 shows the result.

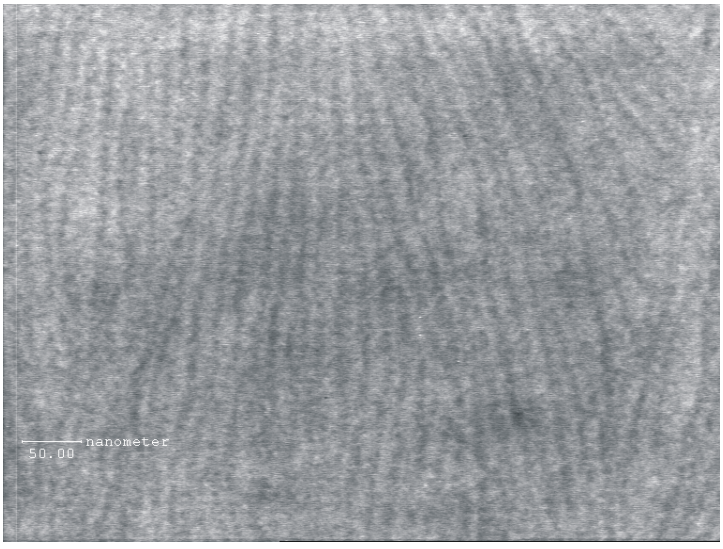

Figure 5.11. *TEM-image of PS20-[Ru]-PEO70 with PF6 counter-ions after dropcasting. The scalebar represents 50 nm.*

From the SAXS/WAXS/POM (Figure 5.9) it is clear that the PEO-block can crystallize. The volume fractions of PS_{20}-[Ru]-PEO_{70} with PF_6 counter-ions reveals that a lamellar morphology can be expected. The TEM-image (Figure 5.11) shows indeed a lamellar arrangement of the block copolymer and is thought to originate

from crystallization of the PEO-block. Due to the fact that the PS-block was selectively stained by RuO_4, it appears dark and consequently the PEO-block appears light, thus locating the metal complexes at the boundaries. The size of the lamellar period as determined by TEM ranges between 15 and 20 nm. This is a reasonable value regarding the short length of both blocks and is also in agreement with the lamellar period as determined by SAXS after isothermal crystallization at 30 °C (= 20 nm). This copolymer on the other hand was not annealed, but nevertheless a similar morphology has been obtained.

5.3.2 Triblock copolymer thin films

The two ABA type of triblock copolymers have been spin-coated and studied as well by AFM (Figure 5.12). In case of PS_{70}-[Ru]-PEB_{70}-[Ru]-PS_{70} (left), a cylindrical morphology is observed upon spin-coating from ethyl acetate, which is a selective solvent for polystyrene. Based on the volume fractions (72% PS, 28% PEB) a cylindrical morphology may be expected. However, calculating the surface area's for the respective blocks based on the AFM-image reveals fractions between 62% and 70% for PS. Of course, the ABA triblock copolymer must contain some AB block copolymer due to the fact that the starting PEB was only 92% *bis*-functional. Recalculation then leads to volume fractions of 67% and 33% for PS and PEB respectively, which is in quite good agreement. The AB-block copolymer impurity is not expected to have a dramatic influence of the morphology, because of its low content and volume fractions that also give rise to a cylindrical morphology. Similar morphologies for this type of triblock copolymers in thin films have been observed.[44-46]

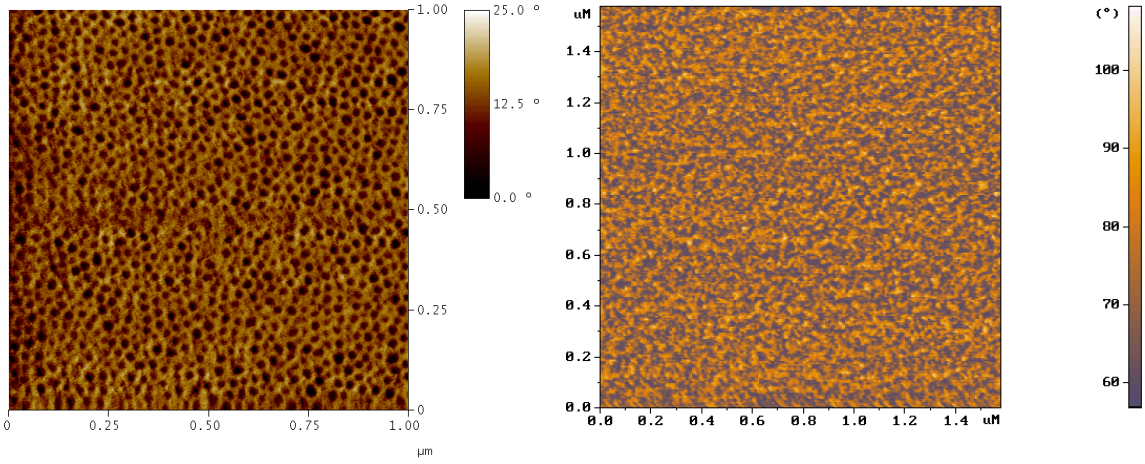

Figure 5.12. *AFM phase images of PS_{70}-[Ru]-PEB_{70}-[Ru]-PS_{70} (left) and of PI_{65}-b-PS_{70}-[Fe]-PS_{70}-b-PI_{65} (right) after spincasting from ethyl acetate and toluene respectively.*

The PI_{65}-*b*-PS_{70}-[Fe]-PS_{70}-*b*-PI_{65} does not reveal a nicely phase separated film (Figure 5.12, right). Annealing will be performed as well as other solvents for spin-coating are going to be tested. It is interesting to note that the starting PI_{65}-*b*-PS_{70} block copolymer reveals a similar type of morphology, which is expected: the volume fractions in the di- and triblock copolymer do not change upon formation of the metal complex. However, ionic interactions may play a role in determining the final morphology, as described in section 5.2.1. Nevertheless, the striking difference in material properties (section 4.6.1) and the NMR-data indicate the successful formation of a triblock copolymer.

5.4 Micelles

Block copolymers form micelles upon dissolution in a selective solvent for one of the blocks. These block copolymer micelles consist of a core formed by the insoluble blocks surrounded by a corona of soluble blocks.[1] The size and shape of micelles are controlled mainly by three independent parameters: the stretching of the core-forming chains, the interfacial tension between the micellar core and the solvent and the repulsions amongst chains in the corona.[47-50] The preparation of micelles can be carried out in several ways. Direct dissolution in the selective solvent is the easiest, but in many cases the copolymer is not directly soluble due to a relatively long solvophobic block. Indirect methods have been developed as exemplified by the work of Eisenberg:[51] the copolymer is dissolved in a common solvent to which a few drops of selective solvent is added to induce micellization. The common solvent is then subsequently replaced by the selective solvent through dialysis. The characteristic features of the accordingly formed micelles strongly depend on the starting common solvent and on the rate of addition of the selective solvent as was recently demonstrated in a cooperation with the university of Frankfurt. These results will be highlighted at the end of section 5.4.1. First, a comparison is made between micelles of PS_{20}-[Ru]-PEO_{70} versus those of covalent analogue and versus those of PS_{20}-[Ru]-PEO_{375} that were prepared by a direct dissolution method. Then micellization of the diblock copolymers of PEB_{70}-[Ru]-PEO_{70} and PFS_{12}-[Ru]-PEO_{70} are described. The PS_{32}-*b*-$P2VP_{13}$-[Ru]-PEO_{70} was used for the preparation of stimuli-responsive triblock copolymer micelles.

5.4.1 Micelles of PS_{20}-[Ru]-PEO_{70} *vs* micelles of covalent PS_{22}-*b*-PEO_{70}

Micelles were prepared by dissolution of the copolymer in DMF and subsequent dialysis against water. The resulting aqueous micelles were characterized by dynamic light scattering. In dynamic light scattering the diffusion of polymers in solution can be studied.[52] It involves the measurement of temporal fluctuations in the intensity of scattered light. The number of photons entering a detector are recorded and analyzed by a digital correlator. The separation in time between photon countings is the correlation time. The autocorrelation function of the intensity at a certain angle can be analyzed and gives rise to the distribution of relaxation times. The decay rates of the relaxation modes in turn provide the translational diffusion coefficients. These can be used for the calculation of the hydrodynamic volume using the Stokes-Einstein approximation. When aggregates of different sizes are present in solution, this requires the deconvolution of the auto-correlation function by e.g. the CONTIN-routine (based on an inverse Laplace transform),[52] which gives information on the distribution of relaxation times in the experimental time correlation functions. Figure 5.13 shows the CONTIN size distribution histograms for the micelles of PS_{20}-[Ru]-PEO_{70} and of PS_{22}-*b*-PEO_{70}. In principle this leads to kinetically frozen micelles because of the vitrification of the PS-block upon addition of the non-solvent.

The latter copolymer shows a single population with a mean hydrodynamic diameter (D_h) of 18 nm. The characteristic size of the micelles is in agreement with commonly reported data for spherical block copolymer micelles. In contrast, two populations are observed for the micelles of PS_{20}-[Ru]-PEO_{70}. The distribution with the highest D_h may be attributed to large clusters of micelles. After 6 weeks of aging the D_h of this distribution has further increased, indicating that the aggregation of the micelles continues in time. Dilution on the other hand does not lead to significant changes in the distributions within the first hour of preparation. The distribution with small D_h

might be attributed to single primary micelles or small clusters of micelles. This will be dealt with in the next paragraphs. First, however, the stability of the micelles is addressed. At high and low temperature, at high and low pH and at high and low ionic strength the UV-spectrum of the micelles does not change (Figure 5.14). This demonstrates the intactness of the metal complex linkage under all these conditions.

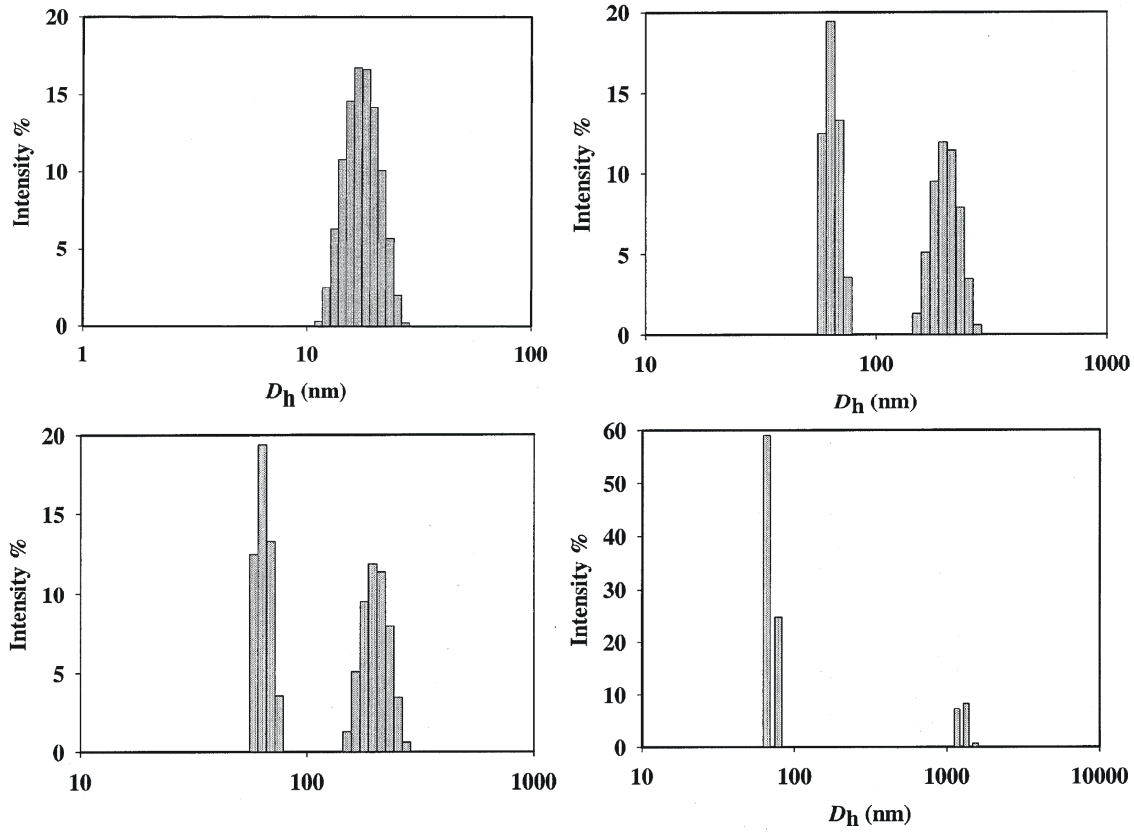

Figure 5.13. *CONTIN size distribution diagrams for PS_{22}-b-PEO_{70} (top left), PS_{20}-[Ru]-PEO_{70} with a concentration of 0.5 g L^{-1} (top right), with a concentration of 0.01 g L^{-1} (bottom left) and after 6 weeks of aging (bottom right).*

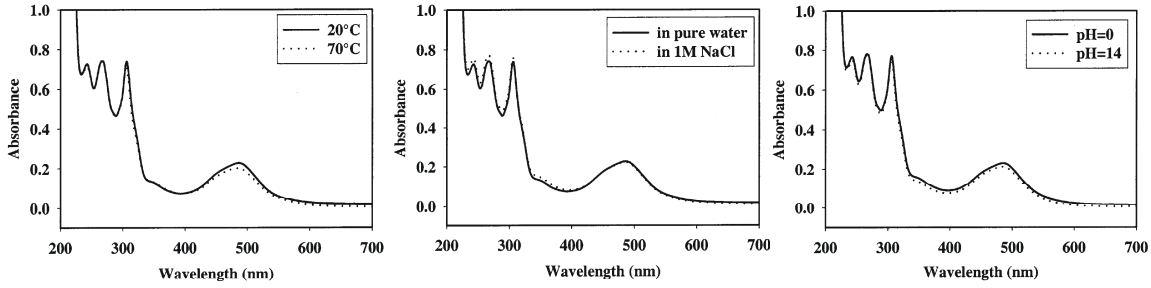

Figure 5.14. *UV-spectra of the micelles in water reveal the stability of the metal complex under different conditions like temperature (left), ionic strength (middle) and pH (right).*

The effect of ionic strength has been studied in more detail. To the initial copolymer solution in DMF, a 1 M salt solution has been added and the DMF solution was dialyzed against the corresponding salt solution. The DLS-spectra revealed in all cases again two distributions, but of particular interest is the D_h of the distribution with the smallest D_h (Table 5.3). The D_h are for all the different salts more or less the same, in the order of 23-24 nm. This is much lower than for the micelles prepared by dialysis against pure water where a D_h of 65 nm was found. The value of 23 nm is

also in much better agreement with the micelles formed by the covalent sample. The small difference may be explained by the presence of the charged metal complexes resulting in a less-closely packed structure because of steric hindrance and possibly in some stretching of the inner PS-block due to electrostatic forces. Anyhow, the size of the micelle is affected by effective screening of ionic interactions by the added salt. Upon addition of salt to the micelles prepared in pure water, only a slight decrease of the D_h can be observed. This decrease depends also to a large extent on the applied counter-ion. Chloride counter-ions are less efficient in reducing D_h when compared to PF_6, SO_4 or PO_4 counter-ions (Figure 5.15). This might be explained by the effective ionic strength at the interface and counter-ion exchange efficiencies.

Table 5.3. *D_h (nm) for the small-size population as measured by DLS and CONTIN-analysis of micelles of PS_{20}-[Ru]-PEO_{70} prepared in 1 M solution of the salt listed below.*

NH_4PF_6	NH_4Cl	NaCl	KCl	Na_3PO_4
23.2	24.4	22.4	22.7	24

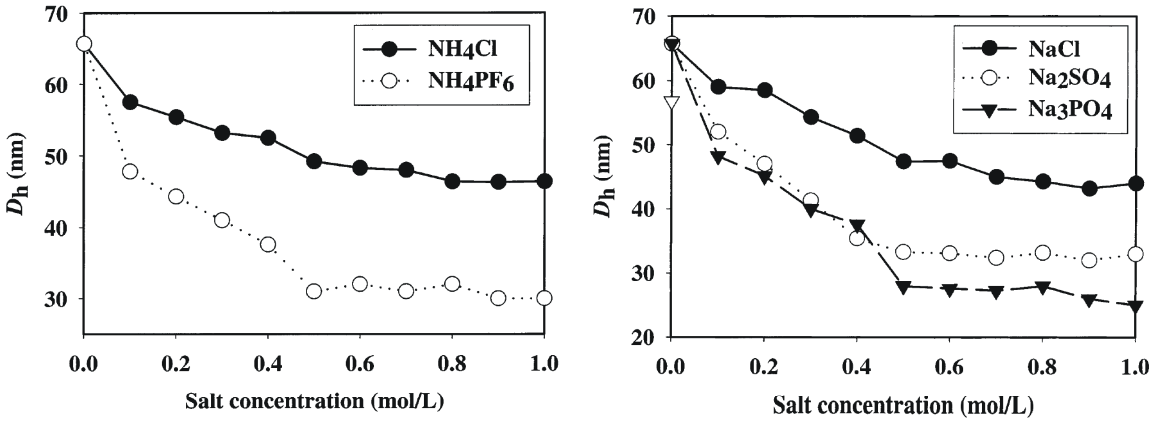

Figure 5.15. *Evolution of the maximum D_h for the small-size populations as measured by DLS from the CONTIN-analysis upon increasing the ionic strength using different counter-ions.*

It is interesting to note that the obtained D_h after addition of salt does not give the same values as obtained for the preparation of the micelles in the corresponding salt solution. This could be due to impossible rearrangements of the copolymer chains due to steric hindrance through the vitrified PS and electrostatic repulsions between the metal complexes whenever salt has been added after micelle preparation. Dialysis of the micellar solution prepared with the salt-solution against pure water resulted again in an increase of the D_h to 57-60 nm. As far as the large clusters of micelles are concerned, they increase in size and in number. Apparently the addition of salt causes a decrease in the solubility of the PEO-chains. As a result they start to aggregate, presumably through coordination of the polymer backbone with the salt.[53] Changes in core radius and aggregation number have also been observed in other systems such as the Pluronics upon the addition of salt.[54]

A D_h of 65 nm is in any case too large to be attributed to single micelles:[1] only fully stretched PS and PEO chains might be able to accommodate such a length. The hypothesis would then be that small clusters of micelles would be responsible for the distribution with a D_h of 65 nm. For this purpose the micelles were investigated by cryo-TEM. This gives direct access to the micellar morphology and eliminates

influences from the drying process.[55] The cryo-TEM images of the PS_{20}-[Ru]-PEO_{70} and PS_{22}-*b*-PEO_{70} samples are shown in Figure 5.16. Individual micelles containing a PS core are seen in both samples. The contrast essentially comes from the PS core, which appears as a darker sphere of a diameter of 10 nm for both samples. The PEO corona could not be easily distinguished for both samples. However, clusters of individual micelles are clearly seen for the PS_{20}-[Ru]-PEO_{70} micelles while only individual micelles are observed for the covalent PS_{22}-*b*-PEO_{70} system, in agreement with the DLS results. Two types of clusters have been detected: a few very large clusters consisting of a large number of micelles, but more frequently small clusters with approx. 2-15 micelles and an overall characteristic size of 60 nm (see arrow in Figure 5.16) could be observed. Dimers, trimers, etc. of individual micelles were also observed in this sample. The small size population observed in DLS is formed not only by isolated micelles but also includes the small clusters seen in cryo-TEM pictures. In this respect, the size of the small cluster seen in Figure 5.16 is ca. 60 nm. This could also explain the polydispersity found in the CONTIN size distribution histograms for the smaller size population. These small clusters can then merge in large size aggregates, as observed by cryo-TEM and DLS. Moreover, these small clusters could break apart, e.g. when salt is added, the size of the PS_{20}-[Ru]-PEO_{70} micelles is dropping from 65 nm to 25 nm. By cryo-TEM additional information about the internal structure of the micelles is obtained. The PS cores are now clearly observed as rather monodisperse spheres with a diameter of 10 nm in the investigated samples. A very important piece of information is obtained whenever the PS_{20}-[Ru]-PEO_{70} micelles are compared to the covalent PS_{22}-*b*-PEO_{70} ones (Figure 4). Actually, no aggregates are formed in the PS_{22}-*b*-PEO_{70} sample, in agreement with DLS results, and the diameter of the PS core is the same for both samples. This indicates that the presence of the charged ruthenium complexes has no influence on the size of the PS cores. However, it does not mean that the aggregation number is the same for the PS_{20}-[Ru]-PEO_{70} and for the covalent micelles. The reason for the formation of only small aggregates of micelles remains unclear.

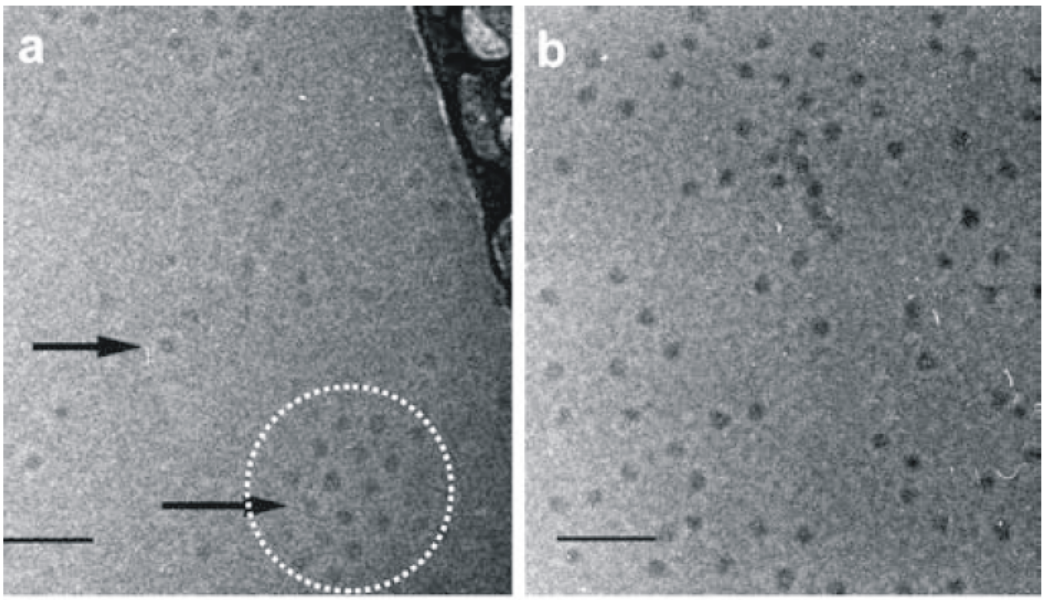

Figure 5.16. *Cryo-TEM micrographs of (a) PS_{20}-[Ru]-PEO_{70} micelles (arrows indicate individual micelle and a small cluster of micelles, respectively) and (b) PS_{22}-b-PEO_{70} micelles. The scale bar represents 100 nm.*

PS_{20}-[Ru]-PEO_{375} was readily soluble in water and formed aqueous micelles, that were characterized by DLS, as shown in Figure 5.17. For the sake of comparison, PS_{20}-[Ru]-PEO_{375} micelles were also prepared by the other method, i.e. dissolution in DMF, addition of water and finally elimination of DMF by dialysis against pure water. This results again in a bimodal distribution of objects, as shown in Figure 5.17. It is worth noting that the two different methods used for PS_{20}-[Ru]-PEO_{375} micelles do not lead exactly to the same micelles/aggregates. Indeed, smaller individual micelles are observed whenever PS_{20}-[Ru]-PEO_{375} is dissolved directly in water. Moreover, no aggregates are found for the system directly prepared in water, which suggests that the direct dissolution of the PS_{20}-[Ru]-PEO_{375} copolymer in water is leading to a system close to equilibrium. Cryo-TEM was also performed on the two PS_{20}-[Ru]-PEO_{375} samples. The PS_{20}-[Ru]-PEO_{375} sample prepared via the DMF/dialysis method gave results similar to the PS_{20}-[Ru]-PEO_{70} micelles, although the individual micelles had a broad size polydispersity. In sharp contrast, spherical micelles with a clear-cut core-shell structure were observed for the PS_{20}-[Ru]-PEO_{375} micelles prepared by direct dissolution in water, as shown in Figure 5.17. Moreover, aggregates of micelles were rarely detected for this sample. The total diameter of the core-shell PS_{20}-[Ru]-PEO_{375} micelles (35 nm) is in good agreement with DLS results.

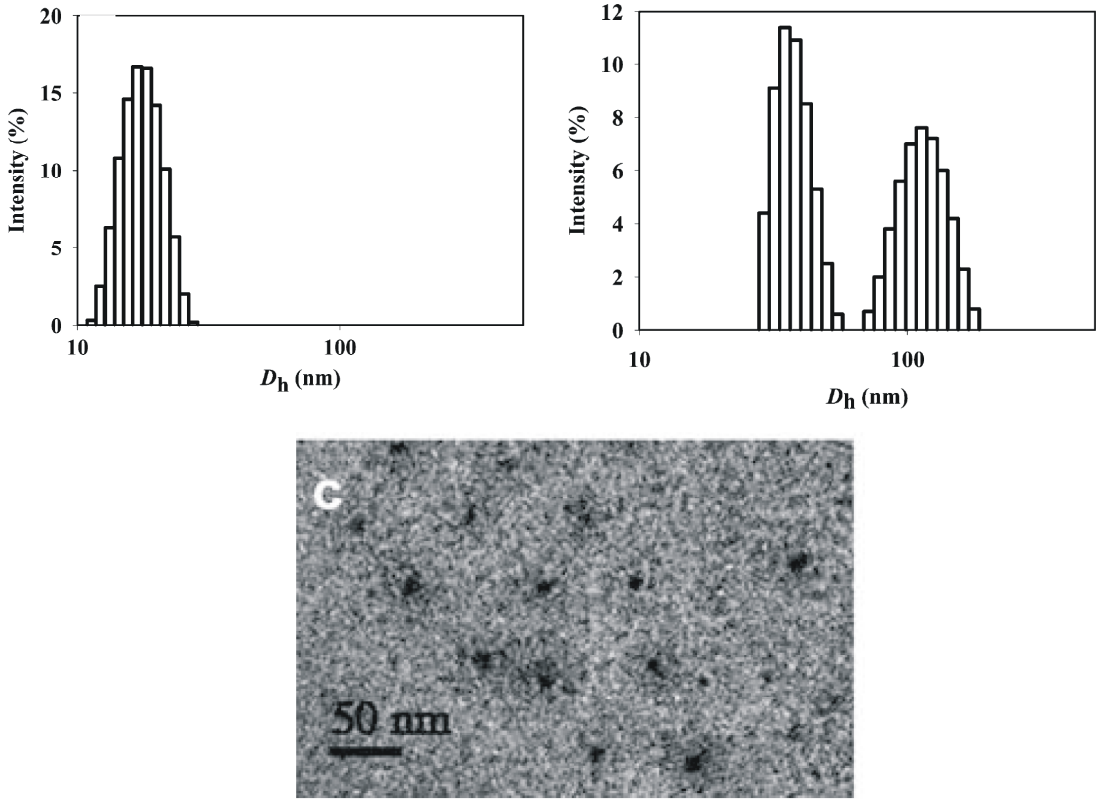

Figure 5.17. *CONTIN size distribution histograms of PS_{20}-[Ru]-PEO_{375} micelles that were prepared directly in water (top left) and by using a non-selective solvent first (top right). The bottom image shows a TEM micrograph that when inspected carefully reveals both the core and the corona of the micelles.*

The observation of the core-shell structure in this system can be explained by a different electron density between the PS core and PEO corona that gives mass thickness contrast in TEM.[56] A recent cryo-TEM investigation of micelles containing a PEO corona showed that a critical polymerization degree of the PEO corona was required for its observation.[56] The less electron-dense PEO block then appears as a

gray corona around the glassy dark PS core. Very few large aggregates were observed by cryo-TEM in the investigated sample, indicating that their number percentage is very low, in agreement with the DLS data shown in Figure 5.17.

A higher homogeneity of the micelles described obviously would be desirable. As mentioned before, the preparation procedure for the PS_{20}-[Ru]-PEO_{70}-micelles was improved by controlled mixing of the solute/DMF phase with water by means of a syringe pump and the rate of mixing was optimized. The same procedure was also applied for PS_{20}-[Ru]-PEO_{375}. In a sedimentation velocity experiment using the analytical ultracentrifuge the curve of relative abundance c(s) versus sedimentation coefficient s for PS_{20}-[Ru]-PEO_{70} micelles prepared previously yielded an essentially bimodal distribution, with a main peak at $s_{20,w}$-values of 9-10 S and a broad, poorly separated peak around 12-14 S. In addition, a small amount of larger particles with broadly distributed s-values was present (Figure 5.18).

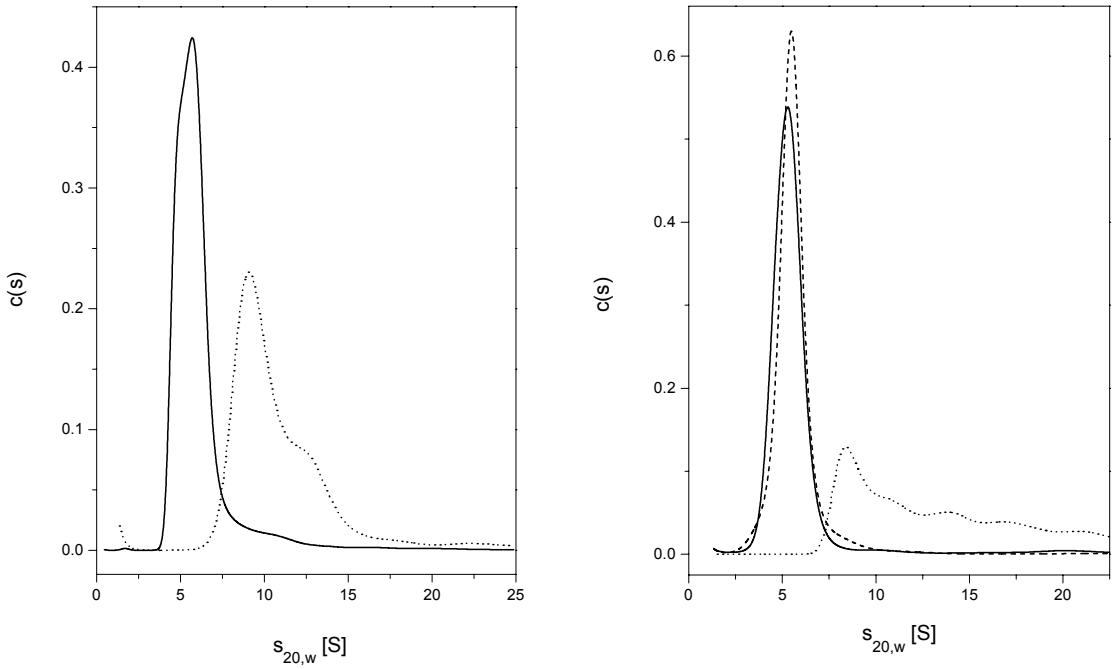

Figure 5.18. *Sedimentation coefficient distributions c(s) (normalised for equal areas under the curves) for PS_{20}-[Ru]-PEO_{70} micelles prepared initially (----) or by mixing the starting solutions by means of a syringe pump (—) (left) and for for two different samples of PS_{20}-[Ru]-PEO_{375} micelles prepared initially by direct dissolution (----), by using a non-selective solvent first (– – –) and by use of a syringe pump (——).*

Distinctly different results were found when the micelles were prepared by the syringe pump: the distributions now were essentially unimodal and nearly symmetrical, and the $s_{20,w}$-value at the maximum of the peak was only around 5.0 S. Also with these samples, however, a few percent of the absorbance was found as broadly distributed material with $s_{20,w}$-values up to approx. 12 S (Figure 5.18). Surprisingly, the c(s) distributions were barely influenced by the rate of water admixing, even when this rate was varied over a large range. Thus, varying the rate of water injection during the first step from 0.2 to 15 µL/min did not significantly influence the peak position of c(s), whereas the relative amount of aggregated material ($s_{20,w}$ > approx. 7 S) slightly increased upon increasing the addition rate. Therefore, a rate of 1.0 µL/min was routinely applied. Sedimentation equilibrium experiments were carried out for the

determination of the molar masses of the micelles. As explained in chapter 4, sedimentation equilibrium experiments give effective molar masses $M_{eff} = M(1-\bar{v}\rho_o)$, where v-bar can be determined by the buoyant density method. This was found to be $\bar{v} = 0.823 \pm 0.005$ mL/g, which is slightly but significantly smaller than the value found with micelles prepared by the earlier procedure (0.837 ± 0.005 mL g^{-1}). The average micelle molar mass is then obtained as 318000 ± 15000 g mol^{-1}. This value corresponds to a number of copolymer molecules in the micelles of around 53, as compared to 72 for the earlier procedure.

For PS_{20}-[Ru]-PEO_{375} a single peak with $s_{20,w}$-values around 5.0 S in sedimentation velocity experiments was observed for samples prepared by direct dissolution in water as well as by using the syringe pump. In sedimentation equilibrium experiments, the curves could be perfectly fitted by a single exponential, thus allowing again $\bar{v}$-determination by the buoyant density method and subsequent determination of the average molar micelle mass M. $\bar{v}$ is obtained from a plot of ρ vs M_{eff} and was found to be 0.830 ± 0.005 mL g^{-1}, which is virtually identical to the value reported for the PEO homopolymer.[57] The average M-value is obtained as 603000 ± 25000 g mol^{-1}. The number of copolymer molecules per micelle is thus only around 31. This indicates that the core of the micelle is much loosely packed than in case of PS_{20}-[Ru]-PEO_{70}, where from the cryo-TEM data similar core sizes were observed.

In summary, micelles composed of block copolymers based on PS and PEO with a metal complex at the block junction give rise to kinetically frozen micelles. Two different size distributions were observed in DLS. Micelles and aggregates were also detected by TEM and AUC. The relative ratio's of aggregate versus primary micelle can be influenced by the preparation method, by the addition of salt and by temperature. Kinetically frozen micelles are obtained because of vitrification of the PS-core and possibly ionic interactions between metal complexes. To further elucidate the influence of ionic interactions, a block copolymer with a low T_g hydrophobic block was used for the preparation of micelles.

5.4.2 Micelles of PEB_{70}-[Ru]-PEO_{70}

This copolymer was described in detail in section 4.6.2. The compound appeared as a waxy solid. DSC revealed the presence of two transitions: the T_g at −56 °C arises from the PEB-block, whereas the melting peak at 49 °C is attributed to the PEO-block. Also PEB_{70}-[Ru]-PEO_{70} was not readily soluble in water and therefore the preparation method as described before was applied. After dialysis, the micelles were analyzed by DLS and AFM. In DLS two populations could again be observed after analysis of the correlation function by the CONTIN-routine, one with a D_h of 32 nm and one with a D_h of 115 nm and these are attributed to primary micelles and aggregates thereof. A value of 32 nm for the diameter of micelles containing a PEB_{70}-core is in good agreement with the expected value. Figure 5.19 shows the CONTIN size distribution histograms, where the intensity is plotted on the y-axis. Actually, since the intensity of the scattered light increases with the size of the scattering centers, the percentage of aggregates can not be calculated properly from the intensity. Rather, a number-averaged calculation should be performed, which can be done using the software. Considering a density of 1 for all species involved, this leads to a number-average of 98 ± 2% of primary micelles. The actual number of aggregates is therefore very small. Dilution of the initial micellar solution from 0.5 to 0.01 g L^{-1} dramatically changes the size distribution, although the mean D_h only

decreases from 58 to 55 nm (Figure 5.18): at low concentrations a single distribution can be observed and this can be explained by a dynamic equilibrium between individual micelles and the aggregates. For micelles of PS_{20}-[Ru]-PEO_{70}, this was not the case.

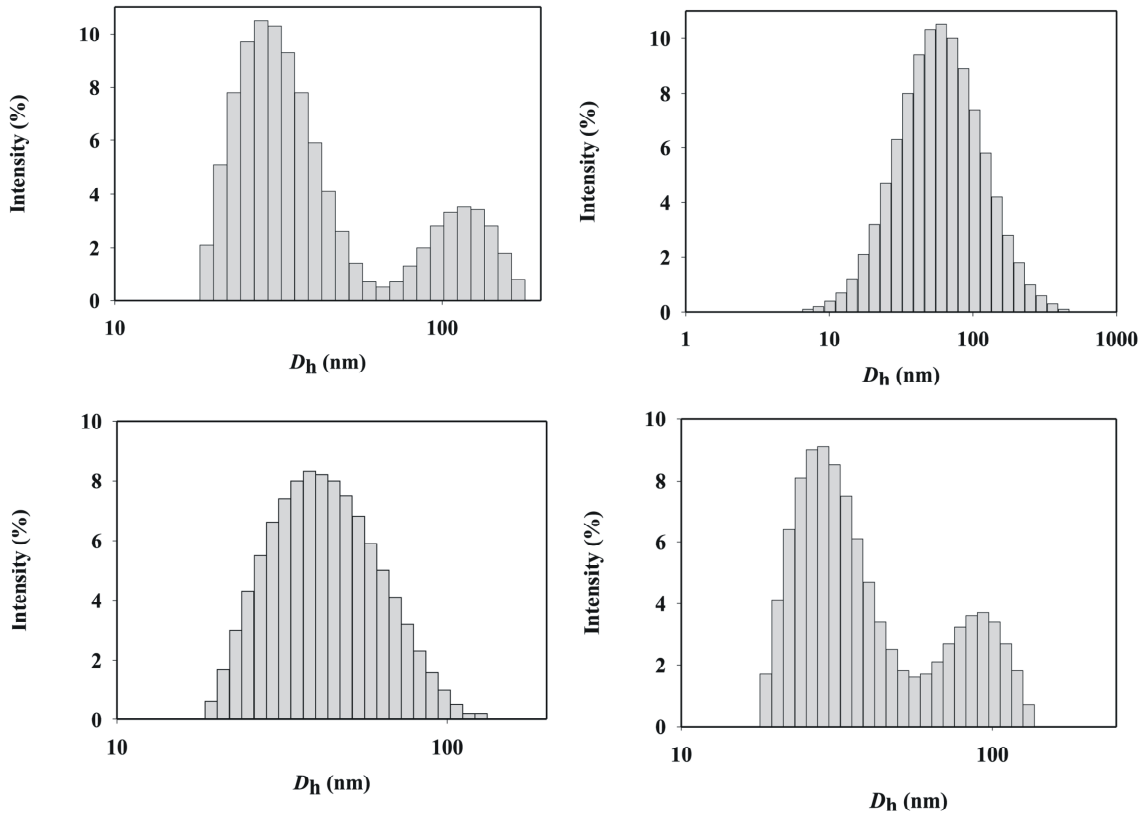

Figure 5.19. *CONTIN size distributions of PEB_{70}-[Ru]-PEO_{70} micelles at a concentration of 0.5 g L^{-1} (top left), at a concentration of 0.01 g L^{-1} (top right), at 65 °C (bottom left) and back at 25 °C (bottom right).*

The influence of temperature was also studied (Figure 5.19). The temperature was increased to 65 °C and again only a single distribution was observed. The D_h of the size distribution was also 32 nm at 65 °C, which indicates that the size of individual micelles is not influenced by temperature. On the other hand, the signal for the aggregates has vanished. Thus, increasing the temperature leads to breakage of the aggregates into individual micelles. Interestingly, cooling the solution to 25 °C again reveals two populations, proving that the equilibrium between individual micelles and their aggregates is truly reversible. A comparison with a covalent analogue should reveal whether influences of ionic aggregation can be accounted for. However, a covalent analogue was not available. Nevertheless, by analogy with the DLS-experiments on PS_{22}-*b*-PEO_{70}, the formation of aggregates will probably not be observed. Therefore micellar aggregation might be attributed to ionic interactions between metal complexes and/or PEO-chains in neighboring micelles. A study of the size of the primary micelles will be more conclusive.

5.4.3 Micelles of PFS_{12}-[Ru]-PEO_{70}

Block copolymers containing poly(ferrocenylsilane) (PFS) blocks have been successfully used to prepare cylindrical micelles in organic solvents, where the core was formed by the self-assembly of the PFS blocks.[58,59] These PFS blocks were combined with polystyrene (PS), poly(dimethylsiloxane) (PDMS) and polyisoprene (PI).[58-62] As a result, diblock and ABA triblock copolymer architectures were prepared. Micelles were formed in organic solvent such as *n*-hexane, in which the PFS blocks are insoluble and self-aggregate into a micellar core while a micellar corona is formed by the PS, PI or PDMS block. Amphiphilic diblock copolymers were also recently prepared in which the PFS blocks still form the micellar core while water-soluble neutral polyethylenoxide (PEO)[63] or poly((*N,N*-dimethylamino)ethyl methacrylate) (PDMAEMA)[64] extent in the water phase. Different morphologies were observed for these micelles: spheres, rods or semi-hollow nanotubes. Spheres were observed when the PFS block was amorphous while cylindrical morphologies were formed for crystallizable PFS blocks. The assumption that the crystallization of PFS is the driving force for the emergence of cylindrical micelles was ascertained by the formation of spherical micelles at temperatures higher than the melting point of the PFS segments.

The formation of PFS_{12}-[Ru]-PEO_{70} was presented in more detail in chapter 4. Micelles were again prepared by addition of water to the copolymer in a non-selective solvent (DMF). Water was added gradually and the scattered intensity was monitored as a function of the added water amount. For a critical added water amount, referred to as the critical water concentration (cwc), a sharp increase in scattered intensity was noted.[65] This indicates that the DMF/H_2O mixture is no longer a good solvent for both blocks and that the water-insoluble blocks (PFS) start to aggregate into micellar cores. The cwc was determined to be 0.55 mL for 1 mL of a 50 g L^{-1} copolymer DMF solution. This cwc is substantially higher than the values observed for crew-cut micelles, in agreement with a larger volume ratio for the hydrophilic block of PFS_{12}-[Ru]-PEO_{70}. An additional amount of water was added after the cwc in order to freeze-in the morphology, as previously discussed by Eisenberg et al.[47-51] DMF was finally eliminated by dialysis against water.

The aqueous micelles formed by PFS_{12}-[Ru]-PEO_{70} were first analyzed by static light scattering (SLS). Since these micelles can be regarded as kinetically frozen aggregates instead of equilibrium micelles, the concentration of free copolymer chains should be extremely low for the investigated solutions. Their contribution to the scattering signals has therefore been neglected. The angular dependence of the SLS data (extrapolated to zero concentration) has been investigated (Figure 5.20). The apparent M_w of the micelles has been determined from the intercept of the straight line shown in Figure 5.19 with the Y-axis and has been found to be $(1.52\pm0.06) \times 10^7$ g/mol. This value leads to a mean aggregation number of about 2500 chains per micelle. This value is too large to be in agreement with spherical micelles for which aggregation numbers are typically around 100.[66] The radius of gyration, R_g, of the micelles has been determined from the slope of the angular dependence of the DLS signal and has been found to be (55±4) nm. This value is also not in agreement with spherical block copolymer micelles. The second virial coefficient A_2 has been determined from the slope of the concentration dependence of the SLS data (extrapolated to zero angle) and was found to be $(5.72\pm0.27) \times 10^{-4}$, indicating that water is a good solvent for the PEO coronal chains.

DLS was used to determine the mean hydrodynamic diameter D_h of the aqueous micelles formed by PFS_{12}-[Ru]-PEO_{70}. The diffusion coefficient for these micelles was found to be approx. 5.5 10^{-8} cm^2/s, corresponding to a mean D_h of (89±1) nm (Stokes-Einstein approximation) while the polydispersity was calculated from the Γ_1/Γ_2^2 ratio and found to be (0.21±0.02).[37] The angular dependence of the apparent diffusion coefficient was also measured. The slope of the angular dependence of D_{app} is related to the shape of the diffusing species and is found to be 0.029, consistent with the value predicted for a rodlike structures (0.03) (Figure 5.20).[58]

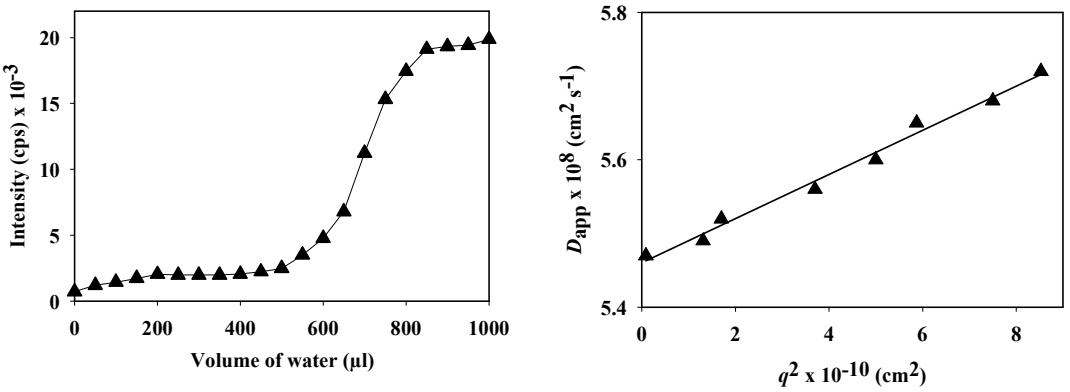

Figure 5.20. *Determination of the critical water concentration (cwc) for PFS_{12}-[Ru]-PEO_{70} aqueous micelles, where the scattered light intensity (in counts per second, cps) is plotted as a function of the added volume of water; the angular dependence of the SLS data extrapolated to zero concentration for PFS_{12}-[Ru]-PEO_{70} aqueous micelles (right).*

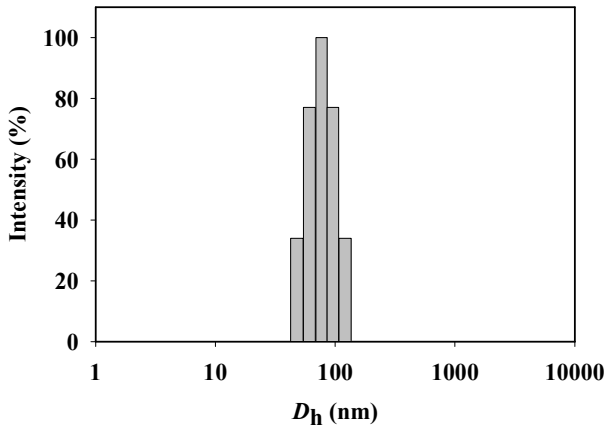

Figure 5.21. *CONTIN size distribution histogram for PFS_{12}-[Ru]-PEO_{70} micelles in water (c = 1 g/L).*

However, the CONTIN size distribution histogram related to the micelles formed by PFS_{12}-[Ru]-PEO_{70} systematically gives a monomodal distribution (Figure 5.21). Rod-like micelles are usually characterized by a two-modes distribution, as a result of the coupling of translational and rotational diffusion.[67] A unimodal distribution can however be observed for very flexible rods.[58]

Information about the inner density profile of the micellar structure can be obtained while considering the R_g/R_h ratio.[68] The theoretical value of this ratio for

monodisperse hard spheres is 0.775, whereas it is 1.5 for Gaussian chains. In case of cylindrical structures, the R_g/R_h ratio strongly depends on the length and thickness of the micelles.[58] The R_g/R_h ratio was found to be 1.24 for the micelles formed by PFS_{12}-[Ru]-PEO_{70}. This is in agreement with the R_g/R_h value of 1.25 previously reported by Liu et al. for cylindrical micelles formed by poly(styrene)-*block*-poly(2-cinnamoylethylmethacrylate) with a cross-linked core in toluene.[69] Very similar conclusions were drawn from the study of PFS-*b*-PDMS micelles in *n*-hexane.[58] In summary, light scattering investigation on the aqueous micelles formed by PFS_{12}-[Ru]-PEO_{70} strongly support the formation of cylindrical or rod-like flexible micelles.

Transmission electron microscopy (TEM) has been used as a tool to characterize the micelles formed by PFS_{12}-[Ru]-PEO_{70}. Since TEM pictures have been obtained on micelles dried on a Formvar film, it can be argued that the structure of the morphology of the micelles has been modified during the drying process. This effect is thought to be limited for the micelles under investigation because they are essentially frozen aggregates that contain crystallizable PFS blocks. Rod-like micelles have been observed by TEM everywhere on the grids, as illustrated in Figure 5.22 for the sample without staining (left Figure). The electronic contrast is thought to originate from the PFS core that contains iron and which is surrounded by the *bis*-terpyridine-ruthenium(II) complexes. The diameter of the core is found to be constant for all these rods and equal to (6±1) nm. This is consistent with the dimension of a core formed by the very short PFS blocks. The length of the rods is highly variable and a mean value of (438±12) nm has been calculated from image analysis. Compared to R_g and R_h values, the contour length of the cylindrical micelles as measured by TEM is much higher. This is in agreement with the formation of highly flexible cylindrical micelles in solution.

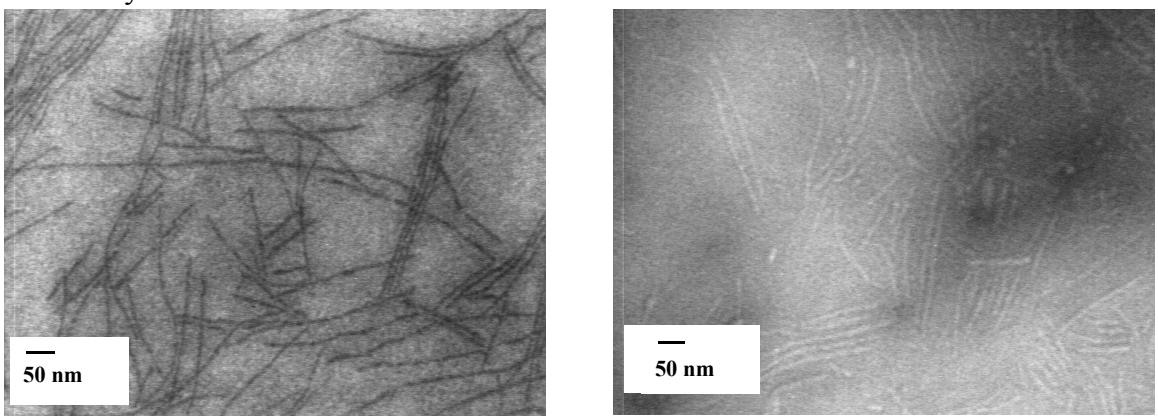

Figure 5.22. *TEM pictures for PFS_{12}-[Ru]-PEO_{70} micelles observed without staining (left) and with staining by phosphotungstic acid (right).*

The micelles have been also negatively contrasted by phosphotungstic acid (see Figure 5.22, right). Provided that the contrasting agent does not penetrate too much into the PEO corona, the core+corona dimension of the micelles can be determined. Since the sample has been prepared in two steps (first deposition of the micelle and drying, second, deposition of a drop of the contrasting agent), the contrasting agent is likely to be located outside the corona of the micelles. The core+corona dimension (in the dried state) has been measured to be (11±1.5) nm. The thickness of the dried collapsed PEO corona is therefore equal to ~2.5 nm. Finally, the cylindrical micelles tends to form bundles, in which they are close packed and oriented parallel to each

others. These aggregates have not been detected by light scattering on the micellar solutions and are therefore thought to be formed during the drying process of the TEM sample preparation. Such a peculiar feature was previously observed in TEM pictures of PFS-*b*-PDMS cylindrical micelles.[58,59]

The formation of cylindrical micelles can be rationalized by three different explanations. The first explanation is applicable for copolymers containing two flexible blocks and has been experimentally developed by e.g. Eisenberg et al.[47-51] The different micellar morphology results from the interplay of three factors, i.e. stretching of the core-forming blocks, surface tension between the micelle core and the solvent outside the core, and interaction between the coronal chains. In a homologous series of diblocks in water, the spheres-to-rods sequence is consistent with the stretching of the core-forming blocks. In spherical micelles, the degree of stretching of the hydrophobic chains is proportional to the radius of the micellar core. The increase of this radius is however limited by the related loss in entropy, until the system becomes unstable and the morphology changes to a cylindrical morphology. The second explanation is related to rod-coil copolymers, thus structures in which a flexible block is linked to a core-forming stiff one.[70] Secondary non-covalent interactions are generally observed between the stiff blocks that tend to orient parallel to each other. This results in cylindrical or lamellar organizations. Rod-like micelles and/or vesicles are then obtained from these copolymers. Due to the crowding of the flexible blocks, finite sized structures can be formed, giving rise to the mushroom aggregates introduced by Stupp et al.[71] The last explanation is related to copolymers in which a flexible block is linked to crystallizable core-forming blocks. In this case, the formation of the cylindrical micelles is caused by the particular orientation of the core-forming chains resulting from the crystallization process. PFS is a core-forming block that is characterized by a strong propensity to crystallization (data about crystallization of PFS can be found in ref. 22). This crystallization process has been previously demonstrated to be at the origin of the cylindrical micelles formed by PFS-containing block copolymer in apolar solvents.[58,59] In order to prove that the aqueous micelles formed by PFS_{12}-[Ru]-PEO_{70} contain a crystallized PFS core, we have first lyophilized the micelles in order to maintain the nanostructures in the bulk state initially formed in solution. These dried micelles have been then measured by differential scanning calorimetry (DSC). Two endotherms were essentially observed in the DSC curves. The first one (52.8±0.1 °C, ΔH = 57.4±0.4 J/g) is related to the melting of the PEO chains which obviously crystallized during the lyophilization process while the second one (122.2±0.2 °C, ΔH = 10±0.2 J/g) corresponds to the melting of the PFS core. The presence of a crystallized PFS core is therefore ascertained in micelles formed by PFS_{12}-[Ru]-PEO_{70}. Aqueous micelles have been previously prepared by PFS-*b*-PEO diblock copolymer with a covalent bond between the two constituent blocks. The degrees of polymerization of both blocks in this PFS-*b*-PEO sample were essentially the same as the ones of the PFS_{12}-[Ru]-PEO_{70} under investigation. Micelles were prepared by direct dissolution of the PFS-*b*-PEO sample in water but large polydisperse spherical micelles were observed for this sample.[63] Clearly the D_h measured by DLS (~160 nm) and the diameter of the micellar measured by TEM (~50 nm) for these spherical micelles are too large to be in agreement with equilibrium spherical dense micelles. From the comparison of PFS-*b*-PEO and PFS_{12}-[Ru]-PEO_{70} micelles, it can be concluded that the *bis*-terpyridine ruthenium(II) complex decreases the solubility of the copolymer in water and has a beneficial effect on the crystallization of the PFS blocks. It should however be noted

that aqueous cylindrical micelles whose characteristic features are quite similar to those of PFS-[Ru]-PEO micelles have been recently reported for a PFS-*b*-PDMAEMA copolymer.[64] The role of the *bis*-terpyridine ruthenium(II) complexes on the ability of the PFS blocks to crystallize is therefore still unclear.

The effect of the addition of salt and the increase of temperature have been investigated on the micellar solution formed by PFS_{12}-[Ru]-PEO_{70}. In addition, the effect of sonication has also been evaluated. Salt was added to the micellar solution (KCl, 1 mol L^{-1}) and the sample was equilibrated for six hours before measurements. The mean D_h was found to be (86±1.5) nm and the polydispersity of the micelles (0.21±0.01). The CONTIN size distribution of the micelles in the presence of KCl is shown in Figure 5.23 (left). The slight decrease in micellar size can be attributed to the desolvation of PEO coronal chains in the presence of salt (salting-out effect). Upon addition of higher amounts of salt, flocculation is observed as a result of the reduced steric stabilization of the poorly solvated PEO chains. Subsequently, the effect of temperature was investigated. The temperature of the surrounding bath of the DLS equipment was raised. After thermal equilibration, the DLS data were collected. The characteristic size of the micelles was poorly affected below 70 °C. For example, a D_h of (80±2) nm and a polydispersity of (0.18±0.01) were noted for the micelles at 65 °C. The CONTIN size distribution histogram is shown in Figure 5.23 (middle). At higher temperature, flocculation was again observed, in agreement with the desolvation of PEO chains at high temperature. Finally, the micellar solution was submitted to ultrasonication for two hours. A deep change in the micellar characteristic features was noted after this treatment. The mean D_h dropped to (65±1.2) nm while the polydispersity increased to (0.28±0.02). The CONTIN size distribution histograms also showed an important decrease in size (Figure 5.23 right).

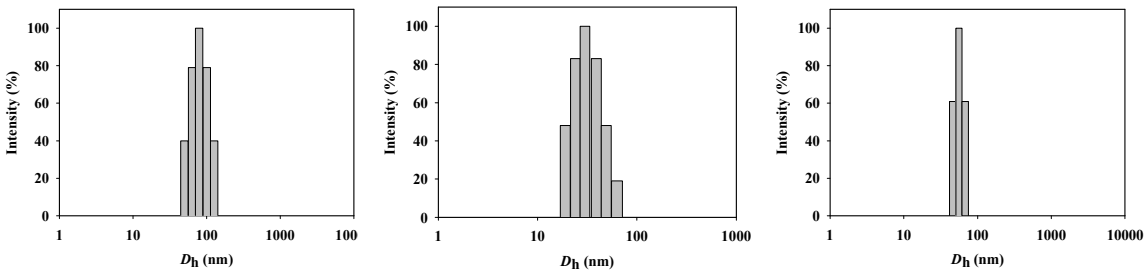

Figure 5.23. *CONTIN size distributions for PFS_{12}-[Ru]-PEO_{70} micelles (c = 0.5 g/L): in 1 mol L^{-1} KCl (left), in water at 65 °C (middle), in water after 2 hours of ultrasonication (right).*

A typical TEM picture of the rods observed after ultrasonication is shown in Figure 5.24. The diameter of the PFS core (5±1 nm) is not affected by this treatment while their length is substantially shorter than the original sample. In this respect, an average length of (138±4 nm) has been calculated from a collection of TEM pictures of ultrasonicated rods. In a previous study on cylindrical micelles formed by PFS-*b*-PDMS copolymers in *n*-hexane, a similar ultrasonication resulted in a significant decrease of the length of the cylindrical micelles. In contrast to our results, the polydispersity of the ultrasonicated rods was considerably reduced compared to the initial PFS-*b*-PDMS cylindrical micelles.

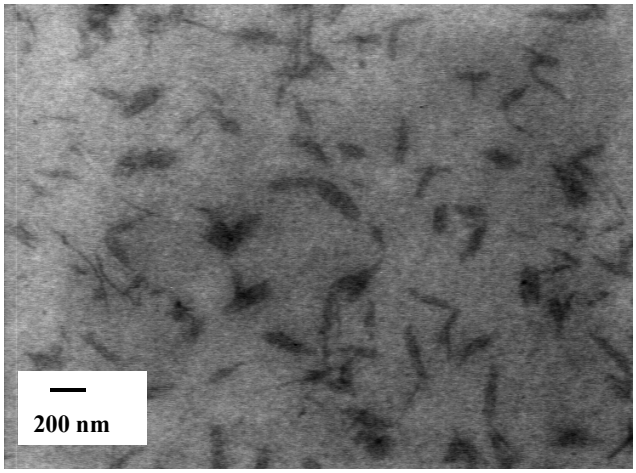

Figure 5.24. *TEM micrograph of the cylindrical micelles of PFS_{12}-[Ru]-PEO_{70} after ultrasonication.*

In summary, micelles of PFS_{12}-[Ru]-PEO_{70} form cylindrical micelles: crystallization of the short PFS blocks is responsible for the cylindrial micelles. Static and dynamic light scattering results were both in agreement with the formation of highly flexible rod-like micelles and could be were visualized by TEM. Their characteristic dimensions were accordingly determined from a collection of pictures. The diameter of the PFS core and of the PEO corona were found to be very small in agreement with the low degree of polymerization of the constituent polymer blocks, while the length of the micelles was large (micrometer range). An increase in temperature or in ionic strength resulted in a decreased water-solubility of the PEO block, which caused in turn flocculation of the micelles. Ultrasonic treatment resulted in a decreased length of the cylindrical micelles while their diameter was not affected.

5.4.4 Micelles of PS_{32}-*b*-$P2VP_{13}$-[Ru]-PEO_{70}

ABC triblock copolymers display a variety of complex morphologies in the bulk.[3,72-75] Nevertheless, little is known up to now about their association behavior in selective solvents of one (or two) of the constituting block(s). In this respect, "three-layer" micelles were previously reported in aqueous media.[76,77] In addition, "crew-cut" micelles were prepared from highly asymmetric ABC copolymers.[78] Recently, an asymmetrical micelle was reported by Erhard et al. in organic solvents.[79] The so-called "Janus" micelle consists of a crosslinked poly(butadiene) core and a corona with a "southern" poly(styrene) and a "northern" poly(methylmethacrylate) hemisphere. Since the "Janus" micelle is the result of the stabilization of a supramolecular organization existing in the bulk state which is then transferred in solution, it must be therefore distinguished from the systems resulting from the direct solubilization of the ABC triblock copolymer in a selective solvent of one of the block. Another important issue regarding these self-assembled systems is their capability to respond to external stimuli such as temperature and/or pH. Recently, the synthesis and characterization of pH-sensitive core-shell-corona (CSC) aqueous micelles made from poly(styrene)-*block*-poly(2-vinylpyridine)-*block*-poly(ethylene oxide) ABC triblock copolymers (PS-*b*-P2VP-*b*-PEO) has been described.[80] The pH-sensitivity of the P2VP shell was used to tune the size of this system from a hydrodynamic diameter of 75 nm at pH > 5 to 135 nm at pH < 5. This effect was attributed to electrostatic repulsion between the charged P2VP blocks at low pH. Temperature- and pH-sensitive CSC micelles were also very recently reported by

Armes et al.[81] Moreover, the shell of these CSC micelles could be selectively cross-linked. The PS_{32}-*b*-$P2VP_{13}$-[Ru]-PEO_{70} ABC triblock copolymer which was described in chapter 4 was used for the preparation of CSC micelles. This was carried out by addition of a 0.1 M HCl solution to a solution of the copolymer in DMF. The metal complex remained intact as judged from the UV/vis spectrum of the micelles. The micellar solution was analyzed by dynamic light scattering (DLS). The CONTIN size distribution histogram revealed two populations, as observed before in case of the micelles of the diblock copolymers. Again, the smaller population with a D_h of 81 nm is attributed to primary micelles while the second one with a D_h of 191 nm is thought to result from the aggregation of individual micelles into larger aggregates (Figure 5.25, left).

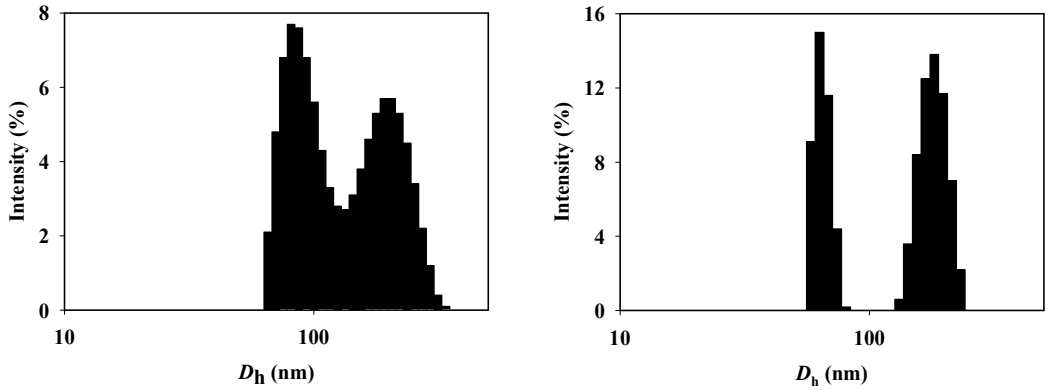

Figure 5.25. *CONTIN size distribution histogram of PS_{32}-b-$P2VP_{13}$-[Ru]-PEO_{70} micelles at pH = 1 (left) and pH = 7 (right).*

The size of the primary micelles does not fall in the usual range of block copolymer micelles,[1] regarding the low molecular weight of the constituting metallo-supramolecular triblocks. For this behavior several explanations can be provided: (I) protonation of the P2VP block, resulting in highly stretched segments; (II) formation of micelles which have a morphology (e.g. rod-like micelles or small vesicles) that differs from the classical spherical star-like shape; (III) formation of non-equilibrium micelles with a loose structure, that require time to reorganize into more compact spherical micelles; and (IV) formation of small clusters as it was also observed in case of the micelles of PS_{20}-[Ru]-PEO_{70}. In this respect, the presence of the charged and bulky *bis*-terpyridine-ruthenium complexes at the interface between the PS-*b*-P2VP and PEO could indeed perturb the packing of the individual amphiphilic macromolecules into a compact micelle. In order to gain additional information about the micellar structure, complementary DLS measurements have been performed. In this respect, the angular dependence of the mean apparent diffusion coefficient (D_{app}) extrapolated to zero-concentration has been investigated for the micelles (Figure 5.26). The slope of the angular dependence of D_{app} was again related to the shape of the diffusing species.[82] The constancy of D_{app} with q^2 can be accounted for the formation of spherical micelles and rules out other morphologies. Indeed, for spherical particles, the rotational motion is not detectable, and D_{app} is independent of q^2.[83]

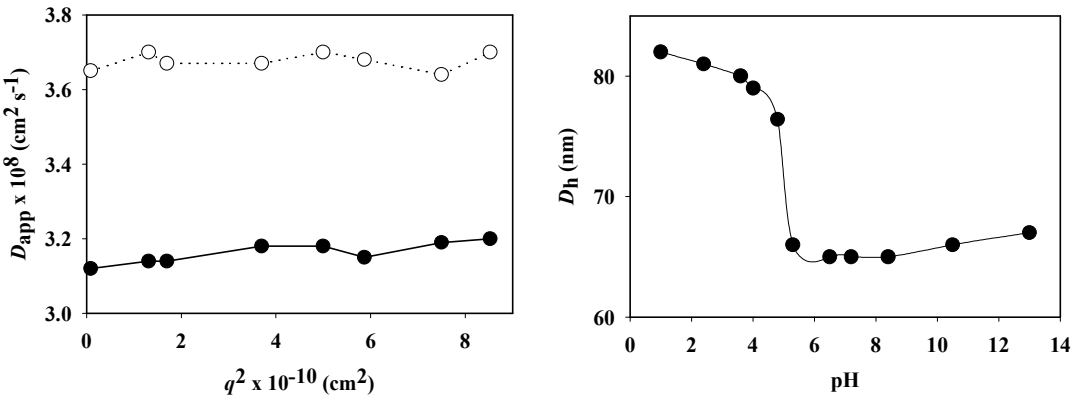

Figure 5.26. *Angular dependence of the apparent diffusion coefficient (D_{app}) of PS_{32}-b-$P2VP_{13}$-[Ru]-PEO_{70} micelles and aggregates at pH = 1 (black dots) and pH = 7 (open dots) (left) and D_h of PS_{32}-b-$P2VP_{13}$-[Ru]-PEO_{70} micelles as a function of pH (right).*

The morphology of the metallo-supramolecular micelles has been examined by TEM (Figure 5.27). Spherical micelles were observed together with larger structures which seem to result from the merging of invididual micelles. No contrasting agent was used for the TEM experiments. The electronic contrast is thought to originate from the ruthenium ions found in the block copolymer structure. This contrast was found to be very uniform within the metallo-supramolecular micelles. Since the micelles were observed in a dried, collapsed state for TEM experiments, the characteristic size of the micelles is much smaller in TEM (ca. 20 nm) than the D_h measured by DLS.

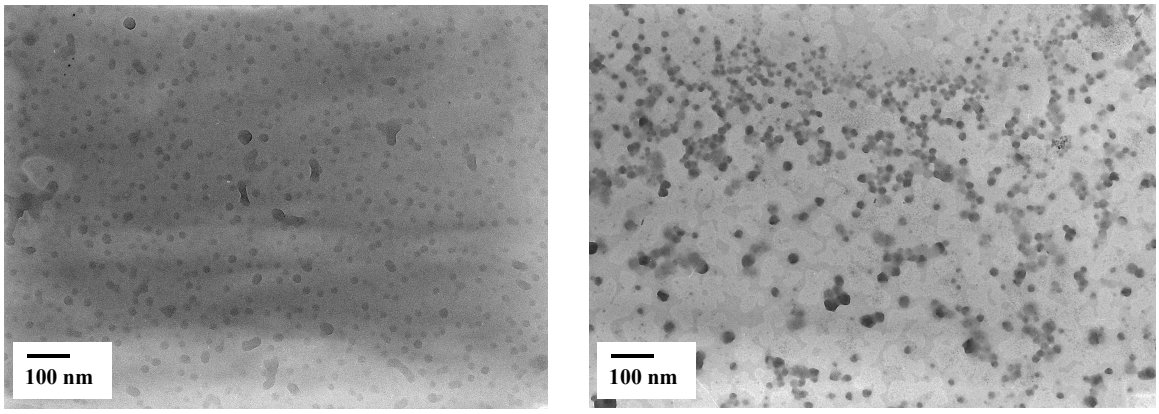

Figure 5.27. *TEM pictures of PS_{32}-b-$P2VP_{13}$-[Ru]-PEO_{70} micelles at pH = 1 (left) and pH = 7 (right).*

The same micelles were subsequently adsorbed on a silicon wafer and investigated utilizing atomic force microscopy (Figure 5.28). Individual micelles and aggregates of micelles were observed, in agreement with the TEM and DLS results. The mean lateral size of the individual micelles was estimated to be around 35 nm in the dried state and is larger than the characteristic size observed by TEM. This is thought to be due to tip convolution effects and to a possible interaction of the adsorbed charged micelles with the charged substrate. In this respect, the height of the adsorbed micelles was estimated to be 18 nm, a value which is in good agreement with the lateral dimensions observed by TEM. In contrast to the morphological characterizations previously obtained on the PS_{200}-*b*-$P2VP_{130}$-*b*-PEO_{495} covalent CSC micelles,[80] the protonated P2VP shell could not be distinguished from the PS core for the PS_{32}-*b*-$P2VP_{13}$-[Ru]-PEO_{70} sample.

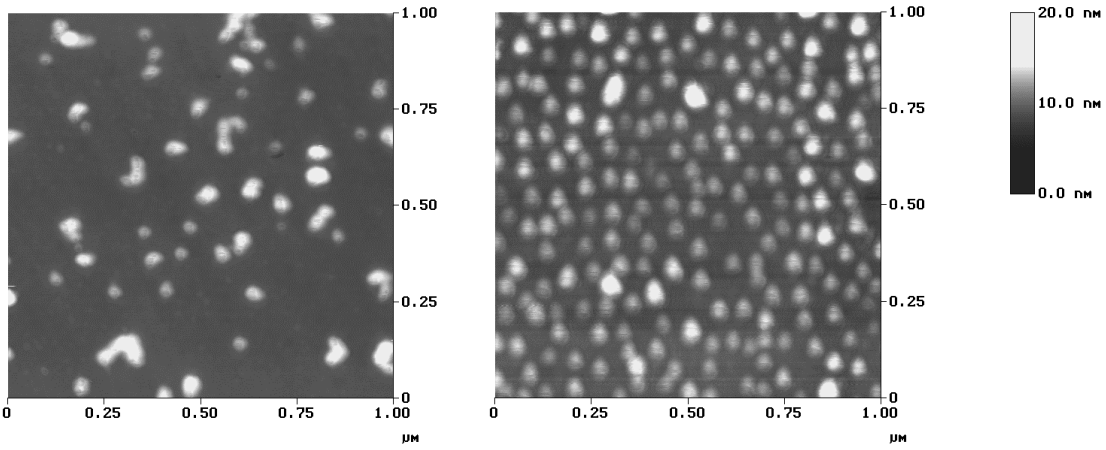

Figure 5.28. *AFM height contrast images of PS_{32}-b-$P2VP_{13}$-[Ru]-PEO_{70} micelles adsorbed on a silicon wafer at pH = 1 (left) and pH = 7 (right).*

In further experiments, the pH of the acidic micellar PS_{32}-*b*-$P2VP_{13}$-[Ru]-PEO_{70} solution was adjusted to neutral value, resulting in the deprotonation of the P2VP blocks. These "neutral" PS_{32}-*b*-$P2VP_{13}$-[Ru]-PEO_{70} micelles were analyzed by DLS and two populations were once again detected in the CONTIN analysis of the experimental correlation function (Figure 5.25, right). The mean size of the primary micelles (D_h = 63 nm) falls in the same range as the results previously obtained on PS_{20}-[Ru]-PEO_{70}. Clustering of the micelles can indeed be suspected again. The D_h of the micelles at neutral pH was lower than the one observed at pH < 5, in agreement with the collapse of the deprotonated P2VP blocks, which are now hydrophobic. In order to prove the reversibility of the size-variation effect, the pH was cycled by adding equimolar amounts of HCl and NaOH to the micellar solution. After each addition of acid or base, the D_h of the micelles was measured. The size-variation effect was not found to be reversible. Moreover, a macroscopic precipitation was observed during the second cycle. This could result from the decreased solubility of the PEO block in the presence of salt. Actually, NaCl is formed during the pH-variation cycles and it is well-know that the addition of salt decreases the solubility of PEO.[53,54] Elimination of the accordingly formed NaCl by dialysis was not successful to restore the solubility of the micelles. The D_h of PS_{32}-*b*-$P2VP_{13}$-[Ru]-PEO_{70} micelles has also been measured as a function of pH at a constant ionic strength (Figure 5.26, right). Two regimes are clearly observed: the "acidic" one with micelles with a D_h of approx. 80 nm and protonated P2VP shell and the "neutral" one with a hydrophobic P2VP shell and a D_h of approx. 65 nm. A sharp transition between both regimes was noted at pH = 5, in agreement with the pKa of P2VP.[82]

The morphology of the PS_{32}-*b*-$P2VP_{13}$-[Ru]-PEO_{70} micelles with the collapsed P2VP shell at neutral pH was also examined by TEM and AFM. Individual micelles and aggregates were again observed. The number of aggregates could be overestimated due to the drying process required for TEM sample preparation. Because of polydispersity it was not possible to see much difference in the size of the micelles formed at pH = 1 or pH = 7. The same conclusion holds for the AFM observation. However, the neutral micelles seem to be more regular in shape compared to the protonated ones. For protonated micelles, electrostatic interactions between the micelles and the substrate could modify their shape compared to the actual situation in solution.[84] The mean lateral size of the adsorbed neutral micelles was determined to

be approx. 30 nm by image analysis. In conclusion, both AFM and TEM characterization techniques were suited to visualize the PS_{32}-*b*-$P2VP_{13}$-[Ru]-PEO_{70} micelles but failed to evidence the structural differences between neutral and protonated micelles. This is thought to mainly result from the low molecular weight of the P2VP block, as discussed earlier. That electrostatic interactions play a major role in the aggregation behavior of PS_{32}-*b*-$P2VP_{13}$-[Ru]-PEO_{70} chains was evidenced by varying the ionic strength in the aqueous micellar solution. For that purpose, different amounts of NaCl were added and the D_h of the micelles was measured, as shown in Figure 5.29.

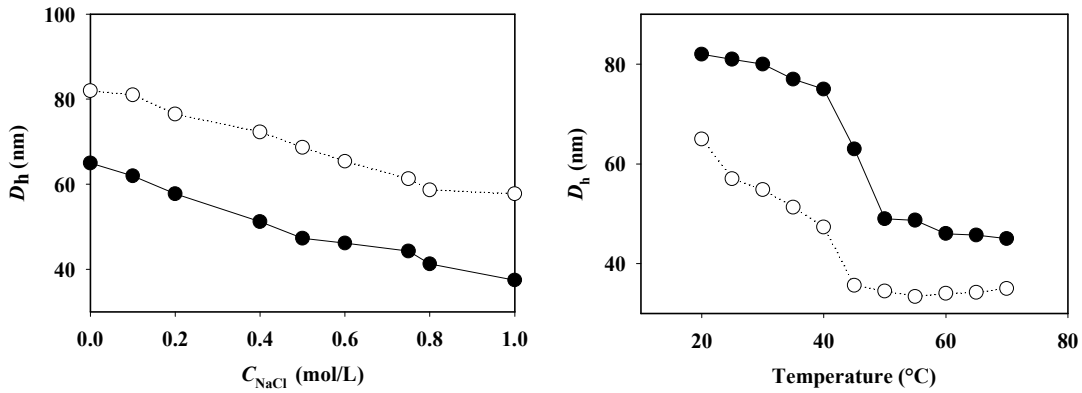

Figure 5.29. *D_h of PS_{32}-b-$P2VP_{13}$-[Ru]-PEO_{70} micelles as a function of added NaCl concentration at pH = 1 (open dots) and pH = 7 (black dots) (left) and D_h of PS_{32}-b-$P2VP_{13}$-[Ru]-PEO_{70} micelles as a function of temperature at pH = 1 (black dots) and pH = 7 (open dots) (right).*

A significant decrease in micelle size was observed when NaCl was added, independent of the actual pH. This merits again the hypothesis that not individual micelles, but small clusters of micelles are present and that the preparation procedure should be optimized. The final size of the neutral and protonated PS_{32}-*b*-$P2VP_{13}$-[Ru]-PEO_{70} micelles is in the range of common block copolymer micelles when 1 mol L^{-1} of NaCl is added. The addition of salt has also an influence on the ratio of micelles to aggregates. Indeed, the addition of a small amount of salt results in an increase of the percentage of micelles. For the protonated micelles, aggregation was totally suppressed. This suggests an equilibrium between micelles and aggregates of micelles which is governed by electrostatic interactions. Residual ions tightly bound to PEO could explain why neutral micelles are also behaving as a polyelectrolyte system. Further addition of salt results in an increase of the percentage of aggregates. This is thought to be due to the reduced solubility of PEO segments as a large amount of salt is added. This results in turn in a decreased water-solubility of PEO and thus to a less effective steric stabilization of the micelles.[85] In parallel to the effect of salt, the effect of temperature on PS_{32}-*b*-$P2VP_{13}$-[Ru]-PEO_{70} micelles was investigated, as shown in Figure 5.29.

These results are qualitatively in agreement with the micelles of PS_{20}-[Ru]-PEO_{70}. The input of thermal energy allows a relaxation of the stretched PEO segments. This is accompanied by a progressive dehydration of PEO, which reduces the steric stabilization of the PEO corona. The reversibility of the salt and temperature effect was also checked. For that purpose, salt was eliminated by dialysis and the D_h of the metallo-supramolecular micelles was measured. The initial D_h was not restored,

meaning that non-equilibrium effects are involved. In the same vain, the initial D_h was not restored when temperature was lowered from 70 to 20 °C, in agreement with non-equilibrium effects. The non-reversibility of the pH-effect has been already discussed before. Moreover, the ratio of micelles to aggregates was also varying with time. All these observations clearly point out that PS_{32}-*b*-$P2VP_{13}$-[Ru]-PEO_{70} micelles are existing in a kinetically frozen state and do not represent a thermodynamic equilibrium.

5.5 Conclusions

The morphology of block copolymers that are held together via a metal complex at the block junction reveals that ionic interactions play a very important role. SAXS-studies on the melt morphology show that indeed the ionic groups associate into multiplets. This multiplet-formation was found to be the dominating driving force for the melt morphology when PF_6 counter-ions were used. By changing the counter-ion to BPh_4, which is less coordinating and much more bulky, the ionic interactions are somewhat reduced. The system is allowed to phase separate into lamellar domains with the metal complexes located at the interface. The first results on the block copolymer library in thin films reveal that indeed different morphologies are being formed. Although far from the thermodynamic equilibrium, this library provides a good start for studying structure-property relationships. In selective solvents block copolymer micelles were obtained. Also here ionic interactions are thought to be responsible for the clustering of the micelles, that independent of the starting block copolymer always gave rise to two populations in DLS regarding size. The presence of large aggregates was further confirmed by analytical ultracentrifugation and TEM. In fact, by cryo-TEM the presence of small aggregates was found to be responsible for the first size distribution in DLS in case of kinetically frozen micelles. Although the procedure for micelle preparation was optimized by controlling the addition rate of water, the micelle formation remains kinetically controlled due to vitrification of the core. Equilibrium micelles were obtained for block copolymers containing a low Tg hydrophobic block. Reversible behavior was found with respect to temperature and concentration. For micelles containing a crystalline core (PFS) cylindrical micelles were obtained and also stimuli-responsive core-shell-corona micelles were found by using an ABC triblock copolymer with a pH-sensitive P2VP block as the shell.

5.6 Outlook

Chapter 1 described the benefits of a copolymer that has a cleavable linkage at the block copolymer interface: terpyridine functionalized nanobeads with high surface area's might be of interest for catalytic application or be used in waste water treatments, whereas the morphology of block copolymers in thin films may be used as a template for the synthesis of nanoporous materials having cylindrical pores of only ~20 nm in size. These pores can be filled through capillary forces and lead to highly regular patterns of nano-dots that are of interest for data storage. The aims of this thesis have been met in so far that block copolymers can indeed be produced by the strategies described. However, as already presented in chapter 2, ruthenium complexes are too stable to become of real application for the purposes mentioned above. Nevertheless, we have tried on many occasions to open the heteroleptic ruthenium complex. The results are unfortunately not very reproducible, although promising effects were observed for the micelles of PEB_{70}-[Ru]-PEO_{70} and PS_{32}-*b*-$P2VP_{13}$-[Ru]-PEO_{70} and for thin films of PS_{300}-[Ru]-PEO_{225}. For the former, a large

excess (> 10^6) of a competitive ligand, hydroxyethylethylenediamino-triacetic acid sodium salt (HEEDTA), was added and heated at 60 ° C for 4 hours. The characteristic color faded and a white precipitate formed. The solution was filtered off and analyzed by DLS and AFM. A D_h of 13 nm was found by DLS, indicating that the diameter of the spherical object has been reduced dramatically (before it was 32 nm). Also, in AFM a decrease from 36 to 18 nm of spherical objects could be observed on spin-coating a very diluted micellar solution onto a silicon wafer (Figure 5.30).

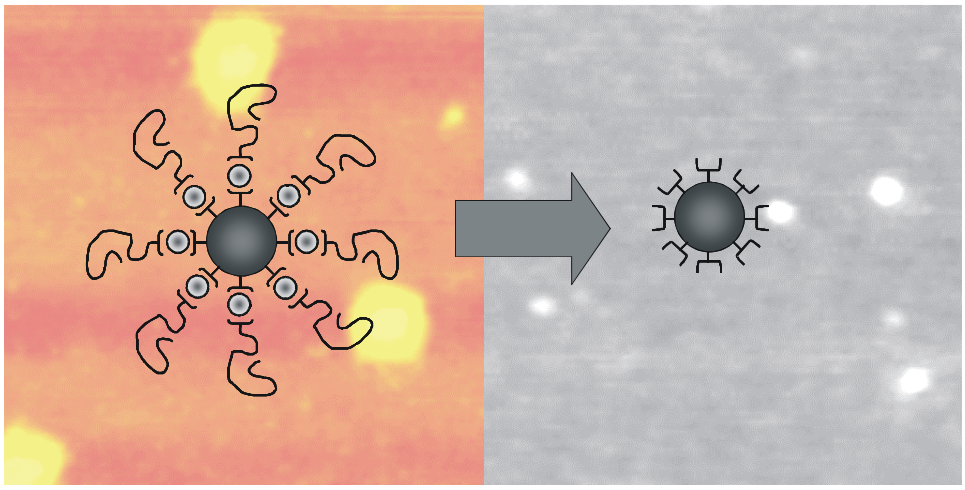

Figure 5.30. *AFM-images before (left) and after opening of the metal complex and dialysis (right), tentatively attributed to a release of the coronal chains and resulting in a terpyridine-functionalized 'nano-bead'. The same scale applies for both images (400 × 400 nm).*

The question that remains however, is if the metal complex has really opened up. HEEDTA is also known to be an oxydant and it could very well be that the PEO-backbone is degraded. This would also lead to smaller spherical objects. Nevertheless, after applying the same treatment to the micelles of PS_{32}-*b*-$P2VP_{13}$-[Ru]-PEO_{70}, addition of Fe^{II}-ions to the colorless solution resulted in a purple color. This indicates the formation of terpyridine-iron(II) complexes and thus proves that terpyridines were present in the micellar solution. PS_{300}-[Ru]-PEO_{225} was spincasted on a silicon wafer from toluene solution and gave rise to a morphology were PEO cylinders were standing upright in a PS-matrix with diameters of ~33 nm. The thin film was slightly crosslinked by deep UV-irradiation to prevent desorption and was subsequently exposed to a solution of $Ce(IV)(SO_4)_2$ in 0.1 M H_2SO_4. Thorough rinsing with water led to the formation of nanopores with holes of at maximum 44 nm deep. By XPS it was confirmed that the PEO-block was removed as well as the PF_6 counter-ions. Moreover, by X-Ray reflectivity measurements the porosity was found to be 17%-22%, which is in good agreement with the PEO volume fraction (20%) (Figure 5.31). This template has subsequently been used for the preparation of titanium nanodots of 5 nm in height in the nanopores. Finally, the polystyrene could be removed.[87] Also here the question remains whether the metal complex is really opened up or that the PEO-backbone is degraded. Experiments on covalent samples have been performed and no degradation of the PEO-block was observed. This merits the hypothesis that the metal complex is opened up, but it could also be cleaved off. Recomplexation efforts with fluorescent europium(III)-ions are currently in progress.

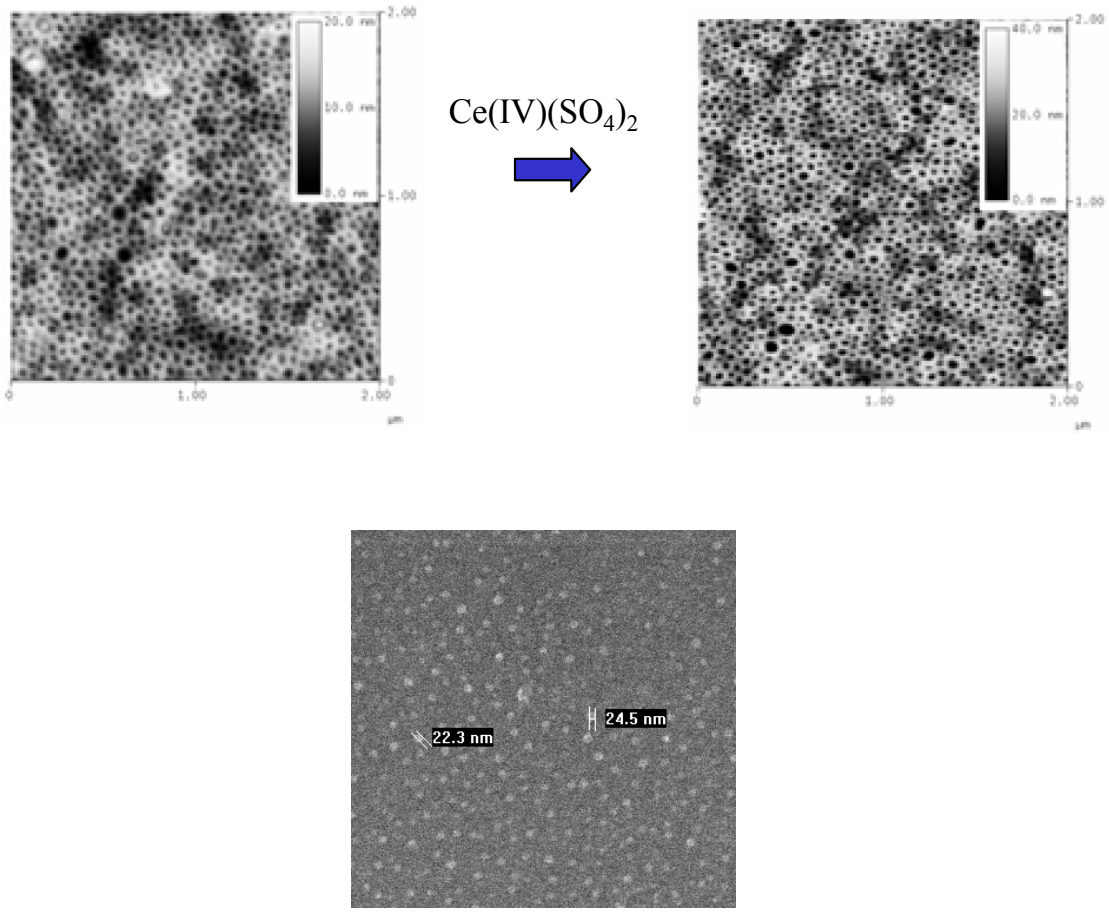

Figure 5.31. *Cylindrical morphology in a thin film of slightly crosslinked PS_{300}-[Ru]-PEO_{225} before (left) and after treatment with $Ce(IV)(SO_4)_2$ and thorough rinsing (right) as observed by AFM. Subsequently the empty cylinders have been metallized with titanium, after which the PS matrix was removed by chloroform. The bottom figure shows a SEM-image, revealing that the diameter of the Ti dots corresponds to the initial diameter of the cylinders.*

In any case, milder conditions are definitely of interest if special polymers with conduction capacities are to be used. For this purpose, the cobalt(III) approach seems worthwhile to develop in more detail. This leads to block copolymers that can be electrochemically labilized and more easily analyzed by NMR-techniques. Of course, the charge is increased to 3+ for such copolymers and ionic interaction may play even larger roles. Nevertheless, the lessons learned on the *bis*-terpyridine ruthenium complexed block copolymers will be invaluable for the understanding and further fine-tuning of the morphologies.

5.7 Experimental part

Small-angle X-ray scattering measurements were conducted using an in-house set-up with a rotating anode X-ray generator (Rigaku RU-H300) operating at 18 kW. By employing two parabolic multilayers mirrors (Bruker, Karlsruhe), a highly parallel beam of a monochromatic CuKα radiation (λ = 0.154 nm) with a divergence of 0.012° was obtained. A Linkam CSS450 shear cell was used as a temperature-controlled sample stage. The SAXS patterns were recorded with a Bruker Hi-Star area detector at a sample-to-detector distance of 1.03 m. The two-dimensional scattering patterns were radially integrated, corrected for the background and then displayed as one-dimensional plots of the intensity as a function of $q = (4\pi/\lambda)\sin\theta$, the modulus of the scattering vector **q**, where θ is half the scattering angle. The collection time was chosen in a way that few hundreds to around 1000 counts were collected at each angular position, giving a statistical error of 3-8%. Wide-angle X-ray scattering measurements were carried out on the same machine. Polarized optical microscopy was performed on a Jeneval polarization microscope equipped with a Linkam THMS 600 heating device with crossed polarizers. Tapping Mode AFM measurements were performed using a MultiMode Scanning Probe Microscope from Digital Instruments, Inc. (Santa Barbara, CA, USA). The samples were probed under minimal force tapping conditions using non contact CSC12 silicon cantilevers (MikroMasch), with a force constant of ~1.75 N/m. TEM images were recorded on a JEOL 2000FX microscope working at 200 kV. TEM samples were prepared by drop-casting of a diluted micellar solution on a Formvar-coated copper grid and equipped with a CCD camera. The samples were prepared by drop-casting of a diluted (0.01 g/L) micellar solution on a Formvar-coated copper grid. The use of contrasting agents for observation is described in the text. Dynamic and static light scattering were carried out on a Brookhaven Instruments Corp. BI-200 apparatus equipped with a BI-2030 digital correlator with 136 channels and a Spectra Physics He-Ne laser with a wavelength λ of 633 nm. A refractive index matching bath of filtered decaline surrounded the scattering cell, and the temperature was controlled at 25 °C. Toluene was used as a reference to determine the Rayleigh ratio. The refractive index increment (dn/dC) was measured with an Optilab DSP interferometric refractometer from Wyatt Technology at 633 nm. A dn/dC of 0.1134 mL/g was found for PFS_{12}-[Ru]-PEO_{70}. All solutions were filtered with a 0.45 μm syringe filter before measurements. The reproducibility of the DLS results was checked by analyzing at least ten times each samples. The standard deviation between these independent measurements was found to be less than 2%. DLS-measurements have also been carried out on a Malvern 4700C apparatus equipped with a Malvern 7032 digital correlator and an Ion Laser Technology argon laser with a wavelength of 488 nm. Although the copolymers were absorbing light at this wavelength, sufficient light was scattered to allow data with good statistics to be obtained. The samples were directly measured without any filtration. Each DLS data resulted from the averaging of ten measurements. Measurements perturbed by dust particles were systematically removed before the averaging. The scattering angle used for the measurements was 90°. A temperature-controlled refractive index matching bath surrounded the scattering cell. In more detail:

Static light scattering (SLS). SLS experiments were carried out in order to determine the average molecular weight, M_w, the radius of gyration, R_g, and the second virial coefficient A_2 by using the relationship:

$$KC/\Delta R(\theta) = [1/M_w + 2A_2C + \ldots]\,[1 + (q^2R_g^2)/3]$$

where C is the concentration, $\Delta R(\theta)$ is the difference between the Rayleigh ratios for the micellar solution and the solvent, K can be expressed as:

$$K = [4\pi n^2/N_A\lambda^4]\,(dn/dC)^2$$

where N_A is Avogadro's number. q is the absolute value of the scattering vector:

$$q = \frac{4\pi n \sin(\frac{\theta}{2})}{\lambda}$$

where θ is the diffusion angle.

Dynamic light scattering (DLS). The second-order correlation function $G_2(t)$ was measured. In the case of a single-exponential decay $G_2(t)$ can be expressed:

$$G_2(t) = B\left[1 + \beta.\exp(-2\Gamma t)\right] = B[1 + \beta|G_1(t)|^2]$$

where B is the baseline, β is an optical constant that depends on the instrument, Γ is the decay rate for the process, t is time, and $G_1(t)$ is the first-order correlation function. Real systems can rarely be described by a single decay. In this case, the method of the cumulants can be used:

$$G_1(t) = \exp\left[-\Gamma_1 t + (\frac{\Gamma_2}{2!})t^2 - (\frac{\Gamma_3}{3!})t^3 + ...\right]$$

where Γ_i is the i^{th} cumulant. The polydispersity index (PDI) of the aggregates was estimated from the $\Gamma_2/\ \Gamma_1^2$ ratio. The Z-average diffusion coefficient over the whole set of aggregates was calculated from the first cumulant:

$$\Gamma_1 = Dq^2$$

where D is the translation diffusion coefficient. The diffusion coefficient extrapolated to zero concentration (D_0) for spherical particles is related to the hydrodynamic diameter, R_h by the Stokes-Einstein equation:

$$D_0 = \frac{k_B T}{6\pi\eta R_h}$$

where k_B is the Boltzmann constant, T is the absolute temperature, and η is the viscosity of the solvent.

The DLS data were also analyzed by the CONTIN routine, a method which is based on a constraint inverse Laplace transformation of the data and which gives access to a size distribution histogram for the aggregates.

Cryo-Transmission Electron Microscopy. Samples were prepared using a newly developed vitrification robot – Vitrobot[86] in which the relative humidity is kept close to saturation to prevent water evaporation from the sample. A drop of the solution (3 μL) was placed on a carbon-coated lacey substrate supported by a TEM 300 mesh copper grid (Ted Pella). After automatic blotting with filter paper, in order to create a thin liquid film over the grid, the grid was rapidly plunged into liquid ethane at its melting temperature. This resulted in a vitrified film. The vitrified specimen was then transferred under a liquid nitrogen environment to a cryo-holder (model 626, Gatan Inc., Warrendale, PA) into the electron microscope, Tecnai 20 - Sphera (FEI), operating at 200 kV with a nominal underfocus of 2-4 micrometer. The working temperature was kept below -175 °C, and the images were recorded on Gatan 794 MultiScan digital camera and processed with Digital Micrograph 3.6.

General procedure for the preparation of the micelles: The copolymer was dissolved in 5 mL DMF to which 5 mL of water was added dropwise. Subsequent dialysis using SpectraPor dialysis bags with a cut-off of 6000-8000 Da was carried out. The final concentration of the copolymer was set to 0.5 g L^{-1}.

5.8 Literature

[1] I. W. Hamley, *The Physics of Block Copolymers*, Oxford University Press, Oxford, **1998**.
[2] F. S. Bates, G. H. Fredrickson, *Annu. Rev. Phys. Chem.* **1990**, *41*, 525-557.
[3] P. Tang, F. Qui, H. Zhang, Y. Yang, *Phys. Rev. E* **2004**, *69*, 0318031-0318038.
[4] A. Eisenberg, J.-S. Kim, *Introduction to ionomers*, John Wiley & Sons, New York, **1998**.
[5] F. Oosawa, *Polyelectrolytes*, Marcel Dekker, New York, **1971**.
[6] A. Eisenberg, *Macromolecules* **1970**, *3*, 147-154.
[7] R.-J. Roe, *Methods of X-Ray and neutron scattering in polymer science*, Oxford University Press, New York, **2000**.
[8] L. Zhu, Y. Chen, A. Zhang, B. H. Calhoun, M. Chun, R. P. Quirk, S. Z. D. Cheng, B. S. Hsiao, F. Yeh, T. Hashimoto, *Phys. Rev. B* **1999**, *60*, 10022-10031.
[9] L. Zhu, S. Z. D. Cheng, B. H. Calhoun, Q. Ge, R. P. Quirk, E. L. Thomas, B. S. Hsiao, F. Yeh, B. Lotz, *Polymer* **2001**, *42*, 5829-5839.
[10] A. Eisenberg, B. Hird, R. B. Moore, *Macromolecules* **1990**, *23*, 4098-4107.
[11] B. Hird, A. Eisenberg, *Macromolecules* **1992**, *25*, 6466-6474.
[12] J.-P. Gouin, C. E. Williams, A. Eisenberg, *Macromolecules* **1989**, *22*, 4573-4578.
[13] R. B. Moore, D. Bittencourt, M. Gauthier, C. E. Williams, A. Eisenberg, *Macromolecules* **1991**, *24*, 1376-1382.
[14] J.-P. Gouin, F. Bossé, D. Nguyen, C. E. Williams, A. Eisenberg, *Macromolecules* **1993**, *26*, 7250-7255.

[15] D. J. Yarusso, S. L. Cooper, *Macromolecules* **1983**, *16*, 1871-1880.
[16] Y. S. Ding, S. R. Hubbard, K. O. Hodgson, R. A. Register, S. L. Cooper, *Macromolecules* **1988**, *21*, 1698-1704.
[17] C. Li, R. A. Register, S. L. Cooper, *Polymer* **1989**, *30*, 1227-1233.
[18] C. E. Williams, T. P. Russell, R. Jérôme, J. Horrion, *Macromolecules* **1986**, *19*, 2877-2884.
[19] Y. Marcus, G. Hefter, *Chem. Rev.* **2004**, *104*, 3405-3452.
[20] R. P. Nieuwhof, A. T. M. Marcelis, E. J. R. Sudhölter, S. J. Picken, W. H. de Jeu, *Macromolecules* **1999**, *32*, 1398-1406.
[21] M. Al-Hussein, W. H. de Jeu, L. Vranichar, S. Pispas, N. Hadjichristidis, T. Itoh, J. Watanabe, *Macromolecules* **2004**, *37*, 6401-6407.
[22] J. Brandup, E. H. Immergut, E. A. Grulke, *Polymer Handbook 4th Ed.*, John Wiley & Sons, New York, **1999**.
[23] W. A. Lopes, H. M. Jaeger, *Nature* **2001**, *414*, 735-738.
[24] M. R. Bockstaller, Y. Lapetnikov, S. Margel, E. L. Thomas, *J. Am. Chem. Soc.* **2003**, *125*, 5276-5277.
[25] S. Yeh, K. Wei, Y. Sun, U. Jeng, K. S. Liang, *Macromolecules* **2003**, *36*, 7903-7907.
[26] R. B. Thompson, V. V. Ginzburg, M. W. Matsen, A. C. Balasz, *Science* **2001**, *292*, 2469-2472.
[27] J. Y. Lee, R. B. Thompson, D. Jasnow, A. C. Balasz, *Macromolecules* **2002**, *35*, 4855-4858.
[28] I. W. Hamley, *Adv. Polym. Sci.* **1998**, *148*, 113-137.
[29] L. Li, Y. Séréro, M. H. J. Koch, W. H. de Jeu, *Macromolecules* **2003**, *36*, 529-532.
[30] G. C. L. Wong, J. Commandeur, H. Fischer, W. H. de Jeu, *Phys. Rev. Lett.* **1996**, *77*, 5221-5224.
[31] M. J. Fasolka, A. M. Mayes, *Annu. Rev. Mater. Res.* **2001**, *31*, 323-355.
[32] D. G. Walton, G. J. Kellogg, A. M. Mayes, P. Lambooy, T. P. Russell, *Macromolecules* **1994**, *27*, 6225-6228.
[33] G. T. Pickett, A. C. Balasz, *Macromolecules* **1997**, *30*, 3097-3103.
[34] M. J. Fasolka, P. Banerjee, A. M. Mayes, G. T. Pickett, A. C. Balasz, *Macromolecules* **2000**, *33*, 5702-5712.
[35] W. H. Tang, *Macromolecules* **2000**, *33*, 1370-1384.
[36] M. W. Matsen, *J. Chem. Phys.* **1997**, *106*, 7781-7791.
[37] H. P. Huinink, J. C. M. Brokken-Zijp, M. A. van Dijk, G. J. A. Sevink, *J. Chem. Phys.* **2000**, *112*, 2452-2462.
[38] P. Mansky, P. M. Chaikin, E. L. Thomas, *J. Mater. Chem.* **1995**, *30*, 1987-1992.
[39] M. Park, C. Harrison, P. M. Chaikin, R. A. Register, D. H. Adamson, *Science* **1997**, *276*, 1401-1404.
[40] H. Yokohama, E. J. Kramer, M. H. Rafailovich, J. Sokolov, S. A. Schwarz, *Macromolecules* **1998**, *31*, 8826-8830.
[41] Z. Lin, D. H. Kim, X. Wu, L. Boosahda, D. Stone, L. LaRose, T. P. Russell, *Adv. Mater.* **2002**, *14*, 1373-1376.
[42] U. Jeong, D. Y. Ryu, J. K. Kim, D. H. Kim, X. Wu, T. P. Russell, *Macromolecules* **2003**, *36*, 10126-10129.
[43] Y. Wang, R. Song, Y. Li, J. Shen, *Surface Science* **2003**, *530*, 136-148.
[44] G. Kim, M. Libera, *Macromolecules* **1998**, *31*, 2569-2577.
[45] A. Knoll, A. Horvat, K. S. Lyakhova, G. Krausch, G. J. A. Sevink, A. V. Zvelindovsky, R. Magerle, *Phys. Rev. Lett.* **2002**, *89*, 035501/1-035501/4.
[46] C. Park, J. Y. Cheng, M. J. Fasolka, A. M. Mayes, C. A. Ross, E. L. Thomas, C. De Rosa, *Appl. Phys. Lett.* **2001**, *79*, 848-850.
[47] K. Yu, A. Eisenberg, *Macromolecules* **1996**, *29*, 6359-6361.
[48] K. Yu, L. Zhang, A. Eisenberg, *Langmuir* **1996**, *12*, 5980-5984.
[49] K. Yu, A. Eisenberg, *Macromolecules* **1998**, *31*, 3509-3518.
[50] K. Yu, C. Bartels, A. Eisenberg, *Langmuir* **1999**, *15*, 7157-7167.
[51] L. Zhang, A. Eisenberg, *Science* **1995**, *268*, 1728-1731.
[52] W. Brown, *Dynamic light scattering*, Oxford University Press, Oxford, **1972**.
[53] R. Kjellander, E. Florin, *J. Chem. Soc. Faraday Trans. 1* **1981**, *177*, 2053-2077.
[54] N. J. Jain, V. K. Aswal, P. S. Goyal, P. Bahadur, *Colloids Surf. A: Physicochem. Eng. Aspects* **2000**, *173*, 85-94.
[55] N. Pinna, K. Weiss, H. Sack-Kongehl, W. Vogel, J. Urban, M. P. Pileni, *Langmuir* **2001**, *17*, 7982-7987.
[56] Y. Zheng, Y.-Y. Won, F. S. Bates, H. T. Davis, L. E. Scriven, Y. Talmon, *J. Phys. Chem. B* **1999**, *103*, 10331-10334.

[57] H. Durchschlag, *Thermodynamic Data for Biochemistry and Biotechnology*, Springer, Berlin, **1986**.
[58] J. A. Massey, K. N. Power-Billard, I. Manners, M. A. Winnik, *J. Am. Chem. Soc.* **1998**, *120*, 9533-9540.
[59] J. A. Massey, K. Temple, L. Cao, Y. Rharbi, J. Raez, M. A. Winnik, I. Manners, *J. Am. Chem. Soc.* **2000**, *122*, 11577-11584.
[60] J. Raez, R. Barjonovu, J. A. Massey, M. A. Winnik, I. Manners, *Angew. Chem. Int. Ed.* **2000**, *39*, 3862-3865.
[61] L. Cao, I. Manners, M. A. Winnik, *Macromolecules* **2001**, *34*, 3353-3360.
[62] R. Resendes, J. A. Massey, K. Temple, L. Cao, K. N. Power-Billard, M. A. Winnik, I. Manners, *Chem. Eur. J.* **2001**, *7*, 2414-2424.
[63] R. Resendes, J. Massey, H. Dorn, M. A. Winnik, I. Manners, *Macromolecules* **2000**, *33*, 8-10.
[64] X.-S. Wang, M. A. Winnik, I. Manners, *Macromol. Rapid Commun.* **2002**, *23*, 210-213.
[65] L. Zhang, H. Shen, A. Eisenberg, *Macromolecules* **1997**, *30*, 1001-1011.
[66] G. Riess, *Prog. Polym. Sci.* **2003**, *28*, 1107-1170.
[67] R. J. Pecora, *J. Chem. Phys.* **1968**, *48*, 4126-4128.
[68] M. Schmidt, W. H. Stockmayer, *Macromolecules* **1984**, *17*, 509-514.
[69] J. Tao, S. Stewart, G. Liu, M. Yang, *Macromolecules* **1997**, *30*, 2738-2745.
[70] M. Lee, B. K. Cho, W. C. Zin, *Chem. Rev.* **2001**, *101*, 3869-3892.
[71] S. I. Stupp, V. LeBonheur, K. Walker, L. S. Li, K. E. Huggins, M. Keser, A. Amstutz, *Science* **1997**, *276*, 384-389.
[72] F. S. Bates, G. H. Fredrickson, *Phys. Today* **1999**, *52(2)*, 32-38.
[73] L. Bronstein, M. Seregina, P. Valetsky, U. Breiner, V. Abetz, R. Stadler, *Polymer Bull.* **1997**, *39*, 361-368.
[74] Y. Mogi, K. Mogi, Y. Matsushita, I. Noda, *Macromolecules* **1992**, *25*, 5412-5415.
[75] C. Auschra, R. Stadler, *Macromolecules* **1993**, *26*, 2171-2174.
[76] J. Kriz, B. Masar, J. Plestil, Z. Tuzar, H. Pospisil, D. Doskocilova, *Macromolecules* **1998**, *31*, 41-51.
[77] C. S. Patrickios, W. R. Hertler, N. L. Abbott, T. A. Hatton, *Macromolecules* **1994**, *27*, 930-937.
[78] G. Yu, A. Eisenberg, *Macromolecules* **1998**, *31*, 5546-5549.
[79] R. Erhardt, A. Böker, H. Zettl, H. Kaya, W. Pyckout-Hintzen, G. Krausch, V. Abetz, A. H. E. Müller, *Macromolecules* **2001**, *34*, 1069-1075.
[80] J.-F.Gohy, N. Willet, S. K. Varshney, J. X. Zhang, R. Jérôme, *Angew. Chem. Int. Ed.* **2001**, *40*, 3214-3216.
[81] S. Liu, J. V. M. Weaver, Y. Tang, N. C. Billingham, S. P. Armes, K. Tribe, *Macromolecules* **2002**, *35*, 6121-6131.
[82] J.-F.Gohy, S. K. Varshney, S. Antoun, R. Jérôme, *Macromolecules* **2000**, *33*, 9298-9305.
[83] R. Xu, M. A. Winnik, F. R. Hallett, G. Riess, M. D. Croucher, *Macromolecules* **1991**, *24*, 87-93
[84] B. Mahltig, J.-F. Gohy, R. Jérôme, M. Stamm, *J. Polym. Sci., Part B Polym. Phys.* **2001**, *39*, 709-718.
[85] D. H. Napper in: *Polymeric Stabilization of Colloidal Dispersions*, Academic Press, London, **1983**.
[86] www.vitrobot.com.
[87] C.-A. Fustin, A. S. Durvey, A. M. Jonas, B. G. G. Lohmeijer, A. Vlad, U. S. Schubert, J.-F. Gohy, manuscript in preparation.

Summary

The research described in this thesis was focused on the introduction of a metal complexating group at the chain end(s) of a polymer backbone in order to connect polymer chains together via the resulting metal complex upon addition of metal ions. The metal complex itself consists of two substituted terpyridine ligands and the metal ions of interest are iron, cobalt, nickel, copper, zinc, ruthenium, cadmium and mercury, all in their 2+-oxidation state. The behavior of the metal-ligand coordination has been investigated in detail by synthesizing model metal complexes. These compounds have been characterized by various spectroscopic techniques, elemental analysis, mass spectrometry and in some cases single crystal X-Ray diffraction. The stability constants of the metal complex formation have been determined by the partition method for zinc(II)-complexes and ^{1}H-NMR-investigations were tried for the derivation of the stability constants of cobalt(II) complexes. MALDI-TOF MS and MS/MS-techniques have been applied for relative binding strength determination of a series of metal complexes. Modeling has rendered some further insights in the metal complex binding. Further studies were focused on the stability of the metal complex by changing the temperature, the pH or the redox state of the metal ion: the latter two could be followed by UV/vis spectroscopy. Heteroleptic metal complexes (bearing a different substituent on each ligand) have been prepared by a two-step synthesis using inert metal complexes of cobalt(III) and ruthenium(II). This lays the foundation for the construction of different polymer architectures, such as polymer *mono*-complexes, simple homo dimers, chain extended polymers, di- and triblock copolymers. For this purpose, the terpyridine ligand needed to be introduced at the chain end(s) of a polymer. Synthetic routes include end group modification of hydroxy end capped polymers by etherification and urethane formation reactions as well as the use of a terpyridine functionalized initiator suitable for the nitroxide mediated controlled radical polymerization of a variety of monomers. The kinetics of the polymerization of styrene, *n*-butylacrylate, 4-vinylpyridine and *N,N*- dimethylacrylamide using this initiator have been studied by gravimetry, GPC and ^{1}H-NMR. At least 10 chemically different polymer backbones can now be prepared with one or two terpyridine end groups. Subsequently these polymers have been connected by the addition of metal ions. Many different architectures could be prepared using the same starting materials, hence the comparison with the LEGO-system. Polymer *mono*-complexes, simple A-A homo dimers, chain-extended polymers and di- and triblock copolymers have been synthesized. Characterization of the molecular weight posed severe challenges, already for the A-A homo dimers, due to the presence of the charged metal complex, but finally analytical techniques such as GPC (using 5 mM NH_4PF_6 in DMF as eluent), non-aqueous capillary electrophoresis (using 5 mM $Ba(ClO_4)_2$ in NMF) and analytical ultracentrifugation (using THF:propylene carbonate-mixtures with 10 mM $[NBu_4][PF_6]$) have been succesfully applied. Furthermore, ^{1}H-NMR and MALDI-TOF MS could be used for studying the composition of the copolymers. Viscosity experiments indicated indeed chain extension upon addition of metal ions to terpyridine-functionalized telechelics.

Block copolymer morphologies were investigated in the bulk, in thin films and in solution. Ionic interactions play an important role in determining the final morphology as evidenced from the small angle X-ray scattering results. Aggregation of the metal complexes into multiplets – as also observed in ionomers – was found to be dependent on the applied counter-ion in case of PS_{20}-[Ru]-PEO_{70} diblock copolymers. More

bulky counter-ions (tetraphenylborates) prevented this aggregation and allowed the block copolymer to phase separate into a lamellar morphology, as expected based on the volume fractions. This phase separation automatically arranges the metal complexes in planes between the two different polymer matrices. Using smaller counter-ions (hexafluorophosphates), ionic aggregation was found to overrule the phase separation between the two blocks. Upon isothermal crystallization from the melt the PEO-blocks start to crystallize and this results in changes in the morphology. A 4 × 4 library of PS_x-[Ru]-PEO_y block copolymers with four different degrees of polymerization in each block was studied by AFM after spin-coating thin films of the copolymers onto a silicon wafer. Block copolymer aqueous micelles were prepared after dialysis of a solution of the block copolymer in a non-selective solvent. This leads in most cases to kinetically frozen micelles, except when using a low T_g block as was demonstrated for PEB_{70}-[Ru]-PEO_{70}. The preparation procedure was improved by controlling the water addition rate. These micelles were studied by a number of techniques such as (cryo)-TEM, AFM, DLS, SLS and analytical ultracentrifugation and where possible compared with their covalent counterparts. In contrast to the covalent block copolymer micelles, two distributions were for all block copolymer micelles observed by DLS-experiments. They have been attributed to primary micelles or small clusters of micelles (as evidenced by cryo-TEM) and larger aggregates of micelles. These findings were corroborated by TEM and AFM. The temperature dependency of the micelles was studied, but more important changes in their hydrodynamic diameters were found by the addition of (different) salt. Ionic interactions between metal complexes on neighboring chains as well as between the ions and the PEO-chains are thought to be responsible for this behavior. Cylindrical micelles were observed in case of PFS_{12}-[Ru]-PEO_{70} using a combination of DLS, SLS and TEM. They are the result of crystallization of the core-forming block (PFS). Stimuli-responsive triblock copolymer micelles were prepared for PS_{32}-*b*-$P2VP_{13}$-[Ru]-PEO_{70}. Protonation of the middle block below pH = 5 led to a expansion of the hydrodynamic diameter as evidenced by DLS-experiments.

An extremely interesting aspect of these block copolymers is that under certain experimental conditions the metal complex may be opened. Although the processes remain currently unclear, this poses an alternative to lithographic techniques through patterning of surfaces on the nano-scale and terpyridine-functionalized ‘nano-beads’ that could be of interest in catalysis or waste water treatment.

Samenvatting

Het onderzoek beschreven in dit proefschrift was gericht op het introduceren van metaal-complexerende groepen aan het keteneinde van polymeren om op deze wijze polymeerketens aan elkaar te koppelen door middel van metaal-ionen. Het metaal complex bestaat uit twee gesubstitueerde terpyridine liganden en de gebruikte metaal ionen waren ijzer, cobalt, nikkel, koper, zink, ruthenium, cadmium en kwik, allen in de 2+ oxidatietoestand. Het gedrag van de metaal-ligand binding is bestudeerd door het synthetizeren van model metaal complexen. Deze verbindingen zijn gekarakteriseerd met verschillende spectroscopische methoden, element analyse, massa spectrometrie en in enkele gevallen met behulp van kristallografie. De stabiliteitsconstanten van het metaal-complexvormingsproces zijn bepaald met behulp van een partitiemethode voor zink(II)-complexen, terwijl ^{1}H-NMR technieken zijn toegepast in een poging deze te achterhalen voor cobalt(II)-complexen. MALDI-TOF MS en MS/MS-technieken zijn gebruikt om de relatieve bindingsterkte van een reeks metaal-complexen ten opzichte van elkaar te bepalen. Modelleren heeft verder bijgedragen aan begrip van het metaal-complexvormingsproces. Verdere studies waren gericht op de stabiliteit van het metaal-complex wanneer de temperatuur, pH en oxidatietoestand van het metaal-ion veranderd werden: de laatste twee konden gevolgd worden met behulp van UV/vis-spectroscopie. Heteroleptische metaal-complexen (met verschillende substituenten op de afzonderlijke liganden) zijn geprepareerd middels een twee-stapssynthese gebruik makend van inerte metaal complexen van cobalt(III) en ruthenium(II). Dit legt het fundament voor de constructie van verschillende polymeerarchitecturen, zoals polymere mono-complexen, homo-dimeren, ketenverlengde polymeren en di en triblok copolymeren. Hiervoor diende de terpyridine ligand aan het keteneinde van een polymeer geintroduceerd te worden. Synthetische strategieën omvatten eindgroep modificatie door middel van veretheringsreacties van hydroxy-functionele polymeren alsmede gecontroleerde radicaal polymerizaties van verschillende monomeren door middel van een terpyridine-gefunctionalizeerde initiator. De kinetiek van de polymerizatie van styreen, *n*-butylacrylaat, 4-vinylpyridine en *N,N*-dimethylacrylamide gebruik makende van deze initiator was bestudeerd met behulp van gravimetrie, GPC en ^{1}H-NMR. Tenminste 10 chemisch verschillende polymeren kunnen nu succesvol gesynthetizeerd worden met een of twee terpyridine eindgroepen. Vervolgens zijn deze polymeren aan elkaar gekoppeld door toevoeging van metaal-ionen. Vele verschillende architecturen kunnen nu geprepareerd worden door gebruik te maken van dezelfde startmaterialen, vandaar de vergelijking met LEGO. Polymere mono-complexen, A-A homo-dimeren, ketenverlengde polymeren en di- en triblokcopolymeren zijn gesynthetizeerd. De karakterisatie van het molecuulgewicht was een uitdaging, zelfs voor de meest eenvoudige A-A homo-dimeren, door de aanwezigheid van de geladen metaal-complexen, maar uiteindelijk zijn technieken zoals GPC (met 5 mM NH_4PF_6 in DMF als eluens), capillaire electrophorese (met 5 mM $Ba(ClO_4)_2$ in NMF als eluens) en analytische ultracentrifuge (met 10 mM $[NBu_4][PF_6]$ in mengsels van THF en propyleencarbonaat) succesvol toegepast. Bovendien, met behulp van ^{1}H-NMR en MALDI-TOF MS was het mogelijk de compositie van de (co)polymeren te bepalen. Viscositeitsexperimenten gaven inderdaad aan dat ketenverlenging plaatsvindt wanneer metaal-ionen worden toegevoegd aan terpyridine-gefunctionalizeerde telechelische polymeren.

Blok copolymeer morfologieen zijn bestudeerd in de bulk, in dunne films en in oplossing. Ionische interacties spelen een belangrijke rol in het bepalen van de uiteindelijke morfologie, zoals aangetoond is met de SAXS-metingen. Aggregatie van de metaal-complexen in multipletten – zoals ook in ionomeren – is afhankelijk van het tegen-ion voor PS_{20}-[Ru]-PEO_{70} blok copolymeren. Grote tegen-ionen, zoals tetraphenylboraat tegen-ionen, verhinderen deze aggregatie en het blok copolymeer is in staat een lamellaire morfologie aan te nemen, zoals ook verwacht wordt op basis van de volume fracties van de blokken. Deze fasescheiding leidt automatisch tot het ordenen van de metaal-complexen in een vlak tussen de twee verschillende polymeermatrices. Wanneer kleinere tegen-ionen werden toegepast, zoals hexafluorofosfaat tegen-ionen, werd de morfologie gedicteerd door de ionische aggregatie en geen fasescheiding tussen de blokken kon worden waargenomen. Isotherme kristallisatie van de blok copolymeer smelt leidt tot kristallisatie van het PEO-blok and dit resulteert vervolgens in andere morfologieen. Een vier bij vier library van PS-[Ru]-PEO blok copolymeren met vier verschillende polymerisatiegraden in elk blok was bestudeerd met behulp van AFM na spin-coaten van dunne films van de copolymeren op silicium wafers. Micellen van verschillende blok copolymeren zijn geprepareerd na dialyse van een oplossing van het betreffende blok copolymeer in een niet-selectief oplosmiddel tegen water. Dit leidt in de meeste gevallen tot micellaire structuren die kinetisch bepaald zijn. Alleen in het geval van PEB_{70}-[Ru]-PEO_{70} konden micellen verkregen worden die in thermodynamisch evenwicht verkeerden wegens het lage T_g blok. De procedure voor het preparen van de micellen is verbeterd door de water toevoegingssnelheid te regelen. De micellen zijn bestudeerd met een scala aan technieken zoals (cryo)-TEM, AFM, DLS, SLS en analytische ultracentrifuge en waar mogelijk zijn ze vergeleken met hun covalente tegenpolen. In tegenstelling tot de covalente blok copolymeer micellen werden twee grootte-distributies waargenomen met behulp van DLS. Deze zijn toegekend aan individuele micellen of kleine clusters van micellen (m.b.v. cryo-TEM) en grotere aggregaten van micellen. Deze bevindingen werden verder onderschreven door TEM en AFM-metingen. De temperatuursafhankelijksheid van de micellen was bestudeerd, echter, belangrijkere verschillen in hydrodynamische diameter van de micellen werd gevonden wanneer verschillende zouten werden toegevoegd. Ionische interacties tussen de metaal-complexen op naburige ketens alsmede tussen het zout en het PEO-blok zouden hier verantwoordelijk voor kunnen zijn. Cylindrische micellen werden verkregen voor PFS_{12}-[Ru]-PEO_{70} door kristallisatie van het kern-vormende polymeerblok (PFS) en zijn gekarakterizeerd met behulp van DLS, SLS en TEM. Stimuli-responsieve triblok copolymeer micellen zijn geprepareerd van PS_{32}-*b*-$P2VP_{13}$-[Ru]-PEO_{70}. Protonatie van het middelste blok bij pH < 5 leidde tot de expansie van de hydrodynamische diameter van de micellen en is geverifieerd met behulp van DLS.

Een zeer belangrijk en interessant aspect van deze blokcopolymeren is dat onder bepaalde condities de metaal-coordinatie ongedaan gemaakt kan worden. Ondanks het feit dat het proces tot nu toe niet volledig begrepen wordt, biedt deze manier een alternatief voor lithografische technieken.

Curriculum vitae

Bas Lohmeijer was born on June 21st 1977 in Groningen. He grew up in the south-western part of the Netherlands, where he obtained his high school diploma (VWO) at Het Juvenaat in Bergen op Zoom. In 1995 he started his study at the Eindhoven University of Technology in chemistry and chemical engineering. From 1998/1999 he took part in an exchange program at the Osaka University in Japan. In 2000 he graduated from the group of professor Meijer in Macromolecular and Organic Chemistry at the Eindhoven University of Technology. In november 2000 he started his PhD-project at the same university in the group of professor Schubert. The most important results of his research are described in this thesis.

Bas Lohmeijer werd geboren op 21 juni 1977 in Groningen. Hij groeide op in het zuidwesten van Nederland, waar hij zijn VWO-diploma haalde aan het Juvenaat in Bergen op Zoom. In 1995 begon hij met zijn studie chemische technologie aan de Technische Universiteit in Eindhoven. In 1998/1999 nam hij deel aan een uitwisselingsprogramma aan de Universiteit van Osaka in Japan. In 2000 studeerde hij af binnen de groep van professor Meijer in macromoleculaire en organische chemie aan de Technische Universiteit in Eindhoven. In november van datzelfde jaar begon hij aan zijn promotie-onderzoek aan dezelfde universiteit in de groep van professor Schubert. De belangrijkste resultaten van zijn onderzoek zijn beschreven in dit proefschrift.

Refereed publications

23. Gohy, Jean-François; Lohmeijer, Bas G. G.; Alexeev, Alexander; Wang, Xiao-Song; Manners, Ian; Winnik, Mitchell A.; Schubert, Ulrich S. **Cylindrical micelles from the Aqueous Self-Assembly of an Amphiphilic Poly(ethylene oxide)-b-Poly(ferrocenylsilane) (PEO-b-PFS) Block Copolymer with a Metallo-Supramolecular Linker at the Block Junction** Chemistry - A European Journal (2004), 10(17), 4315-4323.

22. Vogel, Vitali; Mayer, Gottfried; Lohmeijer, Bas G. G.; Gohy, Jean-François; van den Broek, Jacomina A.; Haase, Winfried; Schubert, Ulrich S.; Schubert, Dieter **Metallo-supramolecular Block Copolymer Micelles: Improved Preparation and Characterisation.** Journal of Polymer Science, Part A: Polymer Chemistry (2004), 42(17), 4458-4465.

21. Lohmeijer, Bas G. G.; Schubert, Ulrich S. **Expanding the supramolecular polymer LEGO system: Nitroxide-mediated living free-radical polymerization as a tool for mono- and telechelic polystyrenes.** Journal of Polymer Science, Part A: Polymer Chemistry (2004), 42(16), 4016-4027.

22. Lohmeijer, Bas G. G.; Gohy, Jean-Francois; Schubert, Ulrich S. **Supramolecular engineering with macromolecules: From defined block copolymers to functional nanomaterials.** Materials Research Society Symposium Proceedings (2004), EXS-1(Architecture and Application of Biomaterials and Biomolecular Materials), 343-345.

19. Regev, Oren; Gohy, Jean-Francois; Lohmeijer, Bas G. G.; Varshney, Sunil K.; Hubert, Dominique H. W.; Frederik, Peter M.; Schubert, Ulrich S. **Dynamic light scattering and cryogenic transmission electron microscopy investigations on metallo-supramolecular aqueous micelles: evidence of secondary aggregation.** Colloid and Polymer Science (2004), 282(4), 407-411.

18. Andres, Philip R.; Hofmeier, Harald; Lohmeijer, Bas G. G.; Schubert, Ulrich S. **Synthesis of 4'-functionalized 2,2':6',2''-terpyridines via the pyridone route: Symmetric and asymmetric bis-complex formation.** Synthesis (2003), (18), 2865-2871.

17. Al-Hussein, M.; Lohmeijer, B. G. G.; Schubert, U. S.; De Jeu, W. H. **Melt Morphology of Polystyrene-Poly(ethylene oxide) Metallo-Supramolecular Diblock Copolymer.** Macromolecules (2003), 36(25), 9281-9284.

16. Meier, Michael A. R.; Lohmeijer, Bas G. G.; Schubert, Ulrich S. **Characterization of defined metal-containing supramolecular block copolymers.** Macromolecular Rapid Communications (2003), 24(14), 852-857.

15. Gohy, Jean-Francois; Lohmeijer, Bas G. G.; Decamps, Brigitte; Leroy, Eric; Boileau, Sylvie; van den Broek, Jacomina A.; Schubert, Dieter; Haase, Winfried; Schubert, Ulrich S. **Synthesis and characterization of metallo-supramolecular micelles.** Polymer International (2003), 52(10), 1611-1618.

14. Vogel, Vitali; Gohy, Jean-Francois; Lohmeijer, Bas G. G.; Van Den Broek, Jacomina A.; Haase, Winfried; Schubert, Ulrich S.; Schubert, Dieter. **Metallo-supramolecular micelles: Studies by analytical ultracentrifugation and electron microscopy.** Journal of Polymer Science, Part A: Polymer Chemistry (2003), 41(20), 3159-3168.

13. Gohy, Jean-Francois; Lohmeijer, Bas G. G.; Schubert, Ulrich S. **From supramolecular block copolymers to advanced nano-objects.** Chemistry--A European Journal (2003), 9(15), 3472-3479.

12. Lohmeijer, Bas G. G.; Schlaad, Helmut; Schubert, Ulrich S. **Synthesis and thermal properties of diblock copolymers utilizing non-covalent interactions.** Macromolecular Symposia (2003), 196(Metal- and Metalloid-Containing Macromolecules), 125-135.

11. Lohmeijer, Bas G. G.; Schubert, Ulrich S. **Water-soluble building blocks for terpyridine-containing supramolecular polymers: Synthesis, complexation, and pH stability studies of poly(ethylene oxide) moieties.** Macromolecular Chemistry and Physics (2003), 204(8), 1072-1078.

10. Meier, Michael A. R.; Lohmeijer, Bas G. G.; Schubert, Ulrich S. **Relative binding strength of terpyridine model complexes under matrix-assisted laser desorption/ionization mass spectrometry conditions.** Journal of Mass Spectrometry (2003), 38(5), 510-516.

9. Lohmeijer, Bas G. G.; Schubert, Ulrich S. **Playing LEGO with macromolecules: Design, synthesis, and self-organization with metal complexes.** Journal of Polymer Science, Part A: Polymer Chemistry (2003), 41(10), 1413-1427.

8. Roy M. A. l'Abee, Leandra L. J. M. Cornelissen, Marta Cueto Diaz, Michel Ligthart, Mariska J. de la Mar, Sanna Wijnans, Bas G. G. Lohmeijer, Ulrich S. Schubert, **High-throughput screening and combinatorial methods: The future of polymer research in industry and academia? A feasibility study**, e-Polymers, (2003), T001 1-30.

7. Gohy, Jean-Francois; Lohmeijer, Bas G. G.; Varshney, Sunil K.; Decamps, Brigitte; Leroy, Eric; Boileau, Sylvie; Schubert, Ulrich S. **Stimuli-Responsive Aqueous Micelles from an ABC Metallo-Supramolecular Triblock Copolymer.** Macromolecules (2002), 35(26), 9748-9755.

6. Lohmeijer, Bas G. G.; Schubert, Ulrich S. **Supramolecular engineering with macromolecules: an alternative concept for block copolymers.** Angewandte Chemie, International Edition (2002), 41(20), 3825-3829.

5. Gohy, Jean-Francois; Lohmeijer, Bas G. G.; Varshney, Sunil K.; Schubert, Ulrich S. **Covalent vs. Metallo-supramolecular Block Copolymer Micelles.** Macromolecules (2002), 35(19), 7427-7435.

4. Gohy, Jean-Francois; Lohmeijer, Bas G. G.; Schubert, Ulrich S. **Reversible metallo-supramolecular block copolymer micelles containing a soft core.** Macromolecular Rapid Communications (2002), 23(9), 555-560.

3. Gohy, Jean-Francois; Lohmeijer, Bas G. G.; Schubert, Ulrich S. **Metallo-Supramolecular Block Copolymer Micelles.** Macromolecules (2002), 35(12), 4560-4563.

2. Brunsveld, Luc; Lohmeijer, Bas G. G.; Vekemans, Jef A. J. M.; Meijer, E. W. **Amplification of chirality in helical supramolecular columns.** Journal of Inclusion Phenomena and Macrocyclic Chemistry (2001), 41(1-4), 61-64.

1. Brunsveld, Luc; Lohmeijer, Bas G. G.; Vekemans, Jef A. J. M.; Meijer, E. W. **Chirality amplification in dynamic helical columns in water.** Chemical Communications (Cambridge) (2000), (23), 2305-2306.

In press:

2. Tziatzios, Christos; Precup, Andrei A.; Lohmeijer, Bas G. G.; Börger, Lars; Schubert, Ulrich S.; Schubert, Dieter **Dimerization of monofunctionalized poly(ethylene oxide) via metal-ligand interactions and hydrogen bonds.** Progress in Colloid And Polymer Science (2004)

1. Lohmeijer, Bas G. G.; Wouters, Daan; Yin, Zhihui; Schubert, Ulrich S. **Metallo-Supramolecular Block Copolymer Libraries: Modular Versatility of the LEGO-System.** Chemical Communications (2004)

Submitted:

1. Al-Hussein, Mahmoud; Lohmeijer, Bas G. G.; de Jeu, W. H.; Schubert, Ulrich S. **Switching the melt morphology of a polystyrene-poly(ethylene oxide) metallo-supramolecular block copolymer using different counter-ions.** Macromolecules

Non-refereed publications:

9. Lohmeijer, Bas G. G.; Schubert, Ulrich S. **Playing LEGO with polymers and nano-objects: The power of metal complex connectors.** Polymeric Materials: Science and Engineering (2004), 91 129-130.

8. Lohmeijer, Bas G. G.; Al-Hussein, Mahmoud; De Jeu, Wim H.; Gohy, Jean-Francois; Schubert, Ulrich S. **Bulk morphology of a metallo-supramolecular block copolymer.** Polymer Preprints (American Chemical Society, Division of Polymer Chemistry) (2004), 45(1), 464-465.

7. Gohy, Jean-Francois; Lohmeijer, Bas G. G.; Schubert, Ulrich S. **Clustering in metallo-supramolecular micelles.** Polymer Preprints (American Chemical Society, Division of Polymer Chemistry) (2004), 45(1), 395-396.

6. Meier, Michael A. R.; Lohmeijer, Bas G. G.; Schubert, Ulrich S. **Recent advances in the characterization of terpyridine based supramolecular polymers.** Polymer Preprints (American Chemical Society, Division of Polymer Chemistry) (2004), 45(1), 389-390.

5. Lohmeijer, Bas G. G.; Schubert, Ulrich S. **Towards metallo-supramolecular ABA triblock and (AB)n multiblock copolymers.** Polymer Preprints (American Chemical Society, Division of Polymer Chemistry) (2004), 45(1), 376-377.

4. Wouters, Daan; Lohmeijer, Bas G. G.; Alexeev, Alexander A.; Saunin, Sergey; Schubert, Ulrich S. **Application of (automated) atomic force microscopy to combinatorial polymer materials research.** Polymeric Materials Science and Engineering (2004), 90 803-804.

3. Lohmeijer, Bas G. G.; Wouters, Daan; Yin, Zhihui; Schubert, Ulrich S. **Block copolymer libraries using supramolecular strategies.** Polymeric Materials Science and Engineering (2004), 90 723-724.

2. Lohmeijer, Bas. G. G.; Gohy, Jean-Francois; Schubert, Ulrich S. **Engineering with macromolecules: From supramolecular chemistry to defined nanomaterials.** Polymer Preprints (American Chemical Society, Division of Polymer Chemistry) (2003), 44(1), 585-586.

1. Lohmeijer, Bas G. G.; Schubert, Ulrich S. **Synthesis of metallo-supramolecular block-copolymers.** Polymeric Materials Science and Engineering (2001), 85 460-461.

Dankwoord

Ook dit proefschrift is niet volledig zonder een woord van dank aan allen die hebben bijgedragen aan het tot stand komen van dit boekje. Allereerst wil ik de leden van de leescommissie - Ian Manners, Ulrich Schubert, Jean-François Gohy en Bert Meijer - van harte bedanken voor hun kritiek op dit proefschrift. Daar is het verhaal een stuk duidelijker van geworden. Uli wil ik van harte bedanken voor alle tijd, suggesties, verbeteringen, ideeen, samenwerkingsverbanden en motivatie gedurende de afgelopen vier jaar. Ik heb een immense bewondering voor de energie die je in je werk steekt en wens je veel geluk in de toekomst met het verder uitbreiden van het onderzoek. I'd like to thank Jean-François for the fruitful cooperation: your fascination for block copolymer morphologies was very motivating and I have learned a great deal about them from you. Your input and feedback regarding the research have been stimulating and have led to several joint publications. I wish you the very best with your new group, but I have no doubts that you will have a lot of success with good science in the (near) future. In that respect, I'd also like to thank Ian Manners, for your criticism on the thesis and the successful cooperation regarding the PFS-PEO block copolymer. From your group/university, many thanks also go out to Xiaosong Wang for providing the hydroxy-functionalized PFS and professor Mitch Winnik for the corrections of the manuscript. Bert, voor alle dingen die je voor mij gedaan hebt wil ik je heel graag bedanken. Dat begon al in 1998, toen ik via jouw contacten met professor Harada de kans kreeg een jaar deel te nemen aan een uitwisselingprogramma aan de Universiteit van Osaka, Japan. Na dat fantastische jaar ben ik in jouw vakgroep afgestudeerd bij Luc Brunsveld. Van jullie fascinatie voor de chemie heb ik destijds een flinke portie meegekregen en was daardoor ook vrij gauw overtuigd een promotie te doen. Ik wil je van harte bedanken voor het deelnemen in de leescommissie en hoop dat je niet te teleurgesteld bent dat ik gekozen heb voor een ander onderwerp als wat jij destijds voorstelde. The results described in this thesis come various sources. I'd like to thank Mahmoud Al-Hussein for all the SAXS measurements on the PS_{20}-[Ru]-PEO_{70} block copolymers in the melt and upon isothermal crystallization. I'm very happy that we met after a presentation in Lunteren and although the results are very promising, I think we are at the beginning of truly understanding and controlling the morphology of these block copolymers. Daarbij wil ik graag Wim de Jeu bedanken voor het inzicht in SAXS en de discussie over isotherme kristallisatie. I'm thankful for the cooperation with the University of Frankfurt. I'd like to thank professor Dieter Schubert to take part in the committee and for the many discussions regarding the characterization by analytical ultracentrifugation. I'd like to thank Christos Tziatzios for the enormous amount of time he has spent in making analytical centrifugation a well-suited technique for studying these polymers. Your work will be very useful in the future. I'm grateful for the many measurements as well as the discussions we had, but I'm also sorry that in some cases I was not able to purify some of the compounds. Many thanks also go out to Gottfried Mayer, Vitali Vogel, Jacomina van den Broek en Winfried Haase for work on the micelles. Kathalijne Oudhoff uit de groep van professor Schoenmakers wil ik graag bedanken voor de vele metingen met capillaire electroforese. Grappig dat wederom na een ontmoeting met een van jouw collega's (Monique) in Lunteren een samenwerking tot stand is gekomen. Inmiddels is hier in Eindhoven een systeem opgezet naar aanleiding van jouw resultaten. Brigitte Décamps, Eric Leroy and Sylvie Boileau I'd like to thank for the TEM-measurements. Irina Suske and professor Salbeck are gratefully acknowledged for the spectroelectrochemical measurements as

described in chapter 2. Guido Kickelbick has performed the X-ray crystallography on some of the model complexes. Thanks for your patience: growing crystals is an really art! I'm grateful to Charles-André Fustin, who is doing great work on patterned surfaces using these block copolymers in thin films. I'd like to thank Pierre Guillet for his efforts and wish you the very best in your PhD under supervision of Jean-François. I hope your time in Eindhoven was a good one! Joost wil ik graag bedanken voor de tijd, uitleg en de metingen met de oude en de nieuwe ESI, Lou en Ralf voor hun hulp met MALDI-TOF MS, GPC en HPLC. Joris, Christian, Andrei, Philip en met name Mike wil ik verder bedanken voor hun MALDI-TOF MS metingen. Mike, ik ben je verder eeuwig dankbaar voor het feit dat je een goed GPC-eluens hebt weten te vinden voor deze geladen polymeren. Dat heeft enorm bijgedragen aan een goede karakterisatie van deze polymeren. Verder was de tijd in Anaheim en Las Vegas erg gezellig. Sorry voor de dinosaurus-foto. Bruce Anderson wil ik bedanken voor de Raman-metingen. Henk Eding dank ik voor de hulp met het opbouwen van het lab op vloer 3 alsmede voor de elementanalyse. Hans Damen bedank ik voor het bestellen van de broodnodige chemicaliën, een taak die later overgenomen is door Antje van den Berg. Caroline Abeln wil bedanken voor het last-minute werk wat betreft elementanalyses. Verder ben ik gezegend geweest met een uitermate zelfstandige en gemotiveerde researchstudent. Brian, van jouw resultaten zijn er een hoop opgenomen in dit proefschrift. Ik heb grote bewondering voor het geduld waarmee je de partitiemethode hebt ontwikkeld en daarnaast de capillaire electroforese hier aan de praat hebt gekregen. Ook Wouter en Ingrid wil ik bedanken voor hun inzet. Lambert, jou wil ik bedanken voor het lekkere kokkerellen en de nano-indentatie resultaten. I'd like to thank Yin and Yankui for synthesizing block copolymers and terpyridine starting materials. Huiqi, Tina, Stephanie, Jörg, Dodo, Dimitri, Issam en Gaby wil ik bedanken voor hun kamergenootschap. Gaby, jou wil ik bedanken voor de afgelopen paar jaar: ze waren fantastisch. Carlos, jouw plotselinge dood was zeer moeilijk te bevatten. De Schubert-groep dank ik voor hun gezelligheid, discussies en samenwerking. Emma dank ik van harte voor al haar inspanningen. Pim, Martijn, Daan, Rolf, Christ, Bas, Frank en Ingmar, als laatste komen jullie aan de beurt. Ik wil jullie van harte bedanken voor alle gezelligheid gedurende de afgelopen jaren. Daan, ik ben blij dat jij mijn paranimf wilt zijn en wens je veel succes met het schrijven van jouw proefschrift. Uiteraard ook nog bedankt voor de vele AFM-plaatjes… Pim, jij hebt de eer de andere paranimf te zijn: ik dank je voor je vriendschap en dat hersencellen gekloond kunnen worden wisten we al langer. Ik ben blij dat ook jij mij terzijde wilt staan tijdens de verdediging. Als laatste wil ik mijn ouders, mijn broers, mijn oma's, opa, ooms, tantes, neefjes en nichtjes bedanken voor hun niet aflatende steun en interesse in al wat ik doe. Met alle liefs,

Bas

This document contains the detailed x-ray crystal structure analysis of bis-terpyridine metal complexes of ligand **4** as described in chapter 2 of the thesis with the following transition metal ions Mn^{II}, Fe^{II}, Ru^{II}, Co^{II}, Ni^{II}, Cu^{II} and Zn^{II}. Also enclosed is the crystal structure of 2,2,5-trimethyl-3-(1-(4'-chloromethyl)phenylethoxy)-4-phenyl-3-azahexane, as described in chapter 3 of the thesis.

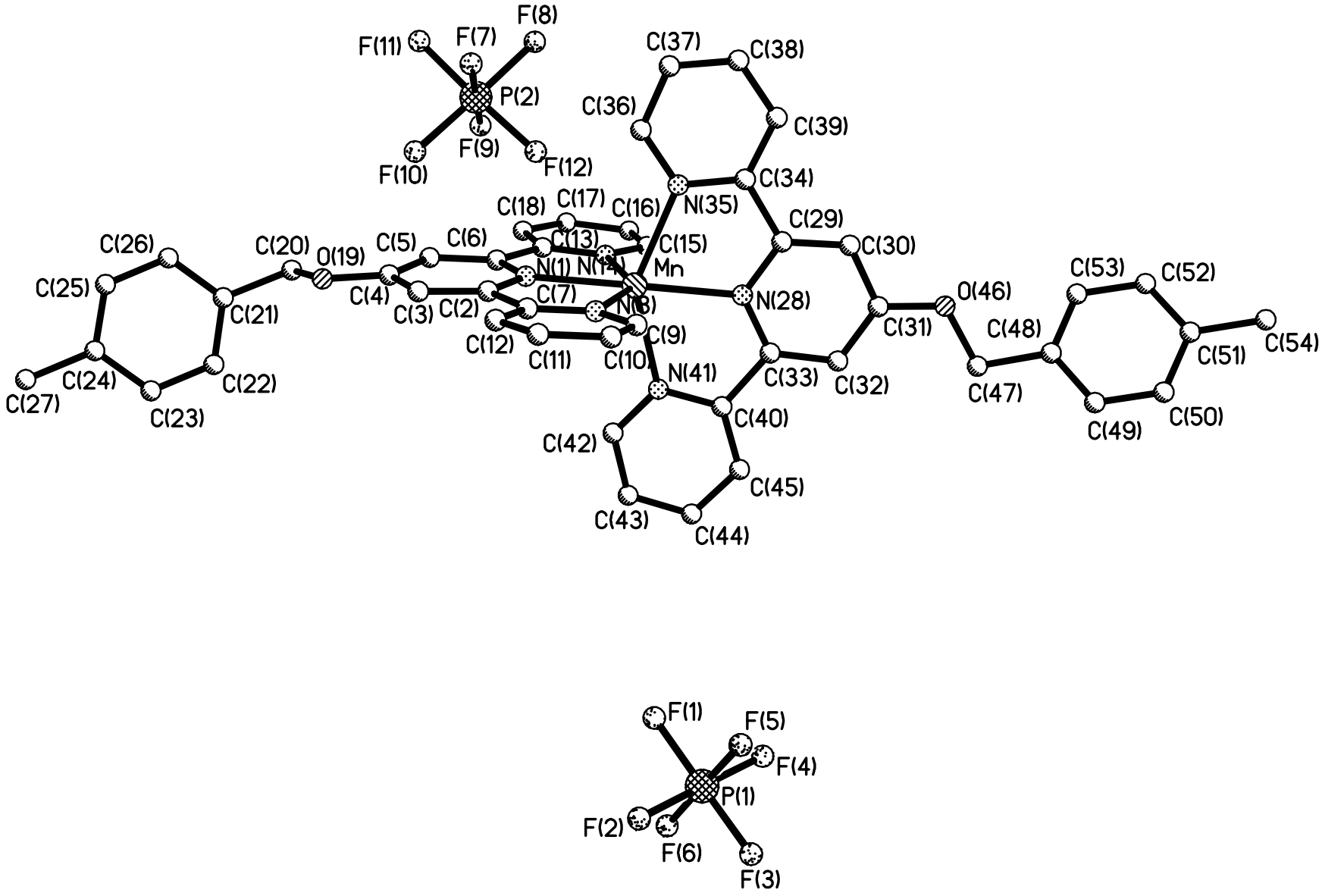
F(8)
F(11)
F(7)
P(2)
F(9)
F(10)
F(12)
C(37)
C(38)
C(36)
C(39)
C(34)
N(35)
C(18)
C(17)
C(16)
C(29)
C(30)
C(26)
C(20)
O(19)
C(5)
C(6)
C(13)
C(15)
C(25)
N(1)
N(14)
Mn
C(4)
C(3)
C(2)
C(7)
N(8)
N(28)
O(46)
C(53)
C(52)
C(21)
C(31)
C(48)
C(54)
C(12)
C(11)
C(10)
C(9)
C(51)
C(24)
C(22)
N(41)
C(33)
C(32)
C(47)
C(27)
C(23)
C(40)
C(50)
C(49)
C(42)
C(45)
C(43)
C(44)
F(1)
F(5)
F(4)
P(1)
F(2)
F(6)
F(3)

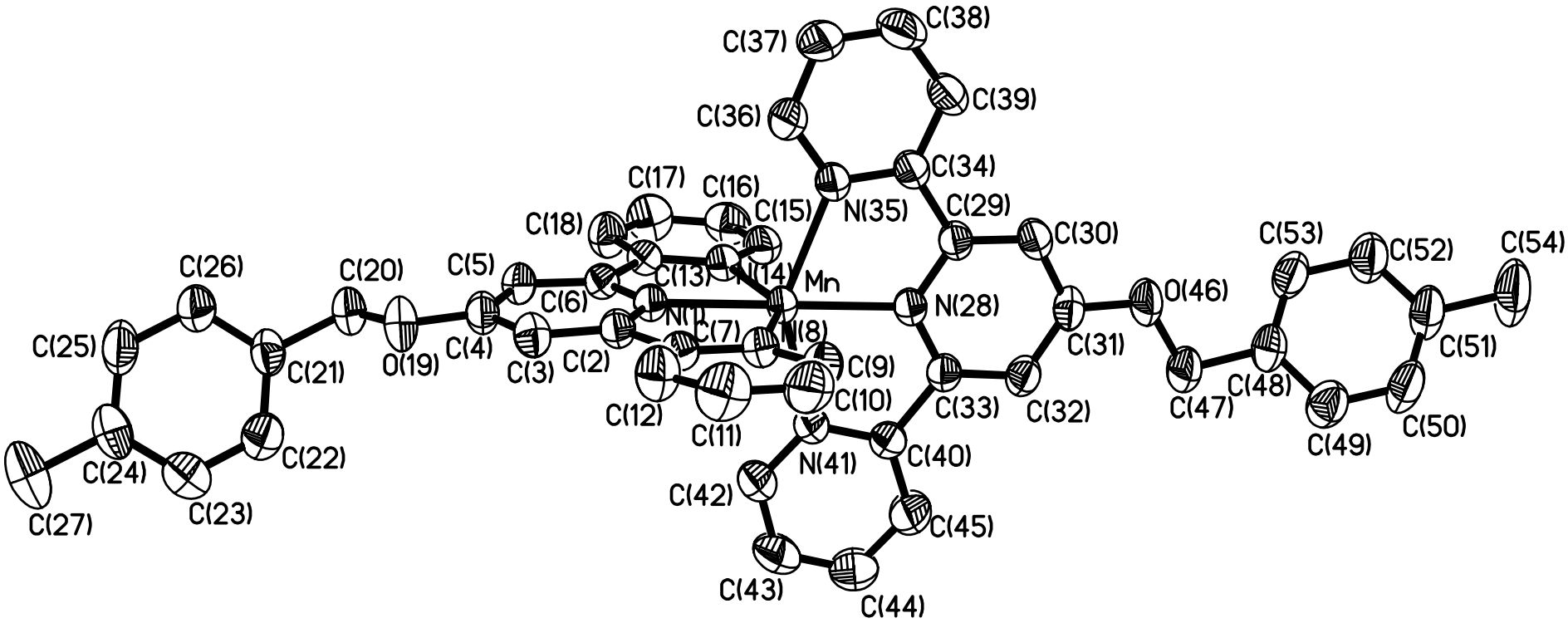
C(38)
C(37)
C(39)
C(36)
C(34)
C(17)
C(16)
C(15)
N(35)
C(29)
C(18)
C(30)
C(53)
C(52)
C(54)
C(26)
C(20)
C(5)
C(13)
C(14)
Mn
O(46)
C(6)
N(28)
C(25)
C(7)
N(8)
C(31)
C(51)
C(21)
O(19)
C(4)
C(3)
C(2)
C(9)
C(48)
C(12)
C(10)
C(33)
C(32)
C(47)
C(11)
C(50)
C(49)
N(41)
C(40)
C(24)
C(22)
C(42)
C(45)
C(27)
C(23)
C(43)
C(44)

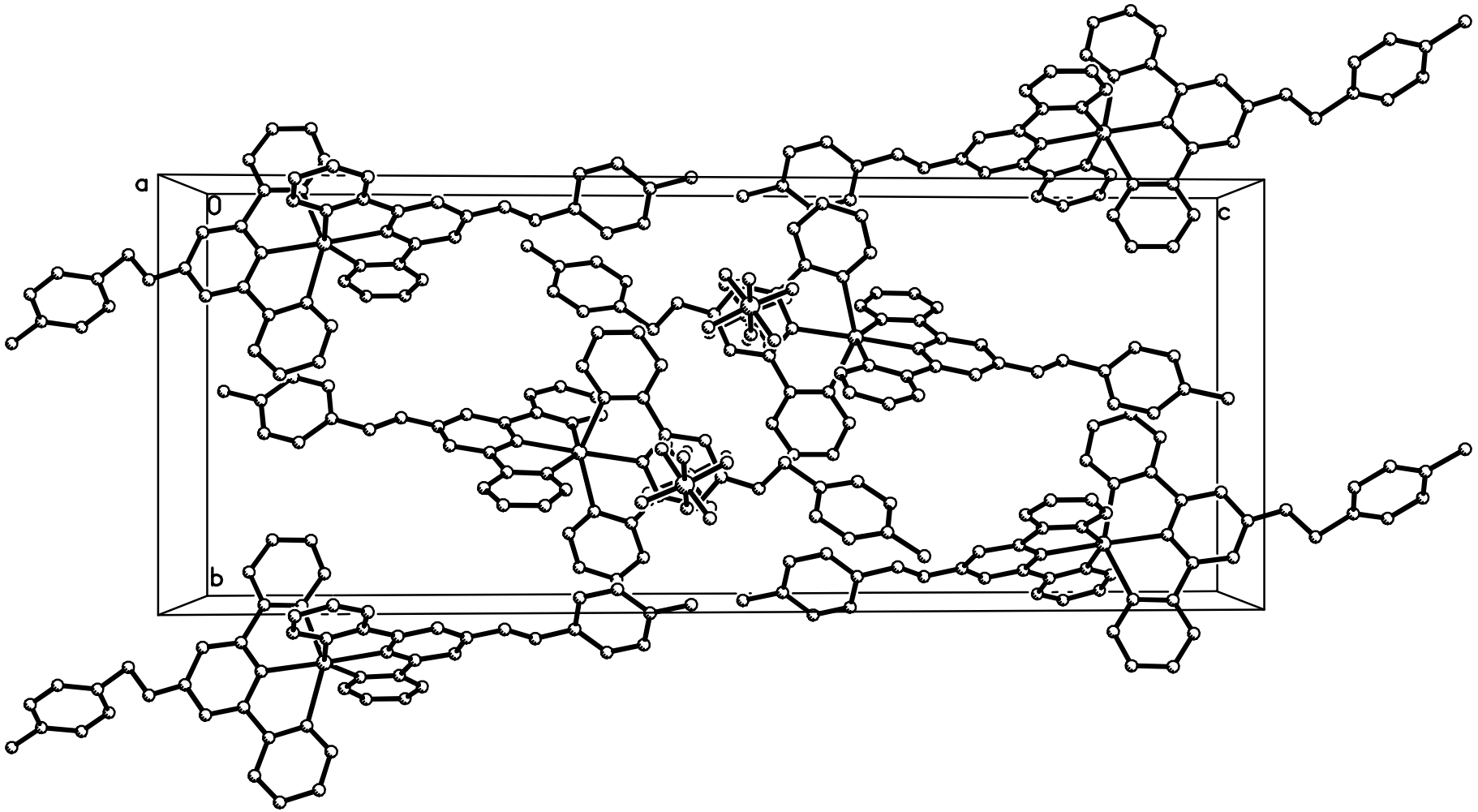
a
0
c
b

Table 1. Crystal data and structure refinement for **4**-Mn-**4**.

Identification code	**4**-Mn-**4**
Empirical formula	C46 H38 F12 Mn N6 O2 P2
Formula weight	1051.70
Temperature	295(2) K
Wavelength	0.71073 A
Crystal system, space group	monoclinic, P2(1)/c
Unit cell dimensions	a = 9.0037(12) A alpha = 90 deg. b = 14.2088(19) A beta = 93.599(3) deg. c = 36.022(5) A gamma = 90 deg.
Volume	4599.3(11) A^3
Z, Calculated density	4, 1.519 Mg/m^3
Absorption coefficient	0.452 mm^-1
F(000)	2140
Crystal size	0.63 x 0.18 x 0.10 mm
Theta range for data collection	2.22 to 28.34 deg.
Limiting indices	-12<=h<=12, -18<=k<=18, -47<=l<=48
Reflections collected / unique	45688 / 11430 [R(int) = 0.0306]
Completeness to theta = 28.34	99.7 %
Max. and min. transmission	0.9562 and 0.7640
Refinement method	Full-matrix least-squares on F^2
Data / restraints / parameters	11430 / 0 / 624
Goodness-of-fit on F^2	1.041
Final R indices [I>2sigma(I)]	R1 = 0.0605, wR2 = 0.1665
R indices (all data)	R1 = 0.0832, wR2 = 0.1831
Largest diff. peak and hole	0.883 and -0.391 e.A^-3

Table 2. Atomic coordinates (x 10^4) and equivalent isotropic displacement parameters (A^2 x 10^3) for **4**-Mn-**4**.
U(eq) is defined as one third of the trace of the orthogonalized Uij tensor.

	x	y	z	U(eq)
Mn	5187(1)	1381(1)	1309(1)	39(1)
N(1)	4764(2)	1607(1)	708(1)	38(1)
C(2)	5119(3)	2437(2)	559(1)	40(1)
C(3)	4758(3)	2639(2)	190(1)	46(1)
C(4)	4034(3)	1962(2)	-34(1)	46(1)
C(5)	3722(3)	1088(2)	118(1)	45(1)
C(6)	4087(2)	951(2)	494(1)	39(1)
C(7)	5898(3)	3106(2)	823(1)	42(1)
N(8)	6042(2)	2825(2)	1178(1)	44(1)
C(9)	6773(3)	3381(2)	1427(1)	55(1)
C(10)	7379(4)	4230(2)	1336(1)	64(1)
C(11)	7227(4)	4521(2)	973(1)	70(1)
C(12)	6468(4)	3959(2)	712(1)	61(1)
C(13)	3717(3)	67(2)	695(1)	41(1)
N(14)	4087(2)	72(2)	1063(1)	42(1)
C(15)	3759(3)	-684(2)	1264(1)	50(1)
C(16)	3060(3)	-1464(2)	1114(1)	59(1)
C(17)	2695(4)	-1471(2)	734(1)	65(1)
C(18)	3025(3)	-701(2)	525(1)	57(1)
O(19)	3679(2)	2232(2)	-386(1)	58(1)
C(20)	2779(3)	1605(2)	-623(1)	55(1)
C(21)	2130(3)	2176(2)	-947(1)	48(1)
C(22)	1014(3)	2822(2)	-897(1)	61(1)
C(23)	377(4)	3325(3)	-1194(1)	67(1)
C(24)	829(3)	3195(2)	-1554(1)	59(1)
C(25)	1938(4)	2551(3)	-1595(1)	68(1)
C(26)	2587(4)	2047(3)	-1300(1)	63(1)
C(27)	111(5)	3730(3)	-1879(1)	88(1)
N(28)	5543(2)	1115(1)	1904(1)	39(1)
C(29)	6789(3)	679(2)	2040(1)	41(1)
C(30)	7042(3)	479(2)	2410(1)	48(1)
C(31)	5990(3)	762(2)	2655(1)	46(1)
C(32)	4710(3)	1214(2)	2517(1)	46(1)
C(33)	4529(3)	1373(2)	2138(1)	40(1)
C(34)	7845(3)	441(2)	1754(1)	43(1)
N(35)	7423(2)	693(2)	1405(1)	42(1)
C(36)	8323(3)	503(2)	1133(1)	52(1)
C(37)	9684(3)	53(3)	1198(1)	65(1)
C(38)	10104(4)	-207(3)	1553(1)	76(1)
C(39)	9186(3)	-9(3)	1835(1)	65(1)
C(40)	3177(3)	1823(2)	1954(1)	45(1)
N(41)	3133(2)	1858(2)	1582(1)	43(1)
C(42)	1930(3)	2211(2)	1394(1)	56(1)
C(43)	735(4)	2554(3)	1567(1)	75(1)
C(44)	778(4)	2542(4)	1945(1)	93(1)
C(45)	2013(4)	2170(3)	2144(1)	81(1)
O(46)	6332(2)	554(2)	3015(1)	61(1)
C(47)	5325(3)	828(2)	3283(1)	58(1)
C(48)	6022(3)	574(2)	3662(1)	53(1)
C(49)	5772(4)	1142(2)	3960(1)	63(1)
C(50)	6393(4)	929(2)	4311(1)	71(1)
C(51)	7270(4)	139(2)	4374(1)	67(1)
C(52)	7500(4)	-432(2)	4074(1)	69(1)
C(53)	6884(4)	-213(2)	3720(1)	63(1)
C(54)	7979(6)	-86(3)	4756(1)	108(2)
P(1)	2788(1)	8630(1)	2408(1)	62(1)
F(1)	3138(6)	7972(2)	2084(1)	183(2)
F(2)	2890(3)	9528(2)	2151(1)	107(1)
F(3)	2457(7)	9274(2)	2732(1)	207(2)
F(4)	2646(3)	7733(1)	2667(1)	83(1)

F(5)	4409(4)	8700(3)	2536(2)	210(3)
F(6)	1134(4)	8533(3)	2291(1)	181(2)
P(2)	9619(1)	2054(1)	296(1)	68(1)
F(7)	11080(3)	2632(2)	281(1)	149(1)
F(8)	10541(3)	1250(2)	509(1)	103(1)
F(9)	8164(3)	1410(2)	304(1)	113(1)
F(10)	8654(4)	2799(3)	70(1)	161(2)
F(11)	9978(3)	1558(2)	-84(1)	115(1)
F(12)	9219(3)	2452(2)	682(1)	126(1)

Table 3. Bond lengths [A] and angles [deg] for **4**-Mn-**4**.

Mn-N(28)	2.1809(19)
Mn-N(1)	2.1970(19)
Mn-N(35)	2.245(2)
Mn-N(8)	2.251(2)
Mn-N(41)	2.253(2)
Mn-N(14)	2.262(2)
N(1)-C(6)	1.334(3)
N(1)-C(2)	1.342(3)
C(2)-C(3)	1.379(3)
C(2)-C(7)	1.488(3)
C(3)-C(4)	1.390(4)
C(4)-O(19)	1.344(3)
C(4)-C(5)	1.393(4)
C(5)-C(6)	1.385(3)
C(6)-C(13)	1.499(3)
C(7)-N(8)	1.339(3)
C(7)-C(12)	1.385(4)
N(8)-C(9)	1.338(3)
C(9)-C(10)	1.371(5)
C(10)-C(11)	1.370(5)
C(11)-C(12)	1.382(4)
C(13)-N(14)	1.347(3)
C(13)-C(18)	1.380(4)
N(14)-C(15)	1.337(3)
C(15)-C(16)	1.368(4)
C(16)-C(17)	1.388(5)
C(17)-C(18)	1.371(4)
O(19)-C(20)	1.447(3)
C(20)-C(21)	1.508(4)
C(21)-C(26)	1.373(4)
C(21)-C(22)	1.382(4)
C(22)-C(23)	1.382(4)
C(23)-C(24)	1.394(5)
C(24)-C(25)	1.369(5)
C(24)-C(27)	1.508(4)
C(25)-C(26)	1.381(4)
N(28)-C(33)	1.334(3)
N(28)-C(29)	1.346(3)
C(29)-C(30)	1.371(3)
C(29)-C(34)	1.483(3)
C(30)-C(31)	1.392(4)
C(31)-O(46)	1.347(3)
C(31)-C(32)	1.383(4)
C(32)-C(33)	1.383(3)
C(33)-C(40)	1.493(3)
C(34)-N(35)	1.340(3)
C(34)-C(39)	1.382(3)
N(35)-C(36)	1.338(3)
C(36)-C(37)	1.388(4)
C(37)-C(38)	1.362(4)
C(38)-C(39)	1.379(4)
C(40)-N(41)	1.341(3)
C(40)-C(45)	1.378(4)
N(41)-C(42)	1.337(3)
C(42)-C(43)	1.366(4)
C(43)-C(44)	1.362(5)
C(44)-C(45)	1.387(5)
O(46)-C(47)	1.421(3)
C(47)-C(48)	1.508(4)
C(48)-C(53)	1.370(4)
C(48)-C(49)	1.374(4)
C(49)-C(50)	1.382(4)
C(50)-C(51)	1.382(5)
C(51)-C(52)	1.376(4)
C(51)-C(54)	1.516(4)
C(52)-C(53)	1.393(4)
P(1)-F(5)	1.505(3)

P(1)-F(3)	1.525(3)
P(1)-F(6)	1.529(3)
P(1)-F(1)	1.543(3)
P(1)-F(2)	1.583(2)
P(1)-F(4)	1.589(2)
P(2)-F(7)	1.555(3)
P(2)-F(12)	1.564(3)
P(2)-F(10)	1.564(3)
P(2)-F(8)	1.583(2)
P(2)-F(11)	1.591(3)
P(2)-F(9)	1.599(3)

N(28)-Mn-N(1)	177.84(8)
N(28)-Mn-N(35)	72.41(7)
N(1)-Mn-N(35)	108.30(7)
N(28)-Mn-N(8)	109.40(7)
N(1)-Mn-N(8)	72.63(7)
N(35)-Mn-N(8)	96.54(8)
N(28)-Mn-N(41)	72.36(7)
N(1)-Mn-N(41)	106.85(7)
N(35)-Mn-N(41)	144.71(7)
N(8)-Mn-N(41)	96.78(8)
N(28)-Mn-N(14)	105.99(8)
N(1)-Mn-N(14)	71.98(7)
N(35)-Mn-N(14)	93.93(8)
N(8)-Mn-N(14)	144.61(7)
N(41)-Mn-N(14)	93.82(7)
C(6)-N(1)-C(2)	119.6(2)
C(6)-N(1)-Mn	120.87(16)
C(2)-N(1)-Mn	119.39(15)
N(1)-C(2)-C(3)	121.3(2)
N(1)-C(2)-C(7)	114.9(2)
C(3)-C(2)-C(7)	123.8(2)
C(2)-C(3)-C(4)	119.3(2)
O(19)-C(4)-C(3)	115.1(2)
O(19)-C(4)-C(5)	125.7(2)
C(3)-C(4)-C(5)	119.2(2)
C(6)-C(5)-C(4)	117.8(2)
N(1)-C(6)-C(5)	122.7(2)
N(1)-C(6)-C(13)	114.4(2)
C(5)-C(6)-C(13)	123.0(2)
N(8)-C(7)-C(12)	121.4(2)
N(8)-C(7)-C(2)	115.7(2)
C(12)-C(7)-C(2)	122.9(2)
C(9)-N(8)-C(7)	118.6(2)
C(9)-N(8)-Mn	123.96(19)
C(7)-N(8)-Mn	117.20(16)
N(8)-C(9)-C(10)	123.1(3)
C(11)-C(10)-C(9)	118.4(3)
C(10)-C(11)-C(12)	119.4(3)
C(11)-C(12)-C(7)	119.1(3)
N(14)-C(13)-C(18)	121.2(2)
N(14)-C(13)-C(6)	115.1(2)
C(18)-C(13)-C(6)	123.7(2)
C(15)-N(14)-C(13)	118.5(2)
C(15)-N(14)-Mn	123.79(17)
C(13)-N(14)-Mn	117.67(16)
N(14)-C(15)-C(16)	123.4(3)
C(15)-C(16)-C(17)	117.9(3)
C(18)-C(17)-C(16)	119.3(3)
C(17)-C(18)-C(13)	119.6(3)
C(4)-O(19)-C(20)	118.3(2)
O(19)-C(20)-C(21)	107.6(2)
C(26)-C(21)-C(22)	118.2(3)
C(26)-C(21)-C(20)	121.4(3)
C(22)-C(21)-C(20)	120.4(3)
C(21)-C(22)-C(23)	120.9(3)
C(22)-C(23)-C(24)	121.3(3)
C(25)-C(24)-C(23)	116.6(3)
C(25)-C(24)-C(27)	122.1(3)
C(23)-C(24)-C(27)	121.2(3)

C(24)-C(25)-C(26)	122.5(3)
C(21)-C(26)-C(25)	120.5(3)
C(33)-N(28)-C(29)	119.0(2)
C(33)-N(28)-Mn	120.71(15)
C(29)-N(28)-Mn	120.30(16)
N(28)-C(29)-C(30)	122.2(2)
N(28)-C(29)-C(34)	114.1(2)
C(30)-C(29)-C(34)	123.6(2)
C(29)-C(30)-C(31)	118.5(2)
O(46)-C(31)-C(32)	125.5(2)
O(46)-C(31)-C(30)	114.9(2)
C(32)-C(31)-C(30)	119.6(2)
C(31)-C(32)-C(33)	118.2(2)
N(28)-C(33)-C(32)	122.5(2)
N(28)-C(33)-C(40)	114.1(2)
C(32)-C(33)-C(40)	123.4(2)
N(35)-C(34)-C(39)	121.1(2)
N(35)-C(34)-C(29)	115.7(2)
C(39)-C(34)-C(29)	123.2(2)
C(36)-N(35)-C(34)	118.9(2)
C(36)-N(35)-Mn	123.63(17)
C(34)-N(35)-Mn	117.41(16)
N(35)-C(36)-C(37)	122.6(2)
C(38)-C(37)-C(36)	118.3(3)
C(37)-C(38)-C(39)	119.6(3)
C(38)-C(39)-C(34)	119.6(3)
N(41)-C(40)-C(45)	120.4(2)
N(41)-C(40)-C(33)	115.6(2)
C(45)-C(40)-C(33)	123.9(2)
C(42)-N(41)-C(40)	119.4(2)
C(42)-N(41)-Mn	123.57(18)
C(40)-N(41)-Mn	116.89(15)
N(41)-C(42)-C(43)	122.7(3)
C(44)-C(43)-C(42)	118.5(3)
C(43)-C(44)-C(45)	119.5(3)
C(40)-C(45)-C(44)	119.4(3)
C(31)-O(46)-C(47)	118.6(2)
O(46)-C(47)-C(48)	107.6(2)
C(53)-C(48)-C(49)	118.5(3)
C(53)-C(48)-C(47)	122.3(3)
C(49)-C(48)-C(47)	119.2(3)
C(48)-C(49)-C(50)	120.6(3)
C(49)-C(50)-C(51)	121.5(3)
C(52)-C(51)-C(50)	117.5(3)
C(52)-C(51)-C(54)	120.8(3)
C(50)-C(51)-C(54)	121.6(3)
C(51)-C(52)-C(53)	121.0(3)
C(48)-C(53)-C(52)	120.8(3)
F(5)-P(1)-F(3)	87.7(3)
F(5)-P(1)-F(6)	177.9(2)
F(3)-P(1)-F(6)	91.8(3)
F(5)-P(1)-F(1)	91.8(3)
F(3)-P(1)-F(1)	179.3(3)
F(6)-P(1)-F(1)	88.7(3)
F(5)-P(1)-F(2)	91.96(18)
F(3)-P(1)-F(2)	89.12(15)
F(6)-P(1)-F(2)	90.10(15)
F(1)-P(1)-F(2)	91.30(16)
F(5)-P(1)-F(4)	89.27(17)
F(3)-P(1)-F(4)	90.37(15)
F(6)-P(1)-F(4)	88.67(14)
F(1)-P(1)-F(4)	89.22(15)
F(2)-P(1)-F(4)	178.65(16)
F(7)-P(2)-F(12)	94.7(2)
F(7)-P(2)-F(10)	93.9(2)
F(12)-P(2)-F(10)	93.79(19)
F(7)-P(2)-F(8)	88.77(17)
F(12)-P(2)-F(8)	88.37(16)
F(10)-P(2)-F(8)	176.4(2)
F(7)-P(2)-F(11)	89.20(18)
F(12)-P(2)-F(11)	174.8(2)

F(10)-P(2)-F(11)	89.37(19)
F(8)-P(2)-F(11)	88.27(16)
F(7)-P(2)-F(9)	176.87(19)
F(12)-P(2)-F(9)	87.46(16)
F(10)-P(2)-F(9)	88.17(19)
F(8)-P(2)-F(9)	89.04(16)
F(11)-P(2)-F(9)	88.50(15)

Symmetry transformations used to generate equivalent atoms:

Table 4. Anisotropic displacement parameters (A^2 x 10^3) for **4**-Mn-**4**.
The anisotropic displacement factor exponent takes the form:
-2 pi^2 [h^2 a*^2 U11 + ... + 2 h k a* b* U12]

	U11	U22	U33	U23	U13	U12
Mn	39(1)	50(1)	27(1)	1(1)	-2(1)	6(1)
N(1)	38(1)	46(1)	31(1)	1(1)	0(1)	3(1)
C(2)	38(1)	48(1)	34(1)	1(1)	0(1)	1(1)
C(3)	49(1)	52(1)	38(1)	6(1)	0(1)	-2(1)
C(4)	44(1)	61(2)	31(1)	3(1)	-1(1)	2(1)
C(5)	48(1)	52(1)	34(1)	-4(1)	-4(1)	1(1)
C(6)	35(1)	48(1)	34(1)	-1(1)	1(1)	4(1)
C(7)	39(1)	49(1)	38(1)	-3(1)	0(1)	3(1)
N(8)	44(1)	51(1)	38(1)	-3(1)	-3(1)	5(1)
C(9)	56(2)	64(2)	45(1)	-12(1)	-9(1)	6(1)
C(10)	64(2)	62(2)	66(2)	-20(2)	-9(2)	-5(2)
C(11)	78(2)	56(2)	75(2)	-6(2)	2(2)	-18(2)
C(12)	73(2)	59(2)	50(2)	3(1)	0(1)	-10(2)
C(13)	38(1)	45(1)	38(1)	0(1)	1(1)	5(1)
N(14)	41(1)	48(1)	37(1)	2(1)	2(1)	5(1)
C(15)	52(1)	54(2)	44(1)	8(1)	5(1)	8(1)
C(16)	62(2)	48(2)	69(2)	12(1)	9(1)	1(1)
C(17)	74(2)	49(2)	70(2)	-3(1)	-1(2)	-10(1)
C(18)	65(2)	55(2)	48(2)	-3(1)	-5(1)	-5(1)
O(19)	68(1)	71(1)	33(1)	8(1)	-8(1)	-11(1)
C(20)	62(2)	67(2)	35(1)	3(1)	-8(1)	2(1)
C(21)	46(1)	62(2)	35(1)	4(1)	-6(1)	-4(1)
C(22)	64(2)	71(2)	48(2)	1(1)	7(1)	3(2)
C(23)	63(2)	69(2)	69(2)	6(2)	-3(2)	11(2)
C(24)	57(2)	66(2)	52(2)	13(1)	-15(1)	-11(1)
C(25)	73(2)	95(2)	35(1)	5(1)	-3(1)	2(2)
C(26)	59(2)	87(2)	41(1)	0(1)	-3(1)	12(2)
C(27)	94(3)	94(3)	73(2)	30(2)	-29(2)	-8(2)
N(28)	38(1)	47(1)	32(1)	1(1)	-1(1)	3(1)
C(29)	39(1)	49(1)	34(1)	1(1)	-2(1)	0(1)
C(30)	45(1)	62(2)	37(1)	5(1)	-4(1)	6(1)
C(31)	52(1)	59(2)	28(1)	2(1)	-2(1)	-4(1)
C(32)	45(1)	60(2)	34(1)	-3(1)	4(1)	1(1)
C(33)	39(1)	47(1)	35(1)	-2(1)	0(1)	1(1)
C(34)	39(1)	52(1)	37(1)	4(1)	0(1)	5(1)
N(35)	40(1)	52(1)	34(1)	4(1)	1(1)	5(1)
C(36)	52(2)	67(2)	39(1)	7(1)	9(1)	10(1)
C(37)	53(2)	89(2)	56(2)	9(2)	17(1)	20(2)
C(38)	51(2)	111(3)	66(2)	20(2)	10(1)	34(2)
C(39)	51(2)	98(2)	46(2)	17(2)	2(1)	26(2)
C(40)	39(1)	55(2)	41(1)	-4(1)	1(1)	5(1)
N(41)	38(1)	52(1)	37(1)	0(1)	0(1)	5(1)
C(42)	49(2)	71(2)	48(2)	3(1)	-2(1)	13(1)
C(43)	50(2)	101(3)	73(2)	5(2)	-2(2)	30(2)
C(44)	62(2)	147(4)	70(2)	-9(2)	12(2)	47(2)
C(45)	62(2)	137(3)	46(2)	-2(2)	12(1)	36(2)
O(46)	64(1)	90(2)	29(1)	8(1)	-1(1)	10(1)
C(47)	64(2)	78(2)	33(1)	4(1)	3(1)	5(2)
C(48)	66(2)	60(2)	32(1)	5(1)	4(1)	-6(1)
C(49)	88(2)	57(2)	46(2)	2(1)	7(2)	4(2)
C(50)	117(3)	61(2)	36(1)	-8(1)	2(2)	1(2)
C(51)	102(3)	58(2)	38(1)	-2(1)	-12(2)	-5(2)
C(52)	100(2)	58(2)	47(2)	0(1)	-9(2)	7(2)
C(53)	90(2)	64(2)	36(1)	-7(1)	1(1)	6(2)
C(54)	184(5)	87(3)	47(2)	-2(2)	-37(2)	9(3)
P(1)	78(1)	61(1)	46(1)	10(1)	-6(1)	-6(1)
F(1)	363(6)	108(2)	88(2)	-6(2)	84(3)	-11(3)
F(2)	167(2)	83(2)	68(1)	28(1)	-16(1)	-41(2)
F(3)	462(8)	85(2)	80(2)	8(2)	64(3)	60(3)
F(4)	102(2)	68(1)	81(1)	26(1)	4(1)	10(1)
F(5)	111(2)	191(4)	315(6)	121(4)	-81(3)	-66(3)

F(6)	104(2)	161(3)	268(5)	137(3)	-66(3)	-21(2)
P(2)	52(1)	91(1)	60(1)	11(1)	4(1)	8(1)
F(7)	95(2)	107(2)	248(4)	-3(2)	38(2)	-27(2)
F(8)	92(2)	125(2)	92(2)	31(1)	9(1)	33(1)
F(9)	76(1)	191(3)	70(1)	6(2)	4(1)	-33(2)
F(10)	145(3)	174(3)	165(3)	80(3)	20(2)	78(2)
F(11)	98(2)	185(3)	65(1)	1(2)	24(1)	13(2)
F(12)	108(2)	164(3)	106(2)	-57(2)	-1(2)	36(2)

Table 5. Hydrogen coordinates (x 10^4) and isotropic displacement parameters (A^2 x 10^3) for **4**-Mn-**4**.

	x	y	z	U(eq)
H(3)	4996	3221	92	55
H(5)	3284	611	-28	53
H(9)	6876	3183	1674	66
H(10)	7880	4599	1517	77
H(11)	7631	5091	903	84
H(12)	6342	4151	465	73
H(15)	4021	-680	1517	60
H(16)	2836	-1974	1263	71
H(17)	2231	-1993	622	77
H(18)	2783	-696	270	68
H(20A)	1989	1334	-487	66
H(20B)	3386	1097	-711	66
H(22)	688	2920	-660	73
H(23)	-368	3760	-1154	81
H(25)	2266	2449	-1832	82
H(26)	3340	1618	-1341	75
H(27A)	868	3969	-2030	133
H(27B)	-457	4244	-1789	133
H(27C)	-535	3317	-2025	133
H(30)	7897	160	2497	58
H(32)	3990	1405	2676	56
H(36)	8025	679	891	63
H(37)	10292	-67	1004	78
H(38)	11004	-515	1605	91
H(39)	9469	-178	2079	78
H(42)	1907	2224	1136	68
H(43)	-90	2791	1429	90
H(44)	-13	2782	2070	111
H(45)	2054	2156	2402	98
H(47A)	4383	503	3239	70
H(47B)	5143	1500	3268	70
H(49)	5179	1675	3926	76
H(50)	6218	1325	4508	86
H(52)	8075	-972	4108	83
H(53)	7060	-606	3521	76
H(54A)	8216	489	4886	162
H(54B)	8874	-442	4731	162
H(54C)	7298	-448	4893	162

Table 6. Torsion angles [deg] for **4**-Mn-**4**.

N(28)-Mn-N(1)-C(6)	-19(2)
N(35)-Mn-N(1)-C(6)	89.77(18)
N(8)-Mn-N(1)-C(6)	-178.96(19)
N(41)-Mn-N(1)-C(6)	-86.98(18)
N(14)-Mn-N(1)-C(6)	1.58(16)
N(28)-Mn-N(1)-C(2)	157.5(19)
N(35)-Mn-N(1)-C(2)	-93.91(18)
N(8)-Mn-N(1)-C(2)	-2.64(17)
N(41)-Mn-N(1)-C(2)	89.34(18)
N(14)-Mn-N(1)-C(2)	177.90(19)
C(6)-N(1)-C(2)-C(3)	2.0(3)
Mn-N(1)-C(2)-C(3)	-174.41(18)
C(6)-N(1)-C(2)-C(7)	-178.8(2)
Mn-N(1)-C(2)-C(7)	4.9(3)
N(1)-C(2)-C(3)-C(4)	-1.1(4)
C(7)-C(2)-C(3)-C(4)	179.7(2)
C(2)-C(3)-C(4)-O(19)	177.7(2)
C(2)-C(3)-C(4)-C(5)	-1.6(4)
O(19)-C(4)-C(5)-C(6)	-176.0(2)
C(3)-C(4)-C(5)-C(6)	3.2(4)
C(2)-N(1)-C(6)-C(5)	-0.1(3)
Mn-N(1)-C(6)-C(5)	176.16(18)
C(2)-N(1)-C(6)-C(13)	-178.5(2)
Mn-N(1)-C(6)-C(13)	-2.2(3)
C(4)-C(5)-C(6)-N(1)	-2.4(4)
C(4)-C(5)-C(6)-C(13)	175.8(2)
N(1)-C(2)-C(7)-N(8)	-4.9(3)
C(3)-C(2)-C(7)-N(8)	174.3(2)
N(1)-C(2)-C(7)-C(12)	173.9(3)
C(3)-C(2)-C(7)-C(12)	-6.8(4)
C(12)-C(7)-N(8)-C(9)	-0.9(4)
C(2)-C(7)-N(8)-C(9)	177.9(2)
C(12)-C(7)-N(8)-Mn	-176.2(2)
C(2)-C(7)-N(8)-Mn	2.7(3)
N(28)-Mn-N(8)-C(9)	5.6(2)
N(1)-Mn-N(8)-C(9)	-175.2(2)
N(35)-Mn-N(8)-C(9)	-68.0(2)
N(41)-Mn-N(8)-C(9)	79.2(2)
N(14)-Mn-N(8)-C(9)	-174.29(19)
N(28)-Mn-N(8)-C(7)	-179.45(17)
N(1)-Mn-N(8)-C(7)	-0.23(17)
N(35)-Mn-N(8)-C(7)	106.94(18)
N(41)-Mn-N(8)-C(7)	-105.81(18)
N(14)-Mn-N(8)-C(7)	0.6(2)
C(7)-N(8)-C(9)-C(10)	0.3(4)
Mn-N(8)-C(9)-C(10)	175.2(2)
N(8)-C(9)-C(10)-C(11)	0.0(5)
C(9)-C(10)-C(11)-C(12)	0.4(5)
C(10)-C(11)-C(12)-C(7)	-1.0(5)
N(8)-C(7)-C(12)-C(11)	1.3(5)
C(2)-C(7)-C(12)-C(11)	-177.5(3)
N(1)-C(6)-C(13)-N(14)	1.6(3)
C(5)-C(6)-C(13)-N(14)	-176.8(2)
N(1)-C(6)-C(13)-C(18)	-179.6(2)
C(5)-C(6)-C(13)-C(18)	2.0(4)
C(18)-C(13)-N(14)-C(15)	-0.4(4)
C(6)-C(13)-N(14)-C(15)	178.4(2)
C(18)-C(13)-N(14)-Mn	-179.1(2)
C(6)-C(13)-N(14)-Mn	-0.3(3)
N(28)-Mn-N(14)-C(15)	0.0(2)
N(1)-Mn-N(14)-C(15)	-179.2(2)
N(35)-Mn-N(14)-C(15)	72.8(2)
N(8)-Mn-N(14)-C(15)	179.88(18)
N(41)-Mn-N(14)-C(15)	-72.8(2)
N(28)-Mn-N(14)-C(13)	178.63(16)
N(1)-Mn-N(14)-C(13)	-0.59(16)
N(35)-Mn-N(14)-C(13)	-108.56(17)

N(8)-Mn-N(14)-C(13)	-1.5(2)
N(41)-Mn-N(14)-C(13)	105.89(17)
C(13)-N(14)-C(15)-C(16)	-0.3(4)
Mn-N(14)-C(15)-C(16)	178.3(2)
N(14)-C(15)-C(16)-C(17)	1.0(4)
C(15)-C(16)-C(17)-C(18)	-0.9(5)
C(16)-C(17)-C(18)-C(13)	0.2(5)
N(14)-C(13)-C(18)-C(17)	0.5(4)
C(6)-C(13)-C(18)-C(17)	-178.3(3)
C(3)-C(4)-O(19)-C(20)	-173.2(2)
C(5)-C(4)-O(19)-C(20)	6.0(4)
C(4)-O(19)-C(20)-C(21)	161.9(2)
O(19)-C(20)-C(21)-C(26)	110.3(3)
O(19)-C(20)-C(21)-C(22)	-72.0(3)
C(26)-C(21)-C(22)-C(23)	0.0(5)
C(20)-C(21)-C(22)-C(23)	-177.8(3)
C(21)-C(22)-C(23)-C(24)	0.4(5)
C(22)-C(23)-C(24)-C(25)	-0.5(5)
C(22)-C(23)-C(24)-C(27)	178.7(3)
C(23)-C(24)-C(25)-C(26)	0.2(5)
C(27)-C(24)-C(25)-C(26)	-179.0(3)
C(22)-C(21)-C(26)-C(25)	-0.3(5)
C(20)-C(21)-C(26)-C(25)	177.4(3)
C(24)-C(25)-C(26)-C(21)	0.2(5)
N(1)-Mn-N(28)-C(33)	-72(2)
N(35)-Mn-N(28)-C(33)	178.7(2)
N(8)-Mn-N(28)-C(33)	87.81(19)
N(41)-Mn-N(28)-C(33)	-3.30(18)
N(14)-Mn-N(28)-C(33)	-92.25(19)
N(1)-Mn-N(28)-C(29)	107(2)
N(35)-Mn-N(28)-C(29)	-1.93(18)
N(8)-Mn-N(28)-C(29)	-92.79(19)
N(41)-Mn-N(28)-C(29)	176.1(2)
N(14)-Mn-N(28)-C(29)	87.15(19)
C(33)-N(28)-C(29)-C(30)	1.0(4)
Mn-N(28)-C(29)-C(30)	-178.4(2)
C(33)-N(28)-C(29)-C(34)	-179.0(2)
Mn-N(28)-C(29)-C(34)	1.6(3)
N(28)-C(29)-C(30)-C(31)	-1.9(4)
C(34)-C(29)-C(30)-C(31)	178.1(2)
C(29)-C(30)-C(31)-O(46)	-178.9(2)
C(29)-C(30)-C(31)-C(32)	1.6(4)
O(46)-C(31)-C(32)-C(33)	-179.9(3)
C(30)-C(31)-C(32)-C(33)	-0.4(4)
C(29)-N(28)-C(33)-C(32)	0.3(4)
Mn-N(28)-C(33)-C(32)	179.71(19)
C(29)-N(28)-C(33)-C(40)	-178.2(2)
Mn-N(28)-C(33)-C(40)	1.2(3)
C(31)-C(32)-C(33)-N(28)	-0.6(4)
C(31)-C(32)-C(33)-C(40)	177.8(2)
N(28)-C(29)-C(34)-N(35)	0.3(3)
C(30)-C(29)-C(34)-N(35)	-179.7(2)
N(28)-C(29)-C(34)-C(39)	-179.9(3)
C(30)-C(29)-C(34)-C(39)	0.2(4)
C(39)-C(34)-N(35)-C(36)	0.0(4)
C(29)-C(34)-N(35)-C(36)	179.8(2)
C(39)-C(34)-N(35)-Mn	178.2(2)
C(29)-C(34)-N(35)-Mn	-1.9(3)
N(28)-Mn-N(35)-C(36)	-179.8(2)
N(1)-Mn-N(35)-C(36)	2.3(2)
N(8)-Mn-N(35)-C(36)	-71.5(2)
N(41)-Mn-N(35)-C(36)	176.9(2)
N(14)-Mn-N(35)-C(36)	74.6(2)
N(28)-Mn-N(35)-C(34)	2.02(18)
N(1)-Mn-N(35)-C(34)	-175.83(18)
N(8)-Mn-N(35)-C(34)	110.34(19)
N(41)-Mn-N(35)-C(34)	-1.2(3)
N(14)-Mn-N(35)-C(34)	-103.52(19)
C(34)-N(35)-C(36)-C(37)	0.0(4)
Mn-N(35)-C(36)-C(37)	-178.2(2)
N(35)-C(36)-C(37)-C(38)	0.5(5)

C(36)-C(37)-C(38)-C(39)	-0.8(6)
C(37)-C(38)-C(39)-C(34)	0.7(6)
N(35)-C(34)-C(39)-C(38)	-0.3(5)
C(29)-C(34)-C(39)-C(38)	179.9(3)
N(28)-C(33)-C(40)-N(41)	3.4(3)
C(32)-C(33)-C(40)-N(41)	-175.0(2)
N(28)-C(33)-C(40)-C(45)	-177.8(3)
C(32)-C(33)-C(40)-C(45)	3.8(5)
C(45)-C(40)-N(41)-C(42)	-1.8(4)
C(33)-C(40)-N(41)-C(42)	177.0(2)
C(45)-C(40)-N(41)-Mn	174.9(3)
C(33)-C(40)-N(41)-Mn	-6.3(3)
N(28)-Mn-N(41)-C(42)	-178.3(2)
N(1)-Mn-N(41)-C(42)	-0.4(2)
N(35)-Mn-N(41)-C(42)	-175.1(2)
N(8)-Mn-N(41)-C(42)	73.4(2)
N(14)-Mn-N(41)-C(42)	-72.8(2)
N(28)-Mn-N(41)-C(40)	5.14(18)
N(1)-Mn-N(41)-C(40)	-176.97(18)
N(35)-Mn-N(41)-C(40)	8.4(3)
N(8)-Mn-N(41)-C(40)	-103.11(19)
N(14)-Mn-N(41)-C(40)	110.71(19)
C(40)-N(41)-C(42)-C(43)	0.9(5)
Mn-N(41)-C(42)-C(43)	-175.5(3)
N(41)-C(42)-C(43)-C(44)	0.6(6)
C(42)-C(43)-C(44)-C(45)	-1.1(7)
N(41)-C(40)-C(45)-C(44)	1.2(6)
C(33)-C(40)-C(45)-C(44)	-177.5(4)
C(43)-C(44)-C(45)-C(40)	0.2(7)
C(32)-C(31)-O(46)-C(47)	-1.2(4)
C(30)-C(31)-O(46)-C(47)	179.3(3)
C(31)-O(46)-C(47)-C(48)	-176.1(2)
O(46)-C(47)-C(48)-C(53)	-35.0(4)
O(46)-C(47)-C(48)-C(49)	145.9(3)
C(53)-C(48)-C(49)-C(50)	0.8(5)
C(47)-C(48)-C(49)-C(50)	180.0(3)
C(48)-C(49)-C(50)-C(51)	-0.6(6)
C(49)-C(50)-C(51)-C(52)	-0.2(6)
C(49)-C(50)-C(51)-C(54)	178.7(4)
C(50)-C(51)-C(52)-C(53)	0.7(6)
C(54)-C(51)-C(52)-C(53)	-178.2(4)
C(49)-C(48)-C(53)-C(52)	-0.3(5)
C(47)-C(48)-C(53)-C(52)	-179.4(3)
C(51)-C(52)-C(53)-C(48)	-0.5(6)

Symmetry transformations used to generate equivalent atoms:

Table 7. Hydrogen bonds for **4**-Mn-**4** [A and deg.].

D-H...A	d(D-H)	d(H...A)	d(D...A)	<(DHA)

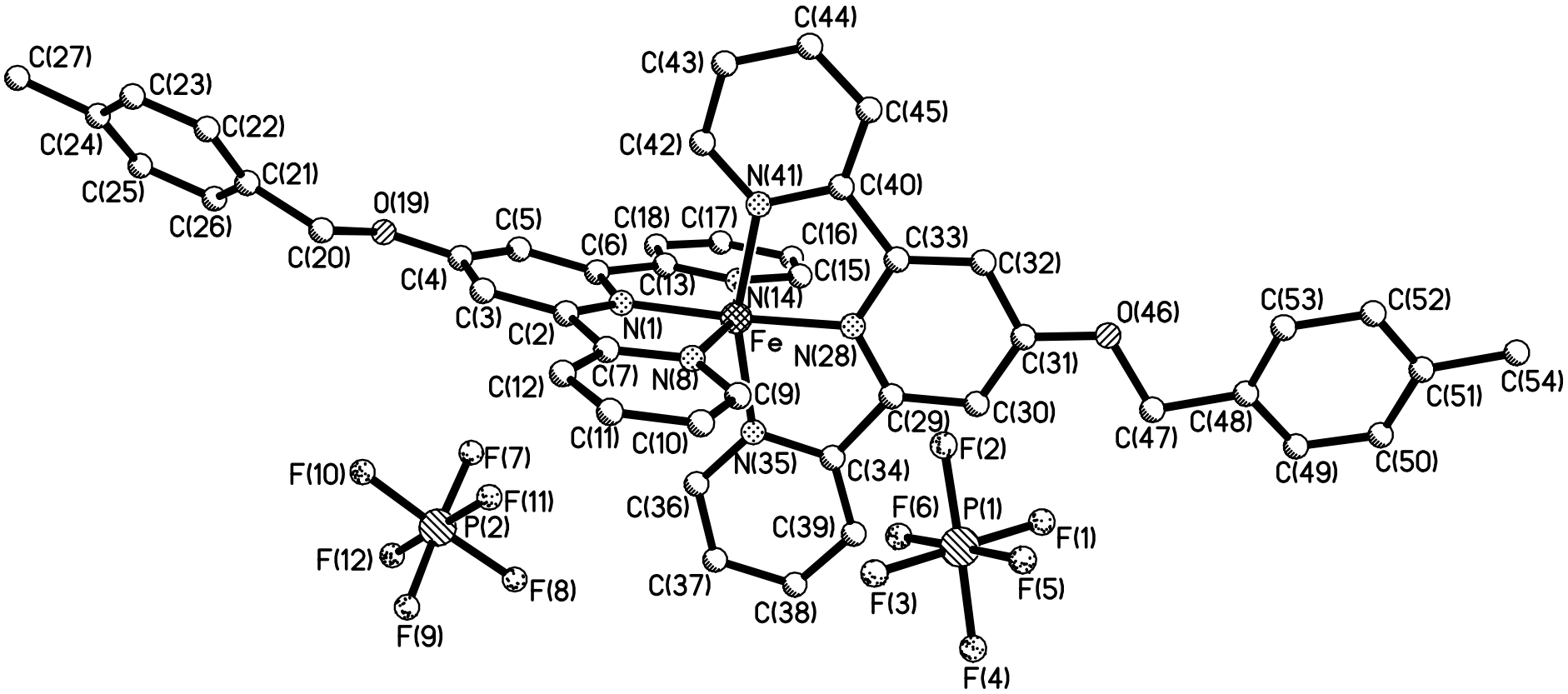
C(44)
C(43)
C(45)
C(42)
N(41)
C(40)
C(27)
C(23)
C(22)
C(24)
C(21)
C(25)
C(26)
O(19)
C(20)
C(5)
C(18)
C(17)
C(16)
C(33)
C(32)
C(6)
C(4)
C(13)
C(15)
N(14)
C(3)
C(2)
N(1)
Fe
N(28)
O(46)
C(53)
C(52)
C(12)
C(7)
N(8)
C(9)
C(31)
C(54)
C(51)
C(11)
C(10)
C(29)
C(30)
C(47)
C(48)
C(49)
C(50)
F(2)
F(7)
F(10)
N(35)
C(34)
F(11)
P(2)
C(36)
F(6)
P(1)
F(1)
C(39)
F(12)
F(5)
C(37)
C(38)
F(3)
F(8)
F(9)
F(4)

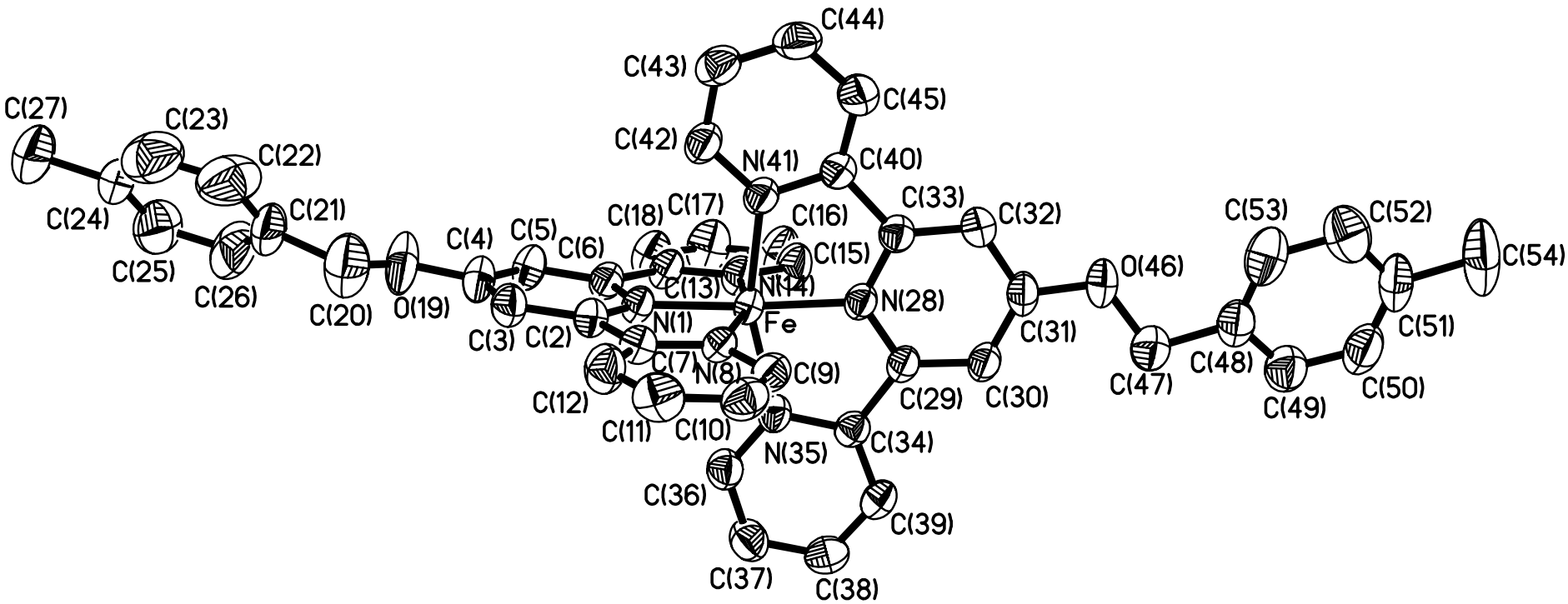
C(44)
C(43)
C(45)
C(27)
C(23)
C(42)
N(41)
C(40)
C(22)
C(33)
C(32)
C(53)
C(52)
C(24)
C(21)
C(18)
C(17)
C(16)
C(15)
C(54)
C(4)
C(5)
C(6)
O(46)
C(25)
C(13)
N(14)
N(28)
C(51)
C(26)
C(20)
O(19)
N(1)
Fe
C(31)
C(3)
C(2)
C(7)
N(8)
C(9)
C(48)
C(47)
C(12)
C(29)
C(30)
C(50)
C(11)
C(10)
C(49)
N(35)
C(34)
C(36)
C(39)
C(37)
C(38)

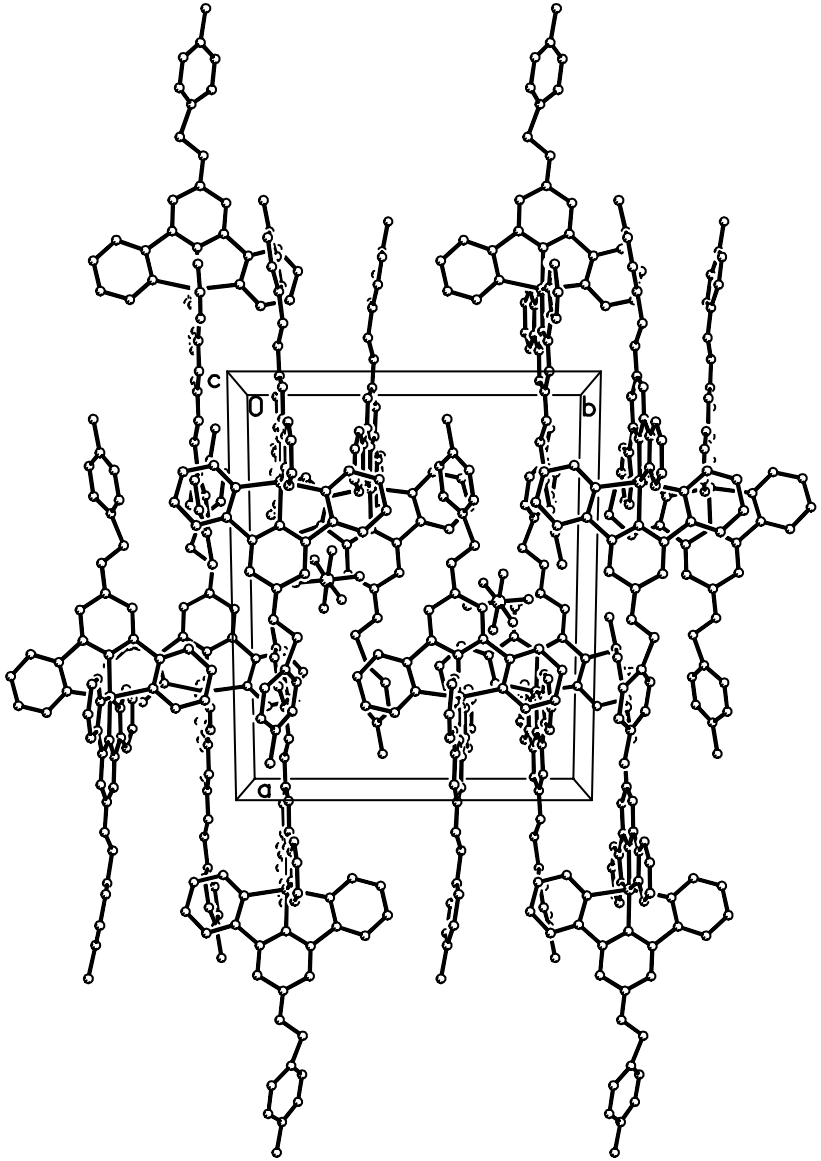
c
0
b
a

Table 1. Crystal data and structure refinement for **4**-Fe-**4**.

Identification code	**4**-Fe-**4**
Empirical formula	C46 H38 F12 Fe N6 O2 P2
Formula weight	1052.61
Temperature	295(2) K
Wavelength	0.71073 A
Crystal system, space group	monoclinic, P2(1)/c
Unit cell dimensions	a = 19.4584(19) A alpha = 90 deg. b = 15.5394(16) A beta = 110.248(2) deg. c = 15.9997(16) A gamma = 90 deg.
Volume	4538.9(8) A^3
Z, Calculated density	4, 1.540 Mg/m^3
Absorption coefficient	0.499 mm^-1
F(000)	2144
Crystal size	0.43 x 0.15 x 0.12 mm
Theta range for data collection	1.94 to 25.99 deg.
Limiting indices	-23<=h<=24, -19<=k<=19, -19<=l<=19
Reflections collected / unique	37243 / 8835 [R(int) = 0.0770]
Completeness to theta = 25.99	99.2 %
Max. and min. transmission	0.9425 and 0.8140
Refinement method	Full-matrix least-squares on F^2
Data / restraints / parameters	8835 / 0 / 622
Goodness-of-fit on F^2	1.013
Final R indices [I>2sigma(I)]	R1 = 0.0662, wR2 = 0.1635
R indices (all data)	R1 = 0.1008, wR2 = 0.1930
Largest diff. peak and hole	1.217 and -0.362 e.A^-3

Table 2. Atomic coordinates (x 10^4) and equivalent isotropic displacement parameters (A^2 x 10^3) for **4**-Fe-**4**.
U(eq) is defined as one third of the trace of the orthogonalized Uij tensor.

	x	y	z	U(eq)
Fe	2410(1)	3705(1)	2595(1)	36(1)
N(1)	3447(2)	3736(2)	3103(2)	39(1)
P(1)	91(1)	1062(1)	2249(1)	62(1)
F(1)	-542(2)	1740(2)	1947(3)	134(2)
P(2)	4732(1)	2507(1)	5930(1)	68(1)
C(2)	3834(2)	3020(2)	3116(2)	42(1)
F(2)	364(2)	1361(3)	1472(2)	118(1)
C(3)	4589(2)	3050(3)	3358(3)	49(1)
F(3)	732(2)	376(2)	2560(3)	100(1)
C(4)	4942(2)	3827(3)	3587(3)	52(1)
F(4)	-160(2)	753(2)	3046(2)	96(1)
C(5)	4538(2)	4571(3)	3583(3)	51(1)
F(5)	-435(2)	363(2)	1633(2)	108(1)
C(6)	3792(2)	4496(2)	3339(2)	43(1)
F(6)	627(2)	1743(2)	2881(2)	88(1)
C(7)	3352(2)	2263(2)	2829(2)	43(1)
F(7)	4636(2)	3432(2)	5486(2)	113(1)
N(8)	2631(2)	2460(2)	2565(2)	39(1)
F(8)	4019(2)	2662(3)	6180(3)	116(1)
C(9)	2147(2)	1810(2)	2328(2)	45(1)
F(9)	4797(2)	1617(2)	6399(3)	129(1)
C(10)	2349(2)	970(3)	2311(3)	54(1)
F(10)	5426(2)	2393(3)	5658(3)	134(2)
C(11)	3084(3)	772(3)	2559(3)	61(1)
F(11)	4229(2)	2117(3)	5014(2)	123(1)
C(12)	3593(2)	1429(3)	2819(3)	57(1)
F(12)	5207(2)	2943(3)	6839(2)	108(1)
C(13)	3261(2)	5200(2)	3252(3)	46(1)
N(14)	2552(2)	4957(2)	2867(2)	45(1)
C(15)	2031(2)	5555(3)	2769(3)	58(1)
C(16)	2191(3)	6393(3)	3056(4)	72(1)
C(17)	2910(3)	6629(3)	3437(4)	72(1)
C(18)	3454(3)	6032(3)	3544(3)	61(1)
O(19)	5675(2)	3927(3)	3806(3)	84(1)
C(20)	6105(3)	3268(4)	3749(5)	94(2)
C(21)	6874(3)	3615(5)	3864(4)	87(2)
C(22)	7185(4)	3317(5)	3326(4)	103(2)
C(23)	7895(4)	3443(4)	3469(5)	99(2)
C(24)	8332(3)	3896(4)	4151(4)	78(2)
C(25)	8032(3)	4274(4)	4696(4)	86(2)
C(26)	7301(3)	4162(5)	4563(4)	105(2)
C(27)	9130(3)	4063(8)	4299(6)	177(5)
N(28)	1377(2)	3711(2)	2027(2)	37(1)
C(29)	944(2)	3627(2)	2515(2)	38(1)
C(30)	191(2)	3645(2)	2125(3)	44(1)
C(31)	-116(2)	3764(2)	1217(3)	47(1)
C(32)	338(2)	3864(3)	710(3)	49(1)
C(33)	1084(2)	3830(2)	1140(2)	41(1)
C(34)	1379(2)	3520(2)	3466(2)	39(1)
N(35)	2115(2)	3523(2)	3644(2)	39(1)
C(36)	2555(2)	3410(3)	4490(3)	48(1)
C(37)	2292(2)	3298(3)	5177(3)	56(1)
C(38)	1544(2)	3313(3)	4997(3)	58(1)
C(39)	1087(2)	3422(3)	4136(3)	50(1)
C(40)	1658(2)	3907(2)	731(2)	44(1)
N(41)	2350(2)	3851(2)	1339(2)	41(1)
C(42)	2904(2)	3876(3)	1015(3)	50(1)
C(43)	2800(2)	3944(3)	122(3)	55(1)
C(44)	2098(3)	4024(3)	-472(3)	58(1)
C(45)	1518(2)	4002(3)	-162(3)	54(1)

O(46)	-840(2)	3810(2)	755(2)	64(1)
C(47)	-1334(2)	3646(3)	1203(3)	64(1)
C(48)	-2109(2)	3773(3)	581(3)	56(1)
C(49)	-2642(3)	3940(3)	938(4)	68(1)
C(50)	-3352(3)	4063(3)	409(4)	72(1)
C(51)	-3569(2)	4056(3)	-494(4)	69(1)
C(52)	-3037(3)	3875(3)	-876(4)	81(2)
C(53)	-2306(3)	3730(3)	-321(4)	75(1)
C(54)	-4349(3)	4234(4)	-1097(5)	111(2)

Table 3. Bond lengths [A] and angles [deg] for **4**-Fe-**4**.

Fe-N(1)	1.897(3)
Fe-N(28)	1.898(3)
Fe-N(35)	1.974(3)
Fe-N(41)	1.986(3)
Fe-N(8)	1.986(3)
Fe-N(14)	1.992(3)
N(1)-C(2)	1.339(5)
N(1)-C(6)	1.347(5)
P(1)-F(1)	1.565(3)
P(1)-F(5)	1.580(3)
P(1)-F(6)	1.582(3)
P(1)-F(2)	1.582(4)
P(1)-F(3)	1.585(3)
P(1)-F(4)	1.589(3)
P(2)-F(9)	1.558(4)
P(2)-F(10)	1.566(4)
P(2)-F(11)	1.576(3)
P(2)-F(12)	1.580(3)
P(2)-F(7)	1.585(4)
P(2)-F(8)	1.591(4)
C(2)-C(3)	1.385(5)
C(2)-C(7)	1.475(5)
C(3)-C(4)	1.375(6)
C(4)-O(19)	1.355(5)
C(4)-C(5)	1.398(6)
C(5)-C(6)	1.371(5)
C(6)-C(13)	1.478(5)
C(7)-N(8)	1.353(4)
C(7)-C(12)	1.380(6)
N(8)-C(9)	1.343(5)
C(9)-C(10)	1.367(6)
C(10)-C(11)	1.380(6)
C(11)-C(12)	1.382(6)
C(13)-N(14)	1.355(5)
C(13)-C(18)	1.382(6)
N(14)-C(15)	1.343(5)
C(15)-C(16)	1.381(6)
C(16)-C(17)	1.367(7)
C(17)-C(18)	1.373(6)
O(19)-C(20)	1.345(7)
C(20)-C(21)	1.542(7)
C(21)-C(22)	1.297(9)
C(21)-C(26)	1.421(9)
C(22)-C(23)	1.335(9)
C(23)-C(24)	1.330(9)
C(24)-C(25)	1.341(8)
C(24)-C(27)	1.511(8)
C(25)-C(26)	1.374(8)
N(28)-C(29)	1.339(4)
N(28)-C(33)	1.347(4)
C(29)-C(30)	1.380(5)
C(29)-C(34)	1.473(5)
C(30)-C(31)	1.379(5)
C(31)-O(46)	1.346(4)
C(31)-C(32)	1.400(6)
C(32)-C(33)	1.377(5)
C(33)-C(40)	1.481(5)
C(34)-N(35)	1.360(4)
C(34)-C(39)	1.384(5)
N(35)-C(36)	1.339(5)
C(36)-C(37)	1.374(6)
C(37)-C(38)	1.383(6)
C(38)-C(39)	1.366(6)
C(40)-N(41)	1.364(5)
C(40)-C(45)	1.367(5)
N(41)-C(42)	1.348(5)
C(42)-C(43)	1.375(6)

C(43)-C(44)	1.373(6)
C(44)-C(45)	1.382(6)
O(46)-C(47)	1.408(5)
C(47)-C(48)	1.505(6)
C(48)-C(53)	1.361(7)
C(48)-C(49)	1.370(7)
C(49)-C(50)	1.361(6)
C(50)-C(51)	1.358(7)
C(51)-C(52)	1.401(8)
C(51)-C(54)	1.516(6)
C(52)-C(53)	1.411(7)

N(1)-Fe-N(28)	176.53(13)
N(1)-Fe-N(35)	102.67(12)
N(28)-Fe-N(35)	80.54(12)
N(1)-Fe-N(41)	96.43(12)
N(28)-Fe-N(41)	80.40(12)
N(35)-Fe-N(41)	160.86(12)
N(1)-Fe-N(8)	80.12(12)
N(28)-Fe-N(8)	101.29(12)
N(35)-Fe-N(8)	90.63(12)
N(41)-Fe-N(8)	91.39(12)
N(1)-Fe-N(14)	80.51(12)
N(28)-Fe-N(14)	98.22(12)
N(35)-Fe-N(14)	90.73(12)
N(41)-Fe-N(14)	93.70(12)
N(8)-Fe-N(14)	160.40(12)
C(2)-N(1)-C(6)	120.1(3)
C(2)-N(1)-Fe	119.6(2)
C(6)-N(1)-Fe	119.7(2)
F(1)-P(1)-F(5)	90.1(2)
F(1)-P(1)-F(6)	91.2(2)
F(5)-P(1)-F(6)	178.6(2)
F(1)-P(1)-F(2)	90.1(3)
F(5)-P(1)-F(2)	91.8(2)
F(6)-P(1)-F(2)	88.78(19)
F(1)-P(1)-F(3)	179.7(3)
F(5)-P(1)-F(3)	90.1(2)
F(6)-P(1)-F(3)	88.61(18)
F(2)-P(1)-F(3)	90.1(2)
F(1)-P(1)-F(4)	91.3(2)
F(5)-P(1)-F(4)	88.97(19)
F(6)-P(1)-F(4)	90.37(18)
F(2)-P(1)-F(4)	178.3(2)
F(3)-P(1)-F(4)	88.4(2)
F(9)-P(2)-F(10)	95.7(3)
F(9)-P(2)-F(11)	91.6(2)
F(10)-P(2)-F(11)	90.9(2)
F(9)-P(2)-F(12)	90.8(2)
F(10)-P(2)-F(12)	91.1(2)
F(11)-P(2)-F(12)	176.8(3)
F(9)-P(2)-F(7)	176.5(3)
F(10)-P(2)-F(7)	87.6(2)
F(11)-P(2)-F(7)	89.6(2)
F(12)-P(2)-F(7)	88.0(2)
F(9)-P(2)-F(8)	86.9(2)
F(10)-P(2)-F(8)	177.4(3)
F(11)-P(2)-F(8)	88.7(2)
F(12)-P(2)-F(8)	89.2(2)
F(7)-P(2)-F(8)	89.9(2)
N(1)-C(2)-C(3)	120.8(3)
N(1)-C(2)-C(7)	111.4(3)
C(3)-C(2)-C(7)	127.8(3)
C(4)-C(3)-C(2)	119.2(4)
O(19)-C(4)-C(3)	123.7(4)
O(19)-C(4)-C(5)	116.5(4)
C(3)-C(4)-C(5)	119.8(4)
C(6)-C(5)-C(4)	118.0(4)
N(1)-C(6)-C(5)	122.0(3)
N(1)-C(6)-C(13)	111.0(3)
C(5)-C(6)-C(13)	127.0(3)

N(8)-C(7)-C(12)	121.9(4)
N(8)-C(7)-C(2)	113.3(3)
C(12)-C(7)-C(2)	124.8(3)
C(9)-N(8)-C(7)	118.0(3)
C(9)-N(8)-Fe	127.0(3)
C(7)-N(8)-Fe	115.0(2)
N(8)-C(9)-C(10)	123.0(4)
C(9)-C(10)-C(11)	119.0(4)
C(10)-C(11)-C(12)	119.0(4)
C(7)-C(12)-C(11)	119.1(4)
N(14)-C(13)-C(18)	122.0(4)
N(14)-C(13)-C(6)	114.0(3)
C(18)-C(13)-C(6)	124.1(4)
C(15)-N(14)-C(13)	118.0(3)
C(15)-N(14)-Fe	127.5(3)
C(13)-N(14)-Fe	114.4(2)
N(14)-C(15)-C(16)	122.6(4)
C(17)-C(16)-C(15)	118.6(4)
C(16)-C(17)-C(18)	120.0(4)
C(17)-C(18)-C(13)	118.8(4)
C(20)-O(19)-C(4)	121.1(4)
O(19)-C(20)-C(21)	109.0(5)
C(22)-C(21)-C(26)	117.1(5)
C(22)-C(21)-C(20)	116.9(6)
C(26)-C(21)-C(20)	125.6(6)
C(21)-C(22)-C(23)	121.8(6)
C(24)-C(23)-C(22)	123.2(6)
C(23)-C(24)-C(25)	117.9(5)
C(23)-C(24)-C(27)	123.3(7)
C(25)-C(24)-C(27)	118.6(7)
C(24)-C(25)-C(26)	120.3(5)
C(25)-C(26)-C(21)	119.3(5)
C(29)-N(28)-C(33)	120.4(3)
C(29)-N(28)-Fe	119.8(2)
C(33)-N(28)-Fe	119.8(2)
N(28)-C(29)-C(30)	121.3(3)
N(28)-C(29)-C(34)	111.1(3)
C(30)-C(29)-C(34)	127.6(3)
C(31)-C(30)-C(29)	118.9(3)
O(46)-C(31)-C(30)	125.1(4)
O(46)-C(31)-C(32)	115.2(3)
C(30)-C(31)-C(32)	119.7(3)
C(33)-C(32)-C(31)	118.3(3)
N(28)-C(33)-C(32)	121.4(3)
N(28)-C(33)-C(40)	111.6(3)
C(32)-C(33)-C(40)	127.0(3)
N(35)-C(34)-C(39)	121.5(3)
N(35)-C(34)-C(29)	113.7(3)
C(39)-C(34)-C(29)	124.8(3)
C(36)-N(35)-C(34)	118.0(3)
C(36)-N(35)-Fe	127.3(3)
C(34)-N(35)-Fe	114.7(2)
N(35)-C(36)-C(37)	122.7(4)
C(36)-C(37)-C(38)	119.2(4)
C(39)-C(38)-C(37)	118.8(4)
C(38)-C(39)-C(34)	119.8(4)
N(41)-C(40)-C(45)	122.8(4)
N(41)-C(40)-C(33)	112.9(3)
C(45)-C(40)-C(33)	124.3(3)
C(42)-N(41)-C(40)	116.6(3)
C(42)-N(41)-Fe	128.1(3)
C(40)-N(41)-Fe	115.3(2)
N(41)-C(42)-C(43)	123.5(4)
C(44)-C(43)-C(42)	118.7(4)
C(43)-C(44)-C(45)	119.3(4)
C(40)-C(45)-C(44)	119.0(4)
C(31)-O(46)-C(47)	118.7(3)
O(46)-C(47)-C(48)	110.1(4)
C(53)-C(48)-C(49)	118.4(4)
C(53)-C(48)-C(47)	123.0(4)
C(49)-C(48)-C(47)	118.6(4)

C(50)-C(49)-C(48)	121.3(5)
C(51)-C(50)-C(49)	122.4(5)
C(50)-C(51)-C(52)	117.5(4)
C(50)-C(51)-C(54)	123.4(5)
C(52)-C(51)-C(54)	119.2(6)
C(51)-C(52)-C(53)	119.6(5)
C(48)-C(53)-C(52)	120.8(5)

Symmetry transformations used to generate equivalent atoms:

Table 4. Anisotropic displacement parameters (A^2 x 10^3) for **4**-Fe-**4**.
The anisotropic displacement factor exponent takes the form:
-2 pi^2 [h^2 a*^2 U11 + ... + 2 h k a* b* U12]

	U11	U22	U33	U23	U13	U12
Fe	26(1)	43(1)	41(1)	1(1)	14(1)	1(1)
N(1)	31(2)	45(2)	45(2)	0(1)	17(1)	1(1)
P(1)	42(1)	58(1)	78(1)	8(1)	10(1)	-10(1)
F(1)	62(2)	90(2)	231(5)	49(3)	25(2)	14(2)
P(2)	55(1)	82(1)	66(1)	2(1)	21(1)	-20(1)
C(2)	35(2)	47(2)	46(2)	3(2)	15(2)	5(2)
F(2)	103(3)	160(4)	82(2)	20(2)	20(2)	-53(2)
C(3)	37(2)	55(2)	54(2)	1(2)	16(2)	7(2)
F(3)	68(2)	86(2)	137(3)	6(2)	22(2)	16(2)
C(4)	31(2)	64(3)	62(2)	-5(2)	15(2)	0(2)
F(4)	88(2)	101(2)	108(2)	1(2)	46(2)	-28(2)
C(5)	34(2)	54(2)	65(2)	-8(2)	17(2)	-9(2)
F(5)	96(2)	98(2)	101(2)	0(2)	-2(2)	-48(2)
C(6)	37(2)	48(2)	46(2)	-1(2)	18(2)	-1(2)
F(6)	80(2)	72(2)	97(2)	-6(2)	15(2)	-26(2)
C(7)	39(2)	48(2)	43(2)	2(2)	15(2)	1(2)
F(7)	146(3)	93(2)	105(3)	17(2)	49(2)	-16(2)
N(8)	33(2)	49(2)	39(2)	1(1)	17(1)	-2(1)
F(8)	79(2)	155(3)	131(3)	-4(3)	58(2)	-17(2)
C(9)	42(2)	52(2)	43(2)	-2(2)	17(2)	-8(2)
F(9)	148(4)	91(3)	131(3)	27(2)	27(3)	-10(2)
C(10)	58(3)	51(2)	55(2)	-3(2)	24(2)	-13(2)
F(10)	90(3)	145(3)	195(4)	-50(3)	86(3)	-21(2)
C(11)	71(3)	43(2)	70(3)	1(2)	26(2)	4(2)
F(11)	125(3)	158(3)	78(2)	-17(2)	28(2)	-78(3)
C(12)	46(2)	52(3)	75(3)	4(2)	22(2)	9(2)
F(12)	101(3)	134(3)	79(2)	-11(2)	16(2)	-39(2)
C(13)	37(2)	47(2)	59(2)	0(2)	23(2)	-1(2)
N(14)	36(2)	44(2)	56(2)	3(1)	19(1)	2(1)
C(15)	41(2)	52(3)	84(3)	4(2)	27(2)	8(2)
C(16)	52(3)	50(3)	119(4)	3(3)	37(3)	11(2)
C(17)	66(3)	42(2)	112(4)	-12(2)	34(3)	-5(2)
C(18)	50(3)	51(2)	86(3)	-9(2)	30(2)	-5(2)
O(19)	33(2)	114(3)	105(3)	-18(2)	23(2)	9(2)
C(20)	59(3)	93(4)	126(5)	0(4)	26(3)	-1(3)
C(21)	32(2)	148(6)	77(4)	8(4)	14(2)	-7(3)
C(22)	105(5)	140(6)	64(3)	-15(4)	27(3)	-48(4)
C(23)	123(6)	97(4)	98(5)	5(4)	66(5)	17(4)
C(24)	41(3)	124(5)	75(3)	26(3)	26(2)	14(3)
C(25)	60(3)	110(5)	77(3)	-12(3)	12(3)	-30(3)
C(26)	73(4)	169(7)	92(4)	-12(4)	51(3)	24(4)
C(27)	48(4)	349(15)	139(7)	86(8)	39(4)	18(6)
N(28)	31(2)	41(2)	44(2)	1(1)	17(1)	2(1)
C(29)	31(2)	39(2)	46(2)	1(2)	16(2)	0(1)
C(30)	31(2)	47(2)	54(2)	5(2)	17(2)	0(2)
C(31)	28(2)	50(2)	58(2)	2(2)	8(2)	0(2)
C(32)	36(2)	61(3)	46(2)	7(2)	10(2)	3(2)
C(33)	37(2)	43(2)	45(2)	3(2)	15(2)	2(2)
C(34)	38(2)	36(2)	45(2)	1(2)	17(2)	1(2)
N(35)	33(2)	43(2)	43(2)	-2(1)	15(1)	4(1)
C(36)	40(2)	57(2)	47(2)	-2(2)	15(2)	4(2)
C(37)	49(2)	75(3)	43(2)	-1(2)	14(2)	12(2)
C(38)	61(3)	75(3)	46(2)	2(2)	28(2)	2(2)
C(39)	39(2)	65(3)	53(2)	2(2)	24(2)	1(2)
C(40)	38(2)	50(2)	45(2)	7(2)	17(2)	3(2)
N(41)	36(2)	45(2)	47(2)	4(1)	19(1)	3(1)
C(42)	39(2)	55(2)	62(2)	7(2)	25(2)	4(2)
C(43)	59(3)	54(2)	63(3)	6(2)	35(2)	8(2)
C(44)	68(3)	67(3)	47(2)	5(2)	30(2)	5(2)
C(45)	49(2)	63(3)	49(2)	3(2)	17(2)	5(2)
O(46)	28(1)	90(2)	69(2)	7(2)	11(1)	3(1)

C(47)	45(2)	76(3)	70(3)	13(2)	19(2)	3(2)
C(48)	41(2)	51(2)	71(3)	4(2)	15(2)	-1(2)
C(49)	53(3)	70(3)	79(3)	15(2)	22(2)	4(2)
C(50)	45(3)	74(3)	100(4)	12(3)	30(3)	-1(2)
C(51)	35(2)	58(3)	100(4)	0(3)	6(2)	-5(2)
C(52)	72(4)	82(4)	76(3)	-12(3)	9(3)	-7(3)
C(53)	51(3)	78(3)	101(4)	-12(3)	33(3)	2(2)
C(54)	42(3)	93(4)	165(6)	2(4)	-8(3)	1(3)

Table 5. Hydrogen coordinates (x 10^4) and isotropic displacement parameters (A^2 x 10^3) for **4**-Fe-**4**.

	x	y	z	U(eq)
H(3A)	4854	2550	3367	59
H(5A)	4768	5101	3741	61
H(9A)	1651	1938	2168	54
H(10A)	1997	539	2135	65
H(11A)	3234	205	2551	73
H(12A)	4091	1310	2986	69
H(15A)	1543	5397	2498	70
H(16A)	1818	6790	2990	86
H(17A)	3030	7193	3625	87
H(18A)	3944	6185	3807	73
H(20A)	5896	2988	3174	113
H(20B)	6137	2847	4209	113
H(22A)	6906	3008	2826	124
H(23A)	8095	3201	3072	119
H(25A)	8319	4614	5166	103
H(26A)	7088	4441	4926	126
H(27A)	9343	4394	4833	266
H(27B)	9171	4376	3801	266
H(27C)	9385	3525	4356	266
H(30A)	-105	3577	2470	52
H(32A)	140	3950	97	59
H(36A)	3059	3407	4617	58
H(37A)	2614	3214	5756	67
H(38A)	1355	3251	5454	70
H(39A)	582	3429	4001	60
H(42A)	3381	3846	1416	60
H(43A)	3197	3936	-75	66
H(44A)	2015	4093	-1077	69
H(45A)	1039	4050	-556	65
H(47A)	-1234	4032	1708	77
H(47B)	-1271	3060	1426	77
H(49A)	-2516	3970	1553	81
H(50A)	-3701	4156	676	86
H(52A)	-3165	3851	-1492	98
H(53A)	-1953	3604	-575	90
H(54A)	-4648	4343	-741	167
H(54B)	-4537	3744	-1473	167
H(54C)	-4357	4728	-1460	167

Table 6. Torsion angles [deg] for **4**-Fe-**4**.

N(28)-Fe-N(1)-C(2)	-107(2)
N(35)-Fe-N(1)-C(2)	95.9(3)
N(41)-Fe-N(1)-C(2)	-82.8(3)
N(8)-Fe-N(1)-C(2)	7.5(3)
N(14)-Fe-N(1)-C(2)	-175.5(3)
N(28)-Fe-N(1)-C(6)	65(2)
N(35)-Fe-N(1)-C(6)	-92.8(3)
N(41)-Fe-N(1)-C(6)	88.5(3)
N(8)-Fe-N(1)-C(6)	178.8(3)
N(14)-Fe-N(1)-C(6)	-4.2(3)
C(6)-N(1)-C(2)-C(3)	-0.9(5)
Fe-N(1)-C(2)-C(3)	170.3(3)
C(6)-N(1)-C(2)-C(7)	-179.6(3)
Fe-N(1)-C(2)-C(7)	-8.3(4)
N(1)-C(2)-C(3)-C(4)	0.0(6)
C(7)-C(2)-C(3)-C(4)	178.3(4)
C(2)-C(3)-C(4)-O(19)	-177.9(4)
C(2)-C(3)-C(4)-C(5)	0.8(6)
O(19)-C(4)-C(5)-C(6)	178.1(4)
C(3)-C(4)-C(5)-C(6)	-0.7(6)
C(2)-N(1)-C(6)-C(5)	1.1(5)
Fe-N(1)-C(6)-C(5)	-170.1(3)
C(2)-N(1)-C(6)-C(13)	178.5(3)
Fe-N(1)-C(6)-C(13)	7.2(4)
C(4)-C(5)-C(6)-N(1)	-0.3(6)
C(4)-C(5)-C(6)-C(13)	-177.2(4)
N(1)-C(2)-C(7)-N(8)	3.8(4)
C(3)-C(2)-C(7)-N(8)	-174.7(3)
N(1)-C(2)-C(7)-C(12)	-176.3(4)
C(3)-C(2)-C(7)-C(12)	5.1(6)
C(12)-C(7)-N(8)-C(9)	3.1(5)
C(2)-C(7)-N(8)-C(9)	-177.1(3)
C(12)-C(7)-N(8)-Fe	-178.0(3)
C(2)-C(7)-N(8)-Fe	1.8(4)
N(1)-Fe-N(8)-C(9)	174.0(3)
N(28)-Fe-N(8)-C(9)	-9.2(3)
N(35)-Fe-N(8)-C(9)	71.2(3)
N(41)-Fe-N(8)-C(9)	-89.7(3)
N(14)-Fe-N(8)-C(9)	165.2(3)
N(1)-Fe-N(8)-C(7)	-4.8(2)
N(28)-Fe-N(8)-C(7)	172.0(2)
N(35)-Fe-N(8)-C(7)	-107.5(2)
N(41)-Fe-N(8)-C(7)	91.5(2)
N(14)-Fe-N(8)-C(7)	-13.6(5)
C(7)-N(8)-C(9)-C(10)	-2.5(5)
Fe-N(8)-C(9)-C(10)	178.7(3)
N(8)-C(9)-C(10)-C(11)	0.9(6)
C(9)-C(10)-C(11)-C(12)	0.2(6)
N(8)-C(7)-C(12)-C(11)	-2.1(6)
C(2)-C(7)-C(12)-C(11)	178.1(4)
C(10)-C(11)-C(12)-C(7)	0.4(7)
N(1)-C(6)-C(13)-N(14)	-6.9(5)
C(5)-C(6)-C(13)-N(14)	170.2(4)
N(1)-C(6)-C(13)-C(18)	172.1(4)
C(5)-C(6)-C(13)-C(18)	-10.8(6)
C(18)-C(13)-N(14)-C(15)	0.3(6)
C(6)-C(13)-N(14)-C(15)	179.4(3)
C(18)-C(13)-N(14)-Fe	-175.2(3)
C(6)-C(13)-N(14)-Fe	3.9(4)
N(1)-Fe-N(14)-C(15)	-175.1(4)
N(28)-Fe-N(14)-C(15)	8.1(4)
N(35)-Fe-N(14)-C(15)	-72.4(4)
N(41)-Fe-N(14)-C(15)	89.0(4)
N(8)-Fe-N(14)-C(15)	-166.3(4)
N(1)-Fe-N(14)-C(13)	-0.1(3)
N(28)-Fe-N(14)-C(13)	-176.9(3)
N(35)-Fe-N(14)-C(13)	102.6(3)

N(41)-Fe-N(14)-C(13)	-96.0(3)
N(8)-Fe-N(14)-C(13)	8.7(5)
C(13)-N(14)-C(15)-C(16)	-1.0(7)
Fe-N(14)-C(15)-C(16)	173.9(4)
N(14)-C(15)-C(16)-C(17)	1.4(8)
C(15)-C(16)-C(17)-C(18)	-1.1(8)
C(16)-C(17)-C(18)-C(13)	0.5(8)
N(14)-C(13)-C(18)-C(17)	-0.1(7)
C(6)-C(13)-C(18)-C(17)	-179.1(4)
C(3)-C(4)-O(19)-C(20)	5.0(7)
C(5)-C(4)-O(19)-C(20)	-173.7(5)
C(4)-O(19)-C(20)-C(21)	169.2(4)
O(19)-C(20)-C(21)-C(22)	-136.6(7)
O(19)-C(20)-C(21)-C(26)	50.3(9)
C(26)-C(21)-C(22)-C(23)	6.7(11)
C(20)-C(21)-C(22)-C(23)	-167.0(6)
C(21)-C(22)-C(23)-C(24)	-1.8(12)
C(22)-C(23)-C(24)-C(25)	-3.0(10)
C(22)-C(23)-C(24)-C(27)	-178.0(7)
C(23)-C(24)-C(25)-C(26)	2.5(9)
C(27)-C(24)-C(25)-C(26)	177.7(7)
C(24)-C(25)-C(26)-C(21)	2.4(10)
C(22)-C(21)-C(26)-C(25)	-6.9(10)
C(20)-C(21)-C(26)-C(25)	166.1(6)
N(1)-Fe-N(28)-C(29)	-156(2)
N(35)-Fe-N(28)-C(29)	1.7(3)
N(41)-Fe-N(28)-C(29)	180.0(3)
N(8)-Fe-N(28)-C(29)	90.5(3)
N(14)-Fe-N(28)-C(29)	-87.6(3)
N(1)-Fe-N(28)-C(33)	22(2)
N(35)-Fe-N(28)-C(33)	179.4(3)
N(41)-Fe-N(28)-C(33)	-2.3(3)
N(8)-Fe-N(28)-C(33)	-91.8(3)
N(14)-Fe-N(28)-C(33)	90.1(3)
C(33)-N(28)-C(29)-C(30)	1.1(5)
Fe-N(28)-C(29)-C(30)	178.8(3)
C(33)-N(28)-C(29)-C(34)	-178.9(3)
Fe-N(28)-C(29)-C(34)	-1.2(4)
N(28)-C(29)-C(30)-C(31)	-1.0(5)
C(34)-C(29)-C(30)-C(31)	179.1(3)
C(29)-C(30)-C(31)-O(46)	-178.7(4)
C(29)-C(30)-C(31)-C(32)	0.1(6)
O(46)-C(31)-C(32)-C(33)	179.6(4)
C(30)-C(31)-C(32)-C(33)	0.6(6)
C(29)-N(28)-C(33)-C(32)	-0.4(5)
Fe-N(28)-C(33)-C(32)	-178.1(3)
C(29)-N(28)-C(33)-C(40)	-180.0(3)
Fe-N(28)-C(33)-C(40)	2.3(4)
C(31)-C(32)-C(33)-N(28)	-0.5(6)
C(31)-C(32)-C(33)-C(40)	179.0(4)
N(28)-C(29)-C(34)-N(35)	-0.4(4)
C(30)-C(29)-C(34)-N(35)	179.5(3)
N(28)-C(29)-C(34)-C(39)	179.7(3)
C(30)-C(29)-C(34)-C(39)	-0.3(6)
C(39)-C(34)-N(35)-C(36)	1.3(5)
C(29)-C(34)-N(35)-C(36)	-178.5(3)
C(39)-C(34)-N(35)-Fe	-178.4(3)
C(29)-C(34)-N(35)-Fe	1.8(4)
N(1)-Fe-N(35)-C(36)	-2.9(3)
N(28)-Fe-N(35)-C(36)	178.4(3)
N(41)-Fe-N(35)-C(36)	173.1(3)
N(8)-Fe-N(35)-C(36)	77.1(3)
N(14)-Fe-N(35)-C(36)	-83.4(3)
N(1)-Fe-N(35)-C(34)	176.8(2)
N(28)-Fe-N(35)-C(34)	-1.9(2)
N(41)-Fe-N(35)-C(34)	-7.2(5)
N(8)-Fe-N(35)-C(34)	-103.2(2)
N(14)-Fe-N(35)-C(34)	96.3(2)
C(34)-N(35)-C(36)-C(37)	-0.5(6)
Fe-N(35)-C(36)-C(37)	179.2(3)
N(35)-C(36)-C(37)-C(38)	-0.8(7)

C(36)-C(37)-C(38)-C(39)	1.3(7)
C(37)-C(38)-C(39)-C(34)	-0.5(7)
N(35)-C(34)-C(39)-C(38)	-0.9(6)
C(29)-C(34)-C(39)-C(38)	179.0(4)
N(28)-C(33)-C(40)-N(41)	-0.8(4)
C(32)-C(33)-C(40)-N(41)	179.7(4)
N(28)-C(33)-C(40)-C(45)	177.7(4)
C(32)-C(33)-C(40)-C(45)	-1.9(6)
C(45)-C(40)-N(41)-C(42)	-1.3(5)
C(33)-C(40)-N(41)-C(42)	177.1(3)
C(45)-C(40)-N(41)-Fe	-179.5(3)
C(33)-C(40)-N(41)-Fe	-1.0(4)
N(1)-Fe-N(41)-C(42)	5.3(3)
N(28)-Fe-N(41)-C(42)	-176.1(3)
N(35)-Fe-N(41)-C(42)	-170.8(3)
N(8)-Fe-N(41)-C(42)	-74.9(3)
N(14)-Fe-N(41)-C(42)	86.1(3)
N(1)-Fe-N(41)-C(40)	-176.8(3)
N(28)-Fe-N(41)-C(40)	1.7(3)
N(35)-Fe-N(41)-C(40)	7.0(5)
N(8)-Fe-N(41)-C(40)	102.9(3)
N(14)-Fe-N(41)-C(40)	-96.0(3)
C(40)-N(41)-C(42)-C(43)	-0.7(6)
Fe-N(41)-C(42)-C(43)	177.1(3)
N(41)-C(42)-C(43)-C(44)	2.6(6)
C(42)-C(43)-C(44)-C(45)	-2.4(6)
N(41)-C(40)-C(45)-C(44)	1.5(6)
C(33)-C(40)-C(45)-C(44)	-176.8(4)
C(43)-C(44)-C(45)-C(40)	0.5(6)
C(30)-C(31)-O(46)-C(47)	-6.3(6)
C(32)-C(31)-O(46)-C(47)	174.8(4)
C(31)-O(46)-C(47)-C(48)	177.2(4)
O(46)-C(47)-C(48)-C(53)	22.4(6)
O(46)-C(47)-C(48)-C(49)	-157.5(4)
C(53)-C(48)-C(49)-C(50)	-0.1(7)
C(47)-C(48)-C(49)-C(50)	179.8(4)
C(48)-C(49)-C(50)-C(51)	-2.1(8)
C(49)-C(50)-C(51)-C(52)	2.8(8)
C(49)-C(50)-C(51)-C(54)	-176.9(5)
C(50)-C(51)-C(52)-C(53)	-1.4(8)
C(54)-C(51)-C(52)-C(53)	178.4(5)
C(49)-C(48)-C(53)-C(52)	1.5(7)
C(47)-C(48)-C(53)-C(52)	-178.4(5)
C(51)-C(52)-C(53)-C(48)	-0.7(8)

Symmetry transformations used to generate equivalent atoms:

Table 7. Hydrogen bonds for **4**-Fe-**4** [A and deg.].

D-H...A	d(D-H)	d(H...A)	d(D...A)	<(DHA)

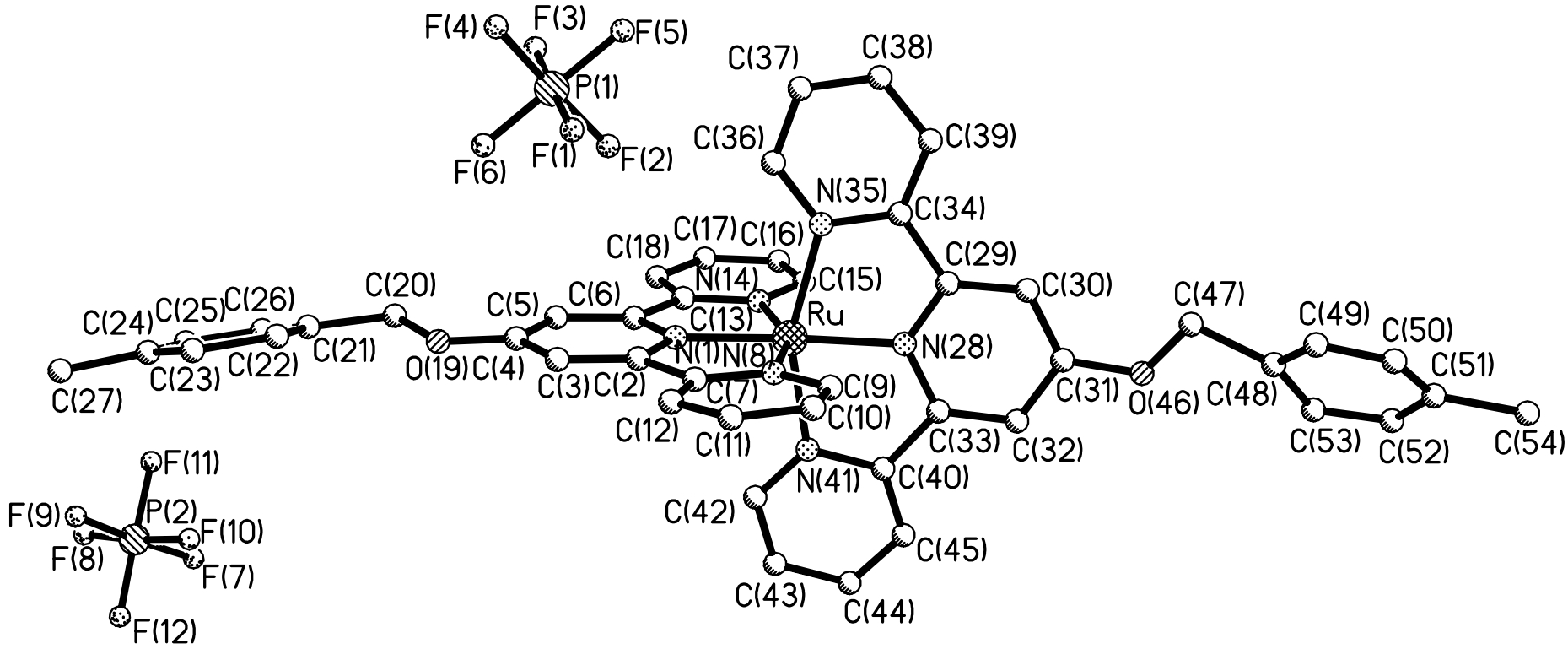
F(4)
F(3)
F(5)
P(1)
F(6)
F(1)
F(2)
C(37)
C(38)
C(36)
C(39)
N(35)
C(34)
C(17)
C(16)
C(18)
C(29)
C(20)
N(14)
C(15)
C(30)
C(24)
C(25)
C(26)
C(5)
C(6)
C(13)
Ru
C(47)
C(49)
C(50)
C(21)
N(1)
N(8)
N(28)
C(51)
C(27)
C(23)
C(22)
O(19)
C(4)
C(3)
C(2)
C(7)
C(9)
C(31)
O(46)
C(48)
C(12)
C(11)
C(10)
C(33)
C(32)
C(53)
C(52)
C(54)
F(11)
N(41)
C(40)
F(9)
P(2)
F(10)
C(42)
F(8)
F(7)
C(45)
C(43)
C(44)
F(12)

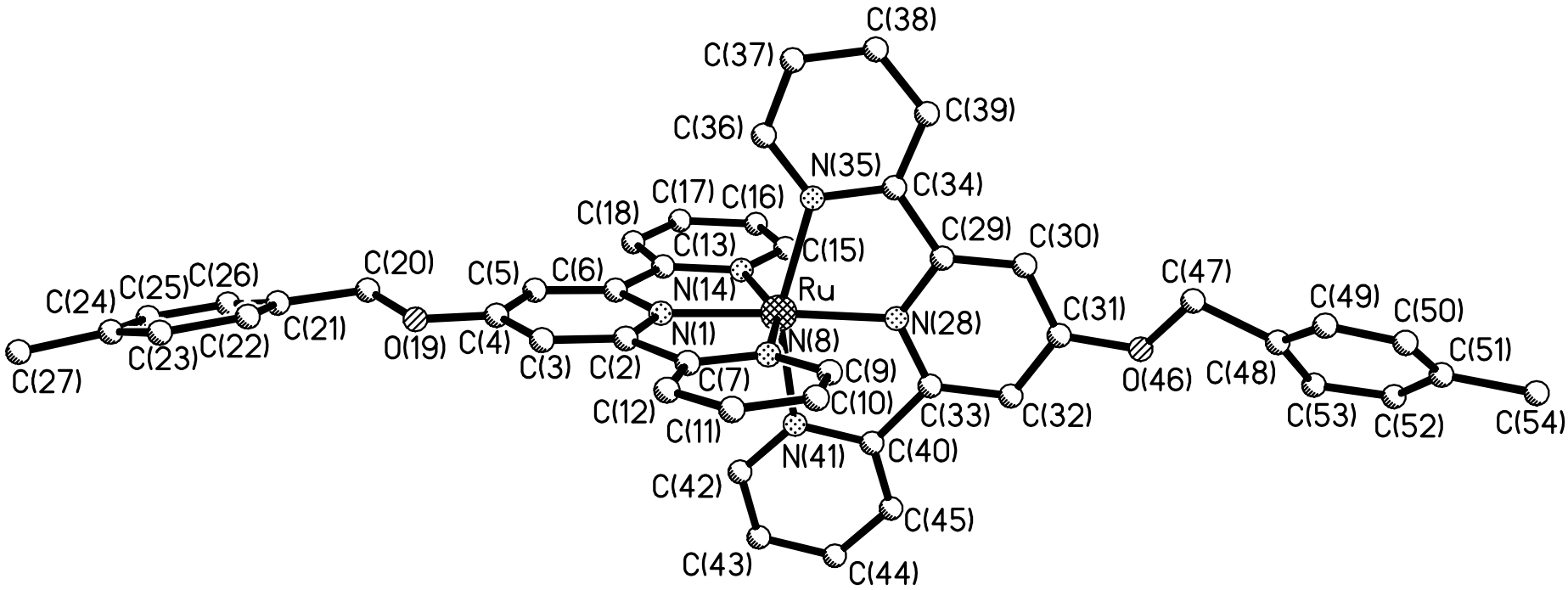
C(38)
C(37)
C(39)
C(36)
N(35)
C(34)
C(17)
C(16)
C(18)
C(29)
C(30)
C(13)
C(15)
C(20)
C(5)
C(6)
N(14)
Ru
C(47)
C(24)
C(25)
C(26)
C(31)
C(49)
C(50)
C(21)
O(19)
C(4)
N(1)
N(8)
N(28)
C(51)
C(27)
C(23)
C(22)
C(3)
C(2)
C(7)
C(9)
O(46)
C(48)
C(12)
C(10)
C(33)
C(32)
C(53)
C(52)
C(54)
C(11)
N(41)
C(40)
C(42)
C(45)
C(43)
C(44)

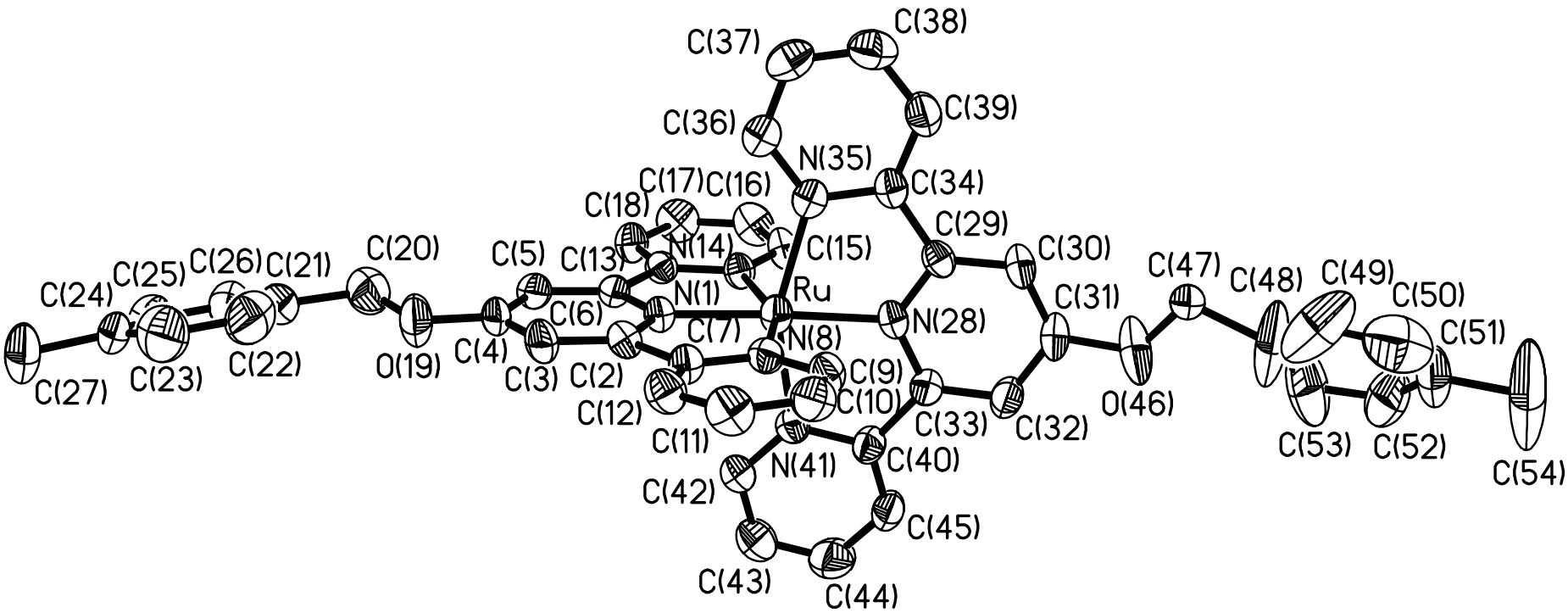
C(37)
C(38)
C(36)
C(39)
N(35)
C(34)
C(17)
C(16)
C(18)
C(29)
C(30)
C(47)
C(48)
C(49)
C(50)
C(51)
C(54)
C(52)
C(53)
O(46)
C(31)
C(32)
C(33)
C(40)
N(41)
C(42)
C(45)
C(43)
C(44)
C(15)
N(14)
C(5)
C(13)
C(20)
C(21)
C(25)
C(26)
C(24)
Ru
N(1)
N(28)
C(6)
C(7)
N(8)
C(9)
C(10)
C(12)
C(11)
C(2)
C(3)
C(4)
O(19)
C(22)
C(23)
C(27)

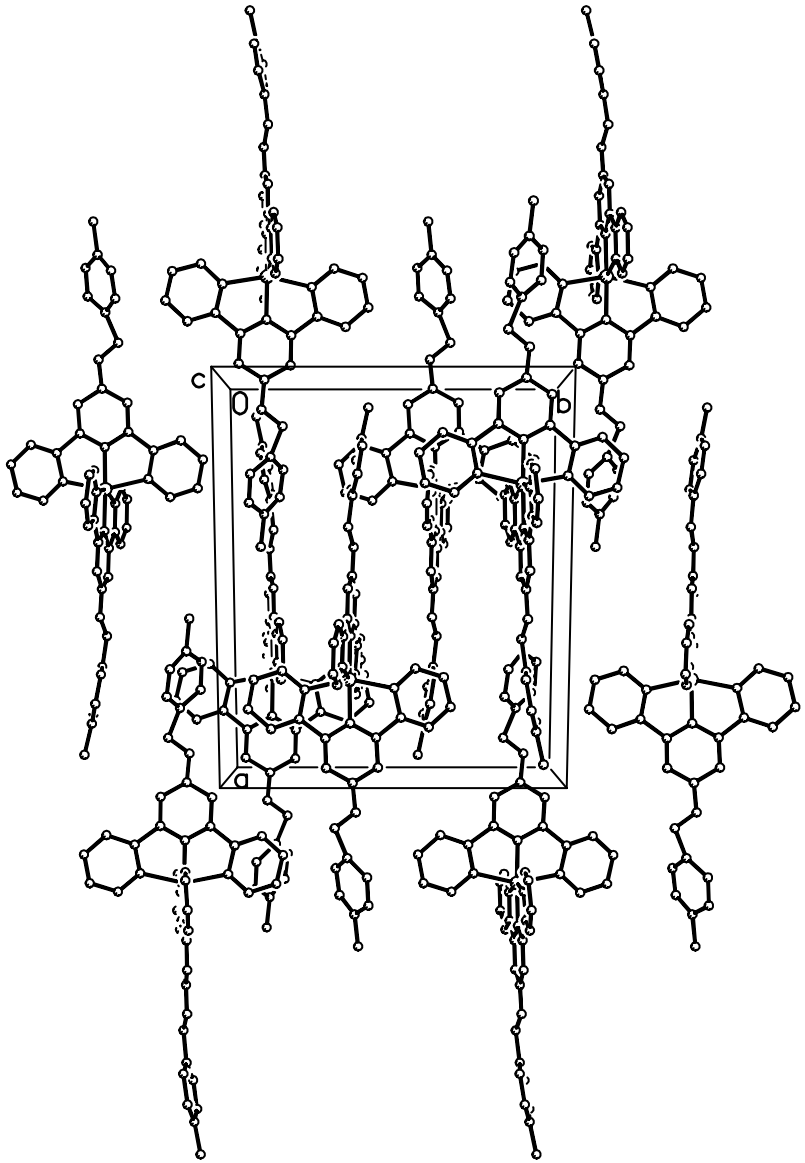
c
0
b
a

Table 1. Crystal data and structure refinement for **4**-Ru-**4**.

Identification code	**4**-Ru-**4**
Empirical formula	C45.50 H37 F12 N6 O2 P2 Ru
Formula weight	1090.82
Temperature	301(2) K
Wavelength	0.71073 A
Crystal system, space group	monoclinic, P2(1)/c
Unit cell dimensions	a = 19.631(2) A alpha = 90 deg. b = 15.5431(18) A beta = 110.454(3) deg. c = 16.0247(19) A gamma = 90 deg.
Volume	4581.2(9) A^3
Z, Calculated density	4, 1.582 Mg/m^3
Absorption coefficient	0.507 mm^-1
F(000)	2200
Crystal size	0.49 x 0.40 x 0.40 mm
Theta range for data collection	2.42 to 23.26 deg.
Limiting indices	-18<=h<=21, -17<=k<=17, -17<=l<=17
Reflections collected / unique	21105 / 6550 [R(int) = 0.0492]
Completeness to theta = 23.26	99.5 %
Max. and min. transmission	0.8229 and 0.7892
Refinement method	Full-matrix least-squares on F^2
Data / restraints / parameters	6550 / 0 / 619
Goodness-of-fit on F^2	1.038
Final R indices [I>2sigma(I)]	R1 = 0.0604, wR2 = 0.1518
R indices (all data)	R1 = 0.0813, wR2 = 0.1665
Largest diff. peak and hole	1.529 and -0.382 e.A^-3

Table 2. Atomic coordinates (x 10^4) and equivalent isotropic displacement parameters (A^2 x 10^3) for **4**-Ru-**4**.
U(eq) is defined as one third of the trace of the orthogonalized Uij tensor.

	x	y	z	U(eq)
Ru	7389(1)	3717(1)	7637(1)	39(1)
N(1)	6318(2)	3738(3)	7047(3)	33(1)
P(1)	5041(1)	1105(1)	7189(1)	58(1)
F(1)	5309(3)	1449(4)	6432(3)	113(2)
C(2)	6019(3)	3847(3)	6158(4)	36(1)
F(2)	5558(2)	1781(2)	7852(3)	83(1)
P(2)	348(1)	7493(1)	9094(1)	66(1)
C(3)	5282(3)	3874(4)	5735(4)	43(1)
F(3)	4795(2)	754(3)	7984(3)	91(1)
C(4)	4837(3)	3793(3)	6242(4)	40(1)
F(4)	4541(2)	400(3)	6556(3)	100(2)
C(5)	5144(3)	3680(3)	7156(4)	41(1)
F(5)	5691(2)	430(3)	7501(4)	94(1)
C(6)	5884(3)	3660(3)	7543(4)	32(1)
F(6)	4404(2)	1768(3)	6897(5)	125(2)
C(7)	6578(3)	3919(3)	5730(4)	37(1)
F(7)	871(3)	7878(4)	9997(3)	121(2)
N(8)	7282(2)	3861(3)	6302(3)	37(1)
F(8)	-319(3)	7606(4)	9401(4)	119(2)
C(9)	7808(3)	3880(3)	5944(4)	41(1)
F(9)	-148(3)	7053(4)	8197(3)	106(2)
C(10)	7673(4)	3938(4)	5056(4)	52(2)
F(10)	1041(3)	7306(4)	8808(4)	114(2)
F(11)	452(3)	6567(3)	9545(4)	110(2)
C(11)	6964(4)	4017(4)	4473(4)	53(2)
C(12)	6412(3)	4001(4)	4831(4)	47(2)
F(12)	276(4)	8382(4)	8621(4)	130(2)
C(13)	6310(3)	3546(3)	8507(4)	33(1)
N(14)	7049(2)	3526(3)	8715(3)	34(1)
C(15)	7469(3)	3396(4)	9563(4)	42(1)
C(16)	7190(3)	3291(4)	10233(4)	51(2)
C(17)	6443(4)	3311(4)	10024(4)	53(2)
C(18)	6006(3)	3445(4)	9154(4)	45(1)
O(19)	4120(2)	3835(3)	5785(3)	63(1)
C(20)	3631(4)	3684(5)	6212(5)	67(2)
C(21)	2848(4)	3797(4)	5581(5)	58(2)
C(22)	2679(4)	3759(5)	4679(7)	79(2)
C(23)	1944(5)	3902(5)	4091(6)	82(2)
C(24)	1421(3)	4065(4)	4471(6)	67(2)
C(25)	1632(4)	4093(5)	5378(6)	74(2)
C(26)	2329(4)	3961(5)	5909(6)	69(2)
C(27)	643(4)	4264(6)	3898(8)	124(4)
N(28)	8467(2)	3736(3)	8146(3)	34(1)
C(29)	8844(3)	3009(3)	8142(3)	34(1)
C(30)	9584(3)	3031(4)	8354(4)	44(1)
C(31)	9947(3)	3807(4)	8582(4)	46(2)
C(32)	9556(3)	4552(4)	8598(4)	46(2)
C(33)	8815(3)	4500(3)	8380(4)	37(1)
C(34)	8372(3)	2245(3)	7869(4)	37(1)
N(35)	7643(2)	2407(3)	7616(3)	35(1)
C(36)	7179(3)	1744(4)	7401(4)	42(1)
C(37)	7404(4)	906(4)	7396(4)	52(2)
C(38)	8133(4)	741(4)	7620(5)	60(2)
C(39)	8621(3)	1413(4)	7867(4)	53(2)
C(40)	8318(3)	5221(3)	8338(4)	40(1)
N(41)	7593(2)	5023(3)	7966(3)	40(1)
C(42)	7106(3)	5638(4)	7922(5)	53(2)
C(43)	7314(4)	6464(4)	8251(6)	71(2)
C(44)	8043(4)	6662(4)	8613(5)	67(2)
C(45)	8541(3)	6030(4)	8656(4)	51(2)

O(46)	10683(2)	3896(4)	8777(4)	83(2)
C(47)	11091(6)	3279(7)	8689(7)	35(2)
C(48)	11849(4)	3646(8)	8798(7)	115(4)
C(49)	12151(7)	3293(8)	8284(6)	118(4)
C(50)	12838(7)	3402(6)	8410(7)	102(3)
C(51)	13280(4)	3850(6)	9085(6)	76(2)
C(52)	13001(4)	4273(6)	9618(5)	78(2)
C(53)	12292(5)	4227(8)	9497(6)	106(3)
C(54)	14097(5)	3958(11)	9232(8)	191(8)

Table 3. Bond lengths [A] and angles [deg] for **4**-Ru-**4**.

Ru-N(1)	1.981(4)
Ru-N(28)	1.985(4)
Ru-N(14)	2.079(4)
Ru-N(8)	2.088(4)
Ru-N(35)	2.100(4)
Ru-N(41)	2.101(4)
N(1)-C(2)	1.350(7)
N(1)-C(6)	1.358(6)
P(1)-F(6)	1.560(5)
P(1)-F(1)	1.575(5)
P(1)-F(4)	1.580(4)
P(1)-F(2)	1.585(4)
P(1)-F(5)	1.592(4)
P(1)-F(3)	1.607(5)
C(2)-C(3)	1.368(8)
C(2)-C(7)	1.486(7)
P(2)-F(12)	1.560(6)
P(2)-F(8)	1.561(5)
P(2)-F(7)	1.571(5)
P(2)-F(9)	1.584(5)
P(2)-F(11)	1.591(5)
P(2)-F(10)	1.607(5)
C(3)-C(4)	1.390(8)
C(4)-O(19)	1.342(7)
C(4)-C(5)	1.387(8)
C(5)-C(6)	1.367(7)
C(6)-C(13)	1.488(7)
C(7)-N(8)	1.368(7)
C(7)-C(12)	1.368(8)
N(8)-C(9)	1.346(7)
C(9)-C(10)	1.356(8)
C(10)-C(11)	1.384(9)
C(11)-C(12)	1.393(8)
C(13)-N(14)	1.371(7)
C(13)-C(18)	1.372(8)
N(14)-C(15)	1.335(7)
C(15)-C(16)	1.375(8)
C(16)-C(17)	1.385(8)
C(17)-C(18)	1.374(8)
O(19)-C(20)	1.382(8)
C(20)-C(21)	1.526(9)
C(21)-C(26)	1.324(10)
C(21)-C(22)	1.366(11)
C(22)-C(23)	1.439(11)
C(23)-C(24)	1.388(11)
C(24)-C(25)	1.365(11)
C(24)-C(27)	1.514(10)
C(25)-C(26)	1.351(10)
N(28)-C(29)	1.351(6)
N(28)-C(33)	1.355(7)
C(29)-C(30)	1.373(7)
C(29)-C(34)	1.475(7)
C(30)-C(31)	1.384(8)
C(31)-O(46)	1.374(7)
C(31)-C(32)	1.393(8)
C(32)-C(33)	1.375(7)
C(33)-C(40)	1.472(7)
C(34)-N(35)	1.369(6)
C(34)-C(39)	1.383(8)
N(35)-C(36)	1.339(7)
C(36)-C(37)	1.375(9)
C(37)-C(38)	1.373(9)
C(38)-C(39)	1.378(9)
C(40)-C(45)	1.371(8)
C(40)-N(41)	1.372(7)
N(41)-C(42)	1.336(7)
C(42)-C(43)	1.393(9)

C(43)-C(44)	1.377(9)
C(44)-C(45)	1.370(9)
O(46)-C(47)	1.288(11)
C(47)-C(48)	1.545(13)
C(48)-C(49)	1.294(15)
C(48)-C(53)	1.466(15)
C(49)-C(50)	1.303(13)
C(50)-C(51)	1.324(13)
C(51)-C(52)	1.337(11)
C(51)-C(54)	1.547(11)
C(52)-C(53)	1.339(10)

N(1)-Ru-N(28)	175.67(17)
N(1)-Ru-N(14)	78.68(17)
N(28)-Ru-N(14)	105.48(17)
N(1)-Ru-N(8)	78.43(17)
N(28)-Ru-N(8)	97.46(17)
N(14)-Ru-N(8)	156.97(17)
N(1)-Ru-N(35)	103.12(17)
N(28)-Ru-N(35)	78.20(17)
N(14)-Ru-N(35)	91.25(16)
N(8)-Ru-N(35)	91.53(16)
N(1)-Ru-N(41)	100.47(17)
N(28)-Ru-N(41)	78.44(17)
N(14)-Ru-N(41)	91.09(16)
N(8)-Ru-N(41)	95.45(17)
N(35)-Ru-N(41)	156.29(17)
C(2)-N(1)-C(6)	120.0(4)
C(2)-N(1)-Ru	120.2(3)
C(6)-N(1)-Ru	119.8(3)
F(6)-P(1)-F(1)	89.6(3)
F(6)-P(1)-F(4)	90.7(3)
F(1)-P(1)-F(4)	92.4(3)
F(6)-P(1)-F(2)	91.3(3)
F(1)-P(1)-F(2)	89.0(3)
F(4)-P(1)-F(2)	177.6(3)
F(6)-P(1)-F(5)	179.2(4)
F(1)-P(1)-F(5)	91.0(3)
F(4)-P(1)-F(5)	89.7(3)
F(2)-P(1)-F(5)	88.3(2)
F(6)-P(1)-F(3)	91.8(3)
F(1)-P(1)-F(3)	178.0(3)
F(4)-P(1)-F(3)	88.9(3)
F(2)-P(1)-F(3)	89.6(3)
F(5)-P(1)-F(3)	87.6(3)
N(1)-C(2)-C(3)	121.4(5)
N(1)-C(2)-C(7)	112.2(5)
C(3)-C(2)-C(7)	126.4(5)
F(12)-P(2)-F(8)	96.3(4)
F(12)-P(2)-F(7)	91.7(3)
F(8)-P(2)-F(7)	91.0(3)
F(12)-P(2)-F(9)	91.1(3)
F(8)-P(2)-F(9)	91.0(3)
F(7)-P(2)-F(9)	176.4(4)
F(12)-P(2)-F(11)	176.5(4)
F(8)-P(2)-F(11)	87.0(3)
F(7)-P(2)-F(11)	89.3(3)
F(9)-P(2)-F(11)	87.8(3)
F(12)-P(2)-F(10)	87.9(3)
F(8)-P(2)-F(10)	175.8(3)
F(7)-P(2)-F(10)	89.2(3)
F(9)-P(2)-F(10)	88.6(3)
F(11)-P(2)-F(10)	88.8(3)
C(2)-C(3)-C(4)	118.7(5)
O(19)-C(4)-C(5)	124.6(5)
O(19)-C(4)-C(3)	115.5(5)
C(5)-C(4)-C(3)	120.0(5)
C(6)-C(5)-C(4)	118.8(5)
N(1)-C(6)-C(5)	121.2(5)
N(1)-C(6)-C(13)	112.3(4)
C(5)-C(6)-C(13)	126.5(5)

N(8)-C(7)-C(12)	121.7(5)
N(8)-C(7)-C(2)	114.9(5)
C(12)-C(7)-C(2)	123.4(5)
C(9)-N(8)-C(7)	117.3(5)
C(9)-N(8)-Ru	128.5(4)
C(7)-N(8)-Ru	114.2(3)
N(8)-C(9)-C(10)	123.4(6)
C(9)-C(10)-C(11)	119.8(5)
C(10)-C(11)-C(12)	117.6(6)
C(7)-C(12)-C(11)	120.2(6)
N(14)-C(13)-C(18)	121.1(5)
N(14)-C(13)-C(6)	114.6(4)
C(18)-C(13)-C(6)	124.3(5)
C(15)-N(14)-C(13)	118.4(5)
C(15)-N(14)-Ru	127.1(4)
C(13)-N(14)-Ru	114.5(3)
N(14)-C(15)-C(16)	122.7(5)
C(15)-C(16)-C(17)	119.0(6)
C(18)-C(17)-C(16)	118.8(5)
C(13)-C(18)-C(17)	120.1(5)
C(4)-O(19)-C(20)	120.0(5)
O(19)-C(20)-C(21)	111.4(6)
C(26)-C(21)-C(22)	119.5(7)
C(26)-C(21)-C(20)	119.7(7)
C(22)-C(21)-C(20)	120.9(7)
C(21)-C(22)-C(23)	120.3(7)
C(24)-C(23)-C(22)	117.8(8)
C(25)-C(24)-C(23)	118.5(7)
C(25)-C(24)-C(27)	120.5(8)
C(23)-C(24)-C(27)	121.0(9)
C(26)-C(25)-C(24)	122.0(8)
C(21)-C(26)-C(25)	121.9(8)
C(29)-N(28)-C(33)	120.6(4)
C(29)-N(28)-Ru	119.5(3)
C(33)-N(28)-Ru	119.3(3)
N(28)-C(29)-C(30)	120.8(5)
N(28)-C(29)-C(34)	112.8(4)
C(30)-C(29)-C(34)	126.4(5)
C(29)-C(30)-C(31)	119.3(5)
O(46)-C(31)-C(30)	123.4(5)
O(46)-C(31)-C(32)	117.0(5)
C(30)-C(31)-C(32)	119.6(5)
C(33)-C(32)-C(31)	119.1(5)
N(28)-C(33)-C(32)	120.6(5)
N(28)-C(33)-C(40)	113.1(4)
C(32)-C(33)-C(40)	126.3(5)
N(35)-C(34)-C(39)	120.4(5)
N(35)-C(34)-C(29)	115.0(4)
C(39)-C(34)-C(29)	124.7(5)
C(36)-N(35)-C(34)	118.8(5)
C(36)-N(35)-Ru	127.4(4)
C(34)-N(35)-Ru	113.8(3)
N(35)-C(36)-C(37)	122.7(5)
C(38)-C(37)-C(36)	118.9(6)
C(37)-C(38)-C(39)	119.3(6)
C(38)-C(39)-C(34)	119.9(6)
C(45)-C(40)-N(41)	120.9(5)
C(45)-C(40)-C(33)	124.2(5)
N(41)-C(40)-C(33)	114.8(5)
C(42)-N(41)-C(40)	118.5(5)
C(42)-N(41)-Ru	127.4(4)
C(40)-N(41)-Ru	113.8(3)
N(41)-C(42)-C(43)	121.9(6)
C(44)-C(43)-C(42)	119.3(6)
C(45)-C(44)-C(43)	118.6(6)
C(44)-C(45)-C(40)	120.7(6)
C(47)-O(46)-C(31)	123.1(7)
O(46)-C(47)-C(48)	109.0(9)
C(49)-C(48)-C(53)	117.8(8)
C(49)-C(48)-C(47)	114.1(11)
C(53)-C(48)-C(47)	127.2(9)

C(48)-C(49)-C(50)	121.7(10)
C(49)-C(50)-C(51)	122.9(9)
C(50)-C(51)-C(52)	118.9(8)
C(50)-C(51)-C(54)	122.0(10)
C(52)-C(51)-C(54)	118.9(10)
C(51)-C(52)-C(53)	121.3(8)
C(52)-C(53)-C(48)	116.9(8)

Symmetry transformations used to generate equivalent atoms:

Table 4. Anisotropic displacement parameters (A^2 x 10^3) for **4**-Ru-**4**.
The anisotropic displacement factor exponent takes the form:
-2 pi^2 [h^2 a*^2 U11 + ... + 2 h k a* b* U12]

	U11	U22	U33	U23	U13	U12
Ru	31(1)	46(1)	39(1)	1(1)	12(1)	1(1)
N(1)	28(2)	37(2)	31(3)	0(2)	9(2)	2(2)
P(1)	41(1)	48(1)	72(1)	7(1)	5(1)	-9(1)
F(1)	103(4)	146(5)	81(3)	19(3)	23(3)	-45(3)
C(2)	35(3)	39(3)	34(3)	1(2)	10(3)	5(2)
F(2)	78(3)	57(2)	93(3)	-4(2)	3(2)	-19(2)
P(2)	55(1)	86(1)	54(1)	3(1)	15(1)	-26(1)
C(3)	33(3)	57(4)	32(3)	5(3)	3(3)	5(3)
F(3)	94(3)	88(3)	98(3)	2(3)	43(3)	-20(3)
C(4)	26(3)	42(3)	45(4)	0(3)	1(3)	1(2)
F(4)	91(3)	91(3)	84(3)	-1(3)	-11(3)	-38(3)
C(5)	36(3)	39(3)	51(4)	2(3)	19(3)	0(2)
F(5)	67(3)	68(3)	130(4)	3(3)	15(3)	11(2)
C(6)	29(3)	31(3)	37(3)	-1(2)	11(2)	0(2)
F(6)	58(3)	75(3)	214(7)	32(4)	12(3)	13(2)
C(7)	34(3)	44(3)	33(3)	2(2)	12(3)	1(2)
F(7)	118(4)	174(5)	64(3)	-21(3)	22(3)	-83(4)
N(8)	36(3)	36(2)	41(3)	4(2)	15(2)	2(2)
F(8)	81(3)	143(5)	150(5)	-36(4)	60(3)	-14(3)
C(9)	37(3)	50(3)	41(3)	5(3)	20(3)	5(3)
F(9)	93(3)	142(4)	70(3)	-7(3)	11(3)	-46(3)
C(10)	55(4)	53(4)	61(4)	6(3)	38(4)	5(3)
F(10)	76(3)	173(5)	104(4)	1(4)	44(3)	-25(3)
F(11)	145(5)	92(3)	95(4)	17(3)	46(4)	-13(3)
C(11)	61(4)	66(4)	38(4)	6(3)	24(3)	6(3)
C(12)	47(4)	54(4)	40(4)	3(3)	13(3)	6(3)
F(12)	159(5)	95(4)	117(5)	27(3)	26(4)	-12(4)
C(13)	33(3)	31(3)	36(3)	-1(2)	15(3)	2(2)
N(14)	31(3)	39(2)	31(3)	-1(2)	12(2)	3(2)
C(15)	30(3)	55(3)	38(3)	-3(3)	8(3)	9(3)
C(16)	58(4)	62(4)	30(3)	-1(3)	13(3)	10(3)
C(17)	64(4)	65(4)	38(4)	3(3)	29(3)	3(3)
C(18)	36(3)	52(3)	49(4)	-1(3)	19(3)	3(3)
O(19)	30(2)	83(3)	70(3)	5(2)	11(2)	5(2)
C(20)	57(5)	71(5)	67(5)	13(4)	14(4)	4(4)
C(21)	45(4)	46(4)	77(5)	1(4)	11(4)	5(3)
C(22)	62(5)	69(5)	121(8)	-20(5)	53(5)	0(4)
C(23)	85(6)	85(6)	59(5)	-10(4)	4(5)	-5(5)
C(24)	33(4)	48(4)	101(7)	1(4)	-1(4)	-7(3)
C(25)	53(5)	73(5)	98(7)	9(5)	30(5)	-6(4)
C(26)	51(5)	75(5)	77(5)	12(4)	16(4)	-4(4)
C(27)	46(5)	96(7)	176(11)	-2(7)	-28(6)	-5(5)
N(28)	27(2)	43(3)	32(2)	1(2)	11(2)	6(2)
C(29)	33(3)	40(3)	27(3)	3(2)	9(2)	7(2)
C(30)	27(3)	55(4)	48(4)	-3(3)	10(3)	8(3)
C(31)	24(3)	66(4)	48(4)	-5(3)	12(3)	0(3)
C(32)	32(3)	51(4)	55(4)	-3(3)	16(3)	-6(3)
C(33)	33(3)	40(3)	39(3)	-1(3)	12(3)	-2(2)
C(34)	32(3)	45(3)	33(3)	2(3)	12(2)	4(3)
N(35)	37(3)	44(3)	25(2)	-1(2)	13(2)	-3(2)
C(36)	43(3)	50(4)	34(3)	-1(3)	14(3)	-5(3)
C(37)	64(5)	51(4)	44(4)	-5(3)	21(3)	-15(3)
C(38)	73(5)	42(4)	68(5)	-1(3)	29(4)	4(3)
C(39)	37(3)	54(4)	61(4)	-2(3)	9(3)	6(3)
C(40)	33(3)	44(3)	45(3)	-1(3)	17(3)	-3(3)
N(41)	36(3)	37(2)	49(3)	4(2)	19(2)	4(2)
C(42)	39(3)	41(3)	77(5)	4(3)	19(3)	6(3)
C(43)	55(5)	50(4)	111(7)	0(4)	33(4)	15(3)
C(44)	70(5)	44(4)	92(6)	-9(4)	33(4)	-3(4)
C(45)	32(3)	47(4)	70(4)	-7(3)	15(3)	-7(3)
O(46)	34(3)	127(5)	85(4)	-19(3)	16(3)	21(3)

C(48)	29(4)	241(14)	70(6)	33(7)	13(4)	-12(6)
C(49)	133(9)	163(10)	54(5)	-9(6)	27(6)	-86(8)
C(50)	152(10)	88(6)	90(8)	1(6)	72(8)	21(7)
C(51)	39(4)	124(7)	69(5)	27(5)	25(4)	17(4)
C(52)	53(5)	100(6)	71(5)	-9(5)	8(4)	-22(4)
C(53)	70(6)	190(11)	71(6)	15(6)	42(5)	48(6)
C(54)	46(6)	400(20)	133(10)	89(12)	41(6)	42(9)

Table 5. Hydrogen coordinates (x 10^4) and isotropic displacement parameters (A^2 x 10^3) for **4**-Ru-**4**.

	x	y	z	U(eq)
H(3)	5082	3946	5121	51
H(5)	4850	3619	7500	49
H(9)	8290	3853	6325	50
H(10)	8055	3924	4840	62
H(11)	6860	4079	3863	64
H(12)	5929	4047	4458	57
H(15)	7970	3376	9706	50
H(16)	7498	3207	10818	61
H(17)	6241	3236	10465	63
H(18)	5504	3467	9002	53
H(20A)	3726	4078	6709	81
H(20B)	3696	3102	6448	81
H(22)	3040	3640	4445	94
H(23)	1823	3886	3476	98
H(25)	1286	4205	5637	89
H(26)	2448	3987	6523	83
H(27A)	318	3965	4127	186
H(27B)	557	4080	3298	186
H(27C)	560	4872	3905	186
H(30)	9839	2529	8343	53
H(32)	9794	5077	8753	55
H(36)	6685	1854	7247	50
H(37)	7067	459	7244	63
H(38)	8296	181	7605	72
H(39)	9117	1307	8031	64
H(42)	6614	5511	7664	63
H(43)	6965	6877	8227	86
H(44)	8193	7212	8825	81
H(45)	9035	6153	8903	61
H(47A)	10876	3017	8106	42
H(47B)	11136	2842	9137	42
H(49)	11870	2952	7812	141
H(50)	13026	3154	8008	123
H(52)	13306	4606	10080	94
H(53)	12090	4549	9842	127
H(54A)	14364	3482	9575	286
H(54B)	14272	4485	9546	286
H(54C)	14163	3973	8666	286

Table 6. Torsion angles [deg] for **4**-Ru-**4**.

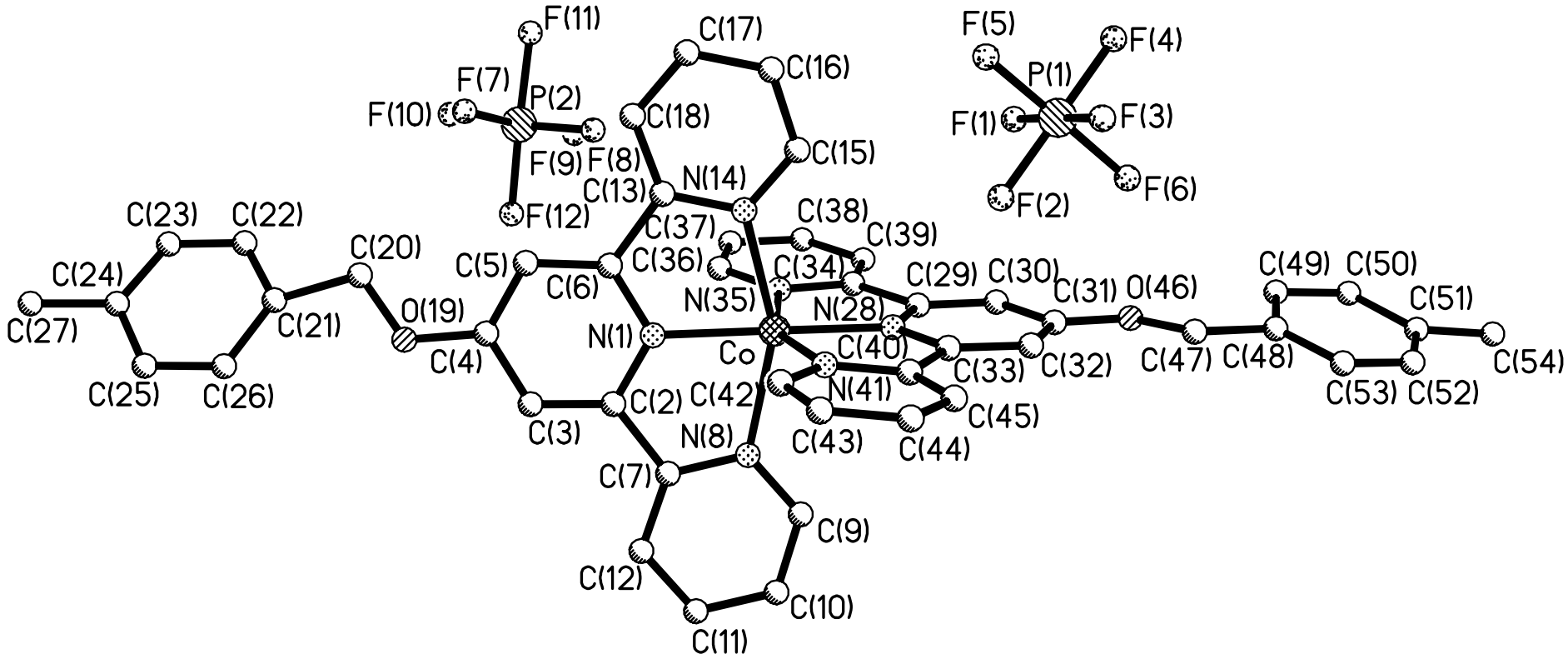
F(11)
F(7)
P(2)
F(10)
F(9)
F(8)
F(12)
C(17)
C(16)
C(18)
C(15)
C(13)
N(14)
C(37)
C(38)
C(39)
C(36)
C(34)
C(29)
C(30)
C(31)
O(46)
C(49)
C(50)
C(51)
C(54)
C(53)
C(52)
C(48)
C(47)
C(32)
C(33)
C(40)
N(28)
N(35)
Co
N(1)
C(5)
C(6)
C(20)
C(23)
C(22)
C(24)
C(27)
C(21)
O(19)
C(4)
C(25)
C(26)
C(3)
C(2)
C(42)
N(41)
C(45)
C(43)
C(44)
N(8)
C(7)
C(9)
C(12)
C(10)
C(11)
F(5)
F(4)
P(1)
F(1)
F(3)
F(6)
F(2)

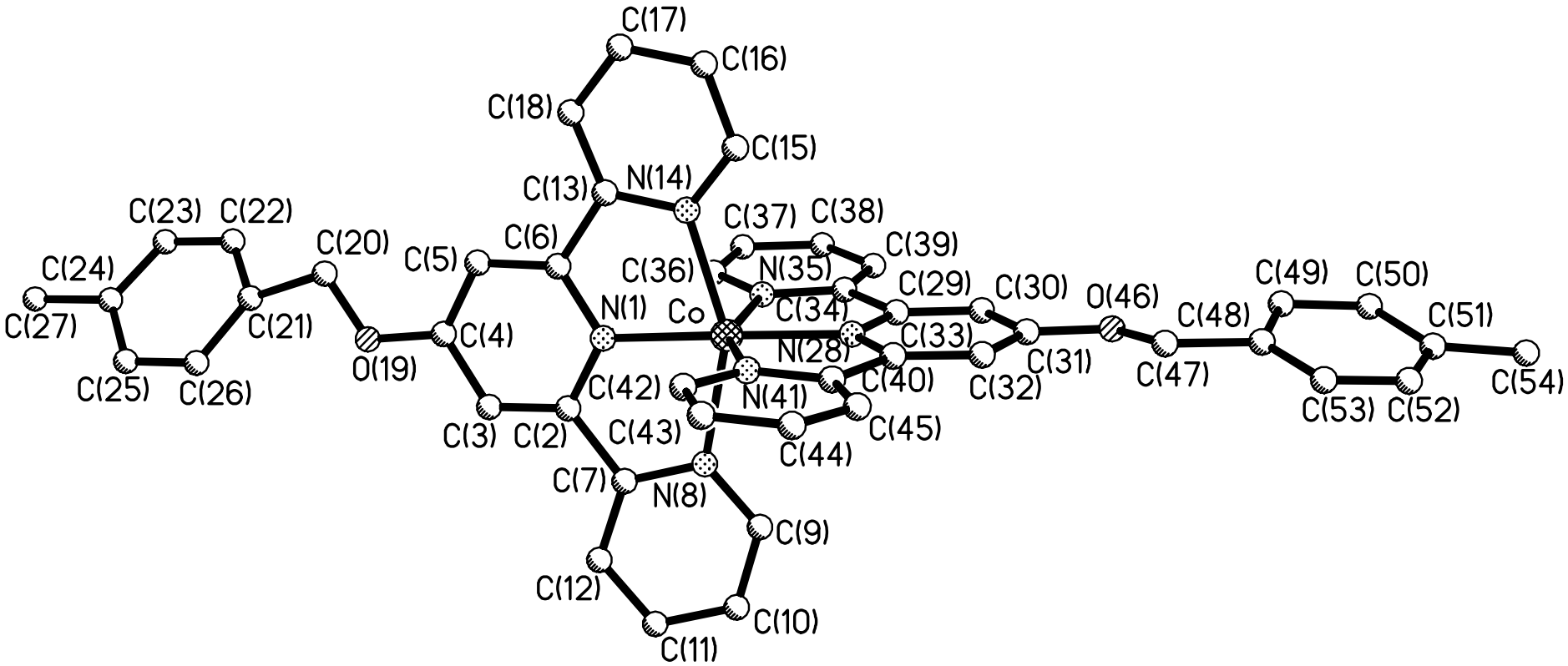
C(17)
C(16)
C(18)
C(15)
C(13)
N(14)
C(23)
C(22)
C(37)
C(38)
C(20)
C(6)
C(5)
C(39)
C(24)
C(36)
N(35)
C(49)
C(50)
C(29)
C(30)
O(46)
C(27)
N(1)
Co
C(34)
C(48)
C(51)
C(21)
C(4)
C(33)
N(28)
C(31)
C(25)
O(19)
C(40)
C(32)
C(47)
C(54)
C(26)
C(42)
N(41)
C(53)
C(52)
C(3)
C(2)
C(43)
C(45)
C(44)
C(7)
N(8)
C(9)
C(12)
C(10)
C(11)

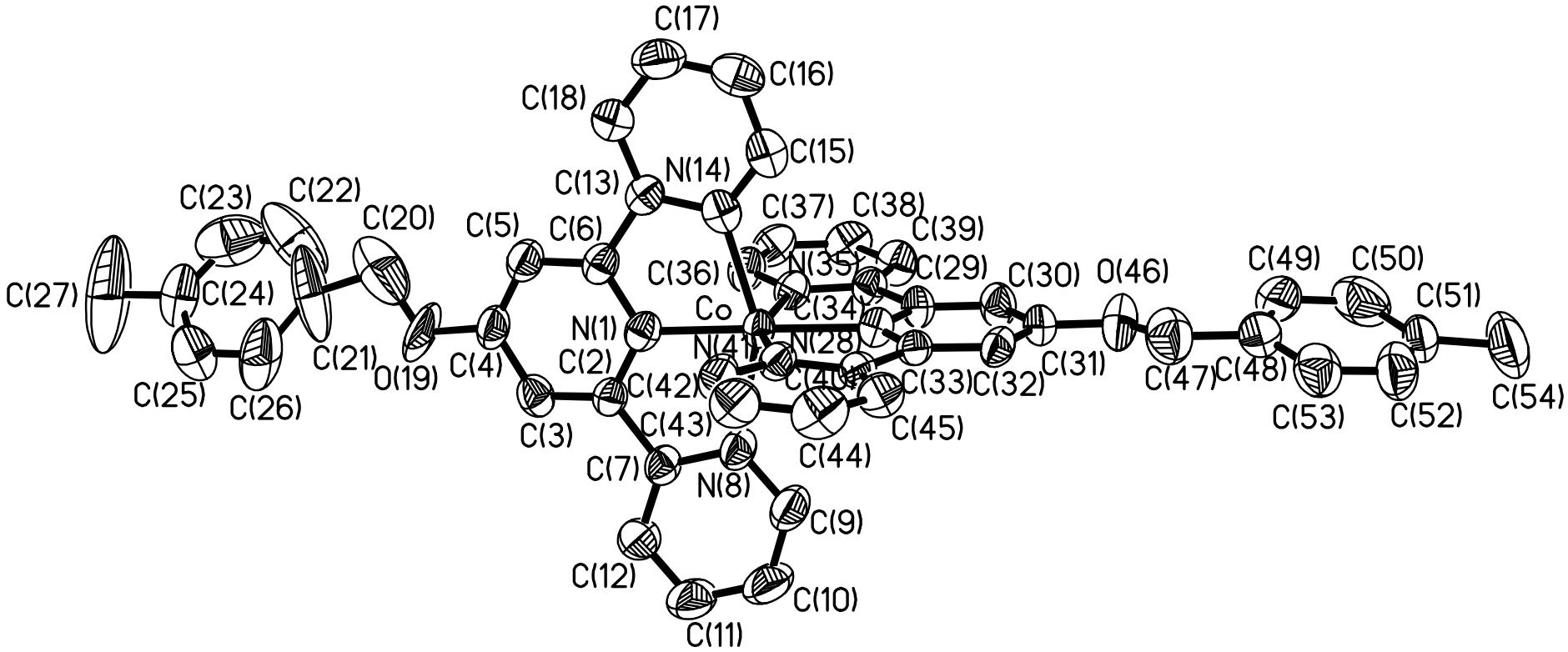
C(17)
C(16)
C(18)
C(15)
N(14)
C(13)
C(23)
C(22)
C(20)
C(5)
C(6)
C(37)
C(38)
C(39)
C(27)
C(24)
C(36)
N(35)
C(29)
C(30)
O(46)
C(49)
C(50)
C(51)
Co
C(34)
N(1)
N(41)
N(28)
C(25)
C(26)
C(21)
O(19)
C(4)
C(2)
C(42)
C(33)
C(32)
C(31)
C(47)
C(48)
C(54)
C(3)
C(43)
C(45)
C(53)
C(52)
C(44)
C(7)
N(8)
C(9)
C(12)
C(10)
C(11)

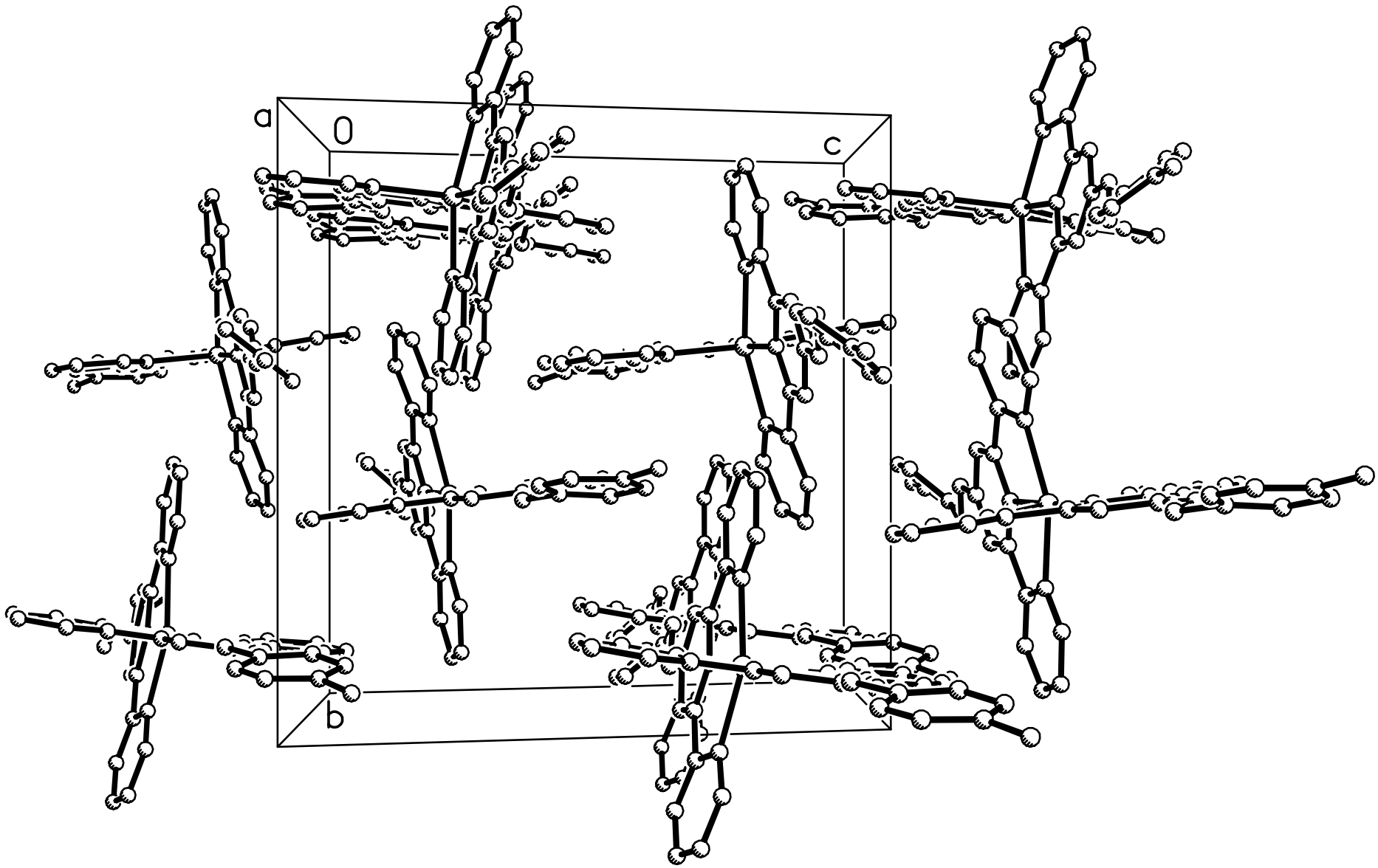
a
0
c
b

Table 1. Crystal data and structure refinement for **4**-Co-**4**.

Identification code	**4**-Co-**4**
Empirical formula	C46 H38 Co F12 N6 O2 P2
Formula weight	1055.69
Temperature	300(2) K
Wavelength	0.71073 A
Crystal system, space group	monoclinic, P2(1)/c
Unit cell dimensions	a = 19.617(5) A alpha = 90 deg. b = 15.492(4) A beta = 110.315(5) deg. c = 16.003(4) A gamma = 90 deg.
Volume	4560.9(18) A^3
Z, Calculated density	4, 1.537 Mg/m^3
Absorption coefficient	0.542 mm^-1
F(000)	2148
Crystal size	0.76 x 0.13 x 0.03 mm
Theta range for data collection	2.42 to 23.30 deg.
Limiting indices	-21<=h<=17, -17<=k<=17, -17<=l<=17
Reflections collected / unique	20929 / 6558 [R(int) = 0.0567]
Completeness to theta = 23.30	99.6 %
Max. and min. transmission	0.9839 and 0.6833
Refinement method	Full-matrix least-squares on F^2
Data / restraints / parameters	6558 / 0 / 624
Goodness-of-fit on F^2	1.092
Final R indices [I>2sigma(I)]	R1 = 0.0784, wR2 = 0.1742
R indices (all data)	R1 = 0.1083, wR2 = 0.1897
Largest diff. peak and hole	1.032 and -0.425 e.A^-3

Table 2. Atomic coordinates (x 10^4) and equivalent isotropic displacement parameters (A^2 x 10^3) for **4**-Co-**4**.
U(eq) is defined as one third of the trace of the orthogonalized Uij tensor.

	x	y	z	U(eq)
Co	7374(1)	3716(1)	7640(1)	37(1)
N(1)	8454(2)	3743(3)	8131(3)	41(1)
P(1)	5031(1)	1114(1)	7173(1)	63(1)
F(1)	5295(3)	1473(4)	6430(4)	126(2)
C(2)	8804(3)	4500(4)	8367(4)	39(1)
F(2)	5540(2)	1788(3)	7838(3)	97(2)
P(2)	9637(1)	2486(2)	5880(1)	73(1)
C(3)	9540(3)	4552(4)	8562(4)	49(2)
F(3)	4786(3)	760(3)	7956(3)	104(2)
C(4)	9926(3)	3813(4)	8534(4)	51(2)
F(4)	4531(3)	426(3)	6539(3)	112(2)
C(5)	9568(3)	3036(4)	8315(4)	51(2)
F(5)	5675(2)	446(3)	7473(4)	106(2)
C(6)	8830(3)	3019(4)	8118(4)	42(2)
F(6)	4397(3)	1773(3)	6906(5)	135(2)
C(7)	8319(3)	5230(4)	8357(4)	43(2)
F(7)	10122(3)	2048(4)	6772(3)	117(2)
N(8)	7605(3)	5042(3)	8007(3)	48(1)
F(8)	8953(3)	2318(4)	6166(4)	127(2)
C(9)	7130(4)	5666(4)	7981(5)	65(2)
F(9)	9118(3)	2870(4)	4994(3)	136(2)
C(10)	7348(4)	6476(4)	8309(6)	79(2)
F(10)	10295(3)	2594(4)	5572(4)	137(2)
C(11)	8072(4)	6664(5)	8668(6)	78(2)
F(11)	9524(3)	1561(4)	5425(4)	124(2)
F(12)	9713(4)	3367(4)	6353(4)	142(2)
C(12)	8561(4)	6030(4)	8686(5)	62(2)
C(13)	8370(3)	2236(4)	7861(4)	41(1)
N(14)	7656(3)	2386(3)	7653(3)	43(1)
C(15)	7202(3)	1723(4)	7440(4)	50(2)
C(16)	7436(4)	884(5)	7422(4)	60(2)
C(17)	8162(5)	737(5)	7624(5)	71(2)
C(18)	8628(4)	1416(4)	7857(5)	60(2)
O(19)	10656(3)	3939(4)	8719(4)	99(2)
C(20)	11042(6)	3295(8)	8653(7)	124(4)
C(21)	11822(4)	3670(10)	8786(7)	133(5)
C(22)	12117(8)	3294(8)	8270(7)	134(5)
C(23)	12817(8)	3375(7)	8401(8)	114(4)
C(24)	13261(4)	3855(7)	9062(6)	80(3)
C(25)	12976(4)	4276(6)	9583(5)	83(2)
C(26)	12256(5)	4209(8)	9444(6)	111(4)
C(27)	14060(5)	3936(12)	9209(8)	215(9)
N(28)	6308(2)	3752(3)	7054(3)	41(1)
C(29)	6013(3)	3860(4)	6166(4)	41(1)
C(30)	5277(3)	3884(4)	5740(4)	51(2)
C(31)	4829(3)	3799(4)	6243(4)	45(2)
C(32)	5138(3)	3688(4)	7153(4)	41(1)
C(33)	5876(3)	3672(3)	7544(4)	37(1)
C(34)	6555(3)	3915(4)	5717(4)	43(2)
N(35)	7256(2)	3851(3)	6286(3)	42(1)
C(36)	7782(3)	3859(4)	5929(4)	52(2)
C(37)	7642(4)	3927(4)	5033(5)	58(2)
C(38)	6939(4)	4017(4)	4463(4)	58(2)
C(39)	6394(4)	4004(4)	4818(4)	54(2)
C(40)	6290(3)	3554(3)	8505(4)	39(1)
N(41)	7013(3)	3517(3)	8702(3)	41(1)
C(42)	7432(4)	3378(4)	9552(4)	55(2)
C(43)	7155(4)	3283(5)	10225(4)	62(2)
C(44)	6416(4)	3324(5)	10017(5)	66(2)
C(45)	5986(4)	3460(4)	9151(4)	52(2)

O(46)	4115(2)	3834(3)	5779(3)	70(1)
C(47)	3635(4)	3691(5)	6216(5)	77(2)
C(48)	2844(4)	3808(4)	5576(5)	62(2)
C(49)	2700(4)	3767(5)	4693(7)	81(2)
C(50)	1959(5)	3915(5)	4104(6)	91(3)
C(51)	1428(4)	4074(5)	4478(7)	71(2)
C(52)	1635(4)	4073(5)	5364(6)	76(2)
C(53)	2326(4)	3954(5)	5905(6)	70(2)
C(54)	647(4)	4256(6)	3902(8)	130(4)

Table 3. Bond lengths [A] and angles [deg] for **4**-Co-**4**.

Co-N(28)	1.973(4)
Co-N(1)	1.988(5)
Co-N(41)	2.079(5)
Co-N(35)	2.108(5)
Co-N(14)	2.132(5)
Co-N(8)	2.140(5)
N(1)-C(2)	1.344(7)
N(1)-C(6)	1.347(7)
P(1)-F(6)	1.551(5)
P(1)-F(1)	1.556(6)
P(1)-F(4)	1.561(5)
P(1)-F(5)	1.573(5)
P(1)-F(2)	1.575(4)
P(1)-F(3)	1.589(5)
C(2)-C(3)	1.369(8)
C(2)-C(7)	1.475(8)
P(2)-F(12)	1.542(6)
P(2)-F(10)	1.543(5)
P(2)-F(9)	1.548(5)
P(2)-F(7)	1.569(5)
P(2)-F(8)	1.582(5)
P(2)-F(11)	1.587(6)
C(3)-C(4)	1.382(8)
C(3)-H(3)	0.9300
C(4)-O(19)	1.372(8)
C(4)-C(5)	1.376(9)
C(5)-C(6)	1.371(8)
C(5)-H(5)	0.9300
C(6)-C(13)	1.481(8)
C(7)-N(8)	1.348(7)
C(7)-C(12)	1.365(8)
N(8)-C(9)	1.333(8)
C(9)-C(10)	1.370(10)
C(9)-H(9)	0.9300
C(10)-C(11)	1.367(10)
C(10)-H(10)	0.9300
C(11)-C(12)	1.366(9)
C(11)-H(11)	0.9300
C(12)-H(12)	0.9300
C(13)-N(14)	1.343(7)
C(13)-C(18)	1.368(8)
N(14)-C(15)	1.325(8)
C(15)-C(16)	1.381(9)
C(15)-H(15)	0.9300
C(16)-C(17)	1.365(10)
C(16)-H(16)	0.9300
C(17)-C(18)	1.359(9)
C(17)-H(17)	0.9300
C(18)-H(18)	0.9300
O(19)-C(20)	1.280(12)
C(20)-C(21)	1.581(12)
C(20)-H(20A)	0.9700
C(20)-H(20B)	0.9700
C(21)-C(22)	1.298(17)
C(21)-C(26)	1.382(15)
C(22)-C(23)	1.322(15)
C(22)-H(22)	0.9300
C(23)-C(24)	1.337(13)
C(23)-H(23)	0.9300
C(24)-C(25)	1.326(11)
C(24)-C(27)	1.507(12)
C(25)-C(26)	1.354(11)
C(25)-H(25)	0.9300
C(26)-H(26)	0.9300
C(27)-H(27A)	0.9600
C(27)-H(27B)	0.9600
C(27)-H(27C)	0.9600

N(28)-C(33)	1.345(7)
N(28)-C(29)	1.346(7)
C(29)-C(30)	1.365(8)
C(29)-C(34)	1.478(8)
C(30)-C(31)	1.390(8)
C(30)-H(30)	0.9300
C(31)-O(46)	1.340(7)
C(31)-C(32)	1.380(8)
C(32)-C(33)	1.365(7)
C(32)-H(32)	0.9300
C(33)-C(40)	1.481(8)
C(34)-N(35)	1.365(7)
C(34)-C(39)	1.370(8)
N(35)-C(36)	1.340(7)
C(36)-C(37)	1.368(9)
C(36)-H(36)	0.9300
C(37)-C(38)	1.371(9)
C(37)-H(37)	0.9300
C(38)-C(39)	1.374(9)
C(38)-H(38)	0.9300
C(39)-H(39)	0.9300
C(40)-N(41)	1.342(7)
C(40)-C(45)	1.368(8)
N(41)-C(42)	1.341(7)
C(42)-C(43)	1.372(9)
C(42)-H(42)	0.9300
C(43)-C(44)	1.372(9)
C(43)-H(43)	0.9300
C(44)-C(45)	1.367(9)
C(44)-H(44)	0.9300
C(45)-H(45)	0.9300
O(46)-C(47)	1.373(9)
C(47)-C(48)	1.545(9)
C(47)-H(47A)	0.9700
C(47)-H(47B)	0.9700
C(48)-C(53)	1.316(10)
C(48)-C(49)	1.343(11)
C(49)-C(50)	1.450(11)
C(49)-H(49)	0.9300
C(50)-C(51)	1.391(11)
C(50)-H(50)	0.9300
C(51)-C(52)	1.333(11)
C(51)-C(54)	1.515(10)
C(52)-C(53)	1.344(10)
C(52)-H(52)	0.9300
C(53)-H(53)	0.9300
C(54)-H(54A)	0.9600
C(54)-H(54B)	0.9600
C(54)-H(54C)	0.9600

N(28)-Co-N(1)	174.54(19)
N(28)-Co-N(41)	77.67(19)
N(1)-Co-N(41)	107.39(18)
N(28)-Co-N(35)	77.83(18)
N(1)-Co-N(35)	97.23(18)
N(41)-Co-N(35)	155.23(18)
N(28)-Co-N(14)	105.09(19)
N(1)-Co-N(14)	77.22(19)
N(41)-Co-N(14)	90.55(17)
N(35)-Co-N(14)	92.35(17)
N(28)-Co-N(8)	101.06(19)
N(1)-Co-N(8)	77.10(19)
N(41)-Co-N(8)	91.01(19)
N(35)-Co-N(8)	97.15(19)
N(14)-Co-N(8)	153.53(19)
C(2)-N(1)-C(6)	120.2(5)
C(2)-N(1)-Co	119.9(4)
C(6)-N(1)-Co	119.4(4)
F(6)-P(1)-F(1)	90.2(4)
F(6)-P(1)-F(4)	90.4(3)
F(1)-P(1)-F(4)	92.8(3)

F(6)-P(1)-F(5)	178.2(4)
F(1)-P(1)-F(5)	91.4(3)
F(4)-P(1)-F(5)	90.4(3)
F(6)-P(1)-F(2)	90.5(3)
F(1)-P(1)-F(2)	88.8(3)
F(4)-P(1)-F(2)	178.2(3)
F(5)-P(1)-F(2)	88.7(3)
F(6)-P(1)-F(3)	90.5(3)
F(1)-P(1)-F(3)	178.0(3)
F(4)-P(1)-F(3)	89.0(3)
F(5)-P(1)-F(3)	87.8(3)
F(2)-P(1)-F(3)	89.4(3)
N(1)-C(2)-C(3)	120.7(5)
N(1)-C(2)-C(7)	113.7(5)
C(3)-C(2)-C(7)	125.6(5)
F(12)-P(2)-F(10)	96.4(4)
F(12)-P(2)-F(9)	91.7(4)
F(10)-P(2)-F(9)	91.3(3)
F(12)-P(2)-F(7)	90.6(3)
F(10)-P(2)-F(7)	91.5(3)
F(9)-P(2)-F(7)	176.1(4)
F(12)-P(2)-F(8)	87.2(4)
F(10)-P(2)-F(8)	176.4(4)
F(9)-P(2)-F(8)	88.6(3)
F(7)-P(2)-F(8)	88.5(3)
F(12)-P(2)-F(11)	176.3(4)
F(10)-P(2)-F(11)	87.1(4)
F(9)-P(2)-F(11)	89.2(3)
F(7)-P(2)-F(11)	88.3(3)
F(8)-P(2)-F(11)	89.3(4)
C(2)-C(3)-C(4)	119.3(6)
C(2)-C(3)-H(3)	120.3
C(4)-C(3)-H(3)	120.3
O(19)-C(4)-C(5)	125.5(6)
O(19)-C(4)-C(3)	114.7(6)
C(5)-C(4)-C(3)	119.8(6)
C(6)-C(5)-C(4)	118.7(6)
C(6)-C(5)-H(5)	120.7
C(4)-C(5)-H(5)	120.7
N(1)-C(6)-C(5)	121.3(6)
N(1)-C(6)-C(13)	113.7(5)
C(5)-C(6)-C(13)	124.9(6)
N(8)-C(7)-C(12)	121.9(6)
N(8)-C(7)-C(2)	114.3(5)
C(12)-C(7)-C(2)	123.7(5)
C(9)-N(8)-C(7)	118.0(5)
C(9)-N(8)-Co	127.5(4)
C(7)-N(8)-Co	114.3(4)
N(8)-C(9)-C(10)	122.1(7)
N(8)-C(9)-H(9)	119.0
C(10)-C(9)-H(9)	119.0
C(11)-C(10)-C(9)	119.7(7)
C(11)-C(10)-H(10)	120.1
C(9)-C(10)-H(10)	120.1
C(12)-C(11)-C(10)	118.4(7)
C(12)-C(11)-H(11)	120.8
C(10)-C(11)-H(11)	120.8
C(7)-C(12)-C(11)	119.8(6)
C(7)-C(12)-H(12)	120.1
C(11)-C(12)-H(12)	120.1
N(14)-C(13)-C(18)	121.0(6)
N(14)-C(13)-C(6)	114.2(5)
C(18)-C(13)-C(6)	124.8(6)
C(15)-N(14)-C(13)	118.7(5)
C(15)-N(14)-Co	126.7(4)
C(13)-N(14)-Co	114.5(4)
N(14)-C(15)-C(16)	122.4(6)
N(14)-C(15)-H(15)	118.8
C(16)-C(15)-H(15)	118.8
C(17)-C(16)-C(15)	118.7(7)
C(17)-C(16)-H(16)	120.7

C(15)-C(16)-H(16)	120.7
C(18)-C(17)-C(16)	118.9(7)
C(18)-C(17)-H(17)	120.6
C(16)-C(17)-H(17)	120.6
C(17)-C(18)-C(13)	120.3(7)
C(17)-C(18)-H(18)	119.8
C(13)-C(18)-H(18)	119.8
C(20)-O(19)-C(4)	118.4(8)
O(19)-C(20)-C(21)	106.0(9)
O(19)-C(20)-H(20A)	110.5
C(21)-C(20)-H(20A)	110.5
O(19)-C(20)-H(20B)	110.5
C(21)-C(20)-H(20B)	110.5
H(20A)-C(20)-H(20B)	108.7
C(22)-C(21)-C(26)	117.6(8)
C(22)-C(21)-C(20)	111.9(12)
C(26)-C(21)-C(20)	129.6(10)
C(21)-C(22)-C(23)	121.6(10)
C(21)-C(22)-H(22)	119.2
C(23)-C(22)-H(22)	119.2
C(22)-C(23)-C(24)	122.2(11)
C(22)-C(23)-H(23)	118.9
C(24)-C(23)-H(23)	118.9
C(25)-C(24)-C(23)	118.1(9)
C(25)-C(24)-C(27)	120.2(10)
C(23)-C(24)-C(27)	121.7(11)
C(24)-C(25)-C(26)	120.1(8)
C(24)-C(25)-H(25)	120.0
C(26)-C(25)-H(25)	120.0
C(25)-C(26)-C(21)	120.3(9)
C(25)-C(26)-H(26)	119.9
C(21)-C(26)-H(26)	119.9
C(24)-C(27)-H(27A)	109.5
C(24)-C(27)-H(27B)	109.5
H(27A)-C(27)-H(27B)	109.5
C(24)-C(27)-H(27C)	109.5
H(27A)-C(27)-H(27C)	109.5
H(27B)-C(27)-H(27C)	109.5
C(33)-N(28)-C(29)	119.9(5)
C(33)-N(28)-Co	119.9(4)
C(29)-N(28)-Co	120.2(4)
N(28)-C(29)-C(30)	121.7(5)
N(28)-C(29)-C(34)	113.6(5)
C(30)-C(29)-C(34)	124.7(5)
C(29)-C(30)-C(31)	118.6(5)
C(29)-C(30)-H(30)	120.7
C(31)-C(30)-H(30)	120.7
O(46)-C(31)-C(32)	125.6(6)
O(46)-C(31)-C(30)	115.1(5)
C(32)-C(31)-C(30)	119.4(5)
C(33)-C(32)-C(31)	119.5(5)
C(33)-C(32)-H(32)	120.3
C(31)-C(32)-H(32)	120.3
N(28)-C(33)-C(32)	121.0(5)
N(28)-C(33)-C(40)	112.8(5)
C(32)-C(33)-C(40)	126.2(5)
N(35)-C(34)-C(39)	121.2(6)
N(35)-C(34)-C(29)	113.7(5)
C(39)-C(34)-C(29)	125.1(5)
C(36)-N(35)-C(34)	117.5(5)
C(36)-N(35)-Co	127.8(4)
C(34)-N(35)-Co	114.7(4)
N(35)-C(36)-C(37)	122.9(6)
N(35)-C(36)-H(36)	118.5
C(37)-C(36)-H(36)	118.5
C(36)-C(37)-C(38)	119.6(6)
C(36)-C(37)-H(37)	120.2
C(38)-C(37)-H(37)	120.2
C(37)-C(38)-C(39)	118.1(6)
C(37)-C(38)-H(38)	120.9
C(39)-C(38)-H(38)	120.9

C(34)-C(39)-C(38)	120.5(6)
C(34)-C(39)-H(39)	119.8
C(38)-C(39)-H(39)	119.8
N(41)-C(40)-C(45)	121.4(5)
N(41)-C(40)-C(33)	113.7(5)
C(45)-C(40)-C(33)	124.9(5)
C(42)-N(41)-C(40)	118.0(5)
C(42)-N(41)-Co	126.2(4)
C(40)-N(41)-Co	115.7(4)
N(41)-C(42)-C(43)	123.0(6)
N(41)-C(42)-H(42)	118.5
C(43)-C(42)-H(42)	118.5
C(44)-C(43)-C(42)	118.5(6)
C(44)-C(43)-H(43)	120.7
C(42)-C(43)-H(43)	120.7
C(45)-C(44)-C(43)	118.8(6)
C(45)-C(44)-H(44)	120.6
C(43)-C(44)-H(44)	120.6
C(44)-C(45)-C(40)	120.4(6)
C(44)-C(45)-H(45)	119.8
C(40)-C(45)-H(45)	119.8
C(31)-O(46)-C(47)	118.8(5)
O(46)-C(47)-C(48)	110.7(6)
O(46)-C(47)-H(47A)	109.5
C(48)-C(47)-H(47A)	109.5
O(46)-C(47)-H(47B)	109.5
C(48)-C(47)-H(47B)	109.5
H(47A)-C(47)-H(47B)	108.1
C(53)-C(48)-C(49)	121.3(7)
C(53)-C(48)-C(47)	119.5(8)
C(49)-C(48)-C(47)	119.2(7)
C(48)-C(49)-C(50)	118.2(7)
C(48)-C(49)-H(49)	120.9
C(50)-C(49)-H(49)	120.9
C(51)-C(50)-C(49)	118.7(8)
C(51)-C(50)-H(50)	120.7
C(49)-C(50)-H(50)	120.7
C(52)-C(51)-C(50)	117.5(7)
C(52)-C(51)-C(54)	121.2(9)
C(50)-C(51)-C(54)	121.3(9)
C(51)-C(52)-C(53)	123.5(8)
C(51)-C(52)-H(52)	118.3
C(53)-C(52)-H(52)	118.3
C(48)-C(53)-C(52)	120.8(8)
C(48)-C(53)-H(53)	119.6
C(52)-C(53)-H(53)	119.6
C(51)-C(54)-H(54A)	109.5
C(51)-C(54)-H(54B)	109.5
H(54A)-C(54)-H(54B)	109.5
C(51)-C(54)-H(54C)	109.5
H(54A)-C(54)-H(54C)	109.5
H(54B)-C(54)-H(54C)	109.5

Symmetry transformations used to generate equivalent atoms:

Table 4. Anisotropic displacement parameters (A^2 x 10^3) for **4**-Co-**4**.
The anisotropic displacement factor exponent takes the form:
-2 pi^2 [h^2 a*^2 U11 + ... + 2 h k a* b* U12]

	U11	U22	U33	U23	U13	U12
Co	29(1)	45(1)	38(1)	1(1)	12(1)	1(1)
N(1)	40(3)	48(3)	39(3)	3(2)	17(2)	6(3)
P(1)	48(1)	50(1)	79(1)	6(1)	6(1)	-8(1)
F(1)	121(4)	156(5)	91(4)	20(4)	26(3)	-48(4)
C(2)	36(3)	44(4)	40(3)	2(3)	15(3)	2(3)
F(2)	90(3)	66(3)	109(4)	-5(3)	2(3)	-18(2)
P(2)	59(1)	98(2)	58(1)	-4(1)	17(1)	27(1)
C(3)	39(4)	58(4)	50(4)	-4(3)	17(3)	-8(3)
F(3)	112(4)	97(4)	110(4)	8(3)	48(3)	-21(3)
C(4)	33(4)	70(5)	49(4)	-4(3)	13(3)	11(3)
F(4)	104(4)	92(3)	98(4)	-3(3)	-16(3)	-37(3)
C(5)	42(4)	59(4)	50(4)	-1(3)	15(3)	11(3)
F(5)	78(3)	76(3)	146(5)	-1(3)	18(3)	19(3)
C(6)	42(4)	50(4)	36(3)	5(3)	14(3)	8(3)
F(6)	66(3)	85(3)	227(7)	39(4)	17(4)	17(3)
C(7)	36(4)	47(4)	53(4)	2(3)	22(3)	0(3)
F(7)	103(4)	161(5)	72(3)	14(3)	11(3)	52(4)
N(8)	37(3)	50(3)	62(3)	4(3)	23(3)	5(2)
F(8)	89(4)	188(6)	116(4)	1(4)	52(3)	25(4)
C(9)	43(4)	56(4)	96(6)	2(4)	27(4)	8(3)
F(9)	132(5)	198(6)	69(3)	22(4)	24(3)	94(4)
C(10)	73(6)	42(4)	127(7)	-4(4)	41(5)	11(4)
F(10)	95(4)	162(5)	180(6)	45(5)	79(4)	25(4)
C(11)	68(5)	43(4)	129(7)	-14(4)	42(5)	-4(4)
F(11)	163(5)	110(4)	103(4)	-24(3)	51(4)	15(4)
F(12)	187(6)	97(4)	120(5)	-21(4)	27(4)	13(4)
C(12)	49(4)	44(4)	95(6)	-5(4)	29(4)	-9(3)
C(13)	47(4)	46(4)	29(3)	6(3)	13(3)	8(3)
N(14)	44(3)	57(3)	31(3)	0(2)	17(2)	-5(3)
C(15)	47(4)	66(5)	40(4)	3(3)	18(3)	-7(4)
C(16)	81(6)	55(4)	48(4)	-6(3)	26(4)	-13(4)
C(17)	88(6)	45(4)	77(5)	-4(4)	23(4)	7(4)
C(18)	53(4)	51(4)	70(5)	-5(4)	11(3)	1(3)
O(19)	52(4)	146(6)	92(4)	-13(4)	18(3)	62(4)
C(20)	103(8)	134(9)	110(8)	-4(7)	4(7)	-52(8)
C(21)	38(5)	303(17)	55(5)	31(8)	11(4)	-47(7)
C(22)	149(11)	170(11)	67(7)	4(7)	19(8)	-104(10)
C(23)	174(12)	94(7)	94(8)	4(6)	73(9)	20(8)
C(24)	51(5)	123(8)	67(5)	28(5)	22(4)	19(5)
C(25)	64(6)	111(7)	67(5)	-11(5)	15(4)	-15(5)
C(26)	58(6)	214(12)	69(6)	-5(7)	31(5)	45(7)
C(27)	58(7)	460(30)	141(11)	109(14)	50(7)	60(11)
N(28)	36(3)	45(3)	41(3)	3(2)	13(2)	4(2)
C(29)	34(3)	51(4)	35(3)	6(3)	7(3)	1(3)
C(30)	42(4)	66(4)	36(3)	0(3)	3(3)	4(3)
C(31)	32(3)	49(4)	46(4)	-1(3)	6(3)	1(3)
C(32)	32(3)	44(3)	52(4)	4(3)	19(3)	5(3)
C(33)	34(3)	35(3)	46(3)	-3(3)	18(3)	-2(3)
C(34)	40(4)	45(4)	42(3)	3(3)	11(3)	4(3)
N(35)	39(3)	47(3)	44(3)	4(2)	18(2)	4(2)
C(36)	43(4)	65(4)	53(4)	6(3)	22(3)	4(3)
C(37)	63(5)	61(4)	61(5)	6(4)	36(4)	11(4)
C(38)	75(5)	66(4)	41(4)	9(3)	30(4)	8(4)
C(39)	58(4)	68(4)	35(3)	8(3)	13(3)	6(3)
C(40)	39(3)	38(3)	38(3)	-2(3)	13(3)	4(3)
N(41)	40(3)	47(3)	37(3)	-2(2)	12(2)	8(2)
C(42)	47(4)	65(4)	48(4)	-1(3)	11(3)	17(3)
C(43)	72(5)	76(5)	35(4)	-3(3)	15(4)	12(4)
C(44)	84(6)	76(5)	46(4)	6(4)	34(4)	9(4)
C(45)	54(4)	61(4)	47(4)	-5(3)	26(3)	0(3)
O(46)	36(3)	89(4)	81(3)	12(3)	15(2)	5(2)

C(47)	63(5)	82(5)	77(5)	8(5)	12(4)	1(4)
C(48)	52(4)	56(4)	71(5)	-2(4)	15(4)	-1(4)
C(49)	60(5)	73(5)	120(8)	-25(5)	45(5)	-4(4)
C(50)	102(7)	90(6)	66(5)	-22(5)	10(5)	-11(5)
C(51)	37(4)	58(4)	103(7)	-6(5)	4(4)	-2(3)
C(52)	48(5)	83(6)	97(7)	7(5)	23(5)	-8(4)
C(53)	62(5)	68(5)	80(5)	8(4)	25(4)	-9(4)
C(54)	51(5)	102(7)	191(11)	-1(7)	-17(6)	-14(5)

Table 5. Hydrogen coordinates (x 10^4) and isotropic displacement parameters (A^2 x 10^3) for **4**-Co-**4**.

	x	y	z	U(eq)
H(3)	9777	5080	8711	58
H(5)	9822	2533	8301	61
H(9)	6636	5548	7731	77
H(10)	7003	6896	8289	95
H(11)	8229	7210	8894	94
H(12)	9057	6142	8923	74
H(15)	6707	1825	7297	60
H(16)	7106	429	7274	72
H(17)	8334	181	7604	85
H(18)	9126	1323	8014	72
H(20A)	10834	3027	8071	149
H(20B)	11069	2867	9106	149
H(22)	11828	2959	7797	160
H(23)	13008	3089	8021	137
H(25)	13270	4619	10045	99
H(26)	12054	4526	9792	133
H(27A)	14241	3394	9084	322
H(27B)	14318	4096	9817	322
H(27C)	14130	4371	8819	322
H(30)	5081	3956	5125	61
H(32)	4844	3625	7497	50
H(36)	8263	3816	6308	63
H(37)	8022	3913	4811	70
H(38)	6834	4085	3854	70
H(39)	5912	4056	4444	65
H(42)	7932	3346	9692	65
H(43)	7462	3192	10809	74
H(44)	6211	3260	10458	79
H(45)	5484	3488	8999	62
H(47A)	3733	4092	6709	93
H(47B)	3699	3109	6456	93
H(49)	3066	3648	4465	97
H(50)	1840	3904	3489	109
H(52)	1282	4160	5622	92
H(53)	2439	3974	6519	84
H(54A)	329	4073	4207	196
H(54B)	532	3948	3350	196
H(54C)	587	4864	3783	196

Table 6. Torsion angles [deg] for **4**-Co-**4**.

N(28)-Co-N(1)-C(2)	65(2)
N(41)-Co-N(1)-C(2)	-92.5(4)
N(35)-Co-N(1)-C(2)	90.2(4)
N(14)-Co-N(1)-C(2)	-179.1(4)
N(8)-Co-N(1)-C(2)	-5.6(4)
N(28)-Co-N(1)-C(6)	-106(2)
N(41)-Co-N(1)-C(6)	96.0(4)
N(35)-Co-N(1)-C(6)	-81.3(4)
N(14)-Co-N(1)-C(6)	9.5(4)
N(8)-Co-N(1)-C(6)	-177.0(4)
C(6)-N(1)-C(2)-C(3)	2.6(8)
Co-N(1)-C(2)-C(3)	-168.8(4)
C(6)-N(1)-C(2)-C(7)	-179.5(5)
Co-N(1)-C(2)-C(7)	9.1(6)
N(1)-C(2)-C(3)-C(4)	-1.5(9)
C(7)-C(2)-C(3)-C(4)	-179.2(6)
C(2)-C(3)-C(4)-O(19)	178.5(5)
C(2)-C(3)-C(4)-C(5)	-0.2(9)
O(19)-C(4)-C(5)-C(6)	-177.8(6)
C(3)-C(4)-C(5)-C(6)	0.7(9)
C(2)-N(1)-C(6)-C(5)	-2.0(8)
Co-N(1)-C(6)-C(5)	169.4(4)
C(2)-N(1)-C(6)-C(13)	178.9(5)
Co-N(1)-C(6)-C(13)	-9.6(6)
C(4)-C(5)-C(6)-N(1)	0.3(9)
C(4)-C(5)-C(6)-C(13)	179.3(6)
N(1)-C(2)-C(7)-N(8)	-8.0(7)
C(3)-C(2)-C(7)-N(8)	169.8(6)
N(1)-C(2)-C(7)-C(12)	170.7(6)
C(3)-C(2)-C(7)-C(12)	-11.5(10)
C(12)-C(7)-N(8)-C(9)	0.6(9)
C(2)-C(7)-N(8)-C(9)	179.4(6)
C(12)-C(7)-N(8)-Co	-175.1(5)
C(2)-C(7)-N(8)-Co	3.7(6)
N(28)-Co-N(8)-C(9)	10.7(6)
N(1)-Co-N(8)-C(9)	-174.6(6)
N(41)-Co-N(8)-C(9)	-67.0(6)
N(35)-Co-N(8)-C(9)	89.6(6)
N(14)-Co-N(8)-C(9)	-160.2(5)
N(28)-Co-N(8)-C(7)	-174.1(4)
N(1)-Co-N(8)-C(7)	0.7(4)
N(41)-Co-N(8)-C(7)	108.3(4)
N(35)-Co-N(8)-C(7)	-95.2(4)
N(14)-Co-N(8)-C(7)	15.0(7)
C(7)-N(8)-C(9)-C(10)	-1.1(11)
Co-N(8)-C(9)-C(10)	174.0(6)
N(8)-C(9)-C(10)-C(11)	0.8(13)
C(9)-C(10)-C(11)-C(12)	0.0(13)
N(8)-C(7)-C(12)-C(11)	0.2(11)
C(2)-C(7)-C(12)-C(11)	-178.5(7)
C(10)-C(11)-C(12)-C(7)	-0.5(12)
N(1)-C(6)-C(13)-N(14)	2.4(7)
C(5)-C(6)-C(13)-N(14)	-176.6(5)
N(1)-C(6)-C(13)-C(18)	-175.4(6)
C(5)-C(6)-C(13)-C(18)	5.6(9)
C(18)-C(13)-N(14)-C(15)	-0.2(8)
C(6)-C(13)-N(14)-C(15)	-178.1(5)
C(18)-C(13)-N(14)-Co	-177.1(5)
C(6)-C(13)-N(14)-Co	5.1(6)
N(28)-Co-N(14)-C(15)	-9.4(5)
N(1)-Co-N(14)-C(15)	175.7(5)
N(41)-Co-N(14)-C(15)	68.0(5)
N(35)-Co-N(14)-C(15)	-87.4(5)
N(8)-Co-N(14)-C(15)	161.4(5)
N(28)-Co-N(14)-C(13)	167.2(4)
N(1)-Co-N(14)-C(13)	-7.7(4)
N(41)-Co-N(14)-C(13)	-115.4(4)

N(35)-Co-N(14)-C(13)	89.2(4)
N(8)-Co-N(14)-C(13)	-22.0(6)
C(13)-N(14)-C(15)-C(16)	-0.2(8)
Co-N(14)-C(15)-C(16)	176.3(4)
N(14)-C(15)-C(16)-C(17)	-0.5(10)
C(15)-C(16)-C(17)-C(18)	1.6(11)
C(16)-C(17)-C(18)-C(13)	-1.9(11)
N(14)-C(13)-C(18)-C(17)	1.2(10)
C(6)-C(13)-C(18)-C(17)	178.9(6)
C(5)-C(4)-O(19)-C(20)	2.9(12)
C(3)-C(4)-O(19)-C(20)	-175.7(8)
C(4)-O(19)-C(20)-C(21)	173.0(6)
O(19)-C(20)-C(21)-C(22)	-142.5(11)
O(19)-C(20)-C(21)-C(26)	49.2(16)
C(26)-C(21)-C(22)-C(23)	4(2)
C(20)-C(21)-C(22)-C(23)	-165.5(10)
C(21)-C(22)-C(23)-C(24)	-0.8(19)
C(22)-C(23)-C(24)-C(25)	-1.7(16)
C(22)-C(23)-C(24)-C(27)	179.5(11)
C(23)-C(24)-C(25)-C(26)	0.5(14)
C(27)-C(24)-C(25)-C(26)	179.3(10)
C(24)-C(25)-C(26)-C(21)	3.1(15)
C(22)-C(21)-C(26)-C(25)	-5.4(18)
C(20)-C(21)-C(26)-C(25)	162.3(11)
N(1)-Co-N(28)-C(33)	-156.3(19)
N(41)-Co-N(28)-C(33)	2.0(4)
N(35)-Co-N(28)-C(33)	178.4(4)
N(14)-Co-N(28)-C(33)	89.3(4)
N(8)-Co-N(28)-C(33)	-86.6(4)
N(1)-Co-N(28)-C(29)	23(2)
N(41)-Co-N(28)-C(29)	-178.2(5)
N(35)-Co-N(28)-C(29)	-1.9(4)
N(14)-Co-N(28)-C(29)	-91.0(4)
N(8)-Co-N(28)-C(29)	93.2(4)
C(33)-N(28)-C(29)-C(30)	-0.5(9)
Co-N(28)-C(29)-C(30)	179.8(5)
C(33)-N(28)-C(29)-C(34)	-178.5(5)
Co-N(28)-C(29)-C(34)	1.8(7)
N(28)-C(29)-C(30)-C(31)	0.3(9)
C(34)-C(29)-C(30)-C(31)	178.0(6)
C(29)-C(30)-C(31)-O(46)	179.7(5)
C(29)-C(30)-C(31)-C(32)	-0.3(9)
O(46)-C(31)-C(32)-C(33)	-179.4(6)
C(30)-C(31)-C(32)-C(33)	0.5(9)
C(29)-N(28)-C(33)-C(32)	0.7(8)
Co-N(28)-C(33)-C(32)	-179.5(4)
C(29)-N(28)-C(33)-C(40)	179.7(5)
Co-N(28)-C(33)-C(40)	-0.5(6)
C(31)-C(32)-C(33)-N(28)	-0.8(8)
C(31)-C(32)-C(33)-C(40)	-179.6(5)
N(28)-C(29)-C(34)-N(35)	-0.3(7)
C(30)-C(29)-C(34)-N(35)	-178.2(6)
N(28)-C(29)-C(34)-C(39)	178.4(6)
C(30)-C(29)-C(34)-C(39)	0.5(10)
C(39)-C(34)-N(35)-C(36)	-1.4(8)
C(29)-C(34)-N(35)-C(36)	177.3(5)
C(39)-C(34)-N(35)-Co	-179.9(5)
C(29)-C(34)-N(35)-Co	-1.1(6)
N(28)-Co-N(35)-C(36)	-176.7(5)
N(1)-Co-N(35)-C(36)	5.6(5)
N(41)-Co-N(35)-C(36)	-168.2(5)
N(14)-Co-N(35)-C(36)	-71.8(5)
N(8)-Co-N(35)-C(36)	83.5(5)
N(28)-Co-N(35)-C(34)	1.6(4)
N(1)-Co-N(35)-C(34)	-176.1(4)
N(41)-Co-N(35)-C(34)	10.1(7)
N(14)-Co-N(35)-C(34)	106.5(4)
N(8)-Co-N(35)-C(34)	-98.2(4)
C(34)-N(35)-C(36)-C(37)	-0.1(9)
Co-N(35)-C(36)-C(37)	178.2(5)
N(35)-C(36)-C(37)-C(38)	2.0(10)

C(36)-C(37)-C(38)-C(39)	-2.3(10)
N(35)-C(34)-C(39)-C(38)	1.1(10)
C(29)-C(34)-C(39)-C(38)	-177.6(6)
C(37)-C(38)-C(39)-C(34)	0.8(10)
N(28)-C(33)-C(40)-N(41)	-2.4(7)
C(32)-C(33)-C(40)-N(41)	176.6(5)
N(28)-C(33)-C(40)-C(45)	179.8(5)
C(32)-C(33)-C(40)-C(45)	-1.3(9)
C(45)-C(40)-N(41)-C(42)	0.4(8)
C(33)-C(40)-N(41)-C(42)	-177.5(5)
C(45)-C(40)-N(41)-Co	-178.0(4)
C(33)-C(40)-N(41)-Co	4.0(6)
N(28)-Co-N(41)-C(42)	178.3(5)
N(1)-Co-N(41)-C(42)	-3.8(5)
N(35)-Co-N(41)-C(42)	169.8(5)
N(14)-Co-N(41)-C(42)	73.0(5)
N(8)-Co-N(41)-C(42)	-80.6(5)
N(28)-Co-N(41)-C(40)	-3.4(4)
N(1)-Co-N(41)-C(40)	174.5(4)
N(35)-Co-N(41)-C(40)	-11.9(7)
N(14)-Co-N(41)-C(40)	-108.7(4)
N(8)-Co-N(41)-C(40)	97.7(4)
C(40)-N(41)-C(42)-C(43)	-0.7(9)
Co-N(41)-C(42)-C(43)	177.6(5)
N(41)-C(42)-C(43)-C(44)	0.6(11)
C(42)-C(43)-C(44)-C(45)	-0.1(11)
C(43)-C(44)-C(45)-C(40)	-0.1(10)
N(41)-C(40)-C(45)-C(44)	0.0(9)
C(33)-C(40)-C(45)-C(44)	177.6(6)
C(32)-C(31)-O(46)-C(47)	-4.8(10)
C(30)-C(31)-O(46)-C(47)	175.2(6)
C(31)-O(46)-C(47)-C(48)	177.0(6)
O(46)-C(47)-C(48)-C(53)	-159.8(7)
O(46)-C(47)-C(48)-C(49)	19.5(10)
C(53)-C(48)-C(49)-C(50)	1.8(12)
C(47)-C(48)-C(49)-C(50)	-177.4(7)
C(48)-C(49)-C(50)-C(51)	-1.3(12)
C(49)-C(50)-C(51)-C(52)	-0.5(12)
C(49)-C(50)-C(51)-C(54)	178.4(7)
C(50)-C(51)-C(52)-C(53)	2.0(12)
C(54)-C(51)-C(52)-C(53)	-176.9(7)
C(49)-C(48)-C(53)-C(52)	-0.5(12)
C(47)-C(48)-C(53)-C(52)	178.8(7)
C(51)-C(52)-C(53)-C(48)	-1.6(12)

Symmetry transformations used to generate equivalent atoms:

Table 7. Hydrogen bonds for **4**-Co-**4** [A and deg.].

D-H...A	d(D-H)	d(H...A)	d(D...A)	<(DHA)

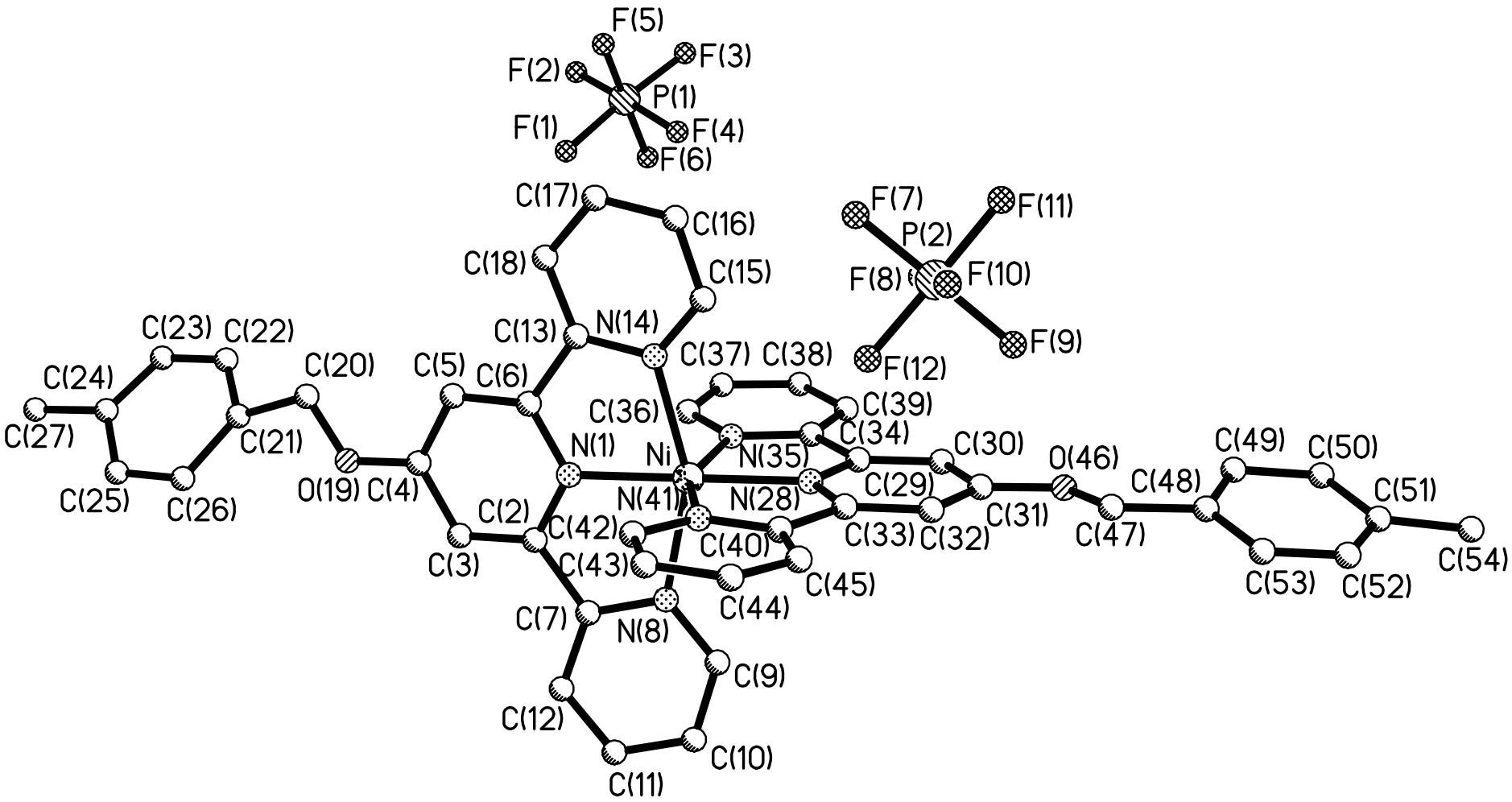
F(5)
F(2)
F(3)
P(1)
F(1)
F(4)
F(6)
F(7)
F(11)
P(2)
F(8)
F(10)
F(9)
F(12)
C(17)
C(16)
C(18)
C(15)
C(23)
C(22)
C(13)
N(14)
C(37)
C(38)
C(24)
C(20)
C(5)
C(6)
C(39)
C(36)
C(27)
C(21)
N(1)
Ni
N(35)
C(34)
C(30)
O(46)
C(49)
C(50)
C(25)
O(19)
C(4)
C(29)
C(48)
C(51)
C(26)
N(41)
N(28)
C(31)
C(2)
C(42)
C(33)
C(32)
C(47)
C(40)
C(3)
C(43)
C(45)
C(54)
C(53)
C(52)
C(44)
C(7)
N(8)
C(9)
C(12)
C(10)
C(11)

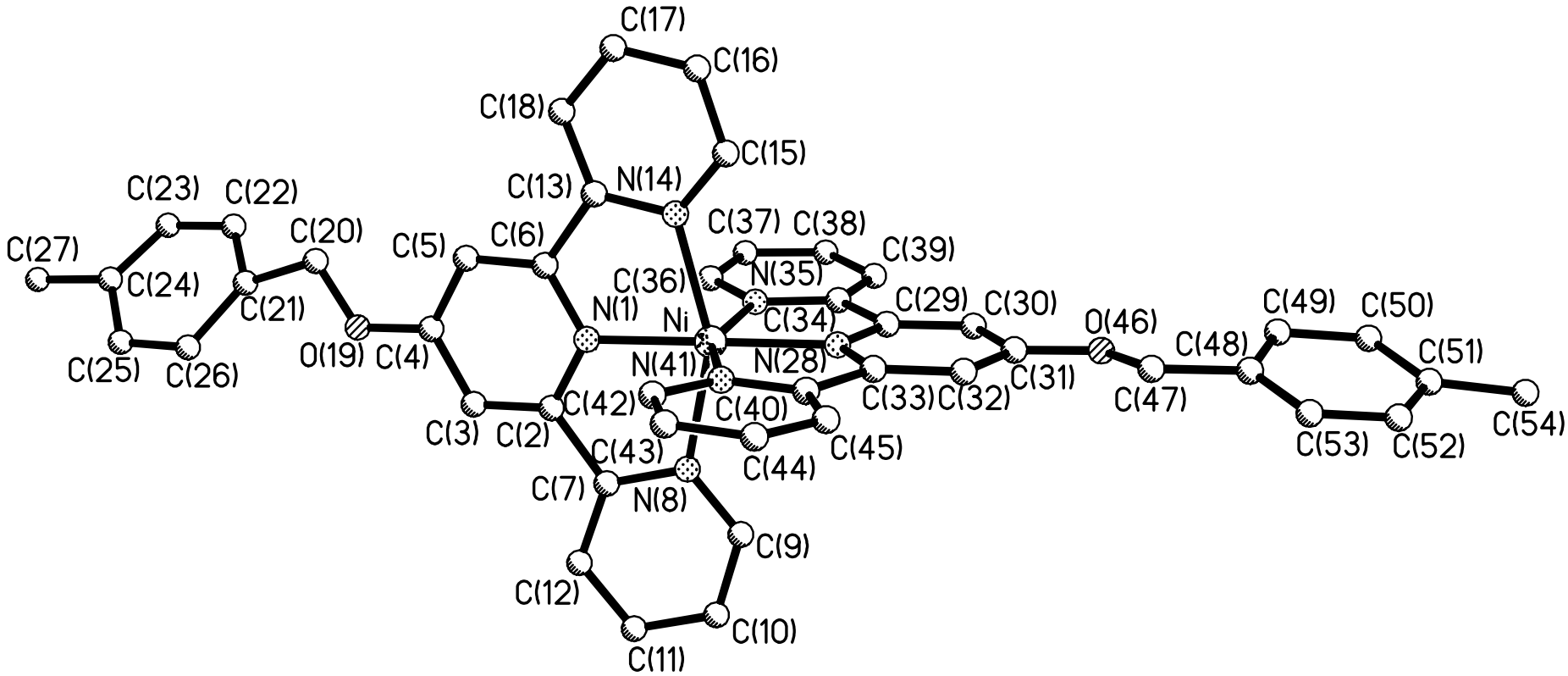
C(17)
C(16)
C(18)
C(15)
C(13)
N(14)
C(23)
C(22)
C(37)
C(38)
C(20)
C(5)
C(6)
C(39)
C(27)
C(24)
C(36)
N(35)
C(29)
C(30)
C(49)
C(50)
C(21)
N(1)
Ni
C(34)
O(46)
C(48)
C(25)
C(26)
O(19)
C(4)
N(41)
N(28)
C(51)
C(31)
C(42)
C(40)
C(33)
C(32)
C(47)
C(3)
C(2)
C(43)
C(45)
C(53)
C(52)
C(54)
C(44)
C(7)
N(8)
C(9)
C(12)
C(10)
C(11)

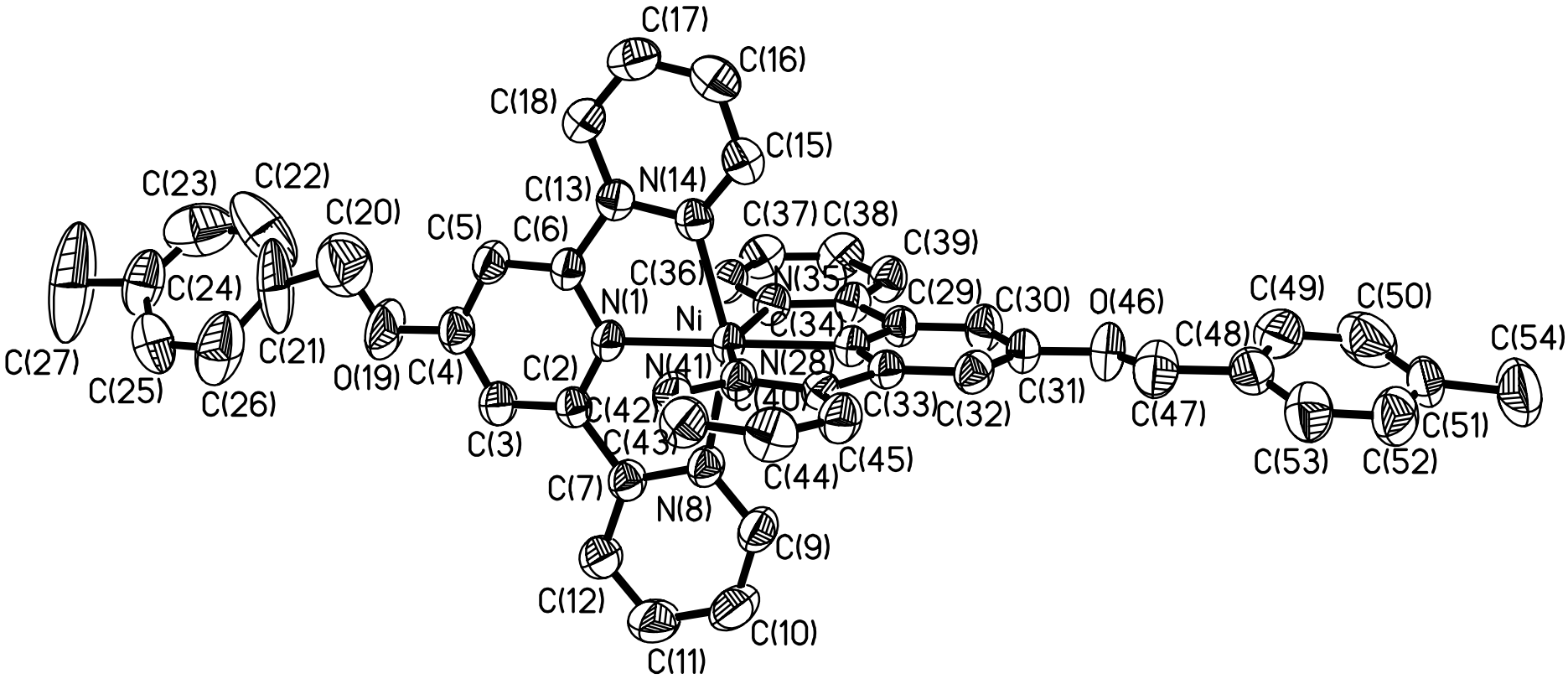
C(17)
C(16)
C(18)
C(15)
C(23)
C(22)
C(13)
N(14)
C(20)
C(5)
C(6)
C(37)
C(38)
C(39)
C(36)
N(35)
C(24)
N(1)
Ni
C(34)
C(29)
C(30)
O(46)
C(49)
C(50)
C(27)
C(21)
O(19)
C(4)
C(2)
N(41)
N(28)
C(48)
C(54)
C(25)
C(26)
C(42)
C(40)
C(33)
C(32)
C(31)
C(47)
C(3)
C(43)
C(44)
C(45)
C(51)
C(53)
C(52)
C(7)
N(8)
C(9)
C(12)
C(10)
C(11)

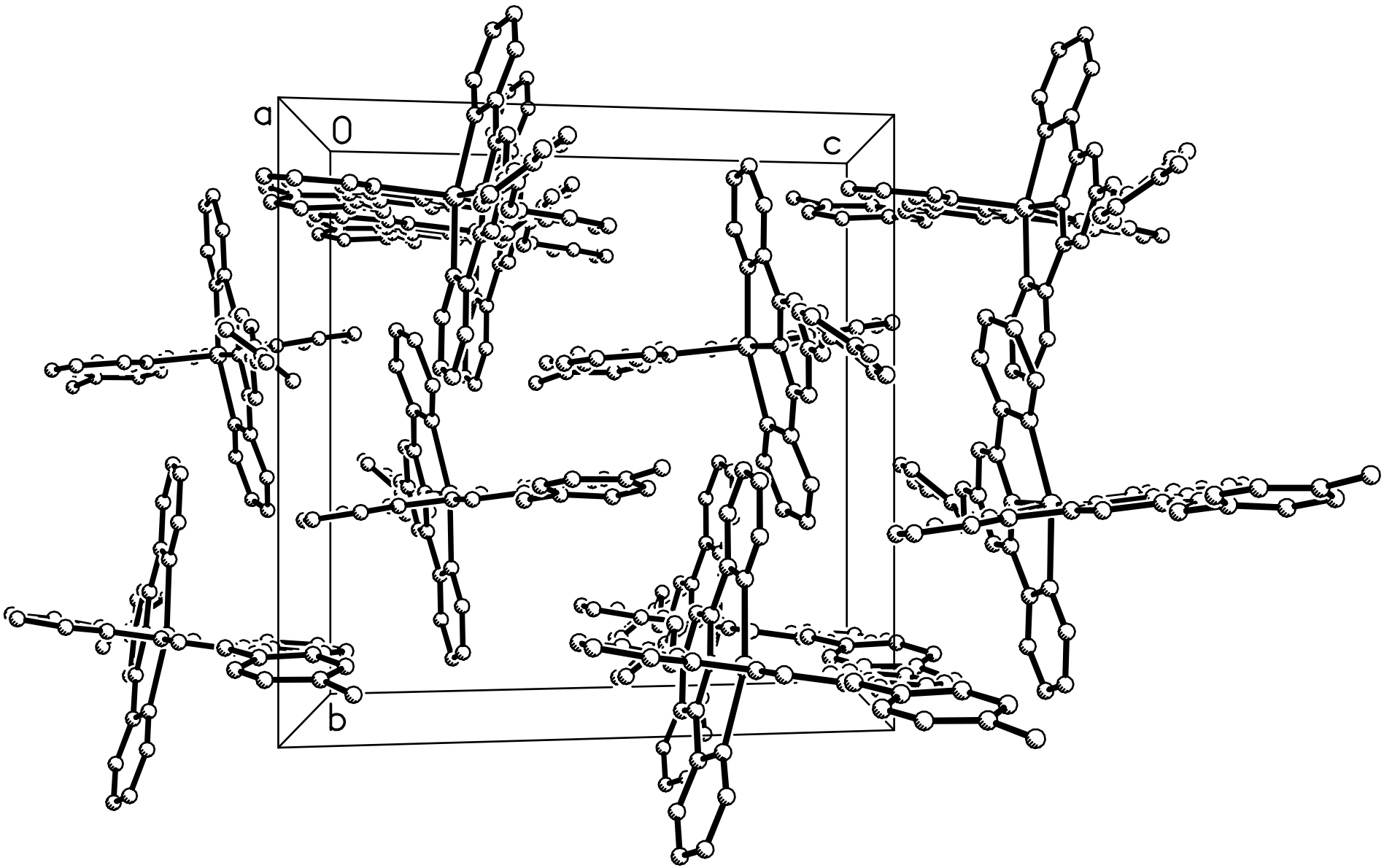
a
0
c
b

Table 1. Crystal data and structure refinement for **4**-Ni-**4**.

Identification code	**4**-Ni-**4**
Empirical formula	C46 H38 F12 N6 Ni O2 P2
Formula weight	1055.47
Temperature	300(2) K
Wavelength	0.71073 A
Crystal system, space group	monoclinic, P2(1)/c
Unit cell dimensions	a = 19.6847(8) A alpha = 90 deg. b = 15.5312(6) A beta = 110.570(1) deg. c = 16.0512(7) A gamma = 90 deg.
Volume	4594.4(3) A^3
Z, Calculated density	4, 1.526 Mg/m^3
Absorption coefficient	0.587 mm^-1
F(000)	2152
Crystal size	0.65 x 0.19 x 0.18 mm
Theta range for data collection	2.41 to 24.71 deg.
Limiting indices	-23<=h<=23, -15<=k<=18, -18<=l<=18
Reflections collected / unique	24253 / 7813 [R(int) = 0.0381]
Completeness to theta = 24.71	99.7 %
Max. and min. transmission	0.9017 and 0.7015
Refinement method	Full-matrix least-squares on F^2
Data / restraints / parameters	7813 / 0 / 624
Goodness-of-fit on F^2	1.048
Final R indices [I>2sigma(I)]	R1 = 0.0624, wR2 = 0.1636
R indices (all data)	R1 = 0.0785, wR2 = 0.1780
Largest diff. peak and hole	1.630 and -0.537 e.A^-3

Table 2. Atomic coordinates (x 10^4) and equivalent isotropic displacement parameters (A^2 x 10^3) for **4**-Ni-**4**.
U(eq) is defined as one third of the trace of the orthogonalized Uij tensor.

	x	y	z	U(eq)
Ni	7385(1)	3714(1)	7649(1)	37(1)
N(1)	8467(2)	3730(2)	8159(2)	38(1)
P(1)	9641(1)	2513(1)	894(1)	72(1)
F(1)	10142(2)	2955(3)	1786(2)	115(1)
P(2)	5031(1)	1109(1)	7179(1)	62(1)
C(2)	8814(2)	4489(2)	8377(2)	41(1)
F(2)	10300(2)	2400(3)	579(3)	129(2)
C(3)	9552(2)	4550(3)	8580(3)	51(1)
F(3)	9112(2)	2133(3)	0(2)	128(2)
C(4)	9935(2)	3808(3)	8553(3)	52(1)
F(4)	8956(2)	2689(3)	1189(3)	121(1)
C(5)	9574(2)	3027(3)	8331(3)	49(1)
F(5)	9717(3)	1633(3)	1374(3)	136(2)
C(6)	8835(2)	3012(2)	8137(2)	40(1)
F(6)	9532(2)	3441(3)	439(3)	120(1)
F(7)	5679(2)	439(2)	7483(3)	102(1)
C(7)	8320(2)	5219(2)	8355(3)	44(1)
N(8)	7605(2)	5034(2)	7986(2)	44(1)
F(8)	5293(2)	1462(3)	6429(3)	123(1)
F(9)	4393(2)	1773(2)	6899(3)	132(2)
C(9)	7129(2)	5655(3)	7950(3)	57(1)
F(10)	4785(2)	753(2)	7961(3)	103(1)
C(10)	7334(3)	6467(3)	8279(4)	74(2)
F(11)	4525(2)	413(2)	6538(2)	108(1)
C(11)	8065(3)	6656(3)	8654(4)	76(2)
F(12)	5548(2)	1784(2)	7848(2)	92(1)
C(12)	8560(2)	6029(3)	8689(3)	60(1)
C(13)	8365(2)	2236(2)	7875(2)	41(1)
N(14)	7650(2)	2392(2)	7638(2)	40(1)
C(15)	7186(2)	1732(3)	7423(3)	46(1)
C(16)	7412(3)	893(3)	7413(3)	57(1)
C(17)	8140(3)	738(3)	7636(3)	66(1)
C(18)	8624(2)	1415(3)	7871(3)	60(1)
O(19)	10659(2)	3897(3)	8729(3)	90(1)
C(20)	11067(4)	3273(5)	8659(5)	112(2)
C(21)	11829(3)	3651(6)	8788(5)	123(3)
C(22)	12118(5)	3290(6)	8269(5)	133(3)
C(23)	12823(5)	3384(5)	8404(5)	111(2)
C(24)	13273(3)	3839(5)	9067(4)	82(2)
C(25)	12993(3)	4270(4)	9585(4)	83(2)
C(26)	12271(3)	4203(6)	9462(4)	115(3)
C(27)	14077(4)	3967(9)	9226(6)	213(7)
N(28)	6312(2)	3743(2)	7058(2)	39(1)
C(29)	6021(2)	3851(2)	6169(2)	41(1)
C(30)	5284(2)	3877(3)	5747(3)	50(1)
C(31)	4833(2)	3793(3)	6245(3)	47(1)
C(32)	5142(2)	3679(2)	7159(3)	44(1)
C(33)	5886(2)	3664(2)	7544(2)	38(1)
C(34)	6571(2)	3917(2)	5731(3)	43(1)
N(35)	7266(2)	3859(2)	6290(2)	43(1)
C(36)	7792(2)	3873(3)	5942(3)	47(1)
C(37)	7646(2)	3939(3)	5038(3)	54(1)
C(38)	6948(3)	4010(3)	4478(3)	59(1)
C(39)	6396(2)	3999(3)	4828(3)	52(1)
C(40)	6301(2)	3547(2)	8510(2)	38(1)
N(41)	7030(2)	3524(2)	8723(2)	39(1)
C(42)	7449(2)	3388(3)	9576(3)	47(1)
C(43)	7169(2)	3287(3)	10238(3)	57(1)
C(44)	6427(3)	3317(3)	10022(3)	60(1)
C(45)	5991(2)	3450(3)	9152(3)	52(1)

O(46)	4120(2)	3829(2)	5787(2)	67(1)
C(47)	3631(3)	3692(3)	6216(4)	70(1)
C(48)	2854(3)	3806(3)	5586(4)	61(1)
C(49)	2694(3)	3764(3)	4694(5)	82(2)
C(50)	1956(4)	3915(4)	4105(4)	92(2)
C(51)	1425(2)	4076(3)	4467(4)	71(2)
C(52)	1633(3)	4078(3)	5371(4)	77(2)
C(53)	2329(3)	3960(3)	5912(4)	72(1)
C(54)	650(3)	4267(5)	3882(6)	126(3)

Table 3. Bond lengths [A] and angles [deg] for **4**-Ni-**4**.

Ni-N(28)	1.989(3)
Ni-N(1)	1.994(3)
Ni-N(41)	2.097(3)
Ni-N(14)	2.120(3)
Ni-N(35)	2.123(3)
Ni-N(8)	2.126(3)
N(1)-C(6)	1.337(5)
N(1)-C(2)	1.345(5)
P(1)-F(5)	1.550(4)
P(1)-F(2)	1.560(4)
P(1)-F(3)	1.562(3)
P(1)-F(1)	1.582(3)
P(1)-F(6)	1.595(4)
P(1)-F(4)	1.602(4)
P(2)-F(9)	1.564(3)
P(2)-F(8)	1.568(4)
P(2)-F(11)	1.580(3)
P(2)-F(7)	1.585(3)
P(2)-F(12)	1.587(3)
P(2)-F(10)	1.594(4)
C(2)-C(3)	1.375(5)
C(2)-C(7)	1.487(5)
C(3)-C(4)	1.387(6)
C(3)-H(3)	0.9300
C(4)-O(19)	1.358(5)
C(4)-C(5)	1.389(6)
C(5)-C(6)	1.376(5)
C(5)-H(5)	0.9300
C(6)-C(13)	1.488(5)
C(7)-N(8)	1.352(5)
C(7)-C(12)	1.384(6)
N(8)-C(9)	1.332(5)
C(9)-C(10)	1.371(6)
C(9)-H(9)	0.9300
C(10)-C(11)	1.383(7)
C(10)-H(10)	0.9300
C(11)-C(12)	1.365(6)
C(11)-H(11)	0.9300
C(12)-H(12)	0.9300
C(13)-N(14)	1.344(5)
C(13)-C(18)	1.375(6)
N(14)-C(15)	1.335(5)
C(15)-C(16)	1.379(6)
C(15)-H(15)	0.9300
C(16)-C(17)	1.372(6)
C(16)-H(16)	0.9300
C(17)-C(18)	1.379(6)
C(17)-H(17)	0.9300
C(18)-H(18)	0.9300
O(19)-C(20)	1.289(8)
C(20)-C(21)	1.554(8)
C(20)-H(20A)	0.9700
C(20)-H(20B)	0.9700
C(21)-C(22)	1.292(12)
C(21)-C(26)	1.414(11)
C(22)-C(23)	1.335(11)
C(22)-H(22)	0.9300
C(23)-C(24)	1.324(10)
C(23)-H(23)	0.9300
C(24)-C(25)	1.330(8)
C(24)-C(27)	1.525(8)
C(25)-C(26)	1.368(8)
C(25)-H(25)	0.9300
C(26)-H(26)	0.9300
C(27)-H(27A)	0.9600
C(27)-H(27B)	0.9600
C(27)-H(27C)	0.9600

N(28)-C(33)	1.338(5)
N(28)-C(29)	1.349(5)
C(29)-C(30)	1.369(5)
C(29)-C(34)	1.487(5)
C(30)-C(31)	1.392(6)
C(30)-H(30)	0.9300
C(31)-O(46)	1.338(5)
C(31)-C(32)	1.389(6)
C(32)-C(33)	1.375(5)
C(32)-H(32)	0.9300
C(33)-C(40)	1.489(5)
C(34)-N(35)	1.350(5)
C(34)-C(39)	1.374(6)
N(35)-C(36)	1.337(5)
C(36)-C(37)	1.379(6)
C(36)-H(36)	0.9300
C(37)-C(38)	1.357(6)
C(37)-H(37)	0.9300
C(38)-C(39)	1.388(6)
C(38)-H(38)	0.9300
C(39)-H(39)	0.9300
C(40)-N(41)	1.354(4)
C(40)-C(45)	1.377(5)
N(41)-C(42)	1.343(5)
C(42)-C(43)	1.367(6)
C(42)-H(42)	0.9300
C(43)-C(44)	1.377(6)
C(43)-H(43)	0.9300
C(44)-C(45)	1.373(6)
C(44)-H(44)	0.9300
C(45)-H(45)	0.9300
O(46)-C(47)	1.383(6)
C(47)-C(48)	1.519(6)
C(47)-H(47A)	0.9700
C(47)-H(47B)	0.9700
C(48)-C(53)	1.333(7)
C(48)-C(49)	1.355(8)
C(49)-C(50)	1.448(8)
C(49)-H(49)	0.9300
C(50)-C(51)	1.386(8)
C(50)-H(50)	0.9300
C(51)-C(52)	1.362(8)
C(51)-C(54)	1.514(7)
C(52)-C(53)	1.353(7)
C(52)-H(52)	0.9300
C(53)-H(53)	0.9300
C(54)-H(54A)	0.9600
C(54)-H(54B)	0.9600
C(54)-H(54C)	0.9600

N(28)-Ni-N(1)	175.59(12)
N(28)-Ni-N(41)	77.88(12)
N(1)-Ni-N(41)	106.32(12)
N(28)-Ni-N(14)	103.90(12)
N(1)-Ni-N(14)	77.60(12)
N(41)-Ni-N(14)	91.39(12)
N(28)-Ni-N(35)	78.00(12)
N(1)-Ni-N(35)	97.86(12)
N(41)-Ni-N(35)	155.74(12)
N(14)-Ni-N(35)	91.88(12)
N(28)-Ni-N(8)	100.79(12)
N(1)-Ni-N(8)	77.96(12)
N(41)-Ni-N(8)	91.34(12)
N(14)-Ni-N(8)	155.18(12)
N(35)-Ni-N(8)	95.67(12)
C(6)-N(1)-C(2)	120.4(3)
C(6)-N(1)-Ni	119.3(2)
C(2)-N(1)-Ni	119.3(2)
F(5)-P(1)-F(2)	96.6(3)
F(5)-P(1)-F(3)	92.3(2)
F(2)-P(1)-F(3)	91.3(2)

F(5)-P(1)-F(1)	90.7(2)
F(2)-P(1)-F(1)	91.0(2)
F(3)-P(1)-F(1)	176.1(3)
F(5)-P(1)-F(6)	176.2(3)
F(2)-P(1)-F(6)	87.0(3)
F(3)-P(1)-F(6)	89.0(2)
F(1)-P(1)-F(6)	87.9(2)
F(5)-P(1)-F(4)	87.0(3)
F(2)-P(1)-F(4)	176.4(3)
F(3)-P(1)-F(4)	88.7(2)
F(1)-P(1)-F(4)	88.9(2)
F(6)-P(1)-F(4)	89.4(2)
F(9)-P(2)-F(8)	89.8(3)
F(9)-P(2)-F(11)	90.3(2)
F(8)-P(2)-F(11)	92.4(2)
F(9)-P(2)-F(7)	178.9(3)
F(8)-P(2)-F(7)	91.1(2)
F(11)-P(2)-F(7)	90.3(2)
F(9)-P(2)-F(12)	91.0(2)
F(8)-P(2)-F(12)	89.0(2)
F(11)-P(2)-F(12)	178.1(2)
F(7)-P(2)-F(12)	88.28(18)
F(9)-P(2)-F(10)	91.2(2)
F(8)-P(2)-F(10)	178.5(2)
F(11)-P(2)-F(10)	88.8(2)
F(7)-P(2)-F(10)	87.9(2)
F(12)-P(2)-F(10)	89.8(2)
N(1)-C(2)-C(3)	121.3(3)
N(1)-C(2)-C(7)	113.2(3)
C(3)-C(2)-C(7)	125.4(3)
C(2)-C(3)-C(4)	118.4(4)
C(2)-C(3)-H(3)	120.8
C(4)-C(3)-H(3)	120.8
O(19)-C(4)-C(3)	116.9(4)
O(19)-C(4)-C(5)	123.2(4)
C(3)-C(4)-C(5)	119.9(4)
C(6)-C(5)-C(4)	118.6(4)
C(6)-C(5)-H(5)	120.7
C(4)-C(5)-H(5)	120.7
N(1)-C(6)-C(5)	121.3(4)
N(1)-C(6)-C(13)	113.2(3)
C(5)-C(6)-C(13)	125.5(3)
N(8)-C(7)-C(12)	121.6(4)
N(8)-C(7)-C(2)	114.8(3)
C(12)-C(7)-C(2)	123.5(3)
C(9)-N(8)-C(7)	118.3(3)
C(9)-N(8)-Ni	127.6(3)
C(7)-N(8)-Ni	113.8(2)
N(8)-C(9)-C(10)	122.8(4)
N(8)-C(9)-H(9)	118.6
C(10)-C(9)-H(9)	118.6
C(9)-C(10)-C(11)	118.9(4)
C(9)-C(10)-H(10)	120.5
C(11)-C(10)-H(10)	120.5
C(12)-C(11)-C(10)	119.0(4)
C(12)-C(11)-H(11)	120.5
C(10)-C(11)-H(11)	120.5
C(11)-C(12)-C(7)	119.4(4)
C(11)-C(12)-H(12)	120.3
C(7)-C(12)-H(12)	120.3
N(14)-C(13)-C(18)	121.3(4)
N(14)-C(13)-C(6)	114.8(3)
C(18)-C(13)-C(6)	123.9(3)
C(15)-N(14)-C(13)	119.1(3)
C(15)-N(14)-Ni	126.8(3)
C(13)-N(14)-Ni	114.1(2)
N(14)-C(15)-C(16)	122.4(4)
N(14)-C(15)-H(15)	118.8
C(16)-C(15)-H(15)	118.8
C(17)-C(16)-C(15)	118.3(4)
C(17)-C(16)-H(16)	120.9

C(15)-C(16)-H(16)	120.9
C(16)-C(17)-C(18)	119.7(4)
C(16)-C(17)-H(17)	120.1
C(18)-C(17)-H(17)	120.1
C(13)-C(18)-C(17)	119.1(4)
C(13)-C(18)-H(18)	120.4
C(17)-C(18)-H(18)	120.4
C(20)-O(19)-C(4)	123.1(5)
O(19)-C(20)-C(21)	107.8(6)
O(19)-C(20)-H(20A)	110.1
C(21)-C(20)-H(20A)	110.1
O(19)-C(20)-H(20B)	110.1
C(21)-C(20)-H(20B)	110.1
H(20A)-C(20)-H(20B)	108.5
C(22)-C(21)-C(26)	117.6(5)
C(22)-C(21)-C(20)	111.9(8)
C(26)-C(21)-C(20)	129.6(7)
C(21)-C(22)-C(23)	121.1(7)
C(21)-C(22)-H(22)	119.4
C(23)-C(22)-H(22)	119.4
C(24)-C(23)-C(22)	123.5(7)
C(24)-C(23)-H(23)	118.2
C(22)-C(23)-H(23)	118.2
C(23)-C(24)-C(25)	117.6(6)
C(23)-C(24)-C(27)	124.5(8)
C(25)-C(24)-C(27)	117.6(7)
C(24)-C(25)-C(26)	120.6(6)
C(24)-C(25)-H(25)	119.7
C(26)-C(25)-H(25)	119.7
C(25)-C(26)-C(21)	119.1(6)
C(25)-C(26)-H(26)	120.5
C(21)-C(26)-H(26)	120.5
C(24)-C(27)-H(27A)	109.5
C(24)-C(27)-H(27B)	109.5
H(27A)-C(27)-H(27B)	109.5
C(24)-C(27)-H(27C)	109.5
H(27A)-C(27)-H(27C)	109.5
H(27B)-C(27)-H(27C)	109.5
C(33)-N(28)-C(29)	120.5(3)
C(33)-N(28)-Ni	119.9(2)
C(29)-N(28)-Ni	119.6(2)
N(28)-C(29)-C(30)	120.6(4)
N(28)-C(29)-C(34)	113.5(3)
C(30)-C(29)-C(34)	125.9(3)
C(29)-C(30)-C(31)	119.5(4)
C(29)-C(30)-H(30)	120.3
C(31)-C(30)-H(30)	120.3
O(46)-C(31)-C(32)	124.8(4)
O(46)-C(31)-C(30)	116.0(4)
C(32)-C(31)-C(30)	119.1(3)
C(33)-C(32)-C(31)	118.6(4)
C(33)-C(32)-H(32)	120.7
C(31)-C(32)-H(32)	120.7
N(28)-C(33)-C(32)	121.6(3)
N(28)-C(33)-C(40)	113.1(3)
C(32)-C(33)-C(40)	125.3(3)
N(35)-C(34)-C(39)	121.8(4)
N(35)-C(34)-C(29)	114.8(3)
C(39)-C(34)-C(29)	123.4(4)
C(36)-N(35)-C(34)	118.3(3)
C(36)-N(35)-Ni	127.5(3)
C(34)-N(35)-Ni	114.2(2)
N(35)-C(36)-C(37)	122.3(4)
N(35)-C(36)-H(36)	118.8
C(37)-C(36)-H(36)	118.8
C(38)-C(37)-C(36)	119.4(4)
C(38)-C(37)-H(37)	120.3
C(36)-C(37)-H(37)	120.3
C(37)-C(38)-C(39)	119.0(4)
C(37)-C(38)-H(38)	120.5
C(39)-C(38)-H(38)	120.5

C(34)-C(39)-C(38)	119.1(4)
C(34)-C(39)-H(39)	120.4
C(38)-C(39)-H(39)	120.4
N(41)-C(40)-C(45)	121.1(3)
N(41)-C(40)-C(33)	114.3(3)
C(45)-C(40)-C(33)	124.6(3)
C(42)-N(41)-C(40)	118.5(3)
C(42)-N(41)-Ni	126.7(2)
C(40)-N(41)-Ni	114.8(2)
N(41)-C(42)-C(43)	122.7(4)
N(41)-C(42)-H(42)	118.7
C(43)-C(42)-H(42)	118.7
C(42)-C(43)-C(44)	118.7(4)
C(42)-C(43)-H(43)	120.6
C(44)-C(43)-H(43)	120.6
C(45)-C(44)-C(43)	119.4(4)
C(45)-C(44)-H(44)	120.3
C(43)-C(44)-H(44)	120.3
C(44)-C(45)-C(40)	119.6(4)
C(44)-C(45)-H(45)	120.2
C(40)-C(45)-H(45)	120.2
C(31)-O(46)-C(47)	120.0(4)
O(46)-C(47)-C(48)	111.4(4)
O(46)-C(47)-H(47A)	109.4
C(48)-C(47)-H(47A)	109.4
O(46)-C(47)-H(47B)	109.4
C(48)-C(47)-H(47B)	109.4
H(47A)-C(47)-H(47B)	108.0
C(53)-C(48)-C(49)	120.0(5)
C(53)-C(48)-C(47)	119.8(5)
C(49)-C(48)-C(47)	120.2(5)
C(48)-C(49)-C(50)	119.3(5)
C(48)-C(49)-H(49)	120.3
C(50)-C(49)-H(49)	120.3
C(51)-C(50)-C(49)	119.1(6)
C(51)-C(50)-H(50)	120.4
C(49)-C(50)-H(50)	120.4
C(52)-C(51)-C(50)	117.3(5)
C(52)-C(51)-C(54)	121.4(6)
C(50)-C(51)-C(54)	121.3(6)
C(53)-C(52)-C(51)	122.8(5)
C(53)-C(52)-H(52)	118.6
C(51)-C(52)-H(52)	118.6
C(48)-C(53)-C(52)	121.5(6)
C(48)-C(53)-H(53)	119.3
C(52)-C(53)-H(53)	119.3
C(51)-C(54)-H(54A)	109.5
C(51)-C(54)-H(54B)	109.5
H(54A)-C(54)-H(54B)	109.5
C(51)-C(54)-H(54C)	109.5
H(54A)-C(54)-H(54C)	109.5
H(54B)-C(54)-H(54C)	109.5

Symmetry transformations used to generate equivalent atoms:

Table 4. Anisotropic displacement parameters (A^2 x 10^3) for **4**-Ni-**4**.
The anisotropic displacement factor exponent takes the form:
-2 pi^2 [h^2 a*^2 U11 + ... + 2 h k a* b* U12]

	U11	U22	U33	U23	U13	U12
Ni	27(1)	45(1)	38(1)	2(1)	11(1)	1(1)
N(1)	28(1)	47(2)	41(2)	1(1)	12(1)	3(1)
P(1)	58(1)	96(1)	59(1)	4(1)	16(1)	-26(1)
F(1)	100(2)	152(4)	76(2)	-12(2)	11(2)	-45(2)
P(2)	44(1)	53(1)	77(1)	6(1)	6(1)	-8(1)
C(2)	35(2)	47(2)	42(2)	-1(2)	13(2)	-2(2)
F(2)	83(2)	159(4)	164(4)	-38(3)	66(3)	-22(2)
C(3)	35(2)	55(2)	62(3)	-3(2)	18(2)	-3(2)
F(3)	119(3)	183(4)	72(2)	-20(2)	21(2)	-80(3)
C(4)	32(2)	67(3)	55(3)	-4(2)	14(2)	-1(2)
F(4)	83(2)	177(4)	114(3)	5(3)	50(2)	-16(2)
C(5)	35(2)	57(2)	53(2)	-2(2)	14(2)	9(2)
F(5)	169(4)	95(3)	126(3)	22(2)	30(3)	-11(3)
C(6)	32(2)	51(2)	37(2)	2(2)	11(2)	4(2)
F(6)	152(4)	109(3)	103(3)	23(2)	47(3)	-19(3)
F(7)	71(2)	76(2)	139(3)	-1(2)	11(2)	13(2)
C(7)	36(2)	46(2)	53(2)	0(2)	18(2)	-2(2)
N(8)	33(2)	45(2)	57(2)	1(2)	18(2)	1(1)
F(8)	117(3)	152(4)	90(3)	21(2)	26(2)	-45(3)
F(9)	63(2)	84(2)	221(5)	37(3)	12(3)	12(2)
C(9)	39(2)	52(3)	80(3)	3(2)	21(2)	6(2)
F(10)	106(3)	99(2)	112(3)	6(2)	49(2)	-20(2)
C(10)	60(3)	50(3)	118(5)	0(3)	39(3)	11(2)
F(11)	97(2)	91(2)	98(2)	-4(2)	-13(2)	-35(2)
C(11)	69(3)	48(3)	113(4)	-13(3)	33(3)	-5(2)
F(12)	86(2)	62(2)	103(2)	-5(2)	3(2)	-20(2)
C(12)	45(2)	50(2)	85(3)	-7(2)	22(2)	-4(2)
C(13)	39(2)	48(2)	36(2)	0(2)	14(2)	4(2)
N(14)	39(2)	48(2)	34(2)	0(1)	12(1)	-1(1)
C(15)	43(2)	57(3)	41(2)	-1(2)	18(2)	-6(2)
C(16)	66(3)	56(3)	51(2)	-3(2)	22(2)	-13(2)
C(17)	73(3)	46(2)	79(3)	-2(2)	27(3)	7(2)
C(18)	47(2)	52(3)	74(3)	-2(2)	14(2)	8(2)
O(19)	36(2)	133(3)	97(3)	-13(2)	22(2)	25(2)
C(20)	89(5)	112(5)	123(6)	-1(4)	22(4)	-12(4)
C(21)	29(2)	270(11)	67(4)	33(5)	13(3)	-14(4)
C(22)	147(7)	170(8)	70(4)	-2(5)	23(5)	-98(6)
C(23)	168(8)	94(5)	91(5)	2(4)	73(6)	14(5)
C(24)	50(3)	129(5)	74(4)	29(4)	31(3)	21(3)
C(25)	56(3)	107(5)	73(4)	0(3)	8(3)	-18(3)
C(26)	73(4)	205(8)	73(4)	0(5)	34(3)	50(5)
C(27)	52(4)	460(20)	141(8)	110(10)	47(5)	57(7)
N(28)	32(2)	44(2)	39(2)	2(1)	12(1)	1(1)
C(29)	35(2)	47(2)	38(2)	1(2)	8(2)	3(2)
C(30)	40(2)	64(3)	39(2)	3(2)	7(2)	5(2)
C(31)	30(2)	51(2)	53(2)	-1(2)	6(2)	2(2)
C(32)	37(2)	47(2)	53(2)	2(2)	21(2)	0(2)
C(33)	32(2)	38(2)	44(2)	-1(2)	13(2)	-1(2)
C(34)	38(2)	48(2)	40(2)	3(2)	12(2)	3(2)
N(35)	38(2)	49(2)	44(2)	4(1)	17(2)	2(1)
C(36)	42(2)	55(2)	49(2)	7(2)	21(2)	5(2)
C(37)	59(3)	58(3)	58(3)	6(2)	35(2)	3(2)
C(38)	68(3)	68(3)	45(2)	10(2)	24(2)	10(2)
C(39)	48(2)	67(3)	40(2)	6(2)	12(2)	8(2)
C(40)	36(2)	38(2)	41(2)	-1(2)	15(2)	1(2)
N(41)	30(2)	47(2)	40(2)	-1(1)	14(1)	2(1)
C(42)	39(2)	59(2)	39(2)	-2(2)	9(2)	8(2)
C(43)	60(3)	71(3)	37(2)	0(2)	14(2)	11(2)
C(44)	65(3)	75(3)	46(2)	3(2)	27(2)	4(2)
C(45)	42(2)	63(3)	53(2)	2(2)	21(2)	3(2)
O(46)	31(2)	89(2)	74(2)	5(2)	8(1)	4(1)

C(47)	50(3)	75(3)	80(3)	12(3)	18(3)	1(2)
C(48)	52(3)	51(3)	70(3)	0(2)	8(2)	-1(2)
C(49)	61(3)	78(4)	116(5)	-25(3)	44(3)	-5(3)
C(50)	98(5)	93(4)	67(4)	-19(3)	6(3)	-11(3)
C(51)	37(2)	57(3)	99(4)	-5(3)	1(3)	-6(2)
C(52)	51(3)	74(3)	108(5)	7(3)	30(3)	-8(2)
C(53)	56(3)	79(3)	79(3)	11(3)	20(3)	-5(2)
C(54)	56(3)	98(5)	176(8)	-2(5)	-19(4)	-2(3)

Table 5. Hydrogen coordinates (x 10^4) and isotropic displacement parameters (A^2 x 10^3) for **4**-Ni-**4**.

	x	y	z	U(eq)
H(3)	9788	5077	8732	61
H(5)	9825	2524	8315	59
H(9)	6637	5534	7690	69
H(10)	6987	6883	8251	89
H(11)	8218	7203	8879	91
H(12)	9055	6144	8936	72
H(15)	6693	1842	7274	56
H(16)	7078	443	7260	69
H(17)	8307	178	7629	79
H(18)	9119	1317	8024	72
H(20A)	10863	3007	8077	134
H(20B)	11105	2839	9107	134
H(22)	11831	2959	7793	159
H(23)	13008	3115	8011	133
H(25)	13290	4621	10035	99
H(26)	12074	4516	9816	138
H(27A)	14299	3420	9213	319
H(27B)	14309	4232	9797	319
H(27C)	14130	4332	8770	319
H(30)	5085	3950	5134	60
H(32)	4852	3614	7504	53
H(36)	8272	3838	6322	57
H(37)	8022	3934	4815	65
H(38)	6841	4064	3868	71
H(39)	5914	4048	4455	63
H(42)	7949	3360	9721	56
H(43)	7473	3200	10823	68
H(44)	6224	3249	10460	72
H(45)	5490	3474	8998	62
H(47A)	3728	4095	6706	84
H(47B)	3693	3114	6460	84
H(49)	3055	3640	4463	98
H(50)	1840	3904	3491	111
H(52)	1282	4164	5627	92
H(53)	2444	3986	6525	86
H(54A)	325	4053	4161	189
H(54B)	546	3992	3315	189
H(54C)	586	4878	3798	189

Table 6. Torsion angles [deg] for **4**-Ni-**4**.

N(28)-Ni-N(1)-C(6)	-100.8(16)
N(41)-Ni-N(1)-C(6)	97.4(3)
N(14)-Ni-N(1)-C(6)	9.6(3)
N(35)-Ni-N(1)-C(6)	-80.6(3)
N(8)-Ni-N(1)-C(6)	-174.8(3)
N(28)-Ni-N(1)-C(2)	67.9(17)
N(41)-Ni-N(1)-C(2)	-93.9(3)
N(14)-Ni-N(1)-C(2)	178.3(3)
N(35)-Ni-N(1)-C(2)	88.1(3)
N(8)-Ni-N(1)-C(2)	-6.1(3)
C(6)-N(1)-C(2)-C(3)	0.2(6)
Ni-N(1)-C(2)-C(3)	-168.3(3)
C(6)-N(1)-C(2)-C(7)	179.1(3)
Ni-N(1)-C(2)-C(7)	10.6(4)
N(1)-C(2)-C(3)-C(4)	0.2(6)
C(7)-C(2)-C(3)-C(4)	-178.6(4)
C(2)-C(3)-C(4)-O(19)	178.0(4)
C(2)-C(3)-C(4)-C(5)	-0.6(6)
O(19)-C(4)-C(5)-C(6)	-177.9(4)
C(3)-C(4)-C(5)-C(6)	0.5(6)
C(2)-N(1)-C(6)-C(5)	-0.3(6)
Ni-N(1)-C(6)-C(5)	168.3(3)
C(2)-N(1)-C(6)-C(13)	-179.5(3)
Ni-N(1)-C(6)-C(13)	-10.9(4)
C(4)-C(5)-C(6)-N(1)	-0.1(6)
C(4)-C(5)-C(6)-C(13)	179.0(4)
N(1)-C(2)-C(7)-N(8)	-10.2(5)
C(3)-C(2)-C(7)-N(8)	168.7(4)
N(1)-C(2)-C(7)-C(12)	169.2(4)
C(3)-C(2)-C(7)-C(12)	-12.0(7)
C(12)-C(7)-N(8)-C(9)	0.1(6)
C(2)-C(7)-N(8)-C(9)	179.4(4)
C(12)-C(7)-N(8)-Ni	-174.0(3)
C(2)-C(7)-N(8)-Ni	5.4(4)
N(28)-Ni-N(8)-C(9)	10.9(4)
N(1)-Ni-N(8)-C(9)	-173.4(4)
N(41)-Ni-N(8)-C(9)	-67.0(4)
N(14)-Ni-N(8)-C(9)	-163.3(3)
N(35)-Ni-N(8)-C(9)	89.7(4)
N(28)-Ni-N(8)-C(7)	-175.7(3)
N(1)-Ni-N(8)-C(7)	0.0(3)
N(41)-Ni-N(8)-C(7)	106.4(3)
N(14)-Ni-N(8)-C(7)	10.1(5)
N(35)-Ni-N(8)-C(7)	-96.9(3)
C(7)-N(8)-C(9)-C(10)	-0.9(7)
Ni-N(8)-C(9)-C(10)	172.3(4)
N(8)-C(9)-C(10)-C(11)	1.0(8)
C(9)-C(10)-C(11)-C(12)	-0.4(9)
C(10)-C(11)-C(12)-C(7)	-0.4(8)
N(8)-C(7)-C(12)-C(11)	0.5(7)
C(2)-C(7)-C(12)-C(11)	-178.8(5)
N(1)-C(6)-C(13)-N(14)	5.0(5)
C(5)-C(6)-C(13)-N(14)	-174.2(4)
N(1)-C(6)-C(13)-C(18)	-174.9(4)
C(5)-C(6)-C(13)-C(18)	6.0(6)
C(18)-C(13)-N(14)-C(15)	2.2(6)
C(6)-C(13)-N(14)-C(15)	-177.6(3)
C(18)-C(13)-N(14)-Ni	-177.6(3)
C(6)-C(13)-N(14)-Ni	2.5(4)
N(28)-Ni-N(14)-C(15)	-10.3(3)
N(1)-Ni-N(14)-C(15)	174.0(3)
N(41)-Ni-N(14)-C(15)	67.6(3)
N(35)-Ni-N(14)-C(15)	-88.4(3)
N(8)-Ni-N(14)-C(15)	163.8(3)
N(28)-Ni-N(14)-C(13)	169.5(2)
N(1)-Ni-N(14)-C(13)	-6.2(2)
N(41)-Ni-N(14)-C(13)	-112.6(3)

N(35)-Ni-N(14)-C(13)	91.4(3)
N(8)-Ni-N(14)-C(13)	-16.4(4)
C(13)-N(14)-C(15)-C(16)	-1.6(6)
Ni-N(14)-C(15)-C(16)	178.2(3)
N(14)-C(15)-C(16)-C(17)	0.1(6)
C(15)-C(16)-C(17)-C(18)	0.7(7)
N(14)-C(13)-C(18)-C(17)	-1.4(7)
C(6)-C(13)-C(18)-C(17)	178.4(4)
C(16)-C(17)-C(18)-C(13)	-0.1(7)
C(3)-C(4)-O(19)-C(20)	-174.5(6)
C(5)-C(4)-O(19)-C(20)	4.0(8)
C(4)-O(19)-C(20)-C(21)	172.4(5)
O(19)-C(20)-C(21)-C(22)	-142.3(8)
O(19)-C(20)-C(21)-C(26)	48.9(11)
C(26)-C(21)-C(22)-C(23)	4.8(13)
C(20)-C(21)-C(22)-C(23)	-165.4(7)
C(21)-C(22)-C(23)-C(24)	0.4(13)
C(22)-C(23)-C(24)-C(25)	-4.8(11)
C(22)-C(23)-C(24)-C(27)	-179.0(8)
C(23)-C(24)-C(25)-C(26)	3.6(10)
C(27)-C(24)-C(25)-C(26)	178.2(7)
C(24)-C(25)-C(26)-C(21)	1.5(11)
C(22)-C(21)-C(26)-C(25)	-5.7(12)
C(20)-C(21)-C(26)-C(25)	162.5(7)
N(1)-Ni-N(28)-C(33)	-160.5(15)
N(41)-Ni-N(28)-C(33)	1.8(3)
N(14)-Ni-N(28)-C(33)	90.2(3)
N(35)-Ni-N(28)-C(33)	179.1(3)
N(8)-Ni-N(28)-C(33)	-87.3(3)
N(1)-Ni-N(28)-C(29)	18.8(18)
N(41)-Ni-N(28)-C(29)	-179.0(3)
N(14)-Ni-N(28)-C(29)	-90.6(3)
N(35)-Ni-N(28)-C(29)	-1.6(3)
N(8)-Ni-N(28)-C(29)	92.0(3)
C(33)-N(28)-C(29)-C(30)	-0.4(5)
Ni-N(28)-C(29)-C(30)	-179.7(3)
C(33)-N(28)-C(29)-C(34)	-179.3(3)
Ni-N(28)-C(29)-C(34)	1.4(4)
N(28)-C(29)-C(30)-C(31)	0.2(6)
C(34)-C(29)-C(30)-C(31)	179.0(4)
C(29)-C(30)-C(31)-O(46)	179.7(4)
C(29)-C(30)-C(31)-C(32)	-0.4(6)
O(46)-C(31)-C(32)-C(33)	-179.3(4)
C(30)-C(31)-C(32)-C(33)	0.8(6)
C(29)-N(28)-C(33)-C(32)	0.8(5)
Ni-N(28)-C(33)-C(32)	-179.9(3)
C(29)-N(28)-C(33)-C(40)	179.9(3)
Ni-N(28)-C(33)-C(40)	-0.9(4)
C(31)-C(32)-C(33)-N(28)	-1.0(6)
C(31)-C(32)-C(33)-C(40)	-179.9(3)
N(28)-C(29)-C(34)-N(35)	0.0(5)
C(30)-C(29)-C(34)-N(35)	-178.9(4)
N(28)-C(29)-C(34)-C(39)	177.7(4)
C(30)-C(29)-C(34)-C(39)	-1.2(6)
C(39)-C(34)-N(35)-C(36)	-0.7(6)
C(29)-C(34)-N(35)-C(36)	177.0(3)
C(39)-C(34)-N(35)-Ni	-178.9(3)
C(29)-C(34)-N(35)-Ni	-1.2(4)
N(28)-Ni-N(35)-C(36)	-176.5(3)
N(1)-Ni-N(35)-C(36)	5.0(3)
N(41)-Ni-N(35)-C(36)	-170.3(3)
N(14)-Ni-N(35)-C(36)	-72.7(3)
N(8)-Ni-N(35)-C(36)	83.6(3)
N(28)-Ni-N(35)-C(34)	1.5(3)
N(1)-Ni-N(35)-C(34)	-176.9(3)
N(41)-Ni-N(35)-C(34)	7.8(5)
N(14)-Ni-N(35)-C(34)	105.3(3)
N(8)-Ni-N(35)-C(34)	-98.4(3)
C(34)-N(35)-C(36)-C(37)	-0.5(6)
Ni-N(35)-C(36)-C(37)	177.5(3)
N(35)-C(36)-C(37)-C(38)	1.4(6)

C(36)-C(37)-C(38)-C(39)	-1.1(7)
N(35)-C(34)-C(39)-C(38)	1.0(6)
C(29)-C(34)-C(39)-C(38)	-176.5(4)
C(37)-C(38)-C(39)-C(34)	0.0(7)
N(28)-C(33)-C(40)-N(41)	-1.3(4)
C(32)-C(33)-C(40)-N(41)	177.7(3)
N(28)-C(33)-C(40)-C(45)	-179.9(4)
C(32)-C(33)-C(40)-C(45)	-0.9(6)
C(45)-C(40)-N(41)-C(42)	1.2(5)
C(33)-C(40)-N(41)-C(42)	-177.5(3)
C(45)-C(40)-N(41)-Ni	-178.6(3)
C(33)-C(40)-N(41)-Ni	2.7(4)
N(28)-Ni-N(41)-C(42)	177.7(3)
N(1)-Ni-N(41)-C(42)	-3.7(3)
N(14)-Ni-N(41)-C(42)	73.8(3)
N(35)-Ni-N(41)-C(42)	171.5(3)
N(8)-Ni-N(41)-C(42)	-81.5(3)
N(28)-Ni-N(41)-C(40)	-2.4(2)
N(1)-Ni-N(41)-C(40)	176.2(2)
N(14)-Ni-N(41)-C(40)	-106.3(3)
N(35)-Ni-N(41)-C(40)	-8.7(4)
N(8)-Ni-N(41)-C(40)	98.3(3)
C(40)-N(41)-C(42)-C(43)	-1.2(6)
Ni-N(41)-C(42)-C(43)	178.6(3)
N(41)-C(42)-C(43)-C(44)	0.7(7)
C(42)-C(43)-C(44)-C(45)	-0.2(7)
C(43)-C(44)-C(45)-C(40)	0.2(7)
N(41)-C(40)-C(45)-C(44)	-0.7(6)
C(33)-C(40)-C(45)-C(44)	177.8(4)
C(32)-C(31)-O(46)-C(47)	-4.3(6)
C(30)-C(31)-O(46)-C(47)	175.6(4)
C(31)-O(46)-C(47)-C(48)	177.2(4)
O(46)-C(47)-C(48)-C(53)	-159.7(4)
O(46)-C(47)-C(48)-C(49)	19.3(7)
C(53)-C(48)-C(49)-C(50)	2.0(8)
C(47)-C(48)-C(49)-C(50)	-177.1(5)
C(48)-C(49)-C(50)-C(51)	-1.7(8)
C(49)-C(50)-C(51)-C(52)	-0.4(8)
C(49)-C(50)-C(51)-C(54)	178.0(5)
C(50)-C(51)-C(52)-C(53)	2.3(8)
C(54)-C(51)-C(52)-C(53)	-176.0(5)
C(49)-C(48)-C(53)-C(52)	-0.1(8)
C(47)-C(48)-C(53)-C(52)	178.9(5)
C(51)-C(52)-C(53)-C(48)	-2.2(8)

Symmetry transformations used to generate equivalent atoms:

Table 7. Hydrogen bonds for **4**-Ni-**4** [A and deg.].

D-H...A	d(D-H)	d(H...A)	d(D...A)	<(DHA)

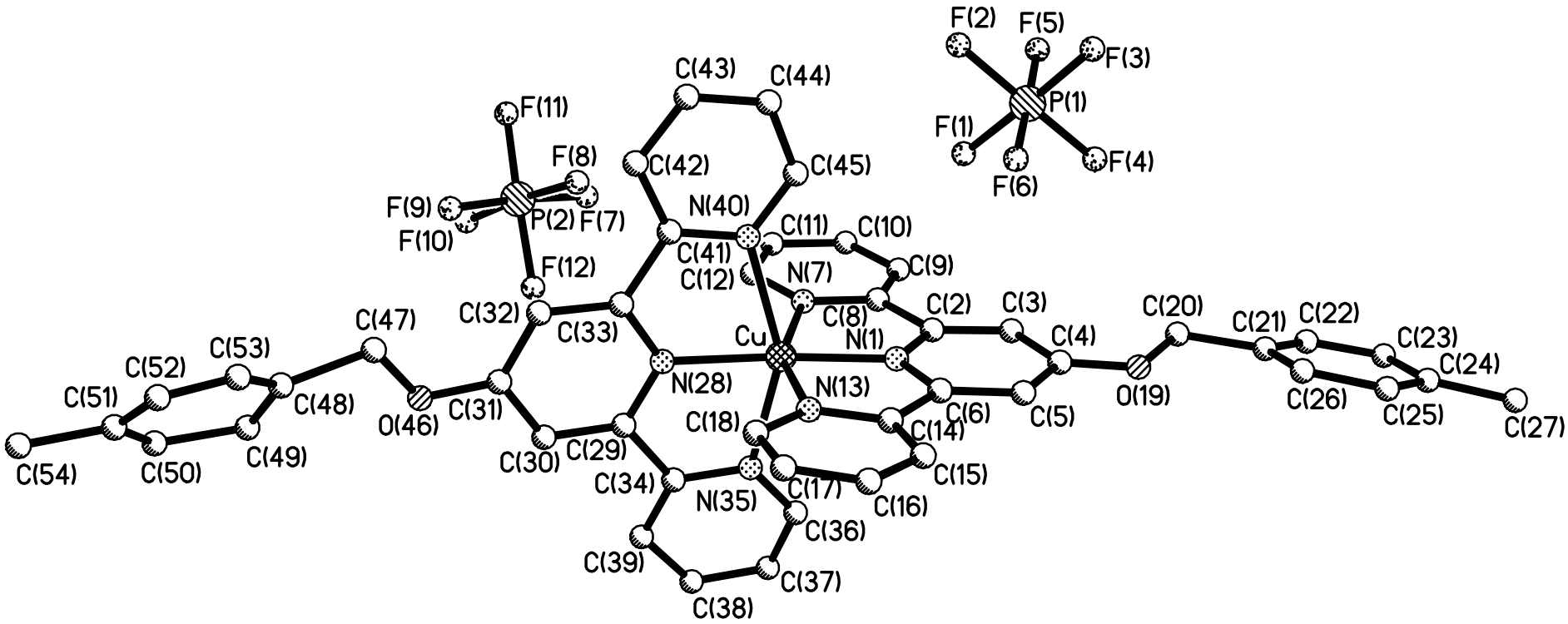
F(2)
F(5)
F(3)
P(1)
F(1)
F(4)
F(6)
C(43)
C(44)
F(11)
F(8)
C(42)
C(45)
F(9)
P(2)
F(7)
N(40)
F(10)
C(11)
C(10)
C(41)
C(9)
F(12)
C(12)
N(7)
C(47)
C(32)
C(33)
C(8)
C(2)
C(3)
C(20)
C(21)
C(22)
C(53)
Cu
N(1)
C(4)
C(23)
C(52)
C(24)
C(51)
N(28)
N(13)
O(19)
C(48)
C(31)
C(6)
C(5)
C(26)
C(25)
O(46)
C(18)
C(14)
C(27)
C(54)
C(50)
C(49)
C(30)
C(29)
C(15)
C(34)
C(17)
N(35)
C(16)
C(36)
C(39)
C(37)
C(38)

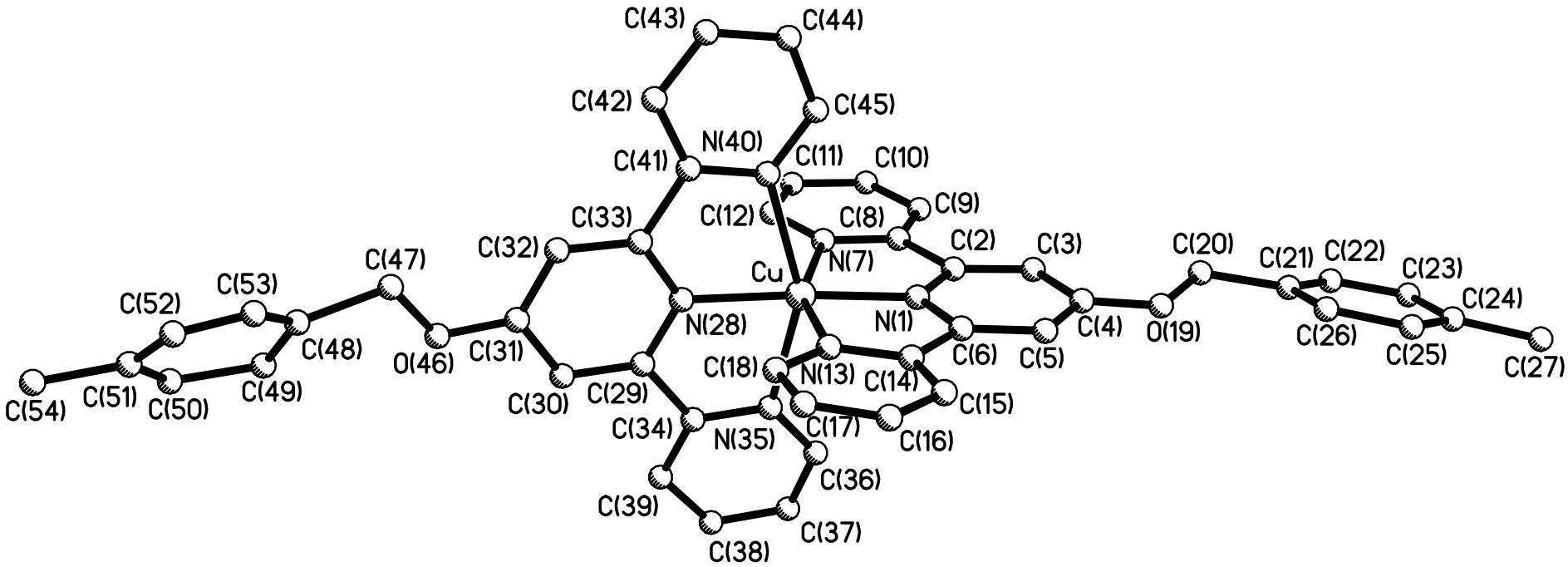
C(43)
C(44)
C(42)
C(45)
N(40)
C(41)
C(11)
C(10)
C(9)
C(12)
C(8)
C(33)
C(32)
N(7)
C(2)
C(3)
C(20)
C(21)
C(22)
C(23)
C(24)
C(47)
C(53)
Cu
C(52)
N(28)
N(1)
C(4)
O(19)
C(26)
C(25)
C(27)
C(48)
O(46)
C(31)
C(18)
N(13)
C(14)
C(6)
C(5)
C(54)
C(51)
C(50)
C(49)
C(30)
C(29)
C(15)
C(34)
C(17)
C(16)
N(35)
C(36)
C(39)
C(37)
C(38)

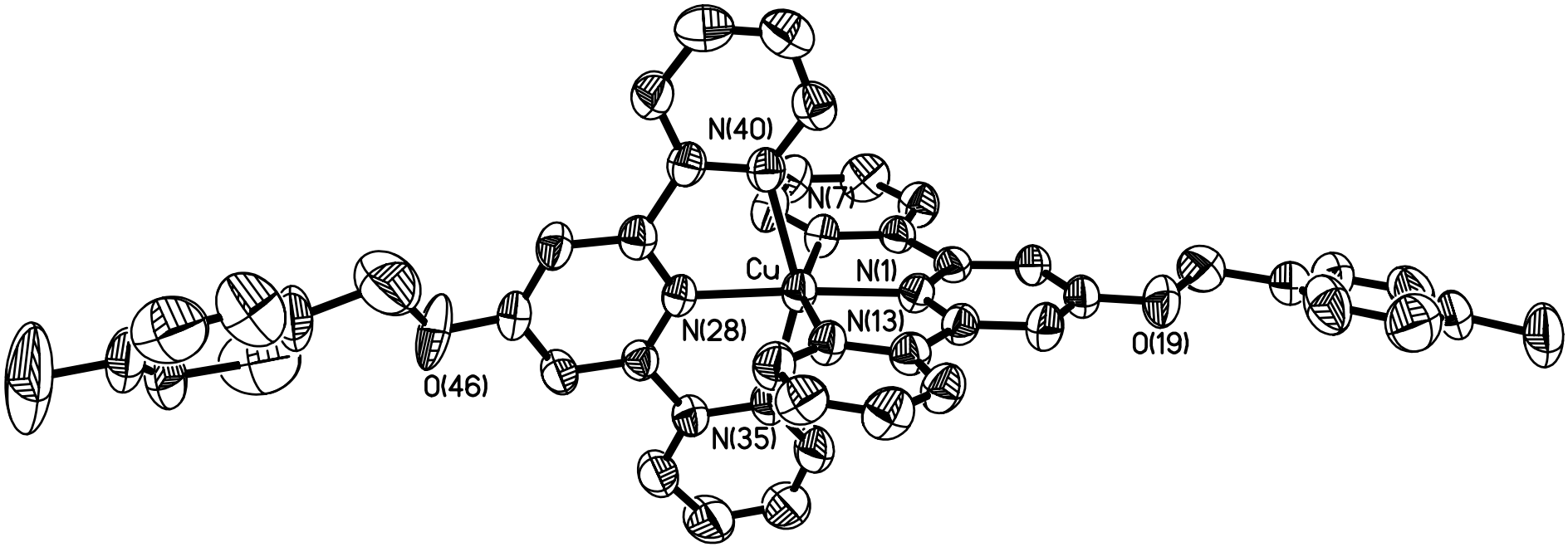
N(40)
N(7)
Cu
N(1)
N(28)
N(13)
O(19)
O(46)
N(35)

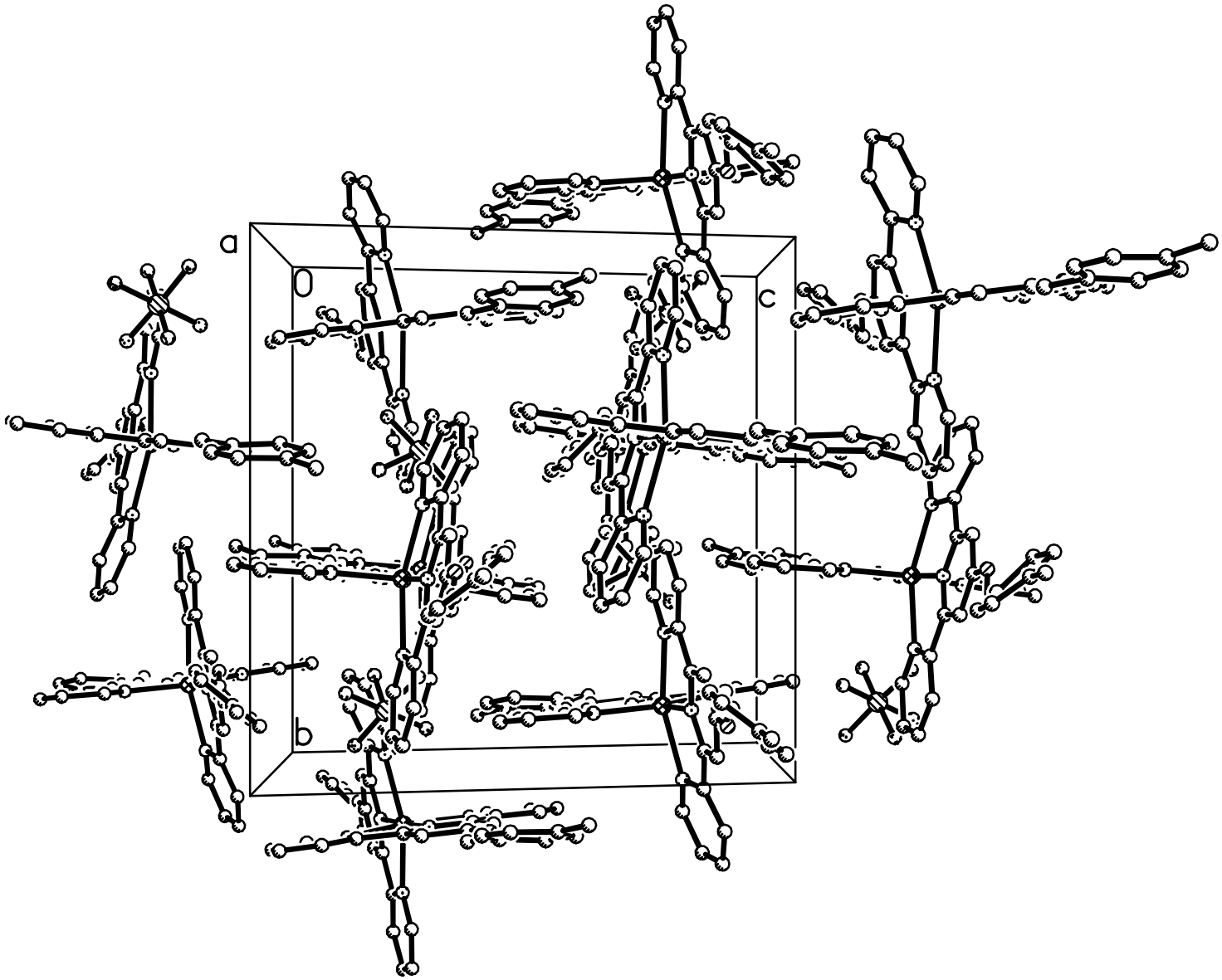
a
0
c
b

Table 1. Crystal data and structure refinement for **4**-Cu-**4**.

Identification code	**4**-Cu-**4**
Empirical formula	C46 H38 Cu F12 N6 O2 P2
Formula weight	1060.30
Temperature	296(2) K
Wavelength	0.71073 A
Crystal system, space group	monoclinic, P2(1)/c
Unit cell dimensions	a = 19.6635(7) A alpha = 90 deg. b = 15.5270(6) A beta = 109.9340(10) deg. c = 16.0390(6) A gamma = 90 deg.
Volume	4603.6(3) A^3
Z, Calculated density	4, 1.530 Mg/m^3
Absorption coefficient	0.639 mm^-1
F(000)	2156
Crystal size	0.23 x 0.12 x 0.10 mm
Theta range for data collection	2.40 to 23.26 deg.
Limiting indices	-21<=h<=20, -17<=k<=14, -17<=l<=17
Reflections collected / unique	15450 / 5345 [R(int) = 0.0381]
Completeness to theta = 23.26	80.9 %
Max. and min. transmission	0.9389 and 0.8670
Refinement method	Full-matrix least-squares on F^2
Data / restraints / parameters	5345 / 0 / 624
Goodness-of-fit on F^2	0.907
Final R indices [I>2sigma(I)]	R1 = 0.0544, wR2 = 0.1363
R indices (all data)	R1 = 0.0797, wR2 = 0.1467
Largest diff. peak and hole	0.894 and -0.325 e.A^-3

Table 2. Atomic coordinates (x 10^4) and equivalent isotropic displacement parameters (A^2 x 10^3) for **4**-Cu-**4**.
U(eq) is defined as one third of the trace of the orthogonalized Uij tensor.

	x	y	z	U(eq)
Cu	7350(1)	6283(1)	2587(1)	44(1)
N(1)	6302(2)	6247(2)	2024(3)	41(1)
P(1)	5020(1)	8865(1)	2166(1)	67(1)
F(1)	5533(2)	8199(2)	2821(3)	102(1)
C(2)	5871(2)	6320(3)	2520(3)	43(1)
F(2)	5668(2)	9540(2)	2446(3)	106(1)
P(2)	9612(1)	7467(1)	5838(1)	81(1)
C(3)	5137(3)	6299(3)	2138(4)	46(1)
F(3)	4515(2)	9557(3)	1541(3)	116(2)
C(4)	4817(3)	6190(3)	1226(4)	51(1)
F(4)	4376(2)	8209(3)	1915(4)	140(2)
C(5)	5277(3)	6122(3)	716(4)	53(1)
F(5)	4780(2)	9234(3)	2950(3)	107(1)
C(6)	6014(3)	6147(3)	1140(3)	44(1)
F(6)	5270(3)	8502(3)	1408(4)	129(2)
N(7)	7002(2)	6477(2)	3688(3)	46(1)
F(7)	8927(2)	7293(4)	6139(3)	128(2)
C(8)	6281(3)	6433(3)	3471(3)	43(1)
F(8)	9082(3)	7838(4)	4953(3)	143(2)
C(9)	5971(3)	6514(3)	4134(4)	56(1)
F(9)	10264(2)	7569(4)	5513(4)	141(2)
F(10)	10091(3)	7015(3)	6724(3)	121(2)
C(10)	6402(3)	6645(4)	4992(4)	67(2)
F(11)	9683(4)	8345(3)	6318(4)	151(2)
C(11)	7139(3)	6696(4)	5198(4)	63(1)
C(12)	7419(3)	6608(3)	4526(4)	55(1)
F(12)	9508(3)	6542(3)	5393(4)	132(2)
N(13)	7247(2)	6160(2)	1234(3)	46(1)
C(14)	6555(3)	6100(3)	683(3)	46(1)
C(15)	6387(3)	6018(3)	-207(4)	56(1)
C(16)	6934(3)	6007(4)	-565(4)	63(2)
C(17)	7626(3)	6091(3)	-20(4)	60(2)
C(18)	7773(3)	6149(3)	881(4)	55(1)
O(19)	4117(2)	6154(3)	773(3)	71(1)
C(20)	3620(3)	6284(4)	1205(5)	74(2)
C(21)	2852(3)	6181(3)	578(5)	66(2)
C(22)	2314(3)	6043(4)	905(5)	73(2)
C(23)	1627(4)	5930(4)	360(6)	81(2)
C(24)	1431(3)	5924(4)	-538(6)	76(2)
C(25)	1979(5)	6070(4)	-887(5)	93(2)
C(26)	2703(4)	6213(4)	-311(6)	83(2)
C(27)	661(4)	5740(5)	-1108(8)	134(4)
N(28)	8427(2)	6265(2)	3097(3)	41(1)
C(29)	8783(2)	5517(3)	3330(3)	43(1)
C(30)	9517(2)	5464(3)	3529(4)	52(1)
C(31)	9912(3)	6194(3)	3493(4)	53(1)
C(32)	9542(2)	6971(3)	3277(4)	52(1)
C(33)	8802(2)	6992(3)	3075(3)	47(1)
C(34)	8316(2)	4770(3)	3342(3)	48(1)
N(35)	7606(2)	4900(3)	2971(3)	51(1)
C(36)	7160(3)	4256(4)	2987(4)	68(2)
C(37)	7394(3)	3482(4)	3365(5)	80(2)
C(38)	8120(4)	3338(4)	3723(6)	87(2)
C(39)	8603(3)	3995(3)	3737(5)	68(2)
N(40)	7656(2)	7684(3)	2615(3)	45(1)
C(41)	8365(2)	7798(3)	2837(3)	46(1)
C(42)	8665(3)	8596(3)	2845(5)	71(2)
C(43)	8209(4)	9302(4)	2623(5)	84(2)
C(44)	7479(4)	9188(4)	2414(4)	69(2)
C(45)	7227(3)	8373(4)	2413(4)	57(1)

O(46)	10624(2)	6098(3)	3661(4)	96(2)
C(47)	11011(5)	6742(6)	3589(8)	133(3)
C(48)	11824(3)	6489(5)	3665(8)	99(3)
C(49)	12155(6)	5846(7)	4317(8)	149(5)
C(50)	12967(3)	5750(5)	4569(5)	83(2)
C(51)	13255(4)	6184(6)	4066(6)	84(2)
C(52)	12839(7)	6663(7)	3411(8)	125(4)
C(53)	12162(6)	6804(6)	3239(6)	113(3)
C(54)	14054(5)	6101(10)	4218(9)	210(7)

Table 3. Bond lengths [A] and angles [deg] for **4**-Cu-**4**.

Cu-N(1)	1.949(4)
Cu-N(28)	1.993(4)
Cu-N(13)	2.119(4)
Cu-N(7)	2.122(4)
Cu-N(35)	2.244(4)
Cu-N(40)	2.253(4)
N(1)-C(6)	1.344(6)
N(1)-C(2)	1.349(6)
P(1)-F(6)	1.563(5)
P(1)-F(4)	1.566(4)
P(1)-F(3)	1.571(4)
P(1)-F(1)	1.571(4)
P(1)-F(2)	1.592(4)
P(1)-F(5)	1.593(4)
C(2)-C(3)	1.363(7)
C(2)-C(8)	1.473(7)
P(2)-F(9)	1.548(4)
P(2)-F(11)	1.549(5)
P(2)-F(8)	1.557(5)
P(2)-F(10)	1.576(5)
P(2)-F(12)	1.586(5)
P(2)-F(7)	1.600(4)
C(3)-C(4)	1.391(8)
C(4)-O(19)	1.322(6)
C(4)-C(5)	1.415(7)
C(5)-C(6)	1.376(7)
C(6)-C(14)	1.486(6)
N(7)-C(12)	1.330(7)
N(7)-C(8)	1.341(6)
C(8)-C(9)	1.400(7)
C(9)-C(10)	1.362(8)
C(10)-C(11)	1.375(8)
C(11)-C(12)	1.374(7)
N(13)-C(18)	1.335(6)
N(13)-C(14)	1.350(7)
C(14)-C(15)	1.357(7)
C(15)-C(16)	1.382(7)
C(16)-C(17)	1.349(8)
C(17)-C(18)	1.378(8)
O(19)-C(20)	1.393(7)
C(20)-C(21)	1.510(9)
C(21)-C(22)	1.348(8)
C(21)-C(26)	1.355(10)
C(22)-C(23)	1.348(10)
C(23)-C(24)	1.358(10)
C(24)-C(25)	1.393(10)
C(24)-C(27)	1.506(9)
C(25)-C(26)	1.426(11)
N(28)-C(29)	1.341(6)
N(28)-C(33)	1.357(6)
C(29)-C(30)	1.372(6)
C(29)-C(34)	1.484(6)
C(30)-C(31)	1.387(7)
C(31)-O(46)	1.339(6)
C(31)-C(32)	1.390(7)
C(32)-C(33)	1.380(7)
C(33)-C(41)	1.492(7)
C(34)-N(35)	1.333(6)
C(34)-C(39)	1.387(7)
N(35)-C(36)	1.336(6)
C(36)-C(37)	1.354(8)
C(37)-C(38)	1.362(9)
C(38)-C(39)	1.389(8)
N(40)-C(41)	1.327(6)
N(40)-C(45)	1.333(6)
C(41)-C(42)	1.370(7)
C(42)-C(43)	1.382(8)

C(43)-C(44)	1.370(9)
C(44)-C(45)	1.358(8)
O(46)-C(47)	1.286(10)
C(47)-C(48)	1.608(11)
C(48)-C(53)	1.208(11)
C(48)-C(49)	1.432(14)
C(49)-C(50)	1.516(12)
C(50)-C(51)	1.319(10)
C(51)-C(52)	1.319(13)
C(51)-C(54)	1.511(10)
C(52)-C(53)	1.282(14)

N(1)-Cu-N(28)	176.04(15)
N(1)-Cu-N(13)	78.87(15)
N(28)-Cu-N(13)	97.84(15)
N(1)-Cu-N(7)	78.40(16)
N(28)-Cu-N(7)	105.01(16)
N(13)-Cu-N(7)	156.97(16)
N(1)-Cu-N(35)	101.67(14)
N(28)-Cu-N(35)	76.47(14)
N(13)-Cu-N(35)	97.40(15)
N(7)-Cu-N(35)	90.74(15)
N(1)-Cu-N(40)	105.69(14)
N(28)-Cu-N(40)	76.49(14)
N(13)-Cu-N(40)	92.23(14)
N(7)-Cu-N(40)	90.38(13)
N(35)-Cu-N(40)	152.28(15)
C(6)-N(1)-C(2)	120.5(4)
C(6)-N(1)-Cu	119.4(3)
C(2)-N(1)-Cu	120.1(3)
F(6)-P(1)-F(4)	90.4(3)
F(6)-P(1)-F(3)	92.8(3)
F(4)-P(1)-F(3)	90.1(3)
F(6)-P(1)-F(1)	89.0(3)
F(4)-P(1)-F(1)	91.2(3)
F(3)-P(1)-F(1)	177.8(3)
F(6)-P(1)-F(2)	91.3(3)
F(4)-P(1)-F(2)	178.3(3)
F(3)-P(1)-F(2)	90.1(2)
F(1)-P(1)-F(2)	88.6(2)
F(6)-P(1)-F(5)	179.0(3)
F(4)-P(1)-F(5)	90.3(3)
F(3)-P(1)-F(5)	88.0(2)
F(1)-P(1)-F(5)	90.3(3)
F(2)-P(1)-F(5)	88.0(3)
N(1)-C(2)-C(3)	120.9(5)
N(1)-C(2)-C(8)	112.9(4)
C(3)-C(2)-C(8)	126.1(4)
F(9)-P(2)-F(11)	97.7(4)
F(9)-P(2)-F(8)	91.7(3)
F(11)-P(2)-F(8)	92.6(3)
F(9)-P(2)-F(10)	92.3(3)
F(11)-P(2)-F(10)	91.1(3)
F(8)-P(2)-F(10)	174.1(3)
F(9)-P(2)-F(12)	86.3(3)
F(11)-P(2)-F(12)	175.7(4)
F(8)-P(2)-F(12)	88.9(3)
F(10)-P(2)-F(12)	87.0(3)
F(9)-P(2)-F(7)	175.7(3)
F(11)-P(2)-F(7)	86.6(3)
F(8)-P(2)-F(7)	88.0(3)
F(10)-P(2)-F(7)	87.7(3)
F(12)-P(2)-F(7)	89.4(3)
C(2)-C(3)-C(4)	120.4(4)
O(19)-C(4)-C(3)	126.6(5)
O(19)-C(4)-C(5)	115.4(5)
C(3)-C(4)-C(5)	117.9(5)
C(6)-C(5)-C(4)	119.0(5)
N(1)-C(6)-C(5)	121.3(4)
N(1)-C(6)-C(14)	114.3(4)
C(5)-C(6)-C(14)	124.4(5)

C(12)-N(7)-C(8)	120.1(4)
C(12)-N(7)-Cu	126.9(3)
C(8)-N(7)-Cu	113.0(3)
N(7)-C(8)-C(9)	119.6(5)
N(7)-C(8)-C(2)	115.5(4)
C(9)-C(8)-C(2)	124.9(4)
C(10)-C(9)-C(8)	119.9(5)
C(9)-C(10)-C(11)	119.5(5)
C(12)-C(11)-C(10)	118.5(6)
N(7)-C(12)-C(11)	122.3(5)
C(18)-N(13)-C(14)	118.4(4)
C(18)-N(13)-Cu	128.1(4)
C(14)-N(13)-Cu	113.5(3)
N(13)-C(14)-C(15)	121.6(4)
N(13)-C(14)-C(6)	114.0(4)
C(15)-C(14)-C(6)	124.4(5)
C(14)-C(15)-C(16)	119.6(5)
C(17)-C(16)-C(15)	119.0(5)
C(16)-C(17)-C(18)	119.3(5)
N(13)-C(18)-C(17)	122.0(5)
C(4)-O(19)-C(20)	119.8(5)
O(19)-C(20)-C(21)	111.4(6)
C(22)-C(21)-C(26)	119.9(6)
C(22)-C(21)-C(20)	119.7(7)
C(26)-C(21)-C(20)	120.3(6)
C(23)-C(22)-C(21)	121.0(7)
C(22)-C(23)-C(24)	123.2(6)
C(23)-C(24)-C(25)	116.6(6)
C(23)-C(24)-C(27)	120.5(8)
C(25)-C(24)-C(27)	122.9(8)
C(24)-C(25)-C(26)	120.2(7)
C(21)-C(26)-C(25)	119.1(6)
C(29)-N(28)-C(33)	119.4(4)
C(29)-N(28)-Cu	120.5(3)
C(33)-N(28)-Cu	119.2(3)
N(28)-C(29)-C(30)	121.7(4)
N(28)-C(29)-C(34)	114.5(4)
C(30)-C(29)-C(34)	123.8(4)
C(29)-C(30)-C(31)	120.1(5)
O(46)-C(31)-C(30)	117.5(5)
O(46)-C(31)-C(32)	124.7(5)
C(30)-C(31)-C(32)	117.8(4)
C(33)-C(32)-C(31)	120.0(4)
N(28)-C(33)-C(32)	120.9(4)
N(28)-C(33)-C(41)	115.7(4)
C(32)-C(33)-C(41)	123.4(4)
N(35)-C(34)-C(39)	122.5(4)
N(35)-C(34)-C(29)	115.7(4)
C(39)-C(34)-C(29)	121.8(4)
C(34)-N(35)-C(36)	118.1(4)
C(34)-N(35)-Cu	111.7(3)
C(36)-N(35)-Cu	129.4(3)
N(35)-C(36)-C(37)	123.2(5)
C(36)-C(37)-C(38)	118.9(5)
C(37)-C(38)-C(39)	119.8(6)
C(34)-C(39)-C(38)	117.4(6)
C(41)-N(40)-C(45)	118.5(4)
C(41)-N(40)-Cu	112.5(3)
C(45)-N(40)-Cu	128.9(3)
N(40)-C(41)-C(42)	122.2(5)
N(40)-C(41)-C(33)	114.7(4)
C(42)-C(41)-C(33)	123.2(4)
C(41)-C(42)-C(43)	118.4(5)
C(44)-C(43)-C(42)	119.5(5)
C(45)-C(44)-C(43)	118.2(6)
N(40)-C(45)-C(44)	123.2(5)
C(47)-O(46)-C(31)	120.4(6)
O(46)-C(47)-C(48)	114.1(7)
C(53)-C(48)-C(49)	119.7(7)
C(53)-C(48)-C(47)	125.6(10)
C(49)-C(48)-C(47)	114.7(9)

C(48)-C(49)-C(50)	116.0(6)
C(51)-C(50)-C(49)	114.9(7)
C(50)-C(51)-C(52)	119.7(7)
C(50)-C(51)-C(54)	119.8(9)
C(52)-C(51)-C(54)	120.4(9)
C(53)-C(52)-C(51)	125.8(9)
C(48)-C(53)-C(52)	122.7(10)

Symmetry transformations used to generate equivalent atoms:

Table 4. Anisotropic displacement parameters (A^2 x 10^3) for **4**-Cu-**4**.
The anisotropic displacement factor exponent takes the form:
-2 pi^2 [h^2 a*^2 U11 + ... + 2 h k a* b* U12]

	U11	U22	U33	U23	U13	U12
Cu	34(1)	53(1)	44(1)	-2(1)	13(1)	-2(1)
N(1)	36(2)	45(2)	41(3)	-3(2)	12(2)	-4(2)
P(1)	47(1)	56(1)	84(1)	-6(1)	4(1)	9(1)
F(1)	95(3)	64(2)	114(4)	5(2)	-5(3)	17(2)
C(2)	39(3)	37(2)	54(3)	-1(2)	18(3)	0(2)
F(2)	77(2)	79(2)	147(4)	1(2)	18(3)	-11(2)
P(2)	63(1)	113(1)	63(1)	-5(1)	16(1)	34(1)
C(3)	35(3)	49(3)	54(3)	-2(2)	16(3)	-2(2)
F(3)	106(3)	99(3)	103(3)	8(2)	-18(3)	40(2)
C(4)	35(3)	50(3)	64(4)	2(2)	10(3)	0(2)
F(4)	69(2)	82(3)	241(7)	-40(3)	17(3)	-12(2)
C(5)	42(3)	66(3)	45(3)	-1(2)	6(3)	-1(2)
F(5)	111(3)	98(3)	113(4)	-13(2)	41(3)	12(2)
C(6)	40(3)	49(3)	41(3)	-2(2)	10(3)	-1(2)
F(6)	125(4)	152(4)	103(4)	-28(3)	30(3)	37(3)
N(7)	36(2)	56(2)	42(3)	1(2)	9(2)	-4(2)
F(7)	92(3)	193(5)	112(4)	1(3)	51(3)	27(3)
C(8)	38(3)	40(3)	53(3)	1(2)	18(3)	0(2)
F(8)	129(4)	216(6)	72(3)	22(3)	18(3)	99(4)
C(9)	50(3)	67(3)	56(4)	-1(3)	25(3)	-4(3)
F(9)	88(3)	175(5)	179(6)	47(4)	70(4)	24(3)
F(10)	105(3)	163(4)	80(3)	17(3)	13(3)	54(3)
C(10)	78(4)	78(4)	55(4)	-3(3)	35(4)	-8(3)
F(11)	180(6)	114(4)	129(5)	-27(3)	12(4)	15(4)
C(11)	64(4)	74(4)	44(3)	2(3)	12(3)	-9(3)
C(12)	44(3)	67(3)	48(4)	3(3)	8(3)	-12(2)
F(12)	162(5)	120(4)	120(4)	-31(3)	55(4)	9(3)
N(13)	37(2)	56(2)	45(3)	-4(2)	14(2)	-4(2)
C(14)	45(3)	51(3)	42(3)	-1(2)	14(3)	0(2)
C(15)	53(3)	70(3)	45(4)	-7(3)	13(3)	-8(3)
C(16)	68(4)	76(4)	47(4)	-7(3)	23(3)	-7(3)
C(17)	67(4)	66(4)	57(4)	-6(3)	34(4)	-7(3)
C(18)	46(3)	64(3)	54(4)	-6(2)	17(3)	-4(2)
O(19)	37(2)	85(3)	84(3)	-10(2)	13(2)	-3(2)
C(20)	65(4)	71(4)	89(5)	-11(3)	28(4)	3(3)
C(21)	52(3)	55(3)	80(5)	-5(3)	8(4)	1(3)
C(22)	53(4)	80(4)	83(5)	-13(3)	19(4)	1(3)
C(23)	53(4)	75(4)	122(7)	0(4)	37(5)	12(3)
C(24)	43(3)	67(4)	98(6)	3(4)	-2(4)	11(3)
C(25)	107(6)	89(5)	69(5)	12(4)	13(5)	3(4)
C(26)	55(4)	87(5)	112(7)	24(4)	33(5)	4(3)
C(27)	55(4)	103(6)	190(11)	5(6)	-26(6)	0(4)
N(28)	34(2)	49(2)	41(2)	0(2)	13(2)	-5(2)
C(29)	38(2)	45(3)	48(3)	2(2)	16(2)	-1(2)
C(30)	38(3)	56(3)	60(4)	7(2)	15(3)	7(2)
C(31)	32(3)	66(3)	56(4)	-1(3)	10(3)	-6(2)
C(32)	36(3)	58(3)	59(4)	3(3)	14(3)	-9(2)
C(33)	40(3)	56(3)	43(3)	-1(2)	15(2)	-2(2)
C(34)	38(3)	53(3)	53(3)	-2(2)	16(2)	1(2)
N(35)	34(2)	52(2)	67(3)	2(2)	15(2)	2(2)
C(36)	42(3)	62(4)	103(5)	-1(3)	29(3)	-6(3)
C(37)	69(4)	52(4)	127(6)	5(4)	43(5)	-11(3)
C(38)	76(4)	50(3)	142(7)	14(4)	48(5)	-1(3)
C(39)	48(3)	57(3)	97(5)	11(3)	23(4)	5(3)
N(40)	40(2)	54(2)	39(3)	2(2)	12(2)	0(2)
C(41)	42(3)	54(3)	38(3)	0(2)	10(2)	-3(2)
C(42)	48(3)	54(3)	101(5)	8(3)	11(4)	-5(3)
C(43)	93(5)	49(4)	108(6)	7(3)	31(5)	-3(3)
C(44)	81(4)	67(4)	61(4)	4(3)	25(4)	16(3)
C(45)	54(3)	71(4)	48(4)	-2(3)	19(3)	10(3)
O(46)	38(2)	144(4)	102(4)	15(3)	20(3)	-42(2)

C(47)	116(7)	122(7)	144(10)	-6(6)	22(7)	36(6)
C(48)	36(3)	98(6)	148(9)	17(5)	13(5)	5(3)
C(49)	197(11)	136(8)	200(11)	-35(8)	177(11)	-50(8)
C(50)	46(3)	118(6)	71(5)	3(4)	5(4)	11(4)
C(51)	44(3)	130(6)	79(5)	-27(4)	23(4)	-18(4)
C(52)	158(10)	124(7)	128(10)	-21(6)	93(9)	-23(7)
C(53)	120(7)	146(8)	79(6)	16(5)	45(6)	29(7)
C(54)	70(6)	400(20)	176(13)	-97(12)	67(8)	-60(8)

Table 5. Hydrogen coordinates (x 10^4) and isotropic displacement parameters (A^2 x 10^3) for **4**-Cu-**4**.

	x	y	z	U(eq)
H(3)	4848	6358	2489	55
H(5)	5083	6062	103	64
H(9)	5472	6479	3990	67
H(10)	6198	6699	5435	81
H(11)	7441	6789	5779	75
H(12)	7917	6641	4662	66
H(15)	5907	5970	-573	68
H(16)	6827	5943	-1173	75
H(17)	8000	6110	-251	72
H(18)	8252	6181	1256	65
H(20A)	3682	6859	1457	89
H(20B)	3710	5874	1687	89
H(22)	2419	6026	1516	88
H(23)	1269	5852	611	98
H(25)	1873	6074	-1498	112
H(26)	3068	6326	-542	100
H(27A)	618	5148	-1292	200
H(27B)	527	6106	-1621	200
H(27C)	346	5849	-775	200
H(30)	9751	4937	3688	62
H(32)	9794	7477	3270	62
H(36)	6664	4343	2726	82
H(37)	7066	3056	3379	96
H(38)	8291	2800	3958	104
H(39)	9099	3918	4001	81
H(42)	9162	8662	2997	85
H(43)	8398	9850	2615	101
H(44)	7165	9655	2276	83
H(45)	6731	8293	2265	69
H(47A)	11032	7157	4048	160
H(47B)	10777	7018	3021	160
H(49)	11887	5508	4571	179
H(50)	13241	5411	5042	99
H(52)	13055	6921	3041	150
H(53)	11922	7164	2767	135
H(54A)	14120	5820	3718	316
H(54B)	14281	5766	4743	316
H(54C)	14270	6663	4289	316

Table 6. Torsion angles [deg] for **4**-Cu-**4**.

N(28)-Cu-N(1)-C(6)	-32(2)
N(13)-Cu-N(1)-C(6)	1.7(3)
N(7)-Cu-N(1)-C(6)	178.0(4)
N(35)-Cu-N(1)-C(6)	-93.7(3)
N(40)-Cu-N(1)-C(6)	90.9(3)
N(28)-Cu-N(1)-C(2)	148(2)
N(13)-Cu-N(1)-C(2)	-178.4(3)
N(7)-Cu-N(1)-C(2)	-2.1(3)
N(35)-Cu-N(1)-C(2)	86.3(3)
N(40)-Cu-N(1)-C(2)	-89.2(3)
C(6)-N(1)-C(2)-C(3)	-0.3(6)
Cu-N(1)-C(2)-C(3)	179.8(3)
C(6)-N(1)-C(2)-C(8)	-179.5(4)
Cu-N(1)-C(2)-C(8)	0.6(5)
N(1)-C(2)-C(3)-C(4)	0.8(7)
C(8)-C(2)-C(3)-C(4)	179.8(4)
C(2)-C(3)-C(4)-O(19)	179.6(4)
C(2)-C(3)-C(4)-C(5)	-1.3(7)
O(19)-C(4)-C(5)-C(6)	-179.4(4)
C(3)-C(4)-C(5)-C(6)	1.4(7)
C(2)-N(1)-C(6)-C(5)	0.4(7)
Cu-N(1)-C(6)-C(5)	-179.7(4)
C(2)-N(1)-C(6)-C(14)	178.4(4)
Cu-N(1)-C(6)-C(14)	-1.7(5)
C(4)-C(5)-C(6)-N(1)	-1.0(7)
C(4)-C(5)-C(6)-C(14)	-178.8(4)
N(1)-Cu-N(7)-C(12)	-178.5(4)
N(28)-Cu-N(7)-C(12)	3.6(4)
N(13)-Cu-N(7)-C(12)	-169.2(4)
N(35)-Cu-N(7)-C(12)	79.8(4)
N(40)-Cu-N(7)-C(12)	-72.5(4)
N(1)-Cu-N(7)-C(8)	3.3(3)
N(28)-Cu-N(7)-C(8)	-174.7(3)
N(13)-Cu-N(7)-C(8)	12.6(6)
N(35)-Cu-N(7)-C(8)	-98.5(3)
N(40)-Cu-N(7)-C(8)	109.2(3)
C(12)-N(7)-C(8)-C(9)	-0.9(7)
Cu-N(7)-C(8)-C(9)	177.5(3)
C(12)-N(7)-C(8)-C(2)	177.7(4)
Cu-N(7)-C(8)-C(2)	-3.9(5)
N(1)-C(2)-C(8)-N(7)	2.4(5)
C(3)-C(2)-C(8)-N(7)	-176.7(4)
N(1)-C(2)-C(8)-C(9)	-179.1(4)
C(3)-C(2)-C(8)-C(9)	1.7(7)
N(7)-C(8)-C(9)-C(10)	0.6(7)
C(2)-C(8)-C(9)-C(10)	-177.8(5)
C(8)-C(9)-C(10)-C(11)	0.0(8)
C(9)-C(10)-C(11)-C(12)	-0.4(9)
C(8)-N(7)-C(12)-C(11)	0.5(7)
Cu-N(7)-C(12)-C(11)	-177.6(4)
C(10)-C(11)-C(12)-N(7)	0.1(8)
N(1)-Cu-N(13)-C(18)	177.5(4)
N(28)-Cu-N(13)-C(18)	-4.7(4)
N(7)-Cu-N(13)-C(18)	168.2(4)
N(35)-Cu-N(13)-C(18)	-82.0(4)
N(40)-Cu-N(13)-C(18)	72.0(4)
N(1)-Cu-N(13)-C(14)	-1.4(3)
N(28)-Cu-N(13)-C(14)	176.4(3)
N(7)-Cu-N(13)-C(14)	-10.7(6)
N(35)-Cu-N(13)-C(14)	99.1(3)
N(40)-Cu-N(13)-C(14)	-107.0(3)
C(18)-N(13)-C(14)-C(15)	0.8(7)
Cu-N(13)-C(14)-C(15)	179.9(4)
C(18)-N(13)-C(14)-C(6)	-178.1(4)
Cu-N(13)-C(14)-C(6)	1.0(5)
N(1)-C(6)-C(14)-N(13)	0.4(6)
C(5)-C(6)-C(14)-N(13)	178.3(5)

N(1)-C(6)-C(14)-C(15)	-178.5(5)
C(5)-C(6)-C(14)-C(15)	-0.6(7)
N(13)-C(14)-C(15)-C(16)	-0.8(8)
C(6)-C(14)-C(15)-C(16)	178.0(5)
C(14)-C(15)-C(16)-C(17)	-1.0(8)
C(15)-C(16)-C(17)-C(18)	2.7(8)
C(14)-N(13)-C(18)-C(17)	1.0(7)
Cu-N(13)-C(18)-C(17)	-177.9(4)
C(16)-C(17)-C(18)-N(13)	-2.8(8)
C(3)-C(4)-O(19)-C(20)	4.3(7)
C(5)-C(4)-O(19)-C(20)	-174.8(5)
C(4)-O(19)-C(20)-C(21)	-177.8(5)
O(19)-C(20)-C(21)-C(22)	161.4(5)
O(19)-C(20)-C(21)-C(26)	-17.5(8)
C(26)-C(21)-C(22)-C(23)	0.4(9)
C(20)-C(21)-C(22)-C(23)	-178.6(6)
C(21)-C(22)-C(23)-C(24)	1.7(10)
C(22)-C(23)-C(24)-C(25)	-2.0(10)
C(22)-C(23)-C(24)-C(27)	176.2(6)
C(23)-C(24)-C(25)-C(26)	0.2(10)
C(27)-C(24)-C(25)-C(26)	-177.9(6)
C(22)-C(21)-C(26)-C(25)	-2.1(9)
C(20)-C(21)-C(26)-C(25)	176.9(6)
C(24)-C(25)-C(26)-C(21)	1.8(10)
N(1)-Cu-N(28)-C(29)	-56(2)
N(13)-Cu-N(28)-C(29)	-89.8(3)
N(7)-Cu-N(28)-C(29)	93.1(3)
N(35)-Cu-N(28)-C(29)	6.0(3)
N(40)-Cu-N(28)-C(29)	179.8(4)
N(1)-Cu-N(28)-C(33)	113(2)
N(13)-Cu-N(28)-C(33)	79.6(3)
N(7)-Cu-N(28)-C(33)	-97.5(3)
N(35)-Cu-N(28)-C(33)	175.4(4)
N(40)-Cu-N(28)-C(33)	-10.8(3)
C(33)-N(28)-C(29)-C(30)	-1.4(7)
Cu-N(28)-C(29)-C(30)	167.9(4)
C(33)-N(28)-C(29)-C(34)	179.2(4)
Cu-N(28)-C(29)-C(34)	-11.4(5)
N(28)-C(29)-C(30)-C(31)	0.1(8)
C(34)-C(29)-C(30)-C(31)	179.4(5)
C(29)-C(30)-C(31)-O(46)	-177.5(5)
C(29)-C(30)-C(31)-C(32)	1.8(8)
O(46)-C(31)-C(32)-C(33)	176.9(5)
C(30)-C(31)-C(32)-C(33)	-2.4(8)
C(29)-N(28)-C(33)-C(32)	0.8(7)
Cu-N(28)-C(33)-C(32)	-168.7(4)
C(29)-N(28)-C(33)-C(41)	-178.1(4)
Cu-N(28)-C(33)-C(41)	12.5(5)
C(31)-C(32)-C(33)-N(28)	1.2(8)
C(31)-C(32)-C(33)-C(41)	180.0(5)
N(28)-C(29)-C(34)-N(35)	11.8(6)
C(30)-C(29)-C(34)-N(35)	-167.5(5)
N(28)-C(29)-C(34)-C(39)	-166.6(5)
C(30)-C(29)-C(34)-C(39)	14.1(8)
C(39)-C(34)-N(35)-C(36)	0.3(8)
C(29)-C(34)-N(35)-C(36)	-178.1(4)
C(39)-C(34)-N(35)-Cu	171.6(4)
C(29)-C(34)-N(35)-Cu	-6.8(5)
N(1)-Cu-N(35)-C(34)	177.3(3)
N(28)-Cu-N(35)-C(34)	0.9(3)
N(13)-Cu-N(35)-C(34)	97.2(3)
N(7)-Cu-N(35)-C(34)	-104.4(3)
N(40)-Cu-N(35)-C(34)	-12.1(5)
N(1)-Cu-N(35)-C(36)	-12.6(5)
N(28)-Cu-N(35)-C(36)	170.9(5)
N(13)-Cu-N(35)-C(36)	-92.7(5)
N(7)-Cu-N(35)-C(36)	65.7(5)
N(40)-Cu-N(35)-C(36)	157.9(4)
C(34)-N(35)-C(36)-C(37)	0.3(9)
Cu-N(35)-C(36)-C(37)	-169.2(5)
N(35)-C(36)-C(37)-C(38)	-2.1(11)

C(36)-C(37)-C(38)-C(39)	3.3(11)
N(35)-C(34)-C(39)-C(38)	0.9(9)
C(29)-C(34)-C(39)-C(38)	179.2(5)
C(37)-C(38)-C(39)-C(34)	-2.7(10)
N(1)-Cu-N(40)-C(41)	-168.9(3)
N(28)-Cu-N(40)-C(41)	7.7(3)
N(13)-Cu-N(40)-C(41)	-89.8(3)
N(7)-Cu-N(40)-C(41)	113.1(3)
N(35)-Cu-N(40)-C(41)	20.8(5)
N(1)-Cu-N(40)-C(45)	8.6(4)
N(28)-Cu-N(40)-C(45)	-174.8(4)
N(13)-Cu-N(40)-C(45)	87.7(4)
N(7)-Cu-N(40)-C(45)	-69.4(4)
N(35)-Cu-N(40)-C(45)	-161.7(4)
C(45)-N(40)-C(41)-C(42)	-1.6(7)
Cu-N(40)-C(41)-C(42)	176.2(4)
C(45)-N(40)-C(41)-C(33)	178.4(4)
Cu-N(40)-C(41)-C(33)	-3.8(5)
N(28)-C(33)-C(41)-N(40)	-4.8(6)
C(32)-C(33)-C(41)-N(40)	176.4(5)
N(28)-C(33)-C(41)-C(42)	175.2(5)
C(32)-C(33)-C(41)-C(42)	-3.6(8)
N(40)-C(41)-C(42)-C(43)	0.7(9)
C(33)-C(41)-C(42)-C(43)	-179.3(5)
C(41)-C(42)-C(43)-C(44)	0.9(10)
C(42)-C(43)-C(44)-C(45)	-1.6(10)
C(41)-N(40)-C(45)-C(44)	0.9(7)
Cu-N(40)-C(45)-C(44)	-176.5(4)
C(43)-C(44)-C(45)-N(40)	0.7(8)
C(30)-C(31)-O(46)-C(47)	176.1(7)
C(32)-C(31)-O(46)-C(47)	-3.2(10)
C(31)-O(46)-C(47)-C(48)	-171.1(7)
O(46)-C(47)-C(48)-C(53)	142.1(11)
O(46)-C(47)-C(48)-C(49)	-39.3(13)
C(53)-C(48)-C(49)-C(50)	13.3(14)
C(47)-C(48)-C(49)-C(50)	-165.4(7)
C(48)-C(49)-C(50)-C(51)	-9.3(11)
C(49)-C(50)-C(51)-C(52)	0.8(12)
C(49)-C(50)-C(51)-C(54)	-176.5(8)
C(50)-C(51)-C(52)-C(53)	5.2(16)
C(54)-C(51)-C(52)-C(53)	-177.4(10)
C(49)-C(48)-C(53)-C(52)	-8.2(17)
C(47)-C(48)-C(53)-C(52)	170.3(10)
C(51)-C(52)-C(53)-C(48)	-1.5(18)

Symmetry transformations used to generate equivalent atoms:

Table 7. Hydrogen bonds for **4**-Cu-**4** [A and deg.].

D-H...A	d(D-H)	d(H...A)	d(D...A)	<(DHA)

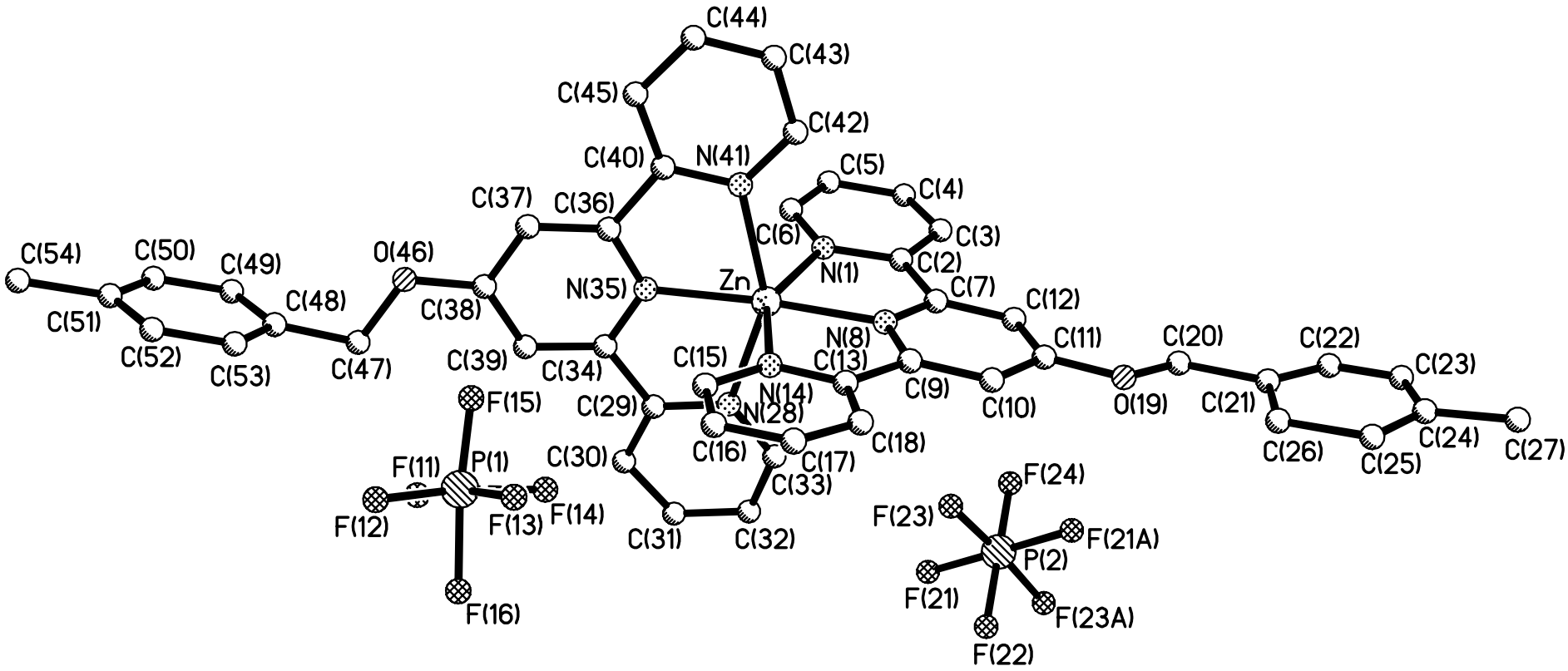
C(44)
C(43)
C(45)
C(42)
C(40)
N(41)
C(5)
C(4)
C(37)
C(36)
C(6)
C(3)
C(54)
C(50)
C(49)
O(46)
N(1)
C(2)
N(35)
Zn
C(7)
C(12)
C(51)
C(48)
C(38)
N(8)
C(11)
C(20)
C(22)
C(52)
C(53)
C(47)
C(39)
C(34)
C(15)
C(13)
C(23)
N(14)
C(9)
C(10)
O(19)
C(21)
F(15)
C(29)
N(28)
C(16)
C(18)
C(24)
C(27)
F(11)
P(1)
C(30)
C(17)
C(26)
C(25)
C(33)
F(24)
F(12)
F(13)
F(14)
C(31)
C(32)
F(23)
F(21A)
P(2)
F(21)
F(23A)
F(16)
F(22)

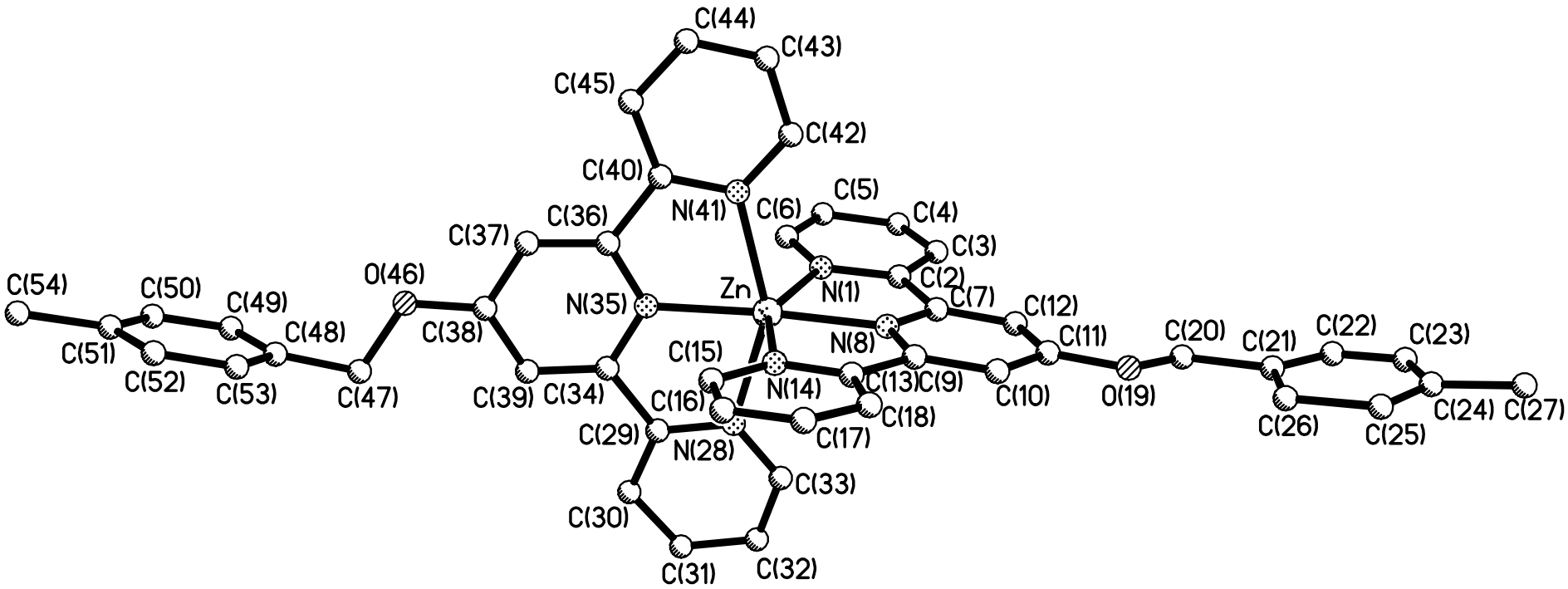
C(44)
C(43)
C(45)
C(42)
C(40)
N(41)
C(6)
C(5)
C(4)
C(36)
C(37)
C(3)
O(46)
C(54)
C(50)
C(49)
Zn
N(1)
C(2)
C(7)
C(12)
N(35)
C(48)
C(38)
N(8)
C(11)
C(20)
C(21)
C(22)
C(23)
C(51)
C(15)
C(52)
C(53)
C(47)
C(39)
C(34)
N(14)
C(13)
C(9)
C(10)
O(19)
C(16)
C(18)
C(24)
C(27)
C(29)
C(17)
C(26)
C(25)
N(28)
C(33)
C(30)
C(31)
C(32)

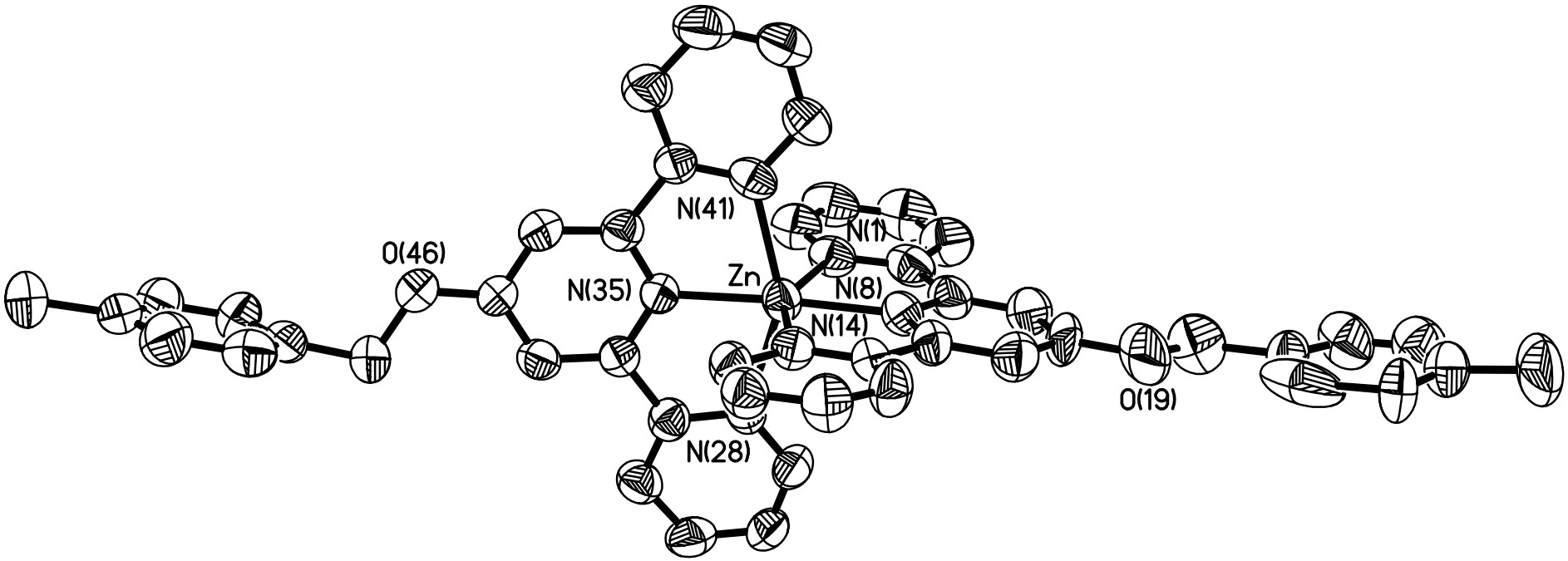
N(41)
N(1)
O(46)
Zn
N(35)
N(8)
N(14)
O(19)
N(28)

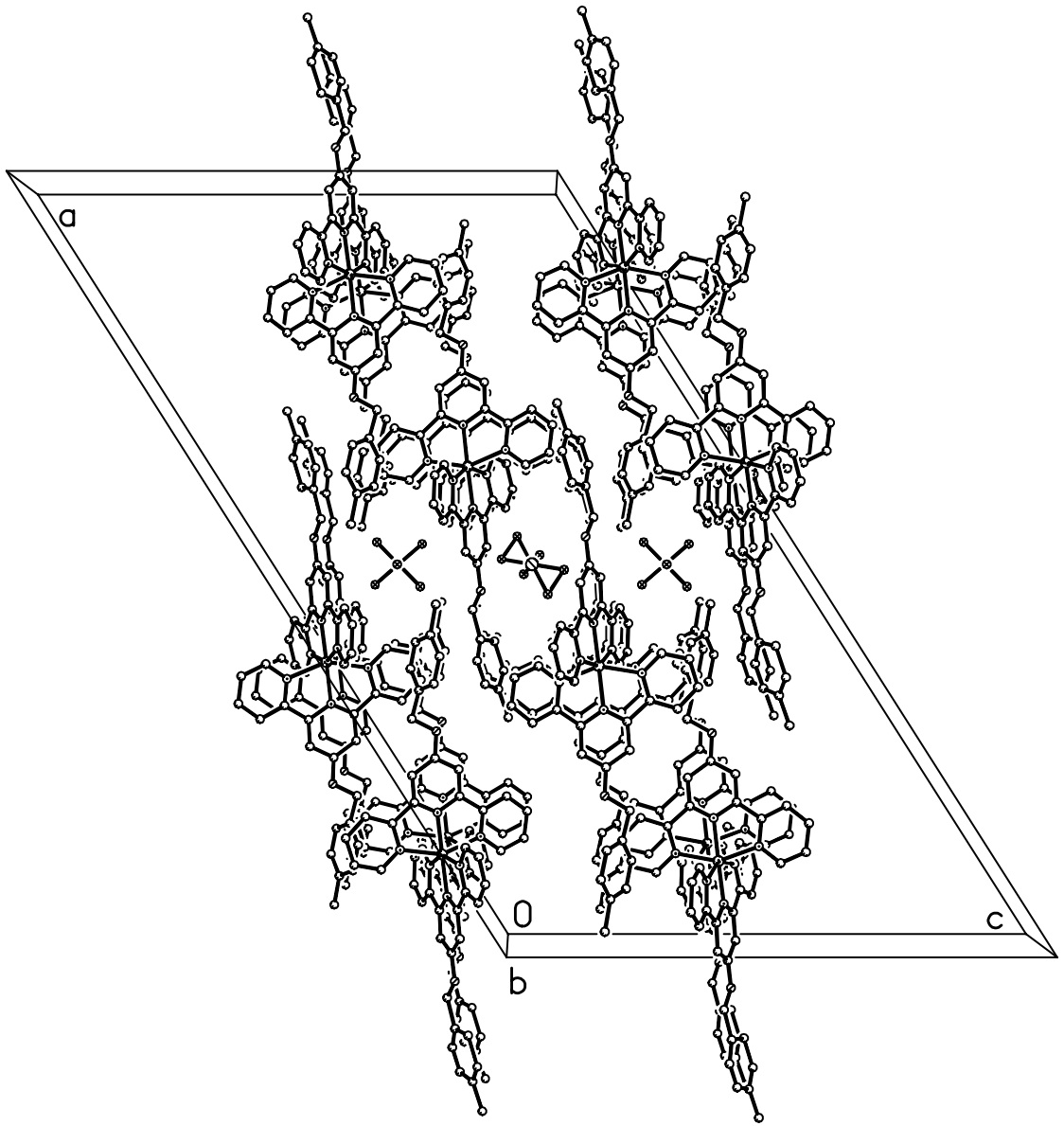
a
0
c
b

Table 1. Crystal data and structure refinement for **4**-Zn-**4**.

Identification code	**4**-Zn-**4**
Empirical formula	C46 H38 F9.50 N6 O2 P2 Zn
Formula weight	1014.63
Temperature	295(2) K
Wavelength	0.71073 A
Crystal system, space group	monoclinic, C2/c
Unit cell dimensions	a = 45.024(9) A alpha = 90 deg. b = 9.1410(18) A beta = 122.40(3) deg. c = 26.577(5) A gamma = 90 deg.
Volume	9235(3) A^3
Z, Calculated density	8, 1.459 Mg/m^3
Absorption coefficient	0.685 mm^-1
F(000)	4140
Crystal size	0.72 x 0.52 x 0.05 mm
Theta range for data collection	2.36 to 20.83 deg.
Limiting indices	-44<=h<=44, -9<=k<=9, -26<=l<=26
Reflections collected / unique	16929 / 3630 [R(int) = 0.0393]
Completeness to theta = 20.83	75.0 %
Max. and min. transmission	0.9666 and 0.6384
Refinement method	Full-matrix least-squares on F^2
Data / restraints / parameters	3630 / 7 / 627
Goodness-of-fit on F^2	1.039
Final R indices [I>2sigma(I)]	R1 = 0.0793, wR2 = 0.2170
R indices (all data)	R1 = 0.0954, wR2 = 0.2354
Largest diff. peak and hole	0.696 and -0.377 e.A^-3

Comment: One of the PF6 anions has two position therefore the occupation factor is 0.5 for each of these molecules.

Table 2. Atomic coordinates (x 10^4) and equivalent isotropic displacement parameters (A^2 x 10^3) for **4**-Zn-**4**.
U(eq) is defined as one third of the trace of the orthogonalized Uij tensor.

	x	y	z	U(eq)
Zn	3732(1)	3162(1)	5041(1)	53(1)
N(1)	3924(2)	1009(7)	5467(3)	59(2)
P(1)	2647(1)	8624(3)	4087(2)	91(1)
C(2)	4287(2)	904(9)	5799(4)	67(2)
P(2)	5000	5006(5)	7500	91(1)
P(2A)	5000	10000	5000	610(20)
C(3)	4442(3)	-405(10)	6097(4)	81(3)
C(4)	4241(3)	-1514(11)	6079(5)	92(3)
C(5)	3877(3)	-1406(10)	5731(5)	80(3)
C(6)	3735(3)	-121(9)	5445(4)	69(2)
C(7)	4478(2)	2195(9)	5775(4)	64(2)
N(8)	4270(2)	3291(6)	5432(3)	56(2)
C(9)	4409(2)	4507(9)	5361(3)	57(2)
C(10)	4773(2)	4661(10)	5643(4)	75(3)
C(11)	4988(2)	3523(11)	6005(4)	73(3)
F(11)	2432(2)	8061(10)	4343(6)	164(4)
C(12)	4838(2)	2302(11)	6077(4)	73(3)
F(12)	2338(3)	9560(15)	3620(5)	202(5)
C(13)	4155(2)	5635(8)	4974(3)	53(2)
F(13)	2908(3)	9289(11)	3946(8)	233(7)
N(14)	3819(2)	5356(6)	4776(3)	51(2)
F(14)	2979(3)	7783(13)	4630(6)	182(4)
C(15)	3574(2)	6340(8)	4442(3)	57(2)
F(15)	2608(4)	7197(12)	3783(7)	220(6)
C(16)	3657(2)	7652(9)	4271(4)	63(2)
F(16)	2729(3)	10029(10)	4529(6)	177(4)
C(17)	3996(2)	7902(9)	4460(5)	74(3)
C(18)	4251(2)	6938(9)	4822(4)	67(2)
O(19)	5344(2)	3758(11)	6263(4)	128(3)
C(20)	5587(3)	2830(12)	6631(6)	96(3)
C(21)	5975(2)	3154(10)	6838(4)	66(2)
F(21)	4708(2)	4998(17)	7641(5)	110(5)
C(22)	6246(3)	2364(13)	7141(5)	91(3)
F(22)	5000	6740(15)	7500	316(19)
C(23)	6550(3)	2636(14)	7274(5)	96(3)
F(23)	4732(2)	5090(19)	6817(4)	126(6)
C(24)	6626(2)	3865(10)	7101(4)	66(2)
F(24)	5000	3361(16)	7500	410(30)
C(25)	6394(2)	4895(10)	6797(4)	72(2)
F(25)	4931(7)	9390(30)	5524(10)	212(14)
C(26)	6008(4)	4584(17)	6616(5)	149(8)
F(26)	4620(5)	10480(30)	4942(12)	199(11)
C(27)	6996(3)	4050(20)	7255(6)	141(6)
F(27)	4874(5)	8620(20)	4736(9)	206(12)
N(28)	3652(2)	4050(7)	5724(3)	56(2)
C(29)	3312(2)	4175(8)	5553(3)	56(2)
C(30)	3217(2)	4586(9)	5950(4)	66(2)
C(31)	3487(2)	4847(10)	6549(4)	77(3)
C(32)	3831(2)	4732(10)	6710(4)	66(2)
C(33)	3900(2)	4315(9)	6291(4)	64(2)
C(34)	3051(2)	3861(8)	4921(3)	49(2)
N(35)	3189(2)	3259(6)	4632(3)	48(2)
C(36)	2987(2)	2985(8)	4041(3)	52(2)
C(37)	2636(2)	3278(8)	3738(4)	62(2)
C(38)	2483(2)	3891(8)	4028(3)	56(2)
C(39)	2699(2)	4177(8)	4638(4)	59(2)
C(40)	3178(2)	2303(7)	3788(3)	51(2)
N(41)	3523(2)	2230(6)	4149(3)	55(2)
C(42)	3718(2)	1652(8)	3954(4)	64(2)
C(43)	3568(3)	1116(10)	3387(4)	73(2)

C(44)	3213(3)	1188(12)	3007(5)	88(3)
C(45)	3008(2)	1809(9)	3200(4)	72(2)
O(46)	2134(1)	4164(7)	3687(2)	71(2)
C(47)	1966(2)	4879(10)	3969(4)	68(2)
C(48)	1600(2)	5158(8)	3500(4)	58(2)
C(49)	1335(2)	4237(10)	3430(4)	71(2)
C(50)	994(3)	4520(14)	3023(6)	98(4)
C(51)	895(3)	5719(17)	2650(5)	107(4)
C(52)	1160(3)	6640(12)	2713(5)	100(4)
C(53)	1507(3)	6359(11)	3135(5)	81(3)
C(54)	506(3)	6030(20)	2195(7)	174(9)

Table 3. Bond lengths [A] and angles [deg] for **4**-Zn-**4**.

Zn-N(8)	2.064(6)
Zn-N(35)	2.080(6)
Zn-N(28)	2.187(7)
Zn-N(41)	2.201(6)
Zn-N(1)	2.203(6)
Zn-N(14)	2.227(6)
N(1)-C(6)	1.318(11)
N(1)-C(2)	1.383(11)
P(1)-F(15)	1.494(11)
P(1)-F(12)	1.536(9)
P(1)-F(13)	1.538(8)
P(1)-F(11)	1.540(10)
P(1)-F(14)	1.612(10)
P(1)-F(16)	1.644(10)
C(2)-C(3)	1.398(12)
C(2)-C(7)	1.482(13)
P(2)-F(24)	1.504(15)
P(2)-F(21)	1.547(8)
P(2)-F(21)#1	1.547(8)
P(2)-F(23)#1	1.552(9)
P(2)-F(23)	1.552(9)
P(2)-F(22)	1.585(14)
P(2A)-F(27)#2	1.410(12)
P(2A)-F(27)	1.410(12)
P(2A)-F(25)	1.675(17)
P(2A)-F(25)#2	1.675(17)
P(2A)-F(26)#2	1.689(16)
P(2A)-F(26)	1.689(16)
C(3)-C(4)	1.343(15)
C(4)-C(5)	1.388(16)
C(5)-C(6)	1.358(13)
C(7)-N(8)	1.341(10)
C(7)-C(12)	1.373(13)
N(8)-C(9)	1.337(10)
C(9)-C(10)	1.396(12)
C(9)-C(13)	1.472(11)
C(10)-C(11)	1.396(13)
C(11)-C(12)	1.372(14)
C(11)-O(19)	1.380(13)
C(13)-N(14)	1.335(9)
C(13)-C(18)	1.398(12)
N(14)-C(15)	1.329(10)
C(15)-C(16)	1.404(12)
C(16)-C(17)	1.347(12)
C(17)-C(18)	1.354(12)
O(19)-C(20)	1.314(13)
C(20)-C(21)	1.552(14)
C(21)-C(22)	1.265(14)
C(21)-C(26)	1.47(2)
C(22)-C(23)	1.245(16)
C(23)-C(24)	1.325(15)
C(24)-C(25)	1.313(12)
C(24)-C(27)	1.498(15)
C(25)-C(26)	1.56(2)
N(28)-C(33)	1.332(10)
N(28)-C(29)	1.348(10)
C(29)-C(30)	1.386(11)
C(29)-C(34)	1.472(11)
C(30)-C(31)	1.411(12)
C(31)-C(32)	1.372(13)
C(32)-C(33)	1.359(12)
C(34)-N(35)	1.338(9)
C(34)-C(39)	1.373(11)
N(35)-C(36)	1.352(10)
C(36)-C(37)	1.363(12)
C(36)-C(40)	1.480(11)
C(37)-C(38)	1.396(12)

C(38)-O(46)	1.352(9)
C(38)-C(39)	1.396(11)
C(40)-N(41)	1.321(10)
C(40)-C(45)	1.397(13)
N(41)-C(42)	1.343(11)
C(42)-C(43)	1.370(13)
C(43)-C(44)	1.359(14)
C(44)-C(45)	1.396(14)
O(46)-C(47)	1.473(10)
C(47)-C(48)	1.459(11)
C(48)-C(53)	1.374(13)
C(48)-C(49)	1.391(12)
C(49)-C(50)	1.348(15)
C(50)-C(51)	1.382(19)
C(51)-C(52)	1.39(2)
C(51)-C(54)	1.530(15)
C(52)-C(53)	1.373(16)

N(8)-Zn-N(35)	174.2(2)
N(8)-Zn-N(28)	103.5(2)
N(35)-Zn-N(28)	75.3(2)
N(8)-Zn-N(41)	105.8(3)
N(35)-Zn-N(41)	75.5(2)
N(28)-Zn-N(41)	150.7(2)
N(8)-Zn-N(1)	76.2(2)
N(35)-Zn-N(1)	109.5(2)
N(28)-Zn-N(1)	95.6(2)
N(41)-Zn-N(1)	91.8(2)
N(8)-Zn-N(14)	75.6(2)
N(35)-Zn-N(14)	98.8(2)
N(28)-Zn-N(14)	93.6(2)
N(41)-Zn-N(14)	93.1(2)
N(1)-Zn-N(14)	151.6(2)
C(6)-N(1)-C(2)	119.1(7)
C(6)-N(1)-Zn	127.7(5)
C(2)-N(1)-Zn	113.2(5)
F(15)-P(1)-F(12)	104.9(9)
F(15)-P(1)-F(13)	95.5(8)
F(12)-P(1)-F(13)	93.6(7)
F(15)-P(1)-F(11)	91.6(7)
F(12)-P(1)-F(11)	91.8(6)
F(13)-P(1)-F(11)	169.7(9)
F(15)-P(1)-F(14)	81.5(8)
F(12)-P(1)-F(14)	173.6(8)
F(13)-P(1)-F(14)	86.7(7)
F(11)-P(1)-F(14)	87.0(6)
F(15)-P(1)-F(16)	170.0(8)
F(12)-P(1)-F(16)	84.3(7)
F(13)-P(1)-F(16)	87.6(7)
F(11)-P(1)-F(16)	84.2(6)
F(14)-P(1)-F(16)	89.3(7)
N(1)-C(2)-C(3)	118.8(9)
N(1)-C(2)-C(7)	115.6(7)
C(3)-C(2)-C(7)	125.5(8)
F(24)-P(2)-F(21)	89.7(6)
F(24)-P(2)-F(21)#1	89.7(6)
F(21)-P(2)-F(21)#1	179.4(12)
F(24)-P(2)-F(23)#1	92.8(7)
F(21)-P(2)-F(23)#1	86.8(6)
F(21)#1-P(2)-F(23)#1	93.2(6)
F(24)-P(2)-F(23)	92.8(7)
F(21)-P(2)-F(23)	93.2(6)
F(21)#1-P(2)-F(23)	86.8(6)
F(23)#1-P(2)-F(23)	174.3(13)
F(24)-P(2)-F(22)	180.000(14)
F(21)-P(2)-F(22)	90.3(6)
F(21)#1-P(2)-F(22)	90.3(6)
F(23)#1-P(2)-F(22)	87.2(7)
F(23)-P(2)-F(22)	87.2(7)
F(27)#2-P(2A)-F(27)	179.999(4)
F(27)#2-P(2A)-F(25)	95.0(9)

F(27)-P(2A)-F(25)	85.0(9)
F(27)#2-P(2A)-F(25)#2	85.0(9)
F(27)-P(2A)-F(25)#2	95.0(9)
F(25)-P(2A)-F(25)#2	180.0(7)
F(27)#2-P(2A)-F(26)#2	94.0(10)
F(27)-P(2A)-F(26)#2	86.0(9)
F(25)-P(2A)-F(26)#2	117.9(12)
F(25)#2-P(2A)-F(26)#2	62.1(12)
F(27)#2-P(2A)-F(26)	86.0(9)
F(27)-P(2A)-F(26)	94.0(10)
F(25)-P(2A)-F(26)	62.1(12)
F(25)#2-P(2A)-F(26)	117.9(12)
F(26)#2-P(2A)-F(26)	180.0(4)
C(4)-C(3)-C(2)	120.2(9)
C(3)-C(4)-C(5)	120.2(8)
C(6)-C(5)-C(4)	117.8(10)
N(1)-C(6)-C(5)	123.8(9)
N(8)-C(7)-C(12)	121.3(8)
N(8)-C(7)-C(2)	114.5(7)
C(12)-C(7)-C(2)	124.2(8)
C(9)-N(8)-C(7)	120.5(7)
C(9)-N(8)-Zn	119.2(5)
C(7)-N(8)-Zn	120.2(6)
N(8)-C(9)-C(10)	120.7(7)
N(8)-C(9)-C(13)	115.7(6)
C(10)-C(9)-C(13)	123.5(8)
C(11)-C(10)-C(9)	118.5(9)
C(12)-C(11)-O(19)	125.9(8)
C(12)-C(11)-C(10)	119.3(7)
O(19)-C(11)-C(10)	114.8(9)
C(11)-C(12)-C(7)	119.6(8)
N(14)-C(13)-C(18)	120.6(7)
N(14)-C(13)-C(9)	115.6(7)
C(18)-C(13)-C(9)	123.7(6)
C(15)-N(14)-C(13)	119.7(6)
C(15)-N(14)-Zn	126.6(5)
C(13)-N(14)-Zn	113.7(5)
N(14)-C(15)-C(16)	121.6(7)
C(17)-C(16)-C(15)	118.2(7)
C(16)-C(17)-C(18)	120.9(8)
C(17)-C(18)-C(13)	119.1(7)
C(20)-O(19)-C(11)	123.5(11)
O(19)-C(20)-C(21)	118.1(10)
C(22)-C(21)-C(26)	119.4(10)
C(22)-C(21)-C(20)	129.3(10)
C(26)-C(21)-C(20)	111.2(10)
C(23)-C(22)-C(21)	127.3(13)
C(22)-C(23)-C(24)	121.3(11)
C(25)-C(24)-C(23)	123.7(9)
C(25)-C(24)-C(27)	119.2(11)
C(23)-C(24)-C(27)	117.1(11)
C(24)-C(25)-C(26)	116.4(9)
C(21)-C(26)-C(25)	111.9(7)
C(33)-N(28)-C(29)	118.4(7)
C(33)-N(28)-Zn	126.6(5)
C(29)-N(28)-Zn	114.5(5)
N(28)-C(29)-C(30)	121.6(7)
N(28)-C(29)-C(34)	115.8(7)
C(30)-C(29)-C(34)	122.6(7)
C(29)-C(30)-C(31)	118.3(8)
C(32)-C(31)-C(30)	119.0(9)
C(33)-C(32)-C(31)	118.6(7)
N(28)-C(33)-C(32)	124.0(7)
N(35)-C(34)-C(39)	121.7(7)
N(35)-C(34)-C(29)	113.8(6)
C(39)-C(34)-C(29)	124.5(7)
C(34)-N(35)-C(36)	121.0(6)
C(34)-N(35)-Zn	119.7(5)
C(36)-N(35)-Zn	118.0(5)
N(35)-C(36)-C(37)	119.6(7)
N(35)-C(36)-C(40)	114.4(6)

C(37)-C(36)-C(40)	125.9(7)
C(36)-C(37)-C(38)	120.8(7)
O(46)-C(38)-C(39)	125.5(7)
O(46)-C(38)-C(37)	116.3(6)
C(39)-C(38)-C(37)	118.3(7)
C(34)-C(39)-C(38)	118.6(7)
N(41)-C(40)-C(45)	121.3(7)
N(41)-C(40)-C(36)	115.9(6)
C(45)-C(40)-C(36)	122.8(7)
C(40)-N(41)-C(42)	120.0(7)
C(40)-N(41)-Zn	114.8(5)
C(42)-N(41)-Zn	125.2(6)
N(41)-C(42)-C(43)	121.6(8)
C(44)-C(43)-C(42)	119.5(9)
C(43)-C(44)-C(45)	119.5(9)
C(44)-C(45)-C(40)	118.1(9)
C(38)-O(46)-C(47)	118.0(6)
C(48)-C(47)-O(46)	107.3(6)
C(53)-C(48)-C(49)	118.2(8)
C(53)-C(48)-C(47)	121.4(8)
C(49)-C(48)-C(47)	120.3(8)
C(50)-C(49)-C(48)	121.3(10)
C(49)-C(50)-C(51)	121.2(10)
C(50)-C(51)-C(52)	117.9(9)
C(50)-C(51)-C(54)	120.2(16)
C(52)-C(51)-C(54)	121.9(16)
C(53)-C(52)-C(51)	120.7(11)
C(52)-C(53)-C(48)	120.7(10)

Symmetry transformations used to generate equivalent atoms:
#1 -x+1,y,-z+3/2 #2 -x+1,-y+2,-z+1

Table 4. Anisotropic displacement parameters (A^2 x 10^3) for **4**-Zn-**4**.
The anisotropic displacement factor exponent takes the form:
-2 pi^2 [h^2 a*^2 U11 + ... + 2 h k a* b* U12]

	U11	U22	U33	U23	U13	U12
Zn	48(1)	49(1)	59(1)	4(1)	28(1)	6(1)
N(1)	73(4)	50(4)	59(4)	4(3)	37(4)	8(3)
P(1)	71(2)	63(2)	155(3)	15(2)	70(2)	5(1)
C(2)	79(6)	63(6)	59(5)	5(4)	38(5)	20(5)
P(2)	64(2)	118(3)	68(2)	0	20(2)	0
P(2A)	670(30)	880(40)	740(30)	-710(40)	680(30)	-690(30)
C(3)	93(6)	57(6)	69(6)	17(4)	28(5)	27(5)
C(4)	127(10)	62(6)	82(7)	28(5)	53(7)	28(6)
C(5)	113(8)	53(5)	86(7)	3(5)	62(7)	5(5)
C(6)	84(5)	55(5)	69(5)	9(4)	42(5)	7(5)
C(7)	62(5)	63(5)	60(5)	2(4)	27(4)	18(4)
N(8)	53(4)	44(4)	61(4)	7(3)	24(3)	15(3)
C(9)	46(4)	57(5)	61(5)	0(4)	25(4)	5(4)
C(10)	62(6)	59(5)	90(6)	-9(5)	32(5)	-1(4)
C(11)	34(5)	80(6)	71(6)	2(5)	5(4)	15(4)
F(11)	140(7)	154(7)	232(11)	53(7)	123(7)	15(5)
C(12)	60(6)	67(6)	64(5)	4(4)	16(5)	23(5)
F(12)	184(9)	294(14)	143(7)	92(8)	96(7)	117(10)
C(13)	43(4)	56(5)	58(4)	-4(4)	27(4)	3(3)
F(13)	251(12)	147(7)	470(20)	103(11)	301(15)	49(8)
N(14)	51(4)	45(3)	55(4)	1(3)	27(3)	0(3)
F(14)	137(7)	180(9)	227(11)	60(8)	96(8)	48(6)
C(15)	52(4)	50(5)	62(5)	5(4)	25(4)	7(4)
F(15)	294(17)	128(7)	255(14)	-55(8)	159(14)	-32(9)
C(16)	59(5)	53(5)	72(5)	5(4)	33(4)	5(4)
F(16)	241(11)	112(6)	224(10)	-22(6)	154(10)	-1(6)
C(17)	68(6)	53(5)	98(7)	9(5)	43(5)	0(4)
C(18)	49(4)	61(5)	86(6)	8(4)	32(4)	-6(4)
O(19)	68(5)	177(8)	87(5)	-10(5)	7(4)	66(5)
C(20)	103(8)	80(6)	113(8)	14(6)	63(7)	7(6)
C(21)	56(5)	79(6)	70(5)	-10(5)	38(5)	-15(5)
F(21)	41(5)	224(14)	78(7)	-19(7)	41(5)	-36(6)
C(22)	89(8)	96(7)	79(7)	23(6)	39(6)	37(7)
F(22)	570(50)	136(13)	500(50)	0	460(50)	0
C(23)	88(8)	104(9)	89(7)	12(6)	43(6)	19(7)
F(23)	39(5)	275(19)	37(5)	14(7)	2(4)	5(7)
C(24)	55(5)	73(6)	61(5)	18(4)	26(4)	9(4)
F(24)	760(80)	129(13)	740(70)	0	670(70)	0
C(25)	41(4)	80(6)	85(6)	25(5)	26(4)	4(4)
F(25)	240(20)	270(30)	250(30)	-170(20)	210(20)	-140(20)
C(26)	170(14)	157(13)	51(6)	-5(7)	15(7)	121(12)
F(26)	135(13)	300(30)	190(20)	-110(20)	108(15)	-131(18)
C(27)	51(6)	235(18)	109(9)	-19(10)	25(6)	26(8)
F(27)	202(15)	310(20)	234(18)	-240(20)	200(16)	-211(18)
N(28)	49(4)	52(4)	68(5)	-1(3)	32(4)	1(3)
C(29)	53(5)	52(4)	56(5)	2(3)	26(4)	2(3)
C(30)	69(5)	73(5)	62(5)	-2(4)	39(5)	8(4)
C(31)	83(7)	80(6)	56(5)	-17(4)	31(5)	-1(5)
C(32)	54(5)	83(6)	52(5)	-14(4)	21(4)	-8(4)
C(33)	48(4)	65(5)	63(6)	-8(4)	18(4)	-5(4)
C(34)	50(4)	45(4)	53(4)	1(3)	29(4)	-1(3)
N(35)	44(3)	48(3)	48(4)	-2(3)	23(3)	-1(3)
C(36)	53(5)	48(4)	57(5)	-4(3)	30(4)	-7(3)
C(37)	56(5)	61(5)	58(5)	-13(4)	23(4)	-3(4)
C(38)	47(5)	60(5)	52(5)	-11(4)	20(4)	-2(4)
C(39)	60(5)	53(4)	69(6)	-10(4)	38(4)	-2(4)
C(40)	52(5)	42(4)	60(5)	-6(3)	30(4)	-5(3)
N(41)	72(5)	45(3)	58(4)	8(3)	41(4)	11(3)
C(42)	75(5)	46(4)	79(6)	9(4)	47(5)	13(4)
C(43)	89(7)	68(6)	82(7)	-11(5)	59(6)	-1(5)
C(44)	105(8)	92(7)	85(7)	-27(5)	64(7)	-15(6)

C(45)	71(5)	72(6)	78(6)	-11(4)	43(5)	-8(4)
O(46)	53(3)	86(4)	61(3)	-20(3)	21(3)	0(3)
C(47)	48(4)	76(5)	73(5)	-9(4)	28(4)	2(4)
C(48)	55(5)	56(5)	67(5)	-8(4)	35(4)	1(4)
C(49)	57(5)	77(6)	69(5)	-7(4)	27(5)	-8(4)
C(50)	57(6)	102(8)	129(10)	-40(8)	45(7)	-18(6)
C(51)	65(7)	128(10)	81(7)	-54(8)	8(6)	26(7)
C(52)	91(8)	74(6)	85(7)	-3(5)	15(7)	22(6)
C(53)	84(7)	72(6)	86(7)	-16(5)	44(6)	-3(5)
C(54)	79(8)	202(16)	139(12)	-76(11)	-10(8)	67(9)

Table 5. Hydrogen coordinates (x 10^4) and isotropic displacement parameters (A^2 x 10^3) for **4**-Zn-**4**.

	x	y	z	U(eq)
H(3)	4685	-510	6307	97
H(4)	4346	-2356	6301	110
H(5)	3734	-2187	5695	96
H(6)	3492	-33	5220	83
H(10)	4869	5504	5592	89
H(12)	4978	1551	6328	87
H(15)	3341	6154	4319	69
H(16)	3483	8329	4034	75
H(17)	4057	8749	4341	89
H(18)	4486	7139	4967	81
H(20A)	5527	1876	6442	115
H(20B)	5575	2759	6983	115
H(22)	6213	1482	7279	109
H(23)	6729	1964	7500	115
H(25)	6457	5764	6695	86
H(26)	5821	5223	6394	178
H(27A)	7088	4963	7459	211
H(27B)	6999	4045	6897	211
H(27C)	7139	3261	7509	211
H(30)	2982	4687	5826	79
H(31)	3433	5093	6830	92
H(32)	4014	4934	7098	80
H(33)	4134	4209	6408	77
H(37)	2496	3068	3333	74
H(39)	2606	4573	4847	70
H(42)	3962	1615	4211	76
H(43)	3707	706	3263	87
H(44)	3108	826	2621	105
H(45)	2765	1891	2945	86
H(47A)	1978	4248	4272	81
H(47B)	2085	5790	4154	81
H(49)	1394	3410	3669	85
H(50)	821	3897	2993	118
H(52)	1101	7455	2468	120
H(53)	1680	6988	3173	97
H(54A)	368	5210	2181	262
H(54B)	471	6167	1809	262
H(54C)	436	6890	2309	262

Table 6. Torsion angles [deg] for **4**-Zn-**4**.

N(8)-Zn-N(1)-C(6)	-176.3(7)
N(35)-Zn-N(1)-C(6)	4.8(7)
N(28)-Zn-N(1)-C(6)	81.2(7)
N(41)-Zn-N(1)-C(6)	-70.5(7)
N(14)-Zn-N(1)-C(6)	-170.4(6)
N(8)-Zn-N(1)-C(2)	4.8(5)
N(35)-Zn-N(1)-C(2)	-174.1(5)
N(28)-Zn-N(1)-C(2)	-97.7(5)
N(41)-Zn-N(1)-C(2)	110.7(5)
N(14)-Zn-N(1)-C(2)	10.8(8)
C(6)-N(1)-C(2)-C(3)	0.5(12)
Zn-N(1)-C(2)-C(3)	179.5(6)
C(6)-N(1)-C(2)-C(7)	177.0(7)
Zn-N(1)-C(2)-C(7)	-4.1(9)
N(1)-C(2)-C(3)-C(4)	-2.9(14)
C(7)-C(2)-C(3)-C(4)	-178.9(9)
C(2)-C(3)-C(4)-C(5)	4.6(16)
C(3)-C(4)-C(5)-C(6)	-4.0(15)
C(2)-N(1)-C(6)-C(5)	0.0(13)
Zn-N(1)-C(6)-C(5)	-178.8(7)
C(4)-C(5)-C(6)-N(1)	1.7(14)
N(1)-C(2)-C(7)-N(8)	0.0(11)
C(3)-C(2)-C(7)-N(8)	176.1(8)
N(1)-C(2)-C(7)-C(12)	179.6(8)
C(3)-C(2)-C(7)-C(12)	-4.3(14)
C(12)-C(7)-N(8)-C(9)	1.9(12)
C(2)-C(7)-N(8)-C(9)	-178.5(7)
C(12)-C(7)-N(8)-Zn	-174.9(7)
C(2)-C(7)-N(8)-Zn	4.7(9)
N(35)-Zn-N(8)-C(9)	-12(3)
N(28)-Zn-N(8)-C(9)	-89.5(6)
N(41)-Zn-N(8)-C(9)	90.0(6)
N(1)-Zn-N(8)-C(9)	177.9(7)
N(14)-Zn-N(8)-C(9)	0.8(6)
N(35)-Zn-N(8)-C(7)	164(2)
N(28)-Zn-N(8)-C(7)	87.3(6)
N(41)-Zn-N(8)-C(7)	-93.2(6)
N(1)-Zn-N(8)-C(7)	-5.3(6)
N(14)-Zn-N(8)-C(7)	177.6(7)
C(7)-N(8)-C(9)-C(10)	0.0(12)
Zn-N(8)-C(9)-C(10)	176.8(6)
C(7)-N(8)-C(9)-C(13)	-180.0(7)
Zn-N(8)-C(9)-C(13)	-3.2(9)
N(8)-C(9)-C(10)-C(11)	-0.5(13)
C(13)-C(9)-C(10)-C(11)	179.4(8)
C(9)-C(10)-C(11)-C(12)	-0.7(14)
C(9)-C(10)-C(11)-O(19)	179.6(8)
O(19)-C(11)-C(12)-C(7)	-177.8(9)
C(10)-C(11)-C(12)-C(7)	2.5(14)
N(8)-C(7)-C(12)-C(11)	-3.1(14)
C(2)-C(7)-C(12)-C(11)	177.3(9)
N(8)-C(9)-C(13)-N(14)	4.8(10)
C(10)-C(9)-C(13)-N(14)	-175.1(8)
N(8)-C(9)-C(13)-C(18)	-176.2(8)
C(10)-C(9)-C(13)-C(18)	3.9(13)
C(18)-C(13)-N(14)-C(15)	-1.5(11)
C(9)-C(13)-N(14)-C(15)	177.6(7)
C(18)-C(13)-N(14)-Zn	176.9(6)
C(9)-C(13)-N(14)-Zn	-4.0(8)
N(8)-Zn-N(14)-C(15)	-179.9(7)
N(35)-Zn-N(14)-C(15)	-1.2(7)
N(28)-Zn-N(14)-C(15)	-76.9(6)
N(41)-Zn-N(14)-C(15)	74.6(6)
N(1)-Zn-N(14)-C(15)	174.2(6)
N(8)-Zn-N(14)-C(13)	1.9(5)
N(35)-Zn-N(14)-C(13)	-179.5(5)
N(28)-Zn-N(14)-C(13)	104.8(5)

N(41)-Zn-N(14)-C(13)	-103.7(5)
N(1)-Zn-N(14)-C(13)	-4.1(8)
C(13)-N(14)-C(15)-C(16)	2.5(11)
Zn-N(14)-C(15)-C(16)	-175.7(6)
N(14)-C(15)-C(16)-C(17)	-0.7(13)
C(15)-C(16)-C(17)-C(18)	-2.2(14)
C(16)-C(17)-C(18)-C(13)	3.1(15)
N(14)-C(13)-C(18)-C(17)	-1.3(13)
C(9)-C(13)-C(18)-C(17)	179.7(8)
C(12)-C(11)-O(19)-C(20)	-1.8(16)
C(10)-C(11)-O(19)-C(20)	177.9(10)
C(11)-O(19)-C(20)-C(21)	173.8(9)
O(19)-C(20)-C(21)-C(22)	-172.7(11)
O(19)-C(20)-C(21)-C(26)	5.1(14)
C(26)-C(21)-C(22)-C(23)	-1.4(18)
C(20)-C(21)-C(22)-C(23)	176.3(12)
C(21)-C(22)-C(23)-C(24)	0(2)
C(22)-C(23)-C(24)-C(25)	2.1(19)
C(22)-C(23)-C(24)-C(27)	-176.7(12)
C(23)-C(24)-C(25)-C(26)	-2.6(15)
C(27)-C(24)-C(25)-C(26)	176.1(10)
C(22)-C(21)-C(26)-C(25)	0.6(13)
C(20)-C(21)-C(26)-C(25)	-177.4(9)
C(24)-C(25)-C(26)-C(21)	1.3(13)
N(8)-Zn-N(28)-C(33)	-12.1(7)
N(35)-Zn-N(28)-C(33)	173.7(7)
N(41)-Zn-N(28)-C(33)	168.9(6)
N(1)-Zn-N(28)-C(33)	65.0(7)
N(14)-Zn-N(28)-C(33)	-88.1(7)
N(8)-Zn-N(28)-C(29)	175.6(5)
N(35)-Zn-N(28)-C(29)	1.4(5)
N(41)-Zn-N(28)-C(29)	-3.4(8)
N(1)-Zn-N(28)-C(29)	-107.3(5)
N(14)-Zn-N(28)-C(29)	99.5(5)
C(33)-N(28)-C(29)-C(30)	0.8(11)
Zn-N(28)-C(29)-C(30)	173.8(6)
C(33)-N(28)-C(29)-C(34)	-179.7(7)
Zn-N(28)-C(29)-C(34)	-6.8(8)
N(28)-C(29)-C(30)-C(31)	-1.3(12)
C(34)-C(29)-C(30)-C(31)	179.3(7)
C(29)-C(30)-C(31)-C(32)	2.1(13)
C(30)-C(31)-C(32)-C(33)	-2.4(13)
C(29)-N(28)-C(33)-C(32)	-1.2(12)
Zn-N(28)-C(33)-C(32)	-173.2(6)
C(31)-C(32)-C(33)-N(28)	2.1(13)
N(28)-C(29)-C(34)-N(35)	10.7(9)
C(30)-C(29)-C(34)-N(35)	-169.9(7)
N(28)-C(29)-C(34)-C(39)	-167.7(7)
C(30)-C(29)-C(34)-C(39)	11.8(12)
C(39)-C(34)-N(35)-C(36)	2.3(10)
C(29)-C(34)-N(35)-C(36)	-176.1(6)
C(39)-C(34)-N(35)-Zn	168.7(5)
C(29)-C(34)-N(35)-Zn	-9.7(8)
N(8)-Zn-N(35)-C(34)	-74(3)
N(28)-Zn-N(35)-C(34)	4.8(5)
N(41)-Zn-N(35)-C(34)	-177.6(6)
N(1)-Zn-N(35)-C(34)	95.7(5)
N(14)-Zn-N(35)-C(34)	-86.6(5)
N(8)-Zn-N(35)-C(36)	93(2)
N(28)-Zn-N(35)-C(36)	171.6(5)
N(41)-Zn-N(35)-C(36)	-10.8(5)
N(1)-Zn-N(35)-C(36)	-97.5(5)
N(14)-Zn-N(35)-C(36)	80.2(5)
C(34)-N(35)-C(36)-C(37)	-2.2(10)
Zn-N(35)-C(36)-C(37)	-168.9(6)
C(34)-N(35)-C(36)-C(40)	-179.4(6)
Zn-N(35)-C(36)-C(40)	14.0(8)
N(35)-C(36)-C(37)-C(38)	1.5(11)
C(40)-C(36)-C(37)-C(38)	178.3(7)
C(36)-C(37)-C(38)-O(46)	178.9(7)
C(36)-C(37)-C(38)-C(39)	-0.8(12)

N(35)-C(34)-C(39)-C(38)	-1.6(11)
C(29)-C(34)-C(39)-C(38)	176.7(7)
O(46)-C(38)-C(39)-C(34)	-178.8(7)
C(37)-C(38)-C(39)-C(34)	0.8(11)
N(35)-C(36)-C(40)-N(41)	-8.5(9)
C(37)-C(36)-C(40)-N(41)	174.5(7)
N(35)-C(36)-C(40)-C(45)	173.6(7)
C(37)-C(36)-C(40)-C(45)	-3.3(12)
C(45)-C(40)-N(41)-C(42)	-0.9(11)
C(36)-C(40)-N(41)-C(42)	-178.8(6)
C(45)-C(40)-N(41)-Zn	177.4(6)
C(36)-C(40)-N(41)-Zn	-0.5(8)
N(8)-Zn-N(41)-C(40)	-168.4(5)
N(35)-Zn-N(41)-C(40)	5.7(5)
N(28)-Zn-N(41)-C(40)	10.5(8)
N(1)-Zn-N(41)-C(40)	115.4(5)
N(14)-Zn-N(41)-C(40)	-92.5(5)
N(8)-Zn-N(41)-C(42)	9.9(6)
N(35)-Zn-N(41)-C(42)	-176.0(6)
N(28)-Zn-N(41)-C(42)	-171.2(5)
N(1)-Zn-N(41)-C(42)	-66.3(6)
N(14)-Zn-N(41)-C(42)	85.8(6)
C(40)-N(41)-C(42)-C(43)	-0.6(11)
Zn-N(41)-C(42)-C(43)	-178.8(6)
N(41)-C(42)-C(43)-C(44)	1.0(13)
C(42)-C(43)-C(44)-C(45)	0.1(15)
C(43)-C(44)-C(45)-C(40)	-1.5(14)
N(41)-C(40)-C(45)-C(44)	2.0(12)
C(36)-C(40)-C(45)-C(44)	179.7(8)
C(39)-C(38)-O(46)-C(47)	2.7(12)
C(37)-C(38)-O(46)-C(47)	-177.0(7)
C(38)-O(46)-C(47)-C(48)	175.4(7)
O(46)-C(47)-C(48)-C(53)	-82.0(10)
O(46)-C(47)-C(48)-C(49)	100.7(9)
C(53)-C(48)-C(49)-C(50)	-1.1(13)
C(47)-C(48)-C(49)-C(50)	176.2(9)
C(48)-C(49)-C(50)-C(51)	1.5(16)
C(49)-C(50)-C(51)-C(52)	-0.9(16)
C(49)-C(50)-C(51)-C(54)	-179.5(10)
C(50)-C(51)-C(52)-C(53)	0.0(17)
C(54)-C(51)-C(52)-C(53)	178.5(10)
C(51)-C(52)-C(53)-C(48)	0.3(16)
C(49)-C(48)-C(53)-C(52)	0.2(14)
C(47)-C(48)-C(53)-C(52)	-177.1(9)

Symmetry transformations used to generate equivalent atoms:
#1 -x+1,y,-z+3/2 #2 -x+1,-y+2,-z+1

Table 7. Hydrogen bonds for **4**-Zn-**4** [A and deg.].

D-H...A	d(D-H)	d(H...A)	d(D...A)	<(DHA)

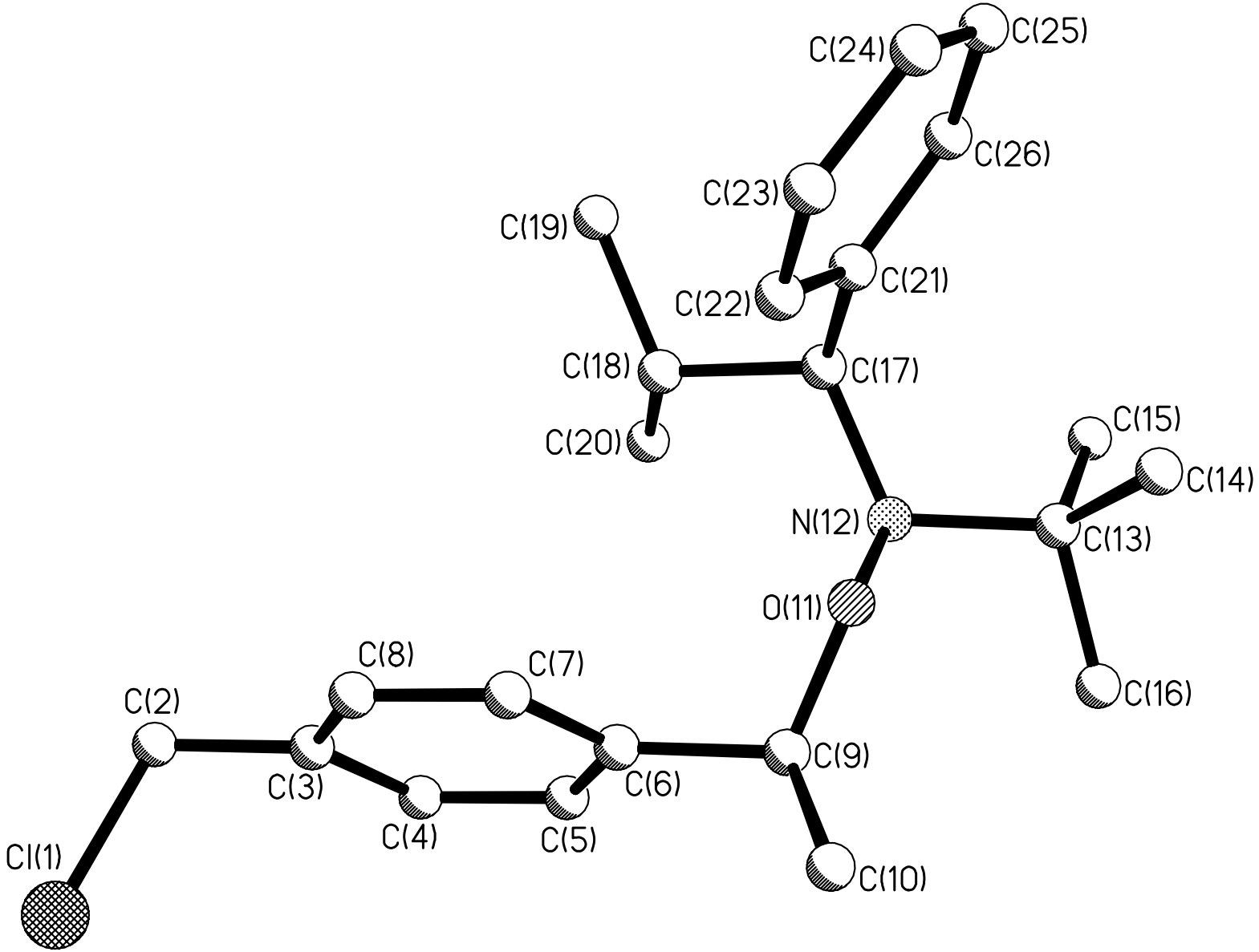
C(24)
C(25)
C(26)
C(23)
C(19)
C(22)
C(21)
C(18)
C(17)
C(20)
C(15)
C(14)
N(12)
C(13)
O(11)
C(16)
C(8)
C(7)
C(2)
C(9)
C(3)
C(6)
C(4)
C(5)
Cl(1)
C(10)

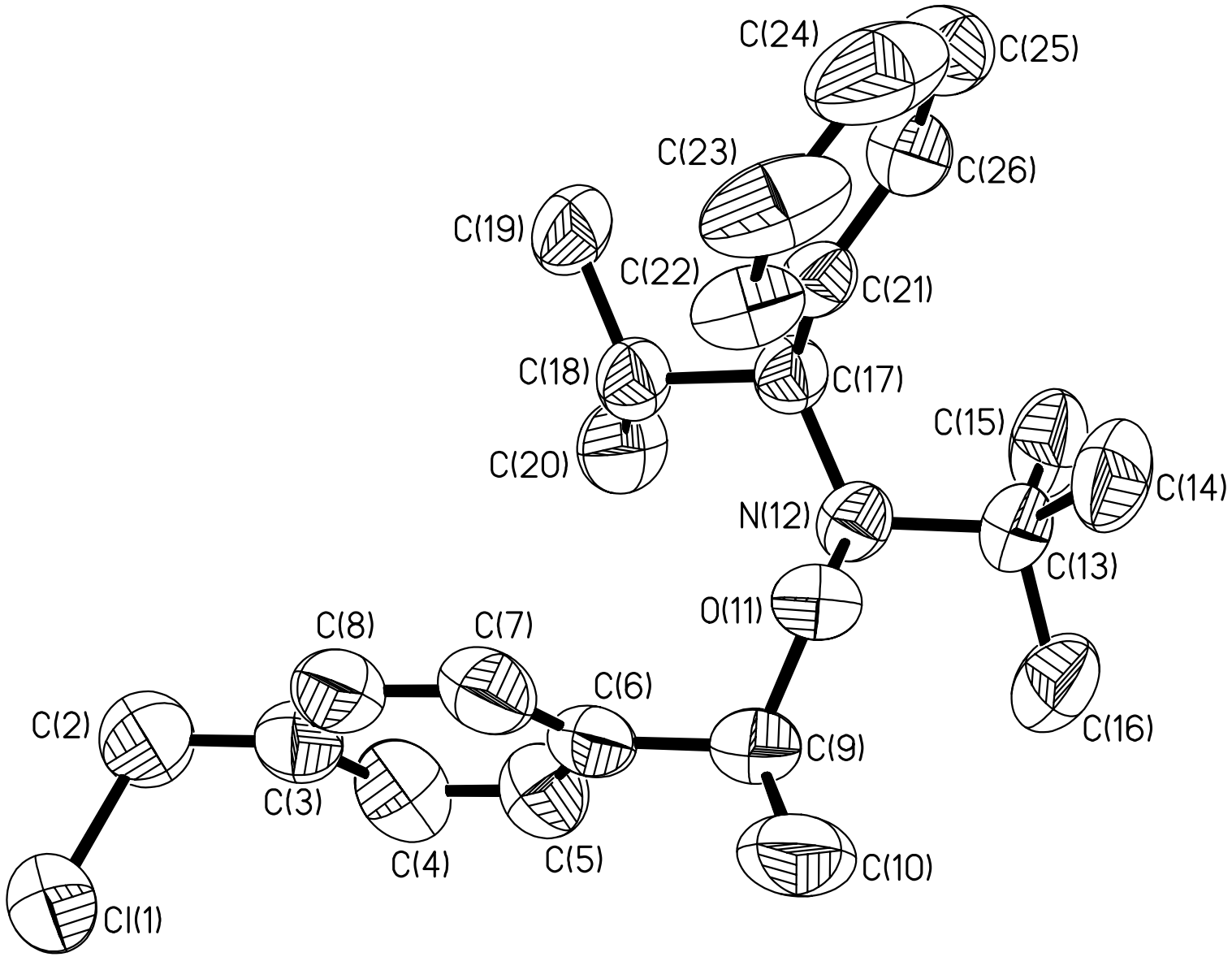
C(24)
C(25)
C(23)
C(26)
C(19)
C(22)
C(21)
C(18)
C(17)
C(20)
C(15)
C(14)
N(12)
C(13)
O(11)
C(8)
C(7)
C(6)
C(16)
C(2)
C(9)
C(3)
C(4)
C(5)
C(10)
Cl(1)

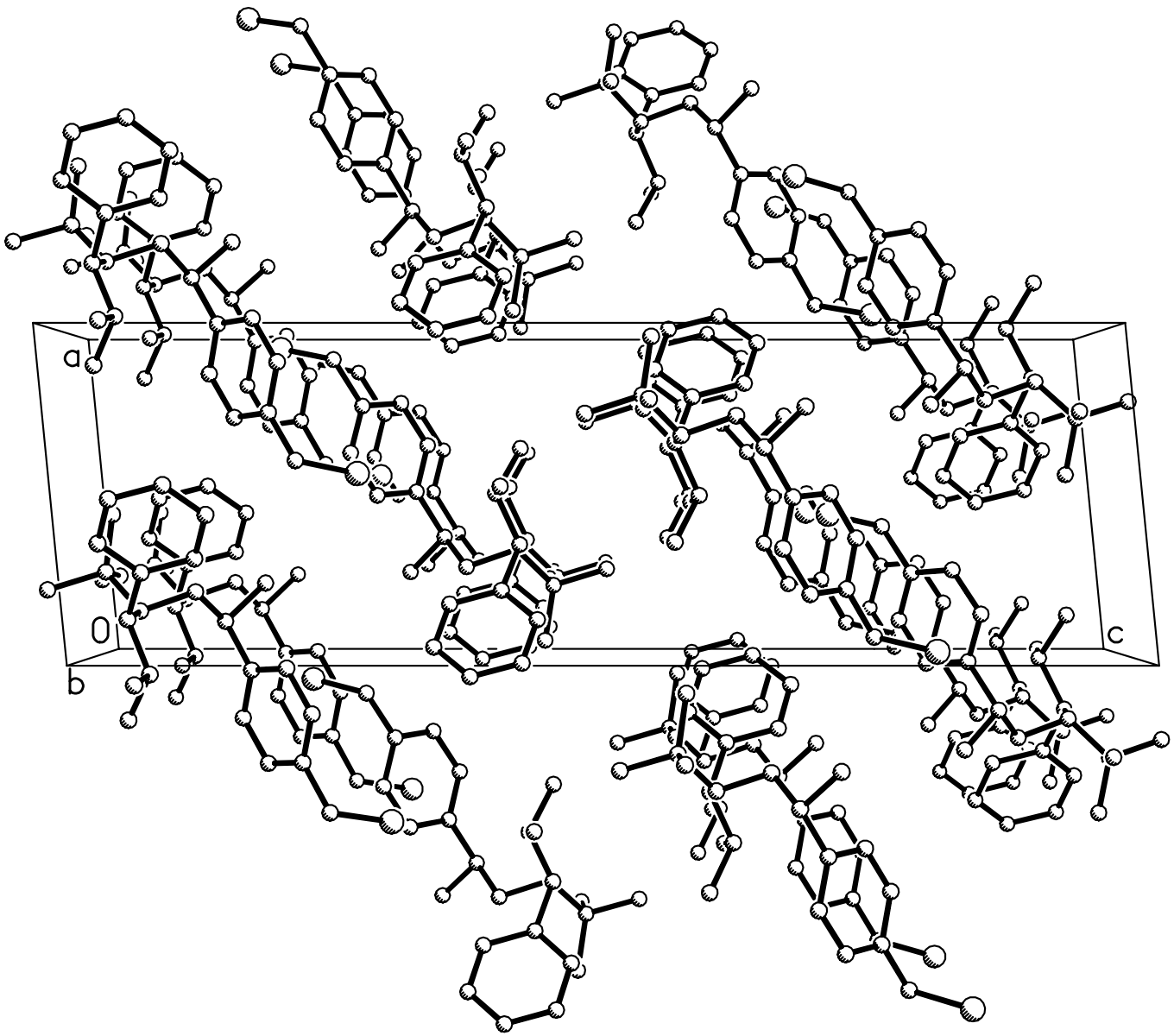
a
0
b
c

Table 1. Crystal data and structure refinement for 2,2,5-trimethyl-3-(1-(4’-chloromethyl)phenylethoxy)-4-phenyl-3-azahexane.

Identification code	2,2,5-trimethyl-3-(1-(4’-chloromethyl)phenylethoxy)-4-phenyl-3-azahexane
Empirical formula	C23 H32 Cl N O
Formula weight	373.95
Temperature	298(2) K
Wavelength	0.71073 A
Crystal system, space group	monoclinic, P2(1)/n
Unit cell dimensions	a = 8.8334(6) A alpha = 90 deg. b = 8.9138(6) A beta = 95.629(2) deg. c = 27.9253(18) A gamma = 90 deg.
Volume	2188.2(3) A^3
Z, Calculated density	4, 1.135 Mg/m^3
Absorption coefficient	0.185 mm^-1
F(000)	808
Crystal size	0.57 x 0.37 x 0.33 mm
Theta range for data collection	2.36 to 24.71 deg.
Limiting indices	-10<=h<=10, -10<=k<=9, -24<=l<=32
Reflections collected / unique	11392 / 3734 [R(int) = 0.0250]
Completeness to theta = 24.71	99.8 %
Max. and min. transmission	0.9413 and 0.9017
Refinement method	Full-matrix least-squares on F^2
Data / restraints / parameters	3734 / 0 / 241
Goodness-of-fit on F^2	1.066
Final R indices [I>2sigma(I)]	R1 = 0.0595, wR2 = 0.1447
R indices (all data)	R1 = 0.0753, wR2 = 0.1541
Largest diff. peak and hole	0.241 and -0.126 e.A^-3

Table 2. Atomic coordinates (x 10^4) and equivalent isotropic displacement parameters (A^2 x 10^3) for 2,2,5-trimethyl-3-(1-(4′-chloromethyl)phenylethoxy)-4-phenyl-3-azahexane.
U(eq) is defined as one third of the trace of the orthogonalized Uij tensor.

	x	y	z	U(eq)
Cl(1)	9405(1)	6324(1)	2136(1)	116(1)
C(2)	9040(4)	7382(4)	2652(1)	112(1)
C(3)	7664(4)	6810(3)	2869(1)	79(1)
C(4)	7778(3)	5723(4)	3217(1)	87(1)
C(5)	6499(3)	5217(3)	3424(1)	77(1)
C(6)	5080(3)	5793(3)	3283(1)	61(1)
C(7)	4970(3)	6868(3)	2929(1)	74(1)
C(8)	6241(4)	7373(3)	2728(1)	86(1)
C(9)	3694(3)	5199(3)	3499(1)	68(1)
C(10)	2600(3)	4420(4)	3125(1)	103(1)
O(11)	2801(2)	6361(2)	3699(1)	59(1)
N(12)	3339(2)	6692(2)	4197(1)	55(1)
C(13)	2237(3)	5981(3)	4509(1)	62(1)
C(14)	578(3)	6393(3)	4379(1)	85(1)
C(15)	2742(3)	6392(4)	5030(1)	89(1)
C(16)	2397(4)	4280(3)	4466(1)	89(1)
C(17)	3513(2)	8351(2)	4242(1)	54(1)
C(18)	5031(2)	8865(3)	4069(1)	60(1)
C(19)	5228(3)	10555(3)	4134(1)	79(1)
C(20)	6365(3)	8045(3)	4335(1)	83(1)
C(21)	2180(2)	9315(2)	4040(1)	57(1)
C(22)	1783(3)	9487(3)	3552(1)	74(1)
C(23)	565(4)	10388(3)	3384(1)	104(1)
C(24)	-250(4)	11135(4)	3697(2)	119(1)
C(25)	134(4)	11006(4)	4179(2)	107(1)
C(26)	1352(3)	10116(3)	4350(1)	78(1)

Table 3. Bond lengths [A] and angles [deg] for 2,2,5-trimethyl-3-(1-(4'-chloromethyl)phenylethoxy)-4-phenyl-3-azahexane.

Cl(1)-C(2)	1.777(3)
C(2)-C(3)	1.500(4)
C(3)-C(4)	1.369(4)
C(3)-C(8)	1.374(4)
C(4)-C(5)	1.393(4)
C(5)-C(6)	1.376(3)
C(6)-C(7)	1.373(3)
C(6)-C(9)	1.513(3)
C(7)-C(8)	1.380(4)
C(9)-O(11)	1.448(3)
C(9)-C(10)	1.520(4)
O(11)-N(12)	1.454(2)
N(12)-C(17)	1.490(3)
N(12)-C(13)	1.509(3)
C(13)-C(14)	1.520(3)
C(13)-C(15)	1.524(4)
C(13)-C(16)	1.529(4)
C(17)-C(21)	1.520(3)
C(17)-C(18)	1.538(3)
C(18)-C(20)	1.517(3)
C(18)-C(19)	1.526(3)
C(21)-C(22)	1.382(3)
C(21)-C(26)	1.386(3)
C(22)-C(23)	1.387(4)
C(23)-C(24)	1.362(5)
C(24)-C(25)	1.359(5)
C(25)-C(26)	1.384(5)

C(3)-C(2)-Cl(1)	111.5(2)
C(4)-C(3)-C(8)	117.7(3)
C(4)-C(3)-C(2)	121.4(3)
C(8)-C(3)-C(2)	120.9(3)
C(3)-C(4)-C(5)	121.1(3)
C(6)-C(5)-C(4)	120.9(3)
C(7)-C(6)-C(5)	117.7(2)
C(7)-C(6)-C(9)	121.9(2)
C(5)-C(6)-C(9)	120.3(2)
C(6)-C(7)-C(8)	121.2(3)
C(3)-C(8)-C(7)	121.4(3)
O(11)-C(9)-C(6)	113.35(18)
O(11)-C(9)-C(10)	105.0(2)
C(6)-C(9)-C(10)	111.8(2)
C(9)-O(11)-N(12)	112.03(16)
O(11)-N(12)-C(17)	107.63(15)
O(11)-N(12)-C(13)	107.33(15)
C(17)-N(12)-C(13)	115.81(17)
N(12)-C(13)-C(14)	114.97(19)
N(12)-C(13)-C(15)	107.78(18)
C(14)-C(13)-C(15)	110.8(2)
N(12)-C(13)-C(16)	107.6(2)
C(14)-C(13)-C(16)	108.4(2)
C(15)-C(13)-C(16)	107.0(2)
N(12)-C(17)-C(21)	117.40(17)
N(12)-C(17)-C(18)	110.80(17)
C(21)-C(17)-C(18)	112.48(18)
C(20)-C(18)-C(19)	110.0(2)
C(20)-C(18)-C(17)	111.3(2)
C(19)-C(18)-C(17)	110.49(19)
C(22)-C(21)-C(26)	117.5(2)
C(22)-C(21)-C(17)	122.7(2)
C(26)-C(21)-C(17)	119.8(2)
C(21)-C(22)-C(23)	120.8(3)
C(24)-C(23)-C(22)	120.4(3)
C(25)-C(24)-C(23)	119.9(3)
C(24)-C(25)-C(26)	120.1(3)
C(25)-C(26)-C(21)	121.2(3)

Symmetry transformations used to generate equivalent atoms:

Table 4. Anisotropic displacement parameters (A^2 x 10^3) for 2,2,5-trimethyl-3-(1-(4'-chloromethyl)phenylethoxy)-4-phenyl-3-azahexane.
The anisotropic displacement factor exponent takes the form:
-2 pi^2 [h^2 a*^2 U11 + ... + 2 h k a* b* U12]

	U11	U22	U33	U23	U13	U12
Cl(1)	143(1)	104(1)	109(1)	-22(1)	60(1)	-34(1)
C(2)	122(3)	104(2)	114(3)	-37(2)	42(2)	-48(2)
C(3)	94(2)	77(2)	69(2)	-23(1)	19(2)	-21(2)
C(4)	66(2)	120(2)	74(2)	-12(2)	0(1)	-1(2)
C(5)	79(2)	87(2)	65(2)	6(1)	6(1)	7(2)
C(6)	71(2)	55(1)	58(1)	-12(1)	9(1)	5(1)
C(7)	86(2)	71(2)	67(2)	-2(1)	14(1)	18(1)
C(8)	125(3)	64(2)	72(2)	-5(1)	32(2)	4(2)
C(9)	74(2)	52(1)	80(2)	-8(1)	16(1)	5(1)
C(10)	93(2)	89(2)	130(3)	-55(2)	21(2)	-11(2)
O(11)	64(1)	53(1)	60(1)	-7(1)	4(1)	4(1)
N(12)	53(1)	55(1)	56(1)	0(1)	2(1)	-7(1)
C(13)	58(1)	62(1)	66(1)	6(1)	8(1)	-13(1)
C(14)	57(2)	90(2)	108(2)	13(2)	11(1)	-20(1)
C(15)	95(2)	105(2)	69(2)	12(2)	15(1)	-31(2)
C(16)	100(2)	67(2)	102(2)	17(2)	19(2)	-17(2)
C(17)	55(1)	56(1)	52(1)	-5(1)	7(1)	-9(1)
C(18)	57(1)	66(1)	58(1)	-8(1)	8(1)	-15(1)
C(19)	82(2)	69(2)	87(2)	-11(1)	20(1)	-30(1)
C(20)	53(1)	91(2)	104(2)	-6(2)	-2(1)	-9(1)
C(21)	52(1)	45(1)	74(2)	-7(1)	10(1)	-10(1)
C(22)	88(2)	51(1)	81(2)	-4(1)	-8(1)	4(1)
C(23)	115(3)	57(2)	129(3)	2(2)	-41(2)	4(2)
C(24)	78(2)	61(2)	212(5)	1(3)	-16(3)	7(2)
C(25)	71(2)	66(2)	188(4)	-16(2)	43(2)	0(2)
C(26)	69(2)	63(2)	107(2)	-12(1)	28(2)	-8(1)

Table 5. Hydrogen coordinates (x 10^4) and isotropic displacement parameters (A^2 x 10^3) for 2,2,5-trimethyl-3-(1-(4'-chloromethyl)phenylethoxy)-4-phenyl-3-azahexane.

	x	y	z	U(eq)
H(2A)	9917	7328	2889	134
H(2B)	8884	8426	2562	134
H(4)	8726	5315	3317	104
H(5)	6606	4479	3660	92
H(7)	4021	7263	2823	89
H(8)	6133	8109	2491	103
H(9)	4025	4479	3753	82
H(10A)	1739	4055	3275	154
H(10B)	3106	3593	2988	154
H(10C)	2262	5119	2875	154
H(14A)	417	7419	4465	127
H(14B)	-56	5752	4550	127
H(14C)	326	6268	4039	127
H(15A)	3824	6270	5090	134
H(15B)	2244	5747	5241	134
H(15C)	2476	7416	5087	134
H(16A)	1992	3964	4150	134
H(16B)	1847	3797	4703	134
H(16C)	3452	4009	4518	134
H(17)	3614	8546	4589	65
H(18)	5014	8634	3726	72
H(19A)	4463	11069	3928	118
H(19B)	6218	10845	4052	118
H(19C)	5130	10816	4463	118
H(20A)	7282	8302	4196	125
H(20B)	6199	6983	4309	125
H(20C)	6458	8333	4668	125
H(22)	2339	8993	3334	89
H(23)	304	10482	3054	125
H(24)	-1068	11734	3582	143
H(25)	-422	11516	4393	128
H(26)	1619	10054	4680	94

Table 6. Torsion angles [deg] for 2,2,5-trimethyl-3-(1-(4'-chloromethyl)phenylethoxy)-4-phenyl-3-azahexane.

Cl(1)-C(2)-C(3)-C(4)	90.1(3)
Cl(1)-C(2)-C(3)-C(8)	-90.4(3)
C(8)-C(3)-C(4)-C(5)	-0.7(4)
C(2)-C(3)-C(4)-C(5)	178.8(3)
C(3)-C(4)-C(5)-C(6)	0.2(4)
C(4)-C(5)-C(6)-C(7)	0.7(4)
C(4)-C(5)-C(6)-C(9)	178.1(2)
C(5)-C(6)-C(7)-C(8)	-1.1(4)
C(9)-C(6)-C(7)-C(8)	-178.4(2)
C(4)-C(3)-C(8)-C(7)	0.3(4)
C(2)-C(3)-C(8)-C(7)	-179.2(2)
C(6)-C(7)-C(8)-C(3)	0.6(4)
C(7)-C(6)-C(9)-O(11)	-56.2(3)
C(5)-C(6)-C(9)-O(11)	126.6(2)
C(7)-C(6)-C(9)-C(10)	62.2(3)
C(5)-C(6)-C(9)-C(10)	-115.0(3)
C(6)-C(9)-O(11)-N(12)	-87.3(2)
C(10)-C(9)-O(11)-N(12)	150.4(2)
C(9)-O(11)-N(12)-C(17)	130.47(17)
C(9)-O(11)-N(12)-C(13)	-104.23(19)
O(11)-N(12)-C(13)-C(14)	-52.9(2)
C(17)-N(12)-C(13)-C(14)	67.3(3)
O(11)-N(12)-C(13)-C(15)	-177.02(19)
C(17)-N(12)-C(13)-C(15)	-56.8(3)
O(11)-N(12)-C(13)-C(16)	67.9(2)
C(17)-N(12)-C(13)-C(16)	-171.8(2)
O(11)-N(12)-C(17)-C(21)	49.7(2)
C(13)-N(12)-C(17)-C(21)	-70.4(2)
O(11)-N(12)-C(17)-C(18)	-81.41(19)
C(13)-N(12)-C(17)-C(18)	158.53(17)
N(12)-C(17)-C(18)-C(20)	-55.3(2)
C(21)-C(17)-C(18)-C(20)	171.12(19)
N(12)-C(17)-C(18)-C(19)	-177.80(19)
C(21)-C(17)-C(18)-C(19)	48.6(3)
N(12)-C(17)-C(21)-C(22)	-71.6(3)
C(18)-C(17)-C(21)-C(22)	58.7(3)
N(12)-C(17)-C(21)-C(26)	111.2(2)
C(18)-C(17)-C(21)-C(26)	-118.5(2)
C(26)-C(21)-C(22)-C(23)	-2.2(4)
C(17)-C(21)-C(22)-C(23)	-179.5(2)
C(21)-C(22)-C(23)-C(24)	0.8(4)
C(22)-C(23)-C(24)-C(25)	0.3(5)
C(23)-C(24)-C(25)-C(26)	0.0(5)
C(24)-C(25)-C(26)-C(21)	-1.5(4)
C(22)-C(21)-C(26)-C(25)	2.6(4)
C(17)-C(21)-C(26)-C(25)	179.9(2)

Symmetry transformations used to generate equivalent atoms:

Table 7. Hydrogen bonds for 2,2,5-trimethyl-3-(1-(4’-chloromethyl)phenylethoxy)-4-phenyl-3-azahexane [A and deg.].

D-H...A	d(D-H)	d(H...A)	d(D...A)	<(DHA)